INTER

International Network on Timber Engineering Research

MEETING FORTY-NINE

GRAZ, AUSTRIA

AUGUST 2016

INTER PROCEEDINGS MEETING FORTY-NINE 2016

INTER - International Network on Timber Engineering Research

2014 the International Network on Timber Engineering Research (INTER) was founded.

Scope
Presentation, discussion and documentation of research results in timber engineering and development of application rules for timber design codes or standards related to timber engineering.
Approach
Annual meetings in different countries/places hosted by meeting participants
Presentation and discussion of papers
Peer review of the abstracts before the meeting and of the papers during the meeting
Decision of the acceptance of the abstracts before the meeting by a well-defined review process
Decision of the acceptance of the papers for the proceedings during the meeting
Publication of the papers and the discussion in proceedings
Rules
All decisions including the appointment of the chairperson or the location of annual meetings are made by the participants attending a meeting.
Membership
Persons contributing to or being interested in research related to timber engineering.

INTER

International Network on Timber Engineering Research

Proceedings

Meeting 49

16 - 19 August 2016

Graz, Austria

Edited by Rainer Görlacher

Timber Scientific Publishing
KIT Holzbau und Baukonstruktionen
Karlsruhe, Germany
2016

Publisher:
Timber Scientific Publishing
KIT Holzbau und Baukonstruktionen
Reinhard-Baumeister-Platz 1
76131 Karlsruhe
Germany
2016

ISSN 2199-9740

Table of Contents

1 List of participants

AUSTRALIA

K Crews	University of Technology Sydney
R Shrestha	University of Technology Sydney

AUSTRIA

M Augustin	Competence Centre holz.bau forschungs gmbh, Graz
R Brandner	Graz University of Technology
J Dröscher	Graz University of Technology
G Flatscher	Graz University of Technology
K Ganster	Graz University of Technology
U Mahlknecht	Competence Centre holz.bau forschungs gmbh, Graz
A Ringhofer	Graz University of Technology
G Schickhofer	Graz University of Technology

CANADA

G Doudak	University of Ottawa
F Lam	University of British Columbia, Vancouver
A Salenikovich	Université Laval, Québec
J-P Tremblay-Auclair	Université Laval, Québec
E Ussher	University of New Brunswick

CHILE

P Gonzalez	University of Santiago of Chile

CHINA

Minjuan He	Tongji University
Zheng Li	Tongji University

CROATIA

M Jelec	University of Osijek
V Rajcic	University of Zagreb

ESTONIA

A Just	Tallinn University of Technology
M Tiso	Tallinn University of Technology

FINLAND

G Fink	Aalto University

FRANCE	
L Franzoni	Ecole des Ponts - Navier
GERMANY	
H J Blaß	Karlsruhe Institute of Technology (KIT)
P Dietsch	Technical University of Munich
M Frese	Karlsruhe Institute of Technology (KIT)
R Görlacher	Karlsruhe Institute of Technology (KIT)
M Kleinhenz	Technical University of Munich
A Kovryga	Technical University of Munich
U Kuhlmann	University of Stuttgart
C Rauschen	Ingenieursozietät Schürmann-Kindmann und Partner Gbr
C Sandhaas	Karlsruhe Institute of Technology (KIT)
W Seim	University of Kassel
P Stapel	Technical University of Munich
ITALY	
A Ceccotti	University of Venice
M Izzi	University of Trieste
JAPAN	
K Kobayashi	Shizuoka University
M Yasumura	Shizuoka University
NEW ZEALAND	
A Hashemi	University of Auckland
R Masoudnia	University of Auckland
L-M Ottenhaus	University of Canterbury
P Quenneville	University of Auckland
F Sarti	University of Canterbury
F Scheibmair	University of Auckland
A Valadbeigi	University of Auckland
P Zarnani	School of Engineering, Computer and Mathematical Sciences
NORWAY	
J Köhler	NTNU Trondheim
SWEDEN	
D Brandon	SP Technical Research Institute of Sweden
A Falk	KTH Royal Institute of Technology
E Serrano	Lund University

SWITZERLAND

T Ehrhart	ETH Zürich
A Frangi	ETH Zürich
S Franke	Bern University of Applied Sciences
R Jockwer	Swiss Federal Laboratories for Material Science (EMPA)
P Palma	Swiss Federal Laboratories for Material Science (EMPA)
R Steiger	Swiss Federal Laboratories for Material Science (EMPA)

UNITED KINGDOM

R Harris	University of Bath
K Ranasinghe	Exova BM TRADA
Wen-Shao Chang	University of Bath
T Reynolds	University of Cambridge
Cong Zhang	University of Bath

USA

J Dolan	Washington State University
M Gershfeld	California State Polytechnic University, Pomona
T Skaggs	American Plywood Association, Tacoma
B Yeh	American Plywood Association, Tacoma

2 Minutes of the Meeting

by F Lam, Canada

CHAIRMAN'S INTRODUCTION

Prof. Hans Blass welcomed the delegates to the International Network of Timber Engineering Research (INTER) in Graz. The meeting in Graz constitutes the 49th meeting of the group including the series of former CIB-W18 meetings. INTER continues the tradition of yearly meetings to discuss research results related to timber structures with the aim of transferring them into practical applications. Chairman thanked G Schickhofer, R. Brander and the timber engineering team for hosting the meeting. This is the 2nd meeting for our group in Graz hosted by G Schickhofer after the 1999 CIB-W18 meeting. The chair announced the sad news that Professor D Barrett from the University of British Columbia passed away on April 5, 2016 and asked for a minute of silence to remember our friend and colleague D Barrett.

There are 22 papers accepted for this meeting. The papers were selected based on a review process for the abstracts with 4 acceptance criteria (state of the art, originality, assumed content, and relation to standards or codes).

Papers brought directly to the meeting would not be accepted for presentation, discussions, or publication. Same rule applies to papers where none of the authors is present or papers which are not defended by one of the authors. The presentations are limited to 20 minutes each, allowing time for meaningful discussions after each presentation. The Chair asked the presenters to conclude the presentation with a proposal or general statements concerning the impact of the research results on existing or future potential applications and development in codes and standards.

The topics covered in this meeting are: Stress grading (1), Timber joints and fasteners (2), Duration of load (1), Timber beams (2), Laminated members (2), Structural stability (7), Fire (3), Statistics and data analysis (1), Serviceability (3). Numbers in parentheses are the number of papers presented in each topic based on initial allocation.

The participants have the possibility of presenting notes towards the end of the technical session. R Görlacher has brought a list of intended note presentations. Participants intending to present notes that are not on the list should notify R Görlacher accordingly.

An address list of the participants was circulated for verification of accuracy.

R Brandner introduced the host organization TU Graz. The organization team is led by G Schickhofer, R Brandner and H Weißnar. He also provided an introduction of Graz, Styria, and TU Graz.

GENERAL TOPICS

None

STRESS GRADING

49 - 5 - 1 Strength Grading of European Beech Lamellas for the Production of GLT and CLT - T Ehrhart, G Fink , R Steiger, A Frangi

Presented by T Ehrhart

H Blass asked were the grading rules checked with verification set outside the material tested. T Ehrhart replied no and only studied short length and would be doing more.

P Stapel asked would there be a difference using the proposed visual rules to establish DAB values used today. T Ehrhart replied no. In 80% of the knots the values would be identical so little difference was observed. Also the knot information was established by looking at the face and assuming the knot will go to the middle of the laminae.

G Ranasinghe commented about the way of measuring KAR and said that in the UK marginal KAR was used because KAR was considered as not too practical.

M Augustin asked how was grain deviation measured. T Ehrhart replied that it was not measured directly and explained the procedure used. He added that it was difficult to quantify although it was important.

TIMBER JOINTS AND FASTENERS

49 - 7 - 1 Impact of Varying Material Properties and Geometrical Parameters on the Reliability of Shear Connections with Dowel Type Fasteners - R Jockwer

Presented by R Jockwer

H Blass commented that steel properties from individual batches would have low coefficient of variation. He asked could the results be made worse by unintentionally having better steel grades leading to low reliability. R Jockwer agreed and replied that the results depended on the ratio of properties of actual and assumed steel grade and the failure mode.

E Serrano discussed the information from Jorissen regarding mixed mode failure. R Jockwer replied that mode 1 fracture energy values were used. He also stated that only if we had pure shear we would have higher fracture energy. If we have stress interaction the fracture energy would drop so mode one would be assumed to be conservative.

P Zarnani commented that the mix mode failure in slide 16 should be better represented. He also questioned the relationship between the coefficients of variation for the material properties and the connection. R Jockwer replied that the issues were considered in the paper with different partial safety factors for brittle and ductile failure modes.

LM Ottenhaus asked about slide 18 where the graph classified on the right side as ductile failure. She asked whether the failure would go into brittle failure mode outside the range of the graph. R Jockwer replied that at the end splitting failure was always present.

F Lam asked about using Ditlevsen's bounds in reliability studies to consider mixed failure modes. R Jockwer replied that the model of establishing the connection capacity already had mixed failure modes considered. F Lam asked whether mode uncertainties were considered. R Jockwer replied that it would be considered in future.

P Quenneville commented the highly manufactured products such as LVL would have low coefficient of variation and the cross layers in some LVL product would change the failure mode. He also asked whether the difference shown in slide 22 was significant. R Jockwer replied that although the number of tests was low the results supported the theoretical model.

K Ranasinghe received clarification of how the 5th percentile values were established from simulation and there was a transition between different failure modes.

T Reynolds and R Jockwer discussed the importance of the influence of material density on failure mode.

G Schickhofer commented one should avoid brittle failure mode and should provide recommendation to avoid brittle failure.

U Kuhlmann commented that some graph for reliability was not clear. R Jockwer replied that the beta values in the range of 5 to 5.5 were for comparison purposes. Also the information was provided as normalized ratios. U Kuhlmann suggested that more information should be provided.

P Dietsch commented that envelope curve showing where additional safety could be achieved would be important for code consideration to guide the development of code provisions to avoid brittle failures.

R Steiger asked why kmod of one was used in the reliability calculations. R Jockwer agreed that the results would be different if a different kmod was used. This would be done in the future.

S Franke commented that the ductile mode consideration would be even more important for example using minimum member thickness.

P Quenneville stated specifying L/d ratio would not be sufficient to ensure ductile behaviour as the number of fasteners would come into play.

49 - 7 - 2 Predicting the Load-Deformation of Bolted Timber Connections up to Failure - Yike Zhang, G M Raftery, P Quenneville

Presented by P Quenneville

M Yasumura asked how Δy was determined. P Quenneville replied only dealing with bolted connections where the definition of Δy was easier from theoretical approach to estimate k_1 and k_2. M Yasumura commented that getting Δy would be difficult from experimental approach.

K Crews suggested that from experimental results sensitivity analysis could be done to check Δy estimates from different approaches.

F Lam asked about the influence of reverse cyclic loading ▯u estimate. P Quenneville replied that from related work using cyclic tests higher capacity was obtained compared to monotonic tests.

A Ceccotti commented about the history of defining ductility for EC8 and it would be useful to study Δu.

LM Ottenhaus added ductility would increase under reversed cyclic conditions for mode 3. F Lam asked would it also increase for mode two. P Quenneville replied that mode of failure could change form mode 3 to mode 2 to l and higher capacity. M Yasumura added low cyclic fatigue failure in steel element could happen in reverse cyclic tests leading to lower ductility.

U Kuhlmann commented that Δu as an absolute value should be considered for ductility and not based on relationship between Δu and Δy.

G Schickhofer commented only glulam and LVL were considered and CLT type should be studied.

A Salenikovich and P Quenneville discussed the use of large fasteners for design.

DURATION OF LOAD

49 - 9 - 1 Long-term Behaviour of Moisture Content in Timber Constructions – Relation to Service Classes - B Franke, S Franke, A Müller, M Schiere

Presented by S Franke

K Crews commented that the work showed different elements in timber could have different service class. He recommended more effort would be needed to use this work. S Franke agreed.

P Dietsch commented that the type of building considered was important. He stated that the resistant based method used to monitor moisture content would not work in frozen timber. S Franke replied that this matter would have to be corrected and temperature of the member would need to be checked.

P Zarnani asked how to explain the high variation in the radial and tangential directions compared to the longitudinal direction. S Franke clarified about the location of the measurements in the specimens and influence of the glue line was not available in the tangential and radial directions so longitudinal direction has the highest transport.

M Augustin asked about the issue related to coating and painting. S Franke replied that in such case coating had no influence because they were applied for protection during transportation.

R Jockwer asked whether it would be possible that the active resistance zone migrated. S Franke replied it would be possible.

P Staple received clarification that the pith location was referenced to all laminates and through the length.

T Reynolds received clarification that the electrodes did not form a path for the moisture.

TIMBER BEAMS

49 - 10 - 1 Tensile Strength Classes for Hardwoods - A Kovryga, P Stapel, J-W G van de Kuilen

Presented by A Kovryga

K Crews commented that no finger joint material was evaluated and in Australia the limiting factor was finger joints with hardwood with delamination and gluing issues. He also commented that in slide 13 there was significant extrapolation and suggested to remove the extrapolation. A Kovryga replied that it was the real data.

G Fink commented that although the values were quite high they could be even higher. He questioned whether testing according to EN 408 was appropriate. A Kovryga agreed as the shorter test span might not be appropriate in terms of location of the weakest parts in the test zone.

K Ranasinghe received clarification that the single knot criterion was not based on UK standards and shear strength had not been analysed. He commented that it would make more sense to declare characteristic density according to species. There were discussions that the tensile strength perpendicular to grain was very high and it was decided to lower the value for design to discourage its use.

A Frangi asked what the coefficient of variation was. A Kovryga replied that the information was in the database.

K Crews commented that one should examine whether too many groups were examined.

F Lam commented that information about yield would be important. A Kovryga replied that each class considered 100 data points and the approach could not provide yield and such information would be obtained in another study on grading.

49 - 10 - 2 Simplified Method to Determine the Torsional Moment Due to Lateral Torsional Buckling - R Hofmann, U Kuhlmann

Presented by U Kuhlmann

R Steiger asked was there an impact for changes in design rules on horizontal bracing. U Kuhlmann replied that a follow up project on horizontal bracing had been performed and results were surprising with uneven distribution of forces amongst the horizontal braces.

P Zarnani and U Kuhlmann discussed flexural buckling and lateral torsional buckling cases.

A Frangi commented about designing bracing system with simplified design method. U Kuhlmann agreed that the old simplified method would be fine.

H Blass asked about recommendation on how to take out the lateral forces. U Kuhlmann replied that in general diagonal bracing was not desirable by owner because of added cost.

K Ranasinghe received clarification that there was no jump between the values for h/b<8 and h/b>8.

LAMINATED MEMBERS

49 - 12 - 1 Displacement Based Determination of Laterally Loaded Cross Laminated Timber (CLT) Wall Systems - G Flatscher, G Schickhofer

Presented by G Flatscher

H Blass asked about reverse cyclic loading. G Flatscher replied that his work only applies to monotonic loading and perhaps reduction in load can be considered in the reverse cyclic cases. There were discussions about displacement versus load capacity. The displacement capacity would be important for inter storey drift considerations. H Blass asked how the authors took into account of the floor reducing the load between the panels. G Flatscher replied that additional tests were conducted to generate data for the model. H Blass commented that high stiffness and capacity of the vertical joint could be used to account for the influence of the floor.

LM Ottenhaus asked about the influence of the failure mode on ductility for cases 1 and 3. G Flatscher replied that rocking and slip were the primary failure modes and ductility might be increased in the angle bracket case.

E Ussher commented that the load distributions depended on the length of the wall and stiffness and asked about influence of vertical load and openings. G Flatscher replied that there could be many influences on the behaviour of the walls but for single family house it is not necessary to consider non-linear analysis and influence of vertical loads was not considered here. He also cited work of Dujic 2007 that considered the influence of opening on the stiffness of the CLT elements.

A Hashemi questioned the lack of hold-downs which might not be true in more complete systems. G Flatscher replied that this could work when the angle bracket are considered as a special hold-down that took both shear and uplift.

M Gershfeld commented about the zipper effect that could happen with a line of connectors. G Flatscher replied that it would also be true for the hold-down case.

S Franke asked what kind of friction was considered. G Flatscher replied that vertical load and additional uplift load were considered and a coefficient of friction of 0.2 was used as a constant for the connections at the base. M Gershfeld commented about influence of interaction between shear and uplift of the angle bracket.

LM Ottenhaus commented that the function of hold-down and angle brackets in reverse cyclic cases to be used as fuse to dissipate energy and/or to carry uplift.

P Zarnani commented also on the need for hold-downs.

A Frangi commented that angle bracket can take shear as well as uplift if sized and designed well and spaced properly. These connection devices were intended for small buildings and lighter structures.

49 - 12 - 2 Structural Analysis of In-Plane Loaded CLT Beams with Holes: FE-Analyses and Parameter Studies - M Jelec, V Rajcic, H Danielsson, E Serrano

Presented by M Jelec

D Brandon commented that about mesh size dependency as small mesh size led to higher stresses. He suggested that fracture mechanics approach should be used. M Jelec agreed.

F Lam suggested that why not use round holes. H Blass agreed that this would reduce the stresses.

P Dietsch commented that the size of the hole would influence stress state and asked what would be the limitations. M Jelec replied that the work was done with respect to available data.

LM Ottenhaus agreed fracture mechanics approach would be appropriate and commented that failure criterion information would be important.

G Schickhofer commented that bigger holes should be considered. Also consideration of the layup of the beams would be important as there would be dependency on the laminae thickness and layup.

P Zarnani added that multiple hole cases and minimum hole spacing should be considered.

R Jockwer asked whether existing provisions in German national code on glulam design could be used. M Jelec replied no as such provisions needed to be validated.

STRUCTURAL STABILITY

49 - 15 - 1 Ambient and Forced Vibration Testing of a Light-frame Timber Building – Conclusions Regarding Design of the Lateral Load Resisting System - R Steiger, G Feltrin, A Sadeghi Marzaleh, S Nerbano

Presented by R Steiger

F Sarti questioned the statement that damping ratio cannot be established accurately from ambient vibration and asked whether the statement referred to ambient vibration measured within one day only. R Steiger responded that the damping ratio depends on amplitude therefore the level of excitation should be close to the design level for estimating damping ratio.

WS Chang commented that results from his paper confirm that amplitude influenced damping. He stated that the use of the shaker may be difficult to identify torsional behaviour. R Steiger explained about the procedures involving the cross correlation parameters and more detailed description of the procedures was available in the cited paper. WS Chang also received clarifications about the accelerometer.

G Doudak asked about comparisons with code equation and agreed that using ambient vibration to estimate damping would be questionable. There were discussions that the level of excitation is significantly higher in models and the structure period would be longer. R Steiger responded that testing of components are on-going with preliminary results indicating a factor of 2 for stiffness compared to code results.

E Ussher commented that damping ratios from ambient vibration can be used for situations where amplitudes are small. He questioned where the exciter influenced the damping estimate. R Steiger responded that the exciter is just an added mass and the additional supports under the floor were uncoupled laterally from the structural system and did not influence the results.

49 - 15 - 2 q-factor Estimation for Timber Blockhaus Buildings - C Bedon, G Rinaldin, M Izzi, M Fragiacomo

Presented by M Izzi

H Blass asked about the static capacity of these joints. M Izzi replied testing was done in Trento. There were discussions related to the presence of tensile stresses perpendicular to grain because of the notches. M Izzi stated that he had not followed the tests but agreed that tensile stresses perpendicular to grain would be important.

G Doudak asked about the influence of friction mechanism. M Izzi replied that gaps could be considered in the model with modifying the load and a gap of 1 mm was considered stable from manufacturers. G Doudak commented it was not clear how the q factor would be affected by the diaphragm rigidity and asked what would be the recommendation for a semi rigid case. M Izzi replied that this had not been investigated in detail yet.

A Frangi commented that the failure mode on connection can be shear and compression. M Izzi discussed the progress in which the mechanism had the lowest value was check first and then go back to model to check the other mechanism.

BJ Yeh commented that service conditions could cause checking of the wood and asked whether the q factor recommended would be appropriate for in service conditions. M Izzi replied yes.

W Seim commented that it was important to study the q factor for this type of structure. He commented that integrating these systems would be important if one had higher q factor. W Seim and M Izzi discussed that additional steel connectors would be needed to avoid integrating factor.

49 - 15 - 3 Simplified Design Procedure for Linear Dynamic Analysis of Multi-storey Lightframe Wood Buildings in Canada - J-P Tremblay-Auclair, A Salenikovich, C Frenette

Presented by J-P Tremblay-Auclair

F Sarti commented that the envelope for overturning looked surprising that less forces was observed with linear analyses. J-P Tremblay-Auclair explained that the stiffness was based on code provisions for the lateral deformation of the shear wall. F Sarti received confirmation that there were plans to compare results with non-linear dynamic analysis in the future.

H Blass commented that this study only considered one specific building. He asked whether tests on load-slip behaviour of the connectors were performed. J-P Tremblay-Auclair replied no and only used literature results on the same material. Also EC 5 equation was chosen because it would be more conservative. H Blass asked how stiffness could be considered conservative. J-P Tremblay-Auclair explained up to a factor of three was observed.

F Lam commented that the conclusion that EU 5 equation would yield conservative results might not always be true. Different buildings and earthquakes could yield different conclusions. More cases should be considered.

W Seim commented about the influence of nail spacing.

G Doudak commented that choice of narrow wall would not meet the requirement of 086. J-P Tremblay-Auclair did not agree as the total height should be considered. A Salenikovich replied that additional information would be available and would be presented to Canadian code committee in future.

J-P Tremblay-Auclair explained the base shear input to LDM was normalized and calibrated to equivalent shear forces.

M Gershfeld asked whether soft story behaviour was seen and commented that it would be a concern in California. F Lam replied in 2009 six storey light wood frame residential building was permitted in the 2009 British Columbia building code. Soft storey behaviour was a concern as shown in computer models. As a practical solution the BC Building code stipulated the amount of shear walls required in the lower two storeys would need to be increased by 20% to prevent soft story behaviour.

A Ceccotti asked about the period of the structure. J-P Tremblay-Auclair replied it was 1.5 sec. A Ceccotti stated that the building was very soft.

49 - 15 - 4 Seismic Performance of CLT Low-rise Structures with Small and Large Wall Elements with Opening - M Yasumura, K Kobayashi, M Okabe

Presented by M Yasumura

M Gershfeld and M Yasumura discussed the details of the corners and no reinforcement was used.

A Ceccotti asked about the difference between yield load and ultimate state. M Yasumura replied that yield point was almost the same as design. A Ceccotti and M Yasumura discussed definition of yield point. A Ceccotti also received clarification about inter storey deflection. M Yasumura discussed the damage at the bottom of the connection also the crack initiation at the corner of the opening.

F Lam and M Yasumura discussed the very consistent hysteresis response predicted by the model under earthquake simulations. M Yasumura stated that more detailed information was available in a recent ASCE paper.

D Dolan commented on incremental dynamic analysis and the importance of post peak response for the collapse considerations could be 14% drift.

V Rajcic asked whether the acceleration of the floor level was measured. M Yasumura responded that it was not a dynamic shake table test.

W Seim asked about the q value for this system and discussed about degradation. M Yasumura responded that the q value should be at least 2.

49 - 15 - 5 Performance of Full-Scale I-Joist Diaphragms - B J Yeh, B Herzog, T Skaggs

Presented by B J Yeh

P Quenneville asked how practical would be the staggered nail pattern. BJ Yeh stated that it is very practical and is being used.

D Dolan commented that the work was referenced to only one manufacturer of LVL with tensile strength perpendicular to grain lower than lumber. There could be variation amongst the many LVL producers. BJ Yeh responded that recommendations from this work only referenced to dimension lumber; LVL should be considered by individual LVL producers as proprietary products. He also commented that higher grade material has higher tendency to split.

G Doudak and BJ Yeh discussed about stiffness of the diaphragm and where it is appropriate to consider the nonlinearity. They also discussed the issues related to the definition of ductility and yield point.

P Zarnani and BJ Yeh discussed the mechanism of shear flow with respect to the diaphragm.

F Lam commented about the importance of species effect rather than density and grade effect that influence splitting.   H Blass added that in EC5 a minimum thickness is needed for species that are prone to splitting.

M Gershfeld suggested the consideration of vertical load when splitting happened. BJ Yeh responded that the influence of vertical load would not have much of an effect.

49 - 15 - 6 Advanced Modelling of CLT Wall Systems for Earthquake Resistant Timber Structures - M Izzi, A Polastri, M Fragiacomo

Presented by M Izzi

G Doudak asked about the interaction between tension and shear and how the model would take into account the interaction. M Izzi responded that the model has shear springs and axial spring and they are uncoupled. G Doudak commented that there were no test results which considered the influence of the floor.   M Izzi replied that the floor was considered not to be able to move in the out of the plane direction and the bending stiffness of the floor was considered as an elastic element.

P Quenneville asked how realistic would be the sliding failure with the presence of perpendicular elements.   M Izzi agreed and the information in the paper was limited to single wall or couple walls in laboratory conditions.

T Reynolds commented that at the 1st floor level the wall might be mounted on the wall rather than the concrete. M Izzi replied the model could be modified to consider such situation.

F Lam commented UBC has data on the interaction between axial and shear load in similar connections. The information would be presented in WCTE 2016.

A Ceccotti questioned about the influence of vertical load between 30 to 40 kN on capacity. M Izzi replied that this was caused by the sliding.   A Ceccotti also questioned the case at zero vertical load the model prediction and test results differed by a factor of 2. There were discussions about the difference of results between the floor and no floor cases.

H Blass received clarification that the displacement was applied at the floor level. M Izzi stated that without floor the failure mode was rocking therefore the failure load was lower.

A Frangi questioned why at zero vertical load where the rocking dominated there was a difference in one case. There was discussion that the connection between the floor and wall could be the limiting factor. A Frangi stated that the proposal to make an improved simplified model was missing in the paper to guide the designers and code. He also commented if we introduced stiffness in design it would add more questions and difficulties. M Izzi replied that more work would be done.

M Gershfeld commented that developing a connection system that could uncouple axial and shear forces would be useful rather than considering the complicated interaction. M Izzi agreed but no system was available.

A Ceccotti commented that it is an important study that could allow us to understand CLT system better; however, we should consider taller and bigger structures with CLT.

49 - 15 - 7 Seismic Resistant Timber Walls with New Resilient Slip Friction Damping Devices - A Hashemi, P Zarnani, A Valadbeigi, R Masoudnia, P Quenneville

Presented by A Hashemi

A Ceccotti commented that in typical CLT system huge acceleration was observed and asked whether this system could reduce the acceleration. A Hashemi responded that this system could reduce acceleration by 80% as presented in the paper.

G Schickhofer stated the test was done in tension and asked what would happen in the case of shear loading. A Hashemi replied that work on this topic will be presented next year.

H Blass commented that this is a good system but asked why such long screws were used at 50 x the diameter. A Hashemi stated that these screws were available at the time and agreed that it was an overdesign and be optimized later.

M Yasumura asked whether such system would be applied to all the wall components in a building. A Hashemi replied probably not. M Yasumura stated that the effect of mixed system needs to be studied.

F Lam commented that low cycle fatigue behaviour of the screws needs to be considered; depending on the stress level they would probably not meet the high cycles cited in the paper. P Quenneville replied that it could be considered later.

T Reynolds and A Hashemi discussed lateral load's dependency on the mass. T Reynolds asked why a 6 m high wall was used with the loading point at mid height. A Hashemi replied the material was conveniently available at the lab.

Z Li stated that friction based devices had been evaluated in Tongji University and asked if these devices needed to be opened up after testing to allow restoration of position. A Hashemi replied that a special lubricant was used so that the device can restore to original position without needing to be opened up.

FIRE

49 - 16 - 1 A Stiffness-Based Approach to Predict the Fire Behavior of Cross Laminated Timber Floors - L Franzoni, D Dhima, A Lebée, F Lyon, G Foret

Presented by L Franzoni

A Frangi commented that he did not agree with the conclusion. He questioned why deflection should be calculated in a fire situation. L Franzoni replied that the paper presented a way to compare experimental data to model and it was not intended as an engineering approach. A Frangi commented that stiffness information would not be needed but only load carrying capacity information. He stated that König's work might not be considered accurately in this paper and Frangi's model was also not intended for calculation of deformations. Frangi suggested if the goal was to look at cases without delamination then one should test with melamine otherwise there would be too many parameters.

G Schickhofer also commented that the paper only considered PU and a general model should consider different adhesives.

49 - 16 - 2 Fire Design of Timber Connections – Assessment of Current Design Rules and Improvement Proposals - P Palma, A Frangi

Presented by P Palma

P Zarnani asked why number of fasteners and spacing of fasteners were not important. P Palma clarified that the number of fasteners were important. P Zarnani asked what type of failure mode was encountered. P Palma responded that side member failures were found. P Zarnani and P Palma discussed that the edge distance would be more important if one had fewer rows but the test results are few to make such claims and failure mode was typically embedment.

P Quenneville asked whether Eurocode allows dowelled only connection. It was clarified that at least one bolt is required. P Quenneville asked whether there would be plans to consider cases with at least one bolt. P Palma stated that some results did not have any bolts but some results did have bolts and that the structural engineer can consider the more conservative results.

P Dietsch commented that kflux factor for nailed connection had two values and there was a big jump from 1.5 to 2.5. He asked if the 280 mm values was a mistake in the code and should be corrected to 440 mm, would it mean that the designs in the past were wrong. P Palma stated that it was an obvious typing error in the code and pointed out the source of the 440 mm values as Holz Brandschutz handbook. P Dietsch questioned the conclusion that side thickness was more important than the gap so what about the situation of fire from below. P Palma responded that in such case all 4 sides are exposed to fire and in the case of fire from below they did not have the information.

U Kuhlmann asked why the bolts were worse than dowels. P Palma responded that the influence of exposed bolt head and nut and washer was the reason.

C Rauschen commented about the negative effect of bolt if one protected the steel plate but not the bolt and would it be okay if 20% capacity was still left. P Palma responded that heat would still travel through the bolt to the protected plate.

J Köhler asked whether the characteristic load was used. P Palma responded that the load ratio was taken as 30% of the mean load.

J Köhler, K Ranasinghe and P Palma discussed about using of the 5% percentile load level might be non-conservative because 95% of the connection would have higher strength.

49 - 16 - 3 Improved Fire Design Model for Timber Frame Assemblies - A Just, M Tiso

Presented by A Just

A Frangi asked with about the possibility to extend the 25 tests by numerical simulations with consideration of the variability. A Just agreed and responded that they could not give numbers for any material and that it was a proposed model approach only. A Frangi commented that companies could do the tests if they were unhappy with the proposed. A Frangi asked whether the authors were sure that the insulation was not falling off. A Just responded that they were not sure and were not dealing with this issue in this approach. He stated that if one did not keep insulation in place then this approach could not be used.

P Zarnani asked about CLT. A Just said that CLT would be a different topic.

K Ranasinghe commented that this proposed approach would require a lot of work to make it usable for designers. He commented that the results in slide 27 suggested that one would need larger cross sections to meet the requirements which would be detrimental to the design. A Just responded that this proposal was neither considered for thin members nor for different material. H Blass added that this meeting is not intended to deliver results to help designers on the spot and the meeting is intended to work on issues related to code.

U Kuhlmann stated that insulation issue is also important for steel structures; in particular, the durability of the insulation has recently been identified as being an issue.

49 - 17 - 1 Reliability of Large Glulam Members - Part 1: Data for the Assessment of Partial Safety Factors for the Bending Strength - M Frese, H J Blaß

Presented by M Frese

J Köhler commented that it was good to propose a size effect for bending strength of glulam. He commented that as this was still artificial data we have to be careful. Because no experiments were conducted it should be mentioned. Choice of distribution function might be better optimized. As comparisons were made with minimum values, this would be sensitive from a probability point of view. M Frese responded that the data were generated for future reliability analysis and the data set would be available for use by reliability experts. J Köhler commented model uncertainties should be considered and more information about the model would be needed to estimate the uncertainties. M Frese responded that a paper will be presented in WCTE 2016 about the model in more detail.

P Dietsch asked about how the model related to experimental evidence and which range could be related. M Frese said that the original data was created in the 1980s on board elements as basic data. There has been a number of series of full scale testing of beams since then to validate the model. This included two series of 20 beams each of two different strength classes and 150 boards and 150 finger joints.

G Fink commented that the characteristic values of the larger beams were not changing as much. The model might not fit the lower tail well. He commented that with a sample size of 1000 beams with low height, one should get some beams with extremely low realizations but this was not seen from the results of the model. He stated that this could be covered by the model uncertainty issue. G Fink and J Köhler and M Frese discussed the importance of variability and the shape of the lower tail of the distribution.

P Quenneville asked about the variability of the loading. M Frese responded this would be a topic for reliability study and not within the scope of this paper.

F Lam commented about the similarity of the k or shape factor between the Canadian study on glulam size effect and this paper. He asked about the effect of width of the laminates. M Frese stated that this was not considered because this was already taken into consideration by grading of the boards. F Lam suggested that study on size effect on shear strength in glulam would also be appropriate.

A Frangi commented that in a study where bending tests were conducted on specimens taken from a failed structure he found a real beam with strength lower than the minimum value. H Blass responded that this could be production error which was not considered in this paper.

Z Li asked about the failure criterion considered in the FEM and what was the size of FEM element considered. M Frese stated that failure of the outmost laminate in tension was considered. The element size in the model was not changed because element size was tied to regression equations used in the basic data set.

G Schickhofer commented that we should consider size effects in our design standards including other properties. M Frese agreed.

P Quenneville commented that large beams are produced with less industrialization. M Frese responded that the quality control for checking of finger joints would be the same for all beam sizes.

P Zarnani asked about the possibility of using the model for LVL. H Blass responded that LVL is a completely different material.

BJ Yeh suggested consideration of width effect because in N America it is a volume consideration.

P Zarnani asked whether the difference was due to grading and not size. M Frese responded no and that in this study only homogeneous beams were considered

V Rajcic commented that it would be a good idea to get data from glulam companies.

49 - 20 - 1 Need to Consider Modal Participation in Vibration Serviceability Design of Cross-Laminated-Timber Slabs - E Ussher, J Weckendorf, K Arjomandi, I Smith

Presented by E Ussher

F Sarti asked about the model of CLT panels and connectivity between the panels. E Ussher replied that axial and rotational springs were employed. F Sarti commented about the higher modes at 100 Hz and that human perceptions would not be sensitive at such high frequency. Ussher commented that they were looking at the acceleration at the high modes.

M Augustin commented that conclusions might not be applicable for heavier floors. E Ussher agreed and replied that this had to be considered in a case by case manner. M Augustin commented that test results in lab could be very different from real situations as the influence of non-load bearing elements could not be considered. E Ussher said that boundary conditions could be adapted and one could also recommend some kind of minimum for design considerations.

49 - 20 - 2 Design Parameters for Lateral Vibration of Multi-Storey Timber Buildings - T Reynolds, A Feldmann, M Ramage, Wen-Shao Chang, R Harris, P Dietsch

Presented by T Reynolds

D Brandon commented about damping versus building height and asked would it be better to separate timber buildings out to see a relationship. T Reynolds replied the reason for not separating the timber from timber concrete system was that the concrete's contribution was considered as part of the system. He agreed that there could be a relationship.

G Doudak asked about the definition of height. T Reynolds clarified it was the height of the building. G Doudak commented that from a dynamic sense the height of the concrete portion in concrete podium cases should not be considered as the building height. T Reynolds agreed that this was a valid point. WS Chang added they could consider only the timber part in such building.

P Quenneville asked whether damping would be related to shear rigidity for shorter buildings. T Reynolds agreed that it would be likely.

A Frangi asked whether the authors would be confident about the proposal based on these unique buildings. T Reynolds replied that it would be important that this work was done so that designers can receive guidance even though the number of cases was limited.

49 - 20 - 3 Design of Timber Floor for Vibration: Some design and Test Questions - Wen-Shao Chang, Haoyu Huang, R Harris

Presented by Wen-Shao Chang

F Sarti commented that the damping ratio reported seems high. WS Chang responded that the contribution of nonstructural elements including partitions and plaster board might have contributed to the high damping. F Sarti asked about comparisons for higher mode damping and commented that the sampling rate of 100

Hz should be related to how high a frequency one would want to capture. WS Chang responded that the sampling rate was taken as 10x the natural frequency.

F Lam commented Nyquest frequency should be used to establish the sampling rate. A discussion of VDV took place. He commented that the measurements at the tail end of the record might be unreliable because of the low signal to noise ratio. WS Chang agreed but they needed the information.

P Dietsch commented that the measured high damping ratio's depended on nonstructural elements and one would need to clarify that the code damping ratios were based on structural elements only. Consideration of the contribution from nonstructural elements towards damping would be future additions. WS Chang responded that the damping level of 2% in the code was too low.

A Ceccotti received clarification that the ½ band method was used to establish damping the paper.

G Schickhofer agreed with P Dietsch that damping at different stages of the building process should be considered. He also agreed that the damping in actual buildings with non-structural elements was much higher than that based on structural elements only. G Schickhofer commented that VDV was very subjective and may be it is a parameter that could be decided by the client.

P Quenneville received clarification that not all floors considered received complaints. WS Chang answered that it was difficult to gain access to floors for evaluation where complaints had already been launched. Experience from engineers (dynamic's experts) indicated that floors with fundamental frequency higher than 10 Hz should perform well.

R Steiger asked about the relationship between damping ratio and amplitude as increase in amplitude tended to lead to increase in damping. WS Chang answered that the excitation was provided via a heel drop test. R Steiger commented that the formulation of VDV is simply a numerical high pass filter. He asked why an exponent of 4 was chosen. WS Chang answered it was based on ISO standard. R Steiger stated that the choice of this factor would be important and could affect the findings. R Harris stated that the issue is that ISO and British standards which are not timber specific standards set the acceptance criteria. EC5 design methods can lead to failures if these failure criteria are considered. This is especially problematic when EC5 does not give guidance for floors with fundamental frequency of less than 8 Hz.

A Ceccotti recalled that EC5 originally used log decrement method to estimate damping. It might have been changed over to modal damping ratio which could be the reason for the difference.

BJ Yeh stated that human response factor is important. WS Chang answered that they have not interviewed the occupants. R Harris added that there are ISO criteria which are not human response based.

T Skaggs asked whether floor k with the low frequency was acceptable by the client. WS Chang answered that he will find out later because the measurements were taken before occupancy.

K Ranasinghe commented about his experience with problematic cases in the UK which indicated that although calculations were satisfied the cases would still typically be settled out of court in favor of the client because it would be difficult to proof that the client was wrong.

A Frangi commented that sound insulation is also very important.

NOTES

Notes were presented.

ANY OTHER BUSINESS

G Schickhofer thanked F Lam and R Görlacher for their contributions.

VENUE AND PROGRAMME FOR NEXT MEETING

M Yasumura invited the group to INTER 2017 in Kyoto Japan August 28 to 31, 2017. Tentative venues for INTER are Tallinn Estonia 2018, Seattle, USA 2019. Munich Germany or Chile 2020.

CLOSE

H Blass would be prepared to act as chair for the group for the next meeting and advised the group to seek a new chair beyond that. K Crew moved that H Blass should extend his chairmanship for one year. The motion passed.

3 INTER Papers, Graz, Austria 2016

49 - 5 - 1	Strength Grading of European Beech Lamellas for the Production of GLT and CLT - T Ehrhart, G Fink , R Steiger, A Frangi
49 - 7 - 1	Impact of Varying Material Properties and Geometrical Parameters on the Reliability of Shear Connections with Dowel Type Fasteners - R Jockwer
49 - 7 - 2	Predicting the Load-Deformation of Bolted Timber Connections up to Failure - Yike Zhang, G M Raftery, P Quenneville
49 - 9 - 1	Long-term Behaviour of Moisture Content in Timber Constructions – Relation to Service Classes - B Franke, S Franke, A Müller, M Schiere
49 - 10 - 1	Tensile Strength Classes for Hardwoods - A Kovryga, P Stapel, J-W G van de Kuilen
49 - 10 - 2	Simplified Method to Determine the Torsional Moment Due to Lateral Torsional Buckling - R Hofmann, U Kuhlmann
49 - 12 - 1	Displacement Based Determination of Laterally Loaded Cross Laminated Timber (CLT) Wall Systems - G Flatscher, G Schickhofer
49 - 12 - 2	Structural Analysis of In-Plane Loaded CLT Beams with Holes: FE-Analyses and Parameter Studies - M Jelec, V Rajcic, H Danielsson, E Serrano
49 - 15 - 1	Ambient and Forced Vibration Testing of a Light-frame Timber Building – Conclusions Regarding Design of the Lateral Load Resisting System - R Steiger, G Feltrin, A Sadeghi Marzaleh, S Nerbano
49 - 15 - 2	q-factor Estimation for Timber Blockhaus Buildings - C Bedon, G Rinaldin, M Izzi, M Fragiacomo
49 - 15 - 3	Simplified Design Procedure for Linear Dynamic Analysis of Multi-storey Lightframe Wood Buildings in Canada - J-P Tremblay-Auclair, A Salenikovich, C Frenette
49 - 15 - 4	Seismic Performance of CLT Low-rise Structures with Small and Large Wall Elements with Opening - M Yasumura, K Kobayashi, M Okabe
49 - 15 - 5	Performance of Full-Scale I-Joist Diaphragms - B J Yeh, B Herzog, T Skaggs
49 - 15 - 6	Advanced Modelling of CLT Wall Systems for Earthquake Resistant Timber Structures - M Izzi, A Polastri, M Fragiacomo
49 - 15 - 7	Seismic Resistant Timber Walls with New Resilient Slip Friction Damping Devices - A Hashemi, P Zarnani, A Valadbeigi, R Masoudnia, P Quenneville

Strength grading of European beech lamellas for the production of GLT & CLT

Thomas Ehrhart, ETH Zürich, Institute of Structural Engineering, Zurich, Switzerland

Gerhard Fink, Aalto University, Department of Civil Engineering, Espoo, Finland

René Steiger, Empa, Swiss Federal Laboratories for Materials Science and Technology, Dübendorf, Switzerland

Andrea Frangi, ETH Zürich, Institute of Structural Engineering, Zurich, Switzerland

Keywords: European beech, strength grading, visual grading characteristics, longitudinal eigenfrequency, strength classes, glued laminated timber, cross laminated timber

1 Introduction

Like in several other Central European countries, the share of European beech wood (*Fagus sylvatica* L.) in the Swiss forests is very high and steadily growing due to forest policy and the progressing climate change. Nowadays, European beech is primarily used in furniture industry and for heating purposes, but not in the construction industry. The best way to process beech logs for structural purposes is still being discussed around the question: To peel or not to peel? For veneered products such as LVL, strength grading is of minor importance due to the high degree of homogenization in the final product; however, grading of the raw material is a key step in the production of glued laminated timber (GLT) and cross laminated timber (CLT).

Previous studies by *Frühwald & Schickhofer* (2004) and *Blass et al.* (2005) have outlined the great potential of European beech timber in terms of strength and stiffness. High mean values of tensile strength $f_{t,0,mean}$ between 62 and 75 N/mm^2 ($f_{t,max} \approx 120$ N/mm^2) and mean values of the modulus of elasticity (MOE) $E_{t,0,mean}$ of approximately 13300-14000 N/mm^2 ($E_{t,0,max} \approx 20000$ N/mm^2) were found. However, the studies also report a large scatter of results, i.e. coefficient of variation COV of up to 0.50 for $f_{t,0}$ and 0.25 for $E_{t,0}$.

The parameters to be accounted for and the limits for visual strength grading of hardwood – including European beech – are specified in DIN 4074-5 (2008). The highest visual strength grade LS 13 corresponds, according to DIN EN 1912 (2012), to the strength grade D 40 (valid for beech wood from Germany). The mechanical and physical properties of D 40 are listed in EN 338 (2016) (selected values in Table 1).

Table 1 Selected mechanical and phyiscal properties according to EN 338 (2016)

Strength grade	$f_{m,k}$ [N/mm²]	$f_{t,0,k}$ [N/mm²]	$E_{m,0,mean}$ [N/mm²]	$E_{m,0,05}$ [N/mm²]	ρ_{mean} [kg/m³]	ρ_k [kg/m³]
D 40	40	24	13000	10900	660	550

The requirements for the production of GLT are defined in EN 14080 (2013), however this standard is restricted to softwood species and poplar. According to EN 14080, the lamellas used for the production of GLT need to be of a certain T-class, i.e. requirements with regard to the 5% fractile value of tensile strength $f_{t,0,l,k}$, the mean value of tensile MOE $E_{t,0,l,mean}$ and the 5% fractile value of density $\rho_{l,k}$ have to be met. Regarding CLT, production requirements are defined in EN 16351 (2015), again limited to softwood species and poplar. So far, there are no European standards available for the production of GLT or CLT made from hardwood (except for poplar).

In Germany, the technical approval Z-9.1-768 (2009) regulates the production of beech GLT for strength classes up to GL 48c. This technical approval represents a major step towards a practical application of beech GLT. However, besides the bending strength, the other prescribed strength- and stiffness properties seem to have been limited to a rather conservative level and hence, do not encourage designers to apply beech GLT in practice.

The present study is part of a research project with the objective of providing the technical basis for the market implementation of high strength GLT made from European beech timber. Strength grading – especially regarding high strength grades – is considered to be of utmost importance for the whole project and therefore is focused on in the first stage.

In order to facilitate the production of GLT of the strength classes GL 40 (= $f_{m,g,05}$ of GLT), GL 48 and GL 55, reliable limits and rules for strength grading of European beech lamellas into the tensile strength grades T 33 (= $f_{t,0,k}$ of the T-class), T 42 and T 50 have to be specified.

2 Material and Methods

2.1 Material

The experimental investigations summarised in this paper were performed on 294 lamellas produced from Swiss grown European beech wood. Planed lamellas with the dimensions $w \cdot t \cdot l$ = 160 x 25 x 3000 mm^3 were ordered in equal shares from four sawmills located north of the Alps in the Cantons Bern, Jura, Aargau and Zurich (Figure 1).

This order strategy was chosen attempting to cover the beech population in Swiss forests adequately and allowing an assessment of the availability of the demanded quality.

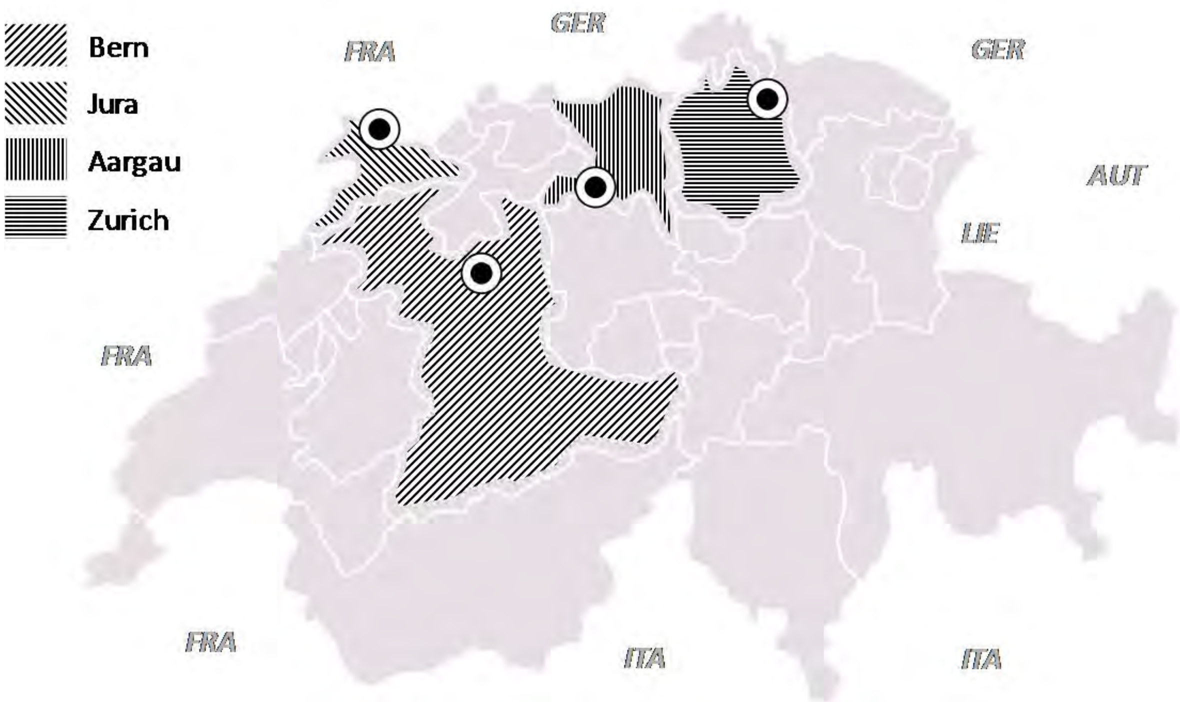

Figure 1 Location of the sawmills in the Swiss Cantons Bern, Jura, Aargau and Zurich

The primary use of GLT and CLT products made from beech is considered to be in service class 1 according to Eurocode 5 (2004), due to the unfavourable behaviour of beech when subjected to changes in humidity. Thus, a moisture content (MC) of 8 ± 2% was defined in this study in order to, at least partially, avoid shrinkage effects.

Frühwald et al. (2003) and *Ohnesorg & Becker* (2006) reported preferable delamination behaviour for thinner lamellas. Therefore, compared to GLT from softwood where lamella thicknesses up to 45 mm are common, a rather low thickness t = 25 mm of the lamellas was chosen as default value for the whole project.

2.2 Methods

2.2.1 Grading criteria

Based on findings by *Frühwald & Schickhofer* (2004) and *Blass et al.* (2005), the following visual indicators were identified in *Ehrhart et al.* (2016) to have a major influence on the tensile strength and stiffness of beech lamellas, and were therefore used in the present study in order to optimize the grading rules.

- *Knots and bark inclusions* quantified by the total knot area ratio (tKAR).
- *Obvious fibre deviation* in lamellas with rift or half rift grain.
- *Wavelike annual ring pattern*.
- *Discolouration* decreasing the surface hardness.

Lamellas containing *wane*, *rot*, *fissures through the thickness*, *pith* and *insect damage* were rejected. The presence of *redheart* was documented but not used in the strength grading process.

According to *Görlacher* (1990), the dynamic MOE E_{dyn} was used as physical indicator when optimising the grading process. Based on the first eigenfrequency f_1 for excitation in the longitudinal direction, the length l and the bulk density ρ_u at a MC of u %, E_{dyn} was calculated:

$$E_{dyn} = 4 \cdot {f_1}^2 \cdot l^2 \cdot \rho_u$$

According to findings by *Frühwald & Schickhofer* (2004), *Blass et al.* (2005) and *Ehrhart et al.* (2016), density does not influence $f_{t,0}$ and $E_{t,0}$ markedly. Thus, density was not considered as indicator in the strength grading process.

For investigations concerning strength grading (see Chapter 3), only characteristics located within the tested length (free length between the clamping jaws of the testing machine) were taken into account. However, the entire lamella (l = 3000 mm) and all present characteristics were considered in questions of economical yield. For both issues, the chosen approach can be considered as conservative.

2.2.2 Definition of pre-grades

In order to simplify the testing process, all lamellas were initially assigned to a pre-grade (A = highest estimated strengths, B, C or Rejects) based on several visual indicators and E_{dyn}. In *Ehrhart et al.* (2016), the requirements and limits for each pre-grade are described in detail. Destructive tensile tests were performed on the randomly selected batches of lamellas listed in Table 2.

Table 2 Number of tested lamellas of the pre-grades A, B, C and Reject

Pre-grade	A	B	C	Rejects
Number of tested lamellas	50	150	50	47

2.2.3 Destructive tensile tests

Destructive tensile tests according to EN 408 (2010) were performed in order to determine $f_{t,0}$ and $E_{t,0}$ of the lamellas (Table 2). 50 lamellas of each pre-grade (A, B and C) and all Rejects were tested with a test length l_t = 2060 mm (≈ 13·w, inner distance between the clamping jaws). Additionally, 50 lamellas of pre-grade B were tested with l_t = 1580 mm (≈ 10·w) and 1100 mm (≈ 7·w) in order to investigate the effect of the test length on the results. A detailed description of the test setup, methods and calculations can be found in *Ehrhart et al.* (2016).

The MC of the specimens was determined using the oven dry method according to EN 13183-1 (2002). $E_{t,0,u}$ and ρ_u were adjusted to the project's reference MC of 8% and the standard reference MC of 12% according to EN 384 (2013). No adjustment is required for $f_{t,0}$.

As specified in EN 14358 (2013), $f_{t,0}$ was assumed lognormally distributed. The maximum likelihood method was used to estimate the distribution parameters that best fit the test data. $E_{t,0}$ and ρ were assumed normally distributed according to EN 14358. The distribution types of $f_{t,0}$ and ρ also correspond to the recommendations provided by the JCSS - Probabilistic Model Code (2006).

3 Results and Discussion

In the following sections, an overview of the mechanical properties of the investigated material is given and the maximum potential and limits of single indicator grading is discussed. The optimized grading limits as well as the related strength, stiffness and density values are presented. Furthermore, the influence of the test length l_t on the measured mechanical properties and the influence of the minimum accepted length l_{min} on the material yield are investigated. Finally, the potential mechanical properties of GLT made from European beech are estimated.

3.1 Overall results

In Figure 2, the empirical distribution of $f_{t,0}$ and $E_{t,0,8}$ (MC = 8%) is shown. The tensile strength was investigated on all lamellas (n = 294). $E_{t,0,8}$ was determined for lamellas of pre-grades A, B and C when tested with a length of l_t = 2060 mm (n = 147). Due to large distortions, three lamellas could not be tested.

A mean tensile strength $f_{t,0,mean}$ = 61 N/mm^2 confirms the great mechanical potential of European beech wood. However, the large scatter in strength (COV = 0.48; $f_{t,0,min}$ = 4.3 N/mm^2, $f_{t,0,max}$ = 132 N/mm^2) clearly evidences the need for reliable strength grading procedures and rules. Comparison to previous studies on $f_{t,0}$ of European beech wood by *Frühwald & Schickhofer* (2004) and *Blass et al.* (2005) indicates, that the investigated population covers the full strength-spectrum.

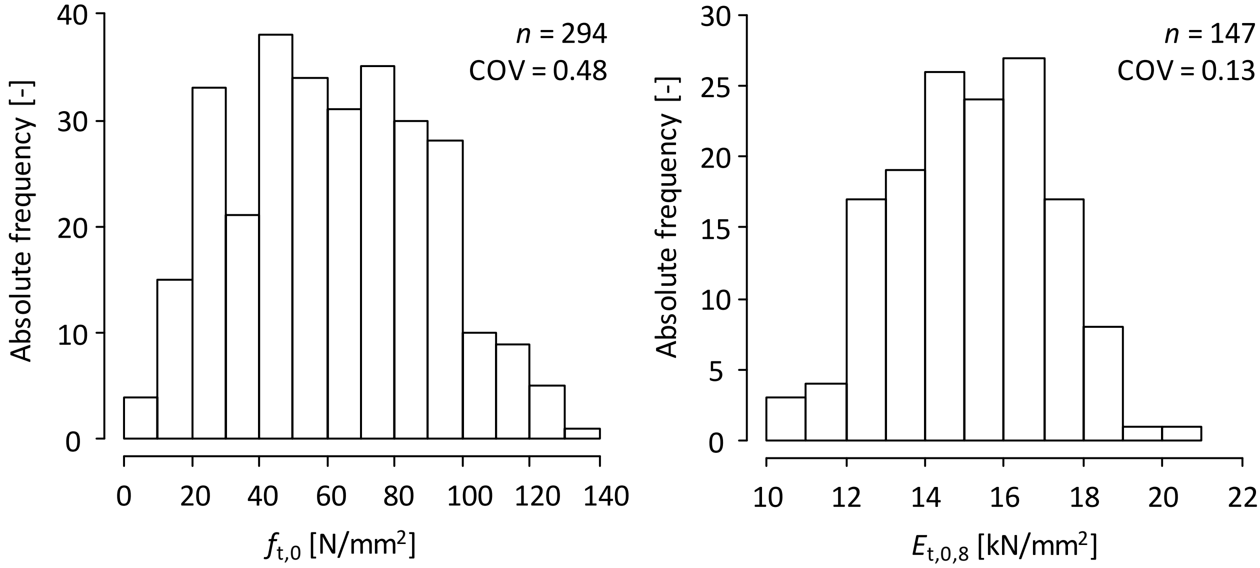

Figure 2 Distribution of the tensile strength $f_{t,0}$ (left) and MOE $E_{t,0,8}$ (right) of the tested European beech lamellas (MC = 8%)

Regarding $E_{t,0,8}$, minimum, mean and maximum values of 10100, 15200 and 20500 N/mm^2 were found (COV = 0.13). These values are just above the values reported by *Frühwald & Schickhofer* (2004) and *Blass et al.* (2005) when adjusting $E_{t,0}$ to the standard reference MC of 12%.

3.2 Single indicator grading (tKAR or E_{dyn}): maximum potential and limits

For the identification of high-strength and stiff lamellas, combined visual and mechanical grading procedures are required as already reported in *Frese & Blass* (2006).

The influence of varying limits for E_{dyn} (lower limit) and tKAR (upper limit) on the 5% fractile value of the tensile strength $f_{t,0,05}$ can be seen in Table 3 (only lamellas tested with l_t = 2060 mm (n = 194) are considered). The bottom row ($E_{dyn,8}$ = all) represents a visual grading method exclusively based on the tKAR-value. The far right column (tKAR = all) represents mechanical grading using E_{dyn} only.

Both approaches lead to unsatisfactory results: Even for the strictest possible visual limit (tKAR = 0), $f_{t,0,05}$ of 50 N/mm^2 cannot be achieved. Regarding the exclusive mechanical grading approach, the requirements for the strength grade T 50 are reached for $E_{dyn,8} \geq 19000$ N/mm^2. However, only 16 out of 194 lamellas (8%) exceed this limit.

In contrast, a grading approach combining both visual and mechanical grading methods leads to significantly better yield especially for high strength levels. A sample of 94 lamellas (= 70 + 64 - 48 + 54 - 48 + 16 - 14, Table 3) with a characteristic tensile strength $f_{t,0,05}$ > 50 N/mm^2 can be found and assigned to the strength grade T 50.

Table 3 Number of specimens and level of characteristic tensile strength $f_{t,0,05}$ depending on the maximum tKAR value and the dynamic MOE $E_{dyn,8}$ (MC = 8%)

$E_{dyn,8}$ [N/mm²]	tKAR [-] 0	≤ 0.05	≤ 0.1	≤ 0.2	≤ 0.3	≤ 0.4	≤ 0.5	all
≥ 20000	4	5	7	7	7	7	7	7
≥ 19000	6	11	14	15	16	16	16	16
≥ 18000	18	28	32	35	36	37	37	37
≥ 17000	35	48	54	60	61	63	63	63
≥ 16000	48	64	73	86	93	95	95	95
≥ 15000	56	74	85	105	116	122	124	124
≥ 14000	70	89	103	126	141	150	152	154
≥ 13000	75	94	110	136	153	165	168	173
≥ 12000	77	97	113	139	158	173	177	185
≥ 11000	77	97	113	140	160	176	181	190
≥ 10000	77	97	113	140	162	178	183	193
all	77	97	113	140	162	179	184	194

$f_{t,0,05}$ [N/mm²]	≥ 50	42 - 50	33 - 42	26 - 33	< 26

3.3 Optimized grading limits

The visual and mechanical grading rules presented hereafter and summarized in Table 4 are based on the assumption that the target T-classes are T 50, T 42 and T 33. Besides the tKAR-value, limits for several additional visual strength indicators – briefly introduced in 2.2.1, specified and investigated in *Ehrhart et al.* (2016) – were defined to complement and further improve the strength grading process. Additional limits to assure the processability of beech lamellas (e.g. regarding distortion and fissures) are defined in DIN 4074-5 (2008) and purposely not described at this point.

Following the proposed grading strategy, the population initially was split into three different visual grades (1 = best, 2, and 3) and Rejects. Due to the high correlation between tKAR and $f_{t,0}$, as well as the influence of fibre deviation and further visual characteristics on $f_{t,0}$, this led to a first separation into groups of different strengths. Subsequently, the lamellas were assigned to the T-classes depending on their visual grade (1, 2 or 3) and $E_{dyn,8}$. Besides further improvement of the strength grading process, this allowed for a precise grading regarding $E_{t,0}$.

Figure 3 shows the cumulated distribution of $f_{t,0}$ (left) and $E_{t,0,8}$ (right) of the classes T 33, T 42, T 50 and Rejects as resulting after the application of the grading rules described above.

Table 4 Limits for the visual and mechanical grading into strength grades T 33, T 42 and T 50

	Visual grade		
Criterion	**Visual 1**	**Visual 2**	**Visual 3**
Knots or bark inclusions	tKAR ≤ 0.05	tKAR ≤ 0.1	tKAR ≤ 0.2
Obvious fibre deviation	-	Unlimited	Unlimited
Wavelike annual ring pattern	-	Unlimited	Unlimited
Redheart	Unlimited	Unlimited	Unlimited
Discolouration			
Surface hardness not reduced	Unlimited	Unlimited	Unlimited
Surface hardness reduced	-	-	Unlimited
Insect damage	-	-	-
Pith	-	-	-
Required $E_{dyn,8}$	**T 33**	**T 42**	**T 50**
Visual 1	≥ 12000	≥ 14000	≥ 16500
Visual 2	≥ 14000	≥ 16500	-
Visual 3	≥ 16500	≥ 18000	-

The large gap of $f_{t,0}$ between the rejected sample and the T-classes shows that the applied grading criteria are efficient to identify weak lamellas (Figure 3, left). Furthermore, $f_{t,0}$ of less than 20% of the Rejects exceeded 40 N/mm^2. The clear separation between the T-classes indicates that the chosen grading approach leads to satisfactory results.

Regarding $E_{t,0,8}$, also a clear separation between the T-classes is found (Figure 3, right). The distribution of $E_{t,0,8}$ can be controlled quite precisely due to the high correlation with E_{dyn} (a coefficient of determination $R^2 = 0.84$ was reported by *Ehrhart et al.* (2016)).

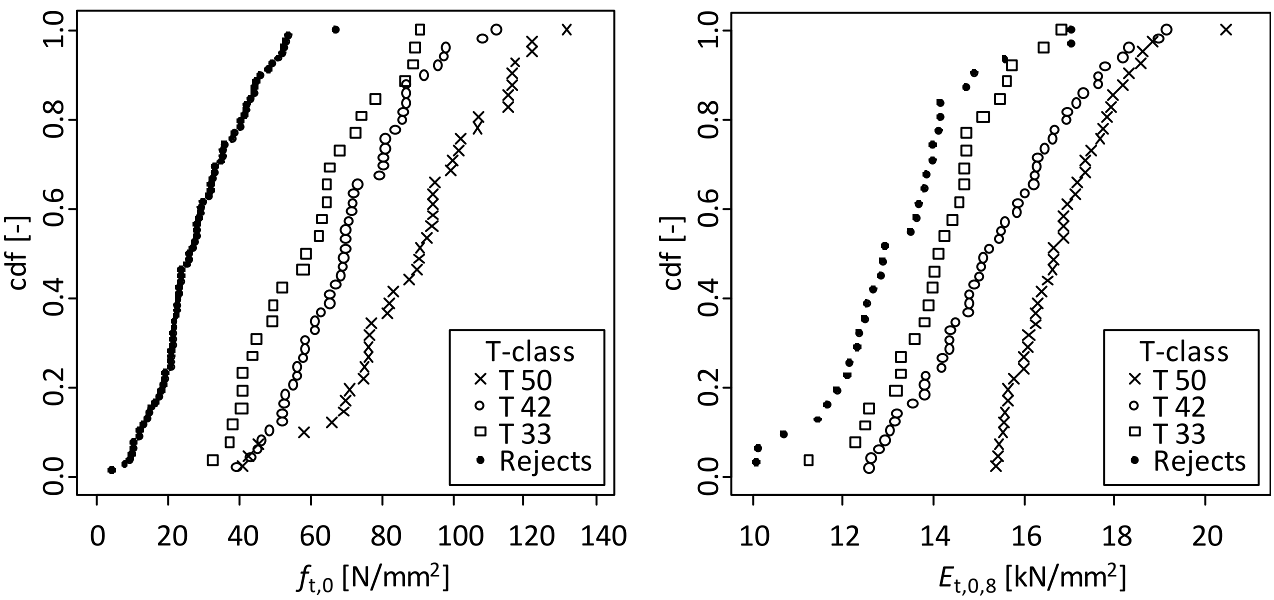

Figure 3 Cumulated distribution (cdf) of tensile strength $f_{t,0}$ (left) and MOE $E_{t,0,8}$ (right) for the resulting T classes T 33, T 42 and T 50 (MC = 8%)

In Table 5, the mechanical properties and densities of the resulting T-classes and Rejects are summarized. Values of $f_{t,0,05}$ slightly higher than targeted resulted when applying the specified grading rules. As no explicit provision concerning the density is made in the grading process, ρ_{mean} and ρ_k of all T-classes is on a similar level.

Table 5 Mechanical properties and density of the resulting T-classes and Rejects for specimens with a test length of 2060 mm (MC = 8%)

		T 33	T 42	T 50	Rejects	All
$E_{t,0,8,mean}$	N/mm^2	**14200**	**15400**	**16900**	13200	15200
$E_{t,0,8,05}{}^{*}$	N/mm^2	12300	12900	15500	10400	12100
COV	-	0.09	0.11	0.07	0.13	0.13
n	-	26	49	41	31	147
$f_{t,0,mean}$	N/mm^2	59.7	70.6	89.3	28.7	56.2
$f_{t,0,05}{}^{**}$	N/mm^2	**34.7**	**45.9**	**54.8**	11.0	16.3
COV	-	0.30	0.24	0.25	0.44	0.53
n	-	26	49	41	78	194
$\rho_{8,mean}$	kg/m^3	**714**	**722**	**739**	720	724
$\rho_{8,05}{}^{*}$	kg/m^3	651	683	673	668	668
COV	-	0.06	0.04	0.05	0.05	0.05
n	-	26	49	41	78	194

* Normal distribution, ** Lognormal distribution

3.4 Influence of the test length l_t

In Figure 4 (left), the cumulated distribution of $f_{t,0}$ for the three different test lengths l_t = 2060, 1580 and 1100 mm are plotted. Each sample consists of 50 specimens of the pre-grade B (n = 48 for l_t = 2060 mm due to strong distortion of two lamellas).

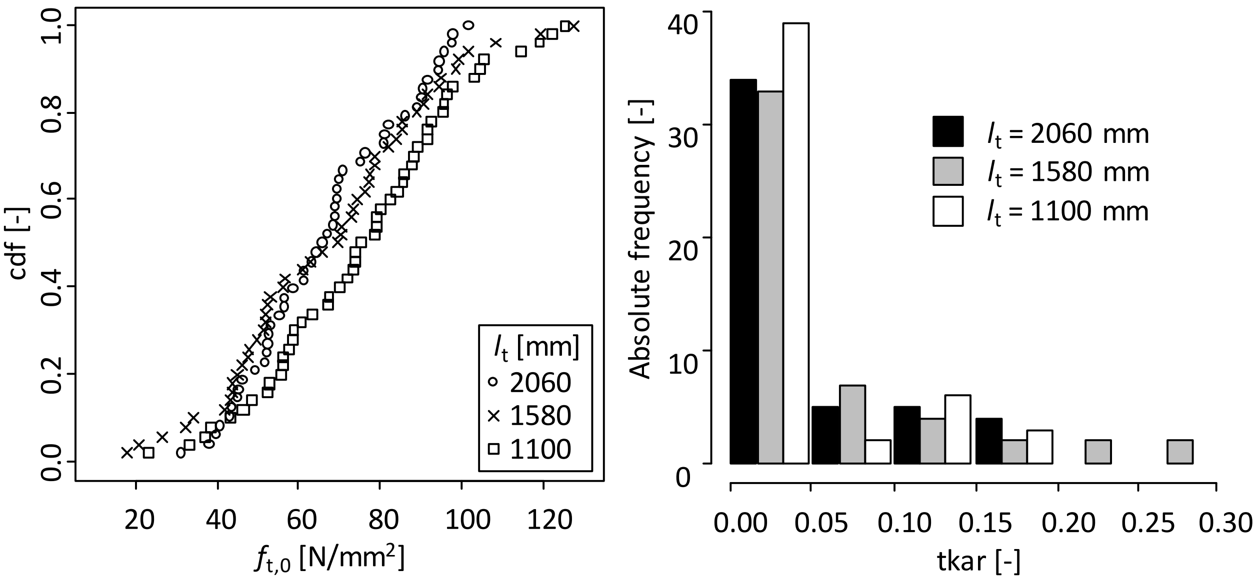

Figure 4 Distribution of tensile strength $f_{t,0}$ (left) and tKAR-values (right) for samples subjected to tensile tests with different test lengths l_t

The mean values of tensile strength of the samples with test lengths of l_t = 2060 mm ($f_{t,0mean}$ = 66.7 N/mm^2) and l_t = 1580 mm ($f_{t,0mean}$ = 67.4 N/mm^2) were found to be almost equal. However, $f_{t,0mean}$ of l_t = 1100 mm is about 13% higher ($f_{t,0mean}$ = 75.8 N/mm^2). This can be due to the different distribution of tKAR-values of the groups, i.e. considerably more lamellas of the l_t = 1100 mm sample showed tKAR-values < 0.05 (78%) compared to l_t = 1580 mm (66%) and l_t = 2060 mm (71%) (Figure 4, right).

Regarding the general adequacy of a test length $l_t \geq 9 \cdot w$, as prescribed in EN 408, two contradictory conclusions (i & ii) can be drawn. (i) As the number of obvious weak points like knots or bark inclusions is much lower in European beech timber compared to most softwoods (see also Chapter 3.5), the location of failure can usually be predicted with high reliability if such a weak point is present. Local failure restricted to a short section of a lamella is observed in many of these cases (Figure 5). Thus, the actual l_t has negligible influence on the tensile strength of lamellas of low visual quality as long as weak points are positioned within the tested length of a lamella.
Increasing lengths l of the lamellas, of course, have also impact on the likelihood of the presence of weak points.

Figure 5 Local failures at obvious weak points

However, (ii) shear failures affecting large parts of lamellas were frequently observed in lamellas with low tKAR-values. Depending on the general and local slope of grain, shear fractures propagate until they reach either the lamella's edge or the clamping jaws. In the second case, shear fracture is supressed in the areas close to the clamping jaws as the deformations in the direction perpendicular to the lamella's axis are restrained (Figure 6). Hence, the shorter l_t, the higher the probability that shear failure reaches and stops at the clamping jaws, which potentially influences $f_{t,0}$.

Figure 6 Shear failure over large parts of a lamella reaching and stopping at the clamping jaws

As a consequence, specification of a minimum test length for the determination of $f_{t,0}$ is of utmost importance for comparability reasons, in particularly when investigating lamellas of high strength grades.

3.5 Influence of the minimum accepted length l_{min} on the material yield

In accordance with findings by *Glos et al.* (2004) and *Frese & Blass* (2006), the number of knots or knot clusters in the investigated beech lamellas (Figure 7, left) was found to be considerably lower compared to spruce lamellas. Thus, finger jointing plays a decisive role when aiming at improving the technical as well as the economical yield as it allows cutting out single weak sections containing large knots or bark inclusions.

This study so far focused on the weakest testable section of the entire lamella in order to grade or reject the lamellas, i.e. single knots or bark inclusions with tKAR-values exceeding the defined limits led to downgrading or rejection of the whole lamella. In several cases, large knots or bark inclusions are located close to the end of lamellas. Thus, cutting them out leads to a significant improvement regarding yield. Depending on the minimum length accepted l_{min} (as technically given by the finger jointing process or economically asked for when considering costs and benefits), a significant proportion of the initially rejected material can be used when l_{min} is specified shorter than 3 m.

In total 87 lamellas (87 x 3 m = 261 m) were rejected due to insufficient visual appearance. Thereof, 68 lamellas showed too large knots or bark inclusions (204 m) and 19 lamellas (57 m) could not be used due to issues like curvature, fissures through the lamellas thickness and wane. The latter were excluded as definitive Rejects, which means that permission of shorter lengths does not affect their classification.

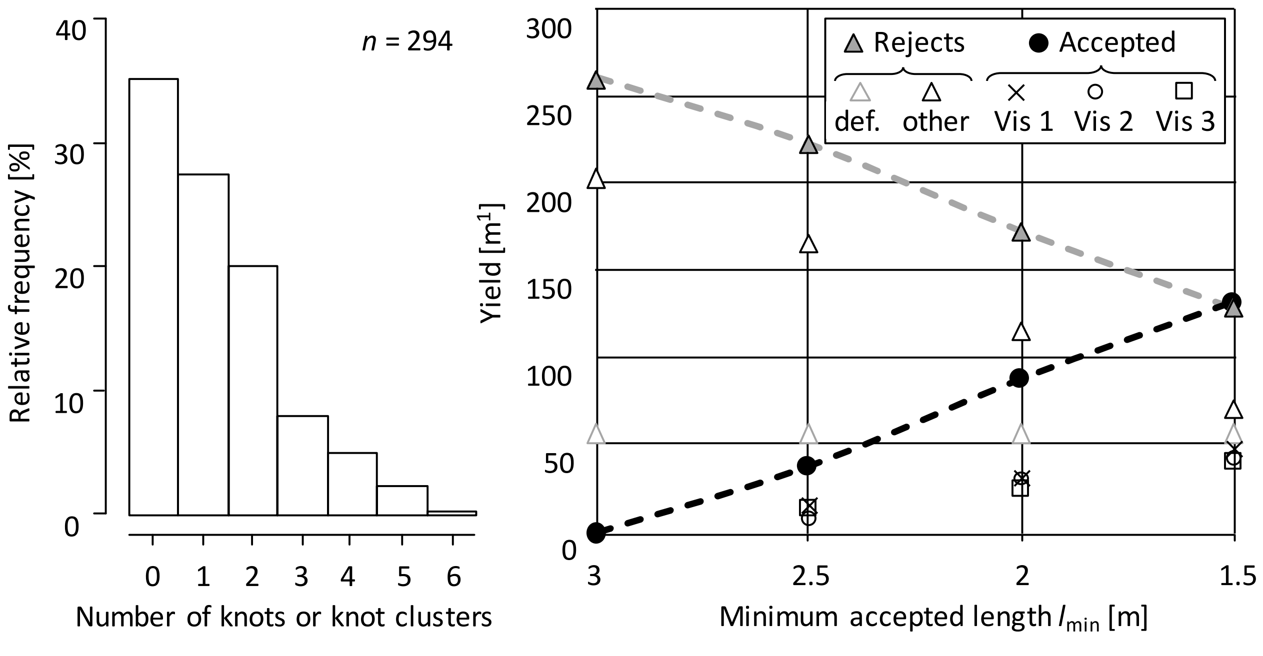

Figure 7 Number of knots or knot clusters per lamella (left) and influence of the minimum accepted length l_{min} on the yield (right)

Figure 7 (right) shows the influence of varying l_{min} on the yield (in running metre m[1]). The group of Rejects is split into *definitive* and *other* (see above). Regarding the accepted material, a distinction is made between the different visual grades (Visual 1, 2 and 3) according to Table 4. Starting from l_{min} = 3 m, the significant reduction of material assigned to the group of Rejects for decreasing l_{min} is obvious. For l_{min} = 1.5 m, more than 50% of the initially rejected material can be used in almost equal parts for the visual grades 1, 2 and 3. Due to the mechanical potential of European beech timber, specification of even shorter lengths could be reasonable in order to achieve higher yield in the strength grades T 42 and T 50.

3.6 Potential mechanical properties of GLT

Numerous models for the derivation of bending strength of GLT ($f_{m,g,k}$) from the lamellas' characteristic tensile strength ($f_{t,l,k}$) and the characteristic strength of finger joints in bending or tension ($f_{m,j,k}$ or $f_{t,j,k}$) are available (*Brandner & Schickhofer*, 2008). However, the use of most of these models is restricted to softwoods and only limited findings regarding the laminating effect of beech GLT on a high strength level are reported in literature. One exception is *Frese & Blass* (2006), presenting a quadratic equation for the estimation of $f_{m,g,k}$ of beech GLT.

According to EN 14080 (2012), $f_{m,g,k}$, the mean value of MOE of GLT ($E_{0,g,mean}$) and its density ($\rho_{g,mean}$) can be calculated based on the lamellas' properties. Although the application of EN 14080 is restricted to softwoods and poplar, it is used at this point to estimate the properties of beech GLT.

Based on the material properties presented in this study and the above-mentioned models it seems realistic to reach the target GLT strength grades. For GL 40, GL 48 and GL 55, expected properties are $E_{0,g,mean} \approx 14300 / 15500 / 17000$ N/mm^2 and $\rho_{g,mean} \approx 730 / 740 / 750$ kg/m^3, respectively (MC = 12%). Due to the small variations between the strength grades, a differentiation regarding the density does not seem to be appropriate.

4 Conclusions

Characteristic tensile strength values $f_{t,0,k}$ of 33, 42 and 50 N/mm^2 can be exceeded when applying the grading rules presented in this paper. Consequently, the investigated European beech lamellas can be assigned to the strength grades T 33, T 42 and T 50. Regarding the mean value of MOE, clear separation between the strength grades was found, i.e. $E_{t,0,8,mean}$ = 14200, 15400 and 16900 N/mm^2, respectively, at the project's reference MC of 8%. The density of all grades is on a very similar level ($\rho_{mean,8} \approx 720$ kg/m^3) as it is not considered as a strength or stiffness indicator in the grading process.

The proposed grading strategy bases on two main parameters – the total knot area ratio (tKAR) and the dynamic MOE (E_{dyn}). Obvious fibre deviation, wavelike annual ring pattern and discolouration are used as complementing visual indicators to further improve the strength grading process. It is shown that a combined grading approach is essential for efficient strength grading, i.e. neither a pure visual nor a pure mechanical grading approach allow reaching the target strength levels.

If single obvious weak points are present, provision of a minimum test length of $9 \cdot w$ is not necessary, as failures occur in very restricted areas. In beech lamellas of higher strength grades, shear failure occurs frequently. The propagation of shear failure is stopped, or at least influenced, at the clamping jaws. Thus, maintaining a minimum test length is clearly necessary.

Strict requirements regarding the maximum size of knots and bark inclusions are essential to reach the target strength classes. In questions of material efficiency, the minimum accepted length l_{min} of lamellas has significant impact on the achievable yield, as the number of knots in European beech timber is substantially lower compared to most softwoods. The reduction of l_{min} from 3 m to 1.5 m approximately halves the volume of rejected material and hence, markedly increases the yield.

Based on the results presented in this study, the target strength classes GL 40, GL 48 and GL 55 appear realistic and reachable. Due to the lack of appropriate models for the observed strength level and/or timber species, the estimated strength and stiffness properties for GLT are subjected to uncertainty.

5 Acknowledgement

The authors acknowledge the support of the Swiss *Federal Office for the Environment FOEN* within the framework of *Aktionsplan Holz*.

6 References

Blass, HJ; Denzler, J; Frese, M; Glos, P; Linsenmann, P (2005): Biegefestigkeit von Brettschichtholz aus Buche; Band 1 der Reihe Karlsruher Berichte zum Ingenieurholzbau; Universitätsverlag Karlsruhe; Karlsruhe, Germany.

Brandner, R; Schickhofer, G (2008): Glued laminated timber in bending: new aspects concerning modelling; Wood Sci Technol (2008) 42:401-425; Springer.

Ehrhart, T; Fink, G; Steiger, R; Frangi, A (2016): Experimental investigation of tensile strength and stiffness indicators regarding European beech timber; Proceedings of 14th World Conference on Timber Engineering WCTE, 2016; Vienna, Austria.

Frese, M; Blass, HJ (2006): Characteristic bending strength of beech glulam; Materials and Structures (2006) 40:3-13; RILEM.

Frühwald, A; Ressel, JB; Bernasconi, A (2003): Hochwertiges Brettschichtholz aus Buchenholz; Abschlussbericht; Universität Hamburg & Bundesforschungsanstalt für Forst- und Holzwirtschaft; Hamburg, Germany.

Frühwald, K; Schickhofer, G (2004): Strength grading of hardwoods; 8th World Conference on Timber Engineering; Lahti, Finland.

Glos, P; Denzler, JK; Linsenmann, PW (2004): Strength and stiffness behaviour of beech laminations for high strength glulam; CIB-W18/37-6-3, Meeting 37; Edinburgh, Scotland.

Görlacher, R (1990): Klassifizierung von Brettschichtholzlamellen durch Messung von Longitudinalschwingungen; Berichte der Versuchsanstalt für Stahl, Holz und Steine der Universität Fridericiana in Karlsruhe; 4. Folge - Heft 21; Karlsruhe, Germany.

Ohnesorg, D; Becker, G (2006): Glueability of beech wood containing red heartwood; 5th IUFRO International Symposium, Wood Structures and Properties; Sielnica, Slovakia.

DIN 4074-5 (2008): Strength grading of wood - Part 5: Sawn hard wood; DIN.

EN 338 (2016): Structural timber - Strength classes; CEN.

EN 384 (2013): Structural timber - Determination of characteristic values of mechanical properties and density; CEN.

EN 408 (2010): Timber structures - Structural timber and glued laminated timber - Determination of some physical and mechanical properties; CEN.

EN 1912 (2012): Structural timber - Strength classes - Assignment of visual grades and species; CEN.

EN 1995-1-1 (2004): Eurocode 5: Design of timber structures - Part 1-1: General - Common rules and rules for buildings; CEN.

EN 13183-1 (2002): Moisture content of a piece of sawn timber - Part 1: Determination by oven dry method; CEN.

EN 14080 (2013): Timber structures - Glued laminated timber and glued solid timber - Requirements; CEN.

EN 14358 (2013): Timber structures - Calculation of characteristic 5-percentile and mean values for the purpose of initial type testing and factory production control; CEN.

EN 16351 (2015): Timber structures - Cross laminated timber - Requirements; CEN.

JCSS (2006): Probabilistic model code Part 3 – Part 3.5: Properties of timber. *http://www.jcss.byg.dtu.dk/Publications/Probabilistic_Model_Code.aspx*

Z-9.1-679 (2009): Allgemeine Bauaufsichtliche Zulassung; BS-Holz aus Buche und BS-Holz Buche Hybridträger; Studiengemeinschaft Holzleimbau e. V.; Wuppertal, Germany.

Discussion

The paper was presented by T Ehrhart

H Blass asked were the grading rules checked with verification set outside the material tested. T Ehrhart replied no and only studied short length and would be doing more.

P Stapel asked would there be a difference using the proposed visual rules to establish DAB values used today. T Ehrhart replied no. In 80% of the knots the values would be identical so little difference was observed. Also the knot information was established by looking at the face and assuming the knot will go to the middle of the laminae.

G Ranasinghe commented about the way of measuring KAR and said that in the UK marginal KAR was used because KAR was considered as not too practical.

M Augustin asked how was grain deviation measured. T Ehrhart replied that it was not measured directly and explained the procedure used. He added that it was difficult to quantify although it was important.

H Blass asked about the G value of 500 MPa in Slide 10 and suggested that shear in buckling would be rolling shear in these walls. C Bedon responded that the chosen value was based on calibration with test results. Preliminary study showed that using a lower G value did not agree with data. Also they did not notice a lot of shear deformation as the rotation was almost a rigid body motion.

G Schickhofer commented that it would be better to consider a minimum requirement rather than such a complicated approach for a simple block wall house.

F Lam asked why the cases with design properties were higher than the cases with mean properties. C Bedon agreed and responded that the process also involved a normalization process.

A Ceccotti asked if the authors checked how far the designs are away from capacities in terms of safety. C Bedon answered that cases where stiffness of walls with large openings can be important and cases where top restraints were not available can also be important.

U Kuhlmann commented that compressive strength versus critical loading is confusing.

Impact of varying material properties and geometrical parameters on the reliability of shear connections with dowel type fasteners

Robert Jockwer
ETH Zürich, Institute of Structural Engineering, Zurich, Switzerland

KEYWORDS: Connection, European Yield Model, brittle failure modes, Reliability

1 Introduction

1.1 Design of connections in timber

Eurocode 5 (EC5, EN 1995-1-1, (CEN, 2004)) applies the load and resistance factored design concept to the design of timber structures. The optimal partial safety factors for achieving the desired failure probability can be determined in dependency of the loading situation and the relevant material parameters as discussed in Kohler et al. (2012). The calibration of these partial safety factors is based mainly on loading situations of timber members in pure bending (Sørensen 2002).
Components consisting of different materials like e.g. timber and steel fasteners in connections may benefit from the much smaller variability of the properties of the steel elements and, hence, from the considerably lower safety factors for the metallic fasteners when evaluating the reliability (Kohler, 2005). In the current EC5 design equations, this benefit amounts to about 15% (Werner, 1993). The reliability based design concept offers a high potential for further enhancement of the currently applied procedures in order to benefit from the full potential of timber and hybrid structures. For a reliable design of connections the entire system of the individual members of the connection has to be assessed with regard to relevant failure modes.

1.2 Importance of ductility for design

Connections are important structural details and are responsible for a large portion of failure events Frühwald et al. (2007). Ductility offers the potential for redistribution of loads in the structure as shown by Dietsch (2011). Different design codes like e.g. DIN 1052 (DIN, 2008) or SIA 265 (SIA, 2012) set the ductile failure mode of a connections as the basis for the design. A detailed discussion of the importance of ductile failure modes in connections can be found in Mischler (1997, 1998).
Due to e.g. geometrical constraints it can be necessary to reduce the dimensions of the connections necessary to achieve ductile failure. This seems adequate especially if the desired

load-carrying capacity can be obtained. However, the in addition also the change in variability of the load-carrying capacity has to be accounted for.
In this paper the impact of ductile and brittle failure modes on the reliability of connections is discussed based on experimental and theoretical studies. It is not intended to evaluate and validate the different design models that exist for ductile and brittle failure modes of connections.

2 Mechanical models and parameters of influence

2.1 Models describing the load-carrying capacity of connections

2.1.1 Models describing the load-carrying capacity of the fasteners: EYM

The resistance of dowel type timber connections is commonly determined as the minimum of the capacities according to the so called European Yield model (EYM) that is based on the studies by Johansen (1949) (Fig. 1). These failure modes describe the embedment failure of the timber and/or the ductile failure of the dowel in dependency of the thickness of the timber members. The relevant material properties are the embedment strength $f_{h,i}$ of the timber members and the yield moment M_y of the fastener. Geometrical parameters are the thickness t_i of the timber members and the diameter d of the fastener.
The load carrying capacity of the different failure modes according to the EYM for a single shear plane in a wood-steel-wood connection is as follows:
Failure mode I: Embedment failure

$$R_{I,i} = f_{h,i} t_i d \tag{1}$$

Failure mode II: Mixed failure

$$R_{II,i} = f_{h,i} t_i d \left[\sqrt{2 + \frac{4M_y}{f_{h,i} d t_i^2}} - 1 \right] \tag{2}$$

Failure mode II: Ductile failure

$$R_{III,i} = \sqrt{4 M_y f_{h,i} d} \tag{3}$$

The resulting load-carrying capacity of the entire connection with a slotted-in steel plate depends on the embedment strength of the timber, the yield moment of the fastener and the thickness of the timber members. Due to its low ductility the failure mode EYM I is considered as brittle when calculating the minimum resistance of the EYM failure modes (Kohler, 2005).

$$R_{connection} = \min\left\{2R_{I,i}, R_{II,i} + R_{II,j}, R_{III,i} + R_{III,j}, R_{II,i} + R_{III,j}\right\} \tag{4}$$

The load-carrying capacity of a connection with multiple fasteners can be calculated using the effective number of fasteners $n_{ef} \leq n$, that accounts for a reduction of load-carrying capacity due to early failure of the connection.

2.1.2 Models describing the load-carrying capacity of the fasteners: Additional models

Comparison between estimated values according to EYM and test results can exhibit considerable difference. Meyer (1957) proposed an additional portion of resistance from friction

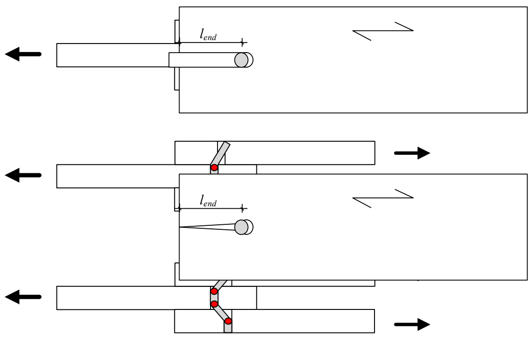

Figure 1: Simplification of failure modes of the EYM fo[illegible]ber-timber connection[illegible]

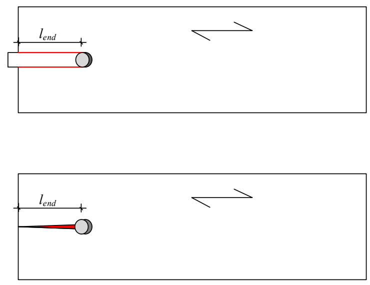

Figure 2: Simplified examples of brittle failure modes due to block tear out (top) and tension perpendicular to grain splitting failure (bottom).

between the timber elements induced by the deformation and relative shorting of the fastener: the rope effect. This rope effect is limited by the axial load-carrying capacity of the fasteners and is neglected en general for dowels. Svensson and Munch-Andersen (2014) discussed the impact of friction between the fastener and the timber increasing the axial force inducing the rope effect.

2.1.3 Models describing the load-carrying capacity of the timber: Jorissen (1998)

Failure modes in the timber members are often characterized by brittle failure mechanisms in shear and tension perpendicular ot the grain (Fig. 2). So far only a design equation for the situation of block shear failure of groups of fasteners is given in the Appendix A of EC5. Additional failure modes with splitting and shear failure of the connection are not accounted for in EC5. Other standards like e.g. Canadian CSA O.86 already consider different brittle failure modes for the design of connections (Quenneville et al., 2006). Nevertheless, brittle failure modes are relevant especially for thin side members of double shear connections and small spacing or end-grain distances.
Geometrical parameters with an impact on the brittle failure of connections are e.g. spacing between fasteners a_1, end-grain distance a_3, edge distances a_4, member thickness t_i. The material parameters with an impact are e.g. shear strength f_v, tension perpendicular to grain strength $f_{t,90}$, stiffness properties (E_0 and G_v) and fracture energies in tension perpendicular to grain $G_{f,I}$ and shear $G_{f,II}$.
Jorissen (1998) presented a fracture mechanics based design approach for brittle failure of a connection (Eq. 5). Due to the complex stress state the fracture process is described by mixed mode fracture with $G_{f,mixed}$. An angle of friction $\phi = 30°$ between dowel and timber is used by Jorissen.

$$R_{split} = 2t_i\sqrt{\frac{G_{f,mixed,i}E_{0,i}d\sin\phi\,(h-d\sin\phi)}{h}} \tag{5}$$

Other more sophisticated fracture mechanics based approaches can be found e.g. in (Schmid et al., 2002).

2.1.4 Models describing the load-carrying capacity of the timber: simplified models

Two very simple models for considering impact of the end-grain distance a_3 are used in the following. The models are based on a simple verification of shear strength f_v (Eq. 6) and tension perpendicular to grain strength $f_{t,90}$ (Eq. 7) in the fracture surface. The model for the resistance against splitting in tension perpendicular to the grain is based on the relation between force F_{90} acting perpendicular to the grain induced by a dowel loaded parallel to the grain by force F_0 as proposed by Jorissen (1998): $F_{90} \approx 0.143 F_0$. The impact of the unequal stress distribution is represented by the stress distribution factors k_v and $k_{t,90}$.

$$R_{v,split} = k_v 2 t_i a_3 f_v \tag{6}$$

$$R_{t,split} = k_{t,90} \frac{1}{0.143} t_i a_3 f_{t,90} \tag{7}$$

As illustrated in Fig. 2 two failure surfaces are assumed in case of shear splitting (Eq. 6) and one in case of tension perpendicular to grain splitting (Eq. 7). The simple model for shear splitting is similar to the model describing block shear failure in Appendix A of EC5. Based on the studies on stress distribution around a fastener by Jorissen (1998) stress distribution factors $k_v = 0.5$ and $k_{t,90} = 1$ are used. The two models in Eq. 6 and 7 can be used in analogy for describing the impact of spacing a_1 on the fracture in tension perpendicular to the grain and in shear.
Schmid et al. (2002) state that mode 1 splitting is most common for $m = 1$ row of fasteners whereas for 2 or more rows plug shear or group tear out failure is more common to occur due to the change in energy release rate in the model of a beam on elastic foundation.

2.2 Material parameters

The determination of different material property values and their impact on the load-carrying capacity of connections with dowel type fasteners was discussed by Werner (1993).
The distribution characteristics of the relevant material property values and a probabilistic assessment of the load-carrying capacaty of shear connections with dowels was presented by Köhler (2007). In the following the most important characteristics of the material property values are summarized.

2.2.1 Embedment strength f_h

The equation in EC5 for the determination of embedment strength parallel to the grain was proposed by Whale and Smith (1986) as follows:

$$f_{h,k} = 0.082 \rho_k (1 - 0.01 d) \tag{8}$$

Additional impacts on the embedment strength like e.g. of the surface roughness of the dowel or the moisture content of the timber are discussed by e.g. Dorn (2012).
The distribution characteristics of embedment strength were determined by Leijten et al. (2004) as summarized in Eq. 9 and Fig. 2. The resulting Eq. 9 yields an embedment strength for GL24h with $\rho_{mean} = 420$ kg/m^3 and $CoV = 10\%$ of $f_{h,mean} = 32.6$ N/mm^2 with $CoV = 16\%$. The mean embedment strength according to Eq. 8 is $f_{h,mean} = 30.3$ N/mm^2 $\rho_{mean} = 420$ kg/m^3.

$$f_h = A \rho^B d^C \varepsilon \tag{9}$$

Table 1: Regression Parameters from Leijten et al. (2004)

Parameter	Type	Mean	stDev
A	Lognormal	0.097	0.23
B	Normal	1.07	0.04
C	Normal	-0.25	0.012
ε	Lognormal	1	0.11

2.2.2 Yield moment M_y

The relevant resistance of a fastener in bending is between the elastic and full plastic bending capacity (e.g. Jorissen and Leijten (2005)). Depending on the failure mode of the EYM and the diameter of the fastener the relevant resisting moment of the fasteners is at different bending angles. The resisting moment of the fastener can be determined in 4 point bending tests e.g. by means of the test equiment presented by Ehlbeck and Werner (1991); Werner (1993). The connection between yield moment of the dowel M_y and yield and tensile strength of the steel is discussed in literature (e.g. Jorissen and Blaß (1998)).
Eq. 10 is given in EC5 and is based on studies by Blaß et al. (2000). Recent studies by Blaß and Colling (2015) show that there can be a considerable difference between steel qualities of different batches. The variation of material properties of the steel within one batch is rather small. Kohler (2005) proposes $CoV \approx 4\%$.

$$M_y = 0.3 f_u d^{2.6} \qquad (10)$$

Table 2: Tensile strength f_u in dependency of steel grades for a $CoV = 4\%$ and lognormal distr. properties

Grade	$f_{y,k}$ [N/mm^2]	$f_{u,k}$ [N/mm^2]	$f_{u,mean}$ [N/mm^2]
S235	$\approx 190-360$	$\approx 360-510$	
4.6	240	400	427
6.6	360	600	641
8.8	640	800	854
ETG 100	$>$ 865	$\approx$960-1100	

2.2.3 Additional material properties and correlations

The distribution characteristics of density ρ, MOE parallel to the grain E_0, shear strength f_v and tension perpendicular to grain strength $f_{t,90}$ are taken from JCSS (2001). Since tension perpendicular to grain strength and shear strength show a pronounced volume effect, and the stressed volume in a connection is rather small compared to other situations in timber structures a rather high value of engineering are higher compared to the values specified in EN 338 (2009a). Aicher et al. (2002) give similar values of tension perpendicular to grain strength for small sized specimen of $V \approx 0.1$ dm^3.
All distribution characteristics used in this study are summarized in Tab. 4.

Table 3: Distribution characteristics of material parameters.

Property	Distribution function	mean	CoV
ρ	Lognormal	420	10%
f_u	Lognormal	e.g. 437	4%
E_0	Lognormal	11500	23%
G_I	Lognormal	0.3	20%
G_{II}	Lognormal	1.05	30%
f_v	Lognormal	5	25%
$f_{t,90}$	Weibul	2	30%

The correlations between the material property values is based on JCSS (2001) (Tab. 4) and Leijten et al. (2004) (Tab. 5).

Table 4: Correlation between material properties values (JCSS, 2001).

	E_0	f_v	$f_{t,90}$
ρ	0.6	0.6	0.4
E_0	-	0.4	0.4
f_v		-	0.6

Table 5: Correlation between embedment strength parameters (Leijten et al., 2004).

	B	C	ε
A	-0.99	-0.24	0
B	-	0.11	0
C		-	0

3 Structural behaviour of a connection

A comparison of the mean load-carrying capacities of the EYM and all splitting failure modes is given in Fig. 3 (a) in dependency of the thickness of the side timber members t_i. The configuration of the connection corresponds to the tests described in Chapter 4.1 with $\rho_{mean} = 420$ kg/m^2 and $f_{u,k} = 400$ N/mm^2. The geometrical parameters of relevance for the load-carrying capacity according to EYM are the thickness of the timber members t_i and the dowel diameter d. The steel quality has an impact only on the load-carrying capacity in failure mode II and III. At the transition between the failure modes II to III the critical slenderness $\lambda_{II/III} = t/d$ for achieving ductile failure can be defined.
The impact of end-grain distance a_3 for a connection with a single fastener is shown in Fig. 3 (b). For small end-grain distance the splitting failure modes cause a reduction of load-carrying capacity.

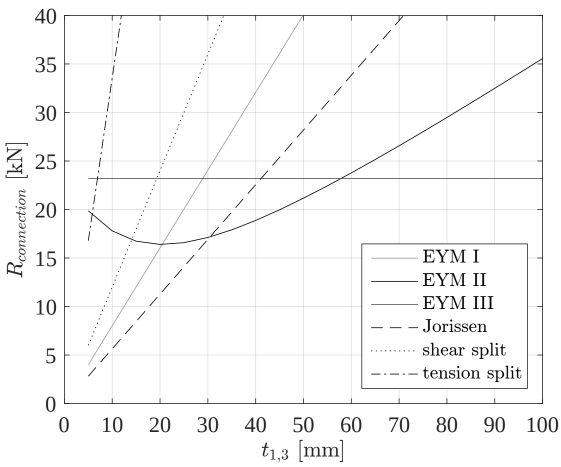

(a)

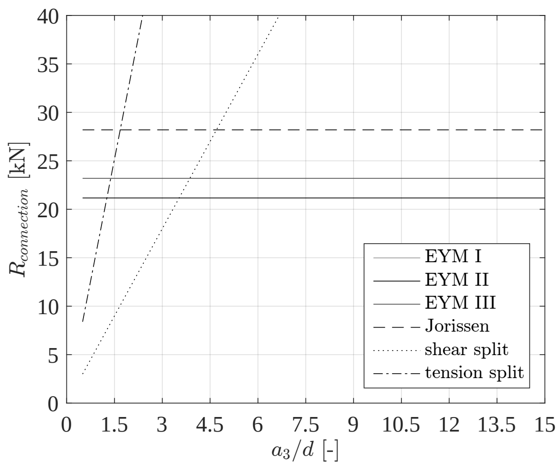

(b)

Figure 3: Load-carrying capacity according to EYM and all splitting failure modes in dependency of side member thickness t_i ($a_3/d = 10$) (a) and of end-grain distance a_3 ($t_i = 50$ mm) (b).

In Fig. 4 the impact of varying material properties different percentile levels on the load-carrying capacity are shown in dependency of the thickness of the side members t_i and the end-grain distance a_3. In addition the coefficient of variation (CoV) are given. It can be seen, that the CoV is highest of the brittle failure modes followed by the failure modes with embedment failure of the dowels. The ductile failure modes of EYM III give the lowest CoV.
In the study presented in this paper it is focused on the interaction of different failure modes and on their impact on the variability of the load-carrying capacity. The absolute value of the individual load-carrying capacity is not studied and validated more detailed.

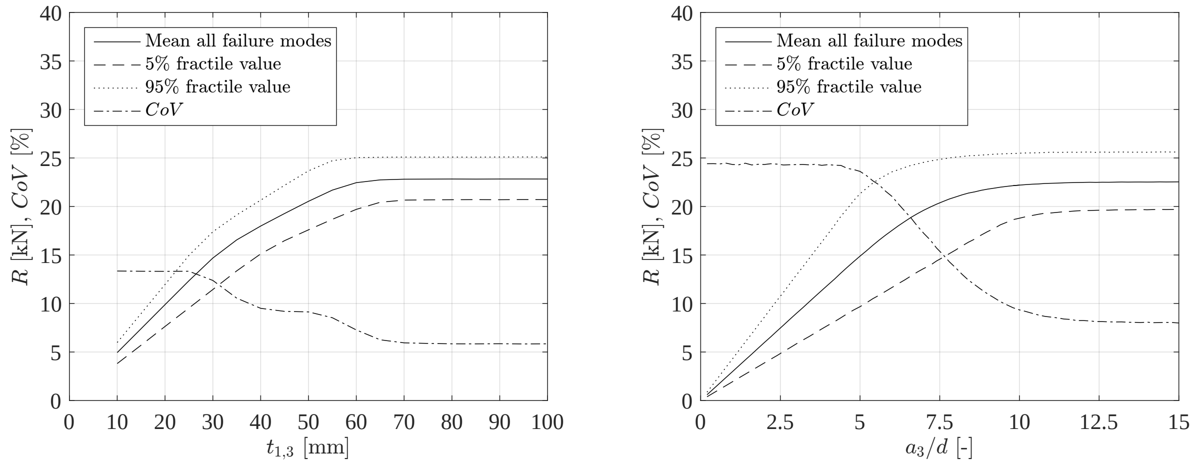

(a) (b)

Figure 4: Relevant load-carrying capacity at mean, 5% and 95% fractile level and corresponding coefficient of variation in dependency of the thickness of the side members t_i ($a_3/d = 10$) (a) and the end-grain distance a_3 ($t_i = 50$ mm) (b).

4 Test results

4.1 Recent tests at ETH Zurich

4.1.1 Geometrie and configuration

In a test series recently carried out at ETH Zurich the impacts of geometrical and material parameters on the load-carrying capacity of dowelled connections with slotted in steel plates was evaluated. The specimen were wood-steel-wood connections with two individual side members. The tests were carried out as pull-pull tests, but only one connection with $d = 12$ mm was tested until failure since the opposite connection with $d = 25$ mm was considerable stronger and exhibited no deformation. No interaction between both connections was neglected due to the large distance of ≈ 200 mm between the last rows of fasteners. The steel plate had a thickness 10 mm.
The side members with a thickness $t = 50$ mm and a width $h = 150$ mm were cut out of boards with the dimensions width/thickness/length 300/50/5000 $[mm]$. The side members were selected based on the density of the timber.
The dowels were cut from round steel of two different steel qualities with a nominal diameter $d = 12$, the effective diameter was in the range of $d \approx 11.90 - 11.95$ mm. The surface of the dowels was smooth but not galvanized.
Three dowels in a row ($n = 3,\ m = 1$) with different spacing and end-distances were tested as summarized in Tab. 6.

Table 6: Spacing and end distance of the test configurations

		a_1		
		$3d$	$4d$	$5d$
	$3d$			x
a_3	$5d$	x	x	x
	$7d$	x*	x	x*

The load was measured by the universal testing machine and the deformation of the two side members with respect to the central steel plate was measured by means of LVDT. The load was applied deformation controlled and failure was reached within approx. 5 min.

In the tests a gap opening between the side members and the central steel plate was observed. That is why the impact of friction due to the rope effect is neglected.

4.1.2 Material properties

The timber for the specimens was selected from a sample of boards with a wide range of density. It was aimed at an equal density of the two side members of the connection. The resulting range of timber density of the specimens is between $\rho = 360 - 520$ kg/m^3.
The properties of the steel of the dowels was controlled in four point bending tests. The distance between load introduction points and support was $l_1 = 50$ mm in 4-point bending. The distance between load introduction points was $l_2 = 72$ mm in 4-point bending. These dimensions are larger than the values specified in EN 409 2009b for 4-point bending with $l_1 \geq 2d$ and $d \leq l_2 \leq 3d$. According to EN 14592 CEN (2008) the maximum angle is $\alpha = 45/d^{0.7} = 7.9°$. The resulting tensile strength calculated according to Eq. 10 is $f_{u,mean} \approx 969$ N/mm^2 for ETG 100 and $f_{u,mean} \approx 581$ N/mm^2 for S235. Especially the tensile strength of the low grade steel S235 is much higher than expected by the specification of the steel quality. They are comparable to the properties of e.g. S355. In total 7 bending tests have been carried out for S235 and 8 for ETG 100. The resulting coefficients of variation of tensile strength are $CoV = 5.8\%$ for S235 and $CoV = 5.1\%$ for ETG 100.

4.1.3 Failure behaviour

In Fig. 5 and 6 the load-deformation behaviour of different configurations up to maximum load F_u are shown. For the specimen with small spacing a_1 and small end-distance a_3 early failure before larger plastic deformation can be seen. Tension perpendicular to grain splitting and/or plug shear failure were the main reasons for this early and brittle failure. For larger spacing and end-distances the larger plastic deformations were achieved.

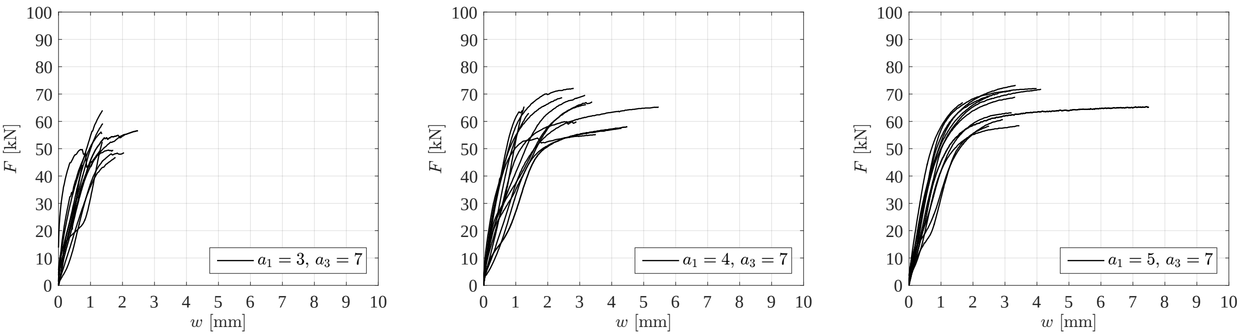

Figure 5: Impact of spacing a_1 on load-deformation behaviour.

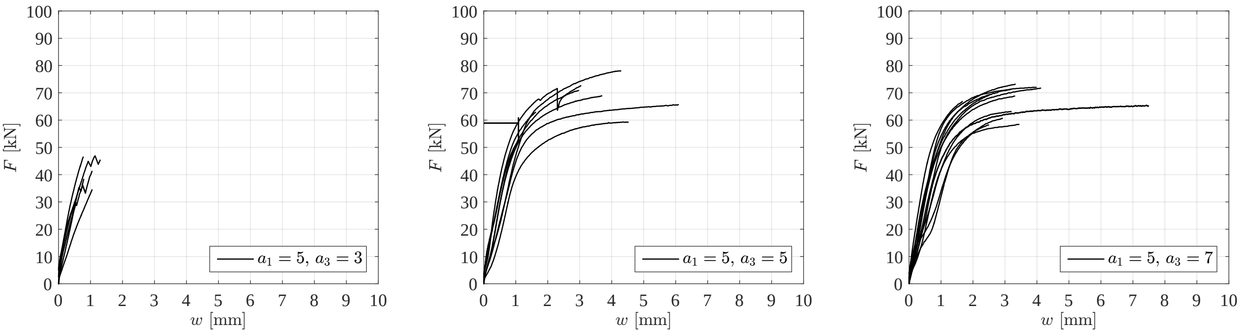

Figure 6: Impact of distance to end-grain a_3 on load-deformation behaviour.

Nevertheless also for large spacing and end-distances splitting and/or plug shear failure occurred at larger deformation. Especially for the configuration with the largest spacing and end-distances large deformations occurred before splitting failure.

4.1.4 Results

In Fig. 7 the load-carrying capacity R_u of the specimens is shown in dependency of the mean density of the side members. An overall large variation can be seen. The regression lines show that in some configurations load-carrying capacity has a clear dependency of the density.

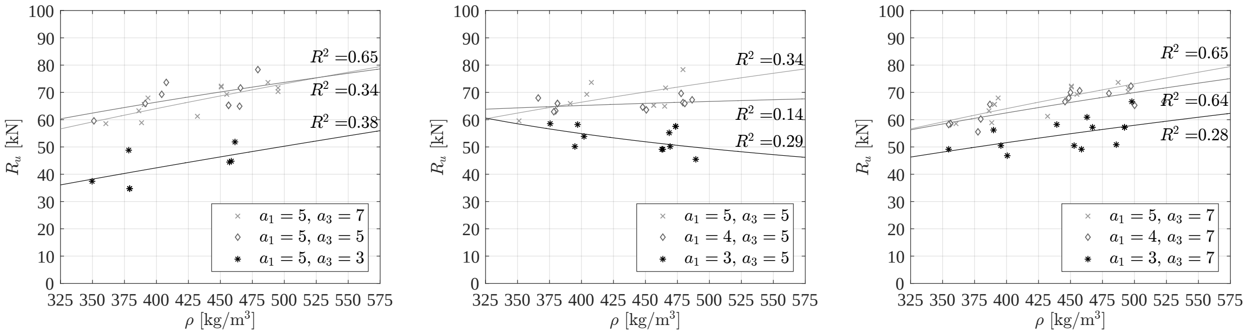

Figure 7: Load carrying capacity R_u in dependency of the mean density of the side members for three different configurations.

In order to allow for a comparison of load-carrying capacity and variation between specimens of different density the results are normalized to a density of $\rho = 420$ kg/m^3 according to Eq. 11.

$$R_{u,420} = R_{u,i} \left(\frac{420 \text{ kg/m}^3}{\rho_i} \right)^k \tag{11}$$

The mean load-carrying capacity $R_{u,mean,420}$ and the parameter k were determined by means of least squares fit. The values and coefficient of determination are given in Tab. 7.

Table 7: Results of the test series. Load-carrying capacity $R_{u,mean,420}$ normalized for a density of $\rho = 420$ kg/m^2 by parameter k with the corresponding coefficient of correlation R^2.

a_1 [-]	a_3 [-]	Steel grade	# [-]	$R_{u,mean,420}$ (CoV) [kN] (%)	k [-]	R^2 [-]
$5d$	$3d$	Low	6	44.0 (12.4%)	0.769	0.38
$3d$	$5d$	Low	10	53.6 (7.4%)	-0.475	0.29
$4d$	$5d$	Low	10	65.5 (3.0%)	0.101	0.14
$5d$	$5d$	Low	8	67.9 (7.0%)	0.464	0.34
$3d$	$7d$	Low	12	52.9 (8.9%)	0.521	0.28
$4d$	$7d$	Low	13	64.1 (5.0%)	0.505	0.64
$5d$	$7d$	Low	12	65.9 (4.8%)	0.594	0.65
$3d$	$7d$	High	7	67.0 (6.2%)	0.165	0.14
$5d$	$7d$	High	8	84.8 (2.9%)	0.555	0.87

The impact of density on the load-carrying capacity varies between the configurations. For several series a parameter $k \approx 0.5$ can be found, which corresponds to the impact of density according to failure mode III of the EYM.
In Tab. 7 the following impact of the geometrical and material parameters on the load carrying capacity and variation can be seen:

- The load carrying capacity decreases with decreasing spacing or end-grain distance.
- The load carrying capacity increases with increasing tensile strength of the steel dowels.
- The variation increases with decreasing spacing and end-grain distance.

4.2 Results from literature

Jorissen (1998) reports a large number of tests with various configurations. The tests were carried out as bolted shear connection in wood-wood-wood. Teflon sheets were used to reduce the impact of the rope effect.
In Fig. 8 the coefficient of variation of the load-carrying capacity $R_{u,420}$ at a density $\rho = 420$ kg/m^3 according to Eq. 11 is shown in dependency of the spacing a_1 of the dowels. The effect of increasing variation with decreasing spacing observed in the tests described in Chapter 4.1 is confirmed by the tests by Jorissen (1998).

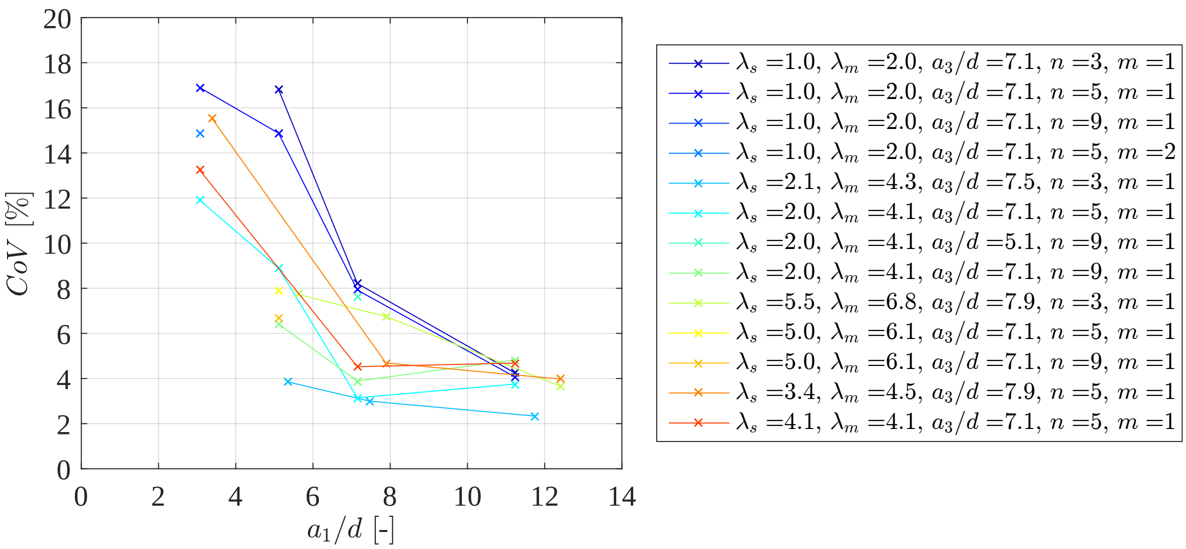

Figure 8: CoV of the load-carrying capacity $R_{u,420}$ at density $\rho = 420$ kg/m^3 for different test series from Jorissen (1998).

The tests were discussed in detail by Jorissen (1998) and Kohler (2005). Jorissen (1998) proposed a reduction factor for accounting for the impact of spacing a_1 on the reduction of load-carrying capacity. Kohler (2005) confirmed the validity of the fracture mechanics design approach for the load-carrying capacity of a single dowel of small slenderness λ. In addition Kohler derived parameters accounting for a model uncertainty of the EYM.
In this paper the considerable impact of spacing a_1 on the variation of load-carrying capacity shall be highlighted. The reason for the increase of variation with decreasing spacing between the dowels is explained by the change of relevant failure mode: for small spacing the material properties of the timber with a the high variation govern the failure whereas for large spacing the steel properties are decisive.

5 Impact of varying material properties on the reliability of connections

According to the load and resistance factored design partial safety factors γ are used in the design equation as e.g. in Eq. 12. The partial safety factor γ_M are calibrated according to the semi-probabilistic design concept in order to account for the variability of the resistance R.

$$z\frac{k_{\mathrm{mod}} \cdot R_{\mathrm{k}}}{\gamma_{\mathrm{M}}} - \gamma_{\mathrm{G}} G_{\mathrm{k}} - \gamma_{\mathrm{Q}} Q_{\mathrm{k}} \geq 0 \tag{12}$$

The impact of the different variability of a lognormal distributed resistance R on the partial safety factor γ_M is shown in Fig. 9 for a target reliability index $\beta = 4.2$. The analysis was performed in Matlab by means of the package UQLab (Marelli et al., 2016). The distribution characteristics of the loads are summarized in Tab. 8.
The load ratio α according to Eq. 9 is for timber structures typically in the range $\alpha \gtrsim 0.5$. For concrete structures with governing permanent loads the range of load ratio α is typically $\alpha \lesssim 0.5$.
The effective partial safety factor for a lognormal distributed resistance with a variation between 20-30% is in the range of $\gamma_M = 1.20 - 1.4$ which fits well the value currently suggested in EC5 $\gamma_M = 1.3$. Kohler et al. (2012) suggest similar partial safety factors for timber structures with different loading situations.

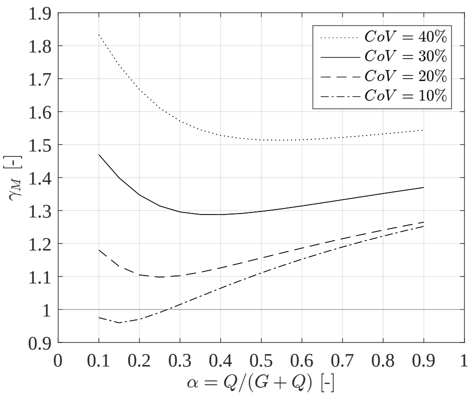

Figure 9: Optimal partical safety factors γ_M .

$$\alpha = \frac{Q}{G+Q} \tag{13}$$

Table 8: Assumed distribution characteristics of loads.

Property	Distr. function	mean	CoV	char. Level	γ
G	Normal	1	10%	50%	$\gamma_G = 1.35$
Q	Gumbel	1	40%	98%	$\gamma_Q = 1.5$

The dimensions and properties of shear connections with dowel type fasteners should be designed in a way to achieve desired reliability of the design. Most beneficial are failure modes that cause a low variability of the load-carrying capacity as e.g. ductile failure of the metal fasteners. As already stated by Jorissen (1998) for the different failure modes of connections with different level of ductility different partial safety factors might be necessary. For the ductile failure mode EYM III with low variability in the range of $\approx 5\%$ it could be benefited from a lower optimal partial safety factor compared to the brittle failure modes due to splitting or plug-shear failure. In order to encourage an economic and reliable design the design of a connection could be based on the ductile failure mode EYM III as it is recommended in Swiss standard SIA 265 (SIA, 2012) and former German standard DIN 1052 (DIN, 2008). For other, brittle failure modes not only the reduction in resistance but also the reduced reliability should be accounted for.

6 Conclusions

From the study presented in this paper, the following conclusions can be drawn:

- connections are complex compounds of different parts and materials exhibiting a wide range of possible failure modes
- the different failure modes are influenced by different geometrical parameters and material properties
- depending on the failure mode these different material properties cause different variability of the resistance of a connection
- the reliability and the resulting optimal partial safety factor depend on the failure mode of the connection and the variability its resistance
- ductile failure modes allow for a low partial safety factor and, hence, an economic design
- brittle failure modes require a larger safety margin

The following conclusions with regard to code relevance can be drawn:

- In order to allow for an economic and reliable design the geometry and configuration of a connection should be chosen in a way to obtain high load-carrying capacity with only a small variability. This can be achieved by sufficiently large spacing, end-distances and timber member thickness (large dowel slenderness λ) in order to reach a failure mode with ductile deformation of the fasteners. This allows to benefit from the small variability of these ductile failure modes and the consequent small partial safety factors.
- The unfavourable brittle failure modes due to splitting or plug-shear failure should be accounted for in the design but charged with sufficient safety margin in order to account for the higher variability and reduced reliability compared to ductile failure modes.
- Reinforcement by means of e.g. self-tapping screws can be a good measure to reduce the risk of brittle failure of dowelled connections due to splitting failure (Bejtka, 2005). It can be used to reduse the variability of load-carrying capacity also for small spacing and end-distances and sustain an adequate level of reliability for this type of connection geometries. Hence, reinforcement of dowel type connections should be accounted for in future version of EC5.

References

Aicher S., Dill-Langer G., Klöck W. (2002): Evaluation of different size effect models for tension perpendicular to grain strength of glulam. In: Proc. of the CIB-W18 Meeting 35, Kyoto, Japan, Paper No. CIB-W18/35-6-1

Bejtka I. (2005): Verstärkung von Bauteilen aus Holz mit Vollgewindeschrauben. PhD thesis, Fakultät für Bauingenieur-, Geo- und Umweltwissenschaften, Universtität Karlsruhe, Karlsruhe, Germany

Blaß H., Colling F. (2015): Load-carrying capacity of dowelled connections . In: Proc. of the INTER Meeting 48, Sibenik, Croatia, Paper No. INTER/48-7-3

Blaß H.J., Biehnhaus A., Krämer V. (2000): Effective bending capacity of dowel-type fasteners. In: Proc. of the CIB-W18 Meeting 33, Delft, The Netherlands, Paper No. CIB-W18/33-7-5

CEN (2004): EN 1995-1-1: Eurocode 5: Design of timber structures - Part 1-1: General - Common rules and rules for buildings. European Committee for Standardization CEN, Bruxelles, Belgium

CEN (2008): EN 14592: Timber structures - Dowel-type fasteners - Requirements. European Committee for Standardization CEN, Bruxelles, Belgium

CEN (2009a): EN 338: Structural timber - Strength classes. European Committee for Standardization CEN, Bruxelles, Belgium

CEN (2009b): EN 409: Timber structures - Test methods - Determination of the yield moment of dowel type fasteners. European Committee for Standardization CEN, Bruxelles, Belgium

Dietsch P. (2011): Robustness of large-span timber roof structures-structural aspects. Engineering Structures 33(11):3106–3112

DIN (2008): DIN 1052: Entwurf, Berechnung und Bemessung von Holzbauwerken - Allgemeine Bemessungsregeln und Bemessungsregeln für den Hochbau. DIN 1052 (2008-12), DIN Deutsche Institut für Normung e.V., Berlin, Germany

Dorn M. (2012): Untersuchungen zum Gebrauchstauglichkeitszustand von Dübelverbindungen im Holzbau. PhD thesis, Technische Universität Wien, Vienna, Austria

Ehlbeck J., Werner H. (1991): Biegegerät zur Prüfung von stiftförmigen Verbindungsmitteln. Tech. rep., Versuchsanstalt für Stahl, Holz und Steine, Abteilung Ingenieurholzbau, Universität Fridericiana Karlsruhe, Karlsruhe, Germany

Frühwald E., Serrano E., Toratti T., Emilsson A., Thelandersson S. (2007): Design of safe timber structures-how can we learn from structural failures in concrete, steel and timber? Tech. rep., Division of Structural Engineering, Lund University, Sweden, tVBK 3053

JCSS (2001): Probabilistic Model Code. Joint Committee on Structural Safety., uRL: http://www.jcss.byg.dtu.dk/

Johansen K.W. (1949): Theory of timber connections. IABSE publications 9:249–262

Jorissen A. (1998): Double shear timber connections with dowel type fasteners. PhD thesis, Technische Universiteit Delft, Delft, The Netherlands

Jorissen A., Blaß H.J. (1998): The fastener yield strength in bending. In: Proc. of the CIB-W18 Meeting 31, Savonlinna, Finland, Paper No. CIB-W18/31-7-6

Jorissen A., Leijten A. (2005): The derivation of design clauses for nailed and bolted joints in Eurocode 5. In: Proc. of CIB-W18 Meeting 38, Karlsruhe, Germany, Paper No. CIB-W18/38-7-5

Kohler J. (2005): A probabilistic framework for the reliability assessment of connections with dowel type fasteners. In: Proc. of the CIB-W18 Meeting 38, Karlsruhe, Germany, Paper No. CIB-W18/38-7-2

Köhler J. (2007): Reliability of timber structures. PhD thesis, IBK ETH Zurich, Zurich, Switzerland

Kohler J., Steiger R., Fink G., Jockwer R. (2012): Assessment of selected Eurocode based design equations in regard to structural reliability. In: Proc. of the CIB-W18 Meeting 45, Växjö, Sweden, Paper No. CIB-W18/45-102-1

Leijten A., Köhler J., Jorissen A. (2004): Review of probability data for timber connections with dowel-type fasteners. In: Proc. of the CIB-W18 Meeting 37, Edinburgh, UK, Paper No. CIB-W18/37-7-13

Marelli S., Sudret B., Lamas C. (2016): Uqlab user manual - structural reliability. Tech. rep., Chair of Risk, Safety and Uncertainty Quantification, ETH Zurich

Meyer A. (1957): Die tragfähigkeit von nagelverbindungen bei statischer belastung. Holz als Roh-und Werkstoff 15(2):96–109

Mischler A. (1997): Influence of Ductility on the Load-Carrying Capacity of Joints with Dowel-Type Fasteners. In: Proc. of the CIB-W18 Meeting 30, Vancouver, BC, Canada, Paper No. CIB-W18/30-37-6

Mischler A. (1998): Bedeutung der Duktilität für das Tragverhalten von Stahl-Holz-Bolzenverbindungen. PhD thesis, IBK ETH Zurich, Zurich, Switzerland

Quenneville P., Smith I., Aziz A., Snow M., Chui Y.H. (2006): Generalised canadian approach for design of connections with dowel fasteners. In: Proc. of CIB-W18 Meeting 39, Florence, Italy, pp CIB–W18/39–7–6

Schmid M., Blaß H.J., Frasson R.P.M. (2002): Effect of distances, spacing and number of dowels in a row on the load carrying capacity of connections with dowels failing by splitting. In: Proc. of the CIB-W18 Meeting 35, Kyoto, Japan, Paper No. CIB-W18/35-7-5

SIA (2012): Standard SIA 265 - Timber Structures. SIA Swiss Society of Engineers and Architects, Zurich, Switzerland

Svensson S., Munch-Andersen J. (2014): Study of the rope-effect on the load-carrying capacity of nailed connections. In: Proc. of the INTER Meeting 47, Bath, UK, Paper No. INTER/47-7-4

Werner H. (1993): Tragfähigkeit von holz-verbindungen mit stiftförmigen verbindungsmitteln unter beräuksichtigung streuender einflußgrößen. PhD thesis, Technische Universität, Karlsruhe, Germany

Whale L., Smith I. (1986): The derivation of design clauses for nailed and bolted joints in Eurocode 5. In: Proc. of CIB-W18 Meeting 19, Florence, Italy, Paper No. CIB-W18/19-7-6

Discussion

The paper was presented by R Jockwer

H Blass commented that steel properties from individual batches would have low coefficient of variation. He asked could the results be made worse by unintentionally having better steel grades leading to low reliability. R Jockwer agreed and replied that the results depended on the ratio of properties of actual and assumed steel grade and the failure mode.

E Serrano discussed the information from Jorissen regarding mixed mode failure. R Jockwer replied that mode 1 fracture energy values were used. He also stated that only if we had pure shear we would have higher fracture energy. If we have stress interaction the fracture energy would drop so mode one would be assumed to be conservative.

P Zarnani commented that the mix mode failure in slide 16 should be better represented. He also questioned the relationship between the coefficients of variation for the material properties and the connection. R Jockwer replied that the issues were considered in the paper with different partial safety factors for brittle and ductile failure modes.

LM Ottenhaus asked about slide 18 where the graph classified on the right side as ductile failure. She asked whether the failure would go into brittle failure mode outside the range of the graph. R Jockwer replied that at the end splitting failure was always present.

F Lam asked about using Ditlevsen's bounds in reliability studies to consider mixed failure modes. R Jockwer replied that the model of establishing the connection capacity already had mixed failure modes considered. F Lam asked whether mode uncertainties were considered. R Jockwer replied that it would be considered in future.

P Quenneville commented the highly manufactured products such as LVL would have low coefficient of variation and the cross layers in some LVL product would change the failure mode. He also asked whether the difference shown in slide 22 was significant. R Jockwer replied that although the number of tests was low the results supported the theoretical model.

K Ranasinghe received clarification of how the 5th percentile values were established from simulation and there was a transition between different failure modes.

T Reynolds and R Jockwer discussed the importance of the influence of material density on failure mode.

G Schickhofer commented one should avoid brittle failure mode and should provide recommendation to avoid brittle failure.

U Kuhlmann commented that some graph for reliability was not clear. R Jockwer replied that the beta values in the range of 5 to 5.5 were for comparison purposes. Also the information was provided as normalized ratios. U Kuhlmann suggested that more information should be provided.

P Dietsch commented that envelope curve showing where additional safety could be achieved would be important for code consideration to guide the development of code provisions to avoid brittle failures.

R Steiger asked why kmod of one was used in the reliability calculations. R Jockwer agreed that the results would be different if a different kmod was used. This would be done in the future.

S Franke commented that the ductile mode consideration would be even more important for example using minimum member thickness.

P Quenneville stated specifying L/d ratio would not be sufficient to ensure ductile behaviour as the number of fasteners would come into play.

Predicting the load-deformation of bolted timber connections up to failure

Y. Zhang, PhD candidate, University of Auckland

G. M. Raftery, Lecturer, University of Auckland

P. Quenneville, Professor of timber design, University of Auckland

Keywords: timber, connection, bolt, resistance, displacement, failure, seismic

1 Introduction

The design of connections is an important portion of the design exercise for timber buildings. For buildings that are subjected to occupancy, wind and or snow loadings, the predictions of the governing resistance can be sufficient. However, prediction of the governing resistance for connections that are subjected to seismic loading is insufficient. For timber connections subjected to seismic loading, it is extremely important to be able to ensure a level of ductility. Thus, one needs to predict the ultimate yielding resistance and the over-capacity of the other failure modes (Park and Priestly, 1992). Finally, it is also important to be able to predict the ultimate displacement so as to have an indication of the ductility, given by Equation (1), that the connection can provide. Thus, engineers need to be able to design timber bolted connections with a known outcome for the ultimate resistance and yield and ultimate displacements, as idealised in Figure 1, to quantify the ductility.

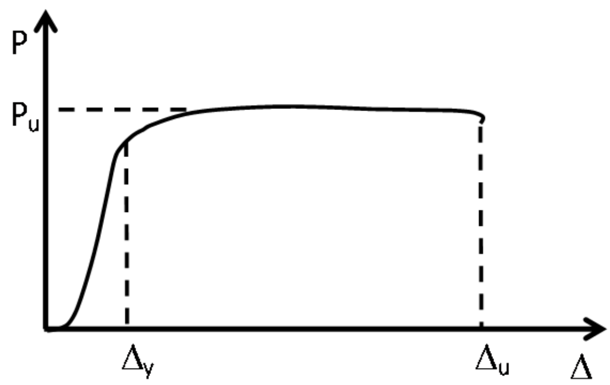

Figure 1. Load-deformation curve for a ductile bolted connection showing ultimate resistance, yield and ultimate displacements.

$$\mu = \frac{\Delta_u - \Delta_y}{\Delta_y} \qquad (1)$$

From past research on bolted connections, it is well known that the ultimate yielding resistance can be well predicted. Research has allowed timber designers to predict the resistance of dowel-type fasteners if their governing mode of failure is yielding (Johansen, 1949). Yielding failure is the result of plastic deformation of the wood fibres alone or in combination with the yielding of the bolt. Described as the European Yield Model (EYM), yielding connections allow plastic deformation to occur through crushing of the wood fibres in bearing (Modes I and II) and the combination of some crushing of the wood fibres and formation of plastic hinges in the steel connector (Modes III and IV), as shown in Figure 2.

The EYM equations predict the yielding capacity of connections, based on these four modes. For non-seismic design, the connection resistance is taken as the minimum capacity of the four EYM modes, if none of the possible brittle failure mode occurs. However, it is recognised that if brittle failures are avoided through design, the ultimate yielding resistance will be given by the resistance of mode I or II, as shown in Figure 3. It is thus imperative to understand connection resistances that are associated with brittle failures in order to avoid them and target the ultimate yielding capacity of the EYM failure modes.

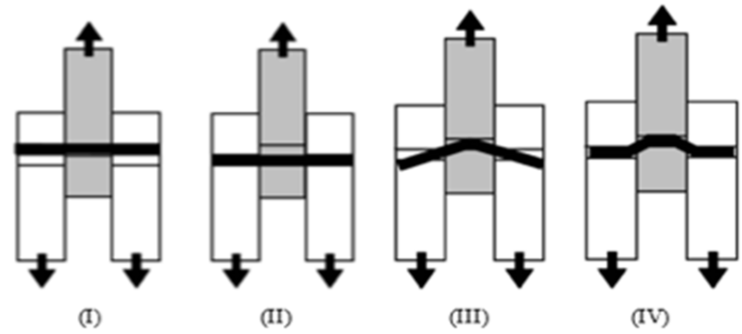

Figure 2. Yielding failure for bolted connections loaded parallel-to-grain (double shear cases).

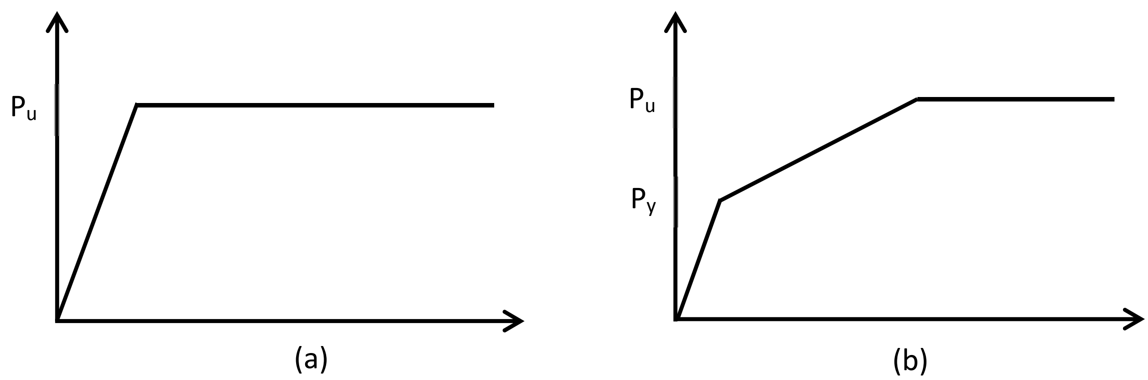

Figure 3. Idealised load-displacement curves for EYM (a) modes I and II and (b) modes III and IV.

Subsequently, secondary failure occurs in one of the brittle failure modes identified in Figure 4 (Jorissen, 1998, Quenneville and Mohammad, 2000). This secondary failure typically occurs suddenly and without warning. Work on brittle failures of bolted connections in recent decades has permitted some form of prediction of the various brittle failure resistances, such as splitting, row shear, group tear-out and net tension (Quenneville and Morris, 2009).

It is understood that the resistance of brittle failure modes can govern the design of timber connections and these brittle failures, if not controlled, can occur at a resistance lower than P_y, or in between P_y and P_u in Figure 3b or below P_u in Figure 3a. Thus, to take full advantage of the maximum ductility that a timber connection can offer, it is thus desirable to ensure that brittle failure mode resistances are well above the resistance of modes I and II of the EYM.

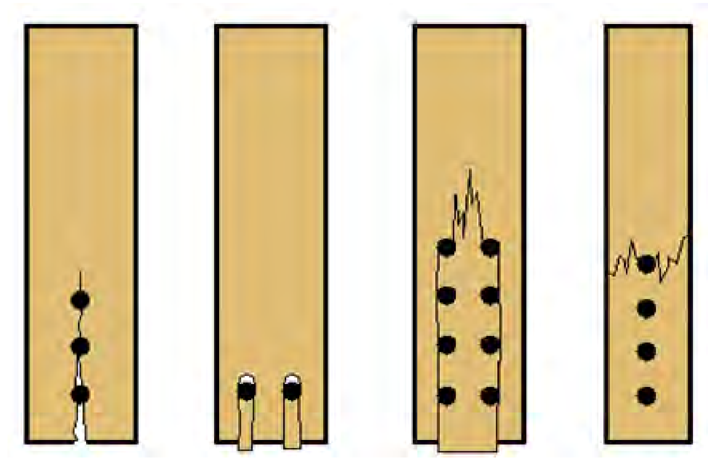

Figure 4. Types of timber bolted connection brittle failure modes.

If this is the case, the only remaining unknown in the determination of a connection's ductility is to quantify the ultimate displacement.

When it comes to a bolted connection displacement, little or no research has allowed anyone to be able to predict the ultimate displacement. Numerous researchers have worked on ductility predictions and many have provided different procedures for determining the yield point from a known bolted connection load-displacement curve (Munoz et al., 2008, Karacabeyli and Cecotti, 1996, Yasamura and Kawai, 1998). However, the prediction of the ultimate displacement is unknown. Until this is possible, determination of the ductility available in a bolted connection will remain only approximate or available for connection configurations that have been tested and replicated in practice. This is a serious impediment for timber designers that need to design timber connections for buildings in seismically-active locations.

Thus, in order to palliate this situation, a research program was undertaken to predict the ultimate displacement of timber bolted connections. It has been observed that for highly ductile connections (with a significant amount of displacement), the final failure mode is brittle. It is thus postulated that the ultimate displacement of a timber bolted connection is related to the over-capacity of the non-governing brittle modes of failure.

2 Methodology

Given that for the design of connections resisting seismic loads, one would ensure that a yielding behaviour would be governing, it would thus mean that the resistance of the other failure modes (splitting, row shear, group tear-out, net tension) would need to be well over the ultimate yielding failure mode resistance (modes I or II, not modes III or IV).

Given that the resistance of the brittle failure modes is directly related to the configuration of the connection, i.e. the amount of wood mobilised in resisting the connection force, the brittle resistance over-capacity will thus be affected and it was postulated that the ultimate displacement would also be affected.

Table 1: Bolted timber connection configurations tested. All Radiata Pine.

series	material	size (mm)	bolt size (mm)	n_r x n	a_{3t} (mm)	a_1 (mm)
1	Glulam	90 x 180	12	2 x 2	36	36
2	Glulam	90 x 180	12	2 x 2	72	72
3	Glulam	90 x 180	12	2 x 2	108	108
4	Glulam	135 x 225	20	2 x 2	80	80
5	Glulam	135 x 225	20	2 x 2	160	160
6	Glulam	135 x 225	20	2 x 2	240	240
7	LVL	45 x 100	12	1	96	---
8	LVL	45 x 100	16	1	128	---
9	LVL	45 x 100	20	1	160	---
10	LVL	45 x 200	20	1	160	---

Note: a_2 is 5d for all glulam configurations

All connection specimens consisted of steel-wood-steel connections. In the case of multi-bolt configurations, the end distance and bolt spacing were set equal to remove any influence of the smaller one of the two variables. Connections were tested in tension only under a monotonic load up to failure. A uniform displacement-control rate was maintained until failure occurred. The tests were performed in accordance with the standard testing procedures outlined in ISO 10984-2:2008. Two linear variable differential transformers (LVDTs) were symmetrically placed at the end of the specimen to measure the average deformation of the timber relative to the steel plates. The test setup for the single bolt in LVL is shown in Figure 5.

Using the load and displacement outputs, the stiffness, resistance and displacement values for each of the connections were identified at multiple points along the curve. The average values and coefficients of variation (COV) were then calculated for each connection type. This allowed the load-deformation behaviour to be modelled.

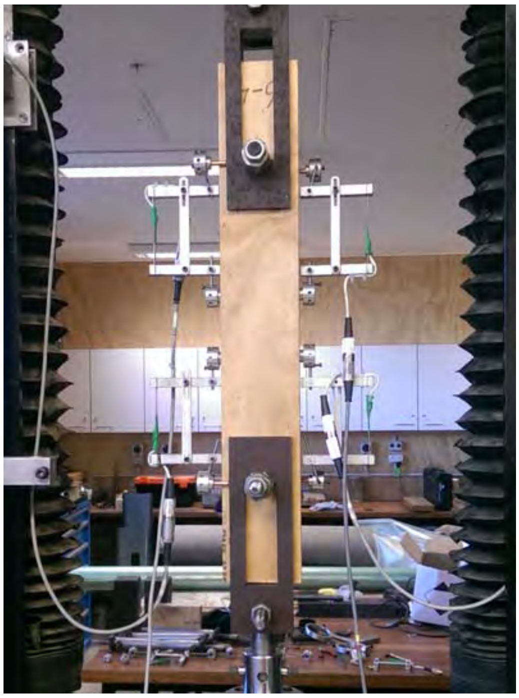

Figure 5. Test set-up for the single bolt tests in LVL.

3 Results and discussion

3.1 Load-displacement response analysis

For the specimens of the first 6 series, the load-displacement response, when mode II governed the resistance, consisted of three distinctive regions, as shown in Figure 6. The behaviour of the connection starts with an elastic phase (1), then moves on to inelastic (2) and subsequently to the plastic one (3). Between each of these regions was a transition zone, where interaction between the two adjacent behaviours was observed.

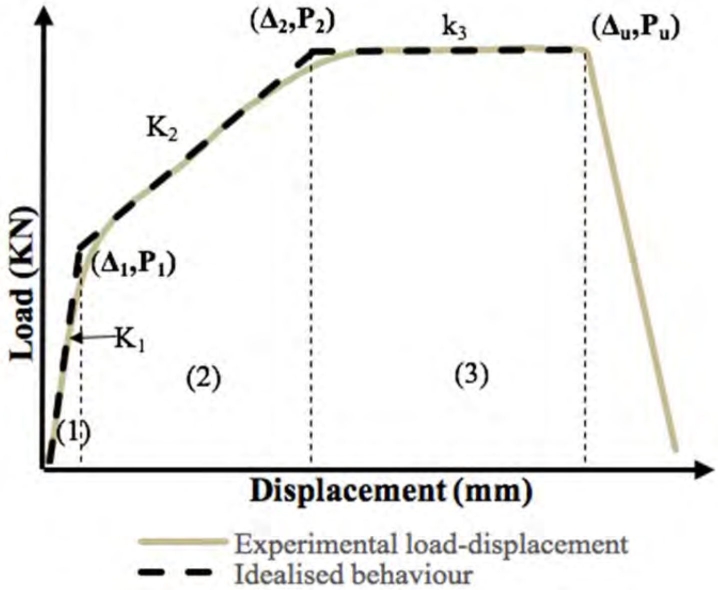

Figure 6. Actual and idealised load-displacement response.

Referring to Figure 6, the initial response is elastic, where recoverable displacement occurs as the connection adjusts to the applied load. As the load increases above a certain level, the connection begins to yield in an inelastic response. This is identified as the point at which the load-displacement curve changes gradient, shown at location (Δ_1, P_1). P_1 is associated with the resistance given from the EYM mode III or IV. Experimental observations demonstrate that at this point the bolts begin to bend. Plastic hinges start to form at specific points, depending on the governing mode III (2 plastic hinges) or IV (4 plastic hinges). As the load increases, the rope effect starts to take place and multiple plastic hinges form along the length of the bolt, multiplying until the entire length is deformed, as shown in Figure 7.

Figure 7. Bolt deformed to ultimate EYM mode II after rope effect, showing multiple plastic hinges.

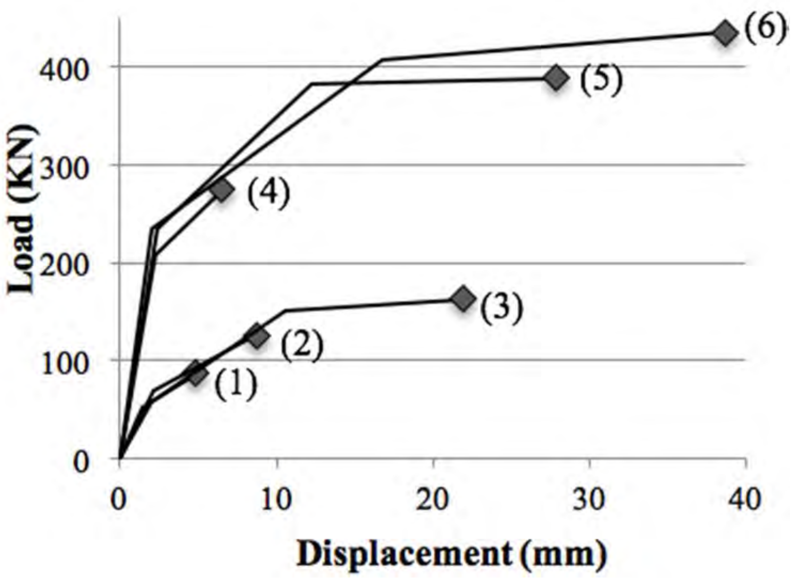

Figure 8. Idealised average load-displacement responses for series 1 to 6.

At this point, shown as location (Δ_2, P_2), no additional bending of the bolt can take place and consequently the timber is forced to fail in embedment. A secondary brittle failure then occurs (Δ_u, P_u), resulting in a sudden decrease in the load capacity of the connection.

The configurations of each of the connections tested influenced the size of each of the behaviour regions, and the point at which failure occurred. Connections of series 1, 2 and 4 failed prior to the plastic region being reached, and hence the ultimate capacity (P_u) was less than P_2. Series 3, 5 and 6 typically failed within the plastic region, which is the desired load-displacement response for seismic connections.

The co-ordinate values and adjoining gradients recorded for the connections were averaged for each of the six configurations, as shown in Figure 8 (series numbers indicated in brackets). It was found that the configurations with the same bolt size and cross-sectional area had similar load-displacement responses.

Classical design philosophy suggests that the capacity of a connection should be defined as the minimum resistance of any given failure mode. The minimum of the EYM mode III and mode IV is determined to be the point at which yielding failure begins to occur. However, testing showed that the capacity of the connection continued to increase after the bolts began to yield (Δ_1, P_1) and a yield plateau only formed when Mode II failure began to occur (Δ_2, P_2). This indicates that the EYM Mode II accurately represent the ultimate

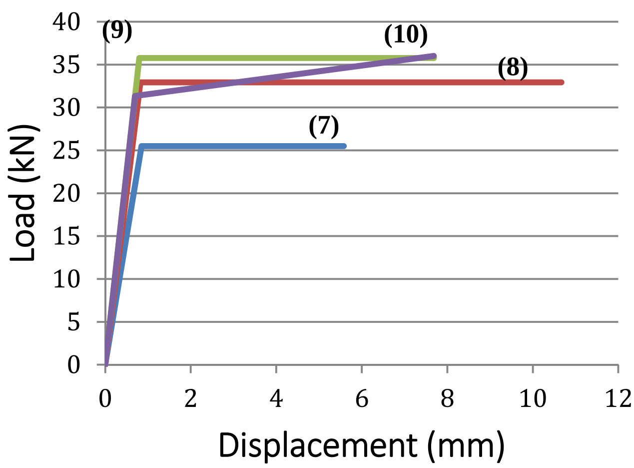

Figure 9: Idealised average load-displacement responses for series 7 to 10.

capacity of those connections for which a brittle failure mode does not governs the resistance.

With regards to the load-displacement relationships for the specimens of series 7 to 10, as shown in Figure 9, the behaviour was slightly different as the cross-section of the specimen and the diameter of the bolts were such that their slenderness ratio is very low and this forced an EYM mode II yielding failure to occur. The ultimate displacement was attained when the specimen failed in splitting.

3.2 Reduced brittle resistance model

Assessment of a failed ductile bolted connection from series 1 to 6, shown in Figure 10, allows one to make the following observations. This specimen exhibited a significant amount of deformation before ultimately rupturing in row shear. As the specimen starts to fail in yielding, timber adjacent to the bolt hole is compressed. This was accompanied by yielding of the bolt as well. As the connection load increased, the compressed zone increased and the connection deformation increased as well. During this additional displacement, the bolt was subjected to the rope effect. The wood fibres adjacent to the deformed bolt shape are bent, and there is a visible line where the fibres have become dislodged from the surrounding timber matrix.

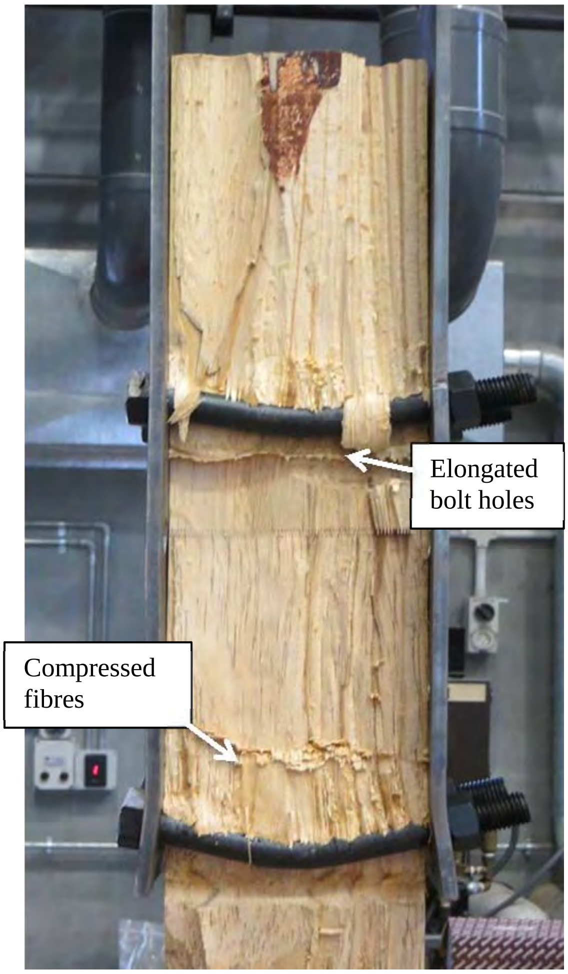

Figure 10. Internal view of connection after secondary failure showing extent of damaged fibres.

This compressed length is damaged and unable to provide resistance shear resistance, resulting in a lower row shear capacity for the connection than that was initially determined for the undamaged specimen. This means that existing brittle failure models which rely on the shear resistance represent an upper bound of their resistance. Thus, as the connection is deforming in a yielding mode, the brittle failure resistances for row shear and group tear-out are decreasing.

The failure hierarchy for series 8 to 10 is almost the same. Series 9 is taken as an example. After the yielding capacity of the connection is reached, a crack is observed next to the bolt hole. This crack is accompanied by crushing of the wood (Figure 11(a)). As the load increased, more wood was crushed but this crack didn't develop further. Instead, new cracks were observed a certain distance away from the centreline of the specimen (Figure 11(b)).

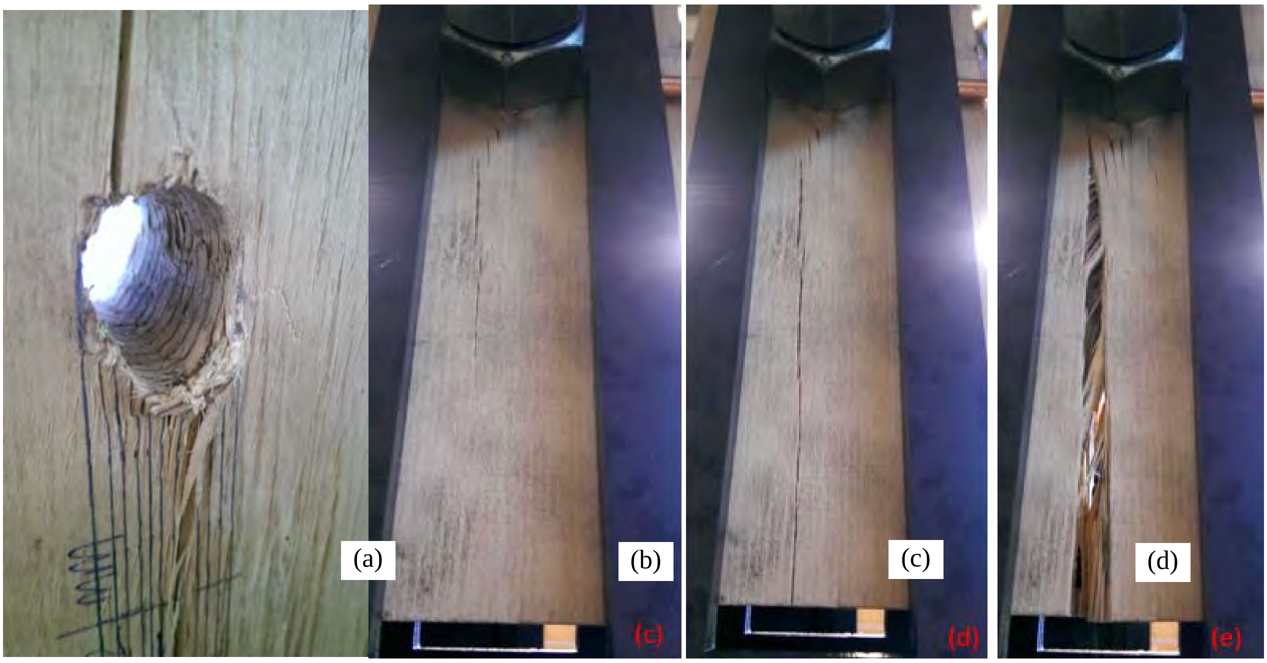

Figure 11. Hierarchy of the splitting failure for specimens of series 7 to 10.

These cracks propagated downwards until another crack occurred at a location closer to the centreline. This became the most significant crack and it gradually spread towards the specimen's end and in most cases, it spread towards the centreline at the same time (Figure 11(c)). Shortly after this crack reached the specimen end, it opened up from the end and this splitting caused the catastrophic failure and the ultimate displacement was attained (Figure 11(d)). The failure hierarchy for series 7 is more or less the same except that a crack initiated from the specimen end well before the final failure. It propagated upwards and along a line close to the centreline. This crack caused the catastrophic failure.

The nature of the failure indicates that failure was probably caused by both tensile stresses perpendicular to grain and shear stresses parallel to grain. The load-displacement curves of the series 7 to 10 only consist of two distinctive regions instead of three regions. The bolts from these tests maintained their original shape throughout the test and no plastic deformation was evident. These observations prove that only EYM mode II was involved. More tests are underway to assess the effect of the end distance on the ultimate displacement when splitting is the secondary failure mode.

Analysis of the secondary failure modes allows one to hypothesise on the causes of the ultimate displacement (Δ_u). The elongation of the bolt holes reduces the volume of timber providing shear or tension perpendicular-to-grain resistance to the connection. This means that splitting, row shear and group tear-out brittle failure resistances decrease with any increase in permanent displacement (inelastic and plastic deformation), as the capacity equations for these failure modes include the end distance (a_{3t}) and bolt spacing (a_1) variables. This differs from the net tension capacity, which remains constant, not being dependent on either of these variables. This hypothesis is best illustrated in Figure 12.

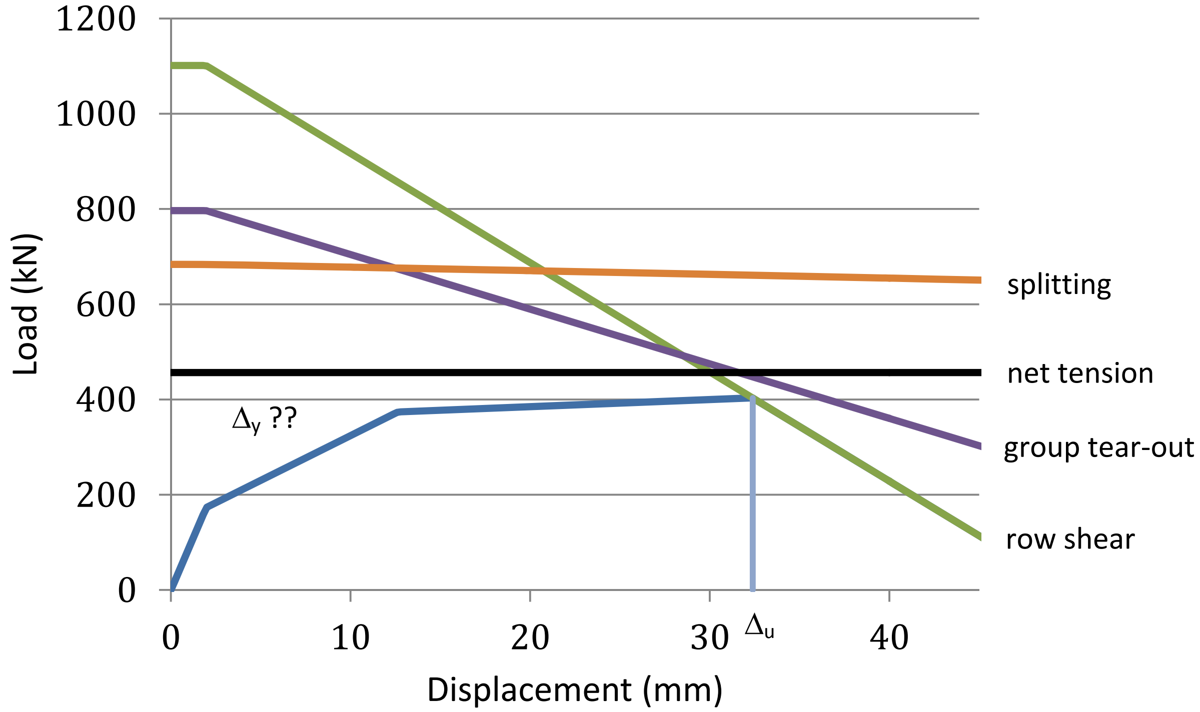

Figure 12. Assumed load-displacement response for a yielding failure with decreasing brittle failure resistances.

Figure 10 also reveals that the compressed length is greater than the permanent displacement. It is not known at this time what is the actual relationship between the connection deformation and the extent of the shear damage zone. In the resistances relationship shown in Figure 12, the decrease in row shear and group tear-out resistances is assumed linear. Further research is underway to establish what is the rate of change of the brittle failure mode resistances.

3.3 Prediction of the ultimate displacement

It is hypothesised that the ultimate displacement of a bolted connection is corresponding to the connection displacement at which the EYM mode II resistance intersects the reducing brittle resistance of splitting, row shear or group tear-out failures.

Using the reduced brittle resistance model in conjunction with the existing EYM, Jacks (2015) and Novis (2015) thus proposed to determine the ultimate displacement (Δ_u) using Equation (2). This equation is only applicable to those connections in which row shear or group tear-out is the governing brittle failure type, and the brittle resistance (P_b) is greater than the ductile resistance ($P_{EYM(II)}$).

$$\Delta_u = \frac{a_c(P_b - P_{EYM(II)})}{FP_b} + \Delta_1 \quad (2)$$

The variables a_c and Δ_1 can be defined according to Equation (2) and Equation (3) respectively. F is an undetermined factor at this point which represents the rate of change of the row shear and group tear-out resistances

$$a_c = \min(a_1, a_{3t}) \quad (3)$$

$$\Delta_1 = P_1 / K_1 \quad (4)$$

Where a_1 and a_{3t} are the bolt spacing and end distance prior to loading, and P_1 and K_1 are identified in Figure 6.

Equation (2) was developed using configurations three and five only, as they were the only connections to fail in the plastic region and be governed by one of the applicable brittle failure types (both failed by row shear). Additional research is required to validate this model.

3.4 Model limitations

Equation (2) is proposed based on the assumption that the plateau of the load-displacement response is horizontal (that the plastic stiffness is zero). The net tension model is also represented by a horizontal relationship which means that it is not theoretically possible for a connection to fail in net tension once it has begun to fail plastically. Nevertheless, a net tension failure was observed during the testing of configuration 6, where friction played a significant role in the resistance of the connection. This increase, when applied in the model, reduces the amount of predicted deformation that will occur before the brittle failure resistance is exceeded. Failure would thus occur on the load-displacement curve at an earlier point than expected, meaning that the model is non-conservative if one assumes zero stiffness in the plastic region.

It is also assumed that the rate of change of the resistances for the brittle failures is constant for both the inelastic and plastic regions. Not enough experimental observations are available to verify these assumptions. More observations of the full connection load-deformation curve (including the ultimate displacement) to quantify the value of F. are being acquired through testing.

3.5 Ductility

As discussed above, seismic design requires knowledge of the ductility of the connection. Therefore, in addition to the ultimate displacement, the displacement at the yield point is also required. The location of the yield point is subjective and as the bolt yielding begins to occur at location (Δ_1, P_1), the entire connection yielding does not occur till the attainment of (Δ_2, P_2). Current models for identifying the yield point do not acknowledge the presence of the inelastic region and hence may not be accurate or neglect the plastic region altogether. Perhaps a review of the yield point location is required in light of this research. However, it is suggested that an appropriate location may be at the intersection of the extended elastic and plastic lines. Verification of the yield point would then allow the ductility to be calculated; as the ratio of the ultimate displacement (calculated using the proposed reduced brittle resistance model) and the displacement at the yield point.

4 Conclusions

This paper presents an analysis of the load-displacement response of bolted timber connections up to failure. A hypothesis for the causation of the ultimate deformation is proposed. From the study, it can be concluded that:

- For ductile seismic design, the EYM mode II best predicts the ultimate capacity. This implies that the use of fasteners with low slenderness is recommended.
- The ultimate displacement occurs at the point where the load-displacement response meets the decreasing resistance of splitting, row shear or group tear-out failure modes.

More testing is underway to evaluate the effect of the end distance on the ultimate displacement for secondary splitting failure.

5 Recommendations

It is recommended that more observations of the full connection load-deformation curve (including the ultimate displacement) be made to quantify the value of F.

6 Acknowledgements

The authors wish to acknowledge the initial research contribution of Sarah Novis and Jessica Jacks, former undergraduate students at the University of Auckland, and the experimental assistance of Mark Byrami and Ross Reichardt.

7 References

ISO 10984-2 (2008): Timber structures – Dowel-type fasteners. Determination of embedding strength and foundation values.

Jacks, J. (2015): Predicting the load-deformation behaviour of bolted timber connections up to failure. Final Year Report submitted in partial fulfilment of the undergraduate degree. Department of Civil and Environmental Engineering, The University of Auckland.

Johansen, K.W. (1949): Theory of Timber Connectors. Publications of the International Association of Bridge and Structural Engineering. No. 9: 249-262. Bern, General Secretariat.

Jorissen, A. (1998): Double Shear Timber Connections With Dowel Type Fasteners, PhD thesis, Delft University Press, The Netherlands, 264 p.

Karacabeili, E., Cecotti, A. (1996): Quasi-static reversed cyclic testing of nailed joints. Proceedings of the International Council for Building and Research, Working Commission W18 – Timber Structures. Paper 29-7-7, Karlsruhe, Germany.

Munoz, w., Mohammad, M., Salenikovich, A. and Quenneville, P. (2008): Determination of yield point and ductility of timber assemblies: in search for a harmonised approach. Proceedings of the WCTE conference, Miyasaki, Japan.

Novis, S. (2015): Predicting the load-deformation behaviour of bolted timber connections prior to failure. Final Year Report submitted in partial fulfilment of the undergraduate degree. Department of Civil and Environmental Engineering, The University of Auckland.

Paulay, T., & Priestley, M. J. N. (1992): Seismic design of reinforced concrete and masonry buildings. New York, Wiley.

Quenneville, J.H.P., and Mohammad, M. (2000): On the failure modes and strength of steel-wood-steel bolted timber connections loaded parallel-to-grain. *Can Journal Civ Engr*, 27, pp. 761-773.

Quenneville, P., & Morris, H. (2009): Proposal for a mechanics-based bolted connection design approach for AS1720.1. Australian Journal of Structural Engineering, 9(3), p. 195-206.

Yasumura, M. and N. Kawai. (1998): Estimating seismic performance of wood-framed structures. Proceedings of 1998 I.W.E.C. Switzerland, Vol. 2, pp. 564-571.

Discussion

The paper was presented by P Quenneville

M Yasumura asked how Δy was determined. P Quenneville replied only dealing with bolted connections where the definition of Δy was easier from theoretical approach to estimate k_1 and k_2. M Yasumura commented that getting Δy would be difficult from experimental approach.

K Crews suggested that from experimental results sensitivity analysis could be done to check Δy estimates from different approaches.

F Lam asked about the influence of reverse cyclic loading Δu estimate. P Quenneville replied that from related work using cyclic tests higher capacity was obtained compared to monotonic tests.

A Ceccotti commented about the history of defining ductility for EC8 and it would be useful to study Δu.

LM Ottenhaus added ductility would increase under reversed cyclic conditions for mode 3. F Lam asked would it also increase for mode two. P Quenneville replied that mode of failure could change form mode 3 to mode 2 to l and higher capacity. M Yasumura added low cyclic fatigue failure in steel element could happen in reverse cyclic tests leading to lower ductility.

U Kuhlmann commented that Δu as an absolute value should be considered for ductility and not based on relationship between Δu and Δy.

G Schickhofer commented only glulam and LVL were considered and CLT type should be studied.

A Salenikovich and P Quenneville discussed the use of large fasteners for design.

Long-term behaviour of moisture content in timber constructions – Relation to service classes

Bettina Franke, Bern University of Applied Sciences

Steffen Franke, Bern University of Applied Sciences

Andreas Müller, Bern University of Applied Sciences

Marcus Schiere, Bern University of Applied Sciences

Keywords: Timber, Structures, Bridges, Moisture content, Service class

1 Introduction

Due to the hygroscopic behaviour of wood, moisture content influences the physical and mechanical properties, when the wood is dried under the fibre saturation point (FSP). Therefore, the correct estimation of the moisture content is important for the design and life cycle of timber structures. The design standards consider this behaviour by three different service classes (SC) according to the annual average moisture content. According to EN 1995-1-1:2004, Eurocode 5 (2004): Service class 1 is characterized by an ambient climate of 20 °C temperature and 65% relative humidity and a moisture content in wood is in average less than 12 M%; in SC 2 the moisture content in wood is in average less than 20 M%; and SC 3 comprises cases with moisture content higher than 20 M%. In SC 1, the relative humidity can be higher than 65% for few weeks per year. National annexes specify the ranges for the service classes differently, e.g. Germany and France. These three classes are a simplification for the planning engineers, because different wood species and wood products react different on climate changes.

The assignment of timber elements to one service class according to the ambient climate condition is one important step for the design of the load carrying capacity and ultimate limit states. However, the development of moisture gradients over the cross section due to daily, weekly or seasonal changes of the climate situation and thus moisture content are not directly considered. For example, an increase of the moisture content leads to moisture induced tension stresses inside the cross section. Thus, when exceeding the very low tension strength perpendicular to grain of wood, the cross section can crack and lead to a reduction of the load carrying capacity for tension perpendicular to the grain or shear, as shown in Figure 1.

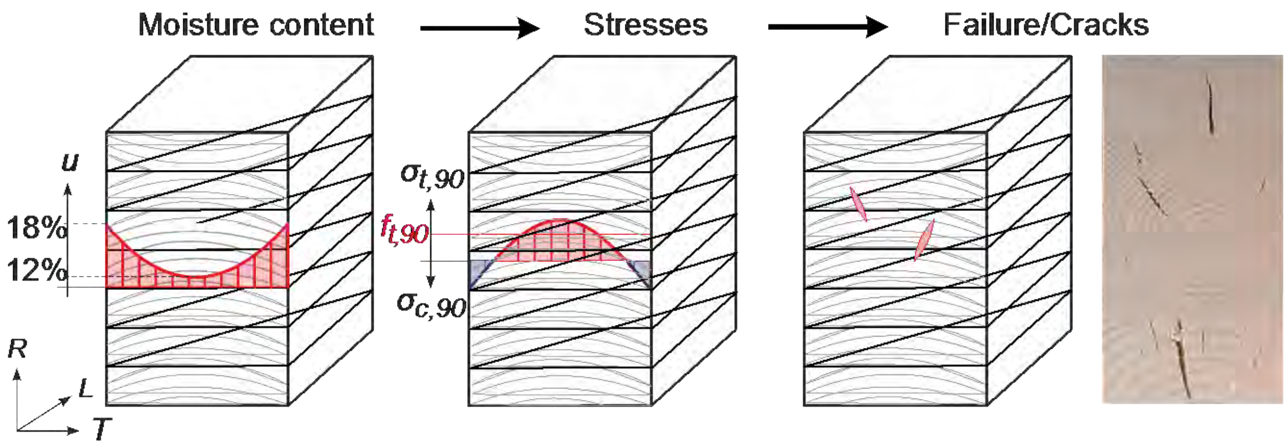

Figure 1: Moisture and stress distribution as well as failure of the cross section for an adsorption process

2 Investigation of the moisture content in wood

2.1 Experimental test series under laboratory conditions

2.1.1 Material and Conditioning

For the observation of the developing moisture content over the cross section, the test series were prepared specifically in the three material axes: radial (R), tangential (T) and longitudinal (L). Furthermore two different sizes (200/200/200 mm and 200/200/800 mm) per material axes were considered, see Figure 2. The side faces of the test specimens were sealed, so that the moisture diffusion only takes place in one material direction. On each specimen, gauges at a depth of 25, 45, 70 and 100 mm from the unsealed surfaces were implemented. For the test series with 200/200/800 mm in size, additional measuring points in a depth of 150, 200, 300 and 400 mm were installed. The specimens were conditioned at 20 °C and 65% relative humidity before and during the preparation and afterwards loaded with 95% relative humidity for a period of about 12 months.

The electrical resistance method was used for the determination of the moisture content using a pair of insulated stainless steel screws as sensor. A Thermofox and Gigamodul from Scanntronik Murgauer GmbH were used to log measurements every 6 hours.

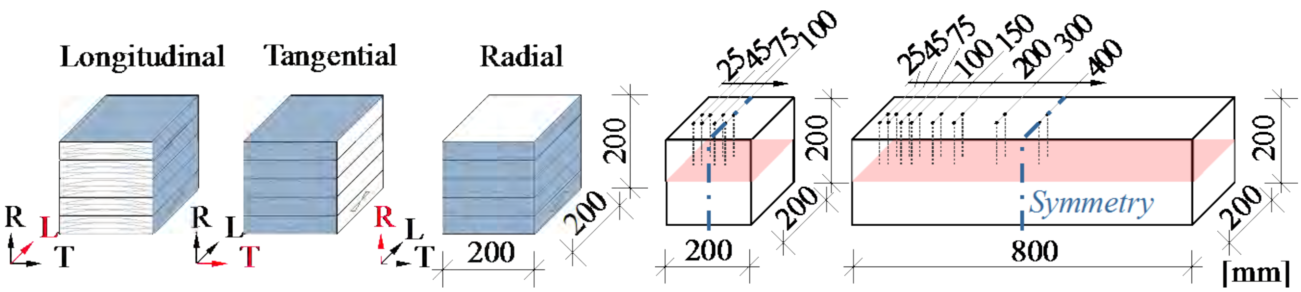

Figure 2: Test specimens with sealed surfaces in blue (top) and position of measuring points for the 200 mm and 800 mm long specimens (bottom)

2.1.2 Results

The moisture distribution in the cross section for the measuring period for the 200/200/200 mm test series are summarized in Figure 3. The diagrams include one curve for each measuring point per material axes. In longitudinal direction, the curves reach soon a plateau. However, in radial and tangential direction, an increase of the moisture content is still present, illustrating the slower process of wetting. It must be pointed out that the plateau reached is at 20 M%, whereas the equilibrium moisture content according to the climate of 20°C/95% is 24 M%. The oven dry method carried out after the tests confirmed a moisture content of 24 M%. It was observed, that the screws showed, even using galvanised steel, some kind of corrosion which may influence the resistance and led to the lower measurement. This could be taken into account by determining an additional time dependent calibration factor. However, the corrosion should not occur and other materials should be used.

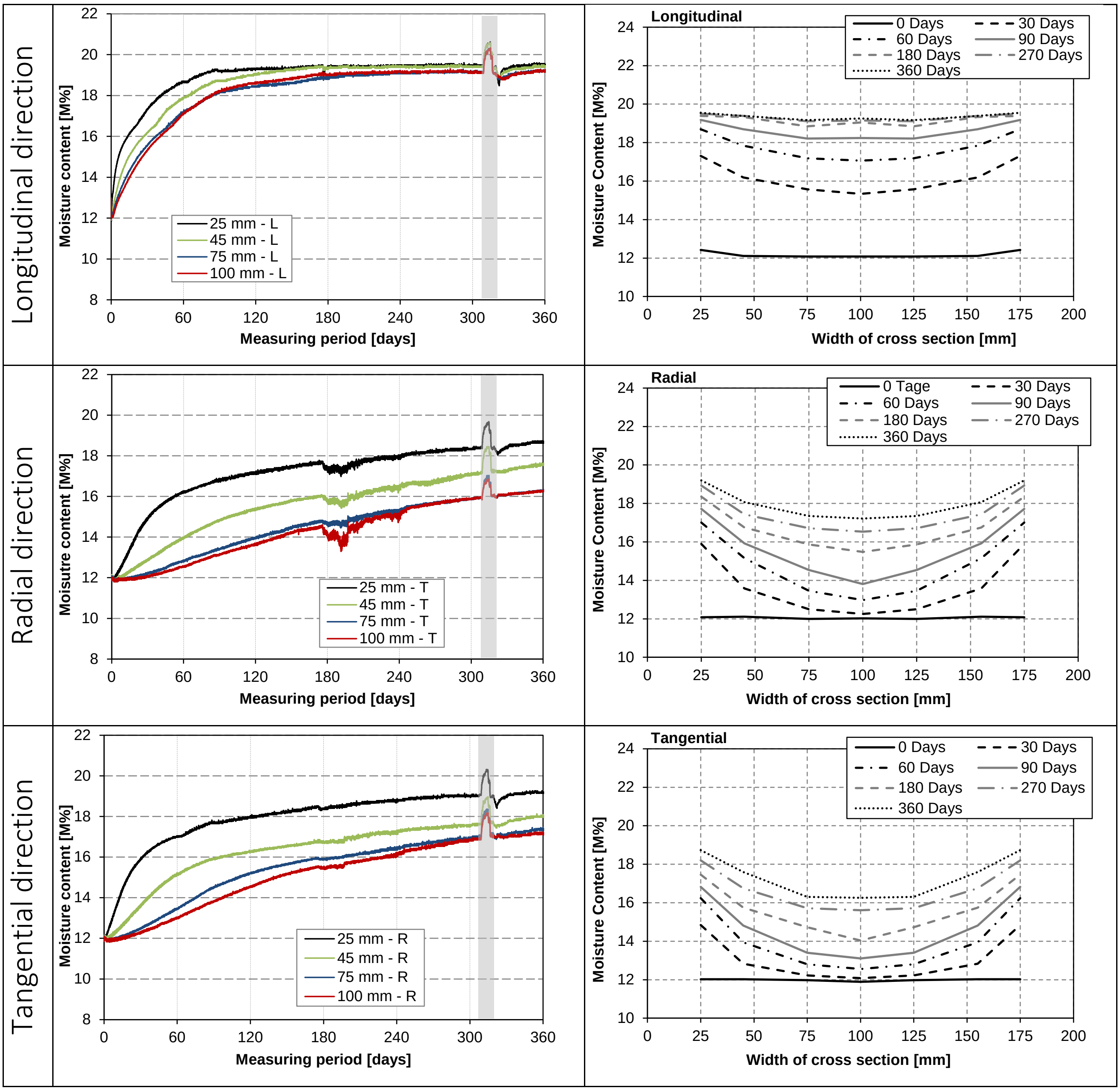

Figure 3: Moisture content development over time and cross section for the three material directions

The distribution of the moisture content over the cross section shows a clear gradient from the surface to the inner part in all three material axes. The increase of the gradient depends on the diffusion direction. For the experimental test series 200/200/800 mm similar results could be observed, as summarized in Franke et al. (2016). The grey shaded time period in the diagrams presents a short break down of the climate chamber within the measuring period.

2.2 Monitoring of timber bridges

2.2.1 General

Timber road bridges where monitored for the assessment of timber members directly exposed to the climate. The Bern University of Applied Sciences, the Institute for Timber construction, Structures and Architecture monitored and assessed six timber bridges in different climate regions of Switzerland, see Figure 4. Table 1 summarizes the main construction details as well as measuring periods and measuring values for each timber bridge. In addition to the direct local measurements at the timber bridges, the climate (air temperature and relative humidity) of close by meteorological stations (Meteo) was observed using data from www.meteoswiss.admin.ch.

Figure 4: Location of timber bridges monitored and close by meteorological stations

Figure 5: Timber road bridge Horen

2.2.2 Results

For the timber bridge Obermatt, the measuring results for the direct ambient climate (air temperature and relative humidity) as well as the moisture content are shown as example in Figure 6 for a period of 41 months. The single data of each parameter are summarized in averaged curves over 14 days. The seasons of the year can be clearly distinguished; the winter season with low temperatures from -5 to 5 °C and higher relative humidity, than the summer season with temperatures of 15 to 20 °C and about 80% relative humidity as well as the two transition seasons spring and fall with the increase respectively decrease of the temperature and the relative humidity reversely.

Table 1: Monitoring details of the timber road bridges

Bridge/Erection Meteo station	Characteristics	Measuring period/ -rate/ -system	Measuring values
Horen 2008 Buchs/Aarau	Beam bridge Spruce Glulam Block glued	since Oct 2009 every 6 hours local system	20 moisture content sensors 1 air temperature sensor 1 relative air humidity sensor
Muotathal 2009 Altdorf	Arch bridge Spruce Glulam Block glued	Oct 2009 - Dec 2011 every 6 hours local system	16 moisture content sensors 4 wood temperature sensors 2 air temperature sensors 2 relative air humidity sensors
Obermatt 2007-2008 Langnau i. E.	Beam bridge Spruce Glulam	Dec 2010-2014 every 6 hours remote system	16 moisture content sensors 4 wood temperature sensors 2 air temperature sensors 2 relative air humidity sensors
Schachenhaus 2000 Langnau i. E.	Timber-concrete composite bridge	Mar 2011-2013 every 6 hours local system	8 moisture content sensors 2 wood temperature sensors 1 air temperature sensor 1 relative air humidity sensor
Luthern 2010 Egolzwil	Spruce glulam Block glued Deck of Kerto-Q	Nov 2009-Sept. 2011 Every 6 hours local system	18 moisture content sensors 1 air temperature sensor 1 relative air humidity sensor
Bubenei 1988 Langnau i. E.	Arch bridge Spruce Glulam, Deck of cross pre stressed glulam	since July 2012 every 12 hours local system	24 moisture content sensors 1 air temperature sensor 1 relative air humidity sensor

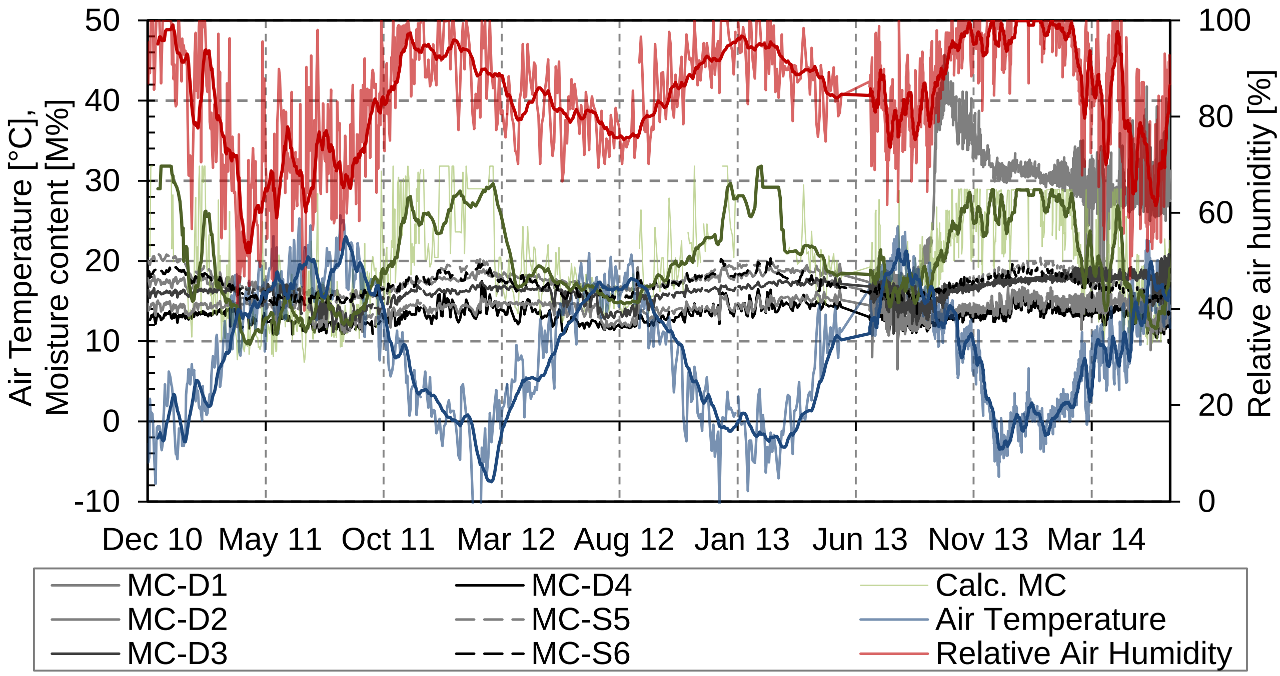

Figure 6: Timber bridge Obermatt, Measured climate and moisture content and calculated equilibirum moisture content

The moisture content is shown for sensors close to the surface (MC-S) and sensors in a depth of 200 mm (MC-D). The equilibrium moisture content calculated according to the measured ambient climate was added as comparison. A time offset according to the moisture diffusion transport and climate duration is not considered. Theoretically, the equilibrium moisture content is valid for the complete cross section by a constant climate. The moisture content measured in the timber cross section follows the seasonal effective climate changes. The response is delayed and with lower variations for both sensor locations at the surfaces and inside compared to the calculated equilibrium moisture content. The moisture content varies between about 14 and 20 M%. The variation of the moisture content at the surface is practically of about 5.5 M% between the summer and winter period. The curves of the moisture content at the inner structure are more evenly distributed and compact to each other, with variations of 2.5 M%. The difference between the inner and outer moisture content of 3 M% results in internal moisture induced stresses. The phase shift between the theoretical calculated equilibrium and measured moisture content is about 2 to 3 months depending on the gradient of climate change and the phase of adsorption or desorption. In general, the measured moisture content did not exceed 20 M%. The behaviour determined and shown for the bridge Obermatt could, in a similar range, also be observed for the other five timber bridges, Franke et al. (2016).

For the planning phase of timber bridges, the analyses of the ambient climate on the bridge and the regional climate by a close by meteorological station are compared. For example Table 2 summarizes the mean, maximum and minimum values for the air temperature, relative humidity and the calculated equilibrium moisture content for the timber bridge Obermatt. The differences in the measured values results in differences in the equilibrium moisture content as well. The mean equilibrium moisture content will be achieved in the inner cross section during the life cycle. After the erection, the ambient climate may induces a moisture gradient in the cross section considering a moisture content of 8 - 12M % from the production line/condition without pre conditioning.

For each timber bridge monitored, the comparison with a nearby meteorological station shows differences which reach up to 6 M%, as summarized in Table 3. For each case, the same measuring period was used wherefore the mean values can differ for the same meteorological station. As conclusion, the local effects regarding the location and the kind of bridge (e.g. water or street crossing) should not be neglected.

Table 2: Timber bridge Obermatt; Comparison of direct measuring at the bridge and meteorological station (meteo)

	Mean Value		Minimum		Maximum		Variation	
Bridge Obermatt	Bridge	Meteo	Bridge	Meteo	Bridge	Meteo	Bridge	Meteo
Temperature [°C]	8.0	8.3	-18.1	-19.1	25.3	31.7	43.4	50.8
Relative humidity [%]	86.8	84.1	34.5	21.8	99.9	100.0	65.4	78.2
Equilibrium moisture content [M%]	20.6	20.3	6.9	4.7	29.0	29.1	22.1	24.3

Table 3: Comparison of the equilibrium moisture content according to the ambient climate measured at the timber bridges or meteorological stations (Meteo) and the moisture content measured

Bridge / Meteo station	Measuring period	Moisture content - mean value			Moisture content - variation		
		Bridge		Meteo	Bridge		Meteo
		Meas.*	Calc.	Calc.	Meas.*	Calc.	Calc.
Mouthatal / Altdorf	15 month	16.6	15.6	15.9	7.5	24.3	25.6
Horen / Buchs	12 month	16.4	15.6	17.5	6.9	23.3	23.6
Luthern / Egolzwil	14 month	13.5	15.7	20.5	8.1	20.2	22.9
Bubenei / Langnau	25 month	22.5	17.2	24.7	5.7	26.6	18.1
Obermatt / Langnau	45 month	18.1	20.6	20.3	8.9	22.1	24.3
Schachenhausen / Langnau	23 month	17.0	15.9	20.5	6.7	21.3	24.3

* Mean value of every measuring point close to the surface

Further, the influences on the ambient climate due to constant shadows, flora, and wind are not insignificant. A positive result is that the moisture content measured is less than the equilibrium moisture content according to the climate of meteorological station.

2.3 Numerical simulations

2.3.1 Numerical model and parameter settings

A 2D numerical model in FE was set up to simulate the moisture diffusion. Linear 4-node plate elements with a regular mesh size of 5 mm were used. The time step size in the calculations was set to a constant interval of 0.1 day. This mesh and time step size was determined through a convergence study, which resulted in an uncertainty of less than 0.1 M% compared to automatic time stepping and 1.25 mm mesh size, Schiere (2016). The inaccuracies occur right after loading, close to the surface of the beam. These inaccuracies do not affect the moisture content developments in the center of the cross section more than the aforementioned inaccuracy of 0.1%.

The modelled beam was loaded as a parallel shaped body, like set up for the experiments and seen in Figure 2. In that way, the material was loaded in its principal material axes.

Moisture diffusion was modelled to be Fickian. In case of wetting processes, Fickian moisture diffusion is expected to give a good approximation of the actual process. In case of drying, non-Fickian moisture diffusion is often preferred over normal Fickian diffusion. This means that extra input parameters have to be given to properly simulate the evaporation of moisture from the wood surface. However, the drying process in the simulation was modelled through a Fickian process as well.

2.3.2 Validation of numerical model

The simulations made with the model were compared to experimental values. This was done for both wetting and drying in the case of a 90 mm wide beam in Jönsson (2004), and for wetting in radial and tangential direction in case of the 200 mm wide beam for the own experiments in Franke et al. (2016).

In this first validation case, the difference between radial and tangential moisture diffusion is difficult to make, because the pith location of each board in the tested glulam beam was close to the board edge. Radial and tangential moisture diffusion is often averaged to one single value, although small differences do exist according to Siau (1971). The wetting and drying was performed from 9 to 16 M% vice versa, see Figure 7. The simulations overlap the moisture content values obtained from experiments. The used diffusion values for wetting and drying were already proposed for the 90 mm wide beam in Angst and Malo (2010).

Diffusion values for validation of the wetting experiments of the 200 mm wide beams were derived in Schiere (2016). The diffusion values for radial moisture diffusion were higher than for tangential diffusion, 2.89e-10 m^2/s and 1.61e-10 m^2/s, respectively. Both were modelled as constant values. The wetting process was simulated from 12 M% to 20 M%, see Figure 8.

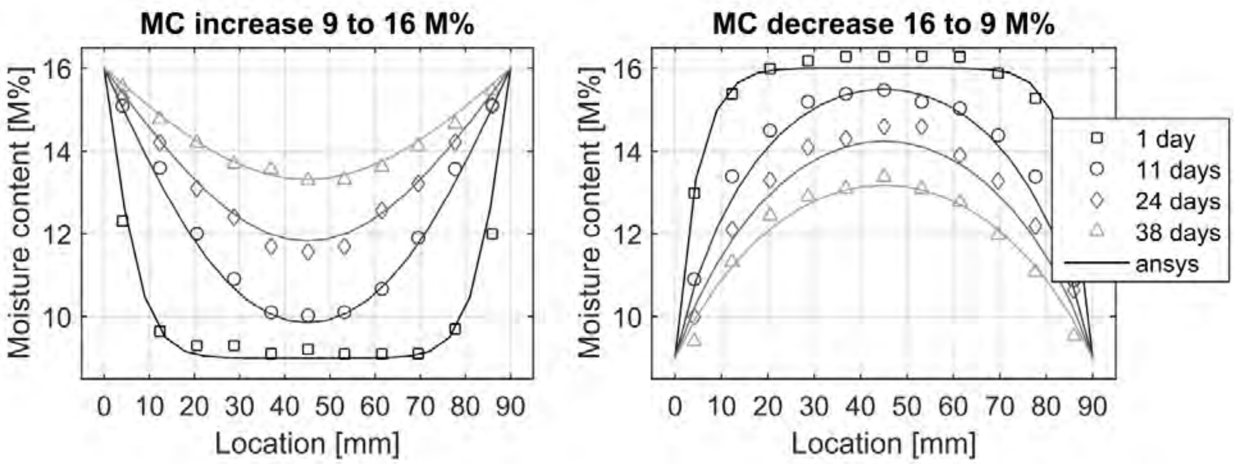

Figure 7: Comparison of experiments and simulations of wetting and drying process of a 90 mm wide beam

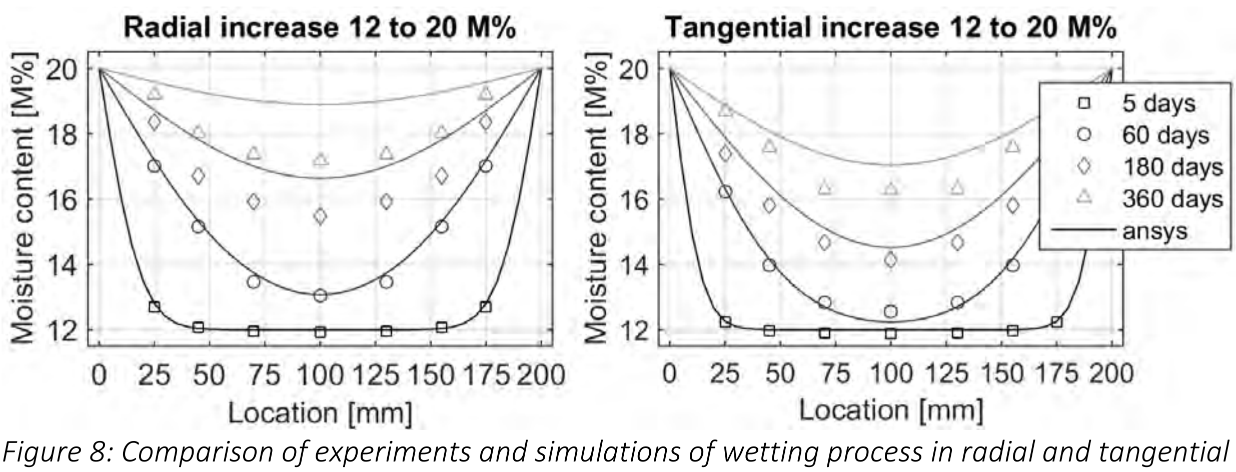

Figure 8: Comparison of experiments and simulations of wetting process in radial and tangential direction of a 200 mm wide beam

Comparisons between simulations and experiments overlap over at least the first 60 days of the experiments very well. Afterwards, differences are observed and they become larger over time, although the differences barely exceed 1 M%. The measurement might also be influenced by corrosion affecting the measured resistance between the gauges, but this is currently under investigation. The differences could also be due to some non-Fickian effects explained by Droin-Josserand et al. (1989) for instance, where moisture diffusion slows down approximately halfway the moisture content increase.

3 Results and relation to standards

3.1 Building types vis a vis service classes

The analysis of the monitoring results observed or published by Gamper et al. (2014), Cruz (2006), Jorge (2014) for different building types and bridges show typical characterizations. In general, the moisture content measured was used where available. In all other cases, the equilibrium moisture content was calculated according to the monitored temperature and relative humidity using the method by Simpson (1973).

In most cases, one service class according to EN 1995-1-1:2004 can clearly be assigned, as shown in Figure 9. However, the building types ice halls, sports halls and swimming pools show a wider variation compared to the other ones. This is related to the specific user profile, e.g. ice halls are not always used over the complete year. Timber bridges show also a wide variation compared to the other ones, but can still be assigned to service class 2, as shown in Figure 10. The timber bridge Bubenei is the only bridge with higher moisture contents which is related to a leaky deck which was reconditioned. In this process, the monitoring system was installed to observe the drying process of the timber structures. These values are not used for further discussions. Figure 10 includes the measured moisture content on timber bridges as mean

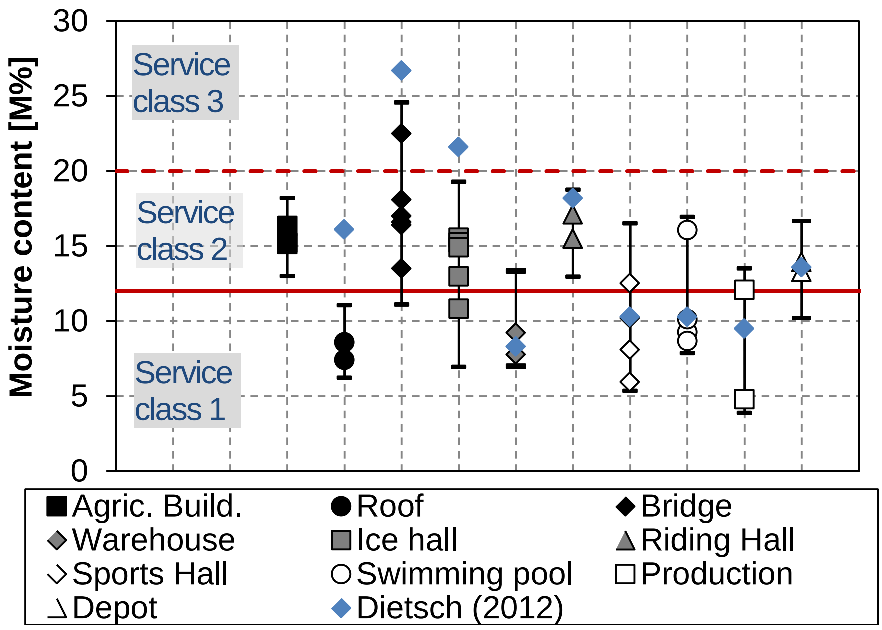

Figure 9: Average moisture content in typical timber building constructions and relation to service classesaccording EN 1995-1-1:2004

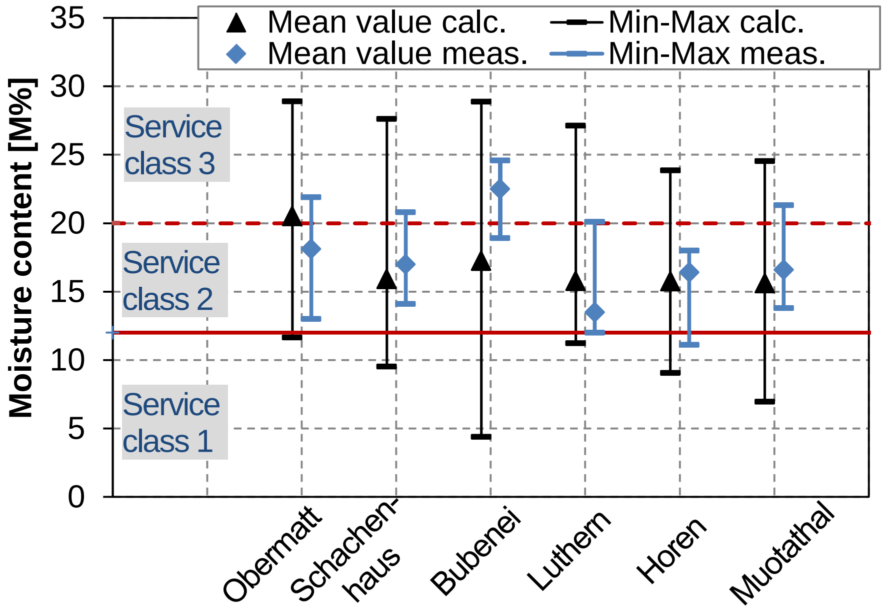

Figure 10: Average moisture content in typical timber building constructions and relation to service classes according EN1995-1-1:2004

values against the measuring points close to the surface and the equilibrium moisture content according to the ambient climate measured. The comparison confirms again that the ambient climate at a bridge has to be considered carefully and that the simply use of information from nearby meteo stations can lead to overestimations of the moisture content.

The results presented are important guidelines for planning engineers, since recommendation of assignment of timber structures to service classes are not available in the standards. The research results presented by Dietsch (2012) confirms the characterizations by building types as shown in Figure 9 where the mean values are included for comparison.

3.2 Distribution over the cross section

The distribution of the moisture content over the cross section could be experimentally and numerically determined during an intensive adsorption process by 20 °C and 95% relative humidity. For two different sizes and three material directions, the distribution over the cross section was determined, as shown in Franke et al. (2016) or in e.g. in Figure 11 and Figure 12. The measured distribution over the cross section was theoretically extended to the surface according to the resulting equilibrium moisture content according to the climate. The distribution of the moisture content along the radial or tangential direction is not converged for a cross section of 200/200/200 mm even after one year of an intensive adsorption process. The analyses of the experimental results show that the moisture content distribution over the cross section can be divided in an active and passive zone.

Daily or weekly climate changes result in a change of moisture content only in the outer zone of the cross section, which is relatively small for example for the cross sections of large timber bridges. Figure 13 and Figure 14 show the moisture content at different material depths for an ice rink and a timber bridge according to the ambient climate measured at the timber structures.

Currently, only a constant service class is used for the design. As proposal, a differentiation of the service class over the cross section, as shown in Figure 15, could be used for the activation of existing load capacities (active zone = SC 3, passive zone = SC 2) and, therefore, increase the capacity of the structure, depending on its location and operational conditions. The question is how to define the size of the active zone. A theoretical analysis using the shrinkage swelling mass show that a difference greater than 1.5 M% is enough that the stress in the wood exceeds the tension strength perpendicular to the grain, as shown Table 4.

Table 4: Theoretical limits of the moisture content for the risk of fracture of the cross section

Material direction	Shrinkage/Swelling mass for Spruce	Modulus of Elasticity E [MPa]	Tension strength f_t [MPa]	Limit of moisture content
Longitudinal	α_L = 0.01 %/M%	10'000	80	> 80 M%
Radial	α_R = 0.19 %/M%	800	2.7	> 1.8 M%
Tangential	α_T = 0.39 %/M%	450	2.7	> 1.5 M%

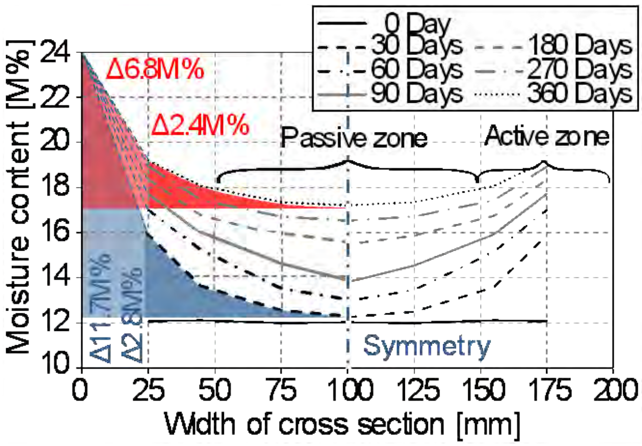

Figure 11: Experimental results of moisture distribution in radial direction for the adsorption process, 200/200/200 mm

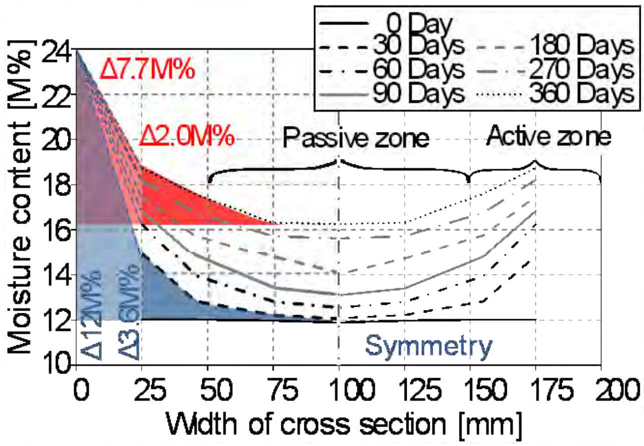

Figure 12: Experimental results of moisture distribution in tangential direction for the adsorption process, 200/200/200 mm

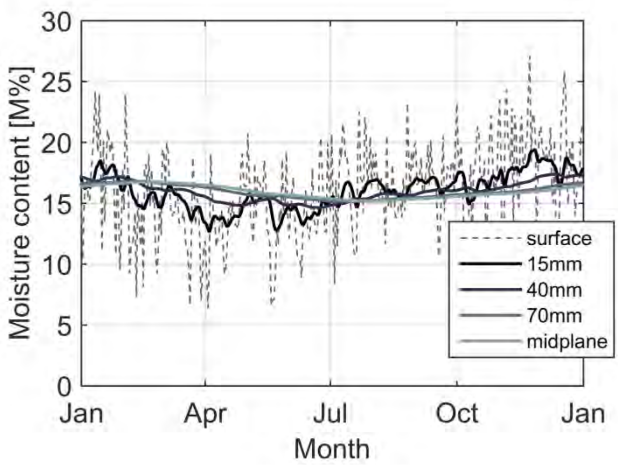

Figure 13: Seasonal moisture content developments on a bridge on a 200 mm wide beam

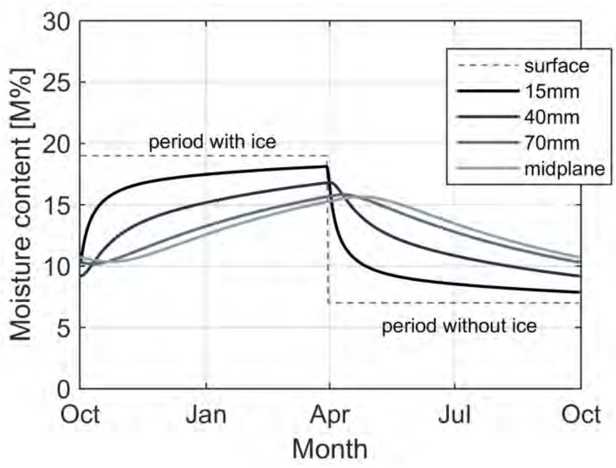

Figure 14: Seasonal moisture content developments in an ice rink in a 200 mm wide beam

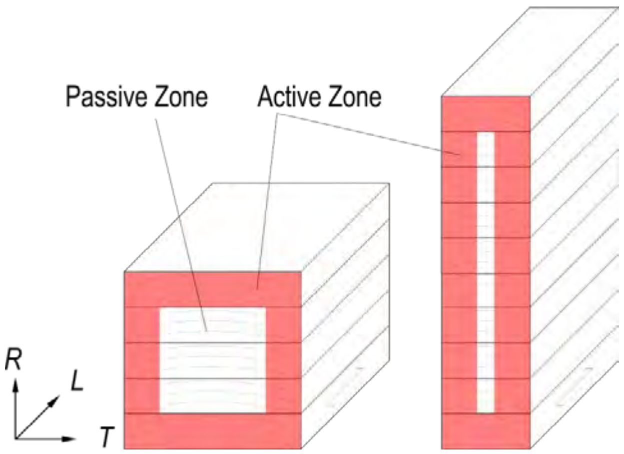

Figure 15: Differentiation of cross section in active and passive zone

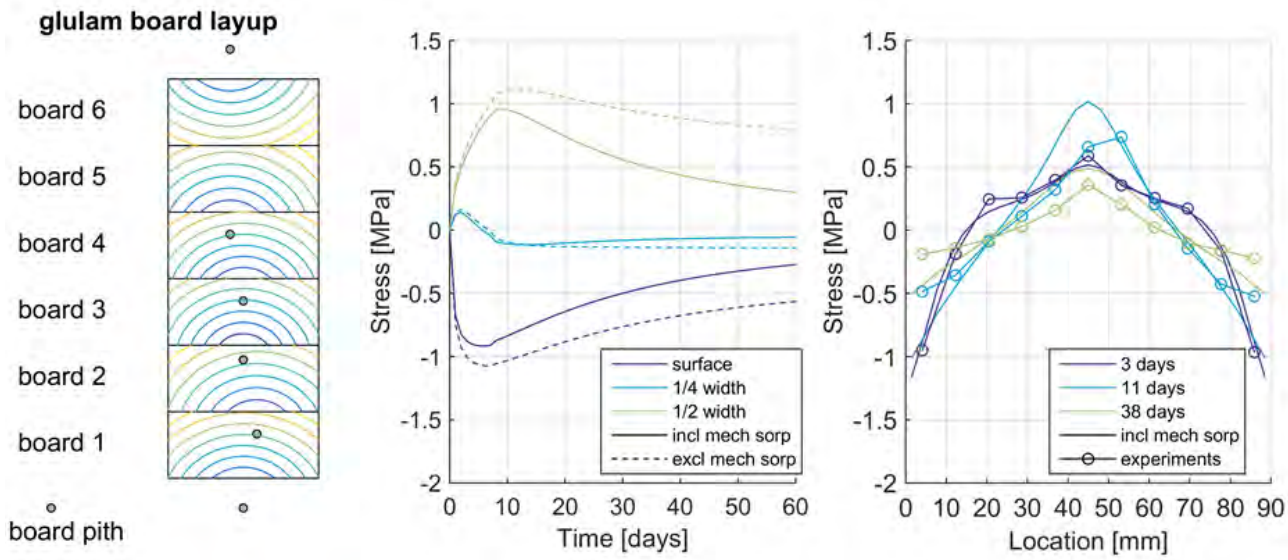

Figure 16: Development of moisture induced stresses in- or excluding time dependent effects in a six layered glulam beam tested in Jönsson (2004).

The real stress distribution is a complex process requiring time dependent parameters. Stress distribution depends on beam width, loading time, pith location of the individual boards, material anisotropy, etc. An example of this stress distribution, calculated as a linear (elastic) distribution and as a non-linear (time dependent) distribution is given in Figure 16. The figure shows the calculated and measured stress distribution in a 90 mm wide and 270 mm high beam, where the pith location is in the order of 1 cm to 2 cm from the individual board edge. The 1D-model explained by Häglund (2008) allows calculation of stress distribution as function of time and allows the comparison between in- and excluding mechano-sorptive stress developments. The time dependent calculations are compared to experimental values given in Jönsson (2004).

4 Recommendation and conclusions

4.1 Erection time period or maintenance/service times

Earlier simulations and validations have shown that the moisture diffusion can be approximated using numerical simulations. The physics behind these complex processes are roughly understood and numerical models should include more than only Fickian moisture diffusion. Although past laboratory experiments focused on a single transient increase and decrease or a cyclic moisture load on wooden beams, real structures operate in more complicated environmental conditions.

As the boards are generally stored, sawn, planed, and glued into glulam beams under moisture contents of approximately 12 M%, it is recommended to investigate the effects this has on the construction and operational events. Relevant questions could be if risk of internal damage due to moisture induced stresses is larger during building construction in winter or in summer periods. Another question could be if better ambient climate control around highly loaded timber elements is required.

This is partly worked out in an example in which various single transient moisture loads are applied to 5 beam sizes with a fixed aspect ratio and board pith location of 50 mm under the board edge, see Figure 17. The stress distribution per time step is calculated over an extended period of time, including time dependent effects. Alongside, an extra variation is made alternating the pith locations by 15 mm from the centreline, see Figure 18.

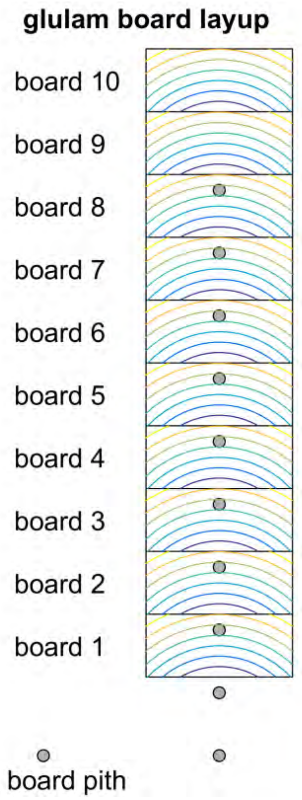

Figure 17: Glulam beam 100/400 mm with pith location on centerline and 50 mm under board edge

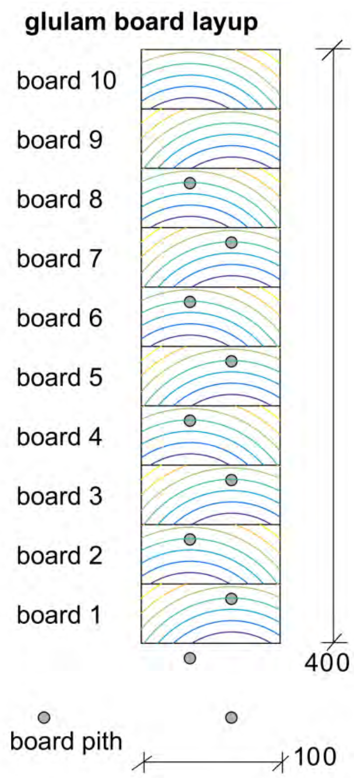

Figure 18: Glulam beam 100/400 mm with alternating pith location on +/- 15 mm from the centerline and 50 mm under board edge

To calculate the stress distribution, the 2D-FE model used earlier was extended and time dependent effects mentioned in Häglund (2008) were included as well. In this case, smaller elements would clearly result in higher accuracies, but calculation times would become longer too. Uncertainties here were expected to be acceptable, in the order maximum 5%, depending on the location, as explained by Schiere (2016).

Examples like Angst-Nicollier (2012) have already shown that the location of the pith with respect to the board edge is important in the development of the stresses during wetting and drying. This is mainly due to the material anisotropy that is high around the pith locations. Different beam widths were considered to see what the relation was between size and maximum stress level was, see Figure 19 (top left). The figure shows the tension stress levels as a function of single load amplitude change and beam width/height. It is observed that under constant loading, tension stress levels of well above 3 MPa can be achieved under extreme wetting conditions. The limit of 1.8 MPa as suggested by Blass and Schmidt (2001) was also drawn in this figure to see where measures are possibly needed to prevent crack generation in the centre of the glulam beam. This line shows that tension stress levels are exceeded at load variations above 9 M% on a 150/600 mm wide/high beam.

Figure 19 on the top right shows that stresses can be reduced more than 10 % by taking care of pith arrangement. Larger pith distances from the board edges will reduce

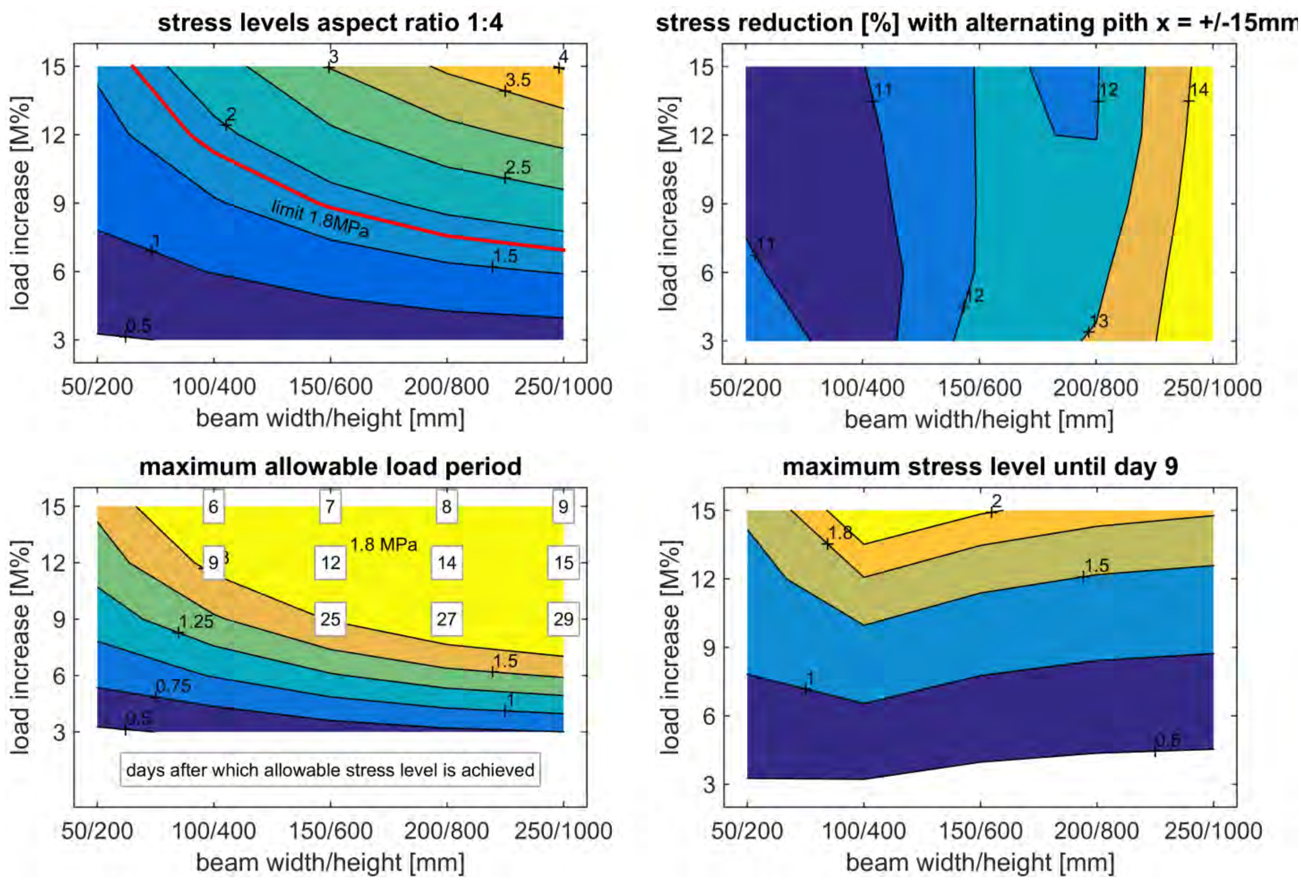

Figure 19: Stress levels, differences of alternating pith locations, maximum allowable loading time, and tension stress levels after 9 days

stress levels as well. Furthermore, larger distances from the beam centreline will also help to reduce the maximum tension stress levels.

Figure 19 (bottom left) further shows the maximum allowable loading time to maintain stress levels under the maximum allowable value of 1.8 MPa. If the maximum stress levels are not achieved at all, no time limit is shown. This figure is useful to have when a building needs to be erected and large changes in ambient climate are expected, or in defining allowable maintenance periods e. g. for ice rinks.

Finally, Figure 19 (bottom right) also shows the maximum stress values in the different beams under different loading up to day nine. This figure explains the maximum stress levels under different loads in case a maintenance event for the structure would last nine days. This could be useful for structures where climate can be controlled, such as a swimming pool perhaps or an indoor ice rink.

The possibility to perform simulations to calculate moisture induced stress developments is a useful tool. Design limits can be simulated and beam dimensions could be chosen upon accordingly, or extra measures could be taken. The possibility to include mechano-sorptive effects, which serves as a stress relaxation, increases the accuracy of the obtained stress levels.

4.2 Conclusion

The analysis of ambient climate data of different building types and timber structures allow a characterization according the building type to service classes. These results support the practical planning engineer and confirm the recommendations in the explanations to DIN1052:2004 by Blaß et al. (2004).

It was shown that the estimation of the moisture content over the cross section can be performed using numerical programs. Furthermore, the numerical simulation could successfully applied to a case study of a bridge and an ice rink. The experimental and numerical results reached to support the scientific as well as the practical engineers.

Finally, introduction of an active and passive zone in structures could enhance the load bearing capacity of structures. As shown through simulations, maximum moisture contents for the inner part of the cross section (passive zone) are below 20 M% and, therefore, belongs to service class 2 where higher modification factors could be applied.

Being able to calculate stress levels in glulam beams due to moisture loads is a useful tool to estimate the risk involving the generation of moisture induced stresses. It is shown that there is an influence of load amplitude and beam dimension, and that higher risks are found in larger beams. It was also confirmed that taking care of pith location in board choice and layup can help to reduce stress levels.

Acknowledgement

The research work was proudly supported by the Federal Office for the Environment (FOEN) and the industry partners Roth AG, Makiol and Wiederkehr, Tiefbauamt des Kanton Bern.

References

Angst-Nicollier V. (2012), Moisture induced stresses in glulam - effect of cross section geometry and screw reinforcement. PhD thesis, NTNU Trondheim, Norway, Doctoral Theses 2012:139.

Angst V. and Malo K. (2010), Moisture induced stresses perpendicular to the grain in glulam: a review and evaluation of the relative importance of models and parameters. Holzforschung, 64(5), p. 609–617

Blaß, HJ, Ehlbeck, J, Kreuzinger, H, Steck G (2004) Erläuterungen zu DIN 1052:2004-08, Entwurf, Berechnung und Bemessung von Holzbauwerken, DGfH, Germany.

Blaß, HJ, Schmidt, M (2001), Querzugfestichkeit von Vollholz und Brettschichtholz, Holz als Roh- und Werkstoff (58), p. 456-466.

Cruz, H, Custódio, J (2006): Durability and temperature effects on bond line, Presentation at COST Action FP 1101, Assessment, Reinforcement and Monitoring of Timber Structures, Trento, Italy.

Dietsch P, Gamper A, Merk M, and Winter S (2015): Monitoring building climate and timber moisture gradient in large-span timber structures, Journal of Civil Structural Health Monitoring 5, p. 153-165.

Dietsch P (2012): Einsatz und Berechnung von Schubverstärkungen für Brettschichtholzbauteile, doctoral thesis, TU München, Germany.

Droin-Josserand A, Taverdet J.M., and Vergnaud J.M. (1989), Modelling the process of moisture adsorption in three dimensions by wood samples of various shapes. Wood Science Technology (23), p. 259–271.

Eurocode 5 (2004): Design of timber structures - Part 1-1: General and rules for buildings. CEN. (EN 1995-1-1).

Franke B, Müller A, Franke S, Magniere N (2016): Langzeituntersuchung zu den Auswirkungen wechselnder Feuchtegradienten in blockverleimten Brettschichtholzträgern, Research Report, ISBN 978-3-9523787-7-9.

Franke B, Franke S, and Müller A (2015): Case studies: long-term monitoring of timber bridges, Journal of Civil Structural Health Monitoring 5, p. 195-202.

Gamper A, Dietsch P, Merk M, Winter S (2014) Gebäudeklima – Langzeitmessung zur Bestimmung der Auswirkungen auf Feuchtegradienten in Holzbauteilen, Research report, TU-München, Germany.

Häglund M (2008): Varying moisture content and eigen-stresses in timber elements. Wood Materials, Science Engineering, pp. 38–45.

Jönsson J (2004): Internal stresses in the cross-grain direction in glulam induced by climate variations, Holzforschung 58, pp. 154–159.

Jorge, L (2013): Environmental and Moisture Measurements, Presentation at COST Action FP 1101, Assessment, Reinforcement and Monitoring of Timber Structures, Trento, Italy.

Siau J.F. (1971), Flow in Wood, Syracuse University Press, Syracuse, New York, U.S.A., first edition.

Simpson W.T. (1973), Predicting equilibrium moisture content of wood by mathematical models, Wood and Fiber, 5(1), p. 41-49.

Schiere M (2016), Moisture diffusion and moisture induced stresses in glulam cross sections, Master Thesis, Bern University of Applied Sciences, Switzerland.

Discussion

The paper was presented by S Franke

K Crews commented that the work showed different elements in timber could have different service class. He recommended more effort would be needed to use this work. S Franke agreed.

P Dietsch commented that the type of building considered was important. He stated that the resistant based method used to monitor moisture content would not work in frozen timber. S Franke replied that this matter would have to be corrected and temperature of the member would need to be checked.

P Zarnani asked how to explain the high variation in the radial and tangential directions compared to the longitudinal direction. S Franke clarified about the location of the measurements in the specimens and influence of the glue line was not available in the tangential and radial directions so longitudinal direction has the highest transport.

M Augustin asked about the issue related to coating and painting. S Franke replied that in such case coating had no influence because they were applied for protection during transportation.

R Jockwer asked whether it would be possible that the active resistance zone migrated. S Franke replied it would be possible.

P Staple received clarification that the pith location was referenced to all laminates and through the length.

T Reynolds received clarification that the electrodes did not form a path for the moisture.

Tensile strength classes for hardwoods

Andriy Kovryga, TU München, Winzererstr. 45, 80797 München, Germany. Email: kovryga@hfm.tum.de

Peter Stapel, TU München, Germany

Jan Willem van de Kuilen, TU München, Germany & TU Delft Fac. of Civil Eng., Netherlands

Keywords: Structural timber, hardwoods, characteristic properties, EN 338, EN 384

1 Introduction

Generally, for structural timber the main properties are listed in a strength class system. In Europe EN 338 (2016) lists available strength class and their respective characteristic properties. Depending on the product application the bending or the tension properties are of main interest. For glulam lamellas, tension classes are preferred as through tension classes the mechanical properties of glulam can be better predicted. Also, machine grading allows for a better prediction of tensile properties compared to bending properties. So far, tension grades were regulated in EN 14081-4. Due to the increased demand on glulam products, the grades were recently analysed, and a tensile class table was introduced in EN 338 (2016). The new strength profiles are the preferred option for glulam production. The requirements for softwood glulam are regulated in EN 14080 (2013).

So far, no tension classes exist for hardwoods. The EN 338 lists for hardwood specimens only so-called “D” classes based on the bending strength. The other properties, like tension strength, are assigned by the default on the safe side using the equations listed in EN 384. For those classes, the ratio tension strength to bending strength is declared on the safe side 0.6. However as shown by Burger & Glos (1997) for higher quality timber higher ratio can be expected.

New tensile classes for hardwoods would allow utilising the properties of hardwoods more efficiently. Whereas the old European standards EN 1194 and EN 14080 (2005) did not regulate species, the most recent version of EN 14080 (2013) is restricted to softwoods only. This means that hardwood glulam producers in Europe face additional costs for obtaining approvals for their products.

In this paper material properties of structural sized medium-dense European hardwoods ash, beech, and maple are presented with regard to the tensile strength classes. Major characteristic properties containing tensile strength, tension modulus of elasticity, density, and their relationships, followed by the relationship between tensile strength and compression and bending strength are analysed. Also, perpendicular to the grain values are presented. A system of Tensile Strength Classes for medium dense European Hardwood is proposed.

2 Tensile strength class system

2.1 General on the strength classes

EN 338 is the European standard for the strength classes and the respective characteristic properties. The classes are defined either on bending or tension tests. Table 1 shows the tensile strength classes for the softwoods exemplarily.

In order to be assigned to a particular strength class, the characteristic properties are to be estimated in accordance with EN 384. EN 384 defines the requirements on the sampling procedure and the calculation of the property values. To assign a sample to class the major characteristic properties including 5th percentile of either tensile or bending strength, the mean static modulus of elasticity, and the 5th percentile of the density are used. If the characteristic properties match the required values for a particular class, the timber may be assigned to this class.

Other material properties are listed for each class in EN 338. Those properties are the bending strength for the tensile classes and the tensile strength for the bending classes, compression strength parallel to the grain direction and so on. The values for these material characteristic are deduced based on equations given in EN 384.

Table 1: Tensile strength classes (T-Classes) for softwoods listed in EN 338 (2016)

	Property	T11	T14	T18	T21	T24	T28	T30
Strength properties [N/mm²]	$f_{m,k}$	17.0	20.5	25.5	29.0	33.0	37.5	40.0
	$f_{t,0,k}$	11.0	14.0	18.0	21.0	24.0	28.0	30.0
	$f_{t,90,k}$	0.4	0.4	0.4	0.4	0.4	0.4	0.4
	$f_{c,0,k}$	18.0	21.0	23.0	25.0	27.0	29.0	30.0
	$f_{c,90,k}$	2.2	2.5	2.7	2.7	2.8	2.9	3.0
	$f_{v,k}$	3.4	4.0	4.0	4.0	4.0	4.0	4.0
Stiffness properties [kN/mm²]	$E_{t,0,mean}$	9.0	11.0	12.0	13.0	13.5	15.0	15.5
	$E_{t,0,k}$	6.0	7.4	8.0	8.7	9.0	10.1	10.4
	$E_{t,90,mean}$	0.3	0.4	0.4	0.4	0.5	0.5	0.5
	G_{mean}	0.6	0.7	0.8	0.8	0.8	0.9	1.0
Density [kg/m³]	ρ_k	320	350	380	390	400	420	430
	ρ_{mean}	380	420	460	470	480	500	520

2.2 Major characteristic properties of hardwoods tested in tension

The ratios between the major strength properties for the T-Classes are derived from the tensile test data for softwoods, mainly spruce and pine. The underlying relationship between the material properties was recently analysed by Denzler (2012), and Bacher & Krzosek (2014). However, EN 338 gives the possibility to assign timber with similar properties into the tensile strength classes.

Even though for hardwoods the assignment to the tensile strength classes is possible, the property relationships differ from softwoods. Firstly, for medium density European hardwoods higher tensile strength values than the ones listed for T-Classes are reported. Glos & Denzler (2006) and Solli (2004) reported, for the highest grade of the visually graded European beech and Scandinavian birch, characteristic strength values that exceed the requirements of the highest T-Class T30.

Second, the relationship between characteristic tensile strength ($f_{t,0,k}$) and characteristic tensile modulus of elasticity ($E_{t,0,mean}$) is different from softwood. For hardwoods with $f_{t,0,k}$ meeting the requirements of the highest T-Class T30, $E_{t,0,mean}$ values below the required 15500 N/mm² are reported by Glos & Denzler for beech (14700 N/mm²) and Solli (2004) for birch (15130 N/mm²). Aicher et al. (2014) reported for chestnut lamellas a characteristic tensile strength of 22.3 N/mm² and $E_{t,0,mean}$ values of 12500 N/mm².

The different ratio of characteristic strength to bending E for hardwoods and softwoods is displayed in the bending strength class system. Hardwood strength classes (D-Classes) indicate lower E values than softwood strength classes, for same bending strength. Green (2005) has pointed on the steeper relationship between bending strength and E for North American hardwoods compared to softwoods. On the contrary, Ravenshorst (2015) indicates a slightly less steep relationship, but in general a rather consistent ratio of all soft- and hardwood species.

However, even within hardwoods differences in material properties and MOR/MOE ratios are reported for species tested in bending. Whereas visually graded oak (Grade LS10+ in accordance with DIN 4074-5) from Germany tested in bending, match the requirements for MOE of D30 (Glos & Denzler 2006), the values for beech and ash exceed the requirements of D30 with 15900 N/mm² and 14000 N/mm² respectively.

2.3 Relationship between values parallel to the grain

The existing strength classes for hardwoods are defined on the bending test basis only. EN 384 gives for hardwoods the $f_{t,0,k}/f_{m,k}$ ratio of 0.6 with tension strength estimated on the safe side, similar to softwoods. However, as Burger & Glos (1997) and Steiger & Arnold (2009) have shown that a higher ratio may apply for higher grades of spruce. Recently, for softwood bending strength classes the higher $f_{t,0,k}/f_{m,k}$ ratio of 0.73 was introduced (EN 338 2016, FprEN 384 2015).

For the softwood T-Classes, the tension strength is determined by tests and bending strength is given from a ratio. In this case, bending strength is taken on the safe side by assuming higher $f_{t,0,k}/f_{m,k}$ ratio of 0.8 (Bacher & Krzosek 2014). To determine the characteristic bending strength of a sample tested in tension is used:

$$f_{m,k} = 3.66 + 1.213 \cdot f_{t,0,k} \tag{1}$$

In ASTMD 1990 (2000) standard, a tension/bending strength ratio of 0.83 for the tension test values is used.

For the compression strength parallel to the grain the following relationship is assumed in FprEN 384 (2015):

$$f_{c,0,k} = 4.3\, f_{m,k}^{\ 0.5} \tag{2}$$

For softwood T-Classes the Eq. 2 was adopted to Eq. 3 under the assumption of 0.6 ratio between $f_{m,k}$ and $f_{t,0,k}$ (Bacher & Krzosek 2014).

$$f_{c,0,k} = 5.5 \cdot f_{t,0,k}^{\ 0.5} \tag{3}$$

2.4 Characteristic properties perpendicular to the grain direction

EN 338 (2016) lists one characteristic tension strength value perpendicular to the grain for all strength classes, distinct for softwoods (0.4 N/mm²) and hardwoods (0.6 N/mm²). The characteristic compression strength perpendicular to the grain is given in FprEN 384 (2015) as a ratio of compression strength to the characteristic density, for both softwoods and hardwoods. For medium dense hardwoods ($\rho_k < 700$ kg/m³) the Eq. 3 is used, while the higher ratio $0.015 \cdot \rho_k$ is assumed for denser hardwoods.

$$f_{c,90,k} = 0.01 \cdot \rho_k \tag{4}$$

The modulus of elasticity perpendicular to the grain is given as a ratio to the E parallel to the grain by the following equation:

$$E_{90,mean} = E_{0,mean}/15 \tag{5}$$

The standard does not distinguish between $E_{t,90}$ and $E_{c,90}$.

3 Materials and methods

3.1 Destructive test data

In this paper, the properties of medium dense hardwoods ash (*Fraxinus excelsior*), European beech (*Fagus sylvatica*) and maple (*Acer sp.*) are analysed with regard to the tensile strength, modulus of elasticity in tension and density. The data sets of different projects on hardwoods carried out at the TU Munich over the past years are used. Table 2 gives an overview of the available data grouped by testing type, cross sections, and free testing length. All specimens, unless otherwise specified, have been tested according to EN 408 (2010) and EN 384 (2010).

Out of 1560 hardwoods tested in tension, 300 beech and 466 ash specimens were tested with the free testing length of 200 mm. The beech specimens were initially used to develop the models for the glulam out of beech by KIT (Blass et al. 2004). The ash specimens were tested in a project of the TU Munich on the mechanical properties of ash for the glulam production (van de Kuilen & Torno 2014). The intention of the small ash specimens was to make them compatible with the Karlsruhe model for glued laminated timber simulations. For those calculations, two test pieces - one for the tension test and the other for the compression test - were cut out of a single beech lamella. Both test pieces are included in the current analysis. The tension strength of the data tested over 200 mm was adjusted to the testing length of 9h using a separate factor for each strength value and is introduced in section 3.3.

To estimate the bending strength to tensile strength ratio, samples with similar cross-section are desirable. Therefore, out of the entire dataset, only one ash sample tested in bending with cross-sections 50×100 mm, 50×150 mm was selected for the determination of this ratio. Although the selected cross-section exceeds the dimensions of the lamellas typically used for the glulam, the 50 mm thickness matches the dimensions of unplaned boards with a final thickness of 36 mm.

Table 2: General overview of data sets, grouped by test type and species

<table>
<tr><th>Type of test</th><th>Species</th><th>Cross sections
b×h (×l) [mm]</th><th>Free length/test span</th><th>N</th></tr>
<tr><td rowspan="5">Tension parallel</td><td>ash</td><td>25×85, 30×100, 35×160,
50×100, 50×150</td><td>765 – 1440 mm (9h)</td><td>519</td></tr>
<tr><td>ash</td><td>25×110, 25×110, 30×150,
25×160, 35×160</td><td>200 mm
(1.2h – 1.8h)*</td><td>466</td></tr>
<tr><td>beech</td><td>30×120, 30×160</td><td>1080 – 1440 mm (9h)</td><td>218</td></tr>
<tr><td>beech</td><td>25×100, 35×100
25×150, 35×150</td><td>200 mm
(1.2h – 1.8h)*</td><td>300</td></tr>
<tr><td>maple</td><td>30×100</td><td>900 (9h)</td><td>57</td></tr>
<tr><td>Bending</td><td>ash</td><td>50×100,50×150</td><td>1800, 2700 mm (18h)</td><td>324</td></tr>
<tr><td rowspan="2">Compression parallel</td><td>ash</td><td>25×110, 25×110, 30×150,
25×160, 35×160</td><td>200 mm (5.7b – 8b)</td><td>457</td></tr>
<tr><td>beech</td><td>25×100, 35×100
25×150, 35×150</td><td>200 mm (5.7b – 8b)</td><td>383</td></tr>
<tr><td rowspan="2">Tension perpendicular</td><td>ash</td><td>45×180×70</td><td>180 mm (h)</td><td>56</td></tr>
<tr><td>beech</td><td>45×180×70</td><td>180 mm (h)</td><td>32</td></tr>
<tr><td rowspan="2">Compression perpendicular</td><td>ash</td><td>45×90×70</td><td>90 mm (h)</td><td>70</td></tr>
<tr><td>beech</td><td>45×90×70</td><td>90 mm (h)</td><td>54</td></tr>
</table>

* below the required free length of 9h

The compression and tensile test tested perpendicular to the grain originate from a project on the strength profiles of middle European hardwoods by Hunger & van de Kuilen (2015) and Westermayr (2014).

3.2 Non-destructive measurements and strength modelling

The non-destructive methods are used to assess timber quality, assign timber to the strength classes and analyse the profiles. Therefore, for all timber pieces both visual and machine grading parameters were measured. The dynamic modulus of elasticity was measured using longitudinal vibration method.

The visible grading criteria listed in the German visual grading standard DIN 4074-5 (2008), rules for boards, were measured. In overall the visual standards contains ten visual criteria to assign timber into the visual grading classes. In the current study, to assign specimens to the visual grades the criteria single knot and knot cluster and the presence of the pith were considered. The single knot (*SK*) is the size of the single knot related to the width and calculated using equation:

$$SK = \frac{\sum a_i}{2w} \tag{6}$$

where a_i is the size of the knot area i measured parallel to the edge of the board. The Knot Cluster (*KC*) is a multiple knot criterion that sums up all *SK* over a length of 150 mm. The edge knot criterion (the penetration depth of the knot) was not considered for the visual grading, as for the glulam lamellas the use of this criterion is optional.

To calculate ratios of tensile strength to both bending and compression strength, the best possible model for the tensile strength prediction was selected. The model included the *SK* – the best single predictor of the tensile strength - and E_{dyn} – the best predictor for the tensile E. Eq. 7 represents the created model.

$$IP\, f_t = a + b \cdot SK + c \cdot E_{dyn} \tag{7}$$

3.3 Adjusting the tensile strength to the free length of 9h

The tension strength of the specimens tested with the free length of 200 mm was adjusted to the free length of 9h using a separate factor for each strength value. Therefore, we assumed that the specimens tested over the free length of 200 mm if tested with the free length of 9h, would observe the same probability distribution the ash and beech specimens tested under the reference conditions. For the ash and beech specimens, the tensile strength was described using a log-normal distribution, as especially in the lower 40 % of the CDF this proved to be the best fit.

To generate a sample of tensile strength tested over the free length of 9h the inverse transformation method is used. This method allows transforming uniform deviates drawn from U (0, 1) into samples drawn from a specified distribution.

In the following $x \sim \ln N(\mu,\sigma^2)$ is the strength of the specimens tested with the free length 9h. The corresponding CDF is described using the Eq. 8:

$$F_x(x) = p \tag{8}$$

For the strength of the specimens (y) tested with the free length of 200 mm the CDF is described as follows:

$$F_y(y) = u \tag{9}$$

with probability $u \sim U(0,1)$.

By applying the inverse CDF to the probability u the sample with the tensile strength tested over 9h is generated:

$$F_x^{-1}(u) = x \tag{10}$$

The ratio $\frac{f_{t,9h,est}}{f_{t,200mm}}$ was calculated for each $f_{t,200mm}$. Figure 1 shows the estimated ratio dependent on tensile strength tested over 200 mm for ash and beech separately.

3.4 Data analysis

The aim of the current analysis is to create optimised profiles for the strength classes with the certain tensile strength to *E* ratio. To conduct the study, the specimens were grouped two times in equal sized groups of 100 specimens each; one time by the tensile *E* and one time by the tensile strength. An ideal grading machine able to determine with 100 % accuracy the tensile *E* in one case and tensile strength in the other case is assumed. The 5th percentile of the tensile strength and density of the grouped specimens are calculated using the ranking method. The calculated values of characteristic tensile strength ($f_{t,0,k}$), $E_{t,0,mean}$ and characteristic density are plotted against each other and compared to the values of T-Classes, listed in EN 338 (2016).

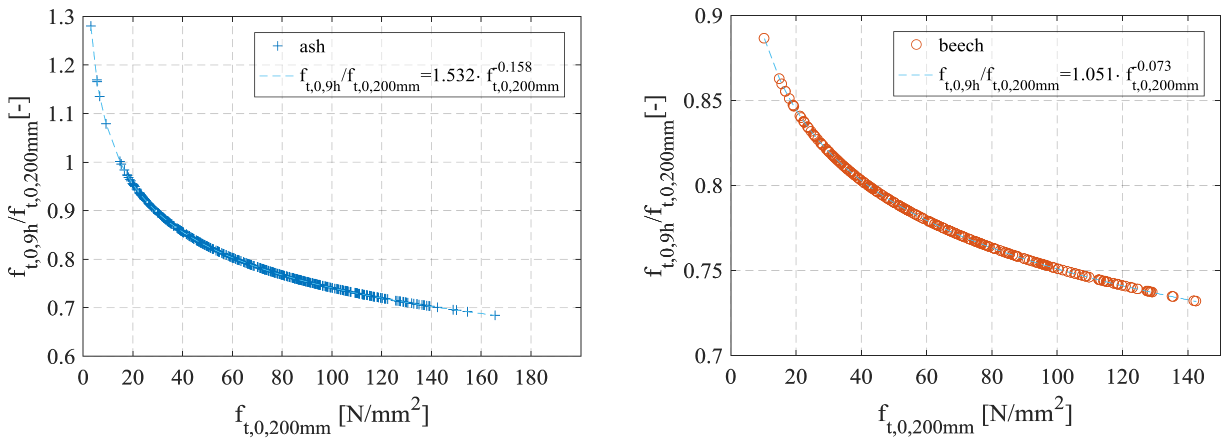

(a) (b)

Figure 1: Ratio of tensile strength tested over 9h to tensile strength tested over 200 mm as a function of tensile strength tested over 200 mm for (a) ash and (b) beech

Additionally, the material property profiles based on tension E and tensile strength are compared to the actual grading results. Therefore, beech, ash, and maple specimens were virtually strength graded. Visual grading was applied according to German visual grading standard DIN 4074-5 with visual grades LS10 and LS13. Machine grading was applied using the indicating property (*IP* f_t) calculated using the Eq. 7. Although the regression model is used here, the model parameters are comparable to the combined visual and machine strength grading introduced by Frese & Blass (2005). Whereas two predictors can compensate each other in the regression model, the combined visual and machine grading does not allow for such interactions by defining separate boundary values for both parameters. Currently, no machine capable to detect knots in hardwoods is industrially available.

The boundaries for the combined visual and machine strength prediction are determined for grading to a single class. The class boundaries were increased stepwise by 10 N/mm² of *IP* f_t and all specimens matching or exceeding those threshold values were assigned to the class. For each group of specimens, the relationship between the material properties has been determined.

The relationship between tension strength and compression strength, as well as tension strength and bending strength, is determined as grouped data. Therefore, first, the tension test data are arranged by the *IP* f_t into equal sized groups of 80 specimens each. In the next step, the compression strength and bending strength data are split using determined *IP* f_t boundaries.

4 Results and discussion

4.1 Tensile strength, tensile E parallel to the grain and density

First, the tensile strength to tensile *E* ratio is analysed in groups of 100 specimens with tensile *E* as indicating property. Compared to the tension classes specified in EN 338, the relationship between tensile strength and $E_{t,0,mean}$ for ash and beech is steeper (Figure 2a). Both species show lower $E_{t,0,mean}$ values compared to the required $E_{t,0,mean}$ of the T-Classes if the same characteristic strength is achieved.

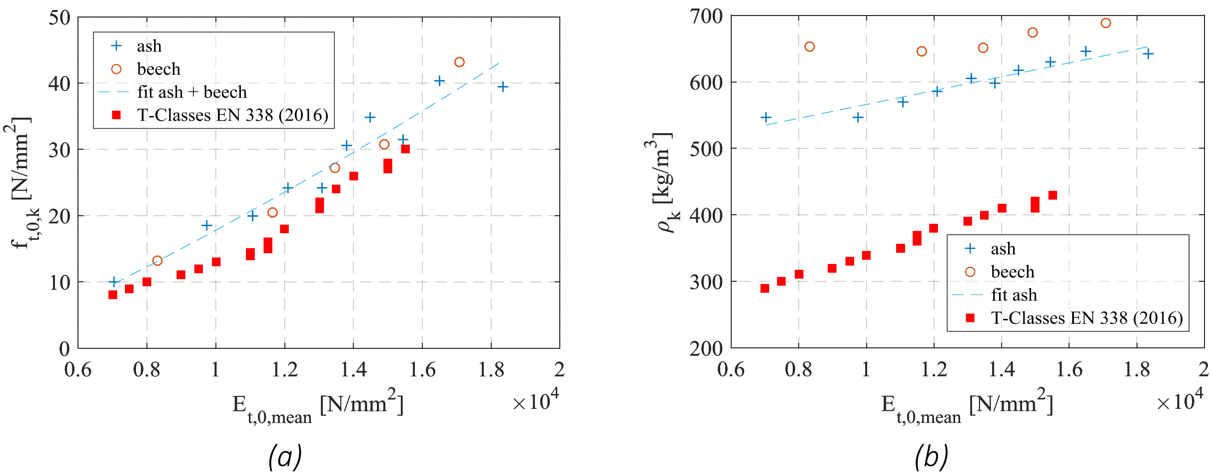

Figure 2: Relationship between (a) $E_{t,0,mean}$ and $f_{t,0,k}$ and (b) between $E_{t,0,mean}$ and ρ_k grouped by $E_{t,0}$

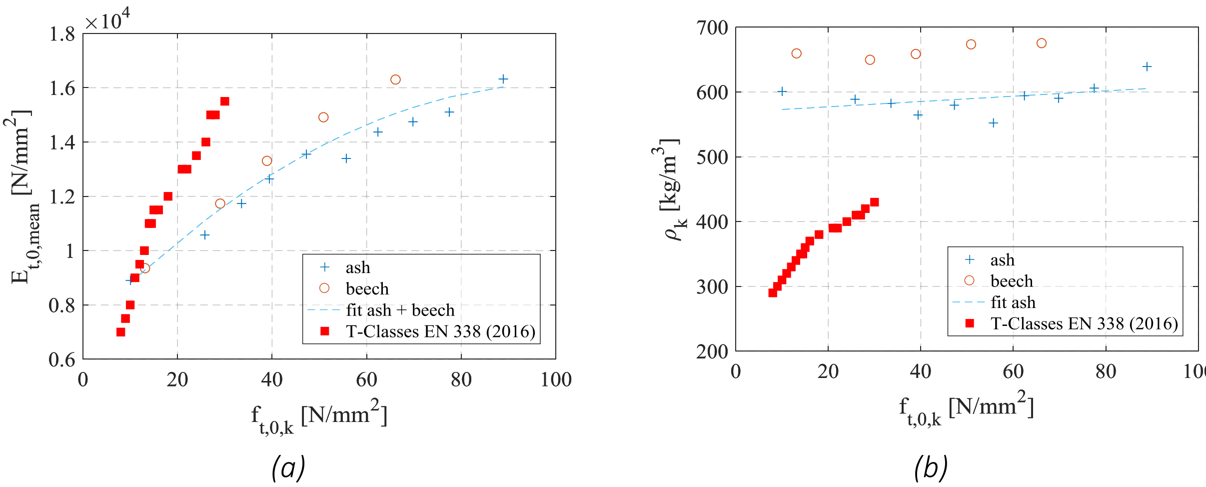

Figure 3: Relationship between (a) $E_{t,0,mean}$ and $f_{t,0,k}$ and (b) between $E_{t,0,mean}$ and ρ_k grouped by $f_{t,0}$

Figure 2b shows the relationship between the $E_{t,0,mean}$ and ρ_k. Both ash and beech show higher characteristic density compared to the values stated in EN 338 (2016). The density of ash is level lower compared to the beech. Therefore, the characteristic density should be increased at least to the values of ash, compared to the softwoods.

If the data are grouped with regard to the tensile strength, the property relationship differs more than that assumed in EN 338. Figure 3 illustrates the relationship between the material properties in this case. Compared to the T-Classes the slope of the line between the characteristic strength and tensile *E* is flatter. For the same characteristic strength as assumed for the T-Classes, lower *E* values are observable. For example, for the characteristic tensile strength of 30 N/mm², a tensile *E* of as little as 11700 N/mm² is obtained, compared to 15500 N/mm² listed for T30.

The relationship between density and tensile strength does not increase continuously. For ash, the density remains on the same level of 600 kg/m³ with some decreases down to 550 kg/m³.

For defining the class values the relationship between tensile *E* and strength should be considered, and, whether the strength or the *E* should be most important grading parameter for the hardwoods presented here.

4.2 The effect of grading on the major characteristic properties

For the deviation of strength class profiles, the material properties of both visually and combined visually - machine strength graded timber are analysed. Figure 4 illustrates $E_{t,0,mean}$ to $f_{t,0,k}$ and $E_{t,0,mean}$ to ρ_k for the visually graded hardwoods. $E_{t,0,mean}$ to $f_{t,0,k}$ does not match the ratios for the softwood T-Classes. If the samples are assigned to the T-Classes, the requirements on the $E_{t,0,mean}$ are not met in each case, making E the grade-limiting property. For LS10 timber with lower tensile strength, the difference between the tested $E_{t,0,mean}$ and required E is even higher.

The $E_{t,0,mean}$ to ρ_k ratio is, as expected, above the values for the T-Classes. Nevertheless, the ratio does not seem to depend on the visual grading procedure. For ash graded to LS13, the density is even lower compared to the specimens assigned to LS10. For beech specimens, the density increases only slightly between LS10 and LS13. These results comply with the fact that density of hardwoods cannot be estimated visually, for instance by growth ring width analysis. Therefore, a single density value for all strength classes, that visually graded hardwoods might be assigned to, is a possible solution.

For a combined visual and machine strength prediction, the relationship between tensile strength and tensile *E* is closer to the T-Classes. However, for the higher *E* values, the tensile strength increases with a higher slope. This increase is similar to the behaviour of tensile strength/tensile E ratio obtained for grouping on the tensile strength (Figure 3). As *IP* f_t predicts both tensile strength (R^2 = 56 %) and tensile E with a high accuracy (R^2 = 59 %), the tensile strength /tensile E ratio of the combined visual and machine grading is similar to the ratios derived on tension *E* and tension strength basis.

The characteristic density of the machine graded hardwoods increases with tensile *E*. The used *IP* f_t includes density as one of the inputs for the E_{dyn} calculation. Therefore, for the higher strength classes, feasible for the machine strength grading using the combined approach, an increase in density values should be allowed.

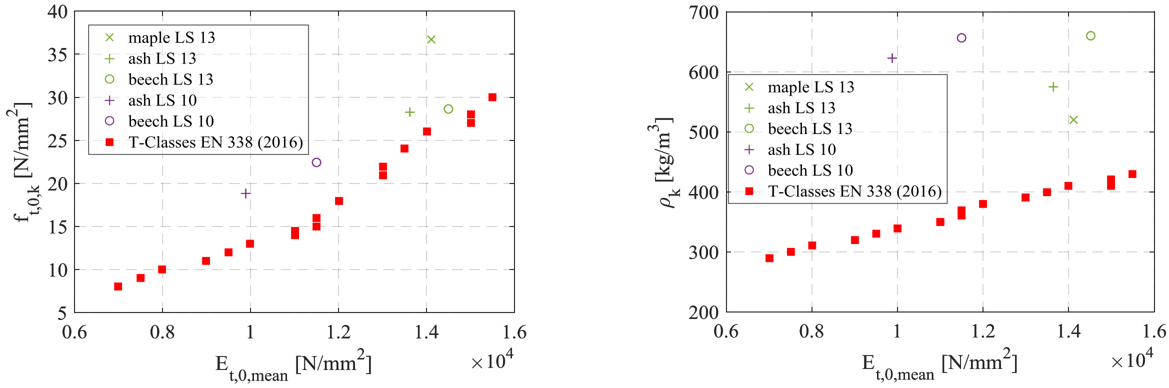

(a) *(b)*

Figure 4: Relationship between (a) $E_{t,0,mean}$ and $f_{t,0,k}$ and (b) between $E_{t,0,mean}$ and ρ_k for the visually graded timber

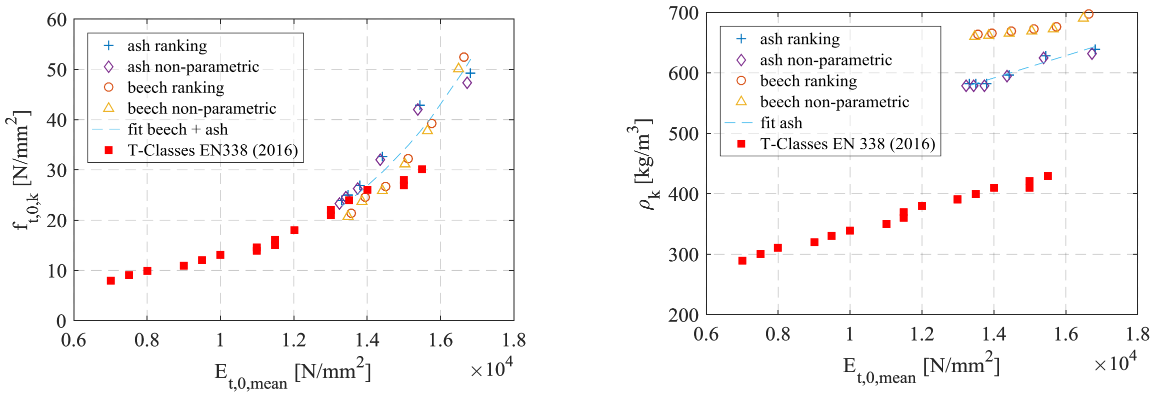

(a) *(b)*

Figure 5 Relationship between (a) $E_{t,0,mean}$ and $f_{t,0,k}$ and (b) between $E_{t,0,mean}$ and ρ_k for the combined visual and machine strength grading of hardwoods to a single class

4.3 Tension strength to bending strength ratio

In the current study, the tension to bending strength ratio was examined for ash specimens of equal dimensions tested in tension and in bending. Figure 6 shows the tension strength to bending strength ratio for the equal sized timber grouped by the IP f_t. The estimated ratio, shown in the figure, is higher than the one for the T-Classes (value equals 1.213). The underlying ratio is close to one of the D-Classes, determined on the safe side for the bending strength and not for the tension strength.

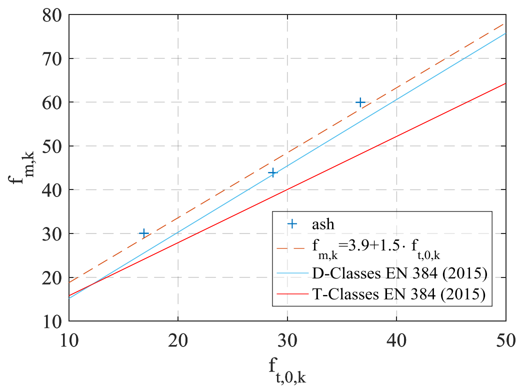

Figure 6: Relationship between tension and bending strength for data grouped by IP f_t

4.4 Tension strength to compression strength ratio

Figure 7 shows the ratio between tension and compression strength obtained for the combined beech and ash data. The estimated equation leads to higher compression strength values compared to the ones listed in EN338 (2016). For the higher strength classes, the fitted equation converges to the one for the softwood T-Classes. If the species are observed separately, both hardwood species tend to behave in a similar way, even though ash seems to have a slightly higher f_c/f_t ratio. For simplicity reasons, it is proposed to apply the equation for softwoods on medium dense hardwoods as well.

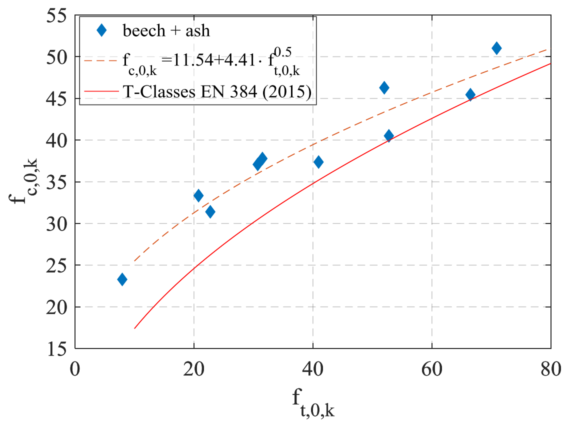

(a)

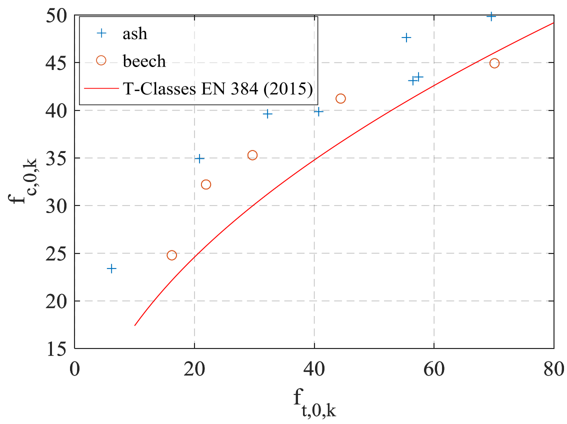

(b)

Figure 7: Relationship between characteristic tensile strength and compression strength for a) joint beech and ash data and b) beech and ash separately, grouped by IP f_t

4.5 Properties perpendicular to the grain direction

Figure 8 shows the relationship between density and both tension and compression strength perpendicular to the grain for ash and beech for the data of Hunger & van de Kuilen (2015) and Westermayr (2014). No correlation between tension strength and density, as well as between compression strength and density for a combination of two species could be found. Only for ash, a correlation of 0.462 between compression strength and density, can be reported. The density values for ash show wide variation if compared to the beech.

The missing correlation between the tensile strength perpendicular to the grain and density does not allow specifying a distinct value for each class. As a consequence, the same value for all classes is sufficient. For the present data, characteristic values for the ash and beech are 3.40 N/mm² and 3.48 N/mm² respectively and exceed the values for solid wood listed in EN 338. Therefore, for all medium dense hardwoods, a single value of 3.4 N/mm² is proposed.

The weak correlation between the density and compression strength does not allow making a significant conclusion on the relationship between these variables. By keeping in mind the low feasibility of visual grading to distinguish between different density levels, same characteristic strength value for the compression strength perpendicular to the grain is essential. For the data of Hunger & van de Kuilen (2015) the characteristic compression strength values are 6.67 N/mm² and 6.77 N/mm² for ash and beech respectively. The results are comparable to the values reported by Huebner (2013) on beech and ash glulam. For the standard, a single characteristic strength value for all classes - 6.6 N/mm² - is proposed.

For both compression and tensile test perpendicular to the grain, the ratio of $E_{90,mean}$ can be compared to the $E_{t,0,mean}$ values of ungraded timber. The ratio ranges from 14.65 to 16.0 for $E_{t,0,mean}$ to $E_{t,90,mean}$ and 12.4 to 13.8 for $E_{t,0,mean}$ to $E_{c,90,mean}$.

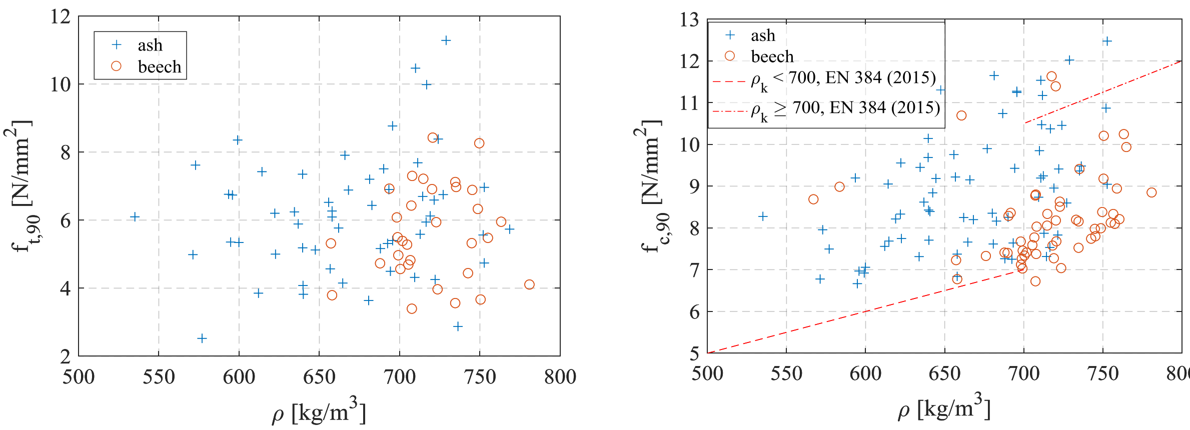

(a) (b)

Figure 8: Relationship between (a) $f_{t,90}$ and ρ and (b) $f_{c,90}$ and ρ

4.6 Proposal for tensile strength profiles for hardwoods

Based on the analysed relationships we propose tensile strength classes for hardwoods named DT-Classes, where “D” stands for hardwoods (“deciduous”) and “T” for tension. Table 3 lists a selection of new classes, which could be extended in both directions using the derived relationships. The tensile E to strength ratio is defined with regard to the tensile E. However, for the classes with a characteristic tensile strength above 30 N/mm² the $E_{t,0,mean}$ to $f_{t,0,k}$ ratio is defined using the combined visual and machine strength prediction. The prediction model integrates both $E_{t,0,mean}$ to $f_{t,0,k}$ ratios derived on the tensile E and tensile $f_{t,0}$ in the best way, by building an intermediate solution between both ratios. This is also a practical way as the design of glulam will be governed by both stiffness and strength. The resulting $f_{t,0,k}$ increases with a higher slope for characteristic strength above 30 N/mm², as illustrated in Figure 9.

Table 3: Proposed tensile strength classes for hardwoods (DT-Classes)

	Property	DT18	DT22	DT25	DT28	DT30	DT34	DT38
Strength properties [N/mm²]	$f_{m,k}$	31	37	41	46	48	55	61
	$f_{t,0,k}$	18	22	25	28	30	34	38
	$f_{c,0,k}$	30	32	34	35	36	37	39
	$f_{t,90,k}$	3.4	3.4	3.4	3.4	3.4	3.4	3.4
	$f_{c,90,k}$	6.6	6.6	6.6	6.6	6.6	6.6	6.6
Stiffness properties [kN/mm²]	$E_{0,mean}$	10	11.5	12.5	13.5	14	15	15.5
	$E_{90,mean}$	0.67	0.77	0.80	0.90	0.93	1.0	1.03
Density [kg/m³]	ρ_k	550	550	550	550	550	610	620

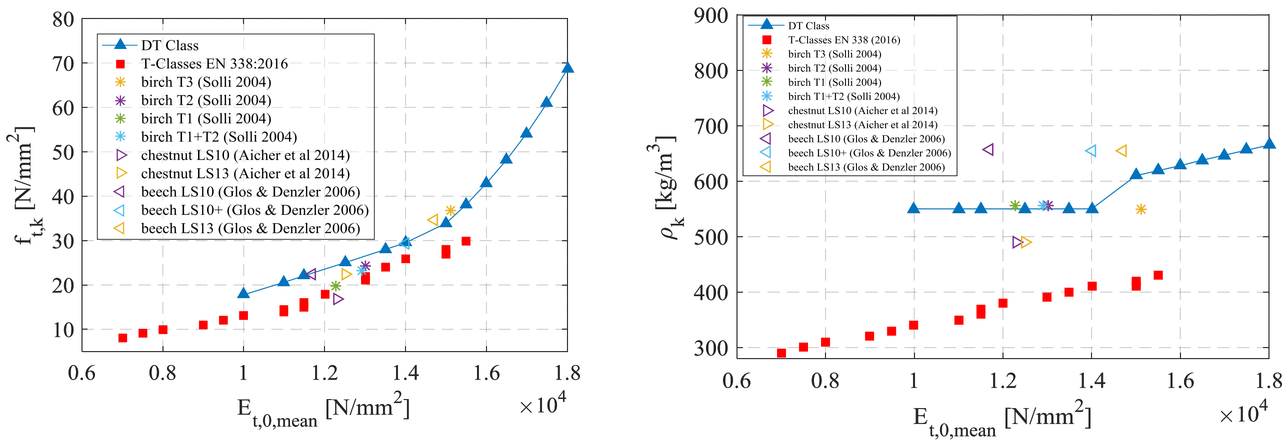

(a) (b)

Figure 9: Relationship between (a) $E_{t,0,mean}$ and $f_{t,0,k}$ and(b) between $E_{t,0,mean}$ and ρ_k for the proposed DT classes in comparison to the T-Classes for softwoods and literature values

If the proposed classes are compared to the literature values in Figure 9, for the highest visual grades of birch, beech and chestnut, the derived profiles match the properties better compared to the current T-Classes. Also higher classes than T30 are possible. However, if the existing system of T-Classes is used for hardwoods, $E_{t,0}$ becomes the grade-limiting property, whereas strength is generally fulfilled. In cases where one of the properties is generally fulfilled, the timber properties are utilised inefficiently.

The selected density profile follows the constant characteristic density value for the strength classes below DT30. Above DT30 the density increases, following the relationship for the machine graded timber. This reflects the fact that the visual grading is not able to distinguish between the different density values. The estimated profiles are shown in Figure 9b in comparison to the existing classes and literature values. For tensile strength below 30 N/mm², the defined threshold value for characteristic density matches the values for birch and beech. Whereas for the characteristic density of chestnut, the value is too high.

This also shows clearly, that determining a single density value for all medium-dense hardwood species might not be easy. The characteristic density of timber analysed here shows high variation and ranges between 520 kg/m³ for LS13 maple to 660 kg/m³ for LS13 beech. For LS13 maple tested in bending, characteristic values as high as 590 kg/m³ are reported by Glos & Torno (2008). For chestnut, a characteristic density of 510 kg/m³ was found by Nocetti et al. (2010). As a consequence, a separate declaration of the density for each combination of species and grade could be the best solution. Already Frühwald & Schickhofer (2005) suggested making density an optional, indicative parameter, rather than a mandatory one.

The relationships between the material properties are derived on medium dense hardwoods ash, beech and maple from Central Europe only. The relationship should be checked on other relevant hardwood specimens, such as oak.

5 Conclusion

In this paper, the material properties of the medium dense European hardwoods tested in tension have been analysed. The material property profiles are examined with regard to tensile E, tensile strength, visual grading and combined visual and machine strength prediction. This allows creating profiles fitting the properties of the selected hardwoods in the best way. These profiles are incorporated in the system of tensile strength classes for hardwoods (DT-Classes) presented here.

The presented DT-Classes are tailored to the material properties of hardwoods and allow, in comparison to the T-Classes an efficient utilisation of timber properties. If the T-Classes are used for hardwoods, the tensile E becomes a grade-limiting property.

Setting a characteristic density value remains a challenging task. High variation in density properties between the hardwoods and the fact that the density of hardwoods cannot be estimated using visual grading rules, compromise the use of density as one of the major characteristic properties for hardwoods. The possibility to declare density separately from the strength classes should be checked.

The ratio of bending strength to tension strength and compression strength to tension strength were checked for hardwoods. This ratio is higher than for softwood T-Classes. For the simplicity reasons the relationships listed in T-Classes for softwoods may also be used for hardwoods.

Based on the available data on compression and tension properties perpendicular to the grain, constant values for $f_{t,90,k}$ and $f_{c,90,k}$ all strength classes are proposed.

6 Acknowledgements

The research was supported by the Federal Ministry of Food and Agriculture of Germany (BMEL).

7 References

Aicher, S., Christian, Z., and Dill-Langer, G. (2014): Hardwood Glulams – Emerging timber products of superior mechanical properties. In: Proceedings of 13th World Conference on Timber Engineering (WCTE 2014), Quebec, Canada, 2014.

ASTMD 1990 (2000): Standard Practice for Establishing Allowable Properties for Visually-Graded Dimension Lumber from In-Grade Tests of Full-Size Specimens.

Bacher, M. and Krzosek, S. (2014): Bending and Tension Strength Classes in European Standards. Forestry and Wood Technology, 88: 14–22.

Blass, H. J., Denzler, J. K., Frese, M., Glos, P. and Linsenmann, P. (2004): Bending strength of beech glulam. Universitätsverlag Karlsruhe. (only available in German)

Burger, N. and Glos, P (1997): Verhältnis von Zug- zu Biegefestigkeit bei Vollholz. Holz als Roh- und Werkstoff, 56 (6): 345–350. (only available in German).

Denzler, J. K. (2012): Harmonised Tensile Strength Classes. Paper 45-5-1. In: Proceedings of the 45th Meeting, CIB-W18, Växjö, Sweden, 2012.

DIN 4074-5 (2008): Strength grading of wood - Part 5: Sawn hardwood.

EN 14080 (2005): Timber structures. Glued laminated timber and glued solid timber. Requirements.

EN 14080 (2013): Timber structures. Glued laminated timber and glued solid timber. Requirements.

EN 338 (2016): Structural timber – Strength classes.

FprEN 384 (2015): Structural timber - Determination of characteristic values of mechanical properties and density.

Frese, M. and Blass, H. J. (2005): Beech glulam strength classes. Paper 38-6-2. In: Proc. of the 38th Meeting, CIB-W-18. Karlsruhe, Germany, 2005.

Frühwald, K. and Schickhofer, G. (2005): Strength grading of hardwoods. In: 14th International Symposium on Nondestructive testing of wood, 198–210.

Glos, P. and Denzler, J. K. (2006): Allocation of Central European Hardwoods into EN 1912. Paper 39-6-1. In: Proc. of the 39th Meeting, CIB-W18, Florence, Italy, 2006.

Glos, P. and Torno, S. (2008): Allocation of domestic maple, ash and poplar species into the European Standard EN 1912. Report Nr. 06517 B, Holzforschung München, Technische Universität München. (only available in German)

Green, D. W. (2005): Grading and Properties of Hardwood Structural Lumber. Chapter 4. In: Ross, R. J. and Erickson J. R. (eds): Undervalued hardwoods for engineered materials and components. Forest Products Society, Madison, 31–55.

Huebner, U. (2013): Mechanische Kenngrößen von Buchen-, Eschen- und Robinienholz für lastabtragende Bauteile. Dissertation. Technische Universität Graz. (only available in German)

Hunger, F. and van de Kuilen, J.-W. G. (2015): Strength profiles of middle European hardwoods. Report Nr. 13508/ "X40”. Holzforschung München, Technische Universität München. (only available in German)

Nocetti, M., Bacher, M., Brunetti, M., Crivellaro, A. and van de Kuilen, J.-W. G. (2010): Machine grading of Italian structural timber: preliminary results on different wood species. Proc. of 11th World Conference on Timber Engineering (WCTE 2010), Riva del Garda, Italy, 2010.

Ravenshorst, G. J. P. (2015): Species independent strength grading of structural timber. PhD thesis. Technische Universiteit Delft, Delft.

Steiger, R. and Arnold, M. (2009): Strength grading of Norway spruce structural timber: Revisiting property relationships used in EN 338 classification system. Wood Sci Technol, 43 (3): 259–278.

van de Kuilen, J.-W. G. and Torno, S. (2014): Material properties of ash for application in glulam. Report Nr. 11508. Holzforschung München, Technische Universität München. (only available in German)

Westermayr, M. (2014): Tensile strength of ash and beech tested perpendicular to the grain. Determining material properties according to EN 408:2010. Bachelor thesis. Holzforschung München, Technische Universität München. (only available in German)

Discussion

The paper was presented by A Kovryga

K Crews commented that no finger joint material was evaluated and in Australia the limiting factor was finger joints with hardwood with delamination and gluing issues. He also commented that in slide 13 there was significant extrapolation and suggested to remove the extrapolation. A Kovryga replied that it was the real data.

G Fink commented that although the values were quite high they could be even higher. He questioned whether testing according to EN 408 was appropriate. A Kovryga agreed as the shorter test span might not be appropriate in terms of location of the weakest parts in the test zone.

K Ranasinghe received clarification that the single knot criterion was not based on UK standards and shear strength had not been analysed. He commented that it would make more sense to declare characteristic density according to species. There were discussions that the tensile strength perpendicular to grain was very high and it was decided to lower the value for design to discourage its use.

A Frangi asked what the coefficient of variation was. A Kovryga replied that the information was in the database.

K Crews commented that one should examine whether too many groups were examined.

F Lam commented that information about yield would be important. A Kovryga replied that each class considered 100 data points and the approach could not provide yield and such information would be obtained in another study on grading.

Simplified method to determine the torsional moment due to lateral torsional buckling

Hofmann, Reiner; formerly University of Stuttgart, Institute of Structural Design

Prof. Dr.-Ing. Kuhlmann, Ulrike; University of Stuttgart, Institute of Structural Design

Keywords: glued laminated timber girders, lateral torsional buckling, imperfections, torsional moment, horizontal bracings

1 Introduction

Glued laminated girders are produced in a variety of types and shapes. Often rather slender girders with wide spans are built. Due to the wide span, a simple verification of direct stresses due to bending and shear stresses caused by shear force does not suffice for the ultimate limit state. Imperfections of the system may generate second order theory effects. These effects increase more than proportionally with the span of the girders. As such slender girders may fail by lateral torsional buckling, the stability analysis of such girders is of high relevance. The usual procedure to verify the lateral torsional stability only refers to the bending moment, see Equation (1) according to *EN 1995-1-1:2004 (2004)*, sec. 6.3.3 and does not consider the torsional moment which is resulting from the bending moment M_d due to effects of second order theory.

$$(M_d{}^{I} / W_y) / (k_{crit} \cdot f_{m,d}) \leq 1{,}0 \tag{1}$$

In order to define the influence of the torsional moment on the shear stresses of glued laminated timber girders at the end support a software has been developed to perform numerical simulations by solving the differential equations, which describe lateral torsional buckling of glued laminated timber girders based on second order theory. This numerical model also takes into account the single supports at the upper chord, which are typical for wide span girders as roof beams with horizontal bracings in order to reduce the relative slenderness of the girder. The results of these investigations are compared to the simplified rule given in *DIN EN 1995-1-1/NA:2010-12 (2010)* for the torsional moment $M_{tor,d}$ as a consequence of the bending moment M_d due to restraint for lateral torsional buckling, see the following equation:

$$M_{tor,d} = M_d / 80 \qquad (2)$$

2 Lateral torsional buckling according to second order theory

A system of three coupled differential equations (Equation (3) to Equation (5)) mathematically describes the lateral torsional buckling of a girder under pure bending, see *Petersen (1980), Roik et al. (1972).*

$$E \cdot I_y \cdot w_{el}^{IV} = 0 \qquad (3)$$

$$E \cdot I_z \cdot v_{el}^{IV} + (M_{yq} \cdot \vartheta_{ges})^{II} = 0 \qquad (4)$$

$$G \cdot I_T \cdot \vartheta_{el}^{II} - E \cdot I_\omega \cdot \vartheta_{el}^{IV} - M_{yq} \cdot \vartheta_{ges}^{II} = 0 \qquad (5)$$

The system of coupled differential equations results from a static equilibrium of a girder with imperfections supported at the ends by effective lateral and torsional restraints. The derivation is based on a simple symmetric cross section, linear-elastic behaviour of material and small deformations. An analytic solution of the system of differential equations is given only for a small number of simple load cases and boundary conditions. The developed software is based on Equation (3) to Equation (5) and solves the bending-torsional problem according to second order theory using the Method of Finite Differences.

3 Basic principles and parameters of the numerical studies

3.1 Situation

In practice, typical girder shapes are parallel-chorded, saddle roof or fish-bellied. Due to manufacturing, the width b is mostly limited to 22 cm and the height h to 200 cm. The span varies between l = 10 and 35 m. The height depends on the span and should amount between l/17 and l/16 according to *Cyron & Sengler (1985)*. As a consequence of these parameters, usually a number of horizontal supports at the upper chord are necessary in order to limit the effective length l_{ef} and the relative slenderness $\boldsymbol{\lambda}_{rel,m}$ and thereby reduce the effects of second order theory.

3.2 Approach of imperfections

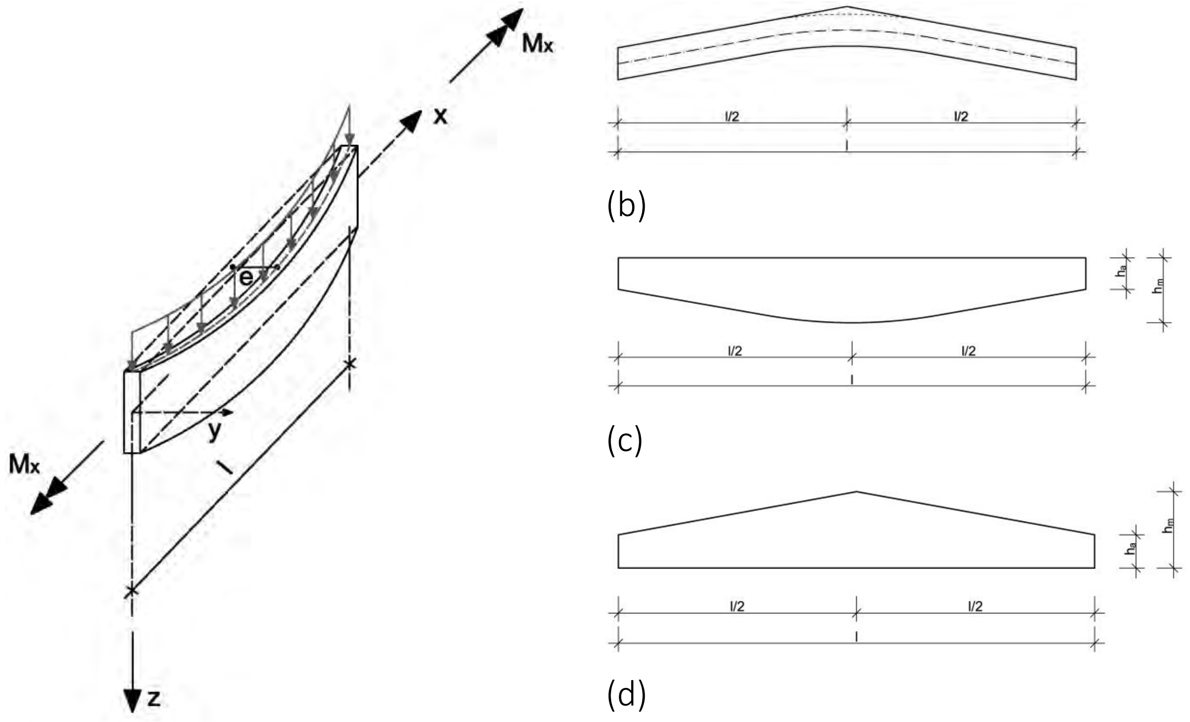

(a)

Figure 3.1. Girder under lateral torsional buckling with constant loading (a) girder with parallel chords and imperfection, (b) Girder with parallel chords and raised lower chord (c) fish-bellied girder (d) saddle roof girder

For calculations according to second order theory, the effects of imperfections have to be taken into account. The German National Annex *DIN EN 1995-1-1/NA:2010-12 (2010)* assumes an eccentricity *e* according to equation (6), see Figure 3.1a)

$$e \leq 0.0025 \cdot l \qquad (6)$$

This should be applied to the girder with an initial sinusoidal curvature between the supports of the structure (scs), acc. to Figure 3.2a).

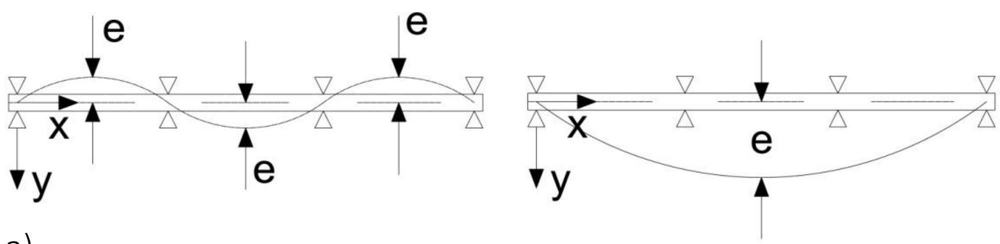

a) b)

Figure 3.2. Top view on a girder with discrete horizontal supports at the upper chord with imperfections of a) sinusoidal curvature between the supports (sds) b) sinusoidal curvature between the end supports(sces).

In general, the imperfections should be applied in the way that leads to the most unfavourable stress distribution in the girder. That is why another initial sinusoidal curvature between the end supports (sces) of the girder according to Figure 3.2b) has also been investigated.

3.3 Considering deflection of horizontal bracings

The imperfect single span girder with rigid discrete horizontal supports is mostly the exceptional case in practice. Very often, the stiffening of wide span girders is realized by horizontal bracings. The horizontal deflection of these horizontal bracings due to external load and lateral load is limited to $l/500$ according to *EN 1995-1-1:2004 (2004), sec. 9.2.5.2.* This minimal demand on the constructive execution of horizontal bracings is implemented as an additional imperfection of the girder, see Figure 3.3, in the computer aided calculation of the deformations and internal forces according to second order theory. With this approach the most unfavourable torsional moments in the cross section at the end supports can be calculated.

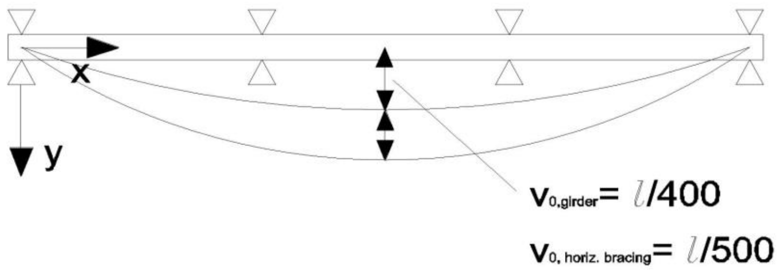

Figure 3.3. Top view on a girder with discrete horizontal supports at the upper chord and imperfections with sinusoidal curvature between the end supports and the deflection due to the horizontal bracing.

The construction detailing of the horizontal bracings and their connection at the end support may cause additional stresses, which are not regarded in the approach presented, see Figure 3.4 and 3.5. In case of a fixation ahead of the forked end support, see Figure 3.4, an additional torsional moment occurs. The verification of these constructions should not neglect these additional stresses.

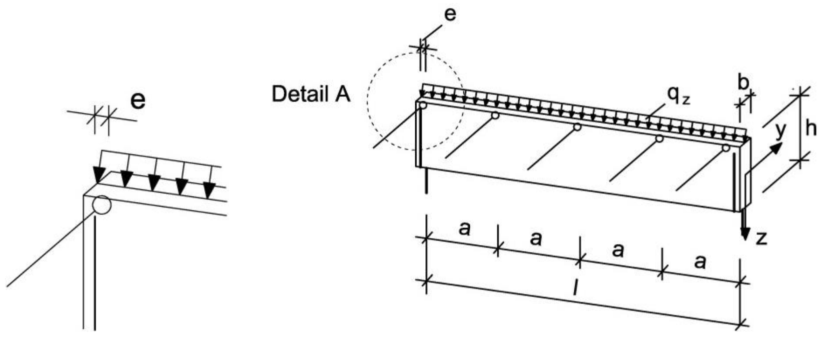

Figure 3.4. Girder under lateral torsional buckling with purlins connected to the girder with the distance a and eaves purlins with an eccentric connection e ahead of the forked end supports.

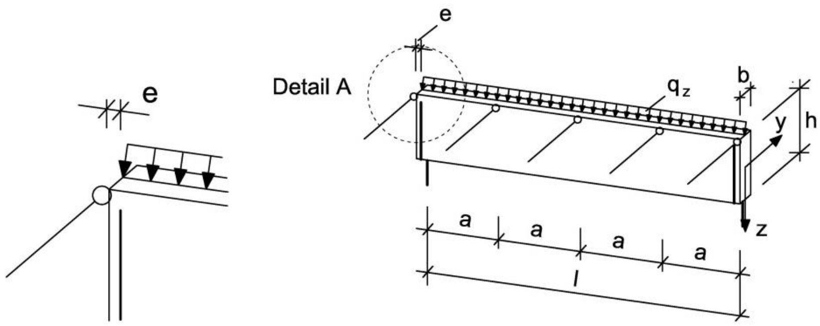

Figure 3.5. Girder under lateral torsional buckling with purlins connected to the girder with the distance a and eaves purlins with an eccentric connection e behind the forked end supports.

The ideal case is the girder under lateral torsional buckling with purlins connected to the girder with the distance *a* and eaves purlins with a direct connection to the forked end supports, as shown in Figure 3.6.

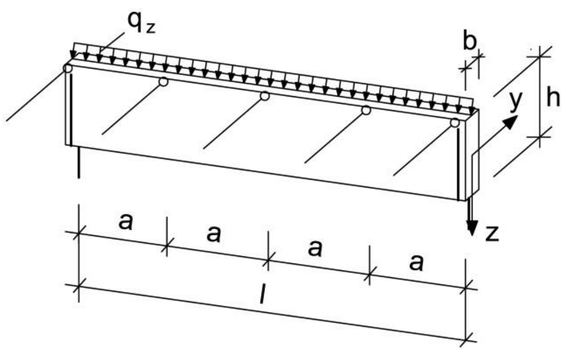

Figure 3.6. Girder under lateral torsional buckling with purlins connected to the girder with the distance a and eaves purlins with an direct connection to the forked end supports.

Due to the direct introduction of the horizontal forces out of the horizontal bracing into the forked end support, an additional torsional moment near the end support cannot occur. In case of a fixation at the compression chord, according to Figure 3.7 the lever arm $z_a = 0$.

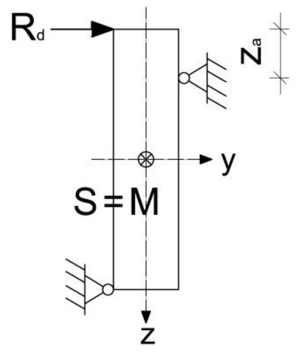

Figure 3.7. Schematic view on the horizontal supports of eaves purlins at the upper chord of a girder under lateral torsional buckling.

3.4 Influence of timber strength

The material properties of the investigated girder also are relevant. In order to calculate the deformations and internal forces due to second order theory, the main properties of material must be given, stiffness depending on the modulus of elasticity $E_{0,05}$ and shear modulus $G_{0,05}$. For the further investigations, the properties of material according to *DIN 1052:2008-12* have been considered for the calculations. The verification of the stresses according to second order theory have been conducted according to *DIN EN 1995-1-1:2010-12* and *DIN EN 1995-1-1/NA:2010-12*. Figure 3.8 shows the factor k_{crit}, which takes into account the reduced bending strength due to lateral torsional buckling dependent on the relative slenderness for bending. The relative slenderness $\lambda_{rel,m}$ for a solid rectangular cross section is calculated to according to equation (7) and (8)

$$\lambda_{rel,m} = (f_{m,k} / \sigma_{m,crit})^{0,5} \quad (7)$$

$$\sigma_{m,crit} = \pi \cdot (E_{0,05} \cdot I_z \cdot G_{0,05} \cdot I_T)^{0,5} / (l_{ef} \cdot W_y) \quad (8)$$

Figure 3.8 shows that the factor k_{crit} does not depend on the strength of timber, so the further investigations can be based on a single class of strength.

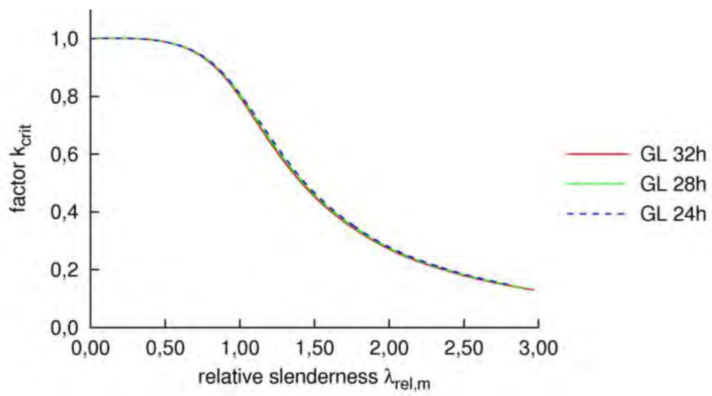

Figure 3.8. Comparison of glued laminated single span girders (h/b = 112/16) built of glulam with varying strength classes according to EN 14080:2013-09 with uniformly distributed load at the upper chord q_{zOG} and a determination of the critical bending stress according to Equation (8).

3.5 Shear strength and modulus of shear of glued laminated timber

The shear strength of glued laminated timber is decisive for the analysis of the torsional moment in lateral torsional stability analysis. *Möhler & Hemmer (1977)* performed a considerable number of experimental series on timber and glued laminated timber girders. For a feasible calculation of the shear stress due to torsion, an isotropic approach for the anisotropic timber has been chosen. The 5%-fractile of torsional strength of square cross section is specified to $f_{tor,k}$ = 3.48 N/mm² for glued laminated timber according to the experiments. The shape of the cross section causes an increase of the torsional resistance of rectangular cross section $h/b \geq 4$, according to *Möhler & Hemmer (1977)* depending on the shape of cross section a shape factor is determined to 1.2. The shear stress due to torsion may be verified with

$$(\tau_{tor,d} / 1.2 \cdot f_{v,d}) \leq 1 \quad (9)$$

which is quite similar to the current verification in *EN 1995-1-1:2004 (2004)*

$$(\tau_{tor,d} / k_{shape} \cdot f_{v,d}) \leq 1 \quad (10)$$

$$\text{with } k_{shape} = \min(1 + 0.15 \cdot h/b;\ 1.3) \quad (11)$$

The shear strength due to the shear force has been investigated in several research projects, see *Glos & Denzler (2004), Schickhofer (2001), Brandner et al. (2007), Klapp & Brüninghoff (2005)*. The characteristic shear strength is determined to

$$f_{v,k} = (h_0 \cdot l_0 / (h \cdot l))^{0.09} \cdot f_{v,k,0} \quad (12)$$

with h_0 = 600 mm and l_0 = 6000 mm

$$f_{tor,k} = 3.5 \text{ N/mm}^2 \quad (13)$$

$$f_{v,k,0} = 2.5 \text{ N/mm}^2 \quad (14)$$

For the following numerical studies shear stresses are verified by

$$(\tau_{tor,d} / (k_{shape} \cdot f_{tor,d})) + (\tau_{y,d} / f_{v,d})^2 + (\tau_{z,d} / f_{v,d})^2 \leq 1 \quad (15)$$

Aside of the shear strength the modulus of shear G and its approach for numerical calculation of deflections and internal forces is decisive for the results. The modulus of shear in timber has been subject of several research projects in the past. Based on *Möhler (1977)* and *Görlacher & Kürth (1994)*, in *Brandner et al. (2007)* a constant value of the shear modulus of $G_{g,mean}$ = 650 N/mm² for glued laminated timber has been derived and is taken into account for the following numerical studies.

4 Results of numerical studies

4.1 Overview

In order to allow for a stability verification according to the equivalent length method without calculating the internal forces according to full 3D second order theory, the results of the numerical studies were analysed and a simplified approach for the torsional moment of the three-dimensional problem of lateral torsional buckling has been derived. The simplified design method also takes into account the effects of horizontal bracings. The internal forces may still be calculated according to first order theory for the stability verification according to the equivalent length method. All the numerical results for the torsional moments in the cross section at the end support in this study depend on the uniformly distributed load q_{zOG} at the upper chord, the span of the girder l, the width b and height h of cross section.

4.2 Straight parallel-chorded glued laminated girders and parallel-chorded girders with a raised bottom chord

The sinusoidal curvature of imperfection between the end supports (see Figure 3.2b)) leads to a higher utilization of shear due to torsional moment in the cross section at the end support than the sinusoidal curvature of imperfection between the supports (see Figure 3.2a)), as shown in *Kuhlmann & Hofmann (2013)*. The influence of the number of horizontal supports of the compression chord in addition to the end supports on the torsional moment at the support due to lateral torsional buckling is quite small. Therefore, the results of the studies of girders with three additional horizontal supports of the compression chord are exemplarily shown in the following. It is assumed that the verification of direct stresses is decisive for the design of the girder. The shear stress $\tau_{y,d}$ due to external load q_{zOG} is very small, so that equation (15) may be reduced to equation (16):

$$(\tau_{tor,d} / (k_{shape} \cdot f_{tor,d})) + (\tau_{z,d} / f_{v,d})^2 \leq 1 \qquad (16)$$

For the further derivation the shear stress due to torsion according to equation (17) may be calculated based on the torsional moment $M_{tor,d}$ due to lateral torsional buckling of a girder with rectangular cross section according to equation (18)

$$\tau_{tor,d} = (3 \cdot \eta_2 \cdot M_{tor,d}) / (h \cdot b^2) \qquad (17)$$

with

η_2 according to Table 1

$M_{tor,d}$ according to equation (18)

h and b as geometrical height and width of section at the point of maximum height

Table 1. Coefficient for the calculation of the torsional moment on a rectangular cross section η_2 according to Szabo (2001)

h/b	**1**	**2**	**3**	**4**	**5**	**6**	**7**	**8**	**9**	**10**
η_2	1,609	1,356	1,247	1,183	1,144	1,117	1,099	1,086	1,075	1,055

The torsional moment due to lateral torsional buckling at the forked end support may be calculated according to equation (18)

$$M_{tor,d} = (k_{tor} \cdot h \cdot b^2 \cdot k_{shape} \cdot f_{tor,d}) / \eta_2 \qquad (18)$$

with

k_{shape} according to equation (11)

$f_{tor,k}$ according to equation (13)

The factor k_{tor} is based on the upper limit value for a certain girder constellation in the numerical studies of *Kuhlmann & Hofmann (2013).* The factor k_{tor} depends on the form of the girder, the relation of height h to width b of the girder at the point of maximum height. The utilization of shear due to torsional moment in the cross section at the end supports of a single span girder with parallel chords and rigid horizontal supports and of single span girders with parallel chords and raised lower chord and rigid horizontal supports does not exceed 12% in the numerical calculations, see Figure 4.1 and Figure 4.2. In this case the factor k_{tor} amounts to a maximum of 0.04, see equation (19)

$$k_{tor} = 0.04 \qquad (19)$$

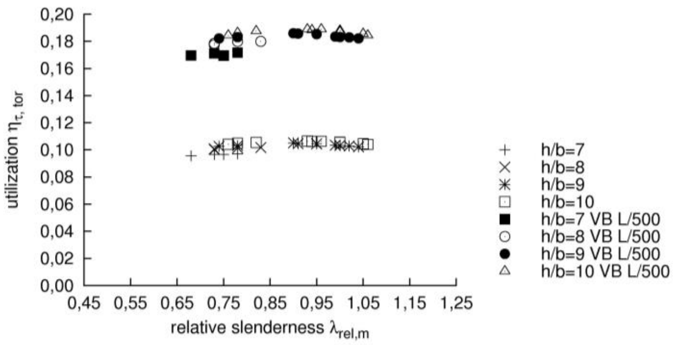

Figure 4.1. Utilization of shear due to torsional moment at the end support of a straight single span girder with parallel chords and three additional horizontal supports at the upper chord according to second order theory with sinusoidal curvature of imperfection between the supports with and without superposed sinusoidal deflection of the horizontal bracing of L/500.

In case of supporting the compression chord by additional horizontal bracings, for which the maximum deflection is limited to l/500, the increased utilization of shear due to torsional moment in the cross section at the end supports can be determined, see Figure 4.1 and Figure 4.2.

The factor k_{tor} for single span girders with parallel chords supported by horizontal bracings and for single span girders with parallel chords and raised lower chord supported by horizontal bracings may be approximated to:

$$k_{tor} = 0.065 \tag{20}$$

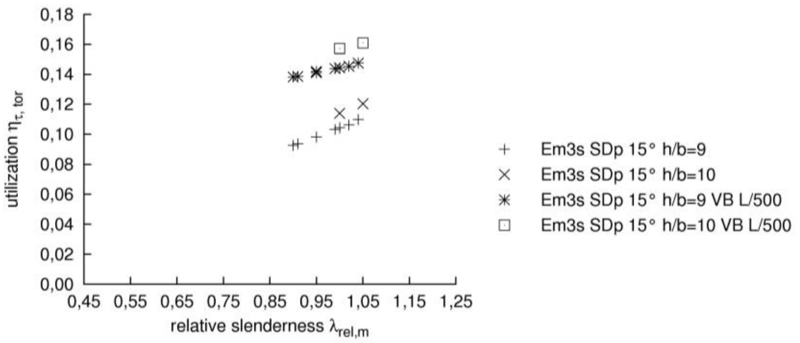

Figure 4.2. Utilization of shear due to torsional moment at the end support of a single span girder with parallel chords, raised lower chord and three additional horizontal supports at the upper chord according to second order theory with sinusoidal curvature of imperfection between the supports(15° inclination of lower chord) and with and without superposed sinusoidal deflection of the horizontal bracing of L/500.

The comparison in Figure 4.3 of the results of the simplified method to estimate the torsional moment in the cross section at the end supports by $M_d/80$, see equation (2), which does not regard any additional horizontal supports, and the torsional moment in the cross section at the end supports calculated by second order theory considering the additional horizontal supports shows the conservatism of the approximation of the torsional moment using $M_d/80$ according to equation (2) in comparison to the real calculation according to second order theory.

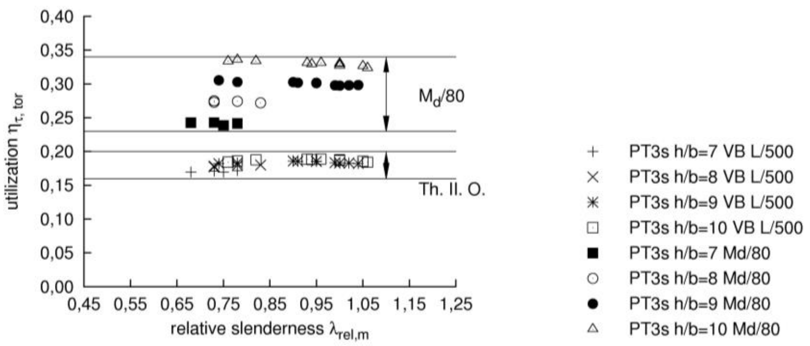

Figure 4.3. Comparison of the utilization of shear due to torsional moment at the end support according to second order theory (Th.II.O.) and the approximation according to equation (2)($M_d/80$) for a straight single span girder with parallel chords with sinusoidal curvature of imperfection between the supports with and without superposed sinusoidal deflection of the horizontal bracing of L/500.

The new method to determine the torsional moment due to lateral torsional buckling according to equation (18) aims to reduce this conservatism. A new approach for the torsional moment in the cross section at the end supports should be efficient but nevertheless safe. Based on the results of the presented research project the torsional moment in the cross section at the end supports is determined with the factor k_{tor} depending on the form of the girder and the *h*/*b*-proportion of each girder at the point of maximum height *h*. The torsional moment in the cross section at the end supports is used to calculate and verify the shear stresses. This completion of the shear stress verification of beams subjected to either bending or combined bending and compression in *EN 1995-1-1:2004 (2004)* takes into account the torsional moment in the cross section at the end supports according to second order theory in a simplified approach and allows a stability verification for lateral torsional buckling according to the equivalent length method based on bending moments according to first order theory.

4.3 Saddle roof and fish-bellied girders

4.3.1 Overview

For saddle roof and fish-bellied girders separate studies were necessary in order to determine the parameters of new simplified approach.

4.3.2 The saddle roof girder

The numerical studies on saddle roof girders with sinusoidal curvature of imperfection between the end supports (see Figure 3.2b)) and with sinusoidal curvature of imperfection between the supports (see Figure 3.2a)) show the highest shear stresses due to torsion for a *h*/*b*-proportion of 10 for saddle roof girders with sinusoidal curvature of imperfection between the supports.

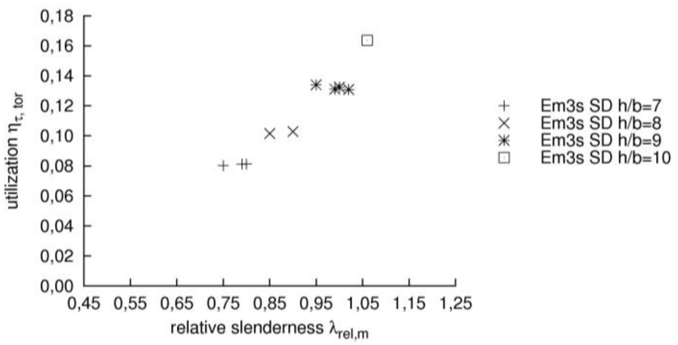

Figure 4.4. Utilization of shear due to torsional moment at the end support of a sattle roof girder (h_a=l/30) with three additional horizontal supports at the upper chord according to second order theory with sinusoidal curvature of imperfection between the supports (see Fig. 3.2a)).

Figure 4.4 shows the results of the numerical studies on saddle roof girders with the height $h_a = l/30$ at the end supports, see Figure 1d). The torsional moment depends on the h/*b*-proportion. The utilization of shear due to torsion amounts for saddle roof girders with $h/b = 7$ to only half of the value for saddle roof girders with $h/b = 10$. In a next step the saddle roof girders with sinusoidal curvature of imperfection between the supports were investigated. The utilization of shear due to torsion for $h/b > 8$ for saddle roof girders with sinusoidal curvature of imperfection between the supports (see Fig. 3.2a)) is higher than for saddle roof girders with sinusoidal curvature of imperfection between the end supports (see Fig. 3.2b)), see Figure 4.5.

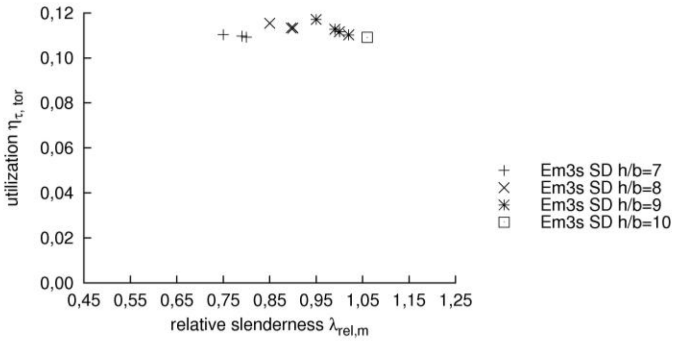

Figure 4.5. Utilization of shear due to torsional moment at the end support of a sattle roof girder (h_a=l/30) with three additional horizontal supports at the upper chord according to second order theory with sinusoidal curvature of imperfection between the end supports (see Fig.3.2b)).

The factor k_{tor} for saddle roof girders with the height $h_a = l/30$ at the end supports and rigid horizontal supports to be applied to calculate the torsional moment at the end supports according to equation (18) is determined to:

For $h/b < 8$ $\quad k_{tor} = 0.037$ (21)

For $h/b \geq 8$ $\quad k_{tor} = 0.0085 \cdot h/b - 0.031$ (22)

For saddle roof girders with compression chords supported by horizontal bracings the utilization of shear due to torsion in the cross section at the end supports increases. The approach for the factor k_{tor} in these cases should be:

For $h/b < 8$ $\quad k_{tor} = 0.067$ (23)

For $h/b \geq 8$ $\quad k_{tor} = 0.008 \cdot h/b + 0.003$ (24)

4.3.3 The fish-bellied roof girder

The numerical studies on fish-bellied girders with sinusoidal curvature of imperfection between the end supports (see Fig. 3.2b)) and with sinusoidal curvature of imperfection between the supports (see Fig. 3.2a)) were divided into two series, one series with the height $h_a = l/20$ of the cross section at the end supports (see Fig. 1c)) and another series with the height $h_a = l/25$ of the cross section at the end supports. Both series show negligible differences in view of the utilization of shear due to torsion. The numerical studies show the highest shear stresses due to torsion for *h*/*b*-

proportion of 10 for fish-bellied girders with sinusoidal curvature of imperfection between the supports, similar to saddle roof girders. For lower h/b -proportions the shear stresses due to torsion are lower, which is also similar to saddle roof girders, the utilization of shear due to torsion for $h/b > 8$ for fish-bellied girders with sinusoidal curvature of imperfection between the supports is higher than for fish-bellied girders with sinusoidal curvature of imperfection between the end supports. The factor k_{tor} for fish-bellied girders with rigid horizontal supports is determined to:

For $h/b < 8$ $\quad k_{\text{tor}} = 0.033$ (25)

For $h/b \geq 8$ $\quad k_{\text{tor}} = 0.0135 \cdot h/b - 0.075$ (26)

For fish-bellied girders with compression chords supported by horizontal bracings the utilization of shear due to torsion in the cross section at the end supports increases. The approach for the factor k_{tor} in these cases should be:

For $h/b < 8$ $\quad k_{\text{tor}} = 0.057$ (27)

For $h/b \geq 8$ $\quad k_{\text{tor}} = 0.0125 \cdot h/b - 0.043$ (28)

5 Conclusions

Based on the results of numerical studies, a new simplified approach is given for the torsional moment induced by lateral torsional buckling in the cross section at the end supports for girder forms quite often used in practise. Based on this approach the utilization of shear due to torsion can be calculated quite easily, without using second order theory for calculating the internal forces and stresses. The stability verification of lateral torsional buckling according to the equivalent length method based on bending moments according to first order theory may be applied as given in *EN 1995-1-1:2004* (2004) for beams subjected to both bending or combined bending and compression. Nevertheless, with the help of the simplified approach for the torsional moment induced by lateral torsional buckling a complete verification of the shear stresses is possible. The approach also considers that the stiffness of the horizontal bracings which support the compression chord is decisive for the torsional moment due lateral torsional buckling in the cross section at the end supports. And also the tapering of the cross section near the end supports of saddle roof and fish-bellied girder leading to a higher utilization of shear due to torsion than for parallel chorded girders is taken into account.

Acknowledgements This research work (17398N) coordinated by the International Association for Technical Issues related to Wood (iVTH e. V.) is supported in the program of “Industriellen Gemeinschaftsforschung (IGF)” and financed by the German Federation of Industrial Research Association (AiF).

6 References

Petersen, C. (1980): Statik und Stabilität der Baukonstruktionen. Publisher Friedr. Vieweg und Sohn, 1980.

Roik et al. (1972): Biegetorsionsprobleme gerader dünnwandiger Stäbe. Publisher Wilhelm Ernst und Sohn, 1972.

Cyron & Sengler (1985): Holzleimbau, Bauen mit Brettschichtholz; published by Informationsdienst Holz, 1985.

Möhler & Hemmer (1977): Verformungs- und Festigkeitsverhalten von Nadelvoll- und Brettschichtholz bei Torsionsbeanspruchung. Holz als Roh- und Werkstoff 35 (1977), pp. 473 – 478.

Glos & Denzler (2004): Kalibrierung der charakteristischen Schubfestigkeitskennwerte für Vollholz in EN 338 entsprechend den Rahmenbedingungen der nationalen Sortiernorm. Technische Universität München, Report No. 04502, August 2004.

Schickhofer, G. (2001): Determination of Shear Strength Values for GLT using Visual and Machine Graded Spruce and laminations. Paper 34-12-6, CIB-W18-Meeting 2001

Brandner et al. (2007): Determination of modulus of shear and elasticity of glued laminated timber related examinations. Paper 40-12-2, CIB-W18-Meeting 2007.

Klapp & Brüninghoff (2005): Shear strength of glued laminated timber. Paper 38-6-3, CIB-W18-Meeting 2005

Möhler, K. (1977): Strength and long-term behaviour of lumbar and glued-laminated timber under torsion loads. Paper 7-6-1, CIB-W18-Meeting 1977.

Görlacher & Kürth (1994): Determination of shear modulus. Paper 27-10-1, CIB-W18-Meeting 1994.

Kuhlmann & Hofmann (2013): Vereinfachte Bemessung von Brettschichtholzträgern variabler Höhe für das Torsionsmoment aus Kippstabilisierung. Research report to IGF-research project 17398N (2013).

Szabó, I. (2001): Höhere Technische Mechanik. 6. Auflage, Springer Verlag 2001.

EN 1995-1-1:2004 (2004): Design of timber structures - Part 1-1: General and rules for buildings. CEN.

DIN EN 1995-1-1:2010-12 (2010): Eurocode 5: Bemessung und Konstruktion von Holzbauten Teil 1-1: Allgemeines – Allgemeine Regeln und Regeln für den Hochbau.

DIN EN 1995-1-1/NA:2010-12 (2010): Nationaler Anhang – National festgelegte Parameter - Eurocode 5: Bemessung und Konstruktion von Holzbauten Teil 1-1: Allgemeines – Allgemeine Regeln und Regeln für den Hochbau.

EN 14080:2013 (2013): Timber structures – Glued laminated timber and glued solid timber – Requirements. CEN.

Discussion

The paper was presented by U Kuhlmann

R Steiger asked was there an impact for changes in design rules on horizontal bracing. U Kuhlmann replied that a follow up project on horizontal bracing had been performed and results were surprising with uneven distribution of forces amongst the horizontal braces.

P Zarnani and U Kuhlmann discussed flexural buckling and lateral torsional buckling cases.

A Frangi commented about designing bracing system with simplified design method. U Kuhlmann agreed that the old simplified method would be fine.

H Blass asked about recommendation on how to take out the lateral forces. U Kuhlmann replied that in general diagonal bracing was not desirable by owner because of added cost.

K Ranasinghe received clarification that there was no jump between the values for $h/b<8$ *and* $h/b>8$*.*

Displacement-Based Determination of Laterally Loaded Cross Laminated Timber (CLT) Wall Systems

Georg Flatscher, Graz University of Technology, Institute of Timber Engineering and Wood Technology

Gerhard Schickhofer, Graz University of Technology, Institute of Timber Engineering and Wood Technology

Keywords: CLT, wall system, connections, analytical model, displacement-based model

1 Introduction

In the past, typical timber structures consisted mainly of several linear elements, i.e. posts and beams and the assumption of simply hinged or rigid joints between these elements usually led to results with an acceptable accuracy in design. Nevertheless, according to section 5 – "Basis of structural analysis" – of European standard EN 1995-1-1 (2004) (also referred to as Eurocode 5) the effect of deformations from connections must also be considered, particularly in statically overdetermined systems. Although not mentioned in Eurocode 5, this requirement is often crucial in designing Cross Laminated Timber (CLT) structures.

As in-plane loaded CLT wall elements are very rigid, the lateral behaviour of the whole building system is critically affected by the number, position and properties of the applied connection systems. Consequently, an adequate consideration of the load-bearing performance of the applied connections is necessary for achieving a well-balanced performance of CLT structures, especially in the case of large horizontal loads, i.e., earthquakes or heavy winds. This is valid, not only for determining the load-bearing capacity but rather for the stiffness and deformation properties. Several experimental campaigns confirm the conditions described and further show significant plastic deformations in single connections – prior to the edges of the tested wall systems; compare e.g. Dujic et al. (2005), Ceccotti et al. (2006), Popovski and Karacabeyli (2011), Gavric (2013), Hummel et al. (2013) and Flatscher et al. (2015).

Some load-based approaches consider a linear elastic- or multi linear load-displacement approximation of the connectors and are offered in literature; see e.g. Gavric et al. (2011), Sustersic and Dujic (2012), Gavric and Popovski (2014) and Gavric et al. (2015). However, load-based models scarcely enable a proper consideration of descending branches in the load-displacement relationship. Hence, a first approach for a displacement-based model is outlined in Flatscher et al. (2014). The present contribution gives a detailed description of a further developed version of this model, which originally is discussed in Flatscher (2016). Subsequently, the new model is verified by comparing its output with experimental test results. Finally, a parameter study including various aspects of CLT structures is conducted and the results are discussed.

2 General comments on CLT wall systems

CLT is an already well known plate-like engineered timber product and is usually composed of an uneven number of layers bonded perpendicularly to each other. An up-to-date report summarising detailed information and references regarding the history, production and properties of CLT is published in Brandner et al. (2016). Thus further information regarding the building material CLT is reduced to essential notes in the respective parts.

In accordance with current calculation models, a CLT wall system includes one CLT element and the connections jointing it to the foundation. Furthermore, if vertical joints connecting adjacent CLT elements in the same plane are used, even more than one CLT element attends the system and the vertical joint must be considered in the calculation as well; compare Figure 2.1.

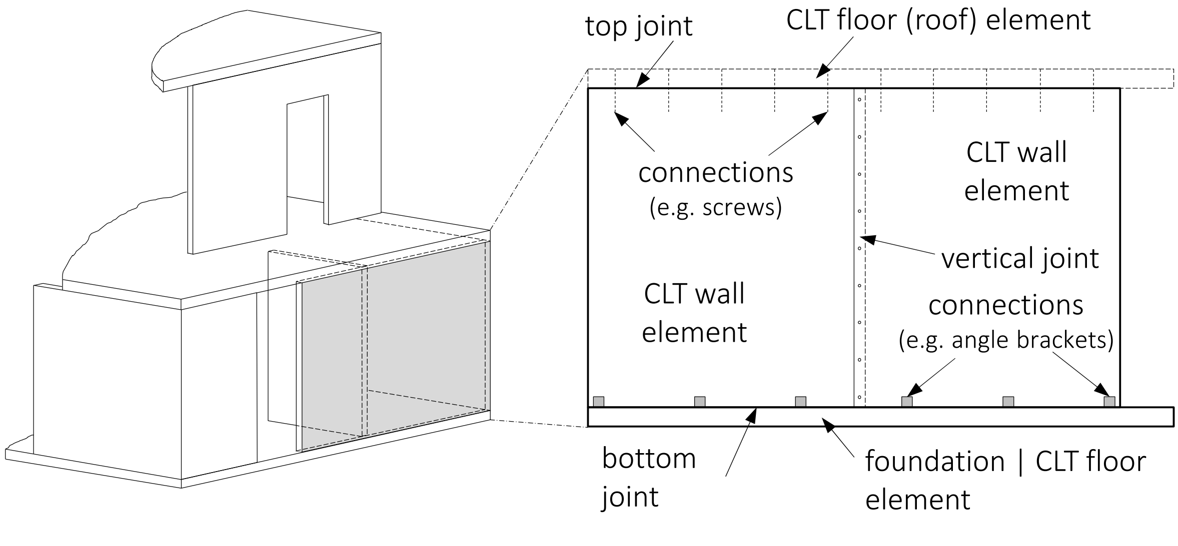

Figure 2.1 Elements defining a CLT wall system; Flatscher (2016).

2.1 Applied fasteners and connections

In Europe the joints within CLT structures are mainly equipped with angle-brackets, hold-downs (using nails or screws as well as bolts as fasteners) and fully or partially threaded self-tapping timber screws. Accommodating this circumstance, several experimental projects regarding these connections are published; compare, e.g., Uibel and Blaß (2007), Flatscher and Schickhofer (2011), Gavric et al. (2011), Bratulic et al. (2014), Tomasi and Smith (2014) and Izzi et al. (2016).

Even if other connection systems are also available, the present discussion solely considers angle-brackets, hold-downs and screws, since the focus is laying on a general description of CLT wall systems and the access to original test data. Nevertheless, the following approaches can be adapted for any other connection system as well.

2.2 Contributions to deflection

When applying a lateral load on the top of a CLT wall system, four contributions to total deflection can be identified: (i) slip (translation), (ii) rocking (rotation), (iii) shear and (iv) bending; compare Figure 2.2 and Equation (1). Although mainly influenced by the characteristics and position of the applied connections, contributions (i) and (ii) are heavily dependent on friction and the acting vertical load as well. Contributions (iii) and (iv), on the other hand, only depend on the characteristics of the used CLT element and are therefore often summarised as 'CLT deformation'.

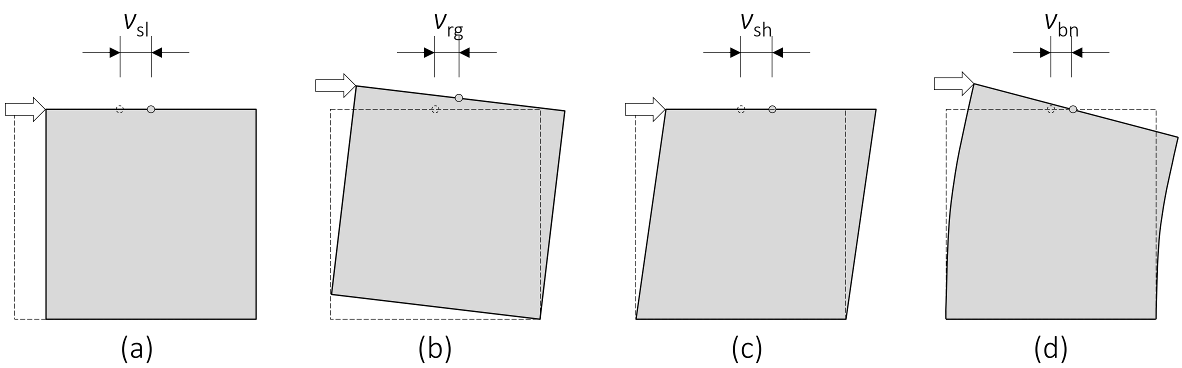

Figure 2.2 Contributions to total lateral deflection of a CLT wall system – (a) slip (rigid body translation); (b) rocking (rigid body rotation); (c) shear deformation of the CLT element; (d) bending deformation of the CLT element; Flatscher (2016).

$$v_{tot} = v_{sl} + v_{rg} + v_{sh} + v_{bn} \tag{1}$$

with

v_{tot} total lateral displacement of a CLT wall system
v_{sl} contribution due to slip (rigid body translation)
v_{rg} contribution due to rocking (rigid body rotation)
v_{sh} contribution due to the shear deformation of the CLT element
v_{bn} contribution due to the bending deformation of the CLT element

3 Displacement-based analytical wall model

As mentioned above, using a displacement-based approach enables a more reliable consideration of load-bearing behaviour in the peak and post peak area. However, such a model requires a displacement-based description of the load-displacement behaviour of considered connections. For this purpose a slightly modified version of the approximation model presented in Flatscher and Schickhofer (2014) is used. The basic function is given in Equation (2); an explaining illustration and the necessary boundary conditions for determining the parameters C_1-C_6 are depicted in Figure 3.1. A more detailed description of the model is included in Flatscher (2016).

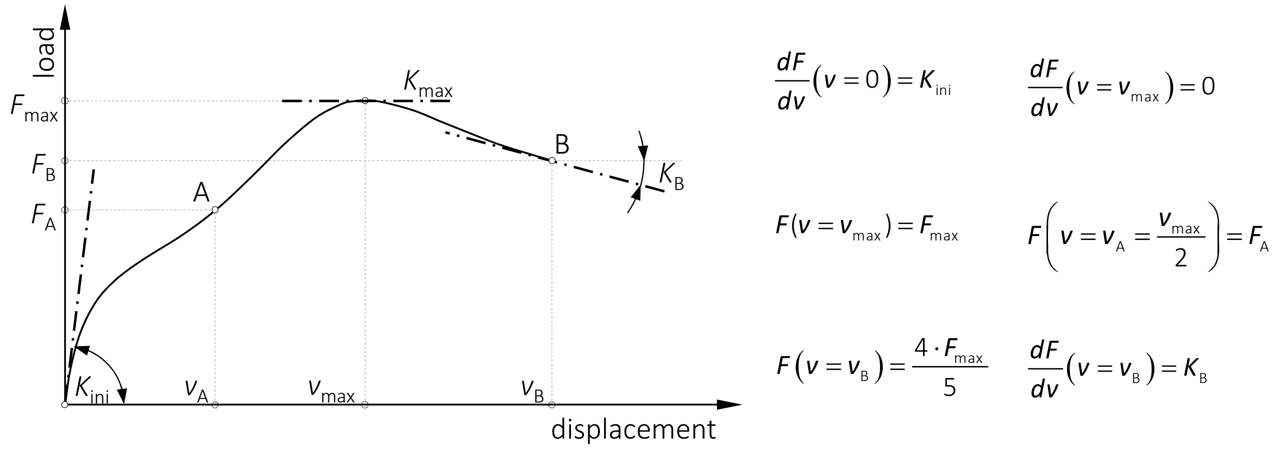

Figure 3.1 Displacment-based approximation model for load-displacement graphs; model and appendant parameters; Flatscher (2016).

$$F(v)=\frac{v+C_1\cdot v^2+C_2\cdot v^3}{C_3+C_4\cdot v+C_5\cdot v^2+C_6\cdot v^3} \tag{2}$$

3.1 Principal mode of operation

Similar to the method for load-based models, a rigid CLT body is assumed when investigating the contributions of connections (slip and rocking); the contributions to total deflection of CLT are determined separately.

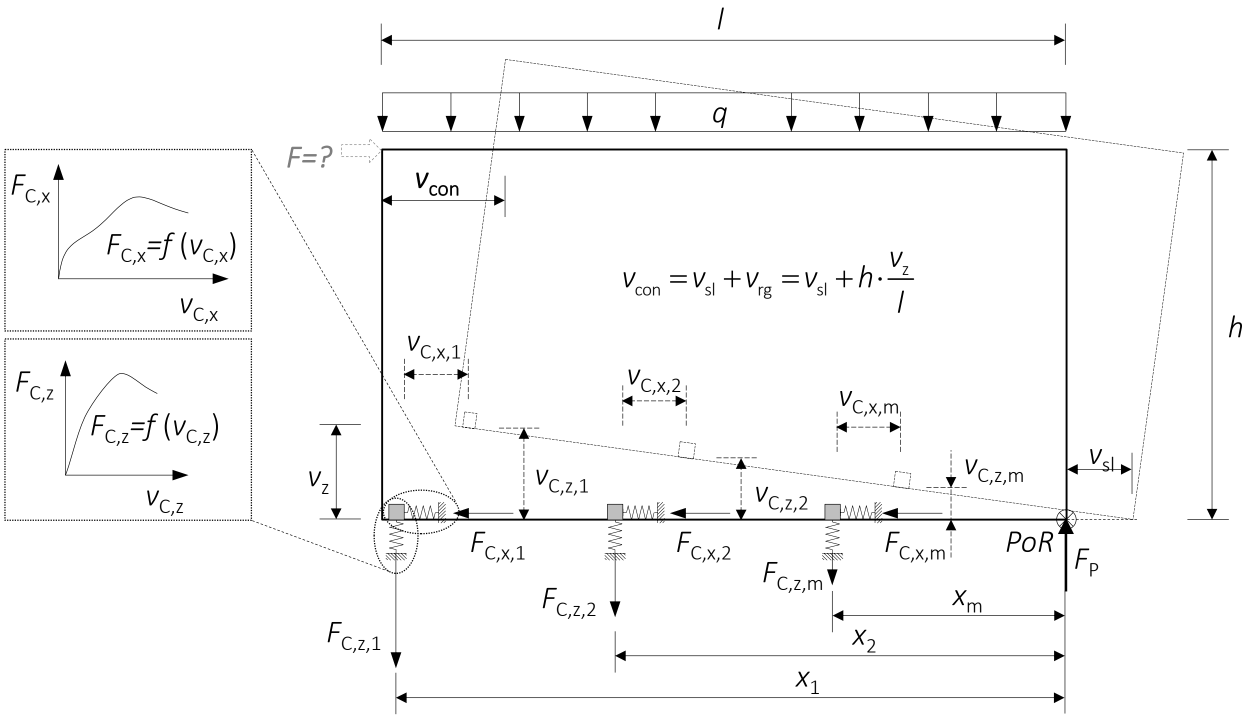

Figure 3.2 Displacement-based approach – overview and notations; Flatscher (2016).

The biggest difference to load-based models is probably the circumstance that the shear and rocking behaviour cannot be determined independently. A possible solution for this circumstance is to fit the ratio between slip and rocking deformations based on experimental results; compare Flatscher et al. (2014). However, since not feasible in practical design, an iterative process is developed for determining this ratio independently from experimental results. Within the following passage this approach is described step by step. For supporting explanations the most important notations are illustrated in Figure 3.2.

- Step 1:
  Estimating the increment of slip and rocking contribution to the applied (connection based) increment of lateral displacement. For this purpose the share parameter p, attending values between 0 and 1, is introduced; compare Equations (3) and (4).

$$v_{sl,i} = v_{sl,i-1} + p \cdot \Delta v_{con,i} \tag{3}$$

$$v_{rg,i} = v_{rg,i-1} + (1-p) \cdot \Delta v_{con,i} \tag{4}$$

with

p share parameter; $0 \leq p \leq 1$ (e.g. $p = 0.5$)

v_{con} increment of connection based lateral deflection

- Step 2:
  Computing lateral and vertical displacements for every connection as expressed in Equations (5) and (6).

$$v_{C,x,m,i} = v_{sl,i} \tag{5}$$

$$v_{C,z,m,i} = x_{m,i} \cdot \frac{v_{rg,i}}{h} \tag{6}$$

with

$v_{C,x,m}$ slip (horizontal) displacement of a connection

$v_{C,z,m}$ uplift (vertical) displacement of a connection

x_m position of m-th connection

- Step 3:
  Determining loads appearing for every connection depending on the respective displacements; compare Equations (7) and (8). For this purpose the application of the proposed approximation model presented above is suggested.

$$F_{C,x,m,i} = f\left(v_{C,x,m,i}\right) \tag{7}$$

$$F_{C,z,m,i} = f\left(v_{C,z,m,i}\right) \tag{8}$$

with

$F_{C,x,m}$ shear load in m-th connection

$F_{C,z,m}$ tension (uplift) load in m-th connection

A quadratic interaction is applied for considering effects resulting from bidirectional loading; compare Eurocode 5. It is assumed in particular that if the available potential for the maximum load is reduced to, e.g., 70 %, the same reduction takes place for any other point at the loading path. In addition, during the incremental determination process the reduction factor for i-th step is forced to be equal or smaller than the same parameter in the step before. Finally, if the connector fails in one direction, the bearing capacity of the other one is also assumed to be zero. The chosen approach for determining the actual potential and the resulting scaled actual loads is given in Equations (9) to (11); see also Flatscher (2016).

$$\left(\frac{F_{\mathrm{C,x,m,i}}}{F_{\mathrm{max,C,x,m}}}\right)^2+\left(\frac{F_{\mathrm{C,z,m,i}}}{F_{\mathrm{max,C,z,m}}}\right)^2\le 1.0 \rightarrow \begin{cases}\delta_{\mathrm{x,m,i}}=\left(1-\left(\frac{F_{\mathrm{C,z,m,i}}}{F_{\mathrm{max,C,z,m}}}\right)^2\right)^{0.5}\\ \delta_{\mathrm{z,m,i}}=\left(1-\left(\frac{F_{\mathrm{C,x,m,i}}}{F_{\mathrm{max,C,x,m}}}\right)^2\right)^{0.5}\end{cases} \tag{9}$$

$$F^*_{\mathrm{C,x,m,i}}=F_{\mathrm{C,x,m,i}}\cdot\delta_{\mathrm{x,m,i}} \tag{10}$$

$$F^*_{\mathrm{C,z,m,i}}=F_{\mathrm{C,z,m,i}}\cdot\delta_{\mathrm{z,m,i}} \tag{11}$$

with

$\delta_{\mathrm{x|z,m}}$ scaling factor considering bidirectional loading

$F^*_{\mathrm{C,x|z,m}}$ scaled actual loads in the connections

- Step 4:
  Computation of the lateral loads on the CLT wall system causal for the assumed displacements as given in Equations (12) and (13). For considering the possible influence of friction as included in Equation (12), it is necessary to determine the actual bearing load F_P as expressed in Equation (14).

$$F_{\mathrm{sl,i}}=\underbrace{\sum\left(F^*_{C,x,m,i}\right)}_{\text{connections}}+\underbrace{F_{\mathrm{P,i}}\cdot\mu_{\mathrm{f}}}_{\text{friction}} \tag{12}$$

$$F_{\mathrm{rg,i}}=\underbrace{\frac{\sum\left(F^*_{C,z,m,i}\cdot x_{\mathrm{m,i}}\right)}{h}}_{\text{connections}}+\underbrace{\frac{q\cdot l^2}{2\cdot h}}_{\text{vertical load}} \tag{13}$$

$$F_{\mathrm{P,i}}=\sum\left(F^*_{C,z,m,i}\right)+q\cdot l \tag{14}$$

with

F_sl lateral load causal for assumed slip

F_rg lateral load causal for assumed rocking

F_P vertical bearing load

μ_f coefficient of friction

- Step 5:
  Since physically only one lateral load F can act at the same time, the constraint given in Equation (15) must be complied with.

$$F_{\mathrm{i}} \overset{!}{=} F_{\mathrm{sl,i}} \overset{!}{=} F_{\mathrm{rg,i}} \qquad (15)$$

  If this condition is satisfied, the shares assumed in step 1 are correct and the calculation ends at this point. Otherwise, steps 1 to 5 must be repeated with a varying share parameter p until equilibrium is reached.

  However, it is also possible that the share parameter will reach its limit (means either 1 or 0) before Equation (15) is fulfilled. This case frequently (but not only) occurs at the very beginning (meaning at small deformations) if one contribution to total deflection is prevented by the boundary conditions (e.g. rocking deformation due to high vertical loads). If so, the minimum of $F_{\mathrm{sl,i}}$ and $F_{\mathrm{rg,i}}$ has to be taken as the relevant load value.

- Step 6:
  Determination of the (elastic) CLT deformations with the actual load F_{i}. For this purpose Equations (16) and (17) for bending and shear are applied, respectively; compare Flatscher (2016). Furthermore, if openings in the CLT wall element have to be considered it is scheduled to use the model described in Dujic et al. (2007) for reducing the relevant stiffness parameters.

$$v_{\mathrm{bn}} = \frac{4 \cdot F \cdot h^3}{E_0 \cdot l^3 \cdot t_{\mathrm{eff}}} \qquad (16)$$

$$v_{\mathrm{sh}} = \frac{F \cdot h}{G^* \cdot l \cdot t_{\mathrm{CLT}}} \qquad (17)$$

  with
  E_0 modulus of elasticity parallel to the grain
  G^* effective shear modulus (compare, e.g., ON B 1995-1-1, 2015)
  t_{eff} effective thickness (sum of vertical CLT layers)
  t_{CLT} total thickness of CLT element

3.2 Considering vertical joints

Based on the thinking in the context of vertical joints documented in Gavric et al. (2015), both coupled and single-coupled behaviour (compare Figure 3.3 (a) and (b), respectively) of CLT wall systems can also be considered in the displacement-based model described here. However, for the sake of simplicity, the following formulas are limited to only one vertical joint of exactly half the length of the CLT element.

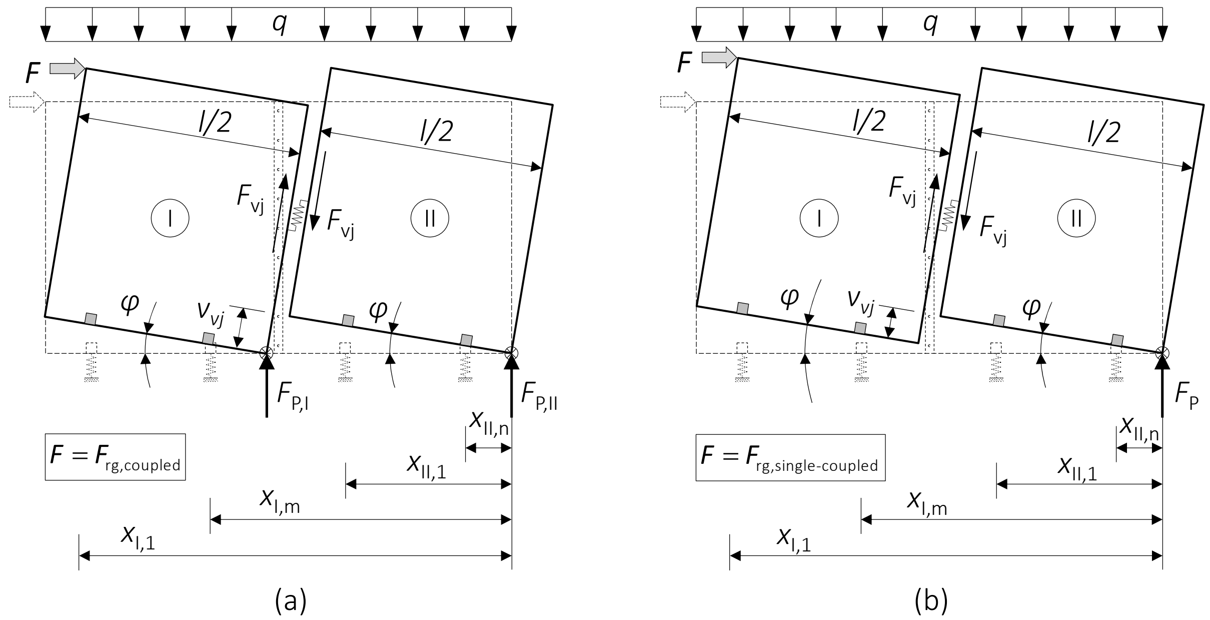

Figure 3.3 CLT wall system including a vertical joint – (a) coupled wall behaviour; (b) single-coupled wall behaviour; Flatscher (2016).

Application of Equation (18) enables determination of rocking displacement in the event of coupled behaviour. The required displacement parameters for determining the corresponding loads in the vertical joint and the connections in the bottom joint are given in Equations (19) to (21).

$$F_{\mathrm{rg,coupled}} = \frac{1}{h} \cdot \left[\sum \left(F_{\mathrm{C,z,I,m}} \cdot \left(x_{\mathrm{I,m}} - \frac{l}{2} \right) \right) + \sum \left(F_{\mathrm{C,z,II,n}} \cdot x_{\mathrm{II,n}} \right) + F_{\mathrm{vj}} \cdot \frac{l}{2} \right] + \frac{q \cdot l^2}{4 \cdot h} \tag{18}$$

$$v_{\mathrm{vj}} = \frac{v_{\mathrm{rg}} \cdot l}{2 \cdot h} \tag{19}$$

$$v_{\mathrm{C,z,I,m}} = x_{\mathrm{I,m}} \cdot \frac{v_{\mathrm{rg}}}{h} - v_{\mathrm{vj}} = v_{\mathrm{rg}} \cdot \left(\frac{x_{\mathrm{I,m}}}{h} - \frac{l}{2 \cdot h} \right) \tag{20}$$

$$v_{\mathrm{C,z,II,n}} = x_{\mathrm{II,n}} \cdot \frac{v_{\mathrm{rg}}}{h} \tag{21}$$

Equations (22) to (24) must be followed for simulating the load-displacement graph of CLT wall systems exhibiting single-coupled behaviour. As can be seen, these expressions require consideration of actual vertical joint displacement. Since this parameter not only influences the resulting lateral but also the uplift deformation of connections, a further iteration is included to the calculation process. As criterion for this computation the actual load in the vertical joint is used; compare Equation (25) and Gavric et al. (2015).

$$F_{\text{rg,single-coupled}} = \frac{v_{\text{rg}}}{h^2} \cdot \left[\sum \left(X_1 \cdot x_{\text{I,m}}^2 \right) + \sum \left(F_{\text{C,z,II,n}} \cdot x_{\text{II,n}} \cdot \frac{h}{v_{\text{rg}}} \right) - \right.$$
$$\left. - \frac{\left(\sum \left(X_1 \cdot x_{\text{I,m}} \right) \right)^2}{\sum \left(X_1 \right) + X_2} \right] + \frac{q \cdot l}{2 \cdot h} \cdot \left(l - \frac{\sum \left(X_1 \cdot x_{\text{I,m}} \right)}{\sum \left(X_1 \right) + X_2} \right) \quad (22)$$

$$X_1 = \frac{F_{\text{C,z,I,m}} \cdot h}{x_{\text{I,m}} \cdot v_{\text{rg}} - v_{\text{vj}} \cdot h} \quad (23)$$

$$X_2 = \frac{q \cdot l + 2 \cdot \sum \left(F_{\text{C,z,I,m}} \right)}{2 \cdot v_{\text{vj}}} \quad (24)$$

$$F_{\text{vj}}(v_{\text{vj}}) = \frac{q \cdot l}{2} + \sum \left(F_{\text{C,z,I,m}} \right) \quad (25)$$

Finally it is worth mentioning that all calculations can be performed with common spread sheet programs (e.g. Microsoft® Excel). This enables a fast and relatively simple application of the suggested approach; see also Flatscher (2016).

4 Comparing analytical and experimental results

Data from three independent research projects conducted at the University of Kassel, the University of Trento and the Graz University of Technology are used for verifying the new model. Experimental tests on connections and wall systems documented in Seim and Hummel (2013), Gavric (2013) and Flatscher et al. (2013) are considered in particular.

Table 4.1. Input parameters for approximating connections' load-displacement relationship.

	Kassel				Trento					Graz			
	AB*		HD**		AB*		HD**		VJ***	AB*		HD**	
	x	*z*	*x*	*z*	*x*	*z*	*x*	*z*	-	*x*	*z*	*x*	*z*
F_{max} [kN]	37.0	35.0	9.8	65.0	27.0	24.0	28.6	46.0	5.5	32.0	36.0	-	50.0
v_{max} [mm]	16.0	16.6	28.0	25.7	28.0	19.7	102.6	19.0	23.0	18.0	21.0	-	18.0
K_{ini} [kN/mm]	10.0	20.0	3.0	30.0	3.0	5.0	1.3	8.0	2.5	5.0	20.0	-	30.0
F_{A} [kN]	29.0	22.4	7.3	48.0	20.5	18.7	16.0	36.0	4.0	23.5	28.0	-	39.0
v_{B} [mm]	22.5	22.2	34.7	30.5	38.0	26.0	106.3	26.0	31.0	25.0	27.0	-	26.5
K_{B} [kN/mm]	-2.30	-1.90	-0.65	-9.00	-1.05	-1.58	-7.75	-2.70	-0.25	-1.65	-3.0	-	-2.0

* AB = angle bracket; ** HD = hold-down; *** VJ = vertical joint connection (behaviour of one single screw); x and z describe the properties for shear and uplift, respectively

In a first step the six parameters necessary for approximating connections' load-displacement relationship are evaluated by fitting the analytical curve-model given in Equation (2) to the respective experimental test data.

The resulting values for the connections used in this paper are given in Table 4.1 for each research project separately. In this context it is important to mention, that the parameter K_{ini} represents the tangential stiffness in the origin and must not be confused with the initial slip (or K_{ser}) usually describing the load-to-displacement ratio at approximately 40 % of F_{max}.

Applying these data sets in principle allows simulating the bulk of CLT wall-configurations explored in the research projects referred to. The present contribution, however, includes only three selected examples; the relevant basic conditions of the chosen samples are listed in Table 4.2.

Table 4.2. Boundary conditions for considered CLT wall-configurations investigated in Seim and Hummel (2013), Gavric (2013) and Flatscher et al. (2013).

	l/h [m]	connections [-]	q [kN/m]	positon of connections (x_m) [m]	vert. joint
W_CLT-1.1*	2.5/2.5	2xHD & 3xAB	10	0.08|0.665|1.25|1.835|2.42	none
Wall 2.2**	2.95/2.95	2xHD & 4xAB	18.5	0.05|0.50|0.95|2.00|2.45|2.90	half lap (20 screws)
WA_A_M01***	2.5/2.5	4xAB	20.8	0.08|0.86|1.64|2.42	none

* University of Kassel; ** University of Trento; *** Graz University of Technology

For an additional verification, the wall-configurations presented here are also simulated in the finite element program RFEM 5 (2015). For this purpose, springs able to simulate the non-linear behaviour of the applied connections are implemented. Furthermore, the CLT elements are modelled as orthotropic surface elements; more detailed information about the FE-model is documented in Flatscher (2016).

When applying the analytical model a constant coefficient of friction equal to 0.2 is used for all walls. Moreover must be mentioned that the interaction as described in section 3.1 is only considered for angle brackets; for hold-downs the respective effect is neglected. This is because an experimental campaign on similar connection systems has shown only a minor loss of axial (uplift) bearing-capacity at lateral (slip) displacement close to 15 mm; compare Pozza et al. (2016). Hence, assuming a quadratic interaction might overestimate the effect of interaction for such connection systems.

Figure 4.1 illustrates the original test curves (top-displacement, slip and uplift) of the chosen samples and the corresponding simulated load-displacement graphs. As can be seen, in principle both the analytical approach and the FE-simulations properly describe the behaviour of all three CLT wall systems. The slightly higher load-carrying capacities resulting from the FE-model are manly caused by the impossibility of considering a proper interaction of shear and uplift springs; see also Flatscher (2016). This circumstance is especially visible at load-slip curves where the FE-model remains elastic, whereby the analytical model also exhibits some plastic deformations.

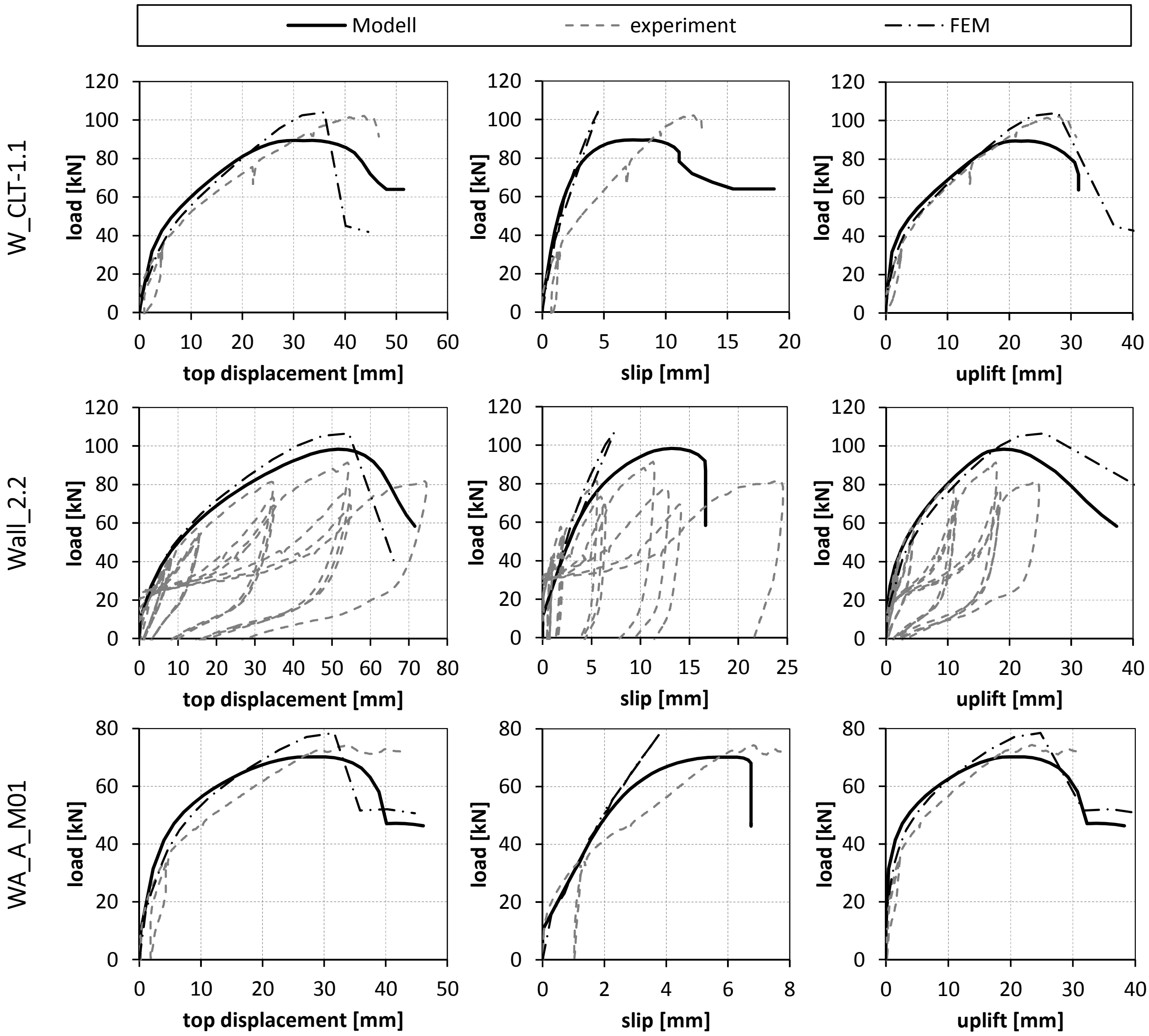

Figure 4.1 Comparison of experimental, analytical and FE generated load-dispalcement curves of three CLT wall systems.

Although not visualised, the behaviour of the vertical joint, connecting the adjacent CLT elements in sample ‘Wall 2.2’, is simulated too. Again, the analytical and the FE-model stand in good agreement to each other and adequately describe the general behaviour during the experiment. Nevertheless, the final deflection is overestimated by both simulations. A possible reason for this fact is described in section 5.2.

However, comparisons with experimental test results certify the quality of the proposed analytical model. The following parameter study is thus based solely on results gathered from the proposed approach.

5 Parameter Study

The parameter study presented here focusses on three topics. Firstly, the effect of wall length and the number of connections on the load-carrying and stiffness properties of CLT wall systems are described. Secondly, the effect of a vertical joint on their lateral behaviour is discussed. Finally, the influence of different connections and calculation models on the load-displacement relationship of the walls as also on the bearing behaviour of the connections considered is briefly covered.

The properties for angle brackets and hold downs are used for all computations as defined in Table 4.1 (Graz). All wall elements are assumed as 5-layered CLT panels with a total thickness of 100 mm (20-20-20-20-20). The modulus of elasticity and the shear modulus are considered with 11,000 N/mm² and 690 N/mm², respectively. The vertical load and the coefficient of friction are also kept constant for all simulations (q = 20 kN/m and μ = 0.2, respectively); further boundary conditions are given in the relevant parts.

5.1 Wall length and number of connections

When analysing horizontally loaded structures rigid floor systems are usually assumed; compare regulations in EN 1998-1 (2004) (also referred to as Eurocode 8). Furthermore, following the suggestions in Follesa et al. (2015), top joints in CLT structures should be over strengthened. As a consequence, all walls within one storey are forced to form the same lateral displacement. Hence, especially in the case of large deformations, the application of initial stiffness values determined at relatively small (and different) displacement levels is questionable. For demonstrating this point a set of three different wall lengths and three different connection distances is simulated. For the sake of simplicity, all the wall systems considered are equipped solely with angle brackets.

Table 5.1. Parameter study on wall geometry and position of connections; geometries and results.

	l/h [m]	n^{*} [-]	a^{**} [m]	F_{max} [kN]	v_{max} [mm]	$K_{0\text{-}40}$ [kN/mm]	$K_{0.5\%}$ [kN/mm]	$K_{0.75\%}$ [kN/mm]	$K_{1.0\%}$ [kN/mm]	v_{CLT} [%]	v_{sl} [%]	v_{rg} [%]
A_1		2	1.50	24.56	46.35	4.48	1.24	0.93	0.76	4	6	90
A_2	1.5/3.0	3	0.75	31.86	49.28	4.34	1.53	1.15	0.95	5	4	91
A_3		4	0.50	39.60	49.92	4.50	1.82	1.39	1.15	7	3	90
B_1		3	1.50	65.09	24.82	14.83	4.05	2.88	2.13	6	30	64
B_2	3.0/3.0	4	1.00	78.69	26.8	15.68	4.80	3.46	2.60	7	26	67
B_3		7	0.50	119.77	28.74	17.34	6.96	5.18	3.99	10	21	69
C_1		4	1.50	111.48	18.78	20.24	7.30	4.89	3.25	8	56	36
C_2	4.5/3.0	6	0.90	146.13	20.57	24.18	9.45	6.45	4.35	9	47	44
C_3		10	0.50	215.23	21.13	30.67	13.60	9.55	6.55	13	40	47

* number of applied connections, ** space between applied connections

Besides geometric boundary conditions, Table 5.1 documents the effective (secant) stiffness at four different levels for every simulated wall. In particular, the load-to-displacement ratio at 40 % of F_{max} ($K_{0\text{-}40} \approx K_{ser}$) and at displacement levels equal to 0.5 %, 0.75 % and 1.0 % of walls' height ($K_{0.5\%}$, $K_{0.75\%}$ and $K_{1.0\%}$, respectively) are given. The corresponding absolute deflections of 15 mm, 22.5 mm and 30 mm represent the maximum interstorey drifts scheduled for damage limitation in Eurocode 8.

As can be seen, the latter mentioned stiffness values are reduced to approximately 25 % on average compared to the corresponding initial stiffness parameters. It must be noticed further that the interstorey drift of 1.0 % forces the walls with lengths of 3.0 and 4.5 m to go beyond v_{max}. This means that they are in their softening branch. Consequently, blindfold application of initial stiffness values (or even K_u according to Eurocode 5) may distinctively underestimate the actual deflections at higher load levels.

Table 5.1 includes further information about the contributions to total deflection when reaching maximum load-carrying capacity (F_{max}). As can be seen, the respective values strongly depend on both the wall geometry and the number of applied connections. As a rule of thumb it can be stated that the longer the wall and the more connections are applied the more sliding becomes the relevant mechanism. Furthermore, the contribution of CLT deformation to total deflection is in most cases below 10 %.

Although current calculation models enable a good approximation of actual wall behaviour, the corresponding computations may be time consuming. As a consequence and since not all design processes require a detailed non-linear analysis, their application may be uneconomic for some cases in practical design. However, distribution of horizontal loads on vertical building elements (primarily walls) must be solved in any case.

A simplified approach often used when designing concrete structures is distribution based on the bending stiffness of wall elements, i.e., their length to the power of 3 (postulated an equal thickness of the walls); compare Bachmann (2002). However, due to the distinct influence of connections, this approach is not feasible for CLT structures.

Table 5.2. Power values for load distribution.

distance between connections	$K_{0\text{-}40}$	$K_{0.5\%}$	$K_{0.75\%}$	$K_{1.0\%}$
a = 1.5 m	1.16	1.54	1.43	1.23
a ≈ 0.9 m*	1.36	1.67	1.55	1.34
a = 0.5 m	1.58	1.74	1.63	1.43

* average of applied spacings for walls A_2, B_2 and C_2

Based on the stiffness properties given in Table 5.1 power values for walls with different lengths but similar distances between applied connections are determined by conducting a least squares fit. As shown in Table 5.2, the resulting exponents range from 1.16 to 1.74. As expected, higher values were reached for more rigid joints (smaller distance between connections) but no distinct tendency becomes evident when considering all four stiffness classes. However, especially for low importance classes (i.e., I or II according to Eurocode 8) lateral loads may be determined based on their length to the power of 1.5 if a minimum spacing between the connections of 1.0 m is satisfied (see normative annex K of ON B 1995-1-1, 2015 and Wallner-Novak et al., 2013).

Nevertheless, it must be stressed that this simplification is only valid if all walls are equipped with similar connections and equal spacings between them. As soon as one of these two conditions is no longer met, the mentioned approach may lead to highly deviating results. Furthermore it must be pointed out that this process does not allow any inference on absolute stiffness values.

5.2 Influence of vertical joints

According to Follesa et al. (2015), defined structural components of CLT structures should be considered as dissipative zones whereat other should be computed with sufficient overstrength(capacity design rules). Moreover, considering vertical joints and designing them for dissipative behaviour is suggested; at least for structures where ductility class high (DCH) is requested.

The positive effect of vertical joints on the displacement capacity of CLT wall systems is undisputed. Nevertheless, it also has to be mentioned that a segmentation of the wall usually reduces their load-carrying capacity, stiffness and energy dissipation; compare Gavric et al. (2015). Moreover, it must be stressed that also the top joint of a CLT wall system must be designed in such a way that the vertical joint is able to act. In other words: an over strengthened connection between the floor and the elements beneath may lock or at least hinder the vertical displacement and consequently reduce the additional displacement capacity.

A CLT wall with 3.0 m in height and 4.0 m in length, equipped with six equally spaced angle brackets is simulated in three different ways for illustrating the circumstances described: (i) with a vertical joint (15 screws; properties as given in Table 4.1), (ii) with a vertical joint and a 'top joint' and (iii) without a vertical joint. In order to consider the influence of the top joint, in case (ii) an additional stiffness for the vertical joint of 3.0 kN/mm is assumed as a first approximation. This value results from a prepared FE-study and, of course, cannot be stated in general.

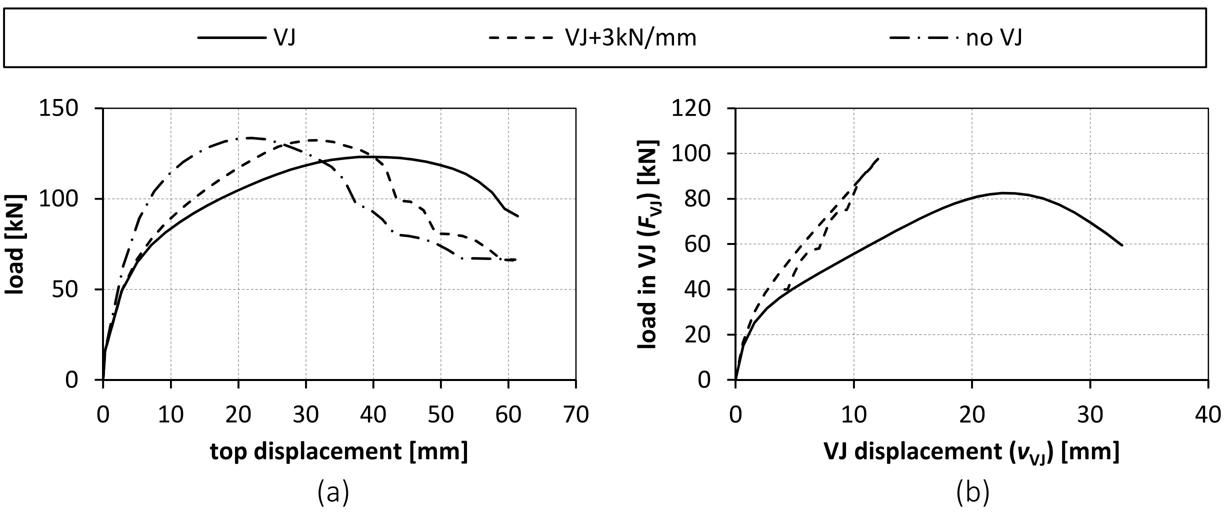

Figure 5.1 Influence of vertical joints on CLT wall systems.

The resulting load-displacement curves for the global behaviour and the vertical joint are depicted in Figure 5.1 (a) and (b), respectively. As expected, integrating a vertical joint improves the displacement property by supporting the rocking behaviour but also slightly reduces the load-carrying capacity. However, as soon as the top joint is considered, displacement occurring in the vertical joint decreases decisively. Moreover, while case (i) exhibits a clear coupled behaviour over the whole loading process, case (ii) switches to a single-coupled behaviour at a total displacement of 26 mm (equates 11.4 mm vertical joint displacement).

5.3 Type of connection and calculation model

Several experimental results confirm that not only hold-downs but also angle-brackets exhibit a distinct load-carrying capacity if loaded in tension (uplift); compare, e.g., Fragiacomo et al. (2011), Gavric et al. (2014) or Flatscher et al. (2015). Nevertheless, hold-downs are still widely used in the practical design of CLT structures. Moreover, some calculation models neglect the uplift capacity of angle-brackets and solely consider hold-downs for preventing uplift of laterally loaded wall systems. Angle brackets, on the other hand, are only used to bear shear loads; compare e.g. Wallner-Novak et al. (2013). Although simple in application, such models lead to relatively high uplift loads in the hold-downs and their transmission to the foundation is often a problematic point in practical design.

Due to this, a further parameter study highlighting the influence of connections and calculation models is performed. In particular three cases are investigated: (i) a wall equipped with two hold-downs and three angle brackets where the hold-downs are considered solely for carrying uplift and the angle brackets for shear; (ii) the same configuration where the uplift capacity of angle brackets is considered too and (iii) a wall without hold-downs but equipped with five angle brackets instead. The corresponding load-displacement diagrams are illustrated in Figure 5.2 and the resulting bearing loads per connection are listed in Table 5.3.

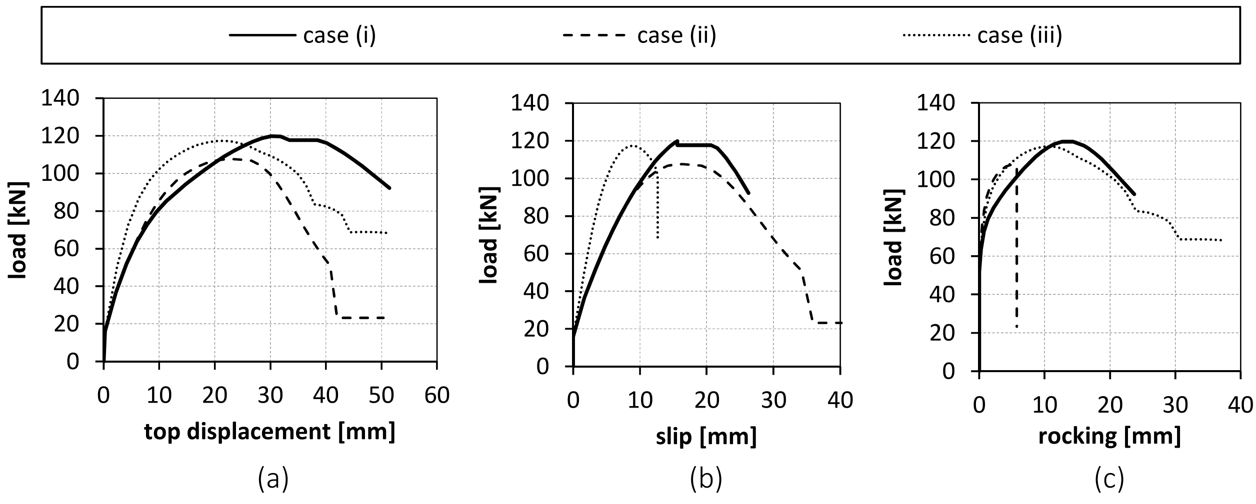

Figure 5.2 Effect of design method and connection type on load-displacement behaviour of a CLT wall system – (a) total deflection; (b) slip contribution; (c) rocking contribution.

As can be seen, the load-displacement graphs for the wall system considered are relatively similar in all three cases, but the slip and rocking contributions vary. Case (i) in particular suggests a balanced behaviour, whereas case (ii) distinctively exhibits slip as the controlling mechanism. In case (iii) rocking caused by the higher shear and slightly lower rocking capacity contributes – in particular after passing the peak load – most to the total deflection.

Table 5.3. Distribution of bearing loads for the single connections.

	connection 1		connection 2		connection 3		connection 4		connection 5	
	shear [kN]	uplift [kN]	shear [kN]	uplift [kN]	shear [kN]	uplift [kN]	shear [kN]	uplift [kN]	shear [kN]	uplift [kN]
Case 1	0	49.82	31.27	0	31.27	0	31.27	0	0	0
Case 2	0	34.86	25.71	4.33	27.41	3.72	29.3	2.81	0	0
Case 3	10.78	22.09	14.67	19.45	17.76	16.36	20.40	12.51	23.62	0

Note: CLT wall l/h = 4.0/3.0m; connections equally distributed (a = 1.0m); q = 20kN/m; coefficient of friction of 0.2

The respective influence on the load distribution for the single connections is probably even more impressive. Taking into consideration the uplift capacity of angle-brackets as implemented in case (ii), the load in the hold-down is reduced to approximately 70 %. In case (iii), where solely angle brackets are applied, the maximum uplift load in the most outer connection even decreases to a ratio of 45 %.

6 Summary and conclusions

A new method for simulating the load-displacement behaviour of various CLT wall systems is presented in the present contribution. The approach uses a continuous and displacement-based approximation of connections' behaviour which finally allows an accurate description of the actual wall behaviour even beyond the peak load.

After verifying the proposed model on experimental results and FE-simulations, a parameter study, focussing on various aspects is conducted. Besides confirming the distinct influence of connections on the behaviour of CLT structures, the study leads to the following main conclusions:

- For low importance classes and in case of similar and equal spaced connections, lateral loads may be disposed basing on the walls' length to the power of 1.5.
- If wall systems are forced to deflections close to permitted interstorey drifts, their secant stiffness decreases significantly. As a consequence, application of initial slip values may essentially underestimate the deflections that actually occur.
- Application of vertical joints does not automatically improve the structural behaviour of CLT buildings. Of course it increases the displacement capacity of CLT wall systems, but on the other hand, load-carrying capacity, stiffness and energy dissipation decrease. Moreover, when determining the behaviour of vertical joints the influence of top joint connections must also be considered; an over strengthened top joint restricts vertical joint displacement.

- Application solely of angle brackets may have a positive influence on load distribution compared to a combination of angle brackets and hold-downs. In particular, it helps in reducing high punctual loads, probably leading to issues when transmitting them to other building components.

Although not mentioned in the present paper, a further point that attracted attention while performing the parameter study is the distinct influence of friction and vertical load on the bearing performance of the CLT wall systems. Further notes regarding these and other points are given in Flatscher (2016).

Finally, although the model presented enables accurate simulation of various wall configurations, it should not be concealed that several effects occurring in CLT structures cannot be considered. In this context, especially the distinct influence of top joints and the bending of floor elements must be mentioned. Moreover, further research on the influence of perpendicular walls is recommended.

7 References

Bachmann, H. (2002), Erdbebensicherung von Bauwerken, 2 edn, Birkhäuser Verlag, Zürich, Switzerland. ISBN: 3-7643-6941-8; (in German).

Brandner, R., Flatscher, G., Ringhofer, A., Schickhofer, G. and Thiel, A. (2016), 'Cross laminated timber (CLT) - overview and development', European Journal of Wood and Wood Products p. 21.

Bratulic, K., Flatscher, G. and Brandner, R. (2014), Monotonic and cyclic behaviour of joints with self-tapping screws in CLT structures, in K.-U. Schober, ed., 'COST Action FP1004, Experimental Research with Timber', University of Bath, Prague, Czech Republic, pp. 1–8.

Ceccotti, A., Lauriola, M. P., Pinna, M. and Sandhaas, C. (2006), SOFIE Project - Cyclic Tests on Cross-Laminated Wooden Panels, in D. A. Bender, D. S. Gromala and D. V. Rosowsky, eds, 'Proceedings of the 9th World Conference on Timber Engineering WCTE2006', Portland, OR, USA.

Dujic, B., Aicher, S. and Zarnic, R. (2005), Racking of Wooden Walls exposed to Different Boundary Conditions, in 'Proceedings of the 38th CIB W18 Meeting - CIB-W18/38-15-6', Stuttgart, Germany.

Dujic, B., Klobcar, S. and Zarnic, R. (2007), Influence of Openings on Shear Capacity of Wooden Walls, in 'Proceedings of the 40th CIB W18 Meeting - CIB-W18/40-15-6', Bled, Slovenia.

EN 1995-1-1 (2004), 'Eurocode 5: Design of timber structures - Part 1-1: General - Common rules and rules for buildings'.

EN 1998-1 (2004), 'Eurocode 8: Design of structures for earthquake resistance - Part 1: General rules, seismic actions and rules for buildings'.

Flatscher, G. (2016), Evaluation and approximation of timber connection properties for displacement-based simulation of CLT wall systems (working title), Doctoral thesis, Graz University of Technology, Graz, Austria. (on going).

Flatscher, G., Bratulic, K., Brandner, R. and Schickhofer, G. (2013), Zusammenfassende und weiterführende Arbeiten zum Verhalten von BSP-Tragwerken bei der Beanspruchungssituation Erdbeben, technical report SGSC 3.1.1_1, holz.bau forschungs gmbh, Graz, Austria. unpublished, (in German).

Flatscher, G., Bratulic, K. and Schickhofer, G. (2014), Screwed joints in cross-laminated timber structures, in 'Proceedings of the 13th World Conference on Timber Engineering WCTE2014', Quebec City, Canada.

Flatscher, G., Bratulic, K. and Schickhofer, G. (2015), 'Experimental tests on cross-laminated timber joints and walls', ICE Journal Structures and Buildings 168(11), 868–877. http://dx.doi.org/10.1680/stbu.13.00085

Flatscher, G. and Schickhofer, G. (2011), Verbindungstechnik in BSP bei monotoner und zyklischer Beanspruchung -Beanspruchung - Statusbericht TU Graz, in '9. Grazer Holzbau-Fachtagung', Graz, pp. G1–G22. (in German).

Flatscher, G. and Schickhofer, G. (2014), Beschreibung der Last-Verschiebungskurven von Verbindungen im Holzbau, in U. Kuhlmann and K. Stephan, eds, 'Holzbau Forschung + Praxis', Stuttgart, Germany. (in German).

Follesa, M., Fragiacomo, M., Vassallo, D., Piazza, M., Tomasi, R., Rossi, S. and Casagrande, D. (2015), A proposal for a new background document of chapter 8 of Eurocode 8, in 'Proceedings of the 2nd INTER Meeting - INTER/48-15-1', Sibenik, Croatia.

Fragiacomo, M., Dujic, B. and Sustersic, I. (2011), 'Elastic and ductile design of multi-storey crosslam massive wooden buildings under seismic actions', Engineering Structures 33(11), 3043–3053.

Gavric, I. (2013), Seismic Behaviour of Cross-Laminated Timber Buildings, Doctoral thesis, Universita degli Studi di Trieste, Trieste.

Gavric, I., Ceccotti, A. and Fragiacomo, M. (2011), Experimental cyclic tests on cross-laminated timber panels and typical connections, in 'Proceedings of the 14th ANIDIS Conference', Bari, Italy.

Gavric, I., Fragiacomo, M. and Ceccotti, A. (2014), 'Cyclic behaviour of typical metal connectors for cross-laminated (CLT) structures', Materials and Structures pp. 1–17. Article in Press.

Gavric, I., Fragiacomo, M. and Ceccotti, A. (2015), 'Cyclic behaviour of CLT wall systems: Experimental tests and analytical prediction models', Journal of Structural Engineering 141(11).

Gavric, I. and Popovski, M. (2014), Design models for CLT shearwalls and assemblies based on connection properties, in 'Proceedings of the 1st INTER Meeting - INTER/47-15-4', Bath, United Kingdom.

Hummel, J., Flatscher, G., Seim, W. and Schickhofer, G. (2013), CLT Wall Elements Under Cyclic Loading – Details for Anchorage and Connection, in R. Harris, A. Ringhofer and G. Schickhofer, eds, 'COST Action FP1004, Focus Solid Timber Solutions – European Conference on Cross Laminated Timber (CLT)', The University of Bath, Graz, pp. 152–165.

Izzi, M., Flatscher, G., Fragiacomo, M. and Schickhofer, G. (2016), 'Experimental investigations and design provisions of steel-to-timber joints with annular-ringed shank nails for Cross-Laminated Timber structures', Construction and Building Materials 122, 446-457.

ON B 1995-1-1 (2015), 'Eurocode 5: Design of timber structures - Part 1-1: General - Common rules and rules for buildings (National specifications for the implementation of ON EN 1995-1-1, national comments and national supplements)'. (in German).

Popovski, M. and Karacabeyli, E. (2011), Seismic Performance of Cross-Laminated Wood Panels, in 'Proceedings of the 44th CIB W18 Meeting - CIB-W18/44-15-7', Alghero, Italy.

Pozza, L., Massari, M., Savoia, M. and Ferracuti, B. (2016), Experimental campaign of mechanical CLT connections subjected to a combination of shear and tension forces, in 'Proceedings of the 3nd International Conference on Structures and Architecture ICSA2016', Guimaraes, Portugal.

RFEM 5 (2015). Structural Analysis and Design Software, Dlubal Software GmbH, Version 5.05.xx. www.dlubal.com

Seim, W. and Hummel, J. (2013), CLT-wall elements - monotonic and cyclic testing, technical report 2D, Universität Kassel, Kassel, Germany. porject: optimberquake.

Sustersic, I. and Dujic, B. (2012), Simplified cross-laminated timber wall modelling for linear-elastic seismic analysis, in 'Proceedings of the 45th CIB W18 Meeting - CIB-W18/45-15-6', Växjö, Sweden.

Tomasi, R. and Smith, I. (2014), 'Experimental characterization of monotonic and cyclic loading responses of CLT panel-to-foundation angle bracket connections', Journal of Materials in Civil Engineering .

Uibel, T. and Blaß, H. J. (2007), Edge joints with dowel type fasteners in cross laminated timber, in 'Proceedings of the 40th CIB W18 Meeting - CIB-W18/40-7-2', Bled, Slovenia.

Wallner-Novak, M., Koppelhuber, J. and Pock, K. (2013), Brettsperrholz Bemessung - Grundlagen für Statik und Konstruktion nach Eurocode, 1. edn, proHolz Austria. ISBN: 978-3-902320-96-4; (in German).

Discussion

The paper was presented by G Flatscher

H Blass asked about reverse cyclic loading. G Flatscher replied that his work only applies to monotonic loading and perhaps reduction in load can be considered in the reverse cyclic cases. There were discussions about displacement versus load capacity. The displacement capacity would be important for inter storey drift considerations. H Blass asked how the authors took into account of the floor reducing the load between the panels. G Flatscher replied that additional tests were conducted to generate data for the model. H Blass commented that high stiffness and capacity of the vertical joint could be used to account for the influence of the floor.

LM Ottenhaus asked about the influence of the failure mode on ductility for cases 1 and 3. G Flatscher replied that rocking and slip were the primary failure modes and ductility might be increased in the angle bracket case.

E Ussher commented that the load distributions depended on the length of the wall and stiffness and asked about influence of vertical load and openings. G Flatscher replied that there could be many influences on the behaviour of the walls but for single family house it is not necessary to consider non-linear analysis and influence of vertical loads was not considered here. He also cited work of Dujic 2007 that considered the influence of opening on the stiffness of the CLT elements.

A Hashemi questioned the lack of hold-downs which might not be true in more complete systems. G Flatscher replied that this could work when the angle bracket are considered as a special hold-down that took both shear and uplift.

M Gershfeld commented about the zipper effect that could happen with a line of connectors. G Flatscher replied that it would also be true for the hold-down case.

S Franke asked what kind of friction was considered. G Flatscher replied that vertical load and additional uplift load were considered and a coefficient of friction of 0.2 was used as a constant for the connections at the base. M Gershfeld commented about influence of interaction between shear and uplift of the angle bracket.

LM Ottenhaus commented that the function of hold-down and angle brackets in reverse cyclic cases to be used as fuse to dissipate energy and/or to carry uplift.

P Zarnani commented also on the need for hold-downs.

A Frangi commented that angle bracket can take shear as well as uplift if sized and designed well and spaced properly. These connection devices were intended for small buildings and lighter structures.

Structural analysis of in-plane loaded CLT beam with holes: FE-analyses and parameter studies

Mario Jelec, Department of Materials and Structures, University of Osijek, Croatia

Vlatka Rajcic, Department of Structures, University of Zagreb, Croatia

Henrik Danielsson, Division of Structural Mechanics, Lund University, Sweden

Erik Serrano, Division of Structural Mechanics, Lund University, Sweden

Keywords: cross laminated timber, CLT, in-plane loading, bending stress, shear stress, FE-analysis, holes, stress concentration, distribution of stress

1 Introduction

Thanks to its crosswise orientation, CLT is a very versatile material capable of carrying both in- and out-of-plane loads and can be used for wall or floor elements as well as for linear members. Despite its obvious benefits, the current status of CLT in European product and standard design still presents a major obstacle for developers, producers and designers, since properties and design for CLT have been regulated via national or international European Technical Approvals (ETAs). A product standard for CLT, EN 16351 (2015) has recently been published, but CLT is still not included in the European timber design code Eurocode 5, so further research, development and standardization work (including regulations for testing, design and execution), is needed (Brandner, 2016).

The aim of this paper is to investigate the performance of CLT beams with and without holes loaded in-plane under various loading conditions with special emphasis on shear loading and the in-plane shear behaviour considering the complex internal structure. CLT beams present a much better solution for beams with holes or notches as compared to glued laminated timber beams thanks to its lay-up where tensile forces perpendicular to the beam axis can be transferred by the transversal layers. In order to have in-depth understanding of the local mechanical behaviour in shear stress transfer between laminations, numerical analyses based on 3D-FE models are used.

FE-based approaches have been used previously for investigations of CLT behaviour (Blass and Görlacher 2002, Bejtka 2011, Flaig 2013) most of them being based on using beam elements or plane elements and not including the influence of e.g. the orthotropic material properties, beam build-up in the out-of-plane direction or stress distribution for various loading condition. Bejtka (2011) conducted comprehensive experimental and numerical analysis on cross and diagonal laminated timber beams, but since the work was focused more on determining bending strength and stiffness, complex shear stress states were not analysed completely.

2 Shear strength of CLT beams loaded in plane

In CLT beams exposed to in-plane loading normal and shear stresses occur. According to Schickhofer et al. (2010), Bogensperger et al. (2010), Flaig and Blass (2013) and Flaig (2013), verification of normal stresses in-plane only takes into account the bending resistance of the net cross section area, here meaning the layers in the direction of stresses. The contribution of the transverse layers (α=90°) is neglected because of the high MOE-ratio $E_0/E_{90}\approx 30$. When it comes to verification of shear strength, calculation of shear stresses is however much more complicated. In general, according to Bogensperger et al. (2007, 2010), Flaig and Blass (2013) and Brandner et al. (2013) three different shear failure mechanisms have to be distinguished for CLT with and without adhesive bonding on the narrow face:

- Failure mode I (FM I) or gross shear failure of the CLT element by shear failures in all layers of CLT with narrow faces bonded layers
- Failure mode II (FM II) or net shear failure of the CLT element by shear failure in net cross sections of CLT
- Failure mode III (FM III) or torsion failure in the crossing areas between orthogonally bonded lamellae involving torsional and unidirectional shear stresses

2.1 Analytical approach

For evaluation of shear stresses in CLT wall element loaded in- plane, an efficient mechanical model for internal stress verification has been evaluated by Moosbrugger et al. (2006) and Bogensperger et al. (2007, 2010). Considering uniform shear loading on wall boundaries, an elementary representative volume sub element (RVSE) has been introduced, which presents the smallest unit cell at intersections between two orthogonal boards whose internal stress state describes the global stress state of the CLT element. In case of CLT beams, which are exposed to both bending and shear loading Flaig (2013) proposed a design procedure for verification of shear stresses, for each of the three failure modes. In case of FM I and FM II, shear stresses τ_{xy}, causing failure parallel and perpendicular to the grain, can be evaluated according to Bernoulli-Euler beam theory using the following expressions:

$$\tau_{xy,gross} = \frac{V_y \cdot S_{z,gross}}{I_{z,gross} \cdot t_{gross}} \qquad \text{(FM I)} \qquad (1)$$

$$\tau_{xy,net} = \frac{V_y \cdot S_{z,net}}{I_{z,net} \cdot t_{net}} \qquad \text{(FM II)} \qquad (2)$$

Maximum values of stresses can be calculated as peak values of the parabolic functions according to equation 3 and 4 (Fig. 1)

$$\tau_{xy,gross,max} = 1{,}50 \cdot \frac{V_y}{h \cdot t_{gross}} \qquad (3)$$

$$\tau_{xy,net,max} = 1{,}50 \cdot \frac{V_y}{h \cdot t_{net}} \qquad (4)$$

An example of shear stress distribution in the longitudinal and transversal layers of a CLT beam, with four lamellae in the longitudinal layers, is shown in Fig. 1. According to Flaig (2013) in case of even number of lamellae in longitudinal layers Eq. 3 overestimates the maximum shear stress in the gross cross section, where in case of odd number of lamellae in longitudinal layers, maximum net shear stresses are overestimated by Eq. 4.

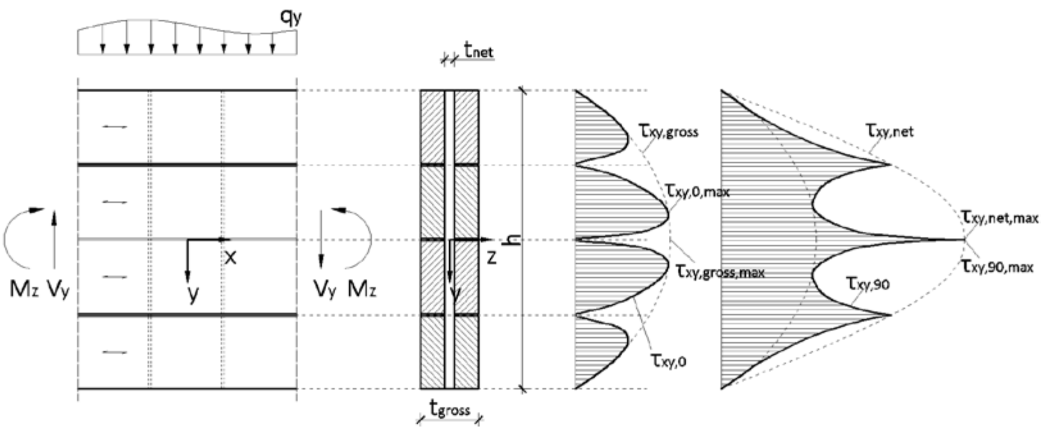

Figure 1. Distribution of shear stresses in the lamellae of CLT beam with four longitudinal lamellae: shear stresses $\tau_{xy,0}$ in longitudinal lamellae (left) and shear stress $\tau_{xy,90}$ in transversal lamellae (right)

In case of FM III, shear stresses originating from three different types of load transfer and acting in the crossing areas between the orthogonally bonded lamellae have to be considered (Flaig, 2013): shear stresses parallel to the beam axis (τ_{zx}), torsional shear stresses (τ_{tor}) and shear stresses perpendicular to the beam axis (τ_{zy}).

The shear stresses parallel to the beam axis, τ_{zx}, are caused by the change in the bending moment. The maximum values of the shear stress component τ_{zx} is found at the outermost lamellae of the beam and can be calculated according to:

$$\tau_{zx} = \frac{6V_y}{b^2 \cdot n_{CA}} \cdot \left(\frac{1}{m^2} - \frac{1}{m^3}\right) \qquad (5)$$

Torsional shear stresses, τ_{tor}, arise due to the eccentricity between the centre lines of adjacent lamellae. Flaig assumed equal torsional moments and hence equal torsional shear stresses for all crossing areas in the beam height direction, based on the condition that the lamellae in the transversal layers are assumed to remain straight in the deformed beam. The maximum torsional shear stress can then be calculated according to:

$$\tau_{tor} = \frac{3V_y}{b^2 \cdot n_{CA}} \cdot \left(\frac{1}{m} - \frac{1}{m^3}\right) \tag{6}$$

Shear stresses perpendicular to the beam axis, τ_{zy}, arise due to external concentrated forces, e.g. support reactions or external forces, or close to holes or notches. For a CLT beam without a hole or a notch and exposed to an external force q_y [N/m] applied to the end grain of the transversal layers, shear stresses can be evaluated according to Eq. 7 (Flaig, 2015).

$$\tau_{zy} = \frac{q_y}{m \cdot b \cdot n_{CA}} \tag{7}$$

In the design of CLT beams each of stress component must be verified with the corresponding shear strength related to relevant shear failure mode. Also, in the crossing areas interaction of shear stresses have to be considered (Flaig, 2013).

3 Shear strength of CLT beams with a hole

Flaig (2013) derived shear stress concentration factors for CLT beams with holes by performing numerical parameter analysis on girder FE-models (isotropic beam-spring models). In later work (Flaig, 2014) some additional idealisations were introduced, such as equal width *b* of all lamellae and constant ratio between the thickness of an individual longitudinal layer and the number of glue lines that the respective layer shares with adjacent transversal layers. The ratios $k_{h,1}$ and $k_{h,2}$, representing ratios of maximum shear stress at the hole to shear stress in an undisturbed beam of equal dimensions, were derived. The following equations for stress verification for CLT beams with holes were derived.

Bending stresses in the middle of the beam span and at the edge of the hole:

$$\sigma_{m,net} = \frac{M}{W_{net}} = \frac{24 \cdot F_{max}}{t_{net,0} \cdot h} \tag{8}$$

$$\sigma_{m,net,h} = \frac{15F_{max} \cdot h^2}{t_{net,0} \cdot (h^3 - h_h^3)} + \frac{3F_{max} \cdot h}{2 \cdot t_{net,0} \cdot h_r^2} \tag{9}$$

Tensile stresses perpendicular to beam axis:

$$F_{t,90} = F_V + F_M = F_{max}\left[\left(\frac{3h_h}{4h} - \frac{h_h^3}{4h^3}\right) + \left(\frac{0.008 \cdot x_h}{h_r}\right)\right] \tag{10}$$

$$\sigma_{t,90} = k_k \cdot \frac{F_{t,90}}{a_r \cdot t_{net,90}}; \text{with } a_r = \min\{b; 0.3(h + h_h)\} \tag{11}$$

Shear stresses (FM I, FM II and FM III):

$$\tau_{xy,gross,h} = 1{,}50 \cdot \frac{V_y}{(h - h_h) \cdot t_{gross}} \tag{12}$$

$$\tau_{xy,net,h} = k_{h2} \cdot \tau_{xy,net,max} = \left[0.103 \cdot \left(\frac{h_h \cdot l_h}{h^2} \cdot m^2\right) + 1.27\right] \cdot \tau_{xy,net,max} \tag{13}$$

$$\tau_{tor,h} = k_{h1} \cdot \tau_{tor} = \left[1.81 \cdot \left(\frac{l_h}{h} \cdot \frac{h_h}{h - h_h}\right) + 1.14\right] \cdot \tau_{tor} \tag{14}$$

$$\tau_{zx,h} = k_{h2} \cdot \tau_{zx} = \left[0.103 \cdot \left(\frac{h_h \cdot l_h}{h^2} \cdot m^2\right) + 1.27\right] \cdot \tau_{zx} \tag{15}$$

$$\tau_{zy,h} = \frac{F_{t,90}}{n_{CA} \cdot a_r \cdot h_r}; \text{with } h_r = \min\{h_{r,top}; h_{r,bottom}\} \tag{16}$$

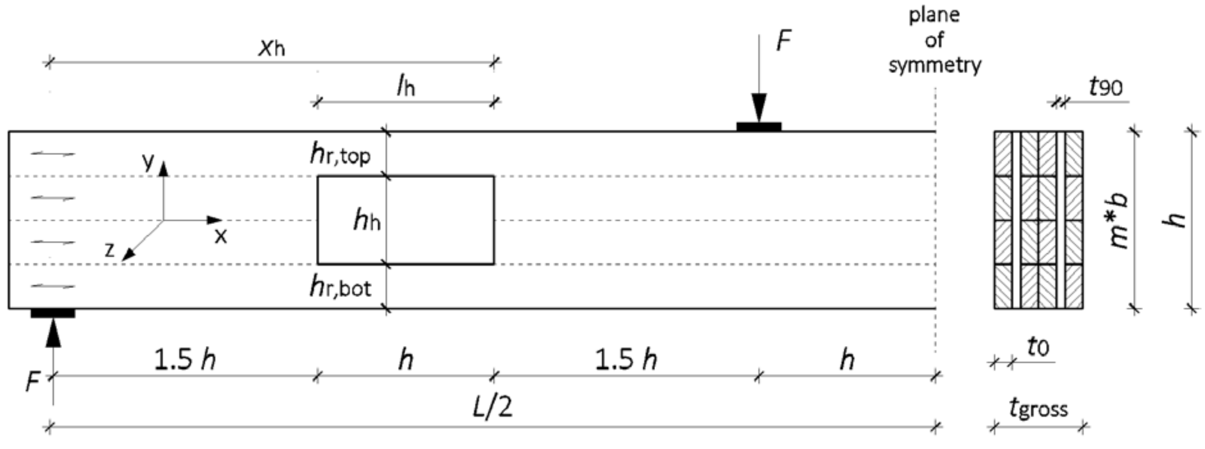

Figure 2. Geometry and layup of analyzed CLT beam

4 Numerical FE-analysis

CLT beams with and without holes were modelled. The CLT is modelled as a layered structure, each layer consisting of laminations (boards). The elements used are second order 3D elements (20-node) with full integration. The boards are assumed to be perfectly bonded only on their flat faces, while no edge bonding is assumed. Instead, a 0.1 mm gap between the boards within one layer is assumed. The perfect bond between the flat face areas of the boards was modelled by using contact elements in combination with perfect bonding and no sliding options of the software used (Ansys 17).The lamination material is assumed to be linear elastic and transverse isotropic. The material parameters are the same as used by Flaig (2014), strength class T14 according to EN 14080 see Table 1. The double symmetry of the test set-up is taken into account and thus only one quarter of each setup is modelled. Element mesh size was uniformly set to 5x5x5 mm^3 in the zones of relevance where stresses were evaluated, while in the more distant areas coarser mesh size was used.

Table 1. Material properties of longitudinal and transversal lamellae in N/mm^2

E_x	E_y	E_z	v_{xy}	v_{yz}	v_{xz}	G_{xy}	G_{yz}	G_{xz}
11000	370	370	0,35	0,35	0,35	690	69	690

5 Discussion and comparison of results

Results from the FE-analysis are presented below. The considered geometries and CLT lay-ups are the same as used for the experimental tests of CLT beams with holes reported by Flaig (2014). The stress values are calculated based on an applied load corresponding to the experimentally found mean failure loads. All stress components given below refer to the coordinate system shown in Fig. 2.

5.1 Bending stress analysis

Structural analysis on CLT beams was performed on six models whose dimensions, geometry and CLT lay-up are presented Table 2. In comparing the numerical results with the analytical, the mean value of bending stresses $\sigma_{m,net}$ over the net area at the mid span of the beam was calculated (Fig. 3) and compared with values obtained by Eq. 8.

Table 2. Dimension and layup of analysed CLT beams in [mm]

Model		h	h_h	h_r	t_{gross}	t_0	t_{90}	b	L	*layup*
without hole	H300	300	-	-	160	30	20	150	3150	l-c-l-l-c-l
	H600	600	-	-	150	30	15	150	6300	l-c-l-l-c-l
with hole	H300-0.4	300	120	90	160	30	20	150	3150	l-c-l-l-c-l
	H300-0.5	300	150	75	160	30	20	150	3150	l-c-l-l-c-l
	H600-0.4	600	240	180	150	30	15	150	6300	l-c-l-l-c-l
	H600-0.5	600	300	150	150	30	15	150	6300	l-c-l-l-c-l

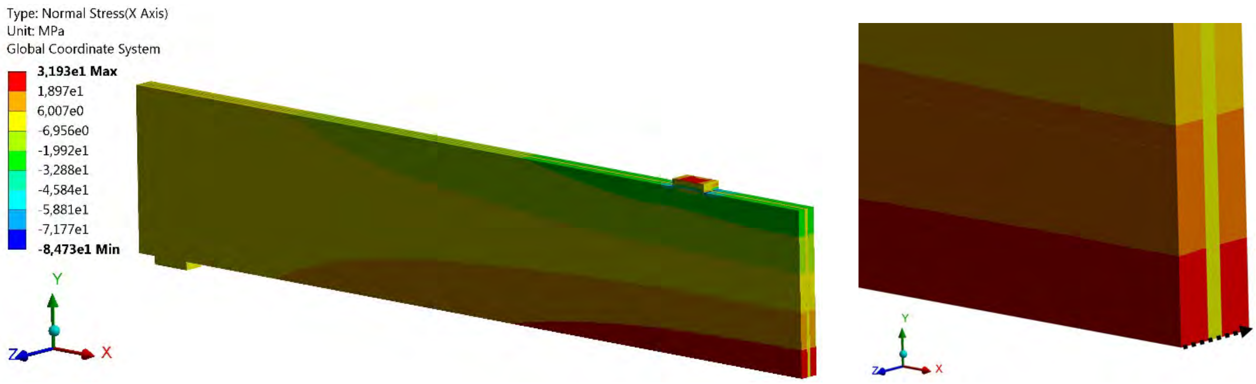

Figure 3. Normal stresses σ_x due to bending for model without hole H600 (left), and the stress path at the mid-span of beam for obtaining mean stress values (right)

In case of CLT beams with holes, additionally bending stresses at the edge of the hole further from the support, $\sigma_{m,net,h}$, were derived and compared with Eq. 9, which was proposed by Flaig (2014). Summarized results are presented in Table 3 and in general, a good agreement is obtained.

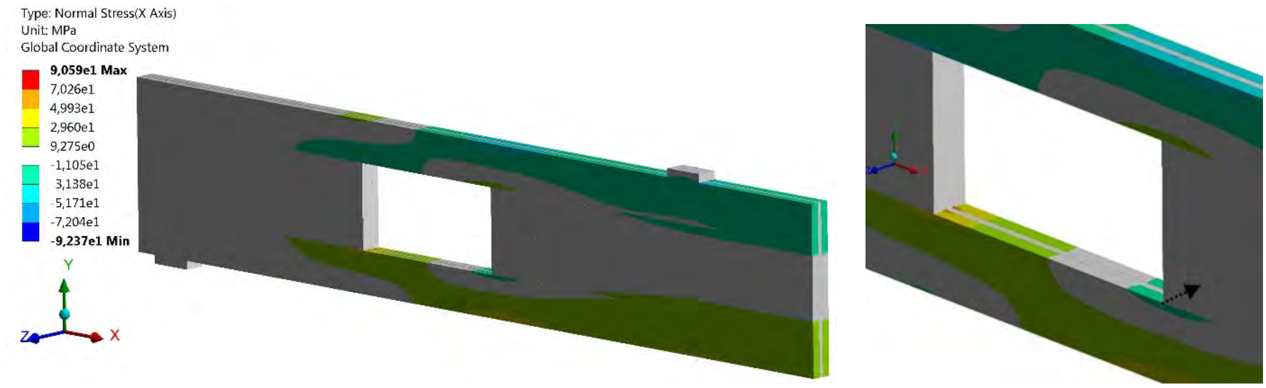

Figure 4. Normal stresses σ_x due to bending for model with hole H600-0.5 (left), and the stress path at the egde of the hole further from support for obtaining mean stress values (right)

Table 3. Summarized results of normal stresses σ_x due to bending

	Model	F_{max} [kN]	Numerical value [N/mm^2]		Analytical value [N/mm^2]	
			$\sigma_{x,net}$	$\sigma_{x,net,h}$	$\sigma_{m,net}$	$\sigma_{m,net,h}$
without hole	H300	59.70	41.59	-	39.80	-
	H600	85.46	29.89	-	28.48	-
with hole	H300-0.4	59.70	40.36	48.29	39.80	54.20
	H300-0.5	64.30	43.47	67.13	42.90	73.50
	H600-0.4	109.76	37.29	47.76	36.62	49.88
	H600-0.5	85.46	28.94	47.05	28.48	48.84

5.2 Tensile stress perpendicular to the beam axis

For CLT beams with holes, tensile stress acting perpendicular to the beam axis at the vertical edges of the holes were calculated according Eq. 10, which is given in the German National Annex (NA) to Eurocode 5 for glulam beams with holes. Since numerical results were mesh size sensitive and high stress concentrations were obtained (Fig. 5), the mean tensile stress in the transversal lamellae at the edges of the holes was calculated according to Eq. 17 and compared with analytical values (Fig. 5).

$$\sigma_{y,90,mean} = \frac{\int \sigma_{y,90}}{A} = \frac{F_{t,90}}{a_r \cdot t_{90}} \tag{17}$$

The tensile stress in the transversal lamellae was calculated using an effective width, a_r, which is chosen as the smaller value of the actual width of the lamellae and the maximum value given in the German NA to EC5 for glulam beams with reinforced holes. The highly non-uniform distribution of tensile stresses is accounted for in the German NA with a factor k_k = 2.0 (Eq. 11).The mean stress from the FE-model was thus compared with the mean analytical value by neglecting the factor k_k. The results are presented in Table 4, showing in general a good agreement with the analytical results.

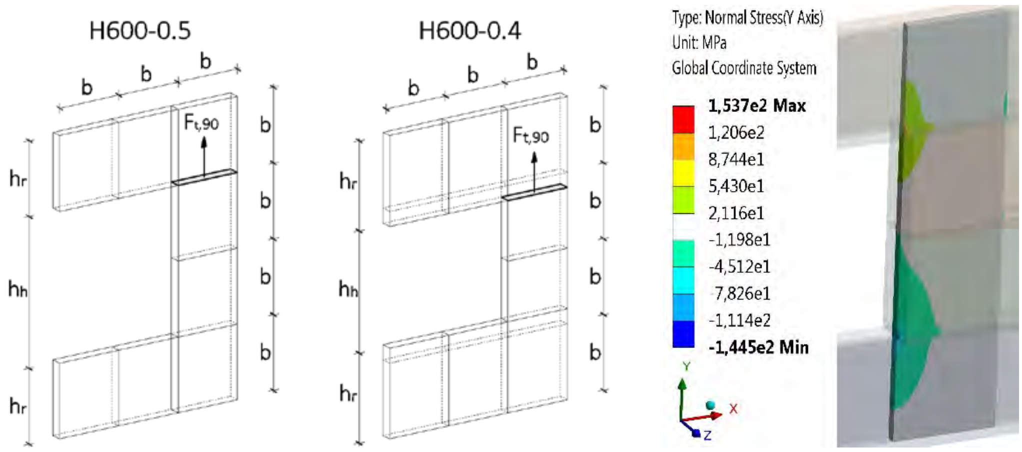

Figure 5. Cross-section area for determining total tensile force perpendicular to beam axis, $F_{t,90}$, (left) and obtained stress concetration at corner of hole for model H600-0.5 (right)

Table 4. Summarized results of tensile stresses perpendicular to beam axis $\sigma_{t,90}$

Model	F_{max} [kN]	Numerical value		Analytical value		
		$F_{t,90}$ [kN]	$\sigma_{t,90,mean}$ [N/mm^2]	$F_{t,90}$ [kN]	$\sigma_{t,90,mean}$ [N/mm^2]	$\sigma_{t,90}$ [N/mm^2]
H300-0.4	59.70	7.99	3.17	10.46	4.15	8.30
H300-0.5	64.30	13.07	4.84	13.11	4.85	9.71
H600-0.4	109.76	19.86	8.82	19.28	8.57	17.14
H600-0.5	85.46	26.40	11.73	18.10	8.04	16.10

5.3 Shear stress analysis

In shear stress analysis, verification of each stress component was done, including shear stresses in gross and net sections as well as over crossing areas of laminations. For models without holes, shear stresses τ_{xy} and τ_{zx} in transversal lamellae located between the load point and support are presented in Fig. 6, while for models with holes shear stresses τ_{xy}, τ_{zx} and τ_{zy} in the first transversal lamellae near the hole are presented in Fig. 7. The distribution of shear stresses τ_{xy} across the beam height is also presented over four different stress paths in Fig. 8, with the following meaning a) at the surface of longitudinal lamellae, b) at the centre of longitudinal lamellae, c) at the surface of transversal lamellae (over crossing areas) and d) at the centre of transversal lamella. Stress paths are marked as black arrows in Fig. 6 and Fig. 7.

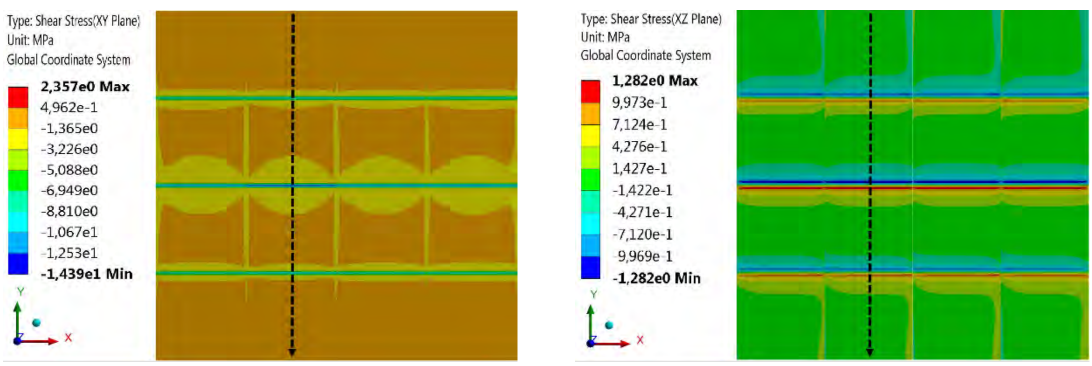

Figure 6. Results of shear stresses τ_{xy} (left) and shear stresses τ_{zx} (right) in model H600

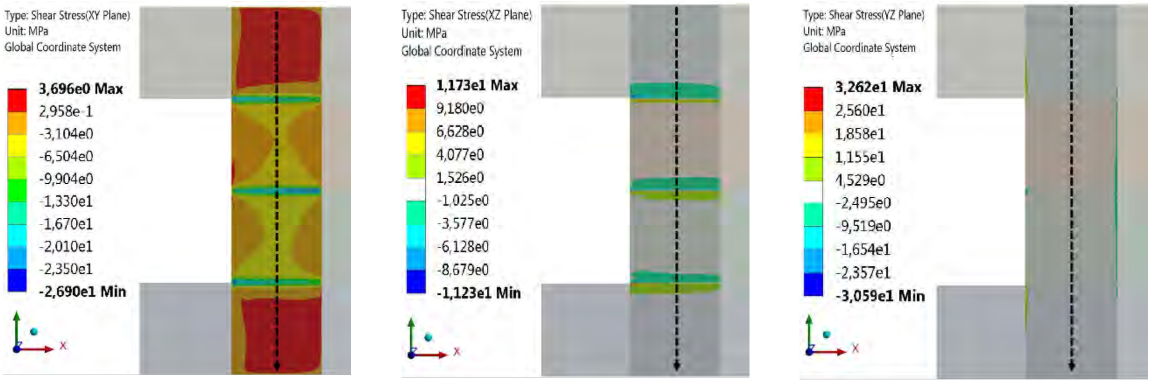

Figure 7. Results of shear stresses τ_{xy}, τ_{zx} and τ_{zy} in model H600-0.5 (from left to right)

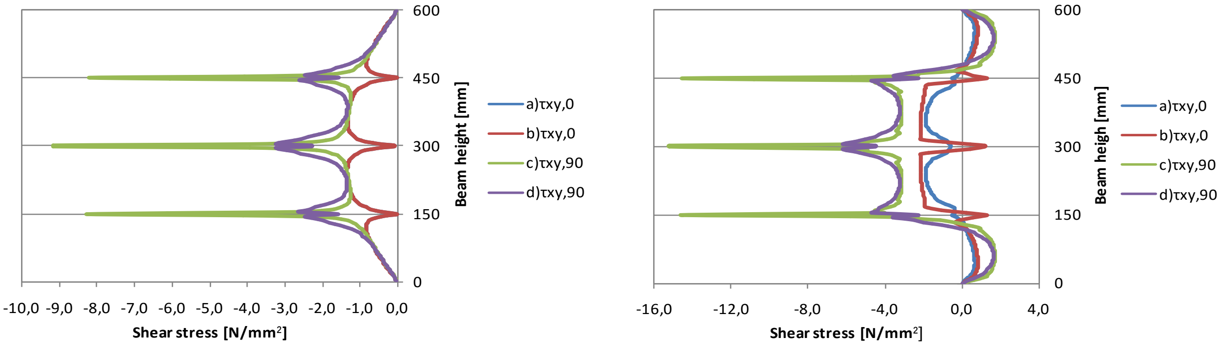

Figure 8. Distribution of shear stresses τ_{xy} across the beam height over four different stress paths (H600 - left, H600 - 0.5 - right)

From the presented distributions some differences may be noticed comparing models with and without holes. In models with holes the distribution of shear of stress τ_{xy} is slightly disturbed due to the small distance to the hole and higher peak values may be noticed. When it comes to shear stress τ_{zx}, from Fig. 9 (left) it may be noticed that for models without holes the maximum value occurs at the center of the beam, which is not in accordance with Flaig`s assumption explained earlier. In case of models with holes, maximum values occur at sections that are coincident with the edges of the hole (Fig. 9 (right)), with concentration of stresses at the corner of the hole. In general, from all the presented graphs, a non-uniform stress distribution may be noticed. From this reason, in verification of each failure mode (FM I, FM II and FM III) mean stresses over appropriate areas or paths were derived and compared with analytical values.

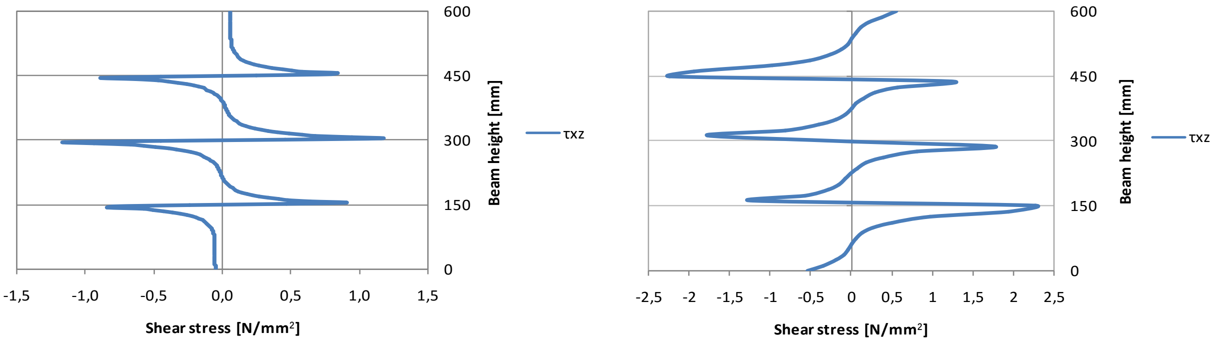

Figure 9. Distribution of shear stresses τ_{zx} across the beam height (H600 - left, H600-0.5 - right)

5.3.1 Verification of FM I

In case of CLT beams without holes, the maximum value of shear stress $\tau_{xy,0}$ along a stress path across the centre of the longitudinal lamellae (curve b) of Fig. 8 (left)) is compared with the analytical values (Eq. 3). For CLT beams with holes, the distribution of shear stresses $\tau_{xy,0}$ over beam height in the section that passes through the hole is presented in Fig. 10. The mean value of gross shear stress over the beam thickness was calculated (Fig. 10) and compared with the analytical equation (Eq. 12). Summarized results are presented in Table 5 and in general, a good agreement is obtained. In the case of model H300 the difference is 11.03%, while the expected error is 25% (Flaig, 2013). For model H600 the difference is smaller, 5.75%, and close to the predicted error 6.3% (Flaig, 2013). For models with holes, differences are even smaller and are for each of the analysed model below 5%.

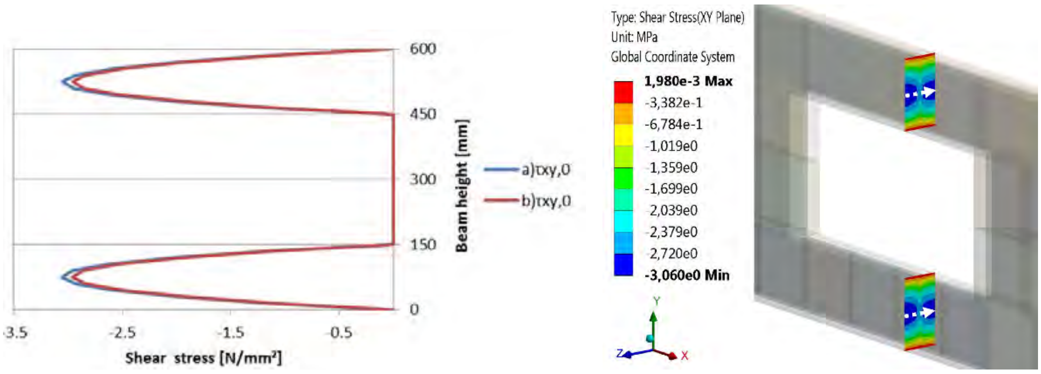

Figure 10. Distribution of shear stress τ_{xy} over beam height (left) and stress path marked as arrow for determining mean values in beam thickness direction (right)

Table 5. Summarized results of shear stresses τ_{xy} for verification of FM I

	Model	F_{max} [kN]	Numerical value [N/mm²]		Analytical value [N/mm²]
			$\tau_{xy,0,max}$	$\tau_{xy,0,mean}$	$\tau_{xy,gross}$
without hole	H300	59.70	1.66	-	1.86
	H600	85.46	1.34	-	1.42
with hole	H300-0.4	59.70	3.48	3.01	3.11
	H300-0.5	64.30	4.54	4.04	4.02
	H600-0.4	109.76	3.10	3.05	3.05
	H600-0.5	85.46	2.96	2.86	2.85

5.3.2 Verification of FM II

In relation to FM II, evaluation of the maximum value of the net shear stress $\tau_{xy,net}$ according to the FE-analyses is problematic since the stress distribution is highly non-uniform and much affected by e.g. the discontinuities introduced by the gaps between the lamellae. Thus, mean values of net shear stresses $\tau_{xy,net}$ across the critical cross sections of the transversal lamellae were obtained by integration of stresses (see Fig. 11). These correspond then to the total (resultant) shear force F_{xy} divided by cross section area of the transversal lamellae according to Eq. 18. Summarized results are presented in Table 6. From presented results, general good agreement is obtained except in the case of model H600-0.4 and H600-0.5 where larger difference may be noticed. Possible reason of that could be influence of mesh size, since using a finer mesh, the numerical values get closer to analytical ones.

$$\tau_{xy,net,mean} = \frac{\int \tau_{xy}}{A} = \frac{F_{xy}}{b \cdot t_{90}} \tag{18}$$

Table 6. Summarized results of net shear stresses τ_{xy} for verification of FM II

	Model	F_{max} [kN]	Numerical value [N/mm²] $\tau_{xy,net,mean}$	Analytical value [N/mm²] $\tau_{xy,net}$
without hole	H300	59.70	7.46	7.36
	H600	85.46	6.76	7.12
with hole	H300-0.4	59.70	11.22	10.71
	H300-0.5	64.30	12.68	11.86
	H600-0.4	109.70	14.96	17.54
	H600-0.5	85.46	12.34	14.91

5.3.3 *Verification of FM III*

In case of FM III, according to Flaig (2013) interaction between shear stresses in beam direction τ_{zx} and torsion shear stresses τ_{tor} should be verified over crossing areas. From the FE-results, the relevant shear stress components can of course be directly evaluated in relation to the corresponding strength values, without decomposing them into transverse, longitudinal and torsional shear. For comparison with analytical expressions, however, mean stress values were calculated by integration of stresses over each crossing area (Fig 11). In that sense, the total (resultant) shear forces F_x and F_y were obtained and divided with crossing areas (Eq. 19 and 20). From the FE-software the torsional moment M_{tor} could be obtained and torsion stresses were calculated according to Eq. 21 (Blass, 2002). Results are given in Table 7.

$$\tau_{zx,\mathrm{cross},mean} = \frac{\int \tau_{zx}}{A_{cross}} = \frac{F_x}{b \cdot b} \tag{19}$$

$$\tau_{zy,\mathrm{cross},mean} = \frac{\int \tau_{zy}}{A_{cross}} = \frac{F_y}{b \cdot b} \tag{20}$$

$$\tau_{tor} = \frac{M_{tor}}{I_p} \cdot \frac{b}{2} \tag{21}$$

From Table 7 it may be noticed that torsional stresses are not equal over each crossing area and for model H600 they are higher close to the neutral axis. In case of shear stress τ_{zy} in models without holes, the obtained numerical values are quite small, in accordance with theoretical background. For models with holes for torsion shear stresses τ_{tor} a larger difference between numerical and analytical results may be noticed. A possible reason for this is the position and size of the hole in relation to crossing areas of first neighbouring vertical lamellae. Other reasons could be the influence gap size between laminations and width of first vertical lamellae near the hole since these parameters were not known completely. Since the analytical approach is based on a girder model, and involves some idealizations, the real arrangement of the longitudinal and transversal laminations is not taken into account. The presented numerical analysis was done on a limited number of models, so a more comprehensive parameter analysis should be carried out to validate the FE-model.

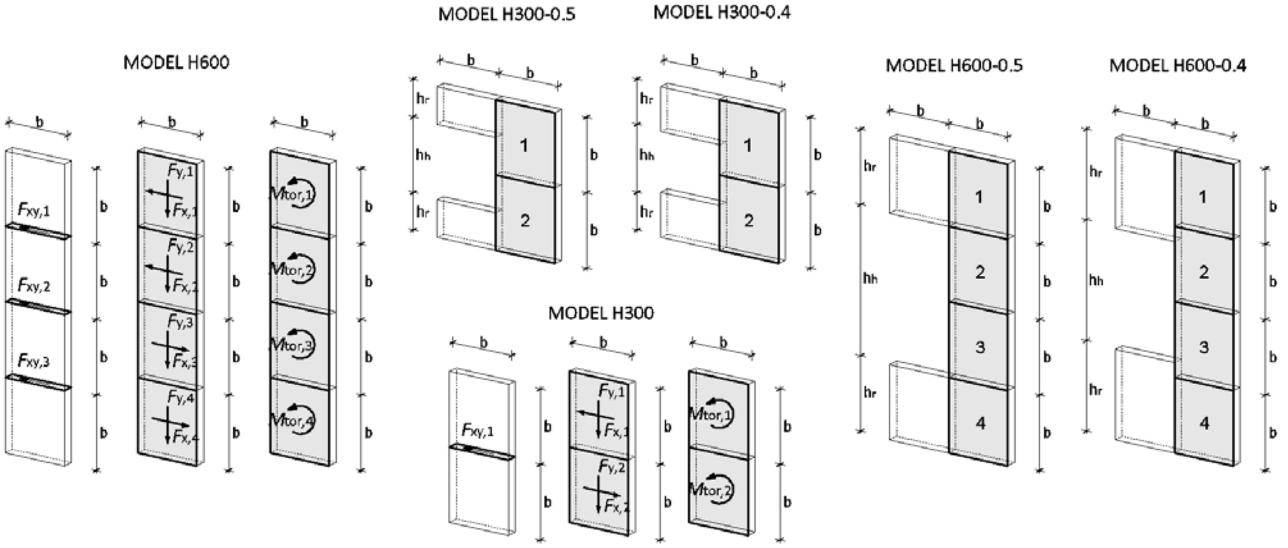

Figure 11. Cross-sectional areas for obtaining resultant forces in verification of FM II and FM III

Table 7. Summarized results of shear stresses over crossing areas for verification of FM III

	Model	F_{max}	Cross. area	Numerical results [N/mm²]			Analytical results [N/mm²]		
				$\tau_{zx,mean}$	τ_{tor}	$\tau_{zy,mean}$	τ_{zx}	τ_{tor}	τ_{zy}
without holes	H300	59.70	1	0.48	0.79	0.06	0.49	0.75	-
			2	0.48	0.79	0.05			
	H600	85.46	1	0.26	0.32	0.04	0.26	0.67	-
			2	0.07	0.69	0.01			
			3	0.07	0.68	0.01			
			4	0.26	0.32	0.05			
with holes	H300-0.4	59.70	1	0.73	1.11	0.25	0.71	1.75	0.29
			2	0.72	1.11	0.29			
	H300-0.5	64.30	1	0.81	1.24	0.43	0.79	2.37	0.51
			2	0.81	1.24	0.51			
	H600-0.4	109.70	1	0.28	0.90	0.38	0.66	2.01	0.35
			2	0.46	0.90	0.35			
			3	0.45	0.91	0.36			
			4	0.29	0.91	0.41			
	H600-0.5	85.46	1	0.49	1.43	0.48	0.55	1.96	0.40
			2	0.13	1.11	0.50			
			3	0.12	1.11	0.50			
			4	0.50	1.43	0.49			

6 Conclusions and further work

In general, for CLT beams without holes, the obtained results are in good agreement with simplified analytical values proposed by Flaig (2013). The main difference relates to the distribution of shear stresses τ_{zx} over the crossing areas per height of CLT beam, where the maximum value is found to be in middle of beam height in contradiction with the assumption of Flaig. For CLT beams with holes, the obtained results are in good agreement with analytical values except the torsion shear stresses over the crossing area of transversal lamellae near the hole. The analytical values were smaller in all cases since they were obtained by Eq.19, which does not consider stress concentrations. The real arrangement of the longitudinal and transversal lamellae in relation to the hole position is a second reason for the difference observed. The analytically derived equations are namely based on idealised girder models which cannot model an arbitrary hole position. In case of tensile stress perpendicular to beam axis, the tensile force was calculated according to German NA to EC5 for glulam beams with holes. Since the failure mechanism for glulam and CLT beams with holes is different, the proposed equations should be validated on a larger number of CLT models. For the presented limited number of models, the agreement between mean values is acceptable, even if high stress concentrations at the corner of the holes were obtained. The presented analyses are a first attempt to contribute to the on-going review process of Eurocode 5 as regards CLT beams with holes. Currently there are no regulations on how to design such beams, so further experimental and numerical investigations are planned.

7 Symbols

t_{gross}	total thickness of CLT beam
t_{90}	thickness of vertical lamellae
t_0	thickness of longitudinal lamellae
t_{net}	smaller of the sum of the thickness of longitudinal and transversal layers
$t_{net,0}$	sum of the thickness of longitudinal lamellae
$t_{net,90}$	sum of the thickness of transversal lamellae
n_{CA}	number of crossing areas within beam thickness
h_h	hole height
l_h	length of hole
b	width of lamellae
x_h	distance of further edge of hole from support
$h_{r,t/b}$	residual height above or below the hole (*t* - top, *b* - bottom)
I_z	second moment of inertia about z-axis
S_z	static moment about z-axis
m	number of longitudinal lamellae within the beam height

8 References

Bejtka, I (2011): Cross (CLT) and diagonal (DLT) laminated timber as innovative material for beam elements. Karlsruher Berichte zum Ingenieurholzbau, Bd. 17, KIT Scientific Publishing

Blass, H-J, Görlacher, R (2002): Zum Trag- und Verformungverhalten von Brettsperrholz-Elementen bei Beanspruchung in Plattenebene. Bauen mit Holz, 12:30-34

Bogensperger, T, Moosbrugger, T, Silly, G (2010): Verification of CLT-plates under loads in plane. In: Proc. 11th World Conference on Timber Engineering, Riva del Garda, Italy.

Bogensperger, T, Moosbrugger, T, Schickhofer, G (2007): New Test Configuration for CLT-Wall Elements under Shear Load. In: Proc. CIB-W18 Meeting 40, Bled, Slovenia, Paper 40-12-3

Brandner, R, Bogensperger, T, Schickhofer, G (2013): In plane Shear Strength of Cross Laminated Timber (CLT): Test Configuration, Quantification and influencing Parameters. In: Proc. CIB-W18 Meeting 46, Vancouver, Canada, Paper 46-12-2

Brandner, R, Flatscher, G, Ringhofer, A, Schickhofer, G, Thiel, A (2016): Cross laminated timber (CLT): overview and development. European Journal of Wood and Wood Products, 74:331-351

DIN EN 1995-1-1/NA (2013) National Annex – Nationally determined parameters – Eurocode 5: Design of timber structures – Part 1-1: General – Common rules and rules for buildings. (DIN)

EN 16351 (2015) Timber structures – Cross laminated timber – requirements (CEN)

EN 14080 (2013) Timber Structures – Glued laminated timber and glued solid timber – Requirements (CEN)

ETA-12/0281, “NORITEC X-LAM” (2012): Cross Laminated Timber (CLT) – Solid wood slab elements to be used as structural elements in buildings”, NORITEC Holzindustrie GmbH, Österreichisches Institut für Bautechnik (OIB).

Eurocode 5 (2004): Design of timber structures - Part 1-1: General and rules for buildings. European Committee for Standardization (EN 1995-1-1)

Flaig, M, Blass, H-J (2013): Shear strength and Shear stiffness of CLT beams loaded in plane. In: Proc. CIB-W18 Meeting 46, Vancouver, Canada, Paper 46-12-3

Flaig, M (2013): Biegeträger aus Brettsperrholz bei Beanspruchung in Plattenbene. Dissertation, Karlsruher Berichte zum Ingenieurholzbau, Bd. 26, KIT Scientific Publishing

Flaig, M (2014): Design of CLT Beams with Rectangular Holes or Notches, In: Proc. 1st INTER Meeting, Bath, United Kingdom, Paper 47-12-4

Flaig, M (2015): In Plattenebene beanspruchte Biegeträger aus Brettsperrholz. Bautechnik, 92:741-749

Moosbrugger, T, Guggenberger, W, Bogensperger, T (2006): Cross Laminated Timber Wall Segments under homogeneous Shear – with and without Openings. In: Proc. 9th World Conference on Timer Engineering, Portland, Oregon, USA

Schickhofer, G, Bogensperger, T, Moosburger, T (2010): BSPhandbuch (CLThandbook: solid timber construction technique with cross laminated timber – verification base on new European standardization concept). Verlag der Technischen Universität Graz (in German)

Discussion

The paper was presented by M Jelec

D Brandon commented that about mesh size dependency as small mesh size led to higher stresses. He suggested that fracture mechanics approach should be used. M Jelec agreed.

F Lam suggested that why not use round holes. H Blass agreed that this would reduce the stresses.

P Dietsch commented that the size of the hole would influence stress state and asked what would be the limitations. M Jelec replied that the work was done with respect to available data.

LM Ottenhaus agreed fracture mechanics approach would be appropriate and commented that failure criterion information would be important.

G Schickhofer commented that bigger holes should be considered. Also consideration of the layup of the beams would be important as there would be dependency on the laminae thickness and layup.

P Zarnani added that multiple hole cases and minimum hole spacing should be considered.

R Jockwer asked whether existing provisions in German national code on glulam design could be used. M Jelec replied no as such provisions needed to be validated.

Ambient and forced vibration testing of a light-frame timber building – Conclusions regarding design of the lateral load resisting system

René Steiger, Glauco Feltrin, Abdola Sadeghi Marzaleh, Stella Nerbano
Empa – Swiss Federal Laboratories for Materials Science and Technology, Structural Engineering Research Laboratory, Dübendorf, Switzerland

Keywords: Experimental modal analysis, ambient vibrations, forced vibrations, light-frame timber building, fundamental period, non-structural component, damping ratio, seismic design, wind design, lateral load resisting system

1 Introduction

When improving the competitiveness of light-frame timber buildings (LFTB) in the multi-storey building market segment, which in many countries is still dominated by masonry and reinforced concrete buildings, efforts are needed in optimizing the structural concept and design with special regard to the lateral load resisting system. In order to meet the requirements in serviceability and structural safety, the lateral load resisting system, has to provide adequate stiffness and load-bearing capacity to the building when subjected to horizontal forces from seismic or wind action. Beside the choice and the detailing of the structural design, the assumed stiffness properties of the slab and wall elements and of the connections strongly impact the calculated estimates of the force distribution in the structure. Hence, with regard to the design of the lateral load resisting system against seismic and wind actions, it is important to know the initial stiffness of a building as well as its dynamic properties as precise as possible.

Available dynamic experimental investigations on LFTB involve shake table tests (*Filiatrault et al.* 2008, 2010; *van de Lindt et al.* 2010; *Sartori et al.* 2012) and on-site experimental investigations of real buildings (*Kohara et al.* 1998; *Ohashi et al.* 1998; *Sato et al.* 2000; *Ellis & Bougard* 2001; *Kharrazi et al.* 2002; *Rainieri et al.* 2010; *Hafeez et al*. 2014) in different stages of construction with ambient vibration tests (AVTs) or forced vibration tests (FVTs), the latter in most cases having been performed with a low-power excitation. In all studies it was found that there is a strong impact of non-structural components (NSC) on the horizontal stiffness of buildings and a remarkable difference between the results from AVTs and FVTs.

In the course of a Swiss National Research Program the unique opportunity arose to experimentally investigate the dynamic properties of a 3-storey LFTB in Switzerland by means of on-site experiments. The tests aimed at identifying natural frequencies and mode shapes as well as the modal damping ratio of the building in its two main directions for horizontal excitations of different amplitudes. In order to identify the impact of NSCs on the dynamic properties of the building the experiments were carried out in two different stages of construction.

The level of seismic action to be accounted for in the design of a specific building mainly depends on the mass (distribution) of the building and on the first natural frequency f_1 or the fundamental period T_1, respectively (*CEN* 2004a). LFTBs compared to reinforced concrete or masonry buildings are expected to be less stiff. If this is true the design of the structure against seismic action could be based on much lower spectral values of horizontal ground acceleration.

Eurocode 8 (*CEN* 2004a) provides equations to estimate T_1 based on the height of the building or based on the lateral elastic displacement of the top of the building due to gravity loads applied in the horizontal direction. These approaches will be compared to the estimations applying the Rayleigh method, MDOF and numerical FE models as well as to the experimental results of the on-site experiments. Finally, conclusions for the seismic design of LFTBs will be drawn.

2 Investigated building

The investigated residential building is 24.00 m in length and 14.60 m in width (Figure 2.1). Above the subterranean garage, made of reinforced concrete (RC), the building is supported by an 11.50 m high LFTB consisting of light-frame timber wall elements (LFTW) with OSB and gypsum fibre board sheathings, timber-concrete composite (TCC) slabs in storeys 1 and 2 and a dowelled-laminated timber (DLT) slab in storey 3. On top of the building there is a rafter roof covered with clay tiles. The staircase, supported by a cross-laminated timber structure, was decoupled from the remaining structure. The elevator shaft in the centre of the staircase was made of self-supporting prefabricated RC elements. Hence, both staircase and elevator shaft did not contribute to the horizontal stiffness of the building. A description of the main structural elements of the building including structural detailing is provided in (*Steiger et al.* 2015).

The building was designed according to the Swiss standards SIA 260, SIA 261, SIA 265 and SIA 265/1 (*SIA* 2003a-c, 2009). The design for wind loads was based on characteristic values of wind force of q_k = 1.07 kN/m^2 on the short side of the building and q_k = 0.68 kN/m^2 on the long side respectively, representing a reference value of dynamic wind pressure of $q_{p,0}$ = 0.90 kN/m^2. The building is located within seismic zone Z 1, where the design value of the horizontal ground acceleration for a return period of 475 years is a_{gd} = 0.60 m/s^2 i.e. 6% g (SIA 2003b). Figure 2.2 shows the elastic response spectra for a damping ratio of ζ = 0.05 given in (*SIA* 2003b). The building is founded on deposits of extensive cemented gravel and sand (i.e. ground type B).

Figure 2.1: Investigated LFTB after completion of construction work (top left) and in construction stage 2 during testing (top right). Short (bottom left) and long side (bottom right) view of the LFTB.

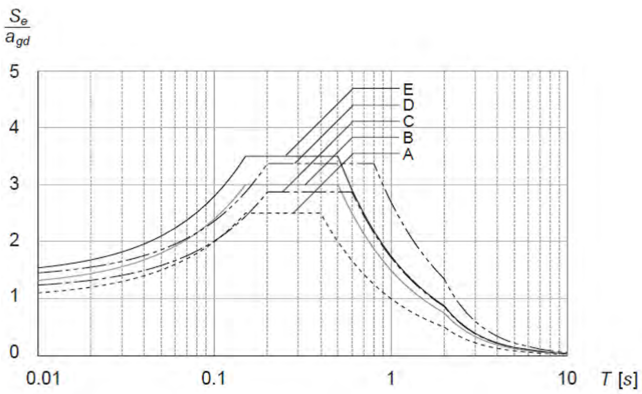

Ground type	Description
A	Firm rock
B	Deposits of extensive cemented gravel and sand and/or over-consolidated soils with a thickness exceeding 30 m
C	Deposits of normally consolidated and uncemented gravel and sand and/or moraine with a thickness exceeding 30 m
D	Deposits of unconsolidated fine sand, silt and clay with a thickness exceeding 30 m
E	Alluvial surface layer of ground classes C or D with a thickness of 5 to 30 m lying above a stiffer layer of the ground classes A or B

Figure 2.2: Elastic response spectra for a damping ratio of ζ = 0.05 according to (SIA 2003b) for ground types A–E.

Design of the building for seismic hazards was made with the force based method assuming a behaviour factor of q = 3 considered for timber buildings with a high ductility (*SIA* 2003c) and a damping ratio of ζ = 0.05 (*SIA* 2003b).

3 Experiments

First AVTs (at different hours during the day) were carried out in order to estimate the natural frequencies of the building. FVTs were then performed by exciting the building with a hydraulic exciter in its two main horizontal directions, however, limiting the excitation to levels where no damages could occur. The exciter consists of a hydraulic actuator which drives a mass guided by a horizontal slide bearing system (*Steiger et al.* 2015). In the experiments the actuator was operated with the maximum mass of 940 kg. Actuator and shaking mass are mounted on a steel rack which is to be bolted to the investigated structure in order to transfer the force. The maximum displacement range of the shaking mass is ±125 mm and the shaking force is constrained by the maximum dynamic actuator force of ±32 kN. The exciter was rigidly anchored to the TCC slab by means of a Hilti® dynamic anchoring set. In order to transfer the excitation forces to the slab without causing damage, the slab had to be reinforced by additional crosswise oriented rebars and the mass of the exciter had to be carried by a series of telescopic metal studs in all storeys underneath the exciter. However, the horizontal stiffness of the building was not affected by this measure.

Exciting the building with as much power as possible required the exciter to be positioned on the 2nd storey (Figure 3.1, left), accounting also for the fact that the attic balcony there offered the only possibility to lift the exciter into the building and out of it after completion of the experiments. The exciter was placed in a room big enough for changing orientation of the exciter in order to excite the building in its two main directions. Figure 3.1 (right) shows the position of the exciter *E* together with centres of mass *M* and stiffness *S* as well as the directions of excitation.

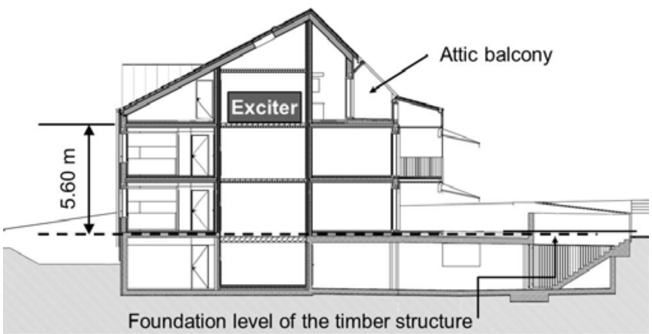

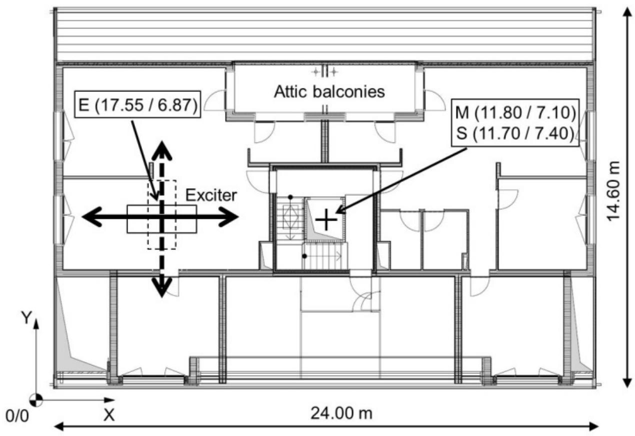

Figure 3.1: Lifting the exciter into the 2nd storey of the building via an attic balcony (left) and final position of the exciter E with respect to centres of mass M and stiffness S (right). Both M and S are located in the centre of the elevator shaft, close to each other.

Since the floors of the LFTB under investigation were very rigid in the in-plane direction (diaphragm), their horizontal motion corresponded to the motion of a rigid body. Such a motion can be decomposed into two translational motions perpendicular to each other and a rotational motion. Hence, it was decided to place the accelerometers at the corners of the floor. Only the upper floors were instrumented but not the reinforced concrete floor of the basement because the large mass and high rigidity of the basement as well as its embedding in the ground produced motions that were order of magnitude smaller than the motion of the floors. In each sensor location the horizontal vibrations were measured in two orthogonal directions (strong and weak building axis). In addition the motion of the exciter mass and the motion of the floor in the direction of the excitation force in the immediate vicinity of the vibration exciter mass were recorded. Detailed information about exact positions of the sensors and their type as well as on data acquisition and signal processing can be taken from (Steiger et al. 2015). Two main stages of construction were investigated, where the key structural elements contributing to the mass and the horizontal stiffness of the building were as described in Table 3.1.

Table 3.1: Investigated stages of construction.

Element	Stage 1	Stage 2
Roof	No clay tiles on the roof yet	
TCC slabs	No sub-flooring installed	
	Shear connections between slab and wall elements installed	
	Fully supported by telescopic studs	Supported underneath the exciter
Façade LFTW	Façade cladding not yet installed	
	Interior gypsum plaster boards not mounted yet	50 % of interior gypsum plaster boards mounted
	Stapled, space between connectors: 500 mm [1)] or 25 mm [2)] respectively	Stapled, space between connectors: 25 mm
	No window and door frames	Window and door frames mounted
	No windows	Windows mounted, closed
	No French windows	French windows mounted, closed
	Hold downs in storey 1 not mounted yet	Hold downs in storey 1 mounted
Internal LFTW	Stapled, space between connectors: 25 mm	
	Gypsum plaster boards not mounted yet	50 % of the gypsum plaster boards mounted
	No door frames	Door frames mounted
	Hold downs in storey 1 not mounted yet	Hold downs in storey 1 mounted

1) Façade walls assigned not to belong to the lateral load resisting system (marked in orange colour in Figure 5.1)

2) Façade walls assigned to be part of the lateral load resisting system (marked in green colour in Figure 5.1)

At both construction stages 1 and 2, an AVT was performed in order to identify the modal parameters at a very low excitation level and to get an overview of the natural frequencies for designing the random excitation signals of the FVTs. Subsequent FVTs consisted of three steps. First, tests were carried out with a broad-band random excitation in order to assess the natural frequencies at different levels of excitation.

This was repeated with a narrow-band random excitation which allowed for a determination of the natural frequencies with an increased precision. Finally the building was subjected to harmonic excitations at various levels with frequencies matching the natural ones in order to determine the modal damping ratios for various amplitudes.

4 Experimental results

4.1 Natural frequencies

The singular values of the cross-correlation matrix (CCM) in the frequency domain are shown in Figure 4.1 and Figure 4.2 for three tests including AVT and the tests at the construction stage 1 with a broad-band random excitation in the transverse and longitudinal directions. They provide a good overview about the excited vibration modes. The singular values of the CCM of AVT disclose the same natural frequencies as the FVT. In the analysis of AVT data vibration mode m4 appears much clearer in the spectrum of the greatest singular value σ_1 since the excitation is not limited to the 2nd floor as in the FVT.

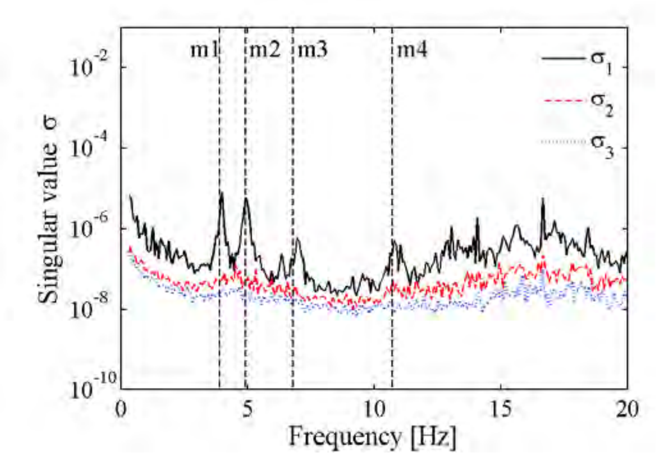

Figure 4.1: Singular values of the cross-correlation matrix σ_1, σ_2, σ_3 of a test with AVT.

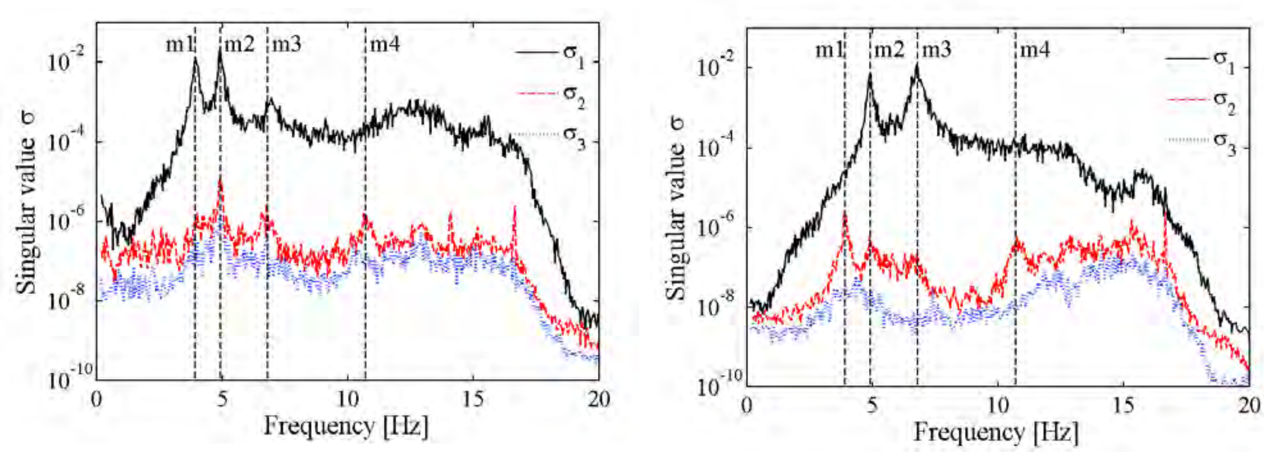

Figure 4.2: Singular values of the cross-correlation matrix σ_1, σ_2, σ_3 of tests with transverse (left) and longitudinal (right) broad band random excitation.

When analysing the progress of CCM values σ_1 and σ_2 three clear peaks can be identified at frequencies of approximately f_1 = 3.9 Hz or T_1 = 0.26 s respectively (m1), f_2 = 4.9 Hz (m2) and f_3 = 6.8 Hz (m3). The greatest singular value σ_1 does not provide any further hint for the existence of additional vibration modes. Analysing the curves of the second greatest singular value σ_2, however, reveals a common peak at f_4 = 10.7 Hz (m4). Since the signal was very weak it is not sure if m4 is really a vibration mode.

4.2 Mode shapes

Figure 4.3 displays the motion of the three floors in the horizontal plane and their decomposition in transverse, longitudinal and rotational motions in modes m1 – m3.

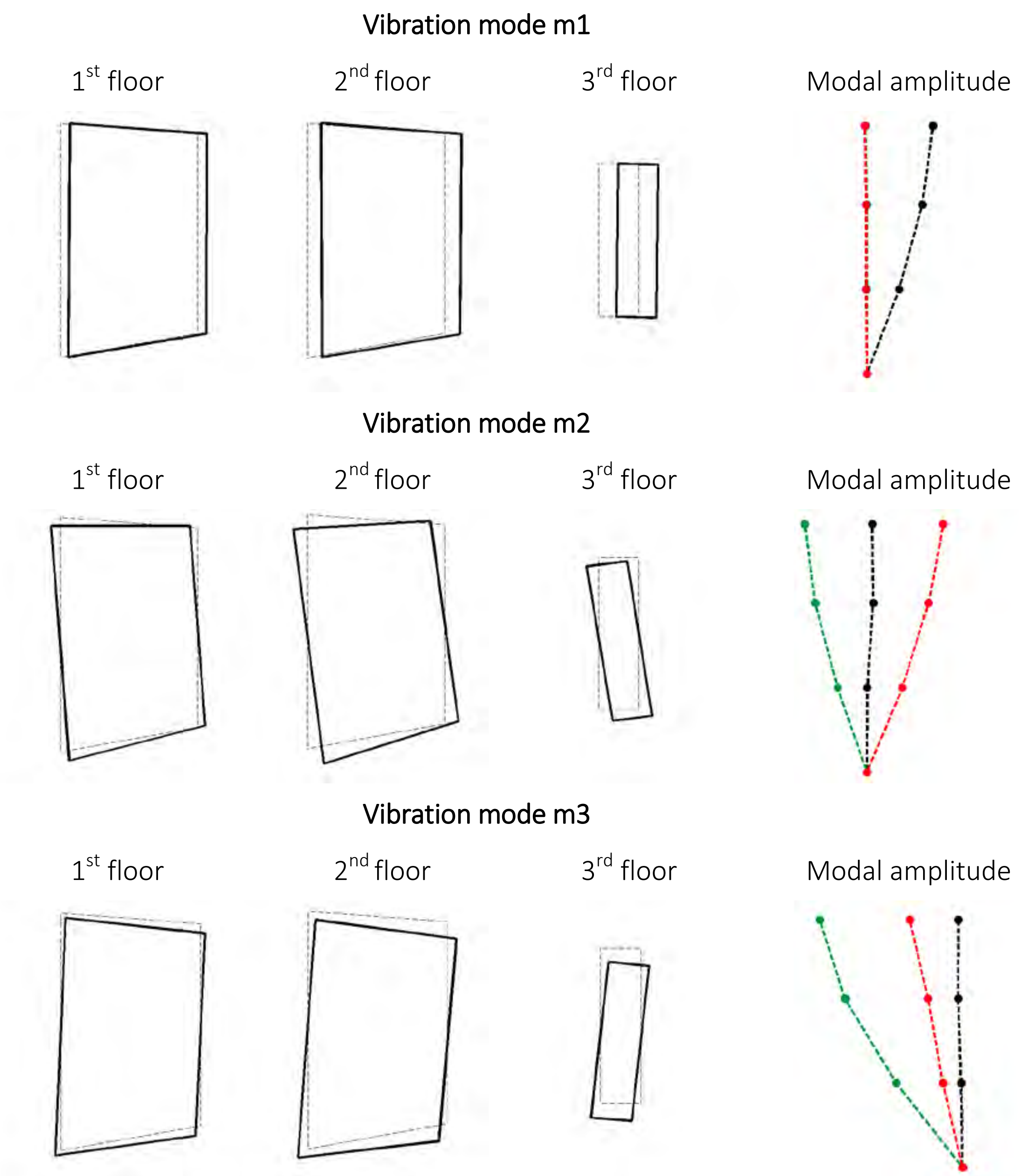

Figure 4.3: Motion of floors in the horizonal plane in vibration modes m1, m2 and m3. Colours in the modal amplitude graph represent: black = motion in the transverse direction, green = motion in the longitudinal direction, red = rotational movement.

The vibration mode m1 is mainly a transverse oscillation. The vibration mode m2 has a strong rotational motion with a smaller but still marked component in the longitudinal direction and a negligible motion in the transverse direction. The vibration mode m3 has a strong motion in the longitudinal direction combined with a small rotational component. Also for this vibration mode the transverse direction is negligible. The vibration mode m4 is the 2nd transverse mode with a negligible longitudinal and a small rotational motion of the 3rd floor.

4.3 Influence of construction stage and vibration amplitude

The tests demonstrated (*Steiger et al.* 2015 and 2016) that NSCs have a significant effect on the natural frequencies and consequently on the overall stiffness of LFTB. This added stiffness is nearly completely lost already at small vibration amplitudes without producing any visible damage and is completely recoverable. Static friction between building components is the most likely mechanism explaining qualitatively such behaviour. The observed increasing damping with increasing vibration amplitudes is also compatible with an incremental conversion of static to sliding friction. Damping ratios identified in our tests were in the range of 0.02 – 0.04.

4.4 AVT vs. FVT

Whereas mode shapes estimated from AVT data turned out to be reliable, natural frequencies and modal damping ratios computed using data from AVT require, because of the extremely small amplitudes, a suitable interpretation in order to provide reliable information about the dynamic properties of the structure. This was also pointed out by *Hafeez et al.* (2014).

In our experiments, in most of the harmonic FVTs in transverse direction of construction stage 2 the acceleration at the 2nd floor exceeded 0.25 ms^{-2} with peaks reaching 0.6 ms^{-2}. Such peak accelerations are abundantly exceeding the vibration serviceability limit of approximately 0.1 ms^{-2} that is recommended by ISO 10137 (*ISO* 2009) for residential buildings subjected to wind loads with a return period of one year. However, the vibration amplitudes achieved during the tests were markedly below the amplitudes that are to be expected during an earthquake. Hence, little can be said about natural frequencies and modal damping ratios at such vibration amplitudes. Shaking table tests (*Filiatrault et al.* 2008 and 2010) showed that an additional significant decrease of stiffness will occur when non-structural components are subjected to damage. It is unknown if this stiffness loss will be able to bridge the huge gap between natural frequencies of the real building and the design model.

5 Estimation of the fundamental period

Force-based seismic design, although known to suffer from several drawbacks (*Filiatrault & Folz* 2002), is still frequently applied in practice, since it is an easy method and not different from e.g. design of a structure against the wind force. The key parameter in the force-based design of a building is its fundamental period. It can be estimated by (1) from equations given in design codes (e.g. *CEN* 2004a), (2) applying the Rayleigh method, (3) analytical calculations on equivalent SDOF or MDOF systems or (4) setting up a 1D-, 2D or 3D numerical model of the building.

5.1 Modelling assumptions

In all calculations, properties (specific mass (or density respectively), MOE, shear modulus) of involved materials solid timber C24, glulam GL24, OSB-3, gypsum-fibre board, concrete C25/30 were taken from product standards and technical approvals. The stiffness of wall and slab elements and of connections (wall-wall, wall-slab, wall-foundation) was estimated by applying specifications and approaches given in Eurocode 5 (*CEN* 2004b), in the former German standard DIN 1052 (*DIN* 2008) and in (*Kessel* 2002).

Furthermore, the subterranean garage (reinforced concrete) was assumed to act as a rigid foundation (dashed line in Figure 2.1) and soil interaction was neglected. The walls marked in colour in Figure 5.1 have been assumed to contribute to stiffening the LFTB in horizontal direction. The mass of the exciter was neglected since being small compared to the mass of TCC slabs.

Figure 5.1: Walls assumed to contribute to stiffening the LFTB in horizontal direction. Walls assigned by the designer to belong to the lateral load resisting system in the course of designing the LFTB are marked in green colour.

Green colour denotes walls being part of the lateral load resisting system as assigned by the designer when designing the building. Since orange coloured walls also contribute to lateral stiffness, models presented in sections 5.2 to 5.5 accounted for both assumptions i.e. there were calculations with green walls only and others with green plus orange walls (Table 5.1). Regarding masses, also contributions by NSCs were considered.

Table 5.1: Overview on the calculations presented in sections 5.2 to 5.5.

Approach / model	Masses	Walls
EC 8, equation (4.6)	–	–
EC 8, equation (4.9)	1	A
Rayleigh method	1	A
MDOF, calculations 1, 2 and 3	1 *2* **2**	A *B* **C**
3D Finite Element Model, calculations 1 and 2	2 *2*	A *B*

1) Permanent loads plus quasi-permanent parts of variable actions according to specifications in the design code SIA 261 (*SIA* 2003b)
2) Masses at the time of on-site experiment
A) Green walls in Figure 5.1
B) Green plus orange walls in Figure 5.1
C) Green plus orange walls in Figure 5.1, orange walls with stiffness reduced by factor 2

5.2 Estimating the fundamental period based on Eurocode 8 approaches

Beside more precise methods to estimate the fundamental period T_1, EC 8 (*CEN* 2004) mentions two simplified methods. For buildings with a height of up to 40 m the value of T_1 (in [s]) may be approximated by the following expression:

$$T_{1,1} = C_t \cdot H^{3/4} \qquad \text{(Equation (4.6) in EC 8)} \qquad (1)$$

C_t is 0.085 for moment resistant steel space frames, 0.075 for moment resistant concrete space frames and for eccentrically braced steel frames and 0.050 for all other structures.

H is the height of the building, in [m], from the foundation or from the top of a rigid basement.

Alternatively EC 8 recommends estimating T_1 (in [s]) using the following equation:

$$T_{1,2} = 2 \cdot \sqrt{d} \qquad \text{(Equation (4.9) in EC 8)} \qquad (2)$$

d is the lateral elastic displacement of the top of the building, in [m], due to gravity loads applied in the horizontal direction. (Note: “gravity loads” may be replaced by the more precise term “permanent loads plus quasi-permanent parts of variable actions”.)

Applying Equations (1) or (2), the fundamental period of the LFTB under investigation would be $T_{1,1,X} = T_{1,1,Y} = 0.31$ s or $T_{1,2,X} = 0.73$ s and $T_{1,2,y} = 1.29$ s respectively. The symbols x and y denote the longitudinal direction and the transverse direction of the building, respectively (Figure 3.1 right).

5.3 Estimating the fundamental period with the Rayleigh method

The designer estimated the fundamental period of the LFTB based on the Rayleigh method (Equation (3)) as $T_{1,\mathrm{R},x} = 0.85$ s and $T_{1,\mathrm{R},y} = 1.0$ s, respectively.

$$T_{1,R} = 2\pi\sqrt{\frac{\sum_{i=1}^{n} m_i u_i^2}{\sum_{i=1}^{n} F_{d,i} u_i}} \tag{3}$$

$F_{d,i}$ is the fictitious horizontal force from permanent loads plus quasi-permanent parts of variable actions on storey i.

m_i is the mass of storey i.

u_i is the horizontal displacement of storey i when subjected to the horizontal force $F_{d,i}$.

5.4 Estimating the fundamental period applying an MDOF system

In this model the building was assumed as a shear story building, in which the slabs were considered rigid. The stiffness of each story in each direction was calculated by summing the stiffness of the walls located in that direction. The wall stiffness was evaluated based on the various deformations, including framing elements, sheathing elements and fasteners, due to horizontal loading. The fundamental period was estimated by solving the differential equation of motion (*Thomson* 1993, *Humar* 2012) of a MDOF system (Figure 5.2.) with 3 lumped masses representing storey and tributary masses as assumed in the design stage as well as in the construction stage of the building when subjected to the dynamic experiments reported in chapter 3.

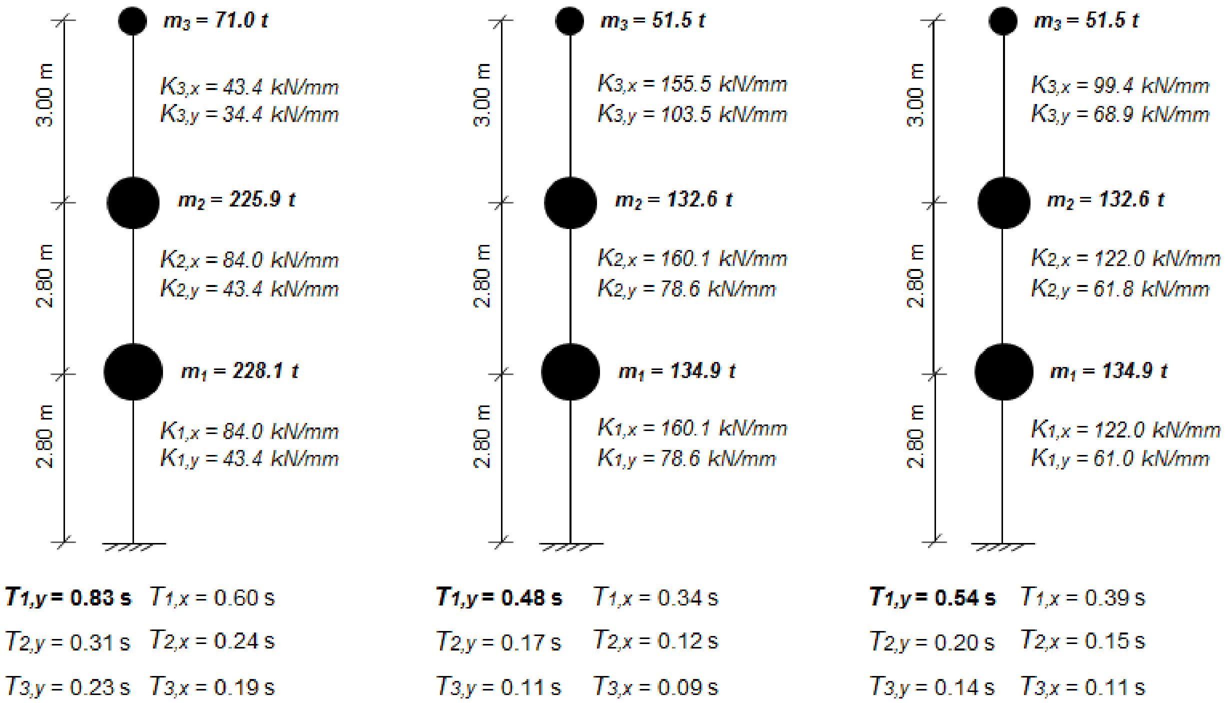

Calculation 1: Design masses and stiffness (green walls only in Figure 5.1)

Calculation 2: Masses and stiffness at the time of on-site experiments (green plus orange walls in Figure 5.1)

Calculation 3: Masses and stiffness at the time of on-site experiments (green plus orange walls Figure 5.1; orange walls with half stiffness)

Figure 5.2: MDOF model of the LFTB with 3 lumped masses: masses and stiffness as assumed in the design (calculation 1) or being present at the time of on-site experiments (calculations 2 and 3).

5.5 Estimating the fundamental period by means of a 3D Finite Element Model

A simplified 3D Finite Element Model in SAP2000® with a flat instead of an inclined roof and neglecting walls with openings was set up. Mode shapes estimated by means of the FE model (Figure 5.3) were equal to those assessed in the experiments (Figure 4.3). The fundamental periods and types of motion estimated with the FE model are listed in Table 5.2.

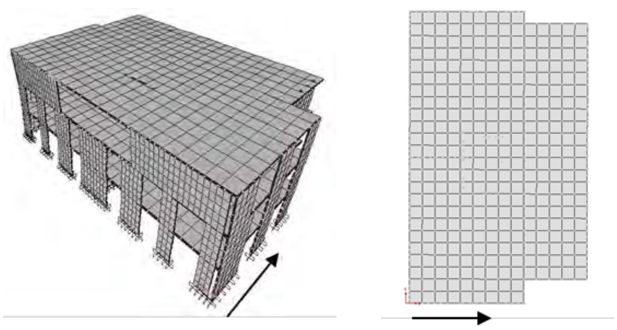

Mode 1: *Translation in transverse direction*

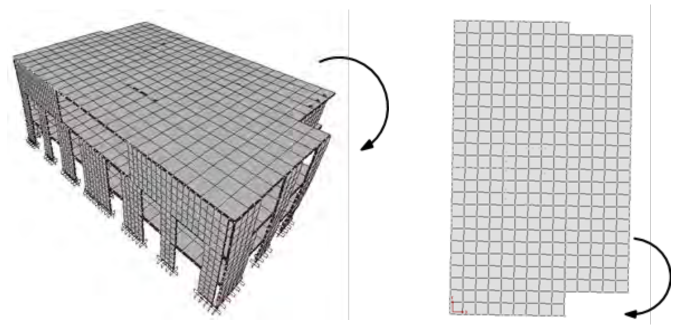

Mode 2: *Torsion* + translation in longitudinal direction

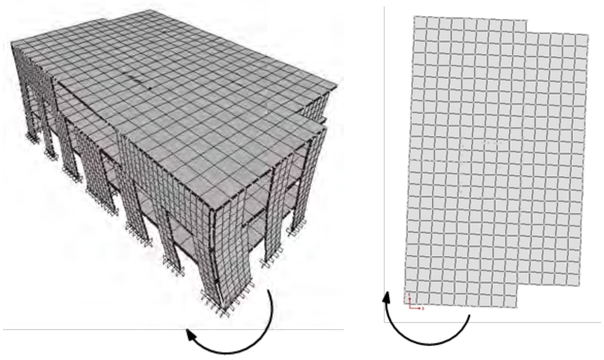

Mode 3: *Torsion* + translation in longitudinal direction

Figure 5.3: Mode shapes estimated by means of the 3D Finite Element model. Italic font indicates the dominating part of motion when the latter consisted of a combination of several motions.

Table 5.2: Fundamental periods and types of motion estimated by means of the 3D Finite Element model with masses at the time of on-site experiments and stiffness assumed when designing the LFTB (green walls according to Figure 5.1, results in brackets) and at the time of on-site experiments (green plus orange walls according to Figure 5.1, results without brackets).

	Unit	**Mode 1**	Mode 2	Mode 3
Fundamental period	[s]	**(0.58) 0.39**	(0.46) 0.34	(0.45) 0.28
Type of motion	[-]	**Translation y**	Torsion	Torsion

6 Estimated natural periods compared to test data

In Figure 6.1 calculated estimates of fundamental periods in transverse direction (which is the decisive case) are compared to the experimental results (red line). The estimates are grouped in those frequently applied during design (green lines) and those requiring more effort in terms of modelling and gathering necessary input data (blue lines). From Figure 6.1 it becomes obvious that there are big differences among estimates themselves and between the estimates and the experiment.

EC 8 equation 4.6 (Equation (1) delivers an estimate (T_1 = 0.31 s) very close to the experimental value (T_1 = 0.26 s). This however, appears having happened by chance, since Equation (1) accounts mainly for the height of the building and does not consider specific properties such as horizontal stiffness. It is not a surprise that the 3D FE model delivered a very good estimate (T_1 = 0.39 s). Also an MDOF calculation with lumped masses and stiffness as present at the time the on-site experiment took place delivers an estimate (T_1 = 0.51 s) closer to the experimental value than other models do.

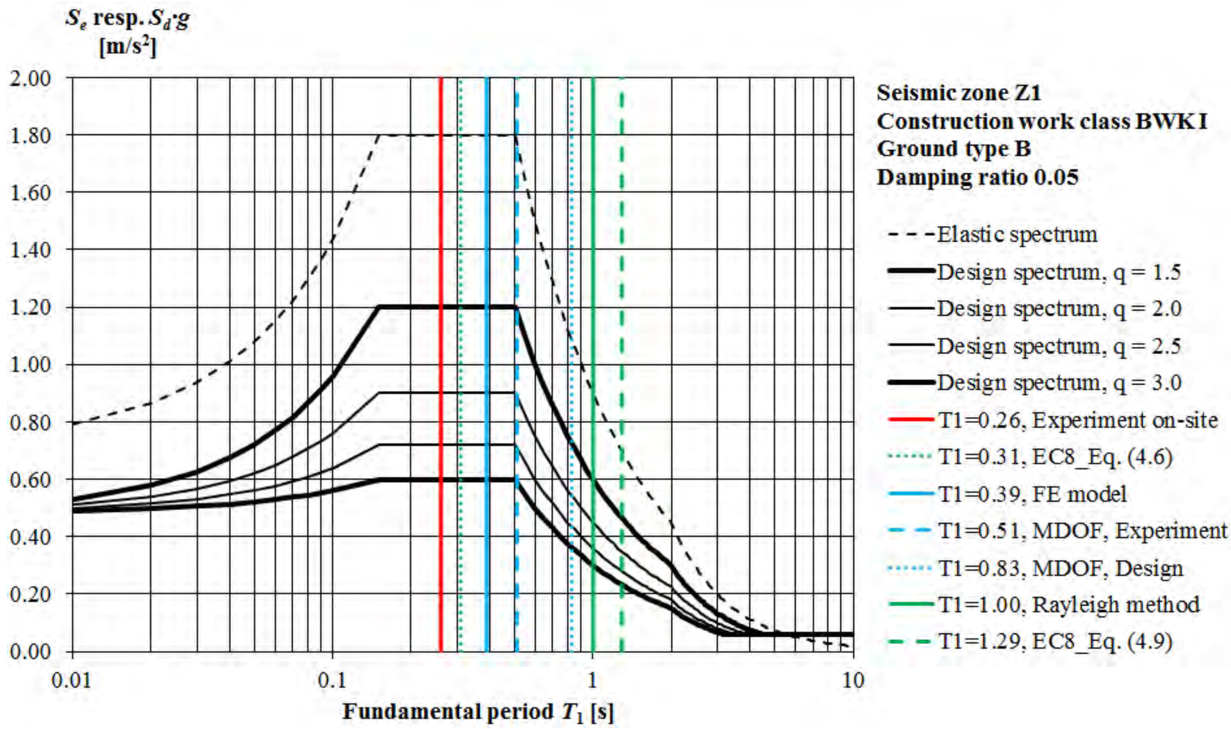

Figure 6.1: Comparison of experimentally derived fundamental period in transverse direction and estimates applying different methods. (The depicted MDOF, Experiment – value (T1 = 0.51) is an averaged value from calculations 2 and 3 shown in Figure 5.2.)

All methods belonging to the "blue group" (Figure 6.1) however, require certain effort in setting up the model and collecting input data. In practice, in order to spare time and costs, designers tend to apply methods as simple as possible and/or to assign only selected walls belonging to the lateral load resisting system. Doing so and estimating the fundamental period with e.g. the Rayleigh method (Equation (3)) or with an MDOF system accounting only for stiffness of walls assigned to be part of the lateral load resisting system delivers wrong estimates of the natural period (T_1 = 1.00 s and T_1 = 0.83 s, respectively). Although requiring already increased effort in calculation, EC 8 equation 4.9 (Equation (2)) delivers the worst estimate.

7 Conclusions and recommendations

From the presented on-site experiments the following conclusions can be drawn:

- With both AVT and FVT, the mode shapes can be identified, whereas it is not possible to assess damping ratios with AVT. Natural frequencies have been found to significantly diminish with increasing amplitude. Therefore, AVT delivers an upper bound of natural frequencies. But also results from FVT shall be assessed critically when estimating fundamental periods for seismic design, since in experiments on real buildings it is not possible to reach amplitudes that occur during a design earthquake.
- Damping ratios identified in the tests were in the range of 0.02 – 0.04. Hence, for seismic or wind design of high-rise LFTB assuming a damping ratio of 0.05 is an appropriate approach.
- In the experiments, a marked impact of friction within and between structural components was observed. However, this is difficult to quantify and to account for in the models when estimating dynamic properties.

Subsequent analyses revealed the following results and allow for formulation of respective recommendations for seismic design of LFTBs:

- Timber structures in general and LFTBs in particular are estimated to exhibit markedly low stiffness and hence, are supposed to allow seismic design based on spectral values lower than the plateau value. Our experiments showed that this was not the case. Hence, the fundamental periods estimated by any model or code equation not falling into the plateau shall be critically assessed.
- Although being a very rough way of estimating the fundamental period, the EC 8 equation $T_{1,1} = C_t \cdot H^{3/4}$ in our case delivered an estimate close to the one identified in the experiments, whereas EC 8 equation $T_{1,2} = 2 \cdot \sqrt{d}$ did not.
- Non-structural walls influence dynamic properties of LFTB to a large extent. Taking into account only their mass but neglecting their contribution to stiffness leads to wrong results with respect to the fundamental period.

Concerning further development of design codes, it is suggested:

- to use in force-based seismic design the plateau value of the response spectra whenever the fundamental periods falling in the descending branch are estimated without a detailed analysis.
- to provide reasonably simple equations allowing a more realistic estimation of fundamental periods for LFTB.

8 Acknowledgement

The presented study was supported by the Swiss Federal Office for the Environment FOEN (Fonds zur Förderung der Wald- und Holzforschung, Project 2012.04) and by the Swiss National Science Foundation SNSF (National Research Program 66 ‘‘Resource Wood’’, Project 406640-136900).

For having given allowance to perform the experiments as well as for having actively supported preparation and execution of the experiments on-site, the authors express their gratitude to the owner of the building, Ferrario Bau AG, Oberglatt and to the involved designers and manufacturer of the building Zindel Brönnimann Ferrario ZBF Architekten AG, Zurich, Pirmin Jung Ingenieure für Holzbau AG, Rain and Artho Holz- & Elementbau AG, St. Gallenkappel.

9 References

DIN 1052 (2008): Entwurf, Berechnung und Bemessung von Holzbauwerken – Allgemeine Bemessungsregeln und Bemessungsregeln für den Hochbau. DIN. Germany.

Ellis, B R, Bougard, A J (2001): Dynamic testing and stiffness evaluation of a six-storey timber framed building during construction. Engineering Structures 23:1232–1242.

Eurocode 8 (2004a): Design of structures for earthquake resistance – Part 1: General rules, seismic actions and rules for buildings. CEN. (EN 1998-1).

Eurocode 5 (2004b): Design of timber structures – Part 1-1: General – Common rules and rules for buildings. CEN. (EN 1995-1-1).

Filiatrault, A & Folz, B (2002): Performance-based design of wood framed buildings. Journal of Structural Engineering ASCE 128:39-47.

Filiatrault, A, Christovasilis, I, Wanitkorkul, A (2008): Experimental seismic investigation of a full-scale wood frame building. In: Structures Congress 2008: Crossing Borders, Vancouver, British Columbia, Canada, April 24–26, 2008.

Filiatrault, A, Christovasilis, I P, Wanitkorkul, A, van de Lindt, J W (2010): Experimental seismic response of a full-scale light-frame wood building. Journal of Structural Engineering ASCE 136:246–254.

Hafeez, G, Mustafa, A, Doudak, G, McClure, G (2014): Predicting the fundamental period of light-frame wood buildings. Journal of Performance of Constructed Facilities ASCE 28:A4014004.

Humar, J L (2012): Dynamics of Structures. CRC Press, Taylor & Francis Group.

ISO 10137 (2009): Bases for design of structures — Serviceability of buildings and walkways against vibrations. ISO, Geneva, Switzerland.

Kessel, M H (2002): Tafeln – Eine elastische, geometrisch lineare Bechreibung. In: Holzbaukalender 2003: 599–632. Bruder Verlag, Karlsruhe, Germany.

Kharrazi, M H K, Ventura, C E, Prion, H G L, Taylor, G W, Lord, J F, Turek, M (2002): Experimental evaluation of seismic response of wood frame residential construction. In: Proceedings of 4th Structural Speciality Conference of the Canadian Society for Civil Engineering, June 5-8, 2002: 1–9.

Kohara, K & Miyazawa, K (1998): Full-scale shaking table test of two-story dwelling houses. In: Proceedings of 5th World Conference on Timber Engineering WCTE, Lausanne-Montreux, Switzerland, August 17–20, 1998: 548–555.

Ohashi, Y, Sakamoto, I, Kimura, M (1998): Shaking table tests of a real-scale wooden house subjected to Kobe earthquake. In: Proceedings of 5th World Conference on Timber Engineering WCTE, Lausanne-Montreux, Switzerland, August 17–20, 1998: 556–563.

van de Lindt, J, Pei, S, Pryor, S E, Shimizu, H, Isoda, H (2010): Experimental seismic response of a full-scale six-story light-frame wood building. Journal of Structural Engineering ASCE 136:1262–1272.

Rainieri, C, Fabbrocino, G, Cosenza, E (2010): Some remarks on experimental estimation of damping for seismic design of civil constructions. Shock and Vibration 17:383–395.

Sartori, T, Casagrande, D, Tomasi, R, Piazza, M (2012): Shake table test on 3-storey light-frame timber buildings. In: Proceedings of 12th World Conference on Timber Engineering WCTE, Auckland, New Zealand, July 16–19, 2012.

Sato, T, Koshihara, M, Kohara, K, Miyazawa, K, Ohashi, Y, Sakamoto, I (2000): Shaking table tests and seismic design method of wooden houses with eccentricity. In: Proceedings of 6th World Conference on Timber Engineering WCTE, Whistler, BC, Canada, July 31–August 3, 2000.

SIA Standard 260 (2003a): Basis of structural design. SIA, Zurich, Switzerland.

SIA Standard 261 (2003b): Actions on structures. SIA, Zurich, Switzerland.

SIA Standard 265 (2003c): Timber structures. SIA, Zurich, Switzerland.

SIA Standard 265/1 (2009): Timber structures – Supplementary specifications, SIA, Zurich, Switzerland.

Steiger, R, Feltrin, G, Weber, F, Nerbano, S, Motavalli, M (2015): Experimental modal analysis of a multi-storey light-frame timber building. Bulletin of Earthquake Engineering. DOI: 10.1007/s10518-015-9828-9.

Steiger, R, Feltrin, G, Weber, F, Nerbano, S, Motavalli, M (2016): On-site dynamic testing of a light-frame timber building. In: Proceedings of 14th World Conference on Timber Engineering WCTE, Vienna, Austria, August 22–25, 2016.

Thomson, W T (1993): Theory of Vibrations. University of California, Santa Barbara, USA.

Discussion

The paper was presented by R Steiger

F Sarti questioned the statement that damping ratio cannot be established accurately from ambient vibration and asked whether the statement referred to ambient vibration measured within one day only. R Steiger responded that the damping ratio depends on amplitude therefore the level of excitation should be close to the design level for estimating damping ratio.

WS Chang commented that results from his paper confirm that amplitude influenced damping. He stated that the use of the shaker may be difficult to identify torsional behaviour. R Steiger explained about the procedures involving the cross correlation parameters and more detailed description of the procedures was available in the cited paper. WS Chang also received clarifications about the accelerometer.

G Doudak asked about comparisons with code equation and agreed that using ambient vibration to estimate damping would be questionable. There were discussions that the level of excitation is significantly higher in models and the structure period would be longer. R Steiger responded that testing of components are on-going with preliminary results indicating a factor of 2 for stiffness compared to code results.

E Ussher commented that damping ratios from ambient vibration can be used for situations where amplitudes are small. He questioned where the exciter influenced the damping estimate. R Steiger responded that the exciter is just an added mass and the additional supports under the floor were uncoupled laterally from the structural system and did not influence the results.

q-factor estimation for timber *Blockhaus* buildings

Chiara Bedon, University of Trieste, Italy

Giovanni Rinaldin, University of Sassari, Italy

Matteo Izzi, University of Trieste & Trees and Timber Institute-CNR IVALSA, Italy

Massimo Fragiacomo, University of L'Aquila, Italy

Keywords: *Blockhaus* structures; *q*-behaviour factor; seismic performance; Finite-Element numerical modelling; three-dimensional models

1 Introduction and state-of-the-art

This paper investigates the structural response and vulnerability of *Blockhaus* buildings under seismic loads. *Blockhaus* systems are widely used in daily practice for the construction of wooden houses or commercial buildings (see for example (Rubner Haus AG SpA)). Native of forested areas, they are often built also in earthquake-prone regions. Several research projects have been carried out, in order to experimentally and/or numerically assess the seismic performance of full-scale structures and small components (Branco & Araújo (2012), *Piazza et al* (2013), *Bedon et al* (2015a), *Bedon et al* (2015b), *Bedon et al* (2015c), *Grossi et al* (2016)). However, the seismic characterization of this construction system requires further investigations and studies, since the current standards for timber structures (e.g. Eurocode 5 (2004) and Eurocode 8 (2004)) do not provide specific recommendations for the calculation of their *q*-behaviour factor.

In this work, based on past research contributions (*Bedon et al* (2015a), (2015b), (2015c)) and full-scale experimental tests (*Piazza et al* (2013)), Finite-Element (FE) investigations are performed on three dimensional *Blockhaus* buildings subjected to seismic loads by means of FE-models implemented in the ABAQUS software package (Simulia (2012)). Parametric simulations are carried out on several building archetypes, characterized by different overall geometrical properties, inter-storey floors (up to 2 levels), number and position of openings, corner joints. Design recommendations are then provided, based on the collected FE results, for a rational estimation of the corresponding *q*-behaviour factor.

2 Finite-Element modelling approach

2.1 Finite-Element assembly

Full three-dimensional *Blockhaus* buildings are investigated by means of a computationally efficient FE modelling approach (see *Bedon et al* (2015b), *Bedon et al* (2015c)). The single *Blockhaus* log-walls are described by a series of rigid beams – representative of the main timber logs – connected at their ends by nonlinear spring elements acting in their axial (Y direction) and transversal (shear – X and Z directions) degrees of freedom and representative of a single carpentry joint (Figure 1).

Based on (*Rinaldin et al* (2013)), each spring represents the mechanical cyclic behaviour of a carpentry joint, resisting shear (sliding in X and Z directions) and compressive (springs in Y direction) forces applied on one-half of each log (see Section 2.2 for the calibration and validation of the modelling assumptions). Once multiple shear walls are assembled together, configurations of real residential or commercial *Blockhaus* buildings can be investigated by properly taking into account the effects of possible geometrical irregularities, window and door openings, building asymmetries, etc.

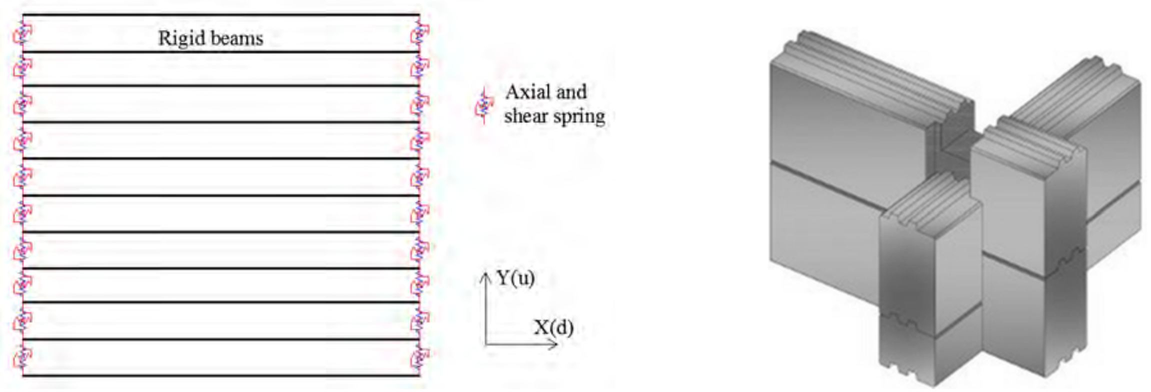

(a) (b)

Figure 1. (a) Schematic view of the typical FE-model for Blockhaus log-walls (Bedon et al (2015b), (2015c)) and (b) reference 'N01' carpentry joint (Rubner Haus AG SpA)

2.2 Finite-Element calibration and validation

The calibration of the springs is carried out towards cyclic experimental tests of single joints (*Grossi et al* (2016)), as also discussed in (*Bedon et al* (2015b), (2015c)). The 3D model of an entire *Blockhaus* building is then validated against the shake-table test results available from the SERIES project (*Piazza et al* (2013)).

Through the current exploratory investigations, a single type of 'Standard' carpentry joints is preliminary considered for all the tested building configurations ('N01' corner joint type, based on (*Bedon et al* (2015b), (2015c))), see Figure 1(b) and Table 1. The effects of the carpentry joint typologies on the global seismic performance of a given *Blockhaus* system, as well as the presence of in-plane fully rigid of flexible inter-storey floors proved in fact to be negligible for the purpose of this study, see Section 4.

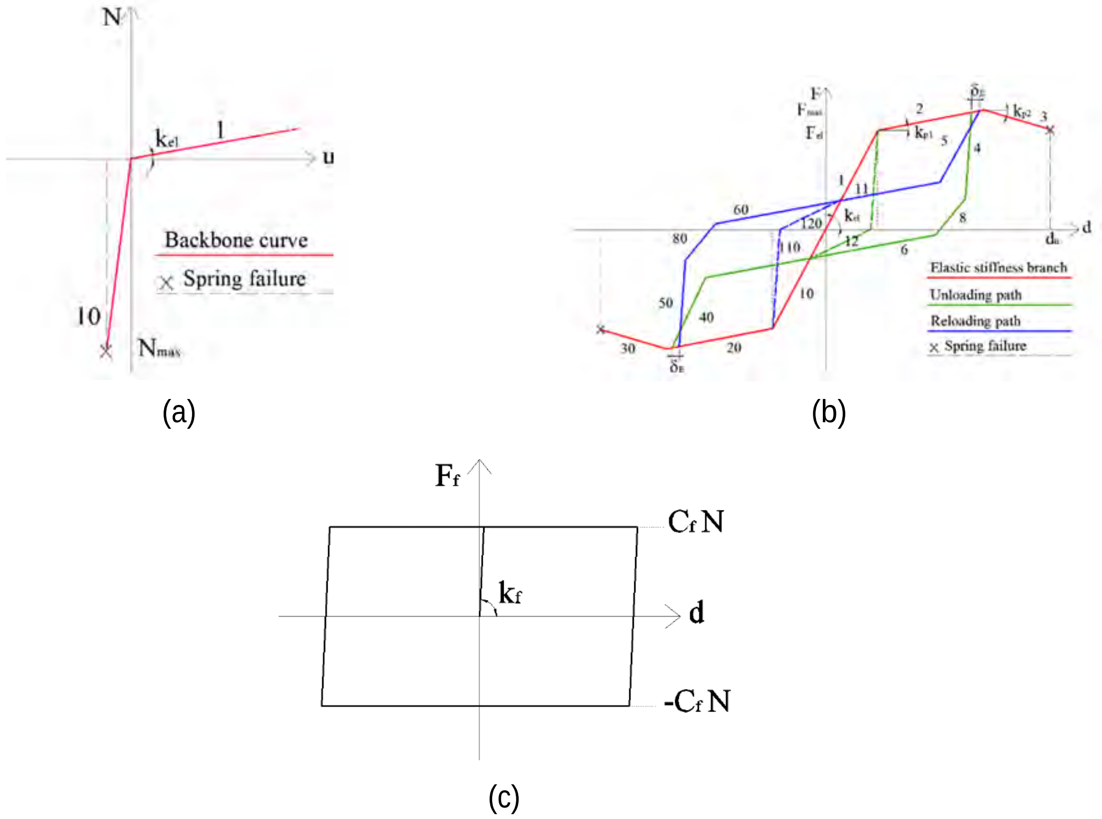

Figure 2. (a) axial DOF, (b) shear DOFs and (c) constitutive law for the friction contribution in the shear DOFs (Rinaldin et al (2013), Bedon et al (2015b), Bedon et al (2015c))

Regarding the mechanical calibration of the non-linear springs representative of a single joint, Figure 2 shows their qualitative behaviour in terms of axial law (Figure 2(a)), shear law (Figure 2(b)) and dynamic friction contribution (Figure 2(c)) respectively. A full description of the FE modelling concept and the N01 calibration can be found in (*Rinaldin et al* (2013), *Bedon et al* (2015b), *Bedon et al* (2015c)). In terms of dynamic friction, see Figure 2(c), the reference value C_f= 0.5 as taken into account through the current parametric study (*Bedon et al* (2015a)).

Table 1. Calibrated input parameters for the simplified FE-model of full 3D Blockhaus buildings, 'N01' type joints, according to (Bedon et al (2015b) and (2015c))

Parameter	Calibrated value	Unit	Load-displacement cyclic response
k_{el}	3.34	kN/mm	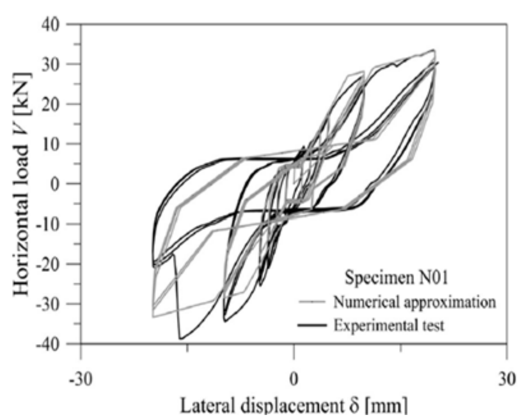
F_{el}	23.01	kN	
k_{p1}	0.49	kN/mm	
F_{max}	33.51	kN	
k_{p2}	-1.47	kN/mm	
k_{sc}	1.5	-	
R_C	0.6	-	
S_C	0.65	-	
d_u	20	mm	
k_{deg}	0.6	-	
α	1	-	
γ	0.0003	-	
gap	1	mm	
k_5	1.2	-	

3 Preliminary validation of the FE modelling assumptions for full 3D *Blockhaus* systems

3.1 The ‘Rusticasa building’ reference case study

A preliminary assessment and validation of the FE modelling approach for full 3D timber log structures was carried out based on some experimental test results available in literature.

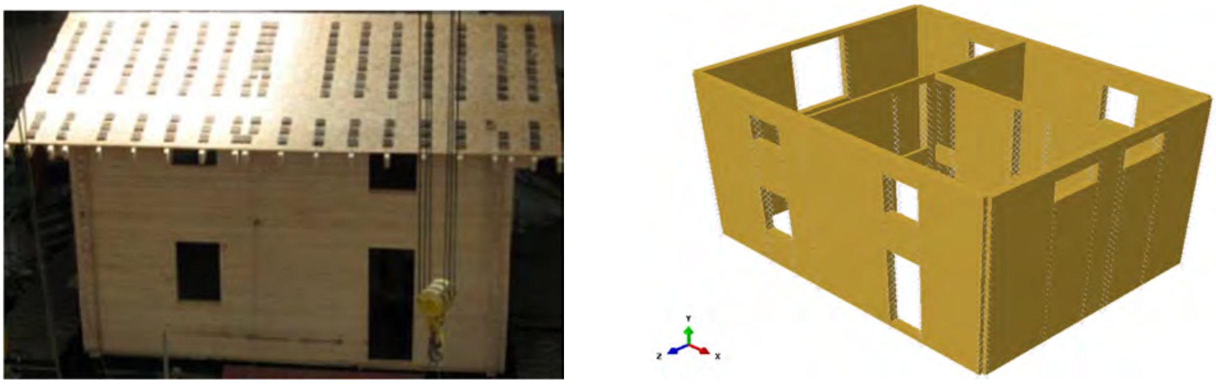

(a) (b)

Figure 3. Rusticasa building. (a) overview of the experimental full-scale specimen (Piazza et al (2013)) and (b) 3D view of the corresponding FE model (ABAQUS (Simulia (2012)))

The ‘Rusticasa building’ has been analysed, the dynamic and seismic performance of which was experimentally investigated within the framework of the SERIES Timber building project ((*Piazza et al* (2013)), see Figure 3(a)). The Rusticasa building is a two-storey log-house, characterized by a 5.64×7.30m rectangular plan and by a total height of 4.40m at the edge of the gable roof and 5.28m at the ridge. The building is almost symmetric along the longitudinal direction, and asymmetric in the transversal direction. The walls are obtained by assembling 160×160mm and 80×160mm logs composed of C24 class spruce. To ensure an in-plane rigid inter-storey floor, 22mm Oriented Strand Board (OSB) sheathing panels supported by timber joists were used. During the experiments, 398 additional steel plates (7.1 kg/each) were equally distributed on the roof to simulate the gravity load. A full description of the Rusticasa building geometry and test methods can be found in (*Piazza et al* (2013)).

In accordance with the FE modelling assumptions described in Section 2, a 3D FE model of the Rusticasa building was implemented in ABAQUS, see Figure 3(b). The geometrical properties of the building were taken from (*Piazza et al* (2013)). The presence of an in-plane fully rigid inter-storey floor was taken into account via a kinematic constraint. The self-weight and the additional permanent loads were applied as nodal masses in the centre of gravity of the first floor and the roof, respectively. The 398 steel plates were also lumped in the centre of gravity of the roof. In terms of mechanical characterization of the carpentry joints, finally, the input parameters corresponding to the N01 joint typology calibrated in Table 1 were used.

3.2 Eigen-value analysis

A preliminary eigenvalue analysis was carried out, so that the predicted fundamental vibration modes could be compared with the corresponding experimental estimations, as obtained via dynamic identification techniques (*Piazza et al* (2013)). The experimental predictions calculated before the shaking table test were considered.

Despite the simplifications of the FE modelling approach, a fairly good correlation was found between numerical and experimental vibration shapes, see Figure 4. Close agreement was also observed in terms of vibration frequencies. Larger discrepancies were obtained for the fourth vibration mode only, hence suggesting the general accuracy of the implemented FE model.

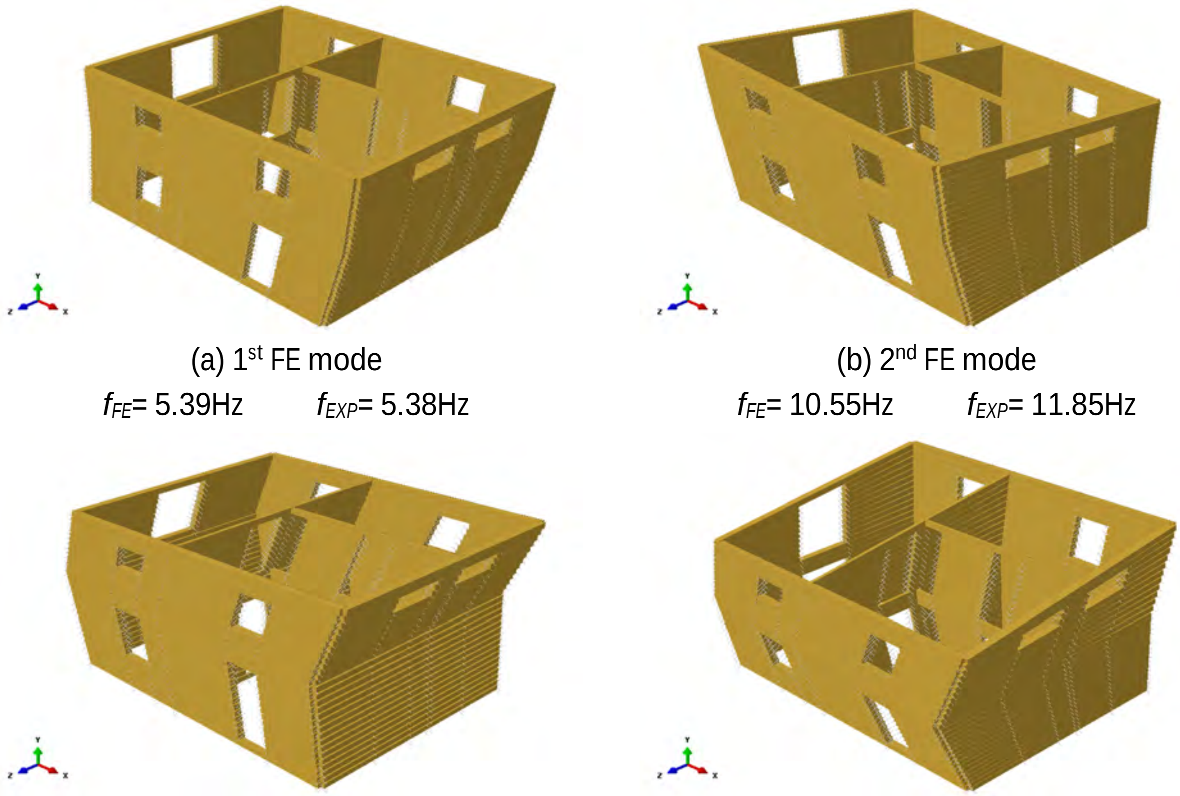

(a) 1st FE mode
f_{FE}= 5.39Hz f_{EXP}= 5.38Hz

(b) 2nd FE mode
f_{FE}= 10.55Hz f_{EXP}= 11.85Hz

(c) 3rd FE mode
f_{FE}= 14.80Hz f_{EXP}= 14.93Hz

(d) 4th FE mode
f_{FE}= 28.62Hz f_{EXP}= 20.53Hz

Figure 4. Numerically predicted fundamental vibration shapes and frequencies for the Rusticasa building (ABAQUS (Simulia (2012)))

3.3 Seismic performance

The same 3D model of the Rusticasa building was then numerically investigated by means of a nonlinear dynamic analysis, in order to assess the seismic performance of the building. The 1979 Montenegro earthquake record was considered as seismic input. Based on (*Piazza et al* (2013)), where several amplitudes for the same seismic record were considered for the full-scale experimental tests, the comparative numerical study was carried out by subjecting the reference FE-model to a low intensity earthquake (PGA= 0.07g), a moderate intensity (0.28g) and a high intensity earthquake (0.5g) respectively. The assessment of the FE predictions towards the full-scale shaking table tests was carried out by comparing the numerically obtained maximum displacements of the 3D FE model and the corresponding experimental measurements (*Piazza et al* (2013)), for some selected control points only. The typical deformed shape was found to be proportional to the first vibration mode of the building, see Figure 4(a). A detailed analysis of the collected predictions highlighted that no structural damage generally occurred in the timber components under the assigned seismic records, either in the full-scale specimen or in the simplified FE model. For the PGA= 0.28g seismic record, the average maximum deformation in the carpentry joints was found to be about 0.5mm, hence comprised within the assigned gap (see the joint calibration of Table 1). Close correlation was found also in terms of local comparisons. For the PGA= 0.28g record, the maximum experimental drift at the ground floor was found to be 0.005%, while the corresponding FE estimation was 0.004%. At the first inter-storey level, the maximum drift was 0.003% and 0.002% for the full-scale experimental tests and the simplified 3D FE model, respectively.

4 Parametric FE investigation

4.1 Selected buildings

Based on the preliminary validation of the 3D modelling approach, an exploratory FE study was carried out by taking into account several building configurations. All the 3D models were assembled and calibrated as described in Section 2. The examined 3D buildings were specifically defined as:

1) “B01” building: single storey *Blockhaus* building, with 4.90×7.10m regular plan and 2.50m height (4.60m at the ridge). The walls are made of 200×200mm, C24 class resistance spruce logs.
2) “B02” building: single storey *Blockhaus* building with symmetric configuration along both the longitudinal and transversal directions. The plan has almost a square shape, with 9.40×10.15m dimensions and 2.66m the height of the building at the edge of the roof (4.10mm at the ridge). The log-walls consist of 80×190mm, C24 spruce elements.
3) “B03” building: single storey system characterized by a markedly asymmetrical geometrical configuration. The plan has overall dimensions of 9.70×11.80m, while the building height is 2.48m (4.10m at the roof edge). The walls are composed of 90×160mm, C24 class, spruce logs.

The presence of an in-plane fully rigid diaphragm at the roof level was preliminary taken into account.

4.2 Dynamic performance evaluation

The B01 to B03 buildings were first analysed via eigenvalue analyses, to explore their dynamic performance. Figure 5 shows the predicted fundamental vibration modes. The corresponding vibration frequencies were found to be equal to 9.95Hz, 9.92Hz and 11.12Hz respectively.

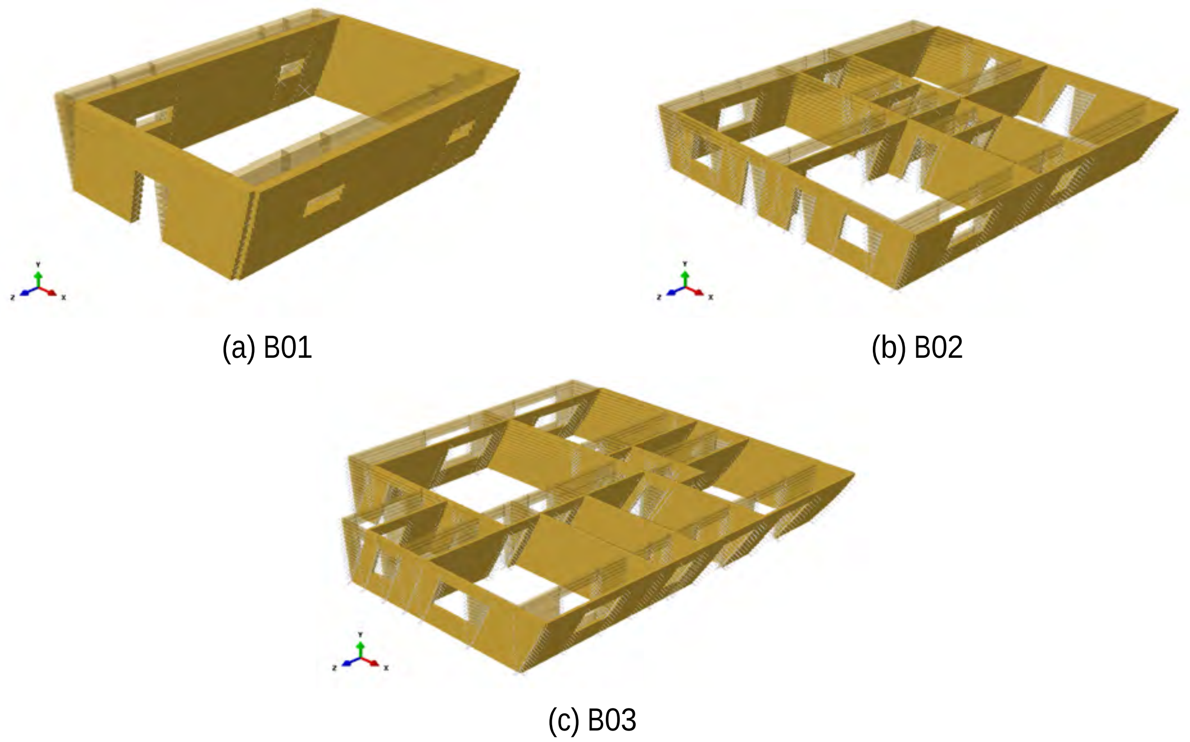

Figure 5. Fundamental vibration modes for the (a) B01, (b) B02 and (c) B03 case study buildings (ABAQUS (Simulia (2012)))

4.3 Seismic performance

The B01 to B03 buildings were then investigated via nonlinear dynamic simulations, under the effects of a set of seven natural seismic earthquake ground motions obtained from REXEL v.3.5 software (*Iervolino et al* (2010)). All the earthquake records were derived by considering PGA= 0.35g, type A soil (e.g. rock soil), topographic category T1 and nominal life of 50 years. A maximum lower and upper tolerance of 10% was considered in the derivation of the seven natural seismic records, see Figure 6(a).

The assessment of the seismic performance of the B01 to B03 systems was carried out by monitoring the maximum inter-storey drifts and the cyclic response of each carpentry joint. A qualitative assessment was also carried out in terms of global deformed shape and possible local failure mechanisms, especially near the openings and the intersections of multiple log-walls. In general, the investigated buildings demonstrated a marked flexibility under the assigned seismic records and an almost global seismic behaviour rather than possible local mechanisms.

The maximum obtained drifts were found to be about 0.0015%, hence in the same order of the Rusticasa building FE model and the corresponding full-scale specimen (see Section 3). A total maximum sliding of 0.7mm was obtained in the carpentry joints, hence comprised within the assigned tolerance gap of 1mm (see Table 1). The effect of such deformations for all the carpentry joints is an almost fully frictional performance for most of them. In terms of overall performance and deformations, finally, an almost stable global behaviour was generally observed, even in the B03 building characterized by a markedly irregular geometry and by a large number of door and window openings (see Figures 6(b) and (c)).

The presence of internal log-walls, in this sense, typically resulted in an increase of stability for the examined systems, and hence in an improved seismic performance.

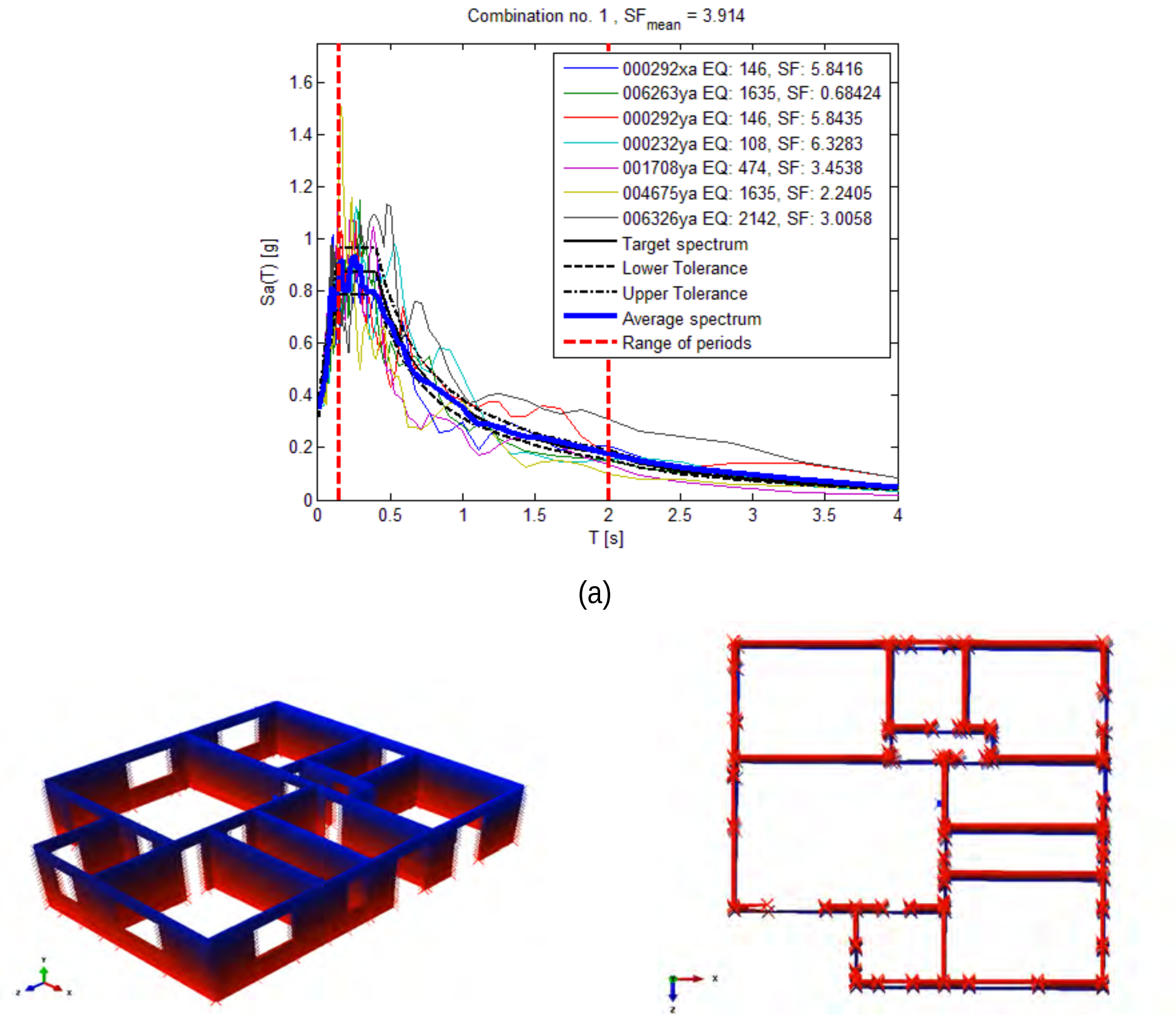

(a)

(b) (c)

Figure 6. (a) Reference set of natural seismic records obtained from REXEL v.3.5, with (b)-(c) typical deformed configuration of the B03 building under seismic events (PGA= 0.35g). Red-to-blue contour plot (scale factor: 5000), 3D and top view (ABAQUS (Simulia (2012)))

4.4 Assessment of most influencing parameters

The B01 case study was further investigated under the PGA= 0.35g seismic records defined in Figure 6, so that the effects of the most influencing parameters on the global and local structural performance of the same geometrical configuration could be further explored.

Based on the main features of the examined structural typology, careful consideration was given to the possible effects deriving from the geometrical properties of the carpentry joints typically used in timber log-wall systems, as well as on the in-plane flexibility of diaphragms and inter-storey floors.

4.4.1 Typology of carpentry joints

A further carpentry joint typology was investigated, for the B01 case study geometrical configuration described in Section 4.1. In accordance with the past FE calibration discussed in (*Bedon et a.* (2015b), (2015c)), the N01 'Standard' joints were replaced by 'Tirol' carpentry joints ('N03' type, based on (*Bedon et al* (2015b) and (2015c)), being characterized by specific geometrical features and cyclic behaviour (Figure 7).

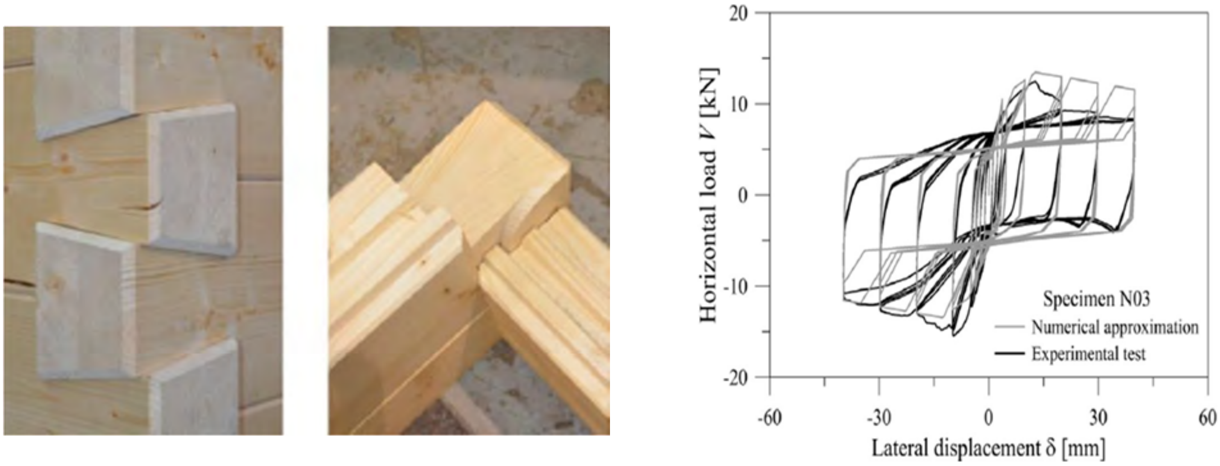

(a) (b)

Figure 7. 'Tirol' carpentry joint (N03 type, in accordance with (Rubner Haus AG SpA, Bedon et al (2015b) and (2015c))). (a) Geometrical configurationa and (b) load-displacement cyclic behavior

Compared to the B01 seismic performance with N01 joints, no differences were observed for the same building geometry with the N03 joint typology in terms of maximum drifts and global seismic performance, under the assigned set of seismic records (PGA= 0.35g). This result can be rationally justified by the occurrence – in the nonlinear dynamic simulations – of maximum deformations in the joints in the order of 0.5mm, i.e. in an almost pure frictional behaviour of the joints themselves.

4.4.2 In-plane flexible diaphragms

The presence of an in-plane flexible diaphragm at the roof level was also taken into account. In most of the cases of practical interest the typical *Blockhaus* roof and inter-storey floor proved to behave as an in-plane fully rigid diaphragm – due to the presence of OSB panels (see also Bedon & Fragiacomo (2015)). Nevertheless, the possible presence of fully flexible roofs and inter-storey floors should be also investigated.

For the B01 case study, a marked increase in maximum drifts was observed after the removal of the in-plane fully rigid diaphragm. Figure 8(a) presents a comparative example of maximum drifts, as obtained from one of the seven assigned seismic records of Figure 6(a). The corresponding deformed shape (*t*= 6.5s) is also proposed in Figures 8(b)-8(c), in the form of red-to-blue contour plot, with evidence of maximum displacements and rotations respectively. In terms of seismic design provisions, it is thus clear that specific rules should be provided for timber log systems with flexible inter-storey floors.

In the current research study, however, only in-plane fully rigid diaphragms were considered. These research outcomes should therefore be further extended.

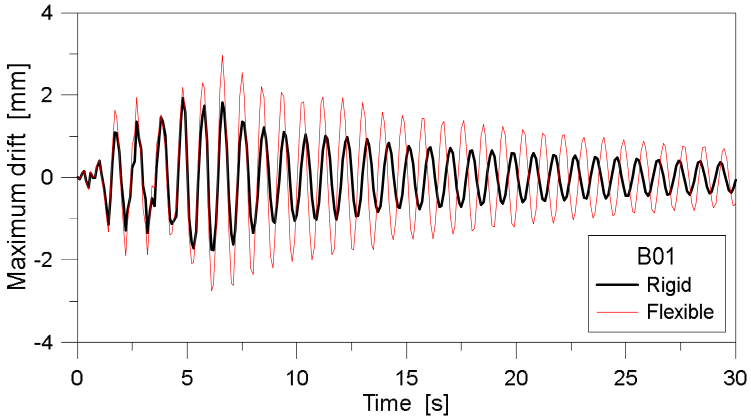

(a)

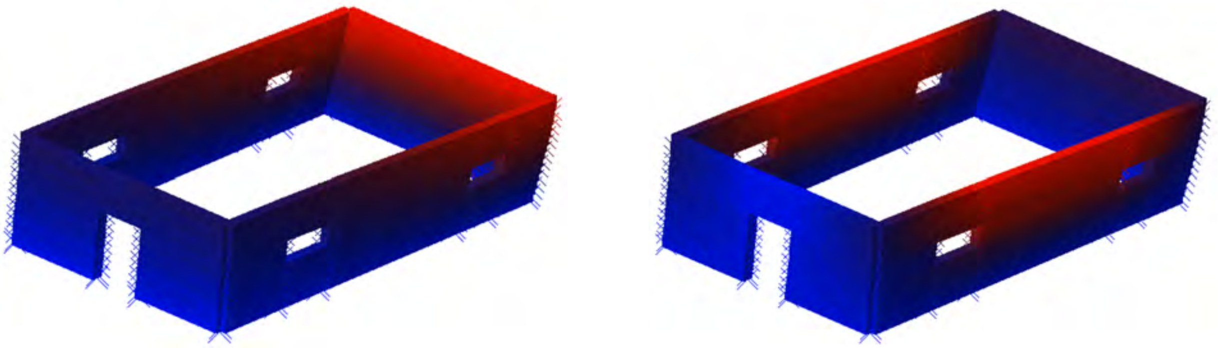

(b) t= 6.5s *(c) t= 6.5s*

Figure 8. Effect of in-plane fully rigid or flexible diaphragm on the sesmic performance of the B01 case study. (a) Monitored maximum drift and corresponding red-to-blue contour plot of (b) displacements and (c) rotational deformations (scale factor: 300, ABAQUS (Simulia (2012)))

5 *q*-factor estimation and design proposal

A final exploratory investigation was carried out, in order to derive a preliminary assessment of the actual dissipative capacity and seismic resistance of timber log-wall structural systems. While in (*Bedon et al* (2015c)) single log-walls under in-plane seismic loads only were considered, in this paper full 3D buildings were analysed.

Although a proper estimation of the *q*-factor is essential in force-based design of structural systems, the current generation of design standards (e.g. Eurocode 5 (2004) and Eurocode 8 (2004)) does not provide recommendations, especially for *Blockhaus* structural systems. Based on the preliminary results of the current study, a value of the *q*-behaviour factor and design provisions for capacity based design (currently missing) are thus provided for possible incorporation in the new generation of the Eurocode 8.

5.1 Classical methodology

Through the parametric study, nonlinear dynamic analyses (NLDA) were carried out on the B01 case study (Figure 5(a)). The previously defined set of seven recorded earthquake ground motions was considered, see Figure 6(a).

For each NLDA simulation, the magnitude of these seismic records was sequentially increased, so that the values representative of (i) the *PGA* leading to a pre-fixed maximum inter-storey drift and (ii) the *PGA* leading to yielding could be collected. In accordance with the past exploratory FE study carried out on single walls only (*Bedon et al* (2015c)), specifically, these reference limit values were defined as:

- $PGA_{u,i}$ (Near Collapse Limit State, NCLS): peak ground acceleration leading to a pre-fixed maximum level of inter-storey drift; and
- $PGA_{y,i}$ (Damage Limit State, DLS): design peak ground acceleration leading to yielding of a single corner joint.

For each *i*-scaled accelerogram, the q_0 value was then estimated as the average ratio of the so collected $PGA_{u,i}$ and $PGA_{y,i}$ peak ground accelerations, so that the corresponding *q*-behaviour factor value is given by:

$$q = q_0 \cdot \gamma_M \tag{1}$$

with γ_M the partial safety coefficient for timber (Eurocode 8 (2004)), assumed equal to 1.3 for dissipative systems, according to a proposal of revision of Section 8 of Eurocode 8 recently published (*Follesa et al* (2015)).

5.1.1 Ultimate configuration (NCLS)

The ultimate limit for the NCLS was preliminary assumed at the attainment of a pre-fixed maximum inter-storey drift δ_{max} derived from standards. In FEMA 356, for example, the NCLS damage configuration for wooden walls corresponds to a 3% transient or permanent inter-storey drift, with severe damage of the primary timber components (i.e. *"Connection loose, nails partially withdrawn; some splitting of members and panels; veneers dislodged"*).

Based on the observed structural response of single log-walls under in-plane seismic loads (see (*Bedon et al* (2015c)) for a detailed discussion of results), as well as on the shake table test results presented in (*Piazza et al* (2013)), a largest ultimate drift was also considered (δ_{max}= 5%). This latter NCLS configuration, although recommended in (FEMA 356) for steel frames only, was in fact rationally applied in this research investigation to *Blockhaus* buildings, due to their intrinsic high flexibility.

5.1.2 Yielding configuration (DLS)

Careful consideration was then also given to the detection of the first yielding configuration for the assigned carpentry joints.

In accordance with (*Bedon et al* (2015c)), the DLS reference configuration was considered as the first yielding for the N01 type joints, i.e. being this latter condition associated – in accordance with Table 1 – to a single joint sliding in the order of ≈8.6mm, i.e. corresponding to a maximum drift of ≈0.04% for the examined buildings.

5.2 Alternative methodology

As an alternative calculation approach, the *q*-behaviour factor was then also calculated for the B01 building system by taking into account the $PGA_{u,i}$ values numerically derived according to in Section 5.1. The corresponding q_0 factor, based on Eq.(1), was then calculated by taking into account the $PGA_{y,i}$ leading the single N01 carpentry joint to shear or compressive failure mechanisms, whatever occurs first.

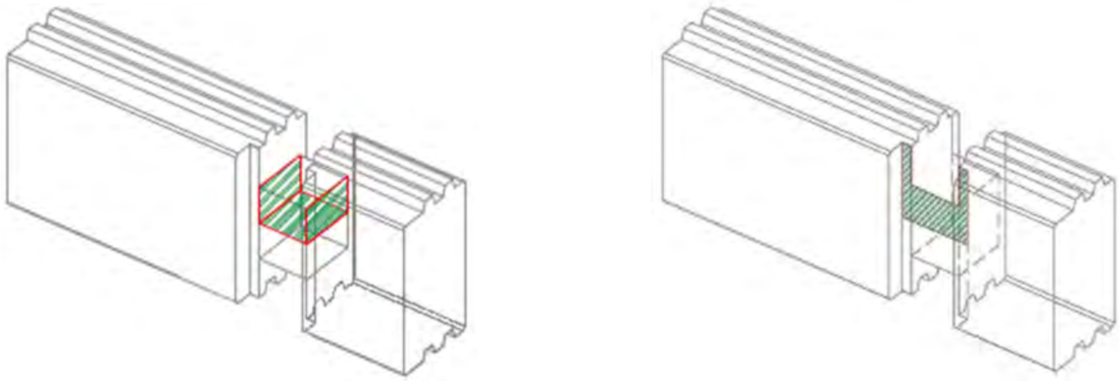

(a) (b)

Figure 9. Reference resisting surfaces for a N01 type carpentry joint (Rubner Haus AG SpA), with evidence of (a) shear or (b) compressive mechanisms

Based on the carpentry geometry displayed in Figure 1, for seismic design, in accordance with the Eurocode 5 provisions (2004) the shear resistance of the joint should be considered as the weakest among the resisting mechanisms, i.e. a pure shear failure mechanism (Figure 9(a)) and a compressive collapse mechanism (Figure 9(b)).

The $PGA_{y,i}$ values, in the current study, were thus derived from the experimental cyclic response of the N01 reference joint (Table 1), as the peak ground acceleration leading – for each *i*-scaled accelerogram –the first joint of the B01 building to a maximum displacement corresponding to the minimum characteristic resistance load:

$$V_{shear,k} = \frac{2}{3} A_{shear} \cdot f_{k,v} \text{ , and} \tag{2a}$$

$$V_{c,90,k} = A_{comp,eff} \cdot f_{c,90,k} \text{ .} \tag{2b}$$

In Eqs.(2a) and (2b), A_{shear} and $A_{comp,eff}$ denote the resisting surfaces (Figure 9), while $f_{k,v}$ and $f_{c,90,k}$ represent respectively the characteristic resistance values of C24 spruce for shear and compression perpendicular to grain.

5.3 Discussion of results

5.3.1 Classical methodology results

In terms of *q*-factor estimation, the main results of the exploratory study are proposed in Figure 10, as obtained by applying the classical methodology (Section 5.1), in terms of PGA_u (Figure 10(a)) and q_0 values (Figure 10(b)) calculated for each *i*-scaled accelerogram. The average values are also proposed as straight lines. The so collected FE data are shown for two NCLS scenarios (δ_{max}= 3% and 5%, Section 5.1.1).

As shown, the obtained FE results generally confirmed the recent findings proposed in (*Bedon et al* (2015c)) for single log-walls subjected to in-plane seismic loads. The NLDA simulations highlighted, in particular, that the assumption of a reference NCLS drift δ_{max}= 3% as conventionally done for wood structures would result in fully neglecting the post-yielding behaviour of the adopted carpentry joints. Consequently, this assumption would result in a q_0-factor equal to ≈1 (Figure 10(b)), i.e. in a final q-factor ≈1.3 (Eq.(1)). For the B01 case study, an average q value of 1.28 at a maximum drift of 3% was in fact obtained. When the ultimate allowable drift is increased to 5%, the carpentry joints activate, hence the intrinsic high flexibility and dissipative capacity of *Blockhaus* buildings is further exploited. For the examined B01 system, a direct effect of this latter assumption is that an average q_0-factor in the order of ≈1.15 was obtained, hence leading to an average q-factor of ≈1.49 (Eq.(1)).

Due to the high deformation capacity of the *Blockhaus* structural system, however, even the assumption of a 5% maximum drift does not fully exploits the potential of the adopted joints, with slidings up to ≈11mm for the reference case study.

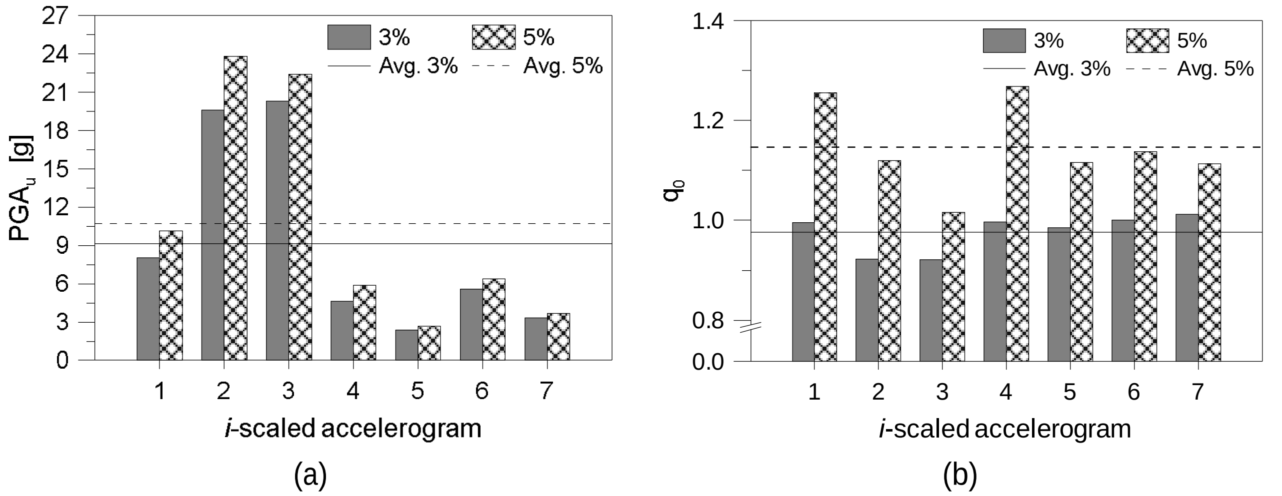

Figure 10. (a) $PGA_{u,i}$ and (b) q_0-factor values numerically derived for the B01 building, in accordance with Section 5.1 (ABAQUS (Simulia (2012))).

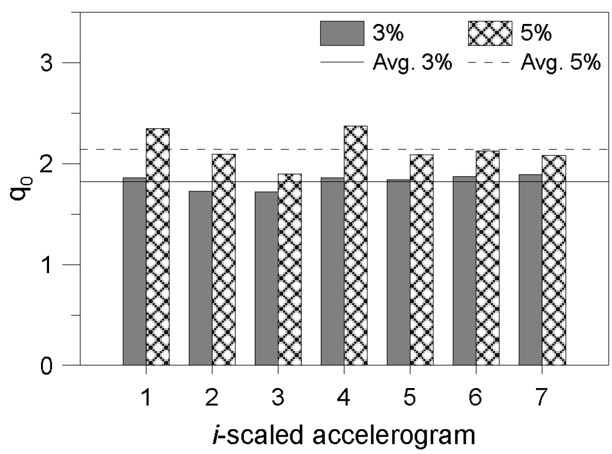

Figure 11. q_0-factor values numerically derived for the B01 building, in accordance with Section 5.2 (ABAQUS (Simulia (2012))).

5.3.2 Alternative methodology results

Following the alternative calculation approach proposed in Section 5.2 for the *q*-factor estimation, totally different predictions were achieved compared to Section 5.3.1, see Figure 11.

For the N01 carpentry joint, the shear collapse mechanism was found to be the weakest one, with $V_{shear,k} \approx$ 12kN the characteristic resistance derived from Eq.(2). Based on the cyclic joint performance of Table 1, a reference yielding displacement ≈4.6mm was taken into account (i.e. maximum total drift ≈2%). An average q_0 value of 1.82 and 2.14 was obtained for a NCLS drift of 3% and 5% respectively, see Figure 11, hence resulting in a *q*-factor in the order of 2.4 and 2.8 (Eq.(1)).

5.4 Design recommendations

The primary observations of the exploratory FE investigations are listed herein after.

- The FE study confirmed the high flexibility and potential of the examined structural system. For the reference NCLS configuration, a maximum inter-storey drift of 5% should be considered, rather than the 3% value usually accepted for wooden structures.
- The geometrical properties of the typical carpentry joints used in *Blockhaus* systems proved to have negligible effects on the overall seismic performance of the examined buildings. This finding directly depends on the presence of small gaps within the single joints, hence on the intrinsic flexibility and pure frictional phenomena in the joints themselves.
- When in-plane fully rigid diaphragms are considered, a *q*-behaviour factor of at least 1.5 should be considered in design for *Blockhaus* systems. The alternative calculation methodology discussed in this paper highlighted that higher dissipative capacities for *Blockhaus* systems – and thus *q*-factors in the order of 2.4-2.8 – can be exploited as long as the yielding configuration is detected as the weakest calculated resisting mechanism of a single joint.
- The presence of fully flexible diaphragms should be also properly explored, since typically resulting in a different global behaviour of the examined buildings, hence in specific *q*-factor values that should be properly calculated.

6 Summary and conclusions

In this paper, an exploratory nonlinear dynamic FE-investigation was proposed for full three-dimensional *Blockhaus* timber buildings. Compared to past research projects of literature, typically focused on the mechanical and seismic characterization of small *Blockhaus* components only or single shear walls under in-plane lateral loads, the novelty of presented study was represented by the application of a simplified but accurate FE-modelling approach to geometrically complex 3D buildings.

At a preliminary stage, the FE-modelling approach was assessed and validated towards the experimental results of full-scale shaking table tests and modal identification measurements carried out on the Rusticasa building (SERIES Project). A good agreement was found between the experimental measurements and the corresponding FE data, both in terms of vibration modes and seismic performance for the same log-wall building.

The nonlinear dynamic investigation was then extended to some selected case studies. The so obtained results were critically discussed for some geometrical configurations of technical interest, in order to investigate the seismic performance and provide a rational estimation of the corresponding q-behaviour factor. In general, the examined geometrical configurations proved to be stable and markedly flexible under the assigned seismic records. It is expected that the current results of the investigation could provide a useful background for the implementation of q-factor values and capacity design rules for *Blockhaus* buildings in the revision of the Eurocode 8 for seismic design. More specifically, it is proposed a q-behaviour factor at least equal to 2.4 for *Blockhaus* systems with in-plane fully rigid inter-storey floors.

7 Acknowledgements

Rubner Haus AG SpA is gratefully acknowledged for the financial and technical support during the experimental investigations on full-scale Blockhaus timber walls and small carpentry joints.

DPC-ReLUIS is also gratefully acknowledged for partially funding the research activity within the framework of the ‘PR4-Timber structures’ project.

Prof. Maurizio Piazza and Dr. Jorge Branco are finally acknowledged for providing technical details on the SERIES Project experiments carried out on the ‘Rusticasa building’.

8 References

Bedon, C., Fragiacomo, M. (2016): Derivation of buckling design curves via FE modelling for in-plane compressed timber log-walls in accordance with the Eurocode 5, European Journal of Wood and Wood Products, *published online*, doi: 10.1007/s00107-016-1083-5

Bedon, C., Fragiacomo, M., Amadio, C., Sadoch, C (2015a): Experimental study and numerical investigation of *Blockhaus* shear walls subjected to in-plane seismic loads. Journal of Structural Engineering, 141(4), doi: 10.1061/(ASCE)ST.1943-541X.0001065

Bedon, C., Rinaldin, G., Fragiacomo, M. (2015b): Non-linear modelling of the in-plane seismic behaviour of timber *Blockhaus* log-walls. Engineering Structures, 91: 112-124

Bedon, C., Rinaldin, G., Fragiacomo, M., Amadio, C. (2015c): Exploratory cyclic and dynamic numerical investigation for the assessment of the seismic vulnerability of

Blockhaus shear walls under in-plane lateral loads. Proceedings of XVI ANIDIS Conference, 13-17 September 2015, L'Aquila, Italy

Branco, J.M., Araújo, J.P. (2012): Structural behaviour of log timber walls under lateral in-plane loads. Engineering Structures, 40(3), 371-382

Eurocode 5 (2004) - Design of timber structures - Part 1-1: General-common rules and rules for buildings. European Committee for Standardisation, CEN, Brussels, Belgium

Eurocode 8 (2004) - Design of Structures for Earthquake Resistance - Part 1: General rules, seismic actions and rules for buildings. European Committee for Standardisation, CEN, Brussels, Belgium

FEMA 356 – Prestandard and commentary for the seismic rehabilitation of buildings, Federal Emergency Management Agency

Follesa, M., Fragiacomo, M., Vassallo, D., Piazza, M., Tomasi, R., Rossi, S., Casagrande, D. (2015): A proposal for a new Background Document of Chapter 8 of Eurocode 8, Proceedings of INTER 2015 Meeting, 2015 Šibenik, Croatia, Paper n°48-7-3

Grossi, P., Sartori, T., Giongo, I., Tomasi, R (2016): Analysis of timber log-house construction system via experimental testing and analytical modelling. Construction and Building Materials, 102(2): 1127-1144

Iervolino, I., Galasso, C., Cosenza, E. (2012): REXEL: computer aided record selection for code-based seismic structural analysis. Bulletin of Earthquake Engineering, 8(2): 339-362. doi: 10.1007/s10518-009-9146-1

Piazza, M., Campos Costa, A., Candeias, P.X., Lourenço, P.B., Branco J.M., Aranha, C. (2013): Seismic performance of multi-storey timber buildings – Rusticasa building – Final Report, SERIES 227887 Timber Buildings Project

Rinaldin, G., Amadio, C., Fragiacomo, M. (2013): A Component approach for the hysteretic behaviour of connections in cross-laminated wooden structures, Earthquake Engineering and Structural Dynamics, 42(13): 2023-2042. Wiley Online Library, doi: 10.1002/eqe.2310

Rubner Haus AG SpA, *www.haus.rubner.com*

Simulia (2012: ABAQUS v.6.12 [Computer Software], Dassault Systems, Providence, RI, USA

Discussion

The paper was presented by M Izzi

H Blass asked about the static capacity of these joints. M Izzi replied testing was done in Trento. There were discussions related to the presence of tensile stresses perpendicular to grain because of the notches. M Izzi stated that he had not followed the tests but agreed that tensile stresses perpendicular to grain would be important.

G Doudak asked about the influence of friction mechanism. M Izzi replied that gaps could be considered in the model with modifying the load and a gap of 1 mm was considered stable from manufacturers. G Doudak commented it was not clear how the q factor would be affected by the diaphragm rigidity and asked what would be the recommendation for a semi rigid case. M Izzi replied that this had not been investigated in detail yet.

A Frangi commented that the failure mode on connection can be shear and compression. M Izzi discussed the progress in which the mechanism had the lowest value was check first and then go back to model to check the other mechanism.

BJ Yeh commented that service conditions could cause checking of the wood and asked whether the q factor recommended would be appropriate for in service conditions. M Izzi replied yes.

W Seim commented that it was important to study the q factor for this type of structure. He commented that integrating these systems would be important if one had higher q factor. W Seim and M Izzi discussed that additional steel connectors would be needed to avoid integrating factor.

Simplified design procedure for linear dynamic analysis of multi-storey light-frame wood buildings in Canada

Jean-Philippe Tremblay-Auclair, Laval University, Quebec, Canada

Alexander Salenikovich, Laval University, Quebec, Canada

Caroline Frenette, cecobois, Quebec, Canada

Keywords: Linear dynamic analysis, seismic design, light-frame shear wall, mid-rise building, linear nail slip.

1 Background

1.1 Introduction

Multi-storey wood construction has been growing in Canada in the last few years due to the low impact of wood buildings on the environment. Currently, the most common method used for seismic design of light-frame wood structures is the equivalent static force procedure (ESFP) of the National Building Code of Canada (NBCC) (NRCC, 2015). Nonetheless, NBCC requires dynamic analysis for structures with irregularities and for structures in high seismic zones. Since it has been authorized to build wood frame structures up to six storeys all over Canada (NRCC, 2015), linear dynamic analysis (LDA) method of the NBCC becomes an increasingly important tool for seismic design. Chen et al. (2014) showed that the dynamic analysis produces a more realistic response of multi-storey light-frame buildings due to consideration of the effect of higher modes of vibration on the distribution of forces and deflections. In fact, the LDA has been a common practice in seismic design of steel and concrete structures for more than 25 years. However, it is rarely used in design of wood frame structures (Karacabeyli and Lum, 2014) because of its limited practicality for low-rise wood buildings. Furthermore, commercial software generally is not adapted to this type of structures for the lack of established procedures to properly determine the stiffness of wood-based systems. Kirkham et al. (2013) have indicated that is the time to have simplified numerical model that can be used by professional engineers. Recently, Newfield et al. (2014) presented a methodology to perform LDA on multi-storey light-frame wood structures using commercial structural software where the stiffness of shear walls is determined using a mechanics-based approach (Newfield et al., 2013) adopted in the Annex A of CSA O86-14 (CSA, 2014) to calculate the light-frame shear wall deflections.

1.2 Nail slip equations

In this section, the nail slip equations of CSA O86-14, NDS 2015 (AWC, 2015a), Eurocode 5 (CEN, 2008) and SIA 265 (2012) for panel-to-wood connections are presented. These equations are used further in this paper to calculate and compare the deflections of shearwalls fabricated with wood structural panels.

1.2.1 CSA O86-14

Clause A.11.7 in the Annex A of CSA O86-14 gives the following nonlinear nail slip equation for light-frame shearwall and diaphragm deflection calculations:

$$e_n = \left(\frac{0.013vs}{d^2}\right)^2 \tag{1}$$

Where e_n is the nail slip, mm; v is the maximum specified shear force per unit length along the diaphragm boundary or top of shearwall, N/mm; s is the nail spacing at panel edges of shearwalls or diaphragms, mm, and d is the nail diameter, mm.

In fact, Eq. (1) has been derived as an approximation from equations previously adopted in the Special Design Provisions for Wind and Seismic (SPDWS) (AWC, 2005). For example, an original equation for the fastener slip in the walls fabricated with dry lumber using 8d common nails was presented in table C4.2.2D (AWC, 2005) as follows (in SI units):

$$e_n = 1.2 \cdot (V_n/938)^{3.018} \tag{2}$$

Where V_n is the maximum specified shear force per nail, N, and the factor 1.2 accounts for the slip in panels other than *Structural I* grade plywood.

1.2.2 NDS 2015

The non-linear nail-slip equations, such Eq. (2), are no longer used in the American design code (SPDWS) (AWC, 2015b). Instead, a single apparent shear stiffness term (G_a) combining the shear stiffness of the sheathing panel and the fastener slip equal to the nail slip at 1.4 times allowable seismic load. According to the SPDWS Commentary (AWC, 2005), the differences are generally negligible for design purposes, although influencing the load distribution assumptions.

Alternatively, one could determine the nail slip using the slip modulus presented in clause 11.3.6 of NDS 2015 for calculation of the group action factor for dowel-type fasteners, which is expressed in SI units as follows:

$$\gamma = 266d^{1.5} \tag{3}$$

Where γ is the slip modulus, N/mm, and d is the nail diameter, mm.

Therefore, the nail slip, e_n (mm), can be determined as follows:

$$e_n = V_n/\gamma \tag{4}$$

Where V_n is the maximum specified shear force per nail, N.

Although the slip modulus presented in Eq. (3) is not currently used to calculate the nail slip in shearwalls, it offers a linear equation for the nail slip, and that is why it has been considered in this project.

1.2.3 Eurocode 5

In Eurocode 5, the slip moduli K_{ser} and K_u for the serviceability limit states and ultimate limit states, respectively, are used to calculate the nail slip. For the nails installed without predrilling, K_{ser} is calculated as follows (clause 7.1):

$$K_{ser} = {\rho_m}^{1.5}d^{0.8}/30 \tag{5}$$

Where K_{ser} is the slip modulus, N/mm; ρ_m is the mean density at 12% MC, kg/m^3, and d is the nail diameter, mm.

For the ultimate limit states:

$$K_u = \ 2K_{ser}/3 \tag{6}$$

Therefore, the nail slip, e_n (mm), is determined as follows:

$$e_n = V_n/K_{ser\ (\mathrm{or}\ u)} \tag{7}$$

Where V_n is the maximum specified shear force per nail, N.

In this project, only the nails without pre-drilling have been considered as the common building practice for shear walls.

1.2.4 SIA 265

In SIA 265, the same Eq. (7) is used to calculate the nail slip as in the Eurocode 5. Slip modulus equations are presented for loading in the parallel and perpendicular directions. For this project, only the equation for loading parallel to grain is considered, as follows:

$$K_{ser,0} = 60d^{1.7} \tag{8}$$

Where $K_{ser,0}$ is the slip modulus for loading parallel to grain, N/mm, and d is the nail diameter, mm.

1.3 Deficiencies of the equivalent static force procedure (ESFP)

The ESFP provides static forces to approximate the seismic behaviour of a structural system simplifying the calculation of its non-linear deflection. Nevertheless, during the development of the ESFP for the NBCC 2005 (NRCC, 2005), Humar and Rahgozar (2000) identified some important concerns with regards to shear walls in multi-storey buildings. The first problem is related to the shear force distribution in the shear walls along the height of the building where shear forces are more dominant at the top and bottom storeys because of the higher mode effect, which cannot be directly accounted for in the ESFP. An F_t factor is used to take this effect into account and to increase the shear force at the roof level. However, Humar and Rahgozar (2000) have demonstrated that the ESFP can still potentially underestimate the shear force by 5 to 10% at the top storeys. It is particularly important in the Eastern Canada where the higher mode effect is more significant due to earthquakes rich in high frequencies. The second problem is related to the overturning moment distribution. According to Humar and Rahgozar (2000), the overturning moment is significantly overestimated in the ESFP for multi-storey shear walls located in the Eastern Canada. The overturning moment is calculated using the shear force calibrated with F_t and M_v factors to consider the effect of higher modes. Then, J_x factor is used to reduce the overturning moment in the lower storeys.

1.4 Linear dynamic analysis (LDA)

Two types of LDA can be performed: time history analysis and modal analysis. Time history analysis allows obtaining the complete information on behaviour of a structure during specific earthquakes. However, this type of analysis being complex and time consuming is rarely used in the design practice nowadays. Modal analysis is much easier to use. In this method, several natural vibration modes of a structure are determined and juxtaposed in order to obtain the maximum forces and displacements using the uniform hazard spectra (UHS). Furthermore, the modal analysis allows designers to analyse in detail the dynamic behaviour of the structure by observing the period, shape and contribution of each individual mode. Therefore, it allows the use of a limited number of modes to design the structure instead of calculating the entire time history response to multiple earthquakes. To determine the number of modes to be used in the analysis of each orthogonal direction of a structure, a common rule is to obtain at least 90% of mass participation in both directions (Karacabeyli and Lum, 2014; Filiatrault et al., 2013).

In comparison with the ESFP, the LDA procedure for multi-storey buildings has the advantage of considering more precisely the effect of higher modes on the behaviour of the structure and therefore better estimates shear forces, overturning moments, inter-storey drifts and total inelastic deflections of shear walls. Furthermore, the NBCC (NRCC, 2010) allows analysing structures with and without irregularities and reduce the accidental torsion for buildings not sensitive to torsion.

1.5 Iterative LDA

Newfield et al. (2014) proposed an iterative LDA procedure (LDA iter.) for the seismic design of multi-storey light-frame wood structures where shear walls are transformed into a series of vertical beam elements of regular cross-section with equivalent properties at each storey (Figure 1). In most commercial structural software, such beam elements can be represented by a section with a depth (*d*) and a width (*b*) of isotropic material with a Young's modulus ($E_{c,eq}$) and a shear modulus (G_p).

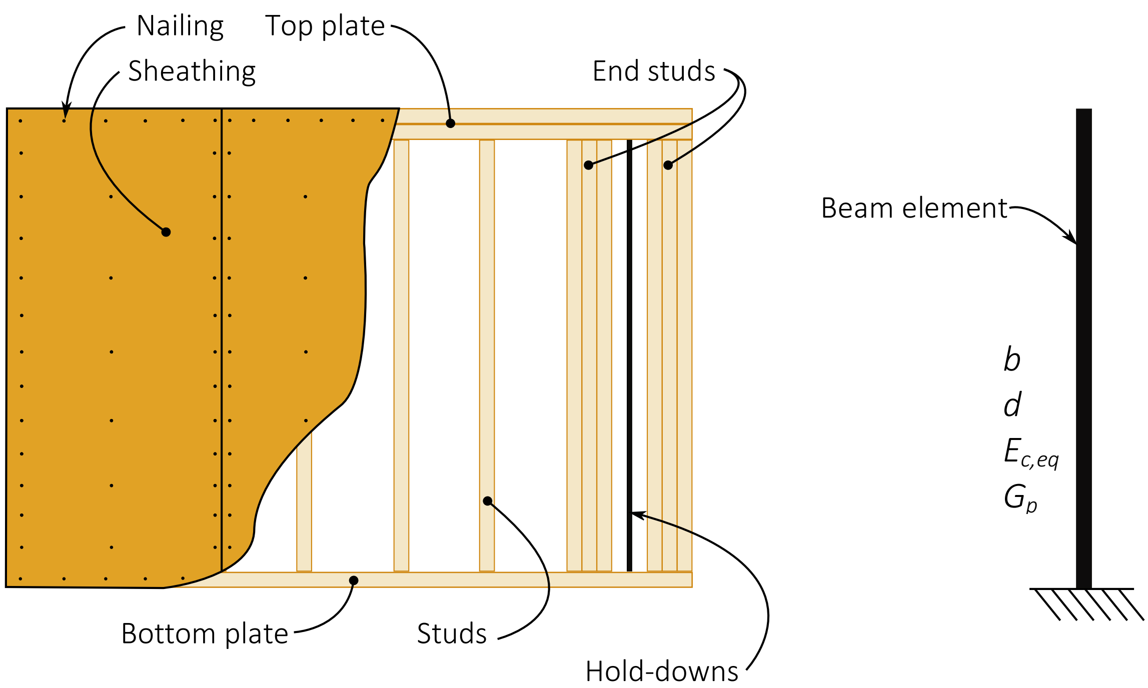

Figure 1: Newfield et al. (2014) light-frame shear wall transformed into beam element with equivalent properties.

This procedure requires a manual iterative adjustment of the element stiffness to account for the non-linear nail slip (e_n) in eq. (9) according to the shear load acting on the wall.

$$G_p = \frac{1.2}{t_{eq}\left(\frac{1}{B_v} + 0.0025\frac{e_n s}{V_n}\right)} \tag{9}$$

Where G_p is the equivalent shear modulus of the wall, N/mm^2; t_{eq} is the equivalent thickness of the wall, mm; B_v is the shear-through-thickness rigidity of the panel, N/mm; e_n is the nail slip, mm; s is the nail spacing, mm; V_n is the shear per nail, N.

1.6 Simplified LDA

The procedure proposed by Newfield et al. (2014) requires to update manually the stiffness properties of each wall at each step, which is time consuming, especially in the design of a whole building. To eliminate the iterations, Tremblay-Auclair (2016) proposed a simplified LDA procedure (LDA simp.) using the apparent shear modulus (G_a), similar to the apparent shear stiffness in the SDWPS (AWC, 2015b), instead of the equivalent shear modulus (G_p) used by Newfield et al. (2014). In this case, the shear resistance of the shear wall is used to calculate the corresponding nail slip and the apparent shear modulus of the wall using the following equation:

$$G_a = \frac{1.2}{t_{eq}\left(\frac{1}{B_v} + 0.0025\,\frac{e_{n,max}s}{V_{n,max}}\right)} \tag{10}$$

Where G_a is the apparent shear modulus of the wall, N/mm^2; $e_{n,max}$ is the nail slip corresponding to the shear resistance of the shear wall, mm; s is the nail spacing, mm; $V_{n,max}$ is the shear per nail corresponding to the shear resistance of the shear wall, N.

Also, the simplification can be achieved if any linear nail slip formula is used in eq. (9).

1.7 Objective

In this paper, we compare the nail slip calculated using formulas presented in section 1.2 with some test results on sheathing-to-framing connections and investigate if the choice of the nail slip formula affects the results of ESFP and LDA analyses. For this purpose, we analysed two light-frame wood shear walls of a six-storey building located in Quebec City. The shear forces, overturning moments and interstorey drifts calculated with ESFP and LDA using the different nail slip formulas are compared and discussed.

2 Case study

Two walls of different aspect ratios, height-to-length, have been selected from the design example of a six-storey light-frame wood building designed by Chaurette et al. (2015) using the ESFP with the CSA O86-14 nonlinear nail slip equation. Figure 2 shows the elevation and the plan of the building highlighting two shear walls analysed in this study. The building is located in Quebec City, in Eastern Canada and the spectrum for modal analysis is presented in Figure 3.

Figure 4 shows configurations of the two walls considered for the comparison of the different nail slip equations in combination with LDA. The two aspect ratios have been chosen based on the work of Tremblay-Auclair (2016). The walls MR8-B and MR11 have an aspect ratio of 6.0 and 1.7, respectively. The height of the first storey is 2.870 m. All intermediate storeys have a height of 2.908 m. The top storey is 3.466 m high to accommodate a flat roof made with light-frame wood trusses. The walls are made of 2 x 6 (38 x 140 mm) studs spaced at 16 in. (0.4 m) c/c; sheathing is blocked; and continuous steel rods are used as overturning restraint. Gun nails of two different sizes have been used, respectively, 0.120 in. (3.05 mm) and 0.131 in. (3.33 mm) of diameter and 2.5 in. (64 mm) and 3.0 in. (76 mm) of length.

Figure 2: Six storey light-frame wood building: (a) elevation and (b) plan (location of the two walls is shown in red)

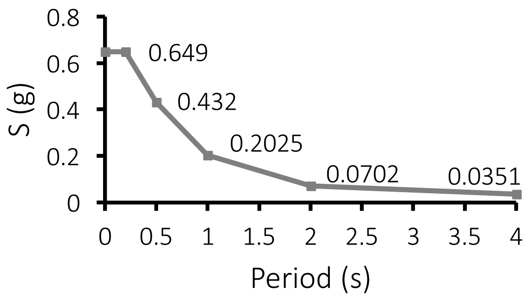

Figure 3: Quebec City response spectrum for soil category D

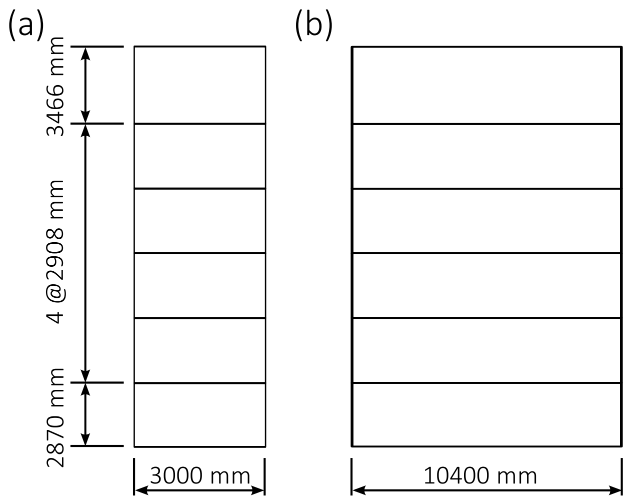

Figure 4: Configuration of walls (a) MR8-B and (b) MR11

3 Results

3.1 Comparison of the nail slip equations

The nail slip relationships presented in section 1.2 are illustrated in Figure 5 for sheathing-to-framing connections with 8d nails. The length of the nail is 2.5 in. (64 mm) and the diameter is 0.120 in. (3.05 mm). Also, results from tests of single nail sheathing-to-framing connections (Salenikovich, 2000; Dolan, 1989) are shown in the figure. The K_0 value represents the initial stiffness of these connections; i. e., the elastic stiffness before the nail begins to yield.

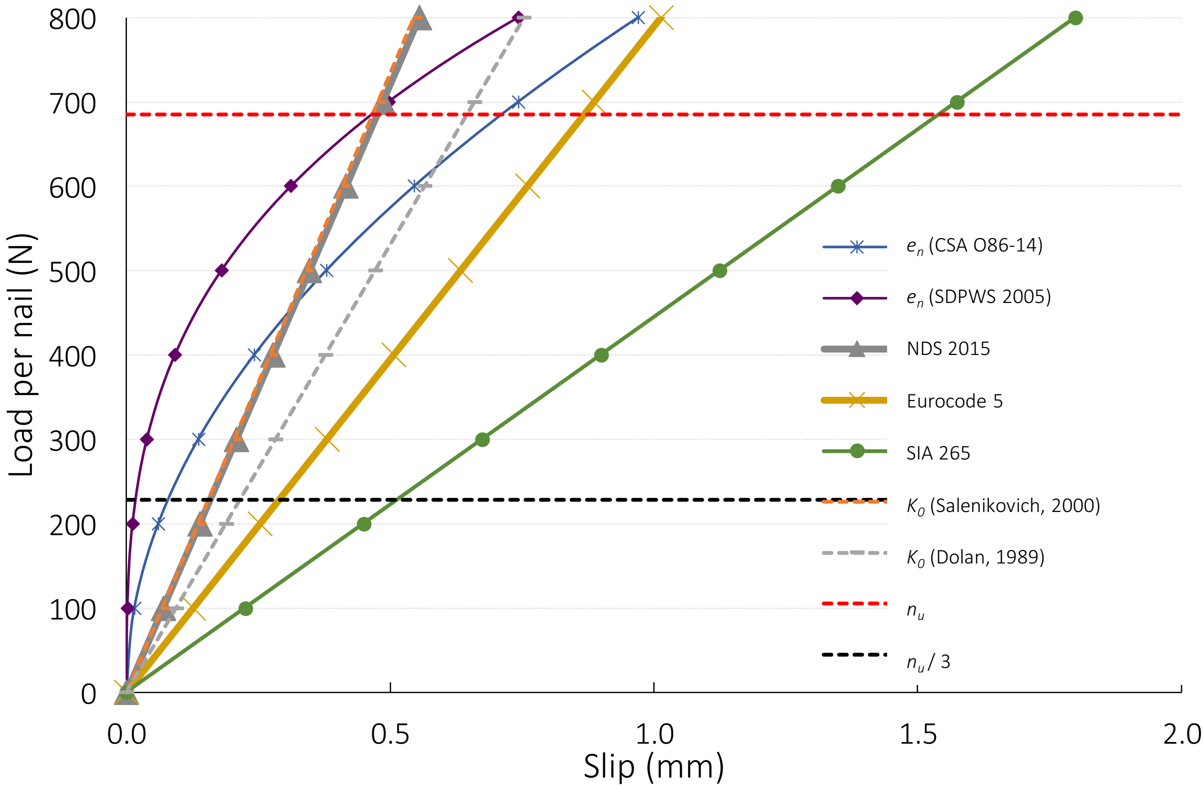

Figure 5: Comparison of nail slip equations for 8d nails (d=3.05 mm and L=64 mm)

It can be observed in Figure 5 that the SIA 265 equation predicts greater slip than all other equations and the test results. The other equations differ 0.4 mm or less from each other and from the test data up to the specified load level (n_u). The NDS 2015 formula based on Eq. (3) and (4) fits well the SDPWS (eq. 2) and the test data of Salenikovich (2000) and shows the least nail slip. The Eurocode 5 formula based on on eq. (5) and (7) appears to be closer to the CSA O86 (eq. 1) and the test data of Dolan (1989).

3.2 Comparison of analyses of two six-storey shear walls

Figure 6 shows the storey shears, (a) and (b), and the overturning moments, (c) and (d), respectively, for the walls MR8-B and MR11 calculated using different methods. The y-axis shows the ratio of the *i*-th storey elevation (H_i) over the total height of the wall (H). The ESFP storey shears and overturning moments are independent of the nail slip equation. The LDA simp. (CSA O86-14) results are obtained using the simplified LDA method where the shear stiffness is calculated from eq. (10) as proposed by Tremblay-Auclair (2016). The LDA (NDS 2015), LDA (Eurocode 5) and LDA (SIA 265) results are obtained using LDA with the shear stiffness from eq. (9) and the corresponding linear nail slip formulas. The LDA iter. (CSA O86-14) results are obtained using the iterative methodology developed by Newfield et al. (2014) with the sear stiffness from eq. (9) and the nonlinear nail slip equation of the CSA O86-14.

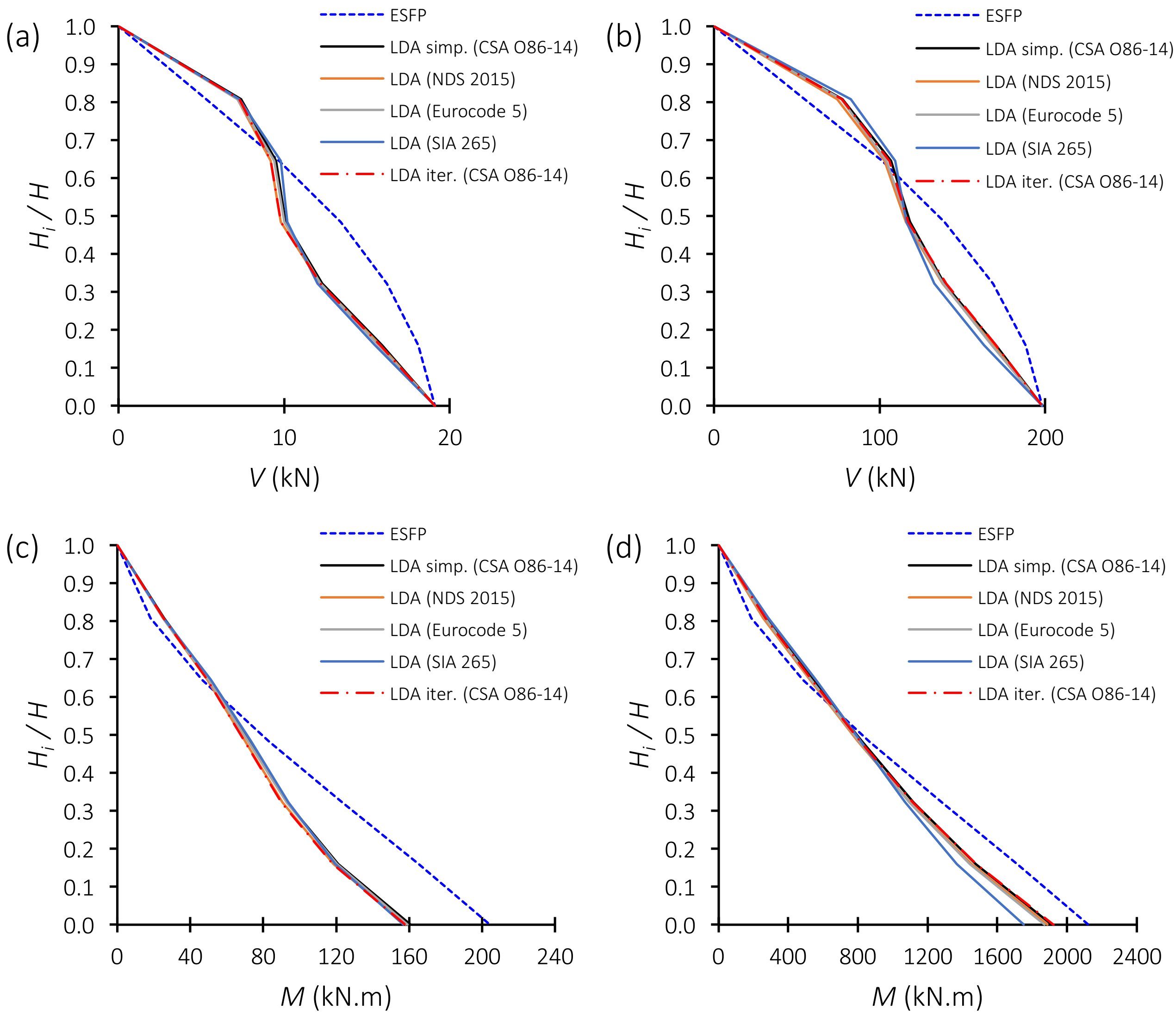

Figure 6: LDA results with the different nail slip equations: (a) MR8-B storey shears; (b) MR11 storey shears; (c) MR8-B overturning moments and (d) MR11 overturning moments.

In this paper, the LDA iter. (CSA O86-14) is considered as the reference, because this method uses the nail slip equation and the methodology to calculate multi-storey shear wall deflection adopted in CSA O86-14 Annex A. In Figure 6 (a and b), it can be observed that all the LDA results are close to each other and they are all calibrated to the same base shear according to the NBCC (NRCC, 2015), which requires that the base shear shall not be less than the ESFP and has to be increased by a factor of 1.2 for combustible construction. Despite the calibration, it can be observed that the ESFP analysis predicts lower storey shear forces at the top storey and higher overturning moments at the first storey relative to all the LDA methods presented in Figure 6. This issue is discussed in more detail in Tremblay-Auclair (2016) and Tremblay-Auclair et al. (2016).

Figure 7 presents the interstorey drifts of the two walls calculated using the different methods. The X-axis represents the interstorey drift as a percentage of the storey height and the Y-axis is the same as the Figure 6. It can be observed that LDA iter. predicts the smallest deflections, except for LDA (NDS 2015) in Figure 7b. Other LDA lines are close to each other, except for the SIA265. The Eurocode 5 and the LDA simp. lines are close to the LDA iter. in both cases and indicate that both methods can be used to perform LDA with sufficient accuracy. The ESFP used with different nail slip formulas produced significantly higher interstorey drifts than the LDA increasing at each level, except for the top storey. This difference is due to the effect of higher modes. Also, it can be observed that higher modes have more impact on the story drift of a wall with a higher aspect ratio. Note that the ESFP (NDS 2015) storey drifts were the closest to the ESFP (CSA O86-14) results.

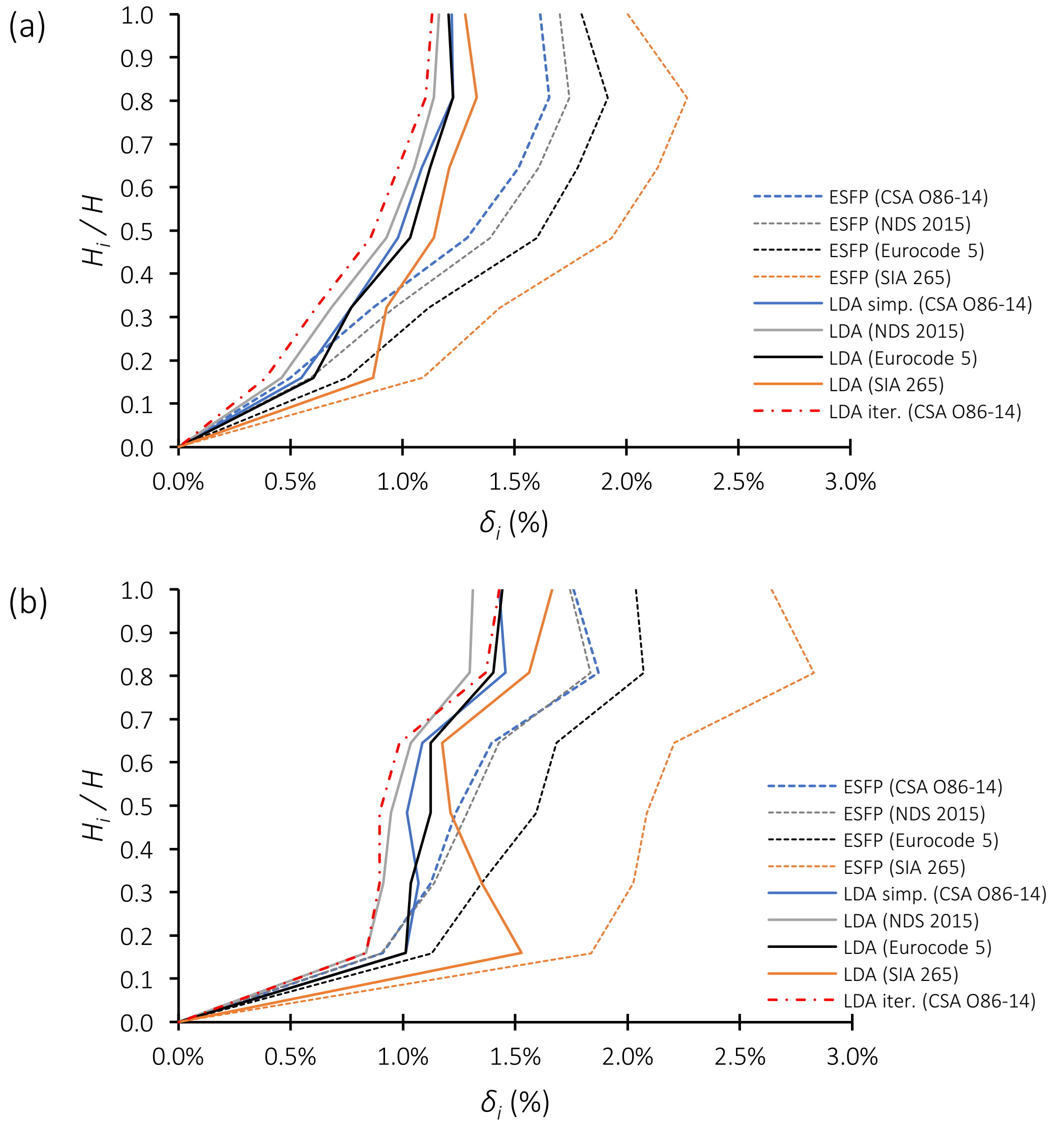

Figure 7: Comparison of LDA results with the different nail slip equations: (a) MR8B interstorey drift and (b) MR11 interstorey drift.

4 Conclusion

The comparison of the nail slip formulas for panel-to-wood nailed connections from four different codes showed little difference between CSA O86-14, NDS 2015 and Eurocode 5, while SIA 265 showed larger nail slip. ESFP and LDA using the four nail slip formulas have been performed on two light-frame shear walls in a six-storey building in Quebec City. The results have shown nearly the same storey shears and overturning moments for all LDA procedures due to the calibration of the base shear required by the NBCC (NRCC, 2015). It has been demonstrated that a simplified LDA procedure with a linear nail slip formula can be used in lieu of the iterative LDA to speed up the design while keeping sufficient accuracy and the advantages of LDA in the analysis of light-frame wood shear walls in mid-rise buildings. The nonlinear nail slip formula of the CSA O86-14 can be approximated with the Eurocode 5 formula with sufficient accuracy of deflection calculations in LDA. As for the ESFP, storey drift predictions have shown to be more sensitive to the nail slip formulas. The storey drifts calculated with the NDS 2015 fastener slip modulus were the closest to the CSA O86-14 predictions. To noted that the ESFP analysis predicted lower storey shear forces at the top storey and higher overturning moments at the first storey relative to the LDA methods. The potential for optimisation of a six-storey light-frame wood building with the LDA is discussed by Tremblay-Auclair et al. (2016).

5 Acknowledgement

This research was sponsored by the Canadian Natural Sciences and Engineering Research Council (NSERC) industrial research chair on ecoresponsible construction in wood (CIRCERB), the Renewable Materials Research Centre (CRMR), the Canadian Natural Sciences and Engineering Research Council (NSERC) and the Fonds de recherche du Québec – Nature et technologies (FRQNT).

6 References

AWC (2005). ASD&LRFD. Wind & Seismic. Special Design Provisions for Wind and Seismic with Commentary. American Wood Council. ANSI/AF&PA SDPWS-2005, Washington DC, USA.

AWC (2015a). NDS. National Design Specification for Wood Construction. American Wood Council. ANSI/AWC NDS-2015, Washington DC, USA.

AWC (2015b). ASD&LRFD. Wind & Seismic. Special Design Provisions for Wind and Seismic. American Wood Council. ANSI/AF&PA SDPWS-2015, Washington DC, USA.

CEN (2008). Eurocode 5 – Design of timber structures - Part 1-1: General – Common rules and rules for design of buildings. EN 1995-1-1:2004/A1:2008.

Chaurette F, Lajoie K and Frenette C (2015): Guide technique sur la conception de bâtiments de 5 ou 6 étages à ossature légère en bois. Cecobois, Quebec City, Canada.

Chen Z, Chui Y H, Doudak G, Chun N and Mohammad M (2014): Simulation of the lateral drift of multi-storey light wood frame buildings based on a modified macro-element model. In Proc. 13th WCTE 2014, Quebec City, Canada.

CSA (2014). CSA O86-14 Engineering Design in Wood. CSA Group, Mississauga, Canada.

Dolan J D (1989): The dynamic response of timber shear walls. PhD thesis, University of British Columbia.

Filiatrault A, Tremblay R, Christopoulos C, Folz B and Pettinga D (2013): Elements of earthquake engineering and structural dynamics. Presse internationales Polytechnique, third edition, Canada.

Humar J and Rahgozar M (2000): Application of uniform hazard spectra in seismic design of multistorey buildings. Canadian Journal of Civil Engineering, 27(3): 563-580, 2000.

Karacabeyli, E and Lum C (2014): Technical guide for design and construction of tall wood buildings in Canada. FPInnovations, Pointe-Claire, Quebec City, Canada. (Special Publication SP-55E).

Kirkham, W, Gupta R and Miller, T (2013): State of the art: Seismic behavior of wood-frame residential structures. Journal of Structural Engineering, 140 (4):04013097.

Newfield G, Ni C and Wang J (2013): A mechanics-based approach for determining deflections of stacked multi-storey wood-based shear walls. Technical report, FPInnovations and Canadian Wood Council, Canada.

Newfield G, Ni C and Wang J (2014): Design of wood frame podium structures using linear dynamic analysis. In Proc. 13th WCTE 2014, Quebec City, Canada.

NRCC (2015): National Building Code of Canada. National Research Council of Canada, Ottawa.

NRCC (2010): National Building Code of Canada. National Research Council of Canada, Ottawa.

NRCC (2005): National Building Code of Canada. National Research Council of Canada, Ottawa.

Salenikovich A J (2000): The racking performance of light-frame shear walls. PhD thesis, Virginia Polytechnic Institute and State University.

SIA 265 (2012) Construction en bois. Société Suisse des Ingénieurs et des Architectes, Zurich.

Tremblay-Auclair J-P (2016): Développement d’une méthode de calcul parasismique pour les bâtiments multiétagés à ossature légère en bois. Master’s thesis, Laval University.

Tremblay-Auclair J-P, Salenikovich A and Frenette C (2016). Potential for design optimisation of a six-storey light-frame wood building using linear dynamic analysis. WCTE 2016 in Vienna, Austria.

Discussion

The paper was presented by J-P Tremblay-Auclair

F Sarti commented that the envelope for overturning looked surprising that less forces was observed with linear analyses. J-P Tremblay-Auclair explained that the stiffness was based on code provisions for the lateral deformation of the shear wall. F Sarti received confirmation that there were plans to compare results with non-linear dynamic analysis in the future.

H Blass commented that this study only considered one specific building. He asked whether tests on load-slip behaviour of the connectors were performed. J-P Tremblay-Auclair replied no and only used literature results on the same material. Also EC 5 equation was chosen because it would be more conservative. H Blass asked how stiffness could be considered conservative. J-P Tremblay-Auclair explained up to a factor of three was observed.

F Lam commented that the conclusion that EU 5 equation would yield conservative results might not always be true. Different buildings and earthquakes could yield different conclusions. More cases should be considered.

W Seim commented about the influence of nail spacing.

G Doudak commented that choice of narrow wall would not meet the requirement of 086. J-P Tremblay-Auclair did not agree as the total height should be considered. A Salenikovich replied that additional information would be available and would be presented to Canadian code committee in future.

J-P Tremblay-Auclair explained the base shear input to LDM was normalized and calibrated to equivalent shear forces.

M Gershfeld asked whether soft story behaviour was seen and commented that it would be a concern in California. F Lam replied in 2009 six storey light wood frame residential building was permitted in the 2009 British Columbia building code. Soft storey behaviour was a concern as shown in computer models. As a practical solution the BC Building code stipulated the amount of shear walls required in the lower two storeys would need to be increased by 20% to prevent soft story behaviour.

A Ceccotti asked about the period of the structure. J-P Tremblay-Auclair replied it was 1.5 sec. A Ceccotti stated that the building was very soft.

Seismic performance of CLT low-rise structures with small and large wall elements with opening

Motoi Yasumura, Shizuoka University, Shizuoka, Japan
Kenji Kobayashi, Shizuoka University, Shizuoka, Japan
Minoru Okabe, Tsukuba Building Research and Testing Laboratory of CBL, Tsukuba

Keywords: 3-ply CLT, Shear walls, Reversed-cyclic lateral load, Aseismic design, failure mode, earthquake-response-analysis, FEM, Opening

1 Introduction

Generally large CLT wall panels including openings are used for CLT structures. However, small wall panels without openings can be also used for the reason of transportation problem, application of large openings, seismic requirements, etc. Large wall elements generally show high stiffness and strength, while small wall elements may produce high ductility which is required for aseismic design. Two identical structures of 6 m length, 4m width and 5.82m height, one consisting of 6-by 2.7m large CLT wall panels and another composed of 1-by 2.7m small CLT wall panels were subjected to static reversed cyclic lateral loads, and the static performance of these structures including different CLT applications were clarified by experiments and numerical analysis (Yasumura et al. 2014). The precedent study focused on the static performance of CLT structures and dynamic properties of these structures were not included. Therefore, time-history earthquake response analysis was conducted on these structures to predict the seismic performance in this paper.

Notification No.611 of Ministry of Land, Infrastructure, Transport and Tourism concerning "the structural method of CLT panel structures" was occasionally published on 1st April 2016. This Technical standards provide aseismic design and calculation methods of CLT panel structures depending on the different use of large and small CLT panels and the ductility of joints connecting CLT wall panels to foundation and upper or lower storey wall panels.

Ductility of joints consisting of steel plates and screws used in this research may be categorised into rather low class. In this research the base shear coefficient C_0 of 1.0 was provisionally applied for the ultimate design of specimen. In the notification No.611 the base shear coefficient for large panel and this type of joints is provided as 0.75.

2 Precondition of experiment

2.1 Model structure

The specimens of two storey structure as shown in Fig. 1 were designed on the supposition of three storey structure as shown in Fig. 2 because of the limitation of test equipment. This procedure brought however many advantages in practice compared to a large scale experiments with three storey specimens using three actuators controlled separately based on the seismic action of each floor level. As the capacity of an actuator 250kN was not enough to push the structure up to the ultimate state, the lateral loads were applied at the top of the specimen (roof level) by two actuators attached at the same level of the reinforced concrete reaction wall. This procedure enabled to realise approximately the same rocking moment and the base shear at the bottom of the specimen as those of assumed three storey structure as shown in Fig. 3. Therefore the weight equivalent to the live and dead loads of the third storey were attached on the roof level of the specimen. This procedure however causes higher shear force on the second storey than that of the assumed three storey structure, the second storey was designed to resist against the lateral force as well as the first storey. This also enabled to know the ultimate state of the second storey.

2.2 Determination of seismic action

The seismic shear force Q_i of each storey of the model structure was calculated

Figure 1 Specimen including 2.6-by 6m CLT wall panels.

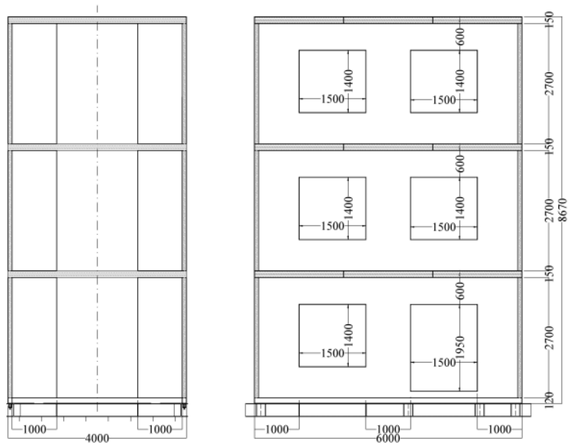

Figure 2 Assumed three storey structure for the full-scale tests.

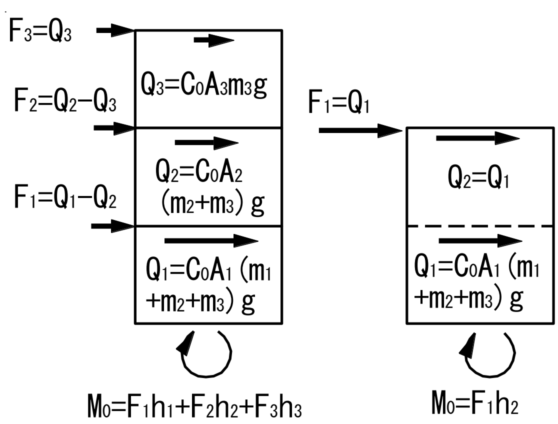

Figure 3 Design concept of specimen. h1, h2, h3: height of 2nd floor, 3rd floor and roof level, respectively.

by the following equation according to BSL(Japanese Building Standard Law).

$$Q_i = C_0 Z R_t A_i \sum_i^N W_i \tag{1}$$

Where, C_0 is the standard shear coefficient, A_i *is* the vertical distribution factor, W_i is the weight of the *i* th storey, *N* is the number of stories, and seismic zone factor *Z* and vibration characteristic factor R_t were set as 1.0.

A_i was calculated with Equations (2) and (3):

$$A_i = 1 + \left(\frac{1}{\sqrt{\alpha_i}} - \alpha_i\right) \cdot \frac{2T}{1+3T} \tag{2}$$

$$\alpha_i = \frac{\sum_i^N W_i}{\sum_1^N W_i} \tag{3}$$

Where, *T* is the natural period (sec.) (0.03H: H=height of structure in meter) and α_i is the ratio of the weight supported by the *i* th story to the weight of the whole building.

It may be a question if the equation (2) is used to calculate the vertical distribution factor A_i for CLT structures, however the horizontal stiffness of CLT structure depends on the stiffness of joints connecting CLT wall panels to the foundation and those are not determined if the horizontal shear force of each storey is not determined. Therefore equation (2) was applied here.

3 Specimens

Specimens are two storey CLT structures of 6m-long, 4m-wide, and 5.82m-high as shown in Figs. 4 and 5. Specimen consisted of 90mm-thick, three-ply CLT wall panels (S60) with *Sugi* lamina (M60) and of 150mm-thick, five-ply CLT floor panels (Mx120) with mixed lamina of *Sugi* (M90) and *Hinoki* (M120), according to the Japan Agricultural Standard, Notification No. 3079 (Ministry of Agriculture, Forestry and Fishery 2013). The two specimens had exactly the same plan and elevation except that the dimension and application of the CLT wall panels were different. One specimen had 6,000mm-long and 2,700mm-high panels with two openings in the first and second stories, and the other consisted of 1,000 mm × 2,700 mm CLT wall panels

Figure 4 Specimen with large CLT wall panels

Figure 5 Specimen with small CLT wall panels

with 1,500 mm × 600 mm and 1,500 mm × 700 mm CLT panels above and under the openings, respectively.

Two 90 mm-thick CLT wall panels with dimensions of 1,000 mm x 2,700 mm installed 2m apart from each other in the perpendicular direction and connected to the longitudinal CLT wall panels with wood screws of 8 mm diameter and 180 mm length (HBS D8-L180) at a spacing of 300 mm were not connected to the sill to avoid reinforcement against the uplift force during lateral loading.

Floor panels with dimensions of 2,000 mm × 4,000 mm were mounted in the perpendicular direction and connected to the top of the lower wall panels with wood screws of 8 mm diameter and 260 mm length (HBS D8-L260) at intervals of 250 mm. Wall panels and floor panels were connected by L- and U-shaped shear connectors. A sill with dimensions of 120 mm × 90 mm was installed under the wall panel of the first story, and the bottom and top of the wall panels were connected to the steel foundation and upper wall panels with U and L- shaped connectors, respectively.

The weights and horizontal shear forces of the assumed three storey structures are shown in Table 1. The weights of 72kN and 126kN were fixed on 2nd floor level and roof level of the specimen, respectively. Total weight of the specimen was 251kN, and the design maximum horizontal capacity of 251kN was assumed considering the base shear coefficient of 1.0. Number of screws for vertical and horizontal joints were calculated by FEM consisting of orthotropic plane elements and linear springs for each joint as shown in Fig.6.

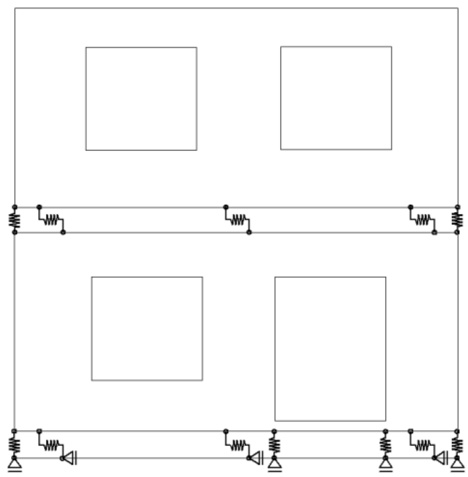

Fig. 6 Boundary conditions for specimen with large wall panels

The vertical tensile forces at the left and right corners of the first storey were respectively 73.4 and 52.3kN for the specimen with large CLT wall panels and 78.8 and 78.5kN for the specimen with small CLT wall panels at the design load of 251kN. The number of vertical restraints used for the specimen with small CLT wall panels was twice as much as that used for the specimen with large CLT wall panels.

Table 1 Weight and lateral seismic force of each storey

Concerned level	Weight W_i (kN)	C_0	A_i	$Q_i = C_0 A_i \sum W_i$ (kN)
3rd story	47.0	1.0	1.616	75.9
2nd story	102.0	1.0	1.204	179.4
1st story	102.0	1.0	1.000	251.0

4 Dynamic analysis

4.1 Modelling of load-displacement relation

The structures were modelled by three damped-mass representing the weight of each story and the hysteresis model proposed in the previous article (M.Yasumura and S.Yasui, 2006) was applied to the simulation.

Figs. 7 to 10 show the load-displacement relationship of first and second storey of specimens with large and small CLT panels. These figures show that the initial stiffness of the specimen with large CLT panels is approximately twice as large as that of the specimen with small CLT panels, and the ultimate displacement of the specimen with small CLT panels showed approximately twice as large as that of specimen with large CLT panels. The load-displacement relations of second storey are very close to those of the first storey in both specimens with large and small CLT panels, however the load-displacement relations with small CLT panels included hysteresis curves with pinching which was not observed in the specimen with large CLT panels.

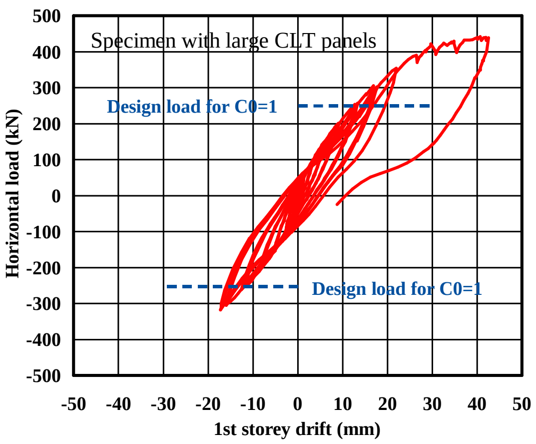

Figure 7 Load-displalement relation of specimen with large panel (1st storey)

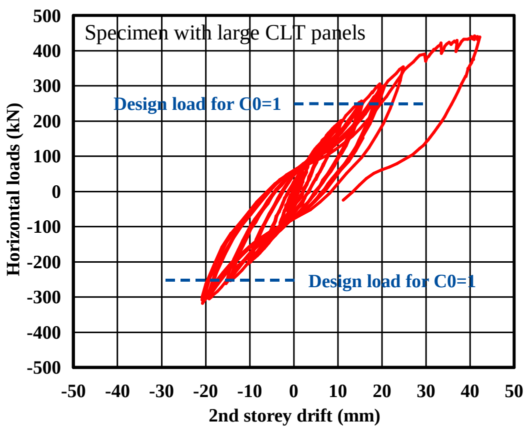

Figure 8 Load-displalement relation of specimen with large panel (2nd storey)

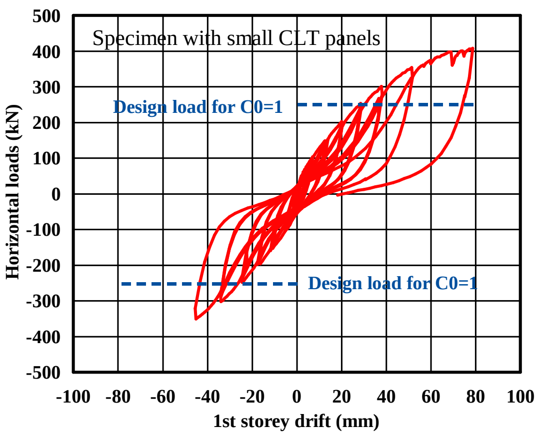

Figure 9 Load-displalement relation of specimen with small panel (1st storey)

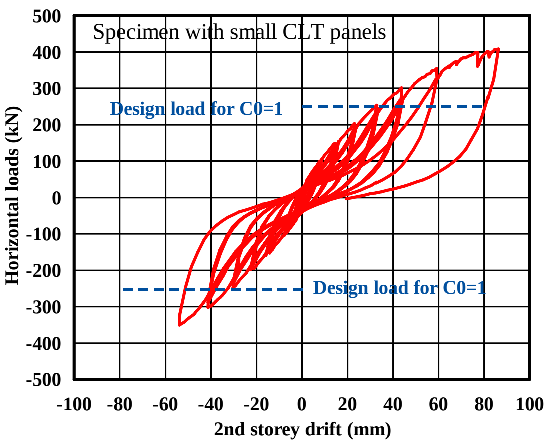

Figure 10 Load-displalement relation of specimen with small panel (2nd storey)

From these observation it was decided to apply the same hysteresis model to first, second and third storeys, but the different types of models to the specimens consisting of large CLT panels and small panels. Fig. 11 shows the model applied to the specimen with small CLT panels.

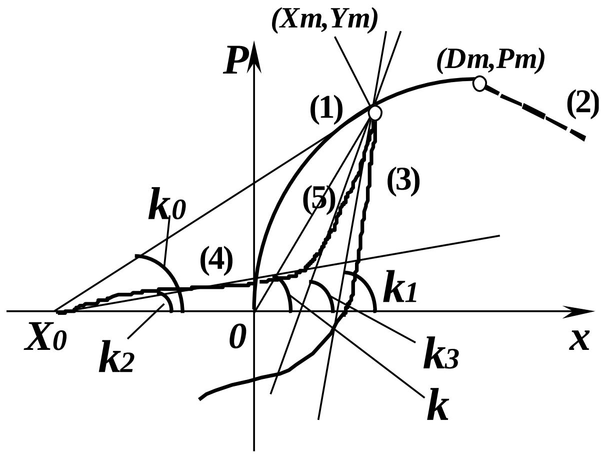

Figure 11 Hysteresis model

This model includes;

1) Loading on the primary curves up to the maximum load.
2) Loading on the primary curves over the maximum load.
3) Unloading from the peak on the primary curve.
4) Reloading with soft spring.
5) Reloading toward the previous peak with hard spring.
6) Unloading from the inner peak.
7) Reloading toward the peak without slips.

The parameters were determined from the experimental results shown in Figs. 7 to 10. The primary curves up to the maximum load (1) and those over the maximum load (2), are expressed as follows;

$$P = (P_0 + C_2 x)(1 - e^{-\frac{C_1 x}{P_0}}) \qquad (1)$$

$$P = Pm - C_3 |x - Dm| \qquad (2)$$

The primary curves over the maximum load was obtained as the straight line determined by the drawn through the points corresponding to Pmax and 0.8Pmax.

Unloading stiffens (3) and the reloading stiffness toward the previous peak (5) were based on the inclination of the straight line determined by the drawn through the origin and the peak on the primary curve (k_0). Reloading stiffness with soft spring (4) was based on the inclination of the straight line determined by the drawn through the peak on the primary curve and the crossing point of the X-axis.

$$k_1 / k = C_4 Xm + 1 \qquad (3)$$

$$k_2 / k_0 = 1 - C_5 |Xm - X_0|^{C_6} \qquad (4)$$

$$k_3 / k = C_7 Xm + 1 \qquad (5)$$

For the specimen with large CLT panels, equations (4) and (5) were removed and *k0* was used for the inclination on reloading toward the previous peak.

4.2 Time history earthquake response analysis

Time-history earthquake response analysis was conducted on the assumed three storey structurs. Lumped mass model was applied for the simulation. The input earthquake ground motions were based on the records of N-S components of the 1940 El Centro and the 1995 JMA Kobe and artificial wave BSL according to the spectrum shown in BSL (Miyake et al., 2010). The damping factor was assumed as 2%. The accelerogram of JMA Kobe NS (0.818G), El Centro NS (0.341G) and BSL (0.579G) were excited on each structure, and then the accelerogram was increased linearly until the maximum displacement response of the first storey attained the ultimate displacement at the experiment*, i.e.* 41mm for specimen with large panel and 78mm for specimen with 78mm.

5 Results and discussion

5.1 Earthquake response of structure

Figure 12 shows the experimental and simulated load-displacement relationships of the 1st storey with large and small wall panels, respectively. Maximum base shear responses of specimens with large and small wall panels obtained from the excitation by BSL (0.579G) were 218.5kN and 191.4kN respectively which were 13% and 24% lower than the design load and 50% and 53% lower than the experimental ultimate loads. Those obtained from the excitation by JMA Kobe NS (0.818G) were 279kN and 298kN which were 11% and 19% higher than the design load and 37% and 27% lower than the experimental ultimate loads. This indicates that the linear calculation with the base shear coefficient C_0=1.0 provides 11 to 23% higher design value than the response by the excitation according to BSL spectrum, but 11 to 19% lower design value than the response from the excitation by JMA Kobe. In any case the base shear responses by JMA KOBE NS were 11 to 23% smaller than the experimental ultimate loads.

Figs. 13 and 14 show the maximum storey drift responses by BSL, JMA KOBE NS and El Centro NS which were scaled up lineally until the response attained the ultimate experimental displacement. The maximum peak ground accelerations corresponding to the ultimate displacement of the first storey with large and small CLT panels were 1.289G and 1.305G for BSL, 1.245G and 1.067G for JMA Kobe NS, and 1.241G and 1.210G for El Centro NS, respectively. The average peak ground acceleration for the ultimate displacement was 1.258G for the specimen with the large wall panels and 1.194G for the small wall panels. Assuming the average peak ground accelerations for the yield point displacements are 0.59G for large and small wall panels, the "q" value for this kind of structure will be calculated as "2.13" and "2.02" for the structure with both large and small CLT wall panels.

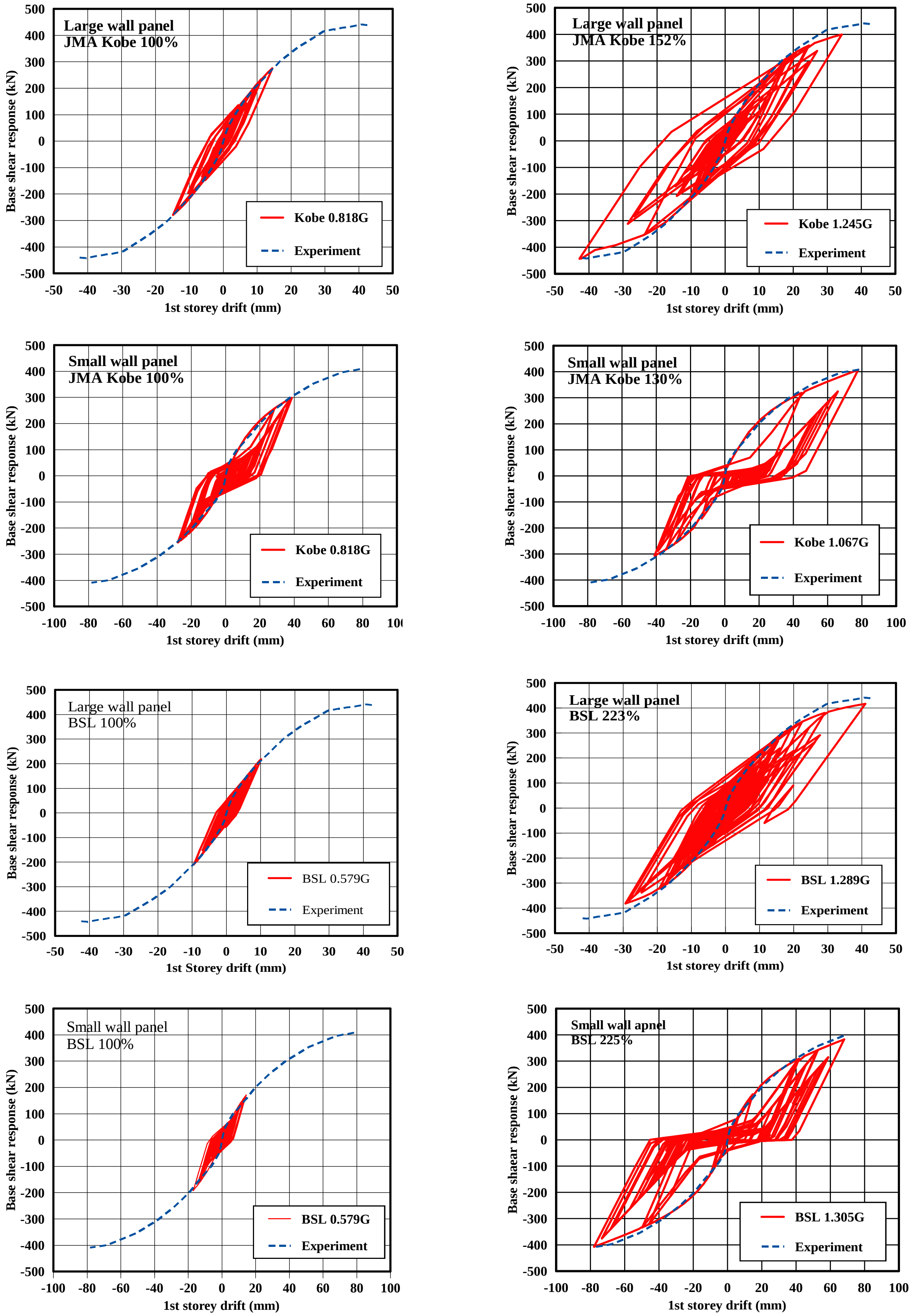

Figure 12 Comparison of simulated results with envelop curves in experiments

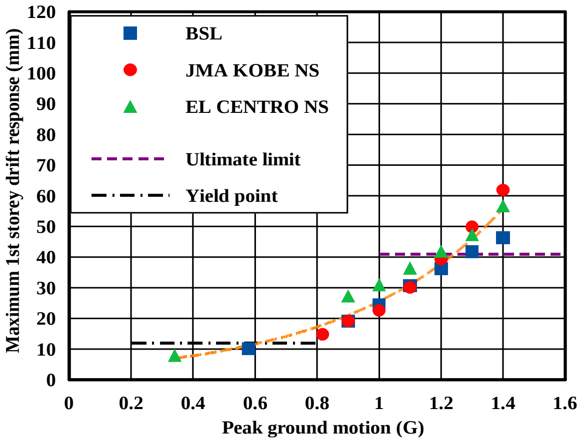

Figure 13 Storey drift response in specimen with large CLT wall panels

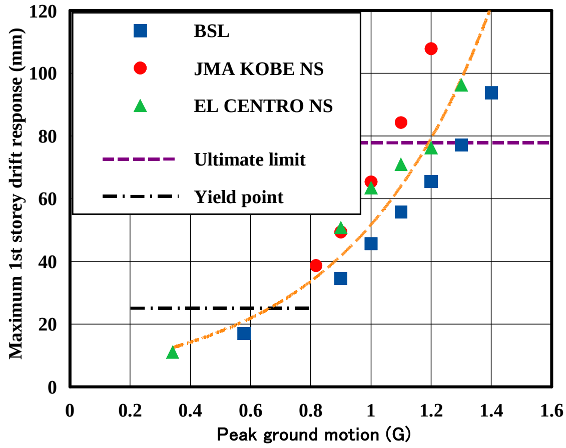

Figure 14 Storey drift response in specimen with small CLT wall panels

5.2 Failure mode

During the reversed cyclic loading on the specimen with large wall panels, the cracks appeared at the corner of openings as shown in Fig.15. In this test, cracks initiated after the design load had been attained, however it is supposed that this failure makes an important effects on the seismic performance of CLT structures. The stress at the corner of opening will be detected by means of FEM as shown in Fig.16. Further study should been conducted on this failure mode to perform the seismic design of CLT structures more precisely (Yasumura et al, 2016).

6 Conclusions

Summarizing the aforementioned results above, the following conclusions were obtained:

- The initial stiffness of specimen with large CLT wall panels was approximately twice as high as that with small CLT wall panels, and the ultimate displacement of the specimen with large wall panels was approximately a half of that with small wall panels.

- Full-size lateral loading tests on CLT structures showed that the ultimate lateral ca-

Figure 15 Crack initiation at the corner of opening

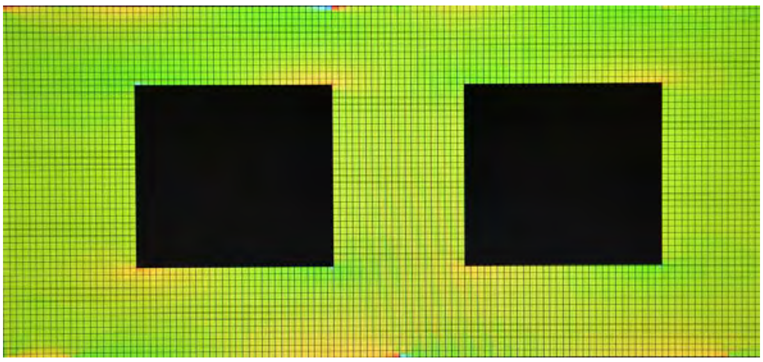

Figure 16 Stress concentration at the corner of openings (stress at x-x direction)

pacity of the structure was 60 to 75% higher than the aseismic design capacity.

・Linear calculation with the base shear coefficient C_0=1.0 provides 11 to 23% higher design value than the dynamic response according to BSL spectrum. The base shear responses by JMA KOBE NS (100%) were 11 to 23% smaller than the experimental ultimate loads.

・The "q" value obtained from the experimental results and dynamic analysis was 2.0 regardless of the size of CLT wall panels.

・Splitting at the corner of openings in large CLT panels may produce an important influence on the seismic performance of CLT structures, and this effect should be considered in aseismic design of CLT structures.

7 Acknowledgement

This work was supported by Forest Agency subsidies for the research project "Structural use of Cross Laminated Timber Made from Regional Wood" and JSPS KAKENHI Grant 26450227.

8 References

1. Motoi Yasumura; Kenji Kobayashi; Minoru Okabe; Tatsuya Miyake; and Kazuyuki Matsumoto (2014) Full-Scale Tests and Numerical Analysis of Low-Rise CLT Structures under Lateral Loading, J. Struct. Eng., DOI: 10.1061/(ASCE)ST.1943-541X.0001348

2. Motoi Yasumura and Shinpei Yasui (2006) Pseudodynamic tests and earthquake response analysis of timber structures I: plywood-sheathed conventional wooden walls with opening, J Wood Sci. 52.63-68

3. Motoi Yasumura and Naohito Kawai (1997) Evaluation of wood framed shear walls subjected to lateral load, Proc. of the 30th CIB-W18 Meeting, paper 30-15-4, pp.1-10, Vancouver, Canada

4. Tatsuya Miyake, Takafumi Nakagawa, Takahiro Tsuchimoto, Hiroshi Isoda and Naohito Kawai (2010) Dependence of Ultimate Seismic Performance on Specifications of Column-end Joints in 3-story Wood Houses, 11th World Conference on Timber Engineering 2010, CNR IVALSA, p.p. 2670-2679, Trentino, Italy

5. Motoi Yasumura, Kenji Kobayashi, Minoru Okabe (2016) Failure analysis of CLT shear walls with opening subjected to horizontal and vertical loads, Proc. WCTE 2016, Vienna, Austria

Discussion

The paper was presented by M Yasumura

M Gershfeld and M Yasumura discussed the details of the corners and no reinforcement was used.

A Ceccotti asked about the difference between yield load and ultimate state. M Yasumura replied that yield point was almost the same as design. A Ceccotti and M Yasumura discussed definition of yield point. A Ceccotti also received clarification about inter storey deflection. M Yasumura discussed the damage at the bottom of the connection also the crack initiation at the corner of the opening.

F Lam and M Yasumura discussed the very consistent hysteresis response predicted by the model under earthquake simulations. M Yasumura stated that more detailed information was available in a recent ASCE paper.

D Dolan commented on incremental dynamic analysis and the importance of post peak response for the collapse considerations could be 14% drift.

V Rajcic asked whether the acceleration of the floor level was measured. M Yasumura responded that it was not a dynamic shake table test.

W Seim asked about the q value for this system and discussed about degradation. M Yasumura responded that the q value should be at least 2.

Performance of Full-Scale I-Joist Diaphragms

Borjen Yeh, Ph.D., P.E.; Ben Herzog; Tom Skaggs, Ph.D., P.E.; APA – The Engineered Wood Association, Tacoma, Washington, U.S.A.

Keywords: Diaphragm, Small-Scale, Full-Scale, I-Joist, Lateral Load Capacity

1 Introduction

Light-frame wood diaphragms constructed with prefabricated wood I-joists have been used in construction of thousands of buildings in North America for more than 30 years. It has always been assumed by the I-joist manufacturers and design engineers that the structural performance of diaphragms constructed with I-joists made of flanges with thickness of 33 mm (1-5/16 inches) or greater will meet the diaphragm design values published in the engineering standard, such as the *Special Design Provisions for Wind and Seismic* (SDPWS) [AWC, 2015], or the U.S. building code [ICC, 2015]. This minimum flange thickness is based on the minimum nail penetration required for the development of full lateral resistance of single nails.

The historical performance in the field supports such an assumption as there have been no reported diaphragm performance issues for those buildings so constructed. However, there are limited full-scale I-joist diaphragm test data that are publically available [Waltz and Dolan, 2010] even though some I-joist manufacturers may have proprietary test data for I-joists made of thin structural composite lumber (SCL) flanges (as thin as 28 mm or 1-1/8 inches in thickness) to demonstrate its structural equivalency to light-frame diaphragms constructed with solid-sawn lumber joists.

In recent years, however, a concern has been raised on the I-joist diaphragm performance based on the experience learned from thin-flange I-joist diaphragm tests. It was reported that I-joist flanges are prone to splitting when subjected to full-scale diaphragm loading, resulting in a reduction in the diaphragm lateral load capacity. In conjunction with a variety of flange sizes, grades, and/or species, the concern over structural performance of I-joist diaphragms has prompted the International Code Council Evaluation Service (ICC-ES), a code evaluation agency in the U.S., to take the position that unless full-scale diaphragm test data are provided, the proprietary code evaluation report (similar to the European Technical Approval, ETA) will not specifically recognize I-joist diaphragm applications regardless of the flange materials and sizes.

To address this deficiency in full-scale I-joist diaphragm test data, APA – The Engineered Wood Association, which represents more than 70% of I-joist production in North America today, initiated a study on I-joist diaphragm performance using both small-scale and full-scale I-joist diaphragm tests. This paper provides the small-scale and full-scale diaphragm test results.

2 Objectives

This study was designed to evaluate the lateral load performance of light-frame diaphragms constructed with prefabricated wood I-joists as the primary framing members. The test results were intended for comparison with diaphragm design values published in the SDPWS or the U.S. code, which were developed based on full-scale diaphragm tests using solid-sawn lumber joists. Due to the small number of full-scale diaphragm tests conducted in this study, it is not the intent of this study to establish new diaphragm design values for I-joist diaphragms. This study was limited to I-joists made of solid-sawn lumber flanges due to the commonality in lumber-flange sizes and grades. However, it is not the intent of this study to preclude the use of the results obtained from this study for I-joists made of structural composite lumber flanges when appropriate.

3 Materials and Methods

3.1 General Consideration

Full-scale diaphragm tests are expensive and time-consuming. With a variety of material variables that could influence the diaphragm lateral load capacities, such as flange species, grade, and dimension, web materials and thickness, floor sheathing thickness, and fastener type and size, it is impractical to conduct full-scale diaphragm tests to quantify the relative influence of each variable to the diaphragm lateral load capacities. As a result, a small-scale test method that can serve as a screening tool to compare the relative diaphragm performance is highly desirable so that the full-scale diaphragm tests can focus only on the diaphragm assemblies with critical variables to save the laboratory time and material cost.

3.2 Small-Scale Diaphragm Tests

The critical connection for a light-frame diaphragm subjected to lateral loads is usually the corner joint where 4 sheathing panels are connected to the same floor (or roof) framing member, as shown in Figure 1. At this location, nails are closely spaced in high density, which is prone to flange splitting. With this in mind, a small-scale test method that can capture the rotation of sheathing panels at the corner joint and the potential for flange splitting was developed by the I-joist industry and has been adopted into ICC-ES *Acceptance Criteria for Prefabricated Wood I-joists*, AC14 [ICC-ES, 2014]. This small-scale test method, through the I-joist industry experience, has demonstrated its capability in screening the material variables that influence the diaphragm lateral load capacities.

Figure 1. Deformation shape of a light-frame diaphragm showing the corner joint as circled

Figure 2 shows the schematic drawings of the small-scale diaphragm assembly. It is understood that the entire diaphragm behaviour can be affected by more than the corner joints. Therefore, this small-scale test results can only be used to provide a relative comparison of the lateral load performance for a range of material variables. An attempt to correlate the small-scale test results to the published diaphragm design values has proven to be challenging.

3.2.1 Test Matrix

In general, there are 3 major wood species or species groups, Douglas-fir (DF), black spruce (BS), and spruce-pine-fir (SPF), which have been used as I-joist lumber flanges in North America. For each wood species or species group, there are different lumber grades. However, the vast majority of production in North America for I-joists made of lumber flanges uses 1650f-1.5E and 2100f-1.8E MSR lumber, or equivalent. Therefore, the matrix developed for this study for small-scale diaphragm tests was based on these 2 lumber grades. For other lumber grades and species, which is relatively rare in commercial production volume, can be evaluated using the data obtained from this study as benchmarks.

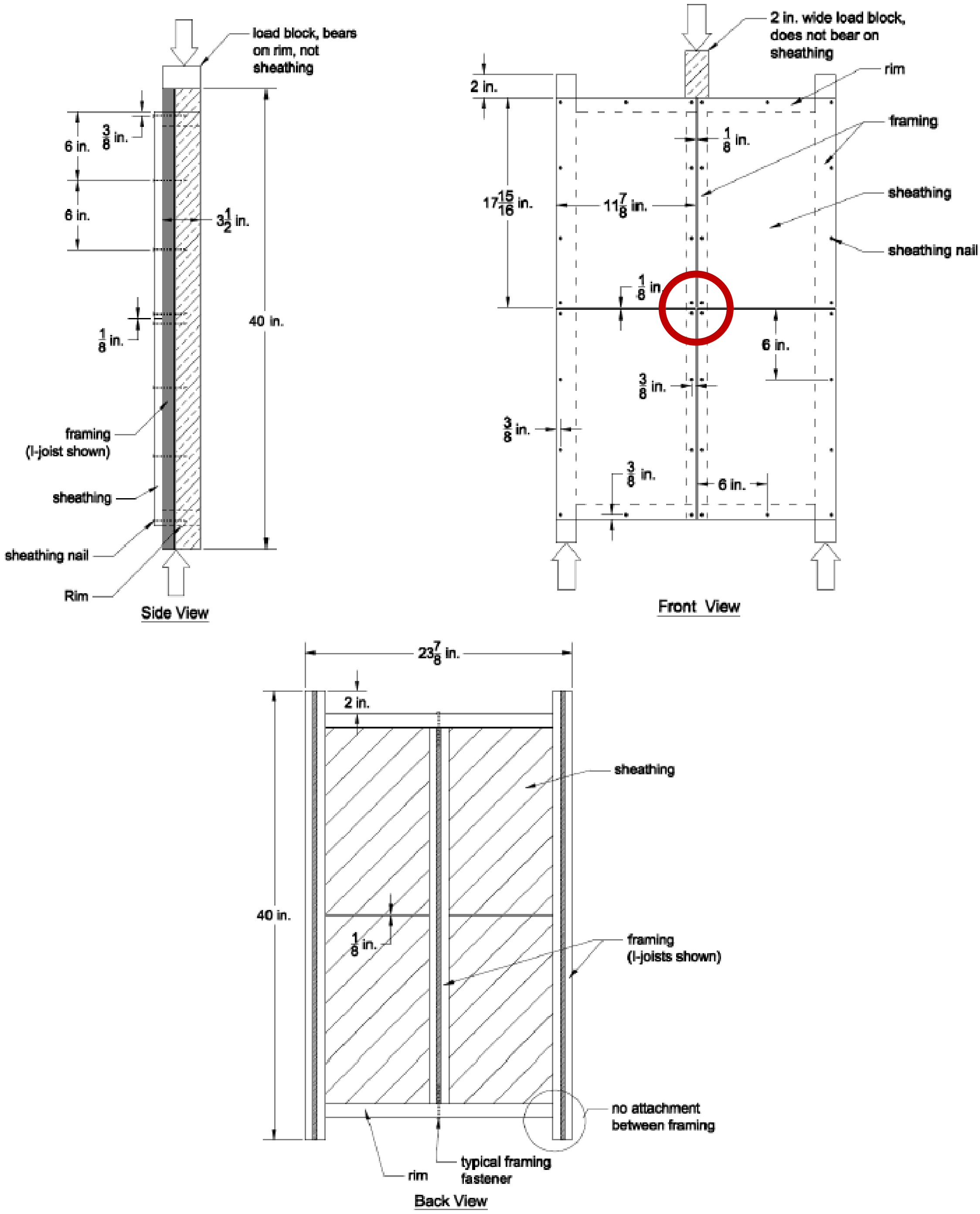

Figure 2. Schematic drawings for small-scale diaphragm test assembly (1 inch = 25.4 mm)

The smallest lumber flange dimension is 38 mm x 64 mm (1-1/2 inches x 2-1/2 inches) in the North American I-joist production today. As such, small-scale diaphragm tests were conducted with this flange size on 1650f-1.5E and 2100f-1.8E flanges (2 flange grades in total) for DF, BS, and SPF (3 species in total). This resulted in 6 small-scale diaphragm test series in total. As previously mentioned, these small-scale diaphragm assemblies were tested to determine the most critical I-joist series for subsequent full-scale diaphragm tests. Figure 3 shows the actual small-scale diaphragm assemblies.


Figure 3. Actual assemblies for small-scale diaphragm tests

3.2.2 Specimen Construction

Ten replicates of each small-scale diaphragm series were tested following ICC-ES AC14 requirements. The sheathing, rim board, and nails were matched for all assemblies tested in this study. A 25-mm (1-inch) thick oriented strand board (OSB) rim board was used as the diaphragm sheathing to reduce the probability of sheathing failure during testing because the intent was to make relative comparison of the diaphragm assembly performance as influenced by the flange splitting.

Laminated strand lumber (LSL) was used as the horizontal rim on the top and bottom of each assembly. The I-joist flange under evaluation included a 51-mm (2-inch) web section and served as the framing member of the assembly. Nails with a shank diameter of 3.8 mm (0.148 inch) and length of 76 mm (3 inches), known as 10d common nails in the U.S., were used to attach the sheathing to the framing (i.e., I-joist flange).

3.2.3 Test Method

All assemblies were tested in the as-received conditions at the APA Research Centre in Tacoma, Washington. As prescribed in ICC-ES AC14, all assemblies were tested within the same time period (± 1 hour) between fabrication and loading. A compressive load was applied to the top of the assembly through a 51-mm (2-inch) wide load block that bore on the rim at the top of the assembly (see Figures 2 and 3). The load block was flush with the rim and centred, and did not bear on the sheathing. At the base, the assembly was supported by a flat test bed on the exterior framing members. The peak load and failure mode of each assembly were recorded.

3.2.4 Test Results for the Small-Scale Diaphragm Assemblies

Test results for the small-scale diaphragm assemblies are summarized in Table 1. All assemblies failed due to framing splitting at the mid-height sheathing-to-framing connection (corner joint). The moisture contents of the flanges from the 6 test series were within 3% of each other, thereby complying with the requirements of ICC-ES AC14 for the purpose of relative performance comparison.

Table 1. Summary statistics for small-scale diaphragm test results [(a)]

	2100f-1.8E MSR			1650f-1.5E MSR		
	DF	BS	SPF	DF	BS	SPF
Observations	10	10	10	10	10	10
Mean, kN (lbf)	23.6 (5300)	26.7 (5995)	26.1 (5863)	25.7 (5767)	23.6 (5299)	25.4 (5711)
COV	0.154	0.064	0.066	0.072	0.093	0.071
Minimum, kN (lbf)	16.3 (3673)	24.3 (5471)	23.7 (5328)	23.2 (5208)	20.6 (4634)	22.1 (4978)
Maximum, kN (lbf)	29.6 (6661)	30.0 (6754)	29.5 (6664)	29.3 (6578)	26.0 (5854)	28.7 (6449)

[(a)] All specimens failed as a result of flange splitting.

As shown in Table 1, the lowest mean peak load was from I-joists made of 1650f-1.5E black spruce flanges and 2100f-1.8E Douglas-fir flanges, as highlighted. While the mean peak load values between these 2 flange series were virtually the same (23.6 kN or 5300 lbf), the coefficient of variation (COV) of the data differed: 9.3% for 1650f-1.5E black spruce and 15.4% for 2100f-1.8E Douglas-fir flanges. As a result, I-joists made of 2100f-1.8E Douglas-fir flanges were selected for the full-scale diaphragm tests due to its higher variability. This was not unexpected as Douglas-fir is known to be more prone to nail splitting than black spruce and spruce-pine-fir. Besides, the higher grade lumber, which is denser, is expected to have a higher nail splitting tendency than the lower grade lumber.

3.3 Full-Scale Diaphragm Tests

The current light-frame diaphragm lateral load capacities published in the SDPWS or the U.S. code were developed based on full-scale diaphragm tests conducted by APA in 1950's through 1970's [Tissell and Elliott, 2000]. There were a variety of diaphragm sizes that were evaluated, ranging from 3.7 m x 12.2 m (12 feet x 40 feet), 7.3 m x 7.3 m (24 feet x 24 feet), to 4.9 m x 14.6 m (16 feet x 48 feet). The higher aspect ratio diaphragms behave like long bending members, while the lower aspect ratio diaphragms act like short shear beams. For the purpose of this study – comparing the diaphragm lateral load capacities with the published values for diaphragms constructed with solid-sawn lumber joists, the full-scale diaphragm tests were conducted using a diaphragm dimension of 7.3 m x 7.3 m (24 feet x 24 feet) in accordance with ICC-ES AC14 to produce the maximum shearing effect.

The sheathing layout, as relative to the loading direction, could affect the diaphragm lateral load capacities. In the SDPWS or U.S. code, the diaphragm design values depend on diaphragm "load cases," as shown in Figure 4. The Canadian code follows the same classification, except that Cases 5 and 6 are not recognized. Overall, diaphragms constructed in accordance with Cases 5 and 6 are considered more critical than other diaphragm configurations due to the existence of continuous panel joints in both loading directions. On the other hand, diaphragms constructed in accordance with Case 1 or Case 2 are considered relatively strong due to its "interlocking" effect with discontinuous panel joints.

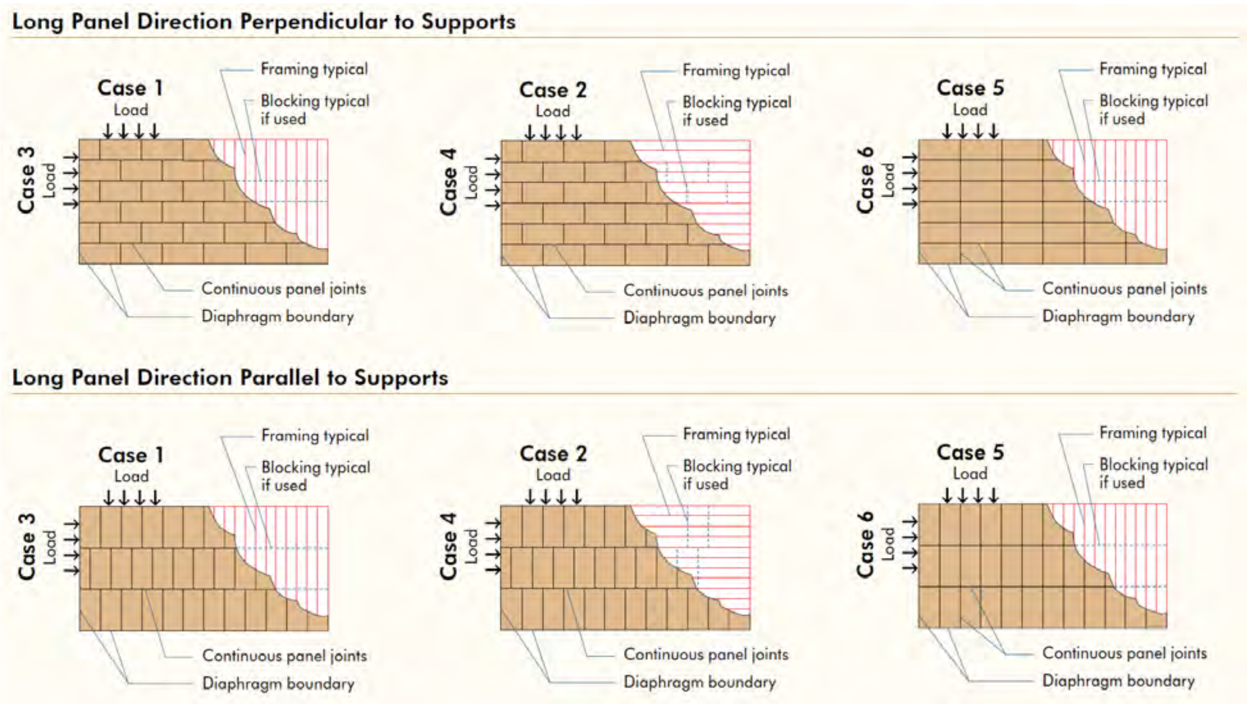

Figure 4. Diaphragm cases in the U.S. building code

In addition to the diaphragm cases, the diaphragm lateral load capacities also depend on sheathing grade and thickness, nail size and spacing, and the presence of panel blocking (i.e., blocked diaphragms) or not (i.e., unblocked diaphragms). For the purpose of this study, a full-scale diaphragm test matrix was developed to cover a range of diaphragm design values, as shown in Table 2.

It is important to note that this test matrix took into account the fact that the closest nail spacing recommended for I-joist flanges is typically limited to 102 mm (4 inches) on centre. In addition, it recognized that the diaphragm lateral load capacities are different between blocked and unblocked diaphragms. As a result, a total of 4 test series were included in the full-scale diaphragm test matrix.

Table 2. Diaphragm Assemblies

Diaphragm ID	Nail	Nail Spacing, mm (in.)			Case	Panel Thickness, mm (in.)	Blocked?
		Field	Diaphragm Boundary	Panel Edges			
1A, 1B, 1C	10d [(a)]	305 (12)	102 (4)	102 (4)	5	15 (19/32)	Yes
2A, 2B			152 (6)	152 (6)	1		No
3A, 3B					5		
4A							Yes

[(a)] 10d nails has 3.8 mm (0.148 inch) in diameter and 76 mm (3 inches) in length.

For Series 1 (Case 5 blocked), which was considered as the most difficult diaphragm configuration for the purpose achieving the targeted design value, 3 replicates were tested to provide a higher data confidence. For Series 2 (Case 1 unblocked) and 3 (Case 5 unblocked), 2 replicates were tested in accordance with ICC-ES AC14. On the other hand, as the test results from Series 1 through 3 were quite convincing, only 1 replicate was tested for Series 4 (Case 5 blocked with a wider nail spacing than Series 1).

3.3.1 Full-Scale Diaphragm Test Setup

The full-scale diaphragm test setup followed the simple-beam method of ASTM E455, *Standard Method for Static Load Testing of Framed Floor or Roof Diaphragm Constructions for Buildings* [ASTM, 2016], as shown in Figure 5, using I-joists conforming to ASTM D5055 [ASTM, 2016] and plywood sheathing conforming to DOC PS1 [DOC, 2009].

During testing, loads from a 1335-kN (300-kip) actuator were distributed into a wide-flange steel beam. From each end of this steel beam, a wide-flange steel beam was used to distribute the load into the diaphragm through 2 load points. V-blocks were used at the connection points to permit the rotation of steel loading beams. At the diaphragm reactions (see Figure 5), bearing plates were installed with a hinge on one end and rollers on the other. A load cell was installed at each reaction point to measure the actual test load up to the diaphragm failure. The diaphragm was retrained from out-of-plane movement by steel plates overlaid with Teflon at parallel edges of the diaphragm.

All diaphragm assemblies were constructed with 241-mm (9-1/2-inch) deep I-joists made of 38 mm x 64 mm (1-1/2 inches x 2-1/2 inches) flanges and 9.5-mm (3/8-inch) OSB web. The I-joists were spaced at 610 mm (24 inches) on centre and sheathed with 15 mm (19/32 inch) plywood floor sheathing. Each diaphragm assembly was suspended on 8 small support blocks sized to maintain the diaphragm in a level horizontal plane. Rollers were placed between the diaphragm assembly and the support blocks to avoid friction. The I-joist right under each load point was reinforced with

1220-mm (4-ft) long filler blocks placed on both sides of I-joists between flanges to prevent localized crushing failures of the diaphragm. The perpendicular joist under the load points was also reinforced with filler blocks. In addition, the corners of the loaded edge and the reaction points of the diaphragm were also reinforced.

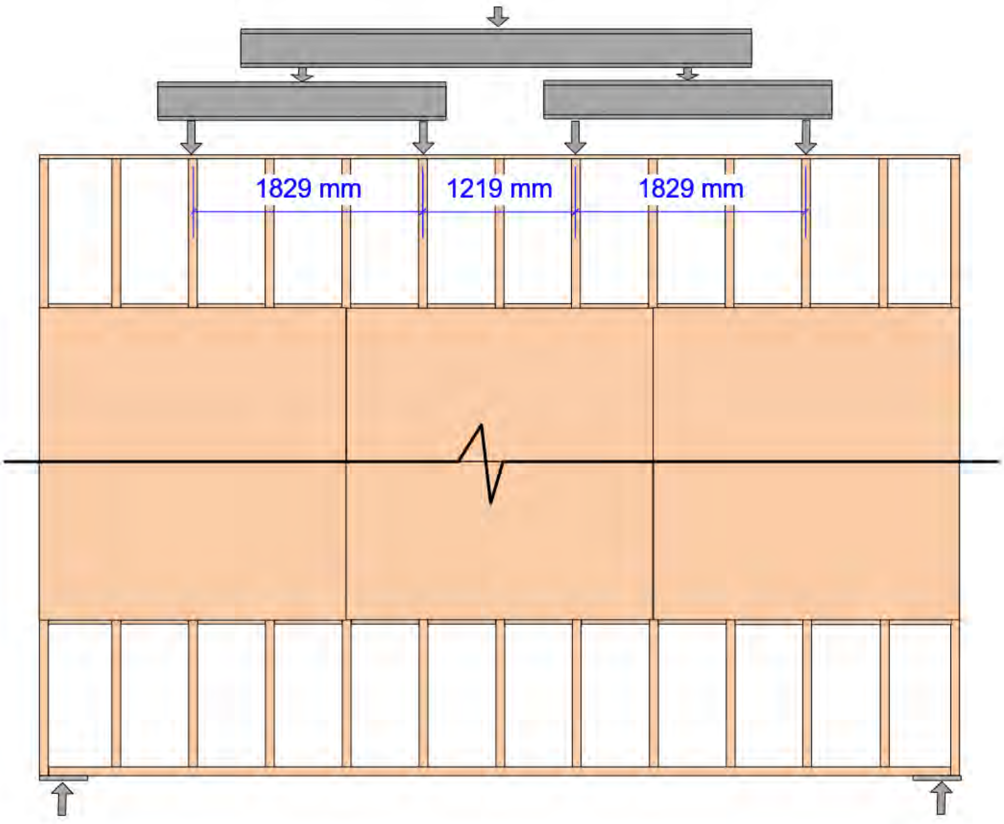

Figure 5. Full-scale diaphragm test setup (1 mm = 0.0394 in.)

For blocked diaphragms, the blocking was provided by 38 mm x 89 mm (1-1/2 inches x 3-1/2 inches) Douglas-fir lumber cut to length to ensure correct joist spacing. The blocking was installed flatwise and held in place using 2 toe-nails of 2.9 mm (0.113 inch) in diameter and 51 mm (2 inches) in length at each end of the lumber blocking.

3.3.2 Test Method

All diaphragm tests were performed in accordance with ASTM E455 at the APA Research Centre in Tacoma, Washington. Two deviations to the standard were noted: (1) the loading on the diaphragms was changed from 2 load points to 4 load points to be consistent with the historical tests used to derive the diaphragm design values in the SDPWS or the U.S. code and (2) deflection measurements were taken at each reaction and mid-span. These deviations are not expected to affect the diaphragm test results.

4 Results and Discussion

4.1 Unsheathed Diaphragm Frame Stiffness

ASTM E455 requires that the bare diaphragm frame (without sheathing) be determined to establish its load-deformation characteristics before attaching the diaphragm sheathing. According to the standard, if the frame has a stiffness equal to or less than 2% of the total diaphragm assembly, no adjustment of test results is necessary. Therefore, stiffness measurements were made on 1 frame each from Series 1, 2, and 3 before the diaphragm sheathing was applied. Table 3 shows the test results.

Table 3. Diaphragm Frame Stiffness Test Results [(a)]

ID	Case	Blocked?	Design Load [(b)], N/mm (lbf/ft)	Stiffness [(b)], N/mm (lbf/in.)	Displacement [(b)], mm (in.)
1	5	Yes	7.0 (480)	32.7 (187)	3.3 (0.131)
2	1	No	4.7 (320)	18.9 (108)	4.8 (0.189)
3	5		3.5 (240)	18.0 (103)	3.3 (0.131)

[(a)] Since the unsheathed frame stiffness for Series 1 is substantially less than 2% of the sheathed diaphragm stiffness, unsheathed diaphragm frame stiffness for Series 4 was considered unnecessary.

[(b)] Value at design load published in the U.S. code, which is based on the peak load divided by 2.8.

As shown in Table 3, the stiffness values of the unsheathed diaphragm frames are small and variable. The frame stiffness was calculated as the slope of a line in the load and displacement plot between the origin (after removal of slack of the system) and the diaphragm design load, which is equal to the peak load divided by 2.8. Comparisons of the unsheathed frame stiffness with that of the corresponding sheathed diaphragms (see Section 4.2 below) show that the unsheathed diaphragm stiffness was substantially lower than 2% of the sheathed diaphragm stiffness. As a result, no adjustments to the diaphragm test results were necessary based on ASTM E455.

4.2 Sheathed Diaphragm Test Results

The typical failure modes for the diaphragms are shown in Figures 6 and 7 for Case 5 blocked and unblocked diaphragms, and Case 1 unblocked diaphragms, respectively. Failure of the diaphragms followed similar mechanisms as that constructed with solid-sawn lumber joists [Tissell and Elliott, 2000]. The primary failure mode was flange splitting caused by panel sheathing rotation, i.e., tension perpendicular-to-grain failure of the top flanges. This was especially true for Series 2 and 3 (unblocked diaphragms). In some instances, it was observed that the sheathing nails yielded and finally failed by tearing out of the panel edge, pulling through the sheathing, or withdrawing from the framing. Severe nail withdrawal was thought to be a result of flange splitting, i.e., splitting occurred first allowing the nails to withdraw. In some instances, panel buckling also occurred (see Figure 6).


Figure 6. Diaphragm failure modes (Case 5 Blocked at left and Case 5 Unblocked at right)


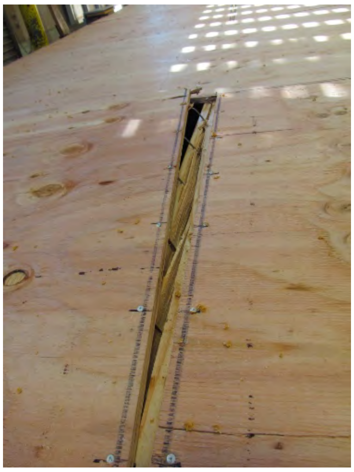

Figure 7. Diaphragm failure modes (Case 1 Unblocked)

A typical load-deformation curve from a diaphragm test is shown in Figure 8. Average peak loads, stiffness at design load, stiffness at two times design load, stiffness at peak load, displacement capacity, and ductility (displacement capacity divided by displacement at design load) are presented in Table 4.

4.3 Discussion

As noted from Table 4, the adjacent nails within a row on the diaphragm boundary for Series 1 were offset (staggered) by 12.7 mm (1/2 inch). This was applied to the tested diaphragms to avoid excessive flange splitting due to the close nail spacing of 102 mm (4 inches). This nail staggering was unnecessary for Series 4 due to an increased nail spacing to 152 mm (6 inches). In addition, as the test results for Series 4, as shown in Table 4, showed a load factor of 3.4, which is significantly greater than the code-recognized minimum load factor of 2.8, only 1 replicate of this assembly was deemed necessary.

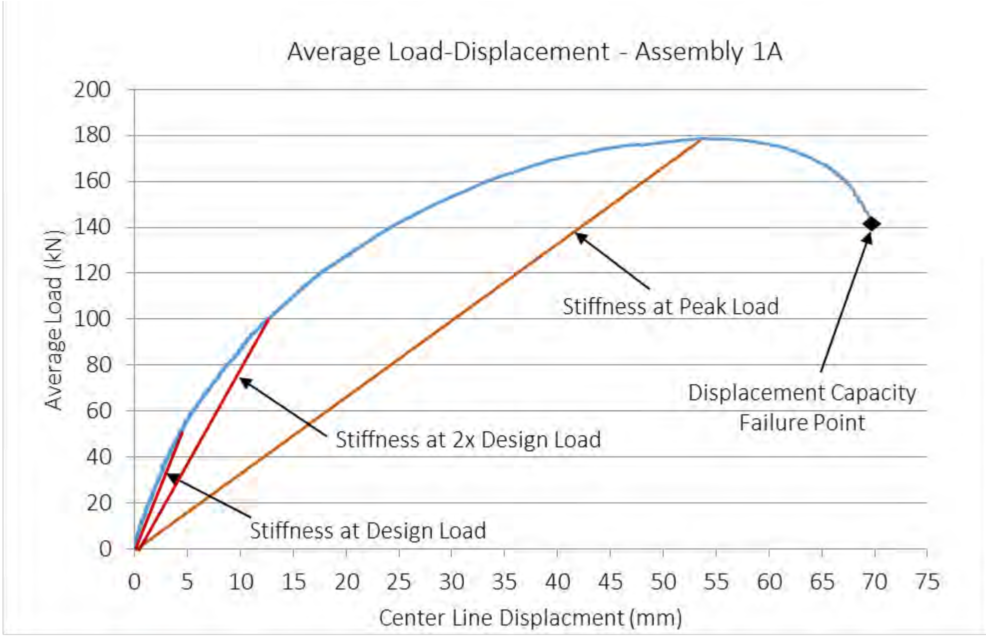

Figure 8. Typical load-displacement curve (1 kN = 224.8 lbf; 1 mm = 0.0394 in.)

It can be also seen from Table 4 that the ductility of the diaphragms is in a range of 14 and 37. Light-frame shear walls are expected to have a ductility of not less than 11, as documented in ASTM D7989 [ASTM, 2015]. Therefore, the I-joist diaphragms tested in this study can be considered to be as ductile as light-frame shear walls.

Test results from Table 4 indicate that the average load factors for Series 1 (Case 5 blocked), 2 (Case 1 unblocked), 3 (Case 5 unblocked), and 4 (Case 5 blocked with a wider nail spacing) are 3.21, 2.99, 3.17, and 3.38, respectively. These load factors exceed the code-recognized minimum load factor of 2.8 for light-frame diaphragms in the U.S. Therefore, the diaphragms constructed with I-joists made of solid-sawn lumber flanges of at least 38 mm x 64 mm (1-1/2 in. x 2-1/2 in.) can be designed with corresponding diaphragm design values published in the U.S. code provided that the nail spacing is not closer than 102 mm (4 inches) on centre. In addition, when the nail spacing is less than 152 mm (6 inches), the adjacent nails within a row on the diaphragm boundary shall be staggered by 12.7 mm (1/2 inch).

5 Conclusions

Results obtained from this study support the following conclusions:

1) Test results obtained from this study show that the diaphragms constructed with I-joists made of solid-sawn lumber flanges of 2100f-1.8E MSR or lower grades, or equivalent, with a minimum dimension of 38 mm x 64 mm (1-1/2

Table 4. Full-Scale Diaphragm Test Results

ID	Case	Blocked?	Design Load (a), N/mm (lbf/ft)	Peak Strength, N/mm (lbf/ft)	Load Factor (b)	Stiffness at Design Load, kN/mm (lbf/in.)	Stiffness at 2x Design Load, kN/mm (lbf/in.)	Stiffness at Peak Load (c), kN/mm (lbf/in.)	Displ. Capacity (d), mm (in.)	Ductility (e)
1A (f)	5	Yes	7.0 (480)	24.4 (1673)	3.49	12.2 (69818)	7.7 (44138)	3.3 (18836)	69.5 (2.74)	16.6
1B (f)				20.6 (1411)	2.94	15.7 (89650)	9.1 (52009)	4.3 (24514)	47.4 (1.87)	14.5
1C (f)				22.3 (1531)	3.19	20.6 (117551)	9.7 (55385)	4.3 (24323)	50.7 (2.00)	20.4
		Mean		22.4 (1538)	3.21	16.2 (92340)	8.8 (50511)	4.0 (22558)	55.9 (2.20)	17.2
2A	1	No	4.7 (320)	14.2 (972)	3.04	7.0 (40104)	3.3 (18652)	1.9 (10761)	68.9 (2.71)	14.2
2B				13.8 (944)	2.95	7.2 (41290)	2.9 (16650)	1.7 (9830)	71.2 (2.80)	15.1
		Mean		14.0 (958)	2.99	7.1 (40697)	3.1 (17651)	1.8 (10295)	70.0 (2.76)	14.6
3A	5	No	3.5 (240)	10.7 (733)	3.05	6.6 (37770)	3.5 (20175)	1.6 (9231)	90.6 (3.57)	23.4
3B				11.5 (791)	3.29	9.3 (52844)	5.0 (28728)	1.8 (10242)	103.0 (4.06)	37.2
		Mean		11.1 (762)	3.17	7.9 (45307)	4.3 (24452)	1.7 (9736)	96.8 (3.81)	30.3
4A	5	Yes	5.3 (360)	17.7 (1210)	3.38	21.5 (122553)	8.1 (46142)	3.1 (17637)	52.7 (2.07)	29.4

(a) As published in the SDPWS or U.S. Code.

(b) Load factor is determined as the ratio between the peak strength and the design load.

(c) Stiffness at peak load is determined as the slope of a line between the origin (after slack of system removed) and the peak load.

(d) Displacement capacity is determined as the diaphragm centre-line displacement where the applied load is equal to 80% of the post-peak load.

(e) Ductility is determined as the ratio between the displacement capacity and the displacement at design load.

(f) Adjacent nails within a row of nails on the diaphragm boundary were offset (staggered) by 12.7 mm (1/2 inch).

inches x 2-1/2 inches) have load factors greater than the code-recognized minimum load factor of 2.8.

2) The diaphragms tested in this study support the use of code-recognized diaphragm design values except that the nails shall not be placed closer than 102 mm (4 inches) on centre and the adjacent nails within a row on the diaphragm boundary shall be staggered by 12.7 mm (1/2 inch) when the nail spacing is less than 152 mm (6 inches).
3) The diaphragms tested in this study exhibit ductility that is comparable with light-frame shear walls.
4) For I-joist series manufactured with proprietary structural composite lumber flanges, the small-scale test results provided in this paper can be used as a benchmark for determining the applicability of these results and whether additional full-scale diaphragm tests are necessary.

6 References

ANSI/AWC (2015). *Special Design Provisions for Wind and Seismic (SDPWS)*. Leesburg, VA.

APA (2016). *Engineered Wood Construction Guide*. Form No. E30. APA – The Engineered Wood Association. Tacoma, Washington.

ASTM International (2015). *Standard Practice for Demonstrating Equivalent In-Plane Lateral Seismic Performance to Wood-Frame Shear Walls Sheathed with Wood Structural Panels*. ASTM D7989. West Conshohocken, PA.

ASTM International (2016). *Standard Method for Static Load Testing of Framed Floor or Roof Diaphragm Constructions for Buildings.* ASTM E455. West Conshohocken, PA.

ASTM International (2016). *Standard Specification for Establishing and Monitoring Structural Capacities of Prefabricated Wood I-Joists*. ASTM D5055. West Conshohocken, PA.

DOC (2009). *Voluntary Product Standard, Structural Plywood*. U.S. Department of Commerce. Washington, D.C.

ICC Evaluation Service, Inc. (2014). *Acceptance Criteria for Prefabricated Wood I-Joists.* AC 14. Brea, CA.

ICC (2015). *International Building Code*. International Code Council. Country Club Hills, IL.

Tissell, J.R. and J.R. Elliott (2000). *Plywood Diaphragms*. APA Research Report 138. APA – The Engineered Wood Association. Tacoma, WA.

Waltz, N. and J.D. Dolan (2010). *I-joist diaphragm systems: performance trends observed with full-scale testing*. Wood Design Focus: Summer/2010.

Discussion

The paper was presented by B J Yeh

P Quenneville asked how practical would be the staggered nail pattern. BJ Yeh stated that it is very practical and is being used.

D Dolan commented that the work was referenced to only one manufacturer of LVL with tensile strength perpendicular to grain lower than lumber. There could be variation amongst the many LVL producers. BJ Yeh responded that recommendations from this work only referenced to dimension lumber; LVL should be considered by individual LVL producers as proprietary products. He also commented that higher grade material has higher tendency to split.

G Doudak and BJ Yeh discussed about stiffness of the diaphragm and where it is appropriate to consider the nonlinearity. They also discussed the issues related to the definition of ductility and yield point.

P Zarnani and BJ Yeh discussed the mechanism of shear flow with respect to the diaphragm.

F Lam commented about the importance of species effect rather than density and grade effect that influence splitting. H Blass added that in EC5 a minimum thickness is needed for species that are prone to splitting.

M Gershfeld suggested the consideration of vertical load when splitting happened. BJ Yeh responded that the influence of vertical load would not have much of an effect.

Advanced modelling of CLT wall systems for earthquake resistant timber structures

Matteo Izzi, University of Trieste, CNR IVALSA Trees and Timber Institute, Italy

Andrea Polastri, CNR IVALSA Trees and Timber Institute, Italy

Massimo Fragiacomo, University of L'Aquila, Italy

Keywords: Cross-Laminated Timber (CLT), CLT wall system, seismic design, non-linear modelling, component approach.

1 Introduction

Cross-Laminated Timber (CLT) is gaining a significant popularity among the structural products as a sustainable alternative to steel and concrete. In comparison with those traditional building materials, CLT has a low carbon footprint and provides comfortable living conditions; moreover, the high strength-to-weight ratio, the prefabrication process and the erection speed are additional key points of its broad diffusion.

Determining the load-carrying capacity of lateral load-resisting systems made of CLT panels (such as CLT wall systems, i.e. CLT walls with mechanical connections) is crucial for both the static and seismic design of CLT structures. However, a calculation method has not yet been included in Eurocode 5 (EN 1995-1-1:2004/A2 2014).

Nowadays, the load-carrying capacity of CLT wall systems is determined with force-based design procedures. However, since the analysis neglects the connections stiffness, those methods do not ensure that the wall system behaves in accordance with the design assumptions. Furthermore, simplified methods neglect some contributions that might affect the response of a CLT wall system, like the friction between the wall and the element that is restrained to and the effect of the overlaying floor.

Based on the above-mentioned issues, this paper proposes a new numerical model of a CLT wall system. The model schematizes the CLT panel as an elastic orthotropic element, while the connections (i.e. hold-downs, angle brackets, and screws) are simulated as non-linear hysteretic springs. The interaction between the CLT panel and the foundation, and between the wall element and the CLT floor restrained on top of it, were specifically addressed in the development of the model.

The study presented herein is carried out considering the experimental tests results obtained by Gavric *et al.* (2015a-2015b-2015c). At first, experimental and numerical results are compared. A parametric study is carried out afterwards, (*a*) by varying the vertical load applied on top of the CLT wall, (*b*) by modifying the aspect ratio of the timber panel, and (c) by simulating a CLT floor screwed on top of the wall. Results are collected in diagrams and compared with a simplified design procedure commonly adopted by practicing engineers and discussed by Pozza *et al.* (2016b), highlighting how those contributions influence the elastic stiffness and the load-carrying capacity of a CLT wall system.

2 State-of-the-art

The mechanical and hysteretic behaviour of CLT structures and their sub-systems (i.e. single-joints and CLT wall systems) were the focus of a large body of research. Monotonic and cyclic tests were carried out on typically used metal connectors and screws (Flatscher *et al.* 2015; Gavric *et al.* 2015a-2015b; Joyce *et al.* 2011; Pozza *et al.* 2016a; Tomasi and Smith 2015). Racking tests were performed on CLT wall systems with various layouts of connections and loads, demonstrating significant ductility and energy dissipation (Dujic *et al.* 2004; Gavric *et al.* 2015c; Hummel *et al.* 2013; Popovski and Karacabeyli 2011). Finally, full-scale tests were carried out on multi-storey CLT buildings under dynamic and quasi-static conditions, providing an insight on the behaviour of CLT structures subjected to earthquake impact (Ceccotti *et al.* 2013; Flatscher and Schickhofer 2015; Popovski and Gavric 2016).
Results of these research projects have highlighted that several factors influence the behaviour of CLT wall systems, including: (*a*) the load-carrying capacity and the in-plane stiffness of the CLT panel; (*b*) the mechanical properties and the layout of the connections; (*c*) the vertical load applied on top of the wall panel; (*d*) the presence of openings and the boundary conditions. Point (*a*) and (*b*) were extensively investigated for both single and multiple CLT wall systems. Due to the high costs of experimental testing and the many variables involved including the size and the aspect ratio of the CLT panel, as well as the various layouts of the connections which may be adopted, there are still several open questions to be addressed concerning points (c) and (d). Some results on these topics were published by Dujic *et al.* (2005; 2007) and, recently, by Sustersic *et al.* (2016).
The experimental data collected during the research programmes were also used as inputs for the development of analytical predictive models (Flatscher *et al.* 2014; Gavric *et al.* 2015c; Pozza *et al.* 2016b), and numerical models of CLT wall systems (Dujic *et al.* 2007; Sustersic and Dujic 2012) and entire CLT structures (Follesa *et al.* 2013; Rinaldin and Fragiacomo 2016; Yasumura *et al.* 2016). In this context, it should be noticed that analytical models are usually employed to predict the mechanical behaviour under monotonic loads, while numerical models can also be used to investigate the hysteretic response under cyclic conditions.
In contrast with the significant findings obtained by the afore-mentioned research projects, design rules for CLT structures and their sub-systems have not yet been included either in Eurocode 5 (EN 1995-1-1:2004/A2 2014) (static design) or in Eurocode 8 (EN 1998-1:2004/A1 2013) (seismic design). Nowadays, the static design of CLT structures is carried out with simplified design procedures and following the pro-

visions included in harmonized technical specifications (like the European Technical Assessments). Regarding the seismic design of CLT structures, the rules prescribed in the current version of Eurocode 8 (EN 1998-1:2004/A1 2013) are very brief and leave room for interpretation. Recently, Follesa *et al.* (2015) have proposed a new version of Chapter 8 of Eurocode 8 (EN 1998-1:2004/A1 2013) where a capacity-based design approach for CLT structures is recommended; however, this proposal has not yet been implemented into the standard.

3 Simplified design procedures

Determining the load-carrying capacity of laterally loaded CLT wall systems is a crucial aspect for both the static and seismic design of CLT structures. However, a calculation method has not yet been prescribed in Eurocode 5 (EN 1995-1-1:2004/A2 2014), and simplified design procedures are required.
Nowadays, practicing engineers perform the ductile design of the dissipative connections and the elastic design of the CLT panel using force-based approaches. The mechanical behaviour of the connections is simplified assuming the hold-downs resist only tension and the angle brackets only shear (Figure 1a).

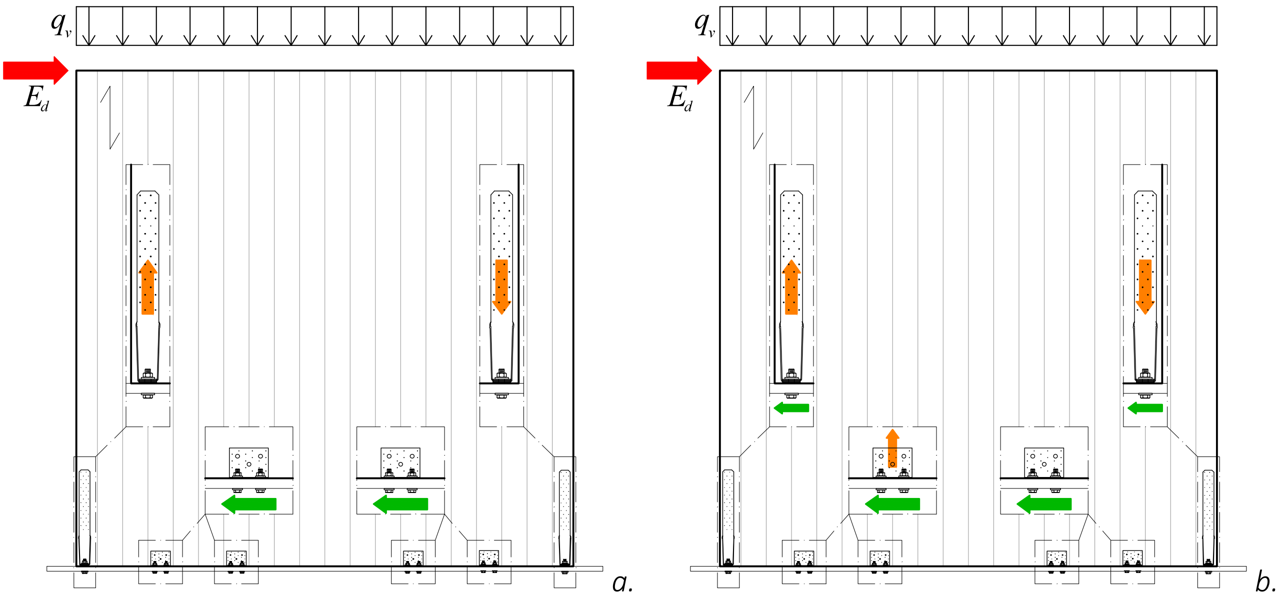

Figure 1. Schematics of a CLT wall system with pushover loading scheme: (a) with metal connectors loaded in a uniaxial state and (b) with the same elements loaded in a biaxial state.

This assumption leads to realistic predictions of the load-carrying capacity only when the CLT panel is much wider than tall, i.e. when the aspect ratio *b*/*h* is greater than one (being *b* the width of the CLT panel and *h* its height). In this situation, the angle brackets are mainly loaded in shear and the hold-downs in tension.
Several issues arise when the width of the CLT panel is comparable to its height, i.e. when the aspect ratio *b*/*h* is close to one; here, both the angle brackets and the hold-downs are simultaneously loaded in shear and tension. Furthermore, connections contribute to the overall response of the wall system, and to the static and dynamic

response of the entire CLT structure, based on their stiffness (Polastri *et al.* 2015). As discussed in Gavric *et al.* (2015a), hold-downs have a relatively weak mechanical behaviour in shear, which provides a minor contribution the lateral load-carrying capacity; on the contrary, angle brackets might be very stiff in both directions and contribute to the lateral load-carrying capacity also in their weaker (i.e. axial) direction (Figure 1b). Therefore, it is not recommended to verify separately the shear and the tensile connections, as the assumption of uniaxial loading might lead to non-realistic predictions of the load-carrying capacity.
It should be also noticed that the simplified design methods fully neglect some contributions that might affect the mechanical behaviour and the dissipation mechanism of a CLT wall system, such as the tangential behaviour between the CLT panel and the foundation and the influence of the overlying floor. In particular, this last contribution is taken into account as a vertical load applied on top of the wall, while its effect on the overall response of the wall system is neglected.

4 Reference CLT wall systems

The numerical simulations presented in Section 6 were carried out using the finite element software package *ABAQUS* (2012), considering the CLT wall systems tested by Gavric *et al.* (2015c) and schematized in Figure 2.

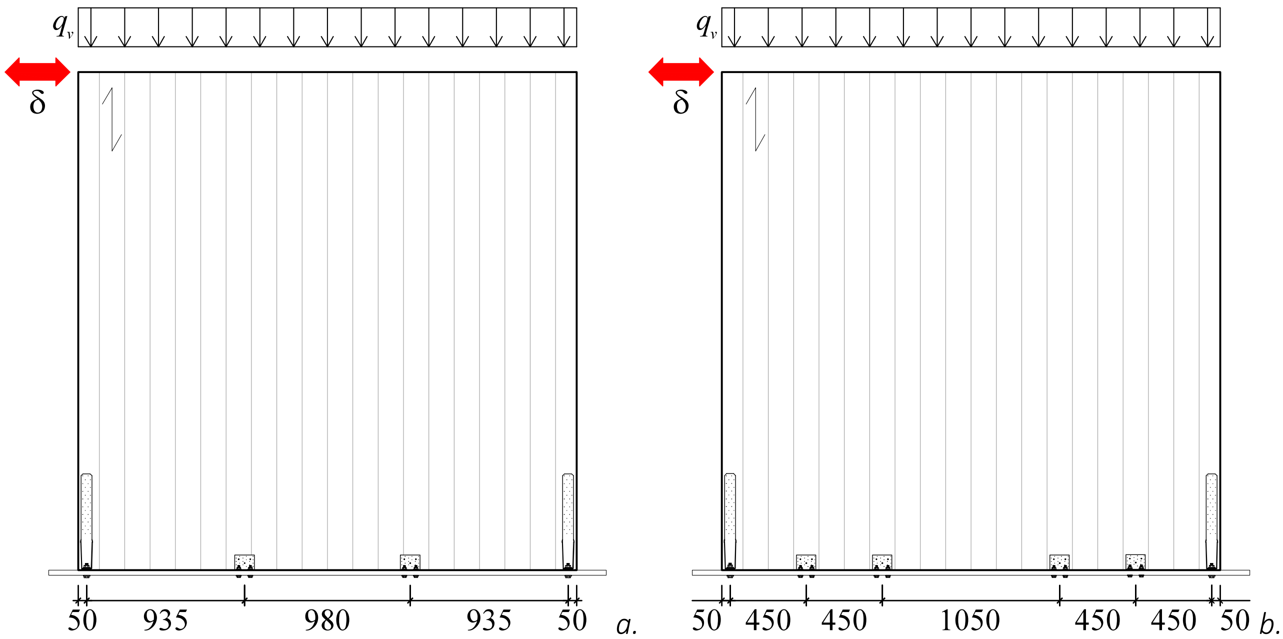

Figure 2. Schematics of the CLT wall systems tested by Gavric et al. (2015c) and considered in the numerical analyses: (a) Wall-A configuration and (b) Wall-B configuration (dimensions in mm).

The first configuration (labelled Wall-A in Figure 2) was assembled using a solid timber panel of size 2950x2950 mm^2, made of five crosswise laminated board layers and a total thickness of 85 mm (17-17-17-17-17); the panel was anchored to a steel foundation with two HTT22 hold-downs (ETA-07/0285 2015) and two AE116 angle brackets (ETA-06/0106 2014). A vertical load q_v = 18.5 kN/m was applied on top of the wall.

The second configuration (labelled Wall-B in Figure 2) was assembled with a similar panel and the same number of hold-downs, while the number of angle brackets was increased to four. Tests on the Wall-B configuration were carried out with two vertical loads: Wall-B1 with q_v = 18.5 kN/m and Wall-B2 with q_v = 9.25 kN/m.
In all the previous cases, the horizontal displacement history δ was applied to the wall by means of a steel profile screwed on top of it. Due to its high flexibility, the contribution of this steel element to the overall behaviour of the system was neglected in the numerical validation of the model. However, the influence of a CLT floor screwed over the wall was analysed in a parametric study.

5 Model description and calibration

The numerical model presented in this contribution aims at overcoming the limits of the simplified design methods, providing realistic predictions of the mechanical and hysteretic behaviour of a CLT wall system. The model presented below simulates a single CLT wall system (i.e. a wall system assembled with a unique panel); however, it can be generalized and used to investigate the behaviour of coupled CLT wall systems (i.e. wall systems assembled with multiple panels, 'coupled' with vertical step joints).
The model schematizes the CLT panel as an elastic orthotropic element, meshed using eight-node brick elements with reduced integration (C3D8R in *ABAQUS*). Table 1 summarizes the material parameters of the CLT panel, taken partly from Brandner *et al.* (2016) and from Ashtari (2012). In the table below the symbols E_x, E_y and E_z denote the moduli of elasticity of the CLT panel; G_{xy}, G_{xz} and G_{yz} the shear moduli while ν_{xy}, ν_{xz} and ν_{yz} are the Poisson's ratios. In the previous symbols, the subscripts *x* and *y* denotes two axis that lay on the plane of the wall, the first one oriented in the parallel to the face lamination of the CLT panel and the second one in the perpendicular direction; finally, the *z* axis is directed in the out-of-plane direction.

Table 1. Material parameters of the CLT panels.

E_x [GPa]	E_y [GPa]	E_z [GPa]	G_{xy} [GPa]	G_{xz} [GPa]	G_{yz} [GPa]	ν_{xy} [-]	ν_{xz} [-]	ν_{yz} [-]
7.10	4.80	0.40	0.65	0.50	0.10	0.075	0.364	0.380

The connections are simulated as non-linear springs with three degrees of freedom by means of a user element subroutine taken from Rinaldin *et al.* (2013). Each degree of freedom represents a displacement component and is calibrated on the results obtained by Gavric *et al.* (2015a-2015b). The hysteresis laws adopted in the simulations are schematized in Figure 3, while Table 2 summarizes the mechanical properties of each connection. The symbol K_{el} denotes the elastic stiffness, F_y the yield load, K_{pl} the stiffness of the inelastic branch and F_{max} the maximum load-carrying capacity.
The mechanical properties were assessed as prescribed in EN 12512:2001/A1 (2005) from the first envelope curve of the experimental data; for each connection system,

those values were used to define the backbone curve of the corresponding hysteresis law (red lines in Figure 3).

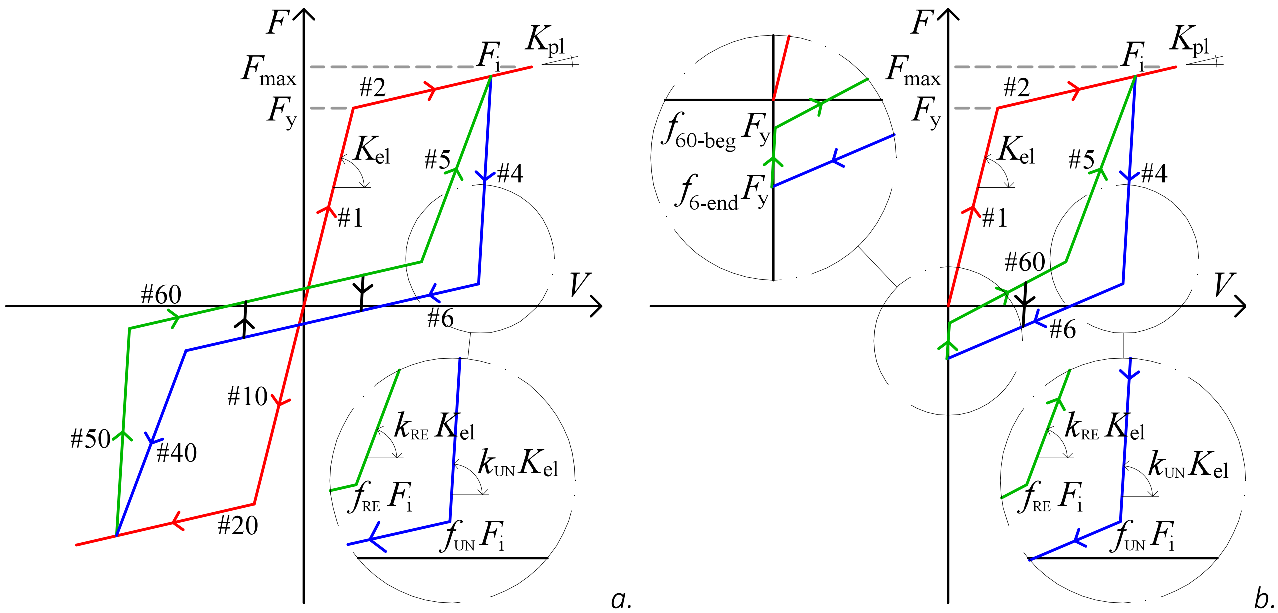

Figure 3. Piecewise-linear laws of the non-linear springs (a) in shear and (b) in tension/withdrawal.

Table 2. Mechanical properties of the connections tested by Gavric et al. (2015a-2015b) (Simpson Strong-Tie AE116 angle bracket and HTT22 hold-down; Rothoblaas HBS10x260 screw).

Property	AE116 shear (n = 7)	AE116 tension (n = 6)	HTT22 shear (n = 6)	HTT22 tension (n = 6)	HBS10x260 in-plane (n = 6)	HBS10x260 out-plane (n = 6)	HBS10x260 withdrawal (n = 6)
K_{el} [kN/mm]	1.90	2.65	0.91	4.65	1.50	1.07	11.14
F_y [kN]	23.13	19.07	9.76	39.13	4.72	5.45	17.69
K_{pl} [kN/mm]	0.26	0.42	0.13	0.70	0.13	0.12	0.78
F_{max} [kN]	27.71	23.47	13.89	47.78	7.72	8.14	31.12

In the table above, the 'in-plane' notation is used to denote the shear behaviour of the screwed joints when the load is applied in the same plane of the CLT panel, while the 'out-plane' notation denotes its behaviour in the perpendicular direction.
The third displacement component of the hold-down and the angle bracket simulates the out-of-plane behaviour of the connectors; without the support of experimental results, those components were modelled as elastic springs and calibrated on the results obtained by Izzi *et al.* (2016), as the withdrawal stiffness of the nails used to anchor the connectors to the CLT panel.

The unloading and reloading paths of the hysteresis laws (blue and green lines in Figure 3, respectively) are governed by four parameters: k_{UN} and k_{RE} control the slope of branches #4 (#40) and #5 (#50); f_{UN} and f_{RE} control the load at the separation points between branches #4 and #6 (#50 and #60) and between branches #6 and #40 (#60 and #5), respectively. Finally, two additional parameters govern the non-symmetric cycle of the tensile/withdrawal springs: $f_{6\text{-end}}$ and $f_{60\text{-beg}}$, respectively. For each test series, these parameters were determined by reproducing the experimental test results using the springs and by minimizing, with the same set of values, the scatter of dissipated energy between experimental and numerical results (see, e.g., Figure 4).

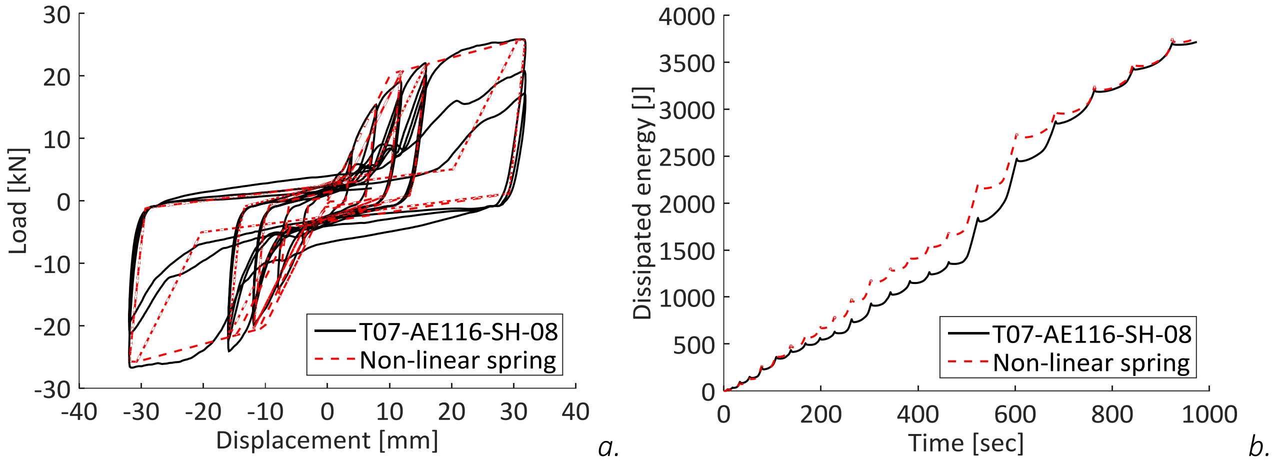

Figure 4. Typical output obtained by calibrating the non-linear hysteretic springs (here referred to a AE116 tested in shear): comparison between (a) loading curves and (b) dissipated energy vs time.

The CLT wall systems tested by Gavric *et al.* (2015c) were anchored to a steel foundation; therefore, numerical analyses were carried out by considering a steel basement placed below the CLT wall. The steel foundation was simulated as an elastic element (with E = 210 GPa and ν = 0.30) and meshed with eight-node brick elements with reduced integration (C3D8R in *ABAQUS*). The interaction between the steel foundation and the CLT wall was modelled as follows: (*a*) the normal behaviour was defined as a unilateral hard contact; (*b*) the tangential behaviour was defined based on a penalty formulation. The afore-mentioned approach could be also employed to simulate the CLT floor screwed on top of the wall.

The non-linear springs are placed at the exact location of the metal connectors in the experimental setups (see Figure 2), and are restrained on one side to the CLT panel and on the other side to the steel foundation. Similarly, the springs used to model the mechanical behaviour of the screws are restrained on one side to the CLT panel and on the other side to the overlaying CLT floor.

6 Numerical analyses and discussions

The numerical model presented in the previous section was validated on the CLT wall systems tested by Gavric *et al.* (2015c) (see Section 4). Simulations were performed in displacement control, acquiring the displacement histories from the tests.

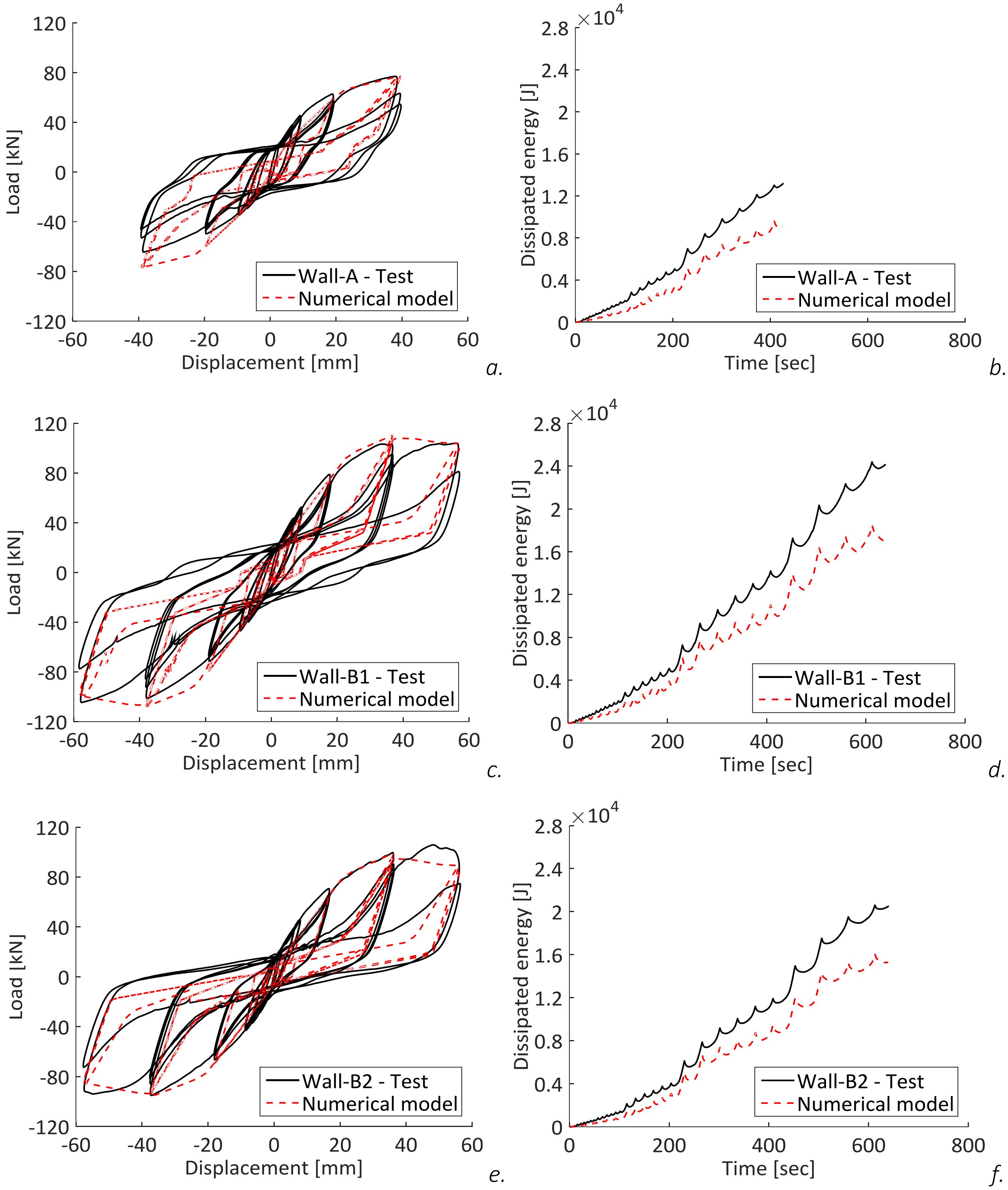

Figure 5. Comparison between experimental and numerical results of the wall systems considered in the analyses, in terms of loading curves and dissipated energy vs time.

In the first set of analyses, the friction between the CLT wall panel and the foundation was neglected. This assumption is coherent with the design approach adopted by practicing engineers and usually leads to conservative results.

Figure 5 shows a comparison between experimental (black solid line) and numerical (red dashed line) results in terms of loading curve and dissipated energy histories. As it is visible from the figure, the numerical model is able to simulate the overall behaviour of the CLT wall system. Differences between experimental and numerical hysteresis cycles might be associated both to minor variations in the mechanical behaviour of the connections and to the lack of friction between the CLT panel and the steel foundation, which has a significant influence on the initial stiffness and the energy dissipation mechanism. Numerical simulations were repeated afterwards by including also the tangential behaviour at the base of the CLT panel; for this purpose, a penalty formulation was adopted with friction coefficient μ_{fr} = 0.20.

Table 3 summarizes the outcomes of this study; it is clear that the tangential behaviour should be taken into account in the analysis to obtain more reliable predictions of the elastic stiffness (K_{el}) and of the energy dissipation (E_d). However, the penalty formulation might lead to higher load-carrying capacities (see, e.g., F_{max} for Wall-A), suggesting the use of more advanced tangential models (e.g. the exponential decay).

Table 3. Comparison between experimental and numerical results, obtained with the proposed model by neglecting and then considering the friction between CLT wall and steel foundation.

CLT wall system	Experimental			Numerical – No friction			Numerical – With friction		
	K_{el} [kN/mm]	F_{max} [kN]	E_d [kJ]	K_{el} [kN/mm]	F_{max} [kN]	E_d [kJ]	K_{el} [kN/mm]	F_{max} [kN]	E_d [kJ]
Wall-A	6.04	76.9	13.2	3.84	76.6	9.1	4.37	93.3	11.5
Wall-B1	6.24	103.9	23.6	4.72	110.3	17.6	5.62	113.3	19.4
Wall-B2	5.80	105.8	20.5	4.01	99.1	15.3	4.60	99.7	16.2

A parametric study was carried out afterwards on the Wall-B configuration. This second set of analyses was aimed at highlighting how the load-carrying capacity and the elastic stiffness of CLT wall systems are influenced by: (*a*) the vertical load (q_v) applied on top of the wall; (*b*) the aspect ratio of the CLT panel; (c) the presence of a floor screwed on top of the wall. Based on the afore-mentioned limitations of the penalty formulation, the contribution due to friction was neglected in this study.

Simulations were performed considering a vertical load q_v varying between zero and 40 kN/m, while three aspect ratios were analysed: b/h = 1 (as in the tests), b/h = 1.5 and b/h = 2. Analyses were repeated afterwards by considering a 150 mm thick and 600 mm wide CLT floor screwed on top of the CLT wall; the floor element was fixed with 18 Rotho Blaas HBS10x260 (ETA-11/0030 2016), equally distributed along the width of the wall. The mechanical properties of the screws are listed in Table 2.

Figure 7 summarizes the results of this parametric study. As mentioned above, analyses were carried out by neglecting the friction between the wall and the steel foundation; therefore, numerical results (solid black lines) were compared with no further modifications with the analytical predictions obtained with a simplified model adopted by practicing engineers and presented in Pozza *et al.* (2016b) (red dashed lines):

$$F_{CLT\ sys} = \min[F_{AB};\ 1/h(F_{HD}b\ q_v b^2/2)] \qquad (1)$$

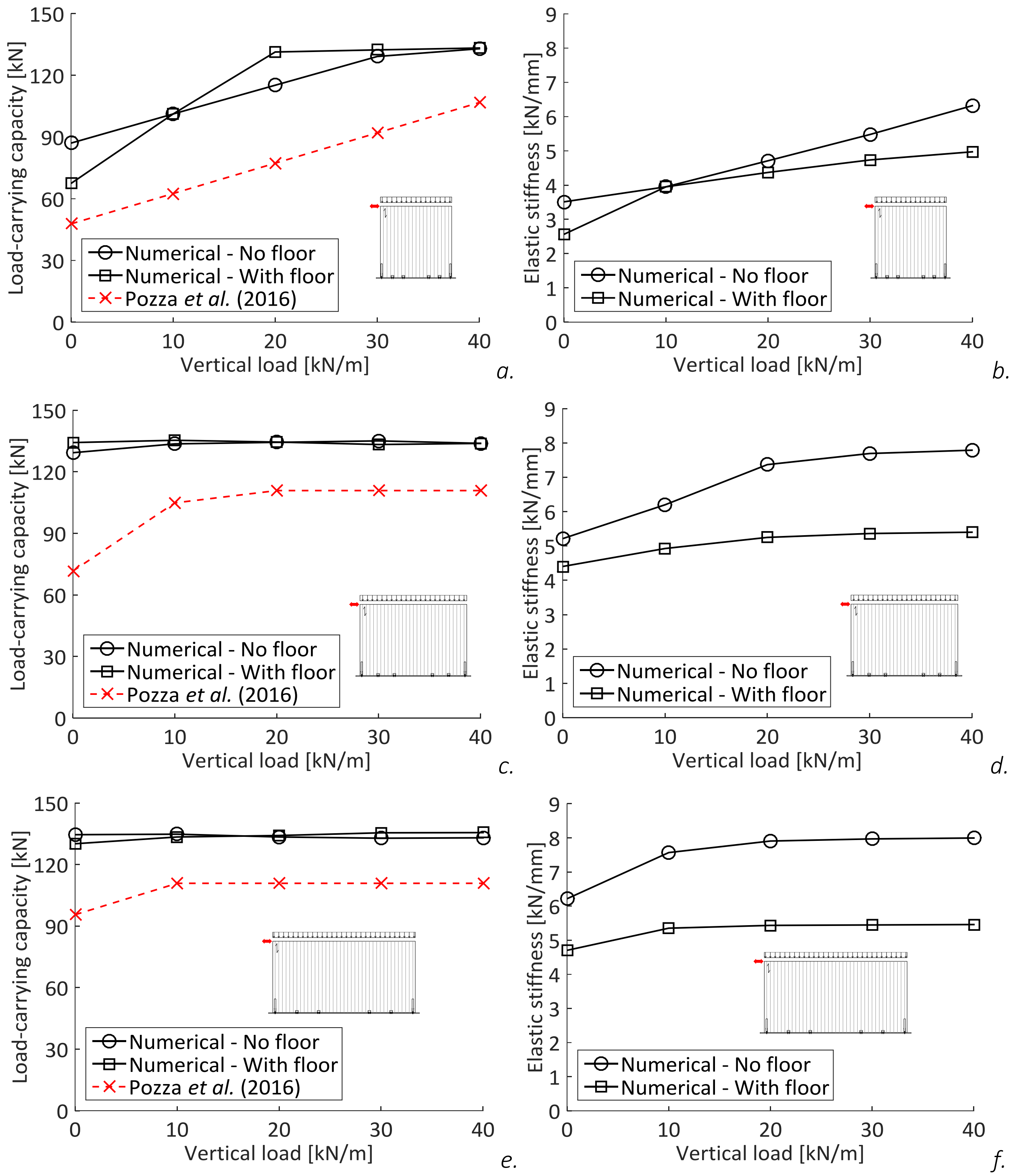

Figure 7. Parametric study showing how the vertical load, the aspect ratio of the wall and a CLT floor on top of it influence the load carrying capacity and the elastic stiffness of a CLT wall system.

In Equation 1, F_{AB} is the load-carrying capacity of the angle brackets, determined by multiplying their number by the experimental shear capacity given in Table 2; similarly, F_{HD} is the experimental tensile capacity of a hold-down given in Table 2, while the other symbols have the same meaning of those used before.

The numerical simulations show that the mechanical behaviour of the wall system is significantly influenced by the aspect ratio of the CLT panel. Rocking occurred in the CLT panel with b/h = 1, whereas all the other cases failed for sliding. Due to the simplified behaviour of the mechanical connections, the model by Pozza *et al.* (2016b)

lead to conservative predictions of the load-carrying capacity; nevertheless, the simplified model provided a correct identification of the failure mechanism in most of the cases analysed. Differences in predicting the failure mechanism were observed for wide walls and when no vertical load was applied. However, this situation is of little practical interest.
The analyses also provided some preliminary information on the influence of a CLT floor screwed on top of a CLT wall system. Based on the mechanical properties and on the layout of connections adopted (Figure 2b), the following considerations can be done: if the wall system fails for sliding (e.g. for $b/h > 1$), the CLT floor has little effects on the load-carrying capacity of the system. A more complex behaviour was observed when the wall system fails due to rocking (e.g. when the aspect ratio $b/h = 1$). In particular, rocking was observed for low values of the vertical load (i.e. for $q_v < 20$ kN/m), while sliding was observed for higher loads. In both situations, the presence of a CLT floor influenced the redistribution of forces within the wall system, limiting the load transferred to the hold-downs.

7 Conclusions

This paper proposed a new numerical model of a CLT wall system, in which the wall is simulated as an elastic orthotropic panel and the connections are modelled as nonlinear hysteretic springs. The model is able to simulate both the contact and the tangential behaviour between the CLT wall and the element that is restrained to; moreover, it allows the simulation of a CLT floor restrained on top of the wall panel.
Numerical results were validated by comparison with similar setups experimentally tested, showing acceptable accuracy. At first, the friction between the CLT wall and the steel foundation that was restrained to was neglected. Its effect on the overall behaviour of the system was investigated afterwards, showing that friction increases the initial stiffness and improves the energy dissipation mechanism, enhancing this last contribution by about 10%.
A parametric study was then carried out, and the influence of the vertical load (q_v) and of the aspect ratio of the CLT wall (b/h) were analysed. Simulations were carried out by neglecting the tangential behaviour at the base of the wall, and were repeated afterwards by considering a CLT floor screwed on top of it. Numerical results were compared with the analytical predictions determined according to a simplified model that is commonly used by practicing engineers. Based on this comparison, it was shown that the simplified model is able to identify the failure mechanism and provides conservative predictions of the load-carrying capacity in most of the cases analysed. Differences between numerical and analytical results can be attributed to the simplifications used to describe the mechanical behaviour of the connections. The simplified model adopts a force-based approach and considers the angle brackets resisting only in shear and the hold-downs only in tension; moreover, the actual stiffness of the connections is neglected. On the other hand, the numerical model adopts

a displacement-based approach and, taking into account the actual stiffness of the connections, is able to simulate both the shear and the tensile behaviour in each connection. Based on the afore-mentioned issues, to obtain realistic predictions of the load-carrying capacity, the adoption of a displacement-based design for CLT wall systems is suggested for implementation in the revised version of Eurocode 5 (EN 1995-1-1:2004/A2 2014).
Analyses provided also some preliminary results on the effect of a screwed floor on top of the CLT wall system. In particular, it was shown that the floor element forces a failure mechanism in sliding and influences the redistribution of forces within the wall system, by reducing the load transferred to the hold-downs.

8 Acknowledgements

This study was carried out while Matteo Izzi was collaborating as Research Assistant at the Trees and Timber Institute of San Michele all'Adige (Italy), the financial support of which is gratefully acknowledged. Giovanni Rinaldin (University of Sassari, Italy) is acknowledged for sharing the user element subroutine employed in the simulations. Chiara Bedon (University of Trieste, Italy) is gratefully acknowledged for the advices, help and collaboration provided while performing the numerical analyses.

9 References

Ashtari S (2012) In-plane Stiffness of Cross-laminated Timber Floors. *MS Thesis*. University of British Columbia, Vancouver, Canada.

Brandner R, Flatscher G, Ringhofer A, Schickhofer G, Thiel A (2016) Cross laminated timber (CLT): overview and development. *European Journal of Wood and Wood Products,* **74**(3): 331-351, doi: 10.1007/s00107-015-0999-5.

Ceccotti A, Sandhaas C, Okabe M, Yasumura M, Minowa C, Kawai N (2013) SOFIE project - 3D shaking table test on a seven-storey full-scale cross-laminated building. *Earthquake Engineering & Structural Dynamics,* **42**(13): 2003-2021, doi: 10.1002/eqe.2309.

Dujic B, Aicher S, Zarnic R (2005) Racking of Wooden Walls Exposed to Different Boundary Conditions. *38th CIB-W18 Meeting*, Karlsruhe, Germany, Paper 38-15-6.

Dujic B, Klobcar S, Zarnic R (2007) Influence of Openings on Shear Capacity of Wooden Walls. *40th CIB-W18 Meeting*, Bled, Slovenia, Paper 40-15-6.

Dujic B, Pucelj J, Zarnic R (2004) Testing of Racking Behavior of Massive Wooden Wall Panels. *37th CIB-W18 Meeting*, Edinburgh, Scotland, Paper 37-15-2.

EN 1995-1-1:2004/A2 (2014) Eurocode 5: Design of timber structures. Part 1-1: General. Common rules and rules for buildings. CEN, Brussels, Belgium.

EN 1998-1:2004/A1 (2013) Eurocode 8: Design of structures for earthquake resistance. Part 1: General rules, seismic actions and rules for buildings. CEN, Brussels, Belgium.

EN 12512:2001/A1 (2005) Timber structures. Test methods. Cyclic testing of joints made with mechanical fasteners. CEN, Brussels, Belgium.

ETA-06/0106 (2014) European Technical Assessment. Three-dimensional nailing plate (timber-to-timber/timber-to-concrete angle bracket). ETA-Denmark, Nordhavn, Denmark.

ETA-07/0285 (2015) European Technical Assessment. Three-dimensional nailing plate (timber to timber and timber to concrete/steel hold downs and post bases). ETA-Denmark, Nordhavn, Denmark.

ETA-11/0030 (2016) European Technical Assessment. Screws for use in timber constructions. ETA-Denmark, Nordhavn, Denmark.

Flatscher G, Bratulic K, Schickhofer G (2014) Screwed Joints in Cross Laminated Timber Structures. *World Conference on Timber Engineering (WCTE)*, Quebec City, Quebec, Canada.

Flatscher G, Bratulic K, Schickhofer G (2015) Experimental tests on cross-laminated timber joints and walls. *Proceedings of the ICE - Structures and Buildings,* **168**(11): 868-877, doi: 10.1680/stbu.13.00085.

Flatscher G, Schickhofer G (2015) Shaking-table test of a cross-laminated timber structure. *Proceedings of the ICE - Structures and Buildings,* **168**(11): 878-888, doi: 10.1680/stbu.13.00086.

Follesa M, Christovasilis IP, Vassallo D, Fragiacomo M, Ceccotti A (2013) Seismic design of multi-storey CLT buildings according to Eurocode 8. *Ingegneria Sismica: International Journal Earthquake Engineering,* **30**(4): 27-53.

Follesa M, Fragiacomo M, Vassallo D, Piazza M, Tomasi R, Rossi S, Casagrande D (2015) A proposal for a new Background Document of Chapter 8 of Eurocode 8. *INTER 2015 Meeting*, Šibenik, Croatia, Paper 48-7-3.

Gavric I, Fragiacomo M, Ceccotti A (2015a) Cyclic behaviour of typical metal connectors for cross laminated (CLT) structures. *Materials and Structures,* **48**(6): 1841-1857, doi: 10.1617/s11527-014-0278-7.

Gavric I, Fragiacomo M, Ceccotti A (2015b) Cyclic behavior of typical screwed connections for cross-laminated (CLT) structures. *European Journal of Wood and Wood Products,* **73**(2): 179-191, doi: 10.1007/s00107-014-0877-6.

Gavric I, Fragiacomo M, Ceccotti A (2015c) Cyclic Behavior of CLT Wall Systems: Experimental Tests and Analytical Prediction Models. *Journal of Structural Engineering,* **141**(11): 04015034(1-14), doi: 10.1061/(ASCE)ST.1943-541X.0001246.

Hummel J, Flatscher G, Seim W, Schickhofer G (2013) CLT Wall Elements Under Cyclic Loading - Details for Anchorage and Connection. *COST Action FP1004, Focus solid timber solutions - European Conference on Cross Laminated Timber (CLT)*, pp: 152-165, Graz, Austria.

Izzi M, Flatscher G, Fragiacomo M, Schickhofer G (2016) Experimental investigations and design provisions of steel-to-timber joints with annular-ringed shank nails for Cross-Laminated Timber structures. *Construction and Building Materials,* **122**: 446-457, doi: 10.1016/j.conbuildmat.2016.06.072.

Joyce T, Smith I, Ballerini M (2011) Mechanical behaviour of in-plane shear connections between CLT wall panels. *44th CIB-W18 Meeting*, Alghero, Italy, Paper 44-7-2.

Polastri A, Pozza L, Loss C, Smith I (2015) Structural characterization of multi-storey CLT buildings braced with cores and additional shear walls. *INTER 2015 Meeting*, Šibenik, Croatia, Paper 48-15-5.

Popovski M, Gavric I (2016) Performance of a 2-Story CLT House Subjected to Lateral Loads. *Journal of Structural Engineering,* **142**(4): E4015006(1-12), doi: 10.1061/(ASCE)ST.1943-541X.0001315.

Popovski M, Karacabeyli E (2011) Seismic Performance of Cross-Laminated Wood Panels. *44th CIB-W18 Meeting*, Alghero, Italy, Paper 44-15-7.

Pozza L, Massari M, Savoia M, Ferracuti B (2016a) Experimental campaign of mechanical CLT connections subjected to a combination of shear and tension forces. *International Conference on Structures and Architecture*, Guimarães, Portugal.

Pozza L, Scotta R, Trutalli D, Polastri A, Smith I (2016b) Experimentally based *q*-factor estimation of cross-laminated timber walls. *Proceedings of the ICE - Structures and Buildings,* **169**(7): 492-507, doi: 10.1680/jstbu.15.00009.

Rinaldin G, Amadio C, Fragiacomo M (2013) A component approach for the hysteretic behaviour of connections in cross-laminated wooden structures. *Earthquake Engineering & Structural Dynamics,* **42**(13): 2023-2042, doi: 10.1002/eqe.2310.

Rinaldin G, Fragiacomo M (2016) Non-linear simulation of shaking-table tests on 3- and 7-storey X-Lam timber buildings. *Engineering structures,* **113**: 133-148, doi: 10.1016/j.engstruct.2016.01.055.

Simulia DS (2012) *ABAQUS 6.12 Documentation*. Providence, Rhode Island, USA.

Sustersic I, Dujic B (2012) Simplified cross-laminated timber wall modelling for linear-elastic seismic analysis. *45th CIB-W18 Meeting*, Växjö, Sweden, Paper 45-15-6.

Sustersic I, Fragiacomo M, Dujic B (2016) Seismic Analysis of Cross-Laminated Multistory Timber Buildings Using Code-Prescribed Methods: Influence of Panel Size, Connection Ductility, and Schematization. *Journal of Structural Engineering,* **142**(4): E4015012(1-14), doi: 10.1061/(ASCE)ST.1943-541X.0001344.

Tomasi R, Smith I (2015) Experimental Characterization of Monotonic and Cyclic Loading Responses of CLT Panel-To-Foundation Angle Bracket Connections. *Journal of Materials in Civil Engineering,* **27**(6): 04014189(1-10), doi: 10.1061/(ASCE)MT.1943-5533.0001144.

Yasumura M, Kobayashi K, Okabe M, Miyake T, Matsumoto K (2016) Full-Scale Tests and Numerical Analysis of Low-Rise CLT Structures under Lateral Loading. *Journal of Structural Engineering,* **142**(4): E4015007(1-12), doi: 10.1061/(ASCE)ST.1943-541X.0001348.

Discussion

The paper was presented by M Izzi

G Doudak asked about the interaction between tension and shear and how the model would take into account the interaction. M Izzi responded that the model has shear springs and axial spring and they are uncoupled. G Doudak commented that there were no test results which considered the influence of the floor. M Izzi replied that the floor was considered not to be able to move in the out of the plane direction and the bending stiffness of the floor was considered as an elastic element.

P Quenneville asked how realistic would be the sliding failure with the presence of perpendicular elements. M Izzi agreed and the information in the paper was limited to single wall or couple walls in laboratory conditions.

T Reynolds commented that at the 1st floor level the wall might be mounted on the wall rather than the concrete. M Izzi replied the model could be modified to consider such situation.

F Lam commented UBC has data on the interaction between axial and shear load in similar connections. The information would be presented in WCTE 2016.

A Ceccotti questioned about the influence of vertical load between 30 to 40 kN on capacity. M Izzi replied that this was caused by the sliding. A Ceccotti also questioned the case at zero vertical load the model prediction and test results differed by a factor of 2. There were discussions about the difference of results between the floor and no floor cases.

H Blass received clarification that the displacement was applied at the floor level. M Izzi stated that without floor the failure mode was rocking therefore the failure load was lower.

A Frangi questioned why at zero vertical load where the rocking dominated there was a difference in one case. There was discussion that the connection between the floor and wall could be the limiting factor. A Frangi stated that the proposal to make an improved simplified model was missing in the paper to guide the designers and code. He also commented if we introduced stiffness in design it would add more questions and difficulties. M Izzi replied that more work would be done.

M Gershfeld commented that developing a connection system that could uncouple axial and shear forces would be useful rather than considering the complicated interaction. M Izzi agreed but no system was available.

A Ceccotti commented that it is an important study that could allow us to understand CLT system better; however, we should consider taller and bigger structures with CLT.

Seismic Resistant Timber Walls with New Resilient Slip Friction Damping Devices

Ashkan Hashemi, The University of Auckland, New Zealand

Pouyan Zarnani, Auckland University of Technology, New Zealand

Armin Valadbeigi, The University of Auckland, New Zealand

Reza Masoudnia, The University of Auckland, New Zealand

Pierre Quenneville, The University of Auckland, New Zealand

Keywords: Cross Laminated Timber, Resilient Slip Friction joint, Self-centring, Seismic resilience, Energy dissipation

1 Introduction

Despite the fact that timber is intrinsically a non-ductile material, timber structures have performed well in terms of seismic performance. This is mainly because of the ductility of the mechanical steel connectors and their interaction with the timber elements. In modern design approaches, these connections are detailed to plastically deform while the timber members stay in the elastic region. Thus, the overall system achieves the required ductility. Latest research about the seismic performance of timber structures has shown that the hysteretic behaviour of the steel connections govern the total seismic performance of the structures. Traditional steel connections available for timber construction are typically comprised of mechanical fasteners such as nails, screws, rivets or bolts which are often subjected to non-recoverable damage in a design level earthquake. Therefore, the connections have to be replaced almost entirely after a severe seismic event.

Passive slip friction connectors including flat steel plates sliding over each other were originally employed in steel structures. Popov et al. (1995) introduced the *symmetric* slotted bolted connections which absorbs the seismic energy through friction during equilateral tension and compression cycles. Popov's comprehensive experiments demonstrated a nearly elastoplastic yet stable hysteretic behaviour. Clifton et al. (2007) proposed the *asymmetric* sliding hinge joint for steel moment resisting frames which had non-rectangular and stable force-deformation behaviour. Filiatrault (1990) utilized the sliding friction devices for timber sheathed shear walls which resulted in a noticeable improvement in the hysteretic behaviour of the walls compared to the conventional timber shear walls. His studies showed that large amount of energy could be absorbed at different lateral drifts up to 1.5%. Loo et al. (2012, 2014, 2015) investigated the application of slip friction hold-downs as a replacement for traditional connectors in timber Laminated Veneer Lumber (LVL) walls. Their experiments showed a considerable improvement in the seismic performance compared to the traditional systems in terms of hysteretic behaviour and residual displacements. Hashemi et al. (2016) extended the application of slip friction connections to rocking Cross Laminated Timber (CLT) coupled wall systems. Their studies demonstrated that coupled walls with friction joints provide superior seismic performance in terms of ductility, energy dissipation and residual deflections compared to similar systems with traditional nailed connections.

This paper introduces a novel timber coupled wall system using innovative Resilient Slip Friction (RSF) joints and CLT panels as a low damage self-centring seismic solution for timber construction. The main objective of this work is to demonstrate how the adoption of the RSF joints in timber walls can improve the ductility of the wall systems while it offers a damage-free ductility zone. The outcomes of this work can be used to recommend more generous behaviour factor (q) compared to what has been proposed by Eurocode 8 (2013) when RSF technology is used.

The experiment carried out on a rocking CLT wall with RSF hold-downs is introduced. Moreover, a simple design procedure for predicting the hysteretic behaviour of the RSF joints in addition to design equations for the coupled wall system are presented. Based on the experimental results, implications to the way in which such a system could be designed in terms of the required ductility and the restoring force are discussed.

2 Resilient Slip Friction (RSF) joint

The energy absorption mechanism of the conventional slip friction connections comprised of sliding flat steel plates has already been proven as one of the most efficient structural damping systems. However, the lack of self-centring behaviour in these joints requires the use of a supplementary system to bring back the structure to its original position after an earthquake, which is always costly. One of the conventional solutions to provide self-centring is the use of post-tensioned tendons up the height of the walls. This solutions has two major disadvantages. Firstly, a significant rate of tendon force loss (30% or more) can take place during the service life of the building which substantially reduces the efficiency of the system and secondly, the post-tension force is highly dependent on the humidity of the environment which is very hard to control in most cases.

In this paper, a novel friction joint is introduced in which the components are arranged in such a way that the damping is achieved as well as self-centring, all in one device. Figure 1 displays the components and the assembly for the Resilient Slip Friction (RSF) joint (2015). The specific shape of the grooves combined with the use of Belleville washers (conical disc springs) and high strength bolts deliver the desirable self-centring behaviour. The angle of the grooves is designed in a way that at the time of unloading, the reversing force caused by the elastically compacted Belleville washers is larger than the resisting friction force between the surfaces. Thus, this force re-centres the slotted plates to their original position.

(a) (b) (c)

Figure 1. RSF joint: a) Cap plates and centre slotted plate b) Belleville spring washers c) Assembly

Based on the free body diagrams and the acting forces shown in Figure 2, a design procedure has been developed to predict the load-deformation behaviour of a symmetric double acting RSF joint (Zarnani et al. 2015). It should be noted that a double acting RSF joint is comprised of two centre slotted plates and two cap plates (see Figure 1(a)). Refer to (Loo et al. 2012) for more information about the differences between the symmetric and asymmetric configurations for slip friction connections. The slip force (F_{slip}) can be determined by Equation 1.

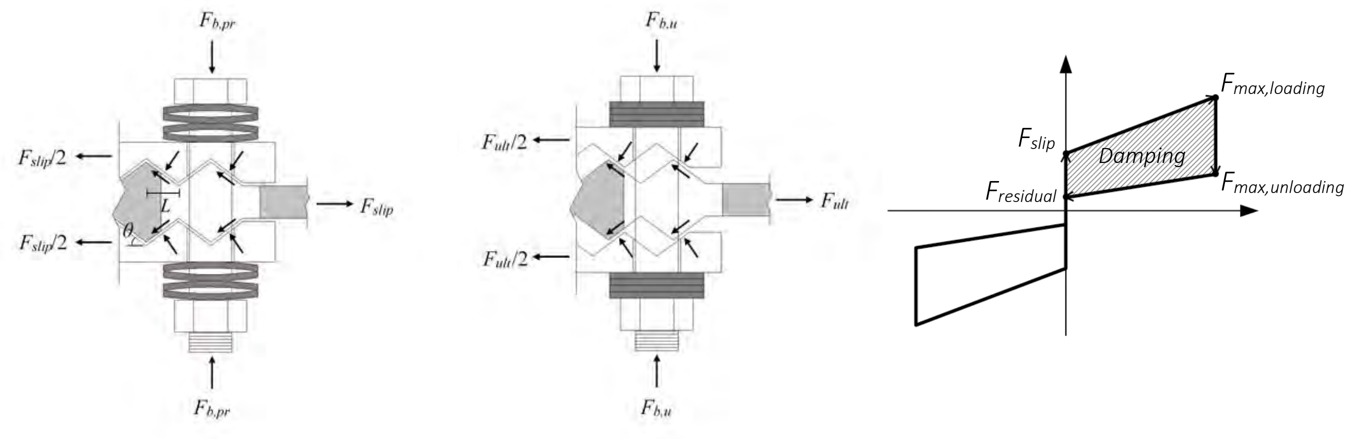

(a) (b) (c)

Figure 2. Schematic view of the symmetric RSF joint: a) Friction plates before slip b) Friction plates at ultimate deflection c) Schematic hysteretic loop

$$F_{slip} = 2n_b F_{b,pr} \left(\frac{\sin\theta + \mu_s \cos\theta}{\cos\theta - \mu_s \sin\theta}\right) \quad (1)$$

Where $F_{b,pr}$ is the clamping force in the bolts caused by the pre-stressing of the Belleville spring washers, n_b is the number of bolts, θ is the angle of the grooves and μ_s is the static coefficient of friction. Figure 2(c) shows the theoretical hysteretic loop for a RSF joint. The residual force in the joint at the end of the unloading can be determined by Equation 2 where μ_k is the kinetic coefficient of friction which can be assumed as $0.85\mu_s$.

$$F_{residual} = 2n_b F_{b,pr} \left(\frac{sin\theta - \mu_k cos\theta}{\cos\theta + \mu_k sin\theta}\right) \quad (2)$$

The ultimate force in loading ($F_{ult,loading}$) and unloading ($F_{ult,unloading}$) can be calculated by replacing μ_s and $F_{b,pr}$ in Equation 1 and Equation 2 with μ_k and $F_{b,u}$, respectively. The ultimate force in the bolts ($F_{b,u}$) can be determined by Equation 2 in which k_s and Δ_s are respectively the total stiffness of the of washers and their maximum deflection when they are fully compressed (the spring washers become flat).

$$F_{b,u} = F_{b,pr} + k_s \Delta_s \quad (3)$$

The maximum deflection in the joint can be calculated by Equation 4 where n_j is the number of joints acting in a series (e.g. n_j equals to 1 for a single acting joint and equals to 2 for a double acting one).

$$\delta_{\max} = n_j \frac{\Delta_s}{\tan\theta} \quad (4)$$

The joint possesses a self-centring characteristic providing that Equation 5 and Equation 6 are satisfied. In Equation 6, L represents the horizontal distance between the top and bottom of a groove.

$$\mu_s < \tan\theta \quad (5)$$

$$L > \frac{\Delta_s}{\sin\theta} \quad (6)$$

3 Experimental testing of a Rocking CLT wall with RSF joints

Experimental tests were conducted on a CLT wall with RSF joints as the hold-down connectors to study the hysteretic behaviour of the wall which represents the performance of the proposed concept in terms of ductility, stability and self-centring capacity.

3.1 The assembly of the RSF hold-downs

The two identical RSF joints used in the test are shown in Figure 3. The RSF hold-downs are implemented in the notches at the bottom corner of the CLT wall. They consist of two centre slotted plate and two cap plates. The cap plates were manufactured using mild steel grade 350 and the centre plates were fabricated with high-strength Bisplate 80 steel. The angle of the grooves was 15 degrees in order to maximize the deformation capacity of the joint. Two 220 mm by 50 mm mild steel stiffener plates had later been welded to the cap plates to reinforce them against out of plane bending.

(a) (b) (c)

Figure 3. The tested RSF hold-down: a) Cap plates and centre slotted plates b) Belleville washers c) Assembly

The RSF joints were designed and built to be able to accommodate a maximum displacement of 65 mm in tension and 15 mm in compression. This was because of the relatively larger displacement demand in tension in comparison to the one in compression in a hold-down connector. These displacement thresholds were determined based on the analytical prediction of the RSF joint behaviour.

3.2 Materials and the test rig

The quasi-static cyclic tests were carried out on a five layer CLT wall with a height of 6000 mm and a width of 2020 mm. The hydraulic actuator was connected to the wall at 3350 mm of height. The CLT panel has five 40 mm thick layers made of MSG8 timber (1999) (200 mm thickness in total). Figure 4 shows the general arrangement of the test setup. The loading protocol displayed in Figure 5(a) was applied to the top of the wall with a loading rate of 1.25 mm/sec. To prove the efficiency of this novel low damage solution, a maximum drift amplitude of 3% was targeted to match the typical design yield limit recommended by the different building codes in the world. Moreover, because of the fact that the conventional beam-column connections with plastic hinges and also the hold-down connections of the shear walls are subjected to severe damage at lateral drifts more that 2%, it was decided to aim for a 3% lateral drift to demonstrate the functionality of the proposed concept. However, if more than 100 mm top displacement (equals to 3% of lateral drift) is demanded by the designer, the RSF joints can be redesigned to meet the required maximum lateral drift.

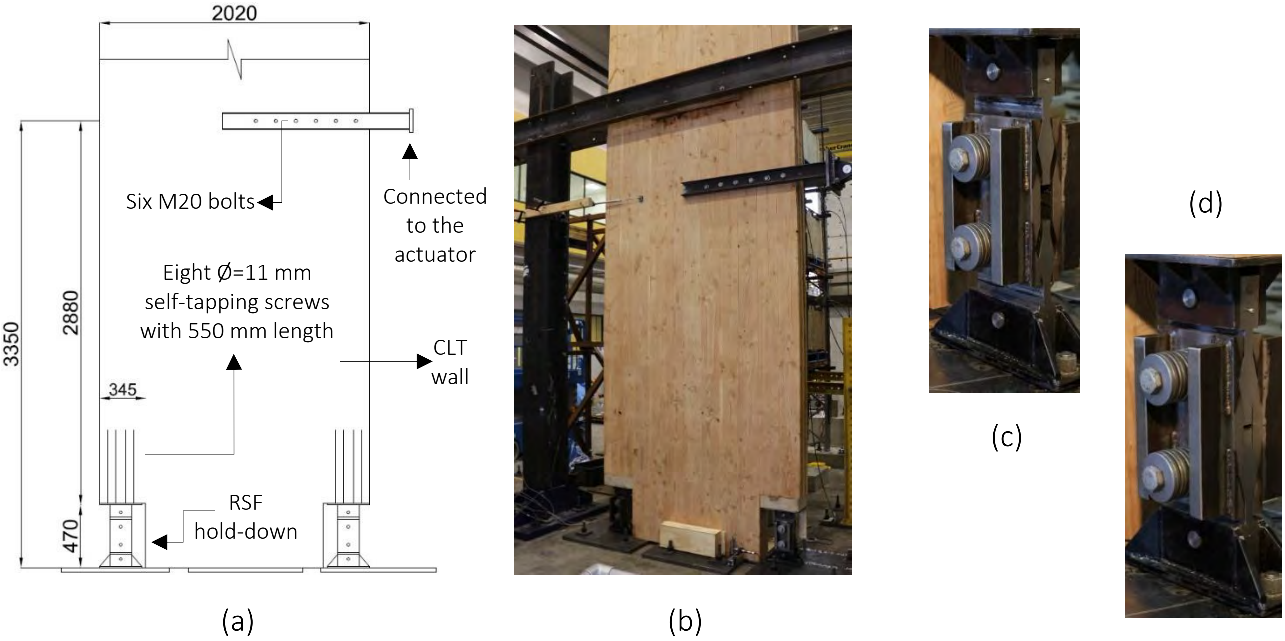

(a) (b)

Figure 4. Experimental testing of rocking CLT wall with RSF joints: a) schematic test setup (dimentions are in mm) b) Test Specimen c) RSF joint deformation in tension d) RSF joint deformation in compression

The authors carried out eight tests in total on the wall. No damage was observed to the wall with no evidence of deterioration in strength or stiffness of the RSF joints. Figure 5(b) shows the typical hysteresis for the wall. For the displayed test, the pre-stressing force was approximately 50% of the maximum force. The flag-shaped hysteresis in Figure 5(b) clearly demonstrates the self-centring behaviour of the tested wall. It should be pointed out that despite the fact that the only applied vertical load was the self-weight of the wall, the wall exhibited a self-centring behaviour. This shows that the self-centring capacity within the proposed concept is independent of the applied gravity loads. Figure 4(b) and 4(c) display the deformed shape of the RSF hold-downs in tension and compression, respectively.

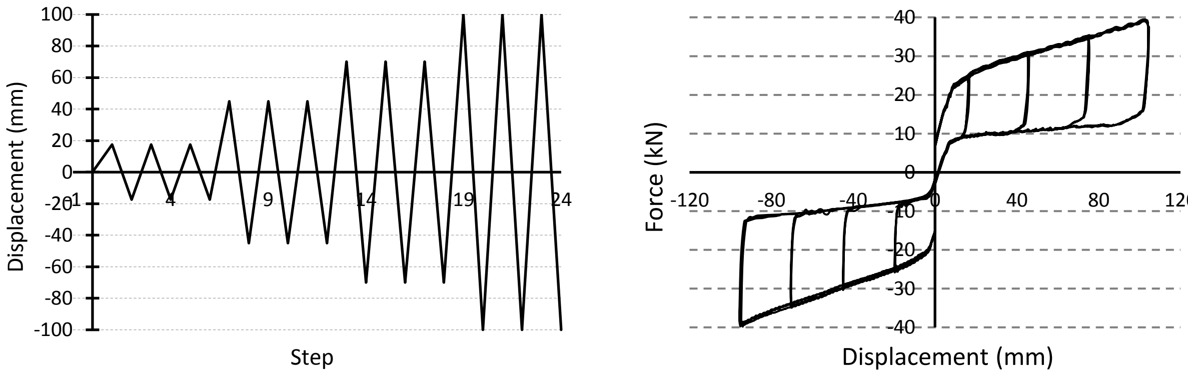

(a) (b)

Figure 5. Experimental results of the rocking CLT wall with RSF joint: a) Load regime b) Load-deformation response

4 Ductility of the timber walls with RSF joints

RSF joints applied to massive rigid timber walls (such as CLT walls), provides a flag-shaped elasto-plastic behaviour. The provided ductility is basically limited by the maximum displacement of the RSF joint. The maximum displacement has to be determined to provide a damage-free ductility during a ULS earthquake or even MCE.

For timber structures in general, the overall ductility (μ) is found by dividing the failure displacement (δ_{max}) by the yield displacement (δ_y). These definitions are displayed in Figure 6(a). For the walls with RSF joints, a similar approach can be adopted to define the total ductility. Figure 5(b) shows that the wall systems with RSF joints offer a damage free ductility zone. This zone is associated with the RSF joints undergoing sliding thereby capping forces below the limit indicated by the designer. The ductility can be defined as $\mu_{rsf}= \delta_{rsf}/ \delta_y$. The designer can decide on an appropriate value for μ_{rsf} corresponding to the relevant code recommendations for drift limits of ULS or MCE. It should be pointed out that the extra ductility (beyond the ductility that is provided by the RSF joints), depends on sufficient overstrength being provided by the other connections within the structures.

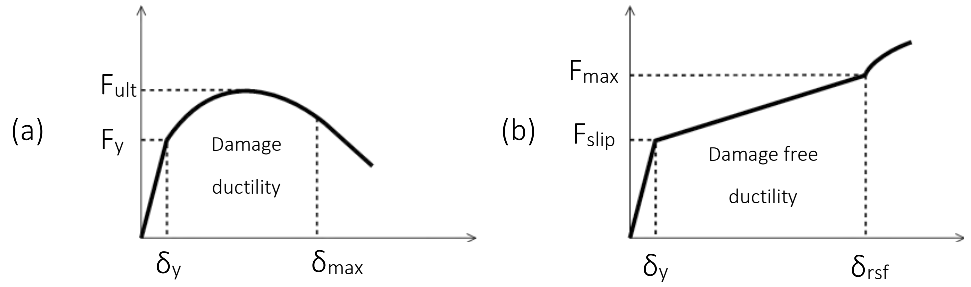

Figure 6. Defenisitons of the Wall strenght and ductility: a) Traditonal systems b) RSF joints

In view of a code application, higher q-factors compared to the recommended values by Eurocode 8 (2013) for seismic design of CLT buildings (q=2) should be allowed when RSF joints are used. This is because the adoption of RSF technology can improve the intrinsic ductility and also the cyclic behaviour of the jointed CLT buildings

5 Numerical modelling of the CLT coupled walls with RSF joints

5.1 The concept of the CLT coupled walls with RSF joints

The proposed system in this section is comprised of coupled CLT walls joined together by two types of RSF joints which are hold-down connections and ductile links. The RSF ductile links connects the CLT wall panels to adjacent walls and/or end steel columns. When two adjacent walls are connected together, the RSF hold-down connects each wall to the foundation. The general arrangement of the proposed concept is displayed in Figure 7. On the brink of rocking, the acting forces on the walls connected to the adjacent CLT wall are the RSF hold-down force (F_H), the sum of RSF ductile link forces ($\sum F_j$) and the vertical loads (W). The acting forces for the walls connected to the end columns are the sum of RSF ductile link forces ($\sum F_j$) and the vertical loads (W). It should be noted that this concept is mainly proposed for structural systems where the lateral load resisting system is separated from the gravity load resisting members. Thus, the only considered vertical load in this study is the self-weight of the CLT walls. However, the proposed system can also be used for structures that include load bearing walls.

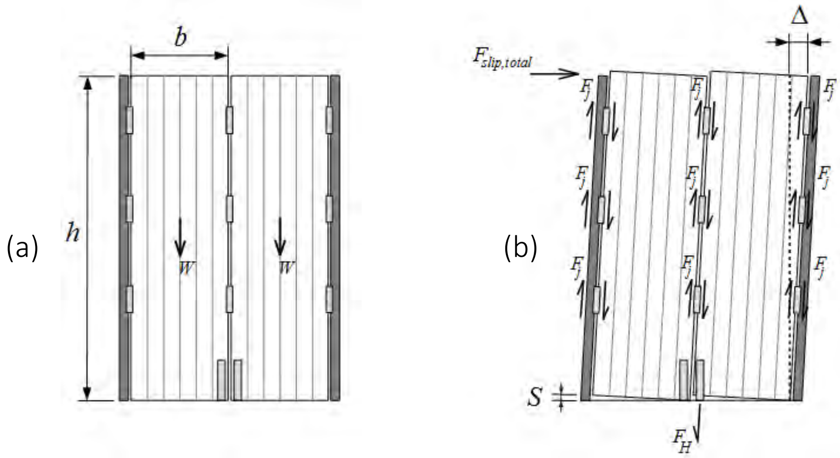

Figure 7. Coupled CLT walls with RSF joints: a) Before Rocking b) After Rocking (Note: Outside columns are restrained from any uplift)

Taking the moments about the rocking point of each wall, the total slip force (F_H + $\sum F_j$) can be determined by Equation 7.

$$F_H + \Sigma F_j = F_{slip}\frac{h}{b} - \frac{W}{2} \tag{7}$$

Where F_H is the slip force of the RSF hold-down, F_j is the slip force for the RSF ductile links, h is the height of the wall, b is the width of the wall, W is the self-weight of the wall and F_{slip} is the applied force at the top of the wall which triggers the slippage in the RSF joints. Note that $F_{slip,total}$ in Figure 7(b) is the applied horizontal slip force at the top of the coupled wall system. If the walls are identical, $F_{slip,total}$ is equally shared between them. However, if the walls within the system have different geometrical or material characteristics, $F_{slip,total}$ is proportional according to their lateral stiffness.

The RSF joints can be designed using Equation 7 considering the fact that for the adjacent walls with RSF hold-downs, the sum of the slip forces of the RSF ductile links has to be equal to the RSF hold-down slip force. Otherwise, the sliding would first initiate in the hold-downs and the walls might be locked together, cancelling the energy absorption potential in the inter-wall ductile links. The slot length for the RSF ductile links between the walls has to be twice that of the RSF hold-downs as they are designed to slide in both upward and downward directions while the hold-downs are intended to only move upward. Accordingly, the slot length for all hold-downs (*S*) and ductile links (*2S*) can be determined by Equation 8 with respect to the required lateral displacement (*Δ*) (see Figure 7(b)). If the walls have different geometry, the slot lengths for the connections within each one of them should be calculated separately.

$$S = \Delta * \frac{b}{h} \tag{8}$$

It should be noted that the RSF hold-downs are rigid connections before slippage. Therefore, the applied horizontal force at the top of the wall (F_{slip}) has to be controlled to not exceed the amount that causes tension failure at the base of the wall.

5.2 Cyclic behaviour of CLT coupled walls with RSF joints

In order to model the RSF joint load-displacement behaviour, the Damper–Friction spring Link element in the SAP2000 software package is adopted. This type of element has proven to be able to accurately represent the cyclic behaviour of a RSF joint providing that its parameters are properly calibrated in accordance with the design parameters of the RSF joint such as the slip force, loading stiffness, maximum loading force, maximum unloading force and the residual force (Hashemi et al. 2016).

The general arrangement of the coupled wall system to be studied under displacement-control cyclic loading using the SAP2000 software package is displayed in Figure 8. The system consists of two identical CLT walls with 8 m height and 2 m length. All of the timber boards within the panel (longitudinal and transverse layers) were assumed to have a thickness of 40 mm, a width of 183 mm and an elastic modulus of 12000 MPa (MSG12 timber along the board's main axis). The density of the timber was assumed as 540 kg/m3. The walls have a thickness of 200 mm. This system includes two 200*200*10 mm steel box columns at the ends assumed to be pinned to the base. The walls are connected to the adjoining panels and/or the adjacent steel columns by RSF ductile links. Furthermore, the walls are attached to the foundation where the two CLT panels are positioned next to each other.

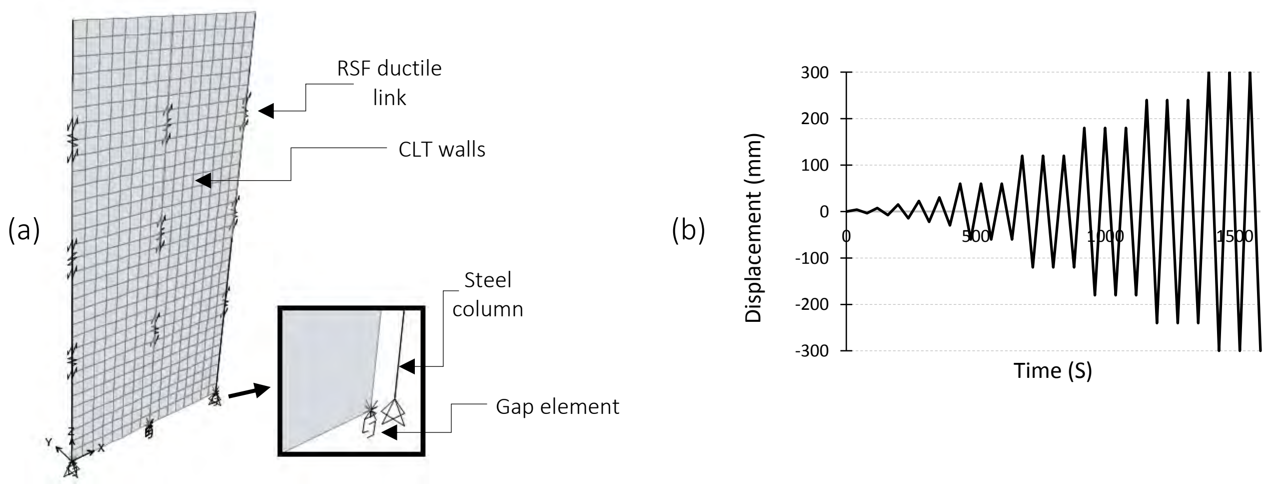

Figure 8. Numerical model of the CLT coupled walls with RSF joints: a) General arrangement b) Displacement-control load schedule

For this study, A 100 kN force applied at the top of the wall system is considered to represent the ULS earthquake force which the RSF joints are designed to resist to. The RSF joints are designed in accordance with the proposed design procedure in section 2 and also Equation 7. Considering a self-weight of 17 kN for each one of the walls, the maximum force for the RSF ductile links attached to the face of the steel columns is 130 kN, the maximum force for the RSF ductile links attached to the adjacent CLT wall is 65 kN and the maximum force for the RSF hold-downs is 195 kN. Note that three RSF ductile links are considered along the height of the walls. In this model, F_{slip} is considered as 50% of the maximum load in the joint ($F_{max,loading}$). Also, the CLT panel is modelled using layered shell element. The calculated design parameters are presented in Table 1. The displacement-control load schedule in Figure 8(a) is applied at the top of the system to evaluate the total load-deformation behaviour. The maximum displacement in the load schedule is 300 mm representing 3.75 % of lateral drift which is recommended by the New Zealand standard for MCE.

Table 1. Calibrated parameters for the numerical model of the RSF joints.

	Slipping stiffness (loading) (N/mm)	Slipping stiffness (Unloading) (N/mm)	Pre-compression displacement (mm)	Stop displacement (mm)
RSF hold-down	1300	281	-75	75
RSF ductile link attached the column	867	187	-75	75
RSF ductile link attached the wall	433	95	-75	75

Figure 9 shows the numerical response of the system under the applied cyclic load regime. It is observable that the RSF hold-downs and the RSF ductile links have a flag-shaped hysteretic behaviour. Figure 9(d) illustrates the total lateral response of the coupled wall system. It can be seen that the system exhibits a self-centring behaviour that can be attributed to the hysteretic behaviour of the RSF joints. It should be emphasized that the only considered vertical load in this model is the self-weight of the wall. This means that the self-centring behaviour of the proposed structural system does not rely on the gravity loads neither on the use of post-tensioned cables. Moreover, Figure 9 evidently demonstrates the low damage characteristic of the proposed system as the hysteretic behaviour remained stable after numerous cycles of loading and unloading. Hence, the bounded area between the hysteretic loops increases over time. This clearly represents a significant rate of energy dissipation which furthers confirms the potential to have a resilient low damage seismic solution. The damage free ductile zone is also observable in Figure 9 which can compared to Figure 6(b).

In this model, F_{slip} is considered as 50% of the maximum load in the joint ($F_{max,loading}$). However, for multi-story buildings, F_{slip} should be specified based on the Ultimate

Limit State (ULS) earthquake loads and the total stiffness of the Belleville washers that are exploited.

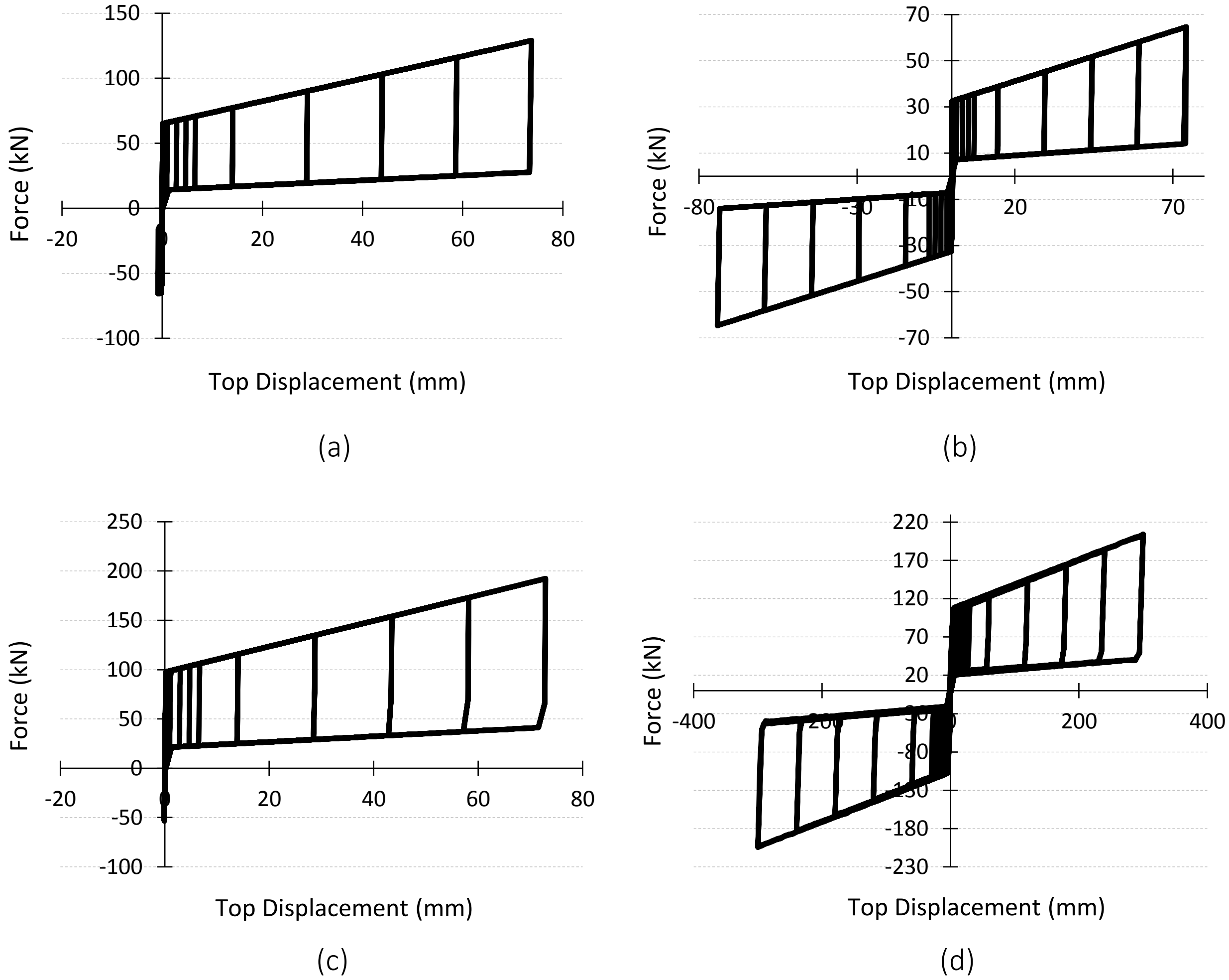

Figure 9. Numerically obtained hysteretic behaviour of the CLT coupled walls with RSF joints: a) RSF ductile link attached to the columns b) RSF ductile link attached to the CLT walls c) RSF hold-down d)Total system

5.3 Seismic performance of CLT coupled walls with RSF joints

In this section, the seismic response of the introduced coupled wall systems with RSF joints are presented. A seismic mass of 18000 kg are assigned to all of the walls in the model at two elevations up the height of the walls (top and middle). Four conventional time-history acceleration records were chosen for the earthquake loading. In accordance with NZS1170 (2002), each record was scaled to match the Christchurch 2500 year return period for MCE and 500 year return period for ULS. A type C soil (shallow soil site) was selected for ground motion scaling. Scale factors were determined with regards to a numerically obtained fundamental period of 0.47 seconds. The fundamental frequency was determined as 2.13 Hz. The scaled peak ground motions for both systems are presented in Table 2. The maximum horizontal displacements at the top of the system are shown in Figure 10. In accordance with

NZS1170.5, the maximum deformation limit of 2.5% (200 mm for this structure) is the reference upper bound applicable to the ULS (1/500 annual period of exceedance for ordinary structures) and a drift limit of 3.75% (300 mm for this structure) is recommended for MCE.

Table 2. Earthquake records and scaling.

Event	Year	PGA (g)	Scaled PGA (g) for ULS	Scaled PGA (g) for MCE
El-Centro	1940	0.31	0.25	0.46
Northridge	1994	0.23	0.28	0.48
Kobe	1995	0.82	0.27	0.55
Christchurch	2011	0.44	0.19	0.48

It is observable that the maximum displacements for all of the selected seismic events has not reached these limits. Moreover, no residual displacement was recorded in any of the time-history analyses demonstrating that the wall system is fully re-centred at the end of the earthquakes.

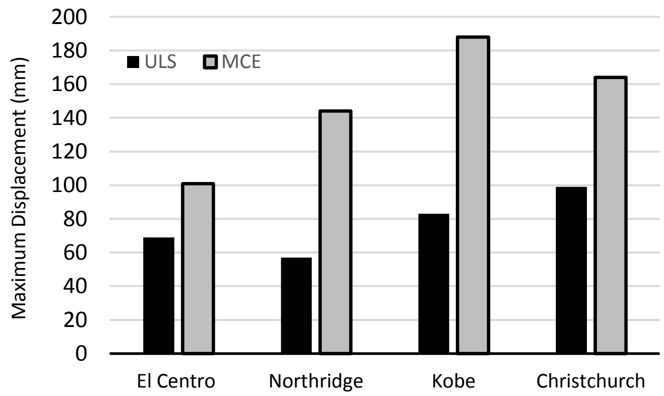

Figure 10. The maximum displacement at the top of the system subjecte to seismic loading

6 Conclusions

Experimental investigations on a rocking CLT wall with Resilient slip friction (RSF) joints as the hold-down connectors proved the feasibility of the concept and the wall demonstrated a stable flag-shaped hysteretic behaviour representing the self-centring characteristic. This is achieved considering the fact that the only applied gravity load was the self-weight of the CLT wall.

The adoption of the RSF joints as a substitute to the the traditional fasteners allows one to significantly improve the seismic response of the CLT rocking walls in terms of ductility and energy absorption capacity. RSF joints allow the available damage free ductility to be determined directly through the maximum displacements (slot lengths) corresponding to a particular lateral drift limit. A design procedure to predict the load-deformation behaviour of the new RSF joints has been introduced in this paper which could serve as a reference as it is validated by large scale experimental tests.

A concept for CLT coupled walls with RSF joints as the hold-down connectors and also as the ductile links between the panels and between the panels and the end steel columns is introduced and numerically simulated. Results confirm that the proposed wall system can be considered as a high ductility class system with respect to the fact that the designer can determine the ductility by specifying the RSF joints design parameters. Moreover, compared to traditional systems, the strength degradation and pinching effect are eliminated.

In view of a code implementation, a more generous behaviour factor (q) can be allowed when dissipative connections such as RSF joints are adopted in CLT buildings. It should be emphasized that the use of RSF joints with predictable and limited behaviour makes the capacity design approach more realistically affordable for design of timber structures.

7 References

A. Hashemi, P. Zarnani, A. Valadbeigi, R. Masoudnia, P. Quenneville. (2016). “Seismic resistant cross laminated timber structures using an innovative resilient friction damping system.” *Proceedings of New Zealand Society for Earthquake Engineering Conference (NZSEE), Christchurch, New Zealand*, Christchurch.

Buchanan, A. H., and Federation, N. Z. T. I. (1999). *Timber design guide*. New Zealand Timber Industry Federation.

Clifton, G. C., MacRae, G. A., Mackinven, H., Pampanin, S., and Butterworth, J. (2007). “Sliding hinge joints and subassemblies for steel moment frames.” *Palmerston North, New Zealand: Proc of New Zealand Society for Earthq Eng Conf*.

Eurocode 8. (2013). “Design of structures for earthquake resistance-part 1: general rules, seismic actions and rules for buildings.”

Filiatrault, A. (1990). “Analytical predictions of the seismic response of friction damped timber shear walls.” *Earthquake engineering & structural dynamics*, Wiley Online Library, 19(2), 259–273.

A. Hashemi, R. Masoudnia, P. Quenneville. (2016). “A Numerical Study of Coupled Timber Walls with Slip Friction Damping Devices.” *Construction and Building Materials*.

Loo, W. Y., Kun, C., Quenneville, P., and Chouw, N. (2014). “Experimental testing of a rocking timber shear wall with slip-friction connectors.” *Earthquake Engineering & Structural Dynamics*, Wiley Online Library, 43(11), 1621–1639.

Loo, W. Y., Quenneville, P., and Chouw, N. (2012). “A numerical study of the seismic behaviour of timber shear walls with slip-friction connectors.” *Engineering*

Structures, Elsevier, 34, 233–243.

Loo, W. Y., Quenneville, P., and Chouw, N. (2015). "Rocking Timber Structure with Slip-Friction Connectors Conceptualized As a Plastically Deformable Hinge within a Multistory Shear Wall." *Journal of Structural Engineering*, American Society of Civil Engineers, E4015010.

New Zealand Standard. (2002). "1170.1: 2002—structural design actions." *Wellington, New Zealand*.

P. Z arnani, P. Quenneville. (2015). "A Resilient Slip Friction Joint. " Provisional Patent no. 7083.

Popov, E. P., Grigorian, C. E., and Yang, T.-S. (1995). "Developments in seismic structural analysis and design." *Engineering structures*, Elsevier, 17(3), 187–197.

Discussion

The paper was presented by A Hashemi

A Ceccotti commented that in typical CLT system huge acceleration was observed and asked whether this system could reduce the acceleration. A Hashemi responded that this system could reduce acceleration by 80% as presented in the paper.

G Schickhofer stated the test was done in tension and asked what would happen in the case of shear loading. A Hashemi replied that work on this topic will be presented next year.

H Blass commented that this is a good system but asked why such long screws were used at 50 x the diameter. A Hashemi stated that these screws were available at the time and agreed that it was an overdesign and be optimized later.

M Yasumura asked whether such system would be applied to all the wall components in a building. A Hashemi replied probably not. M Yasumura stated that the effect of mixed system needs to be studied.

F Lam commented that low cycle fatigue behaviour of the screws needs to be considered; depending on the stress level they would probably not meet the high cycles cited in the paper. P Quenneville replied that it could be considered later.

T Reynolds and A Hashemi discussed lateral load's dependency on the mass. T Reynolds asked why a 6 m high wall was used with the loading point at mid height. A Hashemi replied the material was conveniently available at the lab.

Z Li stated that friction based devices had been evaluated in Tongji University and asked if these devices needed to be opened up after testing to allow restoration of position. A Hashemi replied that a special lubricant was used so that the device can restore to original position without needing to be opened up.

A stiffness-based approach to predict the fire behavior of Cross Laminated Timber floors

L. Franzoni - Laboratoire Navier IFSTTAR, CNRS, UPE – Ecole des Ponts ParisTech

D. Dhima - Centre Scientifique et Technique du Bâtiment (CSTB)

A. Lebée - Laboratoire Navier IFSTTAR, CNRS, UPE – Ecole des Ponts ParisTech

F. Lyon - Centre Scientifique et Technique du Bâtiment (CSTB)

G. Foret - Laboratoire Navier IFSTTAR, CNRS, UPE – Ecole des Ponts ParisTech

Keywords: Structural fire design, Reduced Cross-Section Method, CLT floors, Deflection, Fire tests, One-dimensional charring

1 Introduction

During last decades, the timber construction market has sharply increased, covering also modern residential and commercial buildings within the urban centers. This increase takes benefits from the parallel development of the new massive timber construction method based on Cross Laminated Timber (CLT) panels. These prefabricated thick panels are composed of lumber layers stacked crosswise and glued on their upper and lower faces. The orthogonal lay-up ensures more uniform mechanical and hygroscopic properties along both directions and allows the use of CLT as full-size floor, wall or roof element. The enhanced properties of CLT compared to solid wood make this product competitive with respect to traditional mineral-based construction materials (concrete, masonry) which have a higher environmental impact than wood (Piacenza et al, 2013).

The development of timber structures has to be followed by a progressive increase in knowledge about their fire safety. This is even more important when dealing with relatively recent products such as CLT panels. Indeed, the current version of EN 1995 1-2 (CEN, 2004) includes a fire design method for timber structures derived in the 80's and originally developed for simply supported Glued Laminated Timber (GLT) beams. Such design method, called the Reduced Cross Section Method (RCSM), was originally derived by Schaffer in the 80's (Schaffer, 1984) for GLT by means of simulations validated on available test results. The principle is to use normal properties of wood at ambient conditions combined with a reduced cross section of the timber member due to the fire exposure. The reduction of the cross section is defined with two steps: (i) a first reduction due to a uniform charring rate and (ii) an additional removal of a layer considered to have null mechanical properties (also called zero strength layer - ZSTL or d_0, as in the EN 1995 1-2) in order to take into account the reduced properties of wood in the region close to the char front (Figure 1.1).

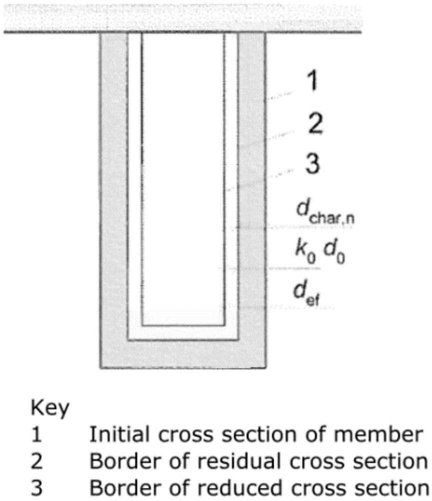

Figure 1.1 Principle of the Reduced Cross Section Method of EN 1995 1-2

The main advantage of the RCSM compared to more advanced calculation methods lies in using normal properties of wood instead of reduced properties. This hypothesis can be applied to timber structures for two main reasons: (i) wood has a very low thermal conductivity and (ii) charred wood protects the intact wood after the char front, acting as an insulating material. This makes simple the approach of the RCSM, which is therefore widely used in practical applications by engineers.

The zero strength layer was originally set to 0.3 inches for bending members (Schaffer, 1984). Subsequently, in EN 1995 1-2 has been reduced to 7 mm and the use for other members than those in bending is implicitly allowed. However, the thickness of the section affected by the thermal gradient depends on the type of the thermal action (ISO or natural fire exposure), the fire duration and the kind of stresses acting on the timber member (tension, compression or shear) (Schmid et al, 2015). Recent studies (Schmid et al, 2012, Schmid et al, 2014, Schmid et al, 2015, Lineham et al, 2016) showed that the predicted behavior of timber members exposed to fire using the RCSM is not always conservative, and the “exact” value of the zero strength layer is difficult to predict since it depends on a multitude of parameters like, for instance, the boundary conditions, the panel’s geometry and the kind of acting stresses. Furthermore, falling-off of layers can occur for the presence of glued interfaces between layers. Indeed, the presence of glue at CLT layers interfaces can influence the fire behavior because of the difference of mechanical properties at high temperatures between glue and timber. When the char front is not yet at the glued interface, the temperature gradient can decrease glue mechanical properties and therefore can lead to premature falling-off of layers and an increase in the charring rate. This phenomenon has been observed in CLT floors exposed to fire in (Frangi et al, 2009), and the proposed approach of EN 1995 1-2 for initially protected surfaces seemed to well reproduce this delamination phenomenon. However, other studies found very few falling-off of layers (Craft et al, 2011), (Osborne et al, 2012) or a falling-off phenomenon that has negligible influence on structural design compared to ambient design of CLT (Klippel et al, 2014). This discrepancy between test results derives from the multitude of parameters influencing the falling-off effect, like the type of glue, the presence of small gaps between boards of each layer, the glue thickness between layers, the panel's lay-up and so on.

Fire tests on loaded timber elements are useful to understand the actual thermal-mechanical behavior of the specimen, but they are expensive, time-consuming and sometimes it is not straightforward to obtain reliable information on the actual load-carrying capacity the specimen. This is also due to the fact that, in most of the cases, the test is stopped before the failure of the specimen for the safety of people and equipment. Therefore, the evolution of panel's deformation during fire exposure is the only information about the variation of mechanical properties during the fire test.

The aim of this paper is to use the measured deflections of three CLT floors exposed to ISO fire (conventional fire tests) for comparing different methods that can be applied for predicting the deflection. In this paper, two existing RCSM approaches, a more refined method and a new RCSM approach based on a zero stiffness layer (ZSSL) are compared.

Even if the existing RCSM approaches were originally derived for predicting the residual load-carrying capacity of timber members, it may be extended to the prediction of deflection, since the stiffness properties are also affected by the thermal gradient after the char front. Moreover, once the panel is designed on the basis of the exiting RCSM for the load-carrying capacity, it could be interesting to investigate about the corresponding deflection predicted using these methods.

First, the available experimental data of bending tests on fire exposed CLT floors is introduced. The subsequent section presents the advanced and simplified modeling in order to reproduce the experimental deflection. Then, the comparison between the predicted and experimental deflection of fire exposed CLT floors is presented. Finally, the results are discussed and the main conclusions are summarized.

2 Fire tests on CLT floors

2.1 Description of fire tests on CLT floors

Three CLT floors from three different producers have been tested in bending while exposed to ISO fire on their lower face in tension. The out-of-plane load remained constant during fire exposure and the panels were simply supported on two sides. Thermocouples were placed in several sections and over the thickness in order to measure the temperature profiles. The deflection was measured with LVDTs at panel mid-span and the displacement rate was constantly monitored. The end of tests was determined when reaching the safety criterion of (i) maximal displacement rate or (ii) when rupture occurred. Moreover, the fire test could also be stopped when reaching an established time of fire exposure without satisfying any safety criterion. Table 2.1 shows the main properties of the fire tests on CLT floors.

All panels were made of Norway spruce (*Picea abies*) lamellas of strength class C24 (CEN, 2009) and glued with one-component polyurethane glue. The panel-to-panel assembling was made with screwed LVL junction and protected with fire insulating joints that ensured the integrity during fire exposure. Suddenly after the end of fire test, the specimen was removed to fire exposure and the fire on its exposed side extinguished with water, which took approximately 6-8 min.

Table 2.1 Properties of the tested specimens of CLT floors

Test number:	1	2	3
Span L [m]	4.2	4.5	4.6
Thickness H [mm]	195	160	182
Total load [kN]	40	40	60
Kind of load	4-points	4-points	Uniform
Distance of point load from supports [m]	1.2	1.2	-
N° of sections with thermocouples	9	1	4
N° of thermocouples per section	9	4	10
Time exposure [min]	150	86	90
Safety criterion reached	Displacement rate	Failure	None

Figure 2.1 presents a typical residual cross section after removing the exceeding charcoal.

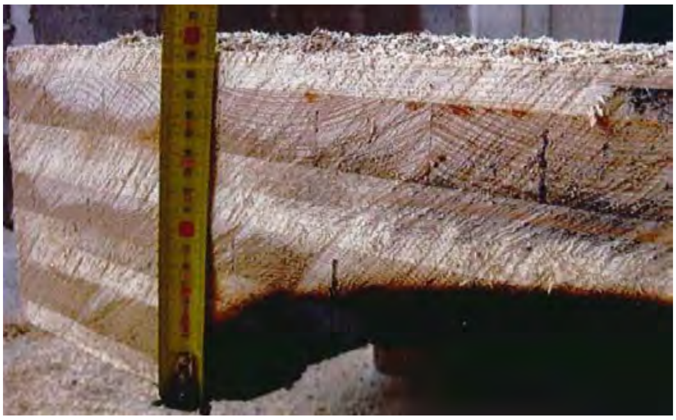

Figure 2.1 Residual cross section of the Test-1 floor

Figure 2.1 shows that there were no alteration of panels' supports geometry due to fire exposure, allowing therefore the hypothesis of respected simple supported boundary condition for the subsequent modeling step.

2.2 Temperature profiles

The temperature evolution within the panels during fire exposure has been measured by means of thermocouples along the cross section. Figure 2.2 presents the position of thermocouples over the thickness for the three tested floors and the directions of each layer. The shielded thermocouples were of type K with a diameter of 1.5mm, drilled inside the specimens by means of an appropriate driller that ensured the perfect straightness and placed in a bore hole having approximately 3mm diameter.

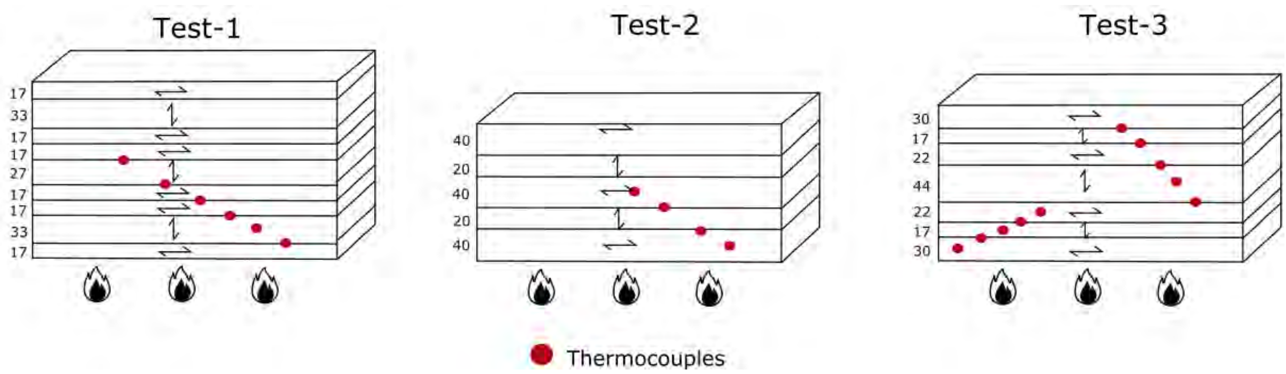

Figure 2.2 Position of thermocouples across the thickness of tested CLT floors. Dimensions in mm

Due to its high number of thermocouples (9 sections along the span and 9 thermocouples per section) and to the certainty of thermocouple position, Test-1 has the most certain documentation on temperature profiles over the CLT thickness. For this reason, in this paper are compared the measured and calculated temperatures only for the Test-1. Concerning the Test-2 and the Test-3 only the comparison of measured and predicted deflections are presented. In Figure 2.3 are plotted the registrations of Test-1 thermocouples placed at 84 mm from the bottom exposed side during the test.

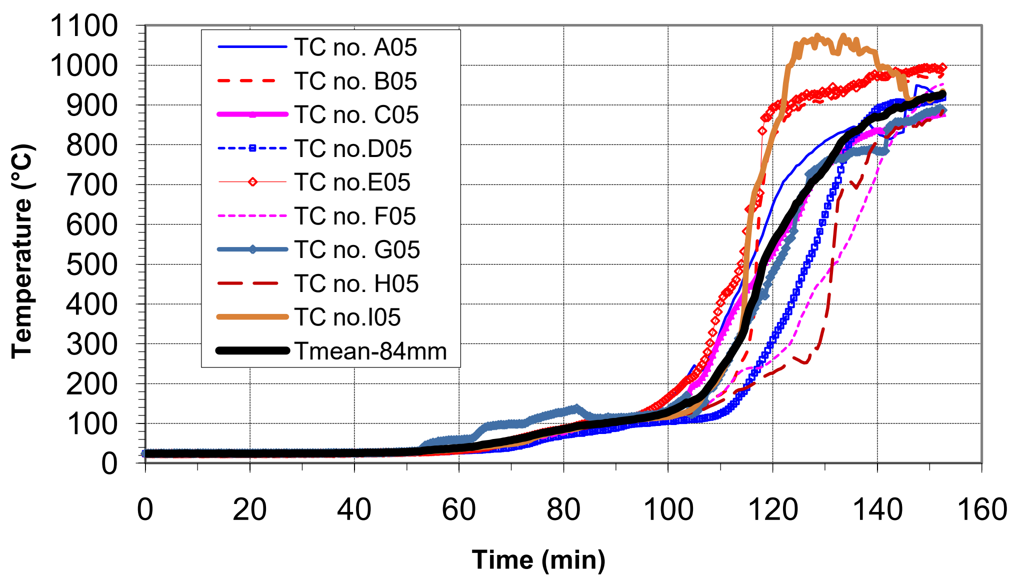

Figure 2.3 Evolution of the measured temperature in Test-1 at 84mm from the bottom side for each of the nine sections and considered mean temperature (solid black line)

The solid black line is the considered mean temperature at 84 mm thickness (between layers 4 and 5, see Figure 2.2) from the nine sections along the panel's span. The significant difference between measured temperatures from different sections derives from the local delamination of timber pieces that yields a local increase of temperatures.

2.3 Charring rates

Starting from the temperature profiles registered by the thermocouples during the test and assuming 300 °C to be the wood charring temperature, one can simply derive the average charring rates $\beta_{mean,i}$ over the CLT thickness. Table 2.2 presents the average computed charring rates for several layers of the three tests during the fire exposure, considering mean temperatures from the available sections. The numbering of layers follows the order of layers exposed to fire.

Table 2.2 Calculated charring rates of the three fire tests from mean measured temperatures. In green the nearly respected charring rate of solid wood according to EN 1995 1-2 (0.65mm/min) while the red gradient shows higher charring rates.

Test-1			Test-2			Test-3		
Layer	Depth [mm]	$\beta_{mean,i} [\frac{mm}{min}]$	Layer	Depth [mm]	$\beta_{mean,i} [\frac{mm}{min}]$	Layer	Depth [mm]	$\beta_{mean,i} [\frac{mm}{min}]$
1	17	0.67	1	40	0.70	1	30	0.61
1/2(2)	16.5	1.38	2	20	1.34	1/2(2)	8.5	1.70
2	33	0.81				2	17	1.15
3	17	0.77				1/2(3)	11	1.35
4	17	0.68				3	22	1.60

For the three tests, the great increase in the charring rate when passing from the first to the second layer clearly shows that a delamination of layers occurred. Moreover, the charring rate within layer 2, directly exposed to fire after the delamination of layer 1, is about the double of the previous charring rate, exactly as established by the design approach of initially protected surfaces of Eurocode 5. Concerning Test-1, the charring rate across interfaces of layers 2/3 and layers 3/4 nearly respected the charring rate of solid wood (0.65 mm/min in EN 1995 1-2) and therefore no significant delamination phenomena should have occurred.

Dealing with Test-2, it was not possible to estimate the charring rates for more than the second layer, due to the shortness of the fire test. Finally, the calculated charring rates for Test-3 highlighted possible delamination phenomena for more than the first layer, leading to a significant increase of mid-span deflection during this Test, as will be presented in the next paragraph. However, the lower certainty on temperature registration for Test-3 compared to Test-1 may somehow overestimate the estimated charring rates.

2.4 Evolution of deflection during fire tests

During the fire tests on loaded CLT floors, the mid-span, deflection was constantly measured by means of Linear Variable Displacement Transducers (LVDT) placed on the upper side in compression. Figure 2.4 plots the evolution of mid-span deflection during fire exposure of the three tested CLT.

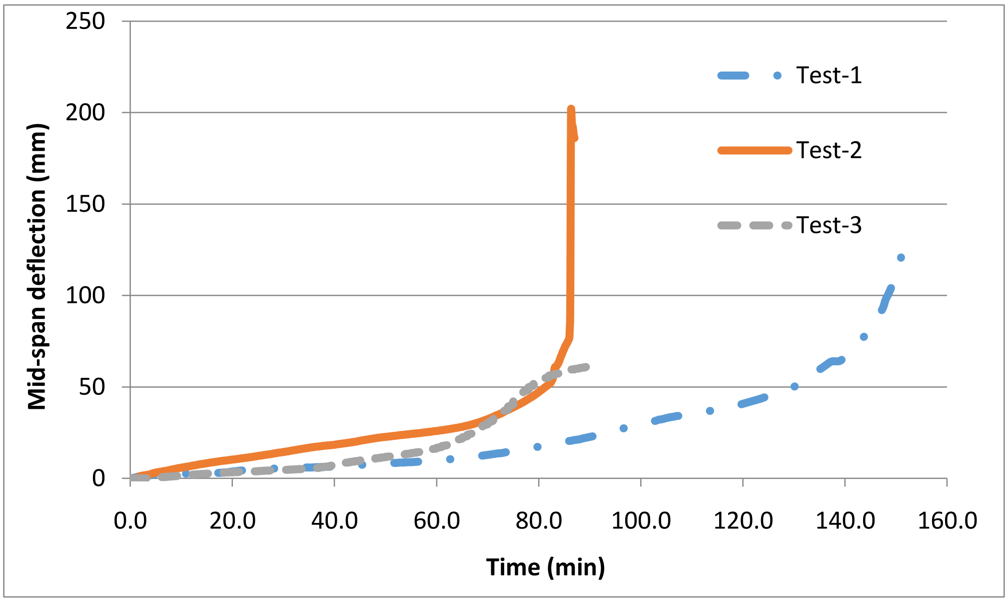

Figure 2.4 Evolution of the mid-span deflection during the three fire tests on CLT floors

Test-1 reached the safety criterion of maximum displacement rate at 150 minutes, highlighted by the acceleration of the increase of its mid-span displacement curve versus time. This means also that the specimen was close to the failure point at that time. The specimen of Test-2 failed on the tension side at 86 min, as the respective displacement curve shows. Finally, Test-3 was stopped after 90 minutes without reaching any safety criterion. The evolution of the mid-span deflection for Test-3 shows some acceleration at about one hour of fire exposure, with a subsequent smoother trend. The calculated charring rates highlighted possible delamination phenomena at this exposure time which can explain the increase in displacement rate. The evolution of Test-1 deflection shows a slight trend variation due to the progressive charring of layers with or without load-carrying capacity. On the contrary, the floor of Test-2 presents a nearly linear trend of deflection variation until the failure, since almost only the first thick longitudinal layer has been affected by the combustion.

3 Modeling

In this section the modeling procedure to reproduce the deflection of tested CLT floors is presented, as well as the design approaches based on the RCSM which will be compared. Two types of advanced modeling are implemented: heat transfer modeling and thermo-mechanical modeling. The heat transfer modeling is based on temperature prediction with SAFIR (SAFIR, 2011) software. Then, the mid-span deflection of the floor is predicted using the Bending-Gradient plate theory for thick plates (Lebée & Sab, 2011), combined with wood's reduced properties by the Eurocode's law (CEN, 2004).

3.1 Advanced modeling of heat transfer

The temperature evolution over the panels' thickness during fire exposure was predicted with SAFIR software. CLT panels were modeled as solid wood, with perfect connections between layers. The density of specimens was measured and values in accordance with the mean value of 420 Kg/m^3 specified in EN 338 (CEN, 2009) have been found. Preliminary analyses investigated on the value to use for moisture content, fitting the predicted temperature to thermocouples registrations for Test-1, leading to the value of 12%. The emissivity (ε) of the modeled wood was set to 0.8, while the coefficients of convection of heated (h_h) and unheated (h_c) surfaces were assumed to be respectively 25 W/m^{2}K and 4 W/m^{2}K. One dimensional uniform mesh of 1 mm was applied as a discretization over the panel thickness for the temperature prediction. Figure 3.1 plots the comparison between predicted and experimental temperature profiles during Test-1 across the specimen thickness.

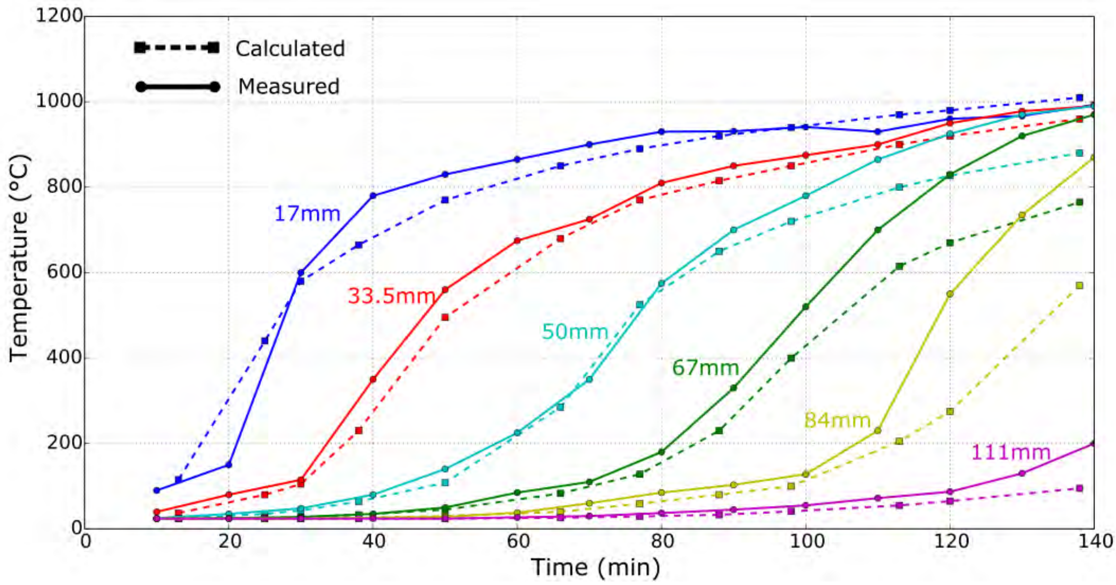

Figure 3.1 Evolution of the predicted and measured temperatures within the floor of Test-1

The falling-off of layer 1 of Test-1 pointed out in Table 2.2 probably leads to the sharp increase of the measured temperatures at 20 minutes at the interface between the first and the second layer (curve for 17mm) and at half-thickness of the second layer (curve for 33.5mm). Globally, the predicted temperatures are in good agreement with the measured values during the fire test. However, for high exposure times (at deep sections), the predicted temperatures are slightly lower than measured temperatures. This can be due to the heat transfer modeled neglecting any falling off of wood during fire exposure. Indeed, even if large detachment of the whole layers were not observed, the local falling of wood pieces was visible during testing and could lead to a progressive increase of measured temperatures.

3.2 Thermo-mechanical modeling

The thermo-mechanical behavior of CLT floors has been modeled with a “multilayer” model, with each layer having the mesh thickness of 1 mm. Wood is an orthotropic material with three principal axes and therefore its elastic behavior is defined by three Young’s moduli, three shear moduli and three Poisson’s ratios. However, since within timber boards of CLT is not possible to know the local orientation of wood axes, wood can be modeled as a transversely isotropic material (Franzoni et al, 2016a), (CEN, 2009) having only a longitudinal (*0*) and transverse (*90*) direction. Further analyses highlighted the negligible influence of Poisson’s ratios on the deflection prediction and therefore are set to zero. Since no characterization of the raw material has been done, the elastic moduli of wood according to strength class C24 of EN 338 (CEN, 2009) and a *rolling* shear modulus (G_{90}) of 50 MPa were considered (Table 3.1).

Table 3.1 Stiffness properties of C24 strength class timber according to EN 338 (2009)

Modulus of Elasticity	E_0	E_{90}	G_0	G_{90}
Stiffness [MPa]	11000	370	690	50

Once the temperature profile is established for each considered exposure time, the elastic moduli changed as a function of temperature using the reduction coefficient $k_{\theta,E}$ given by the EN 1995 1-2 (CEN, 2004) laws (Figure 3.2).

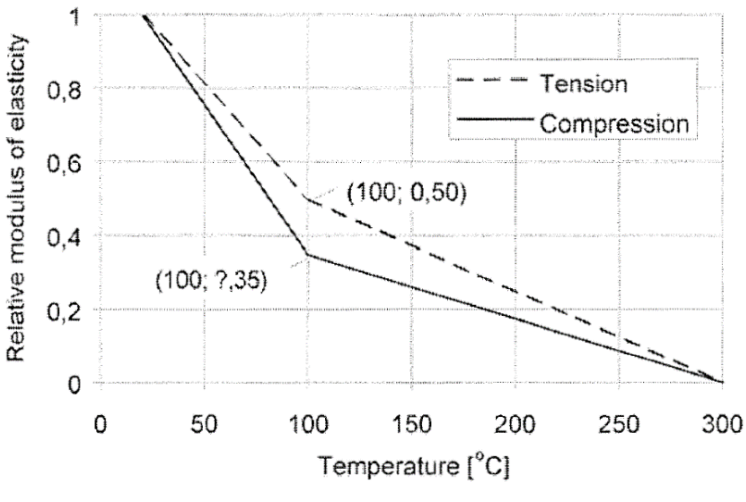

Figure 3.2 Effect of temperature on modulus of elasticity parallel to grain of softwood (Eurocode 5, 2004)

Different reductions of Young's modulus for the upper or lower part of the CLT floor, that work respectively in compression and in tension, have been taken into account. Since no reduction coefficient of the shear moduli has been given in the Eurocode, the same law as compressive Young's modulus has been adopted for them. Finally, with the reduced properties for each 1mm mesh, the mid-span deflection is computed with the Bending-Gradient plate theory for thick layered plates (Lebée & Sab, 2011). This theory is an extension to laminated plates of the Reissner-Mindlin theory for thick homogeneous plates. Contrary to the Kirchhoff-Love theory of thin plates, this theory consider non-negligible transverse shear deformation of the cross section, taking into account the shear compliance of the panel for the deflection prediction. Therefore transverse shear effects, which sometimes play a crucial role in CLT panels in bending, can be well predicted with this approach. The Bending-Gradient plate model has been recently applied to predict the mechanical behavior of regularly spaced CLT panels (Franzoni et al, 2016b) and the buckling of CLT (Perret et al, 2016). According to this method, the layers are homogenized with a semi-analytical procedure in order to obtain the equivalent out-of-plane bending and shear stiffnesses of the panel. This calculation is performed at each increment of exposure time in order to predict the evolution of mid-span deflection.

3.3 Reduced Cross Section modeling

Since recent studies pointed out that the current version of the RCSM is not always conservative, several attempts to improve the RCSM without changing its simple approach have been done. In the next paragraphs, three methods to determine the geometry of the effective cross section are presented. Once the effective geometry is established, properties at ambient conditions of C24 timber from EN 338 are combined with the plate theory in order to predict the mid-span deflection according to the RCSM.

3.3.1 Existing approaches

- **RCSM-1.** The first existing RCSM approach has been derived by (Schmid et al, 2012) fitting results of advanced numerical simulations on timber members in bending. According to this method, the charring rate is uniform as prescribed in EN 1995 1-2 (0.65 mm/min), while the ZSTL (d_0) is derived as a function of panel's total thickness and of the exposed side. Applying this approach to the three tested panels leads to the following values of d_0: Test-1 = 11 mm; Test-2 = 10.7 mm; Test-3 = 10.8 mm.
- **RCSM-2.** The second simplified design model (Frangi et al, 2009) is based on the initially protected surfaces approach of the Eurocode, in order to take into account the delamination phenomenon already discussed. Hence, a double charring rate (1.3 mm/min) is considered after the complete charring of each layer

(delamination moment), until the char depth exceeds 25 mm. Beyond these 25 mm of char depth, the charring rate returns at 0.65 mm/min. Within this method, the value of ZSTL (d_0) was not established; hence the value set by EN 1995 1-2 (7mm) is combined with RCSM-2.

3.3.2 New suggested RCSM approach

More than the two presented existing models, a new simplified approach based on the RCSM is suggested in this paper (RCSM-3). The principle is to define the reduced section of the floors taking into account the reduction factor for modulus of elasticity $k_{\theta,E}$. In other words, the basic idea is to calculate the reduced thickness of each discretized mesh by the advanced modeling as a function of the temperature calculated with Safir software. Then, for each fire exposure time, the zero stiffness layer (ZSSL) of the floor is the sum of all reduced thicknesses of meshes. Figure 3.3 presents the basic principle of the stiffness-based approach of RCSM-3

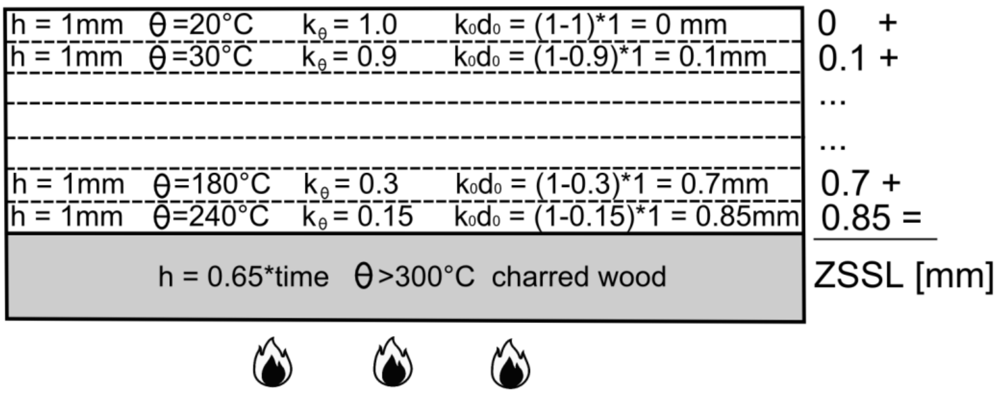

Figure 3.3 Principle of the suggested derivation of the zero stiffness layer. ϑ = temperature

The suggested derivation of the ZSSL is therefore based on the hypothesis that at established reduction of stiffness corresponds the same reduction of geometry (or "loss of material"). The studies of (Franzoni et al, 2016b) and (Franzoni et al, 2016c) showed that this hypothesis is valid when dealing with the bending deflection, without contribution of transverse shear. On the contrary, such hypothesis is not anymore valid concerning the transverse shear deflection. However, since the geometry and the lay-up of the considered panels yield a low contribution (in the range of 10%-12%) of transverse shear to the global deflection, this principle can be applied to the tested floors with a low margin of error. When plotting the estimated ZSSL for the three tests versus the exposure time, the plot of Figure 3.4 can be found. From Figure 3.4 it is clear that the ZSSL increases during exposure time, reaching values much higher than the constant 7 mm prescribed in EN 1995 1-2.

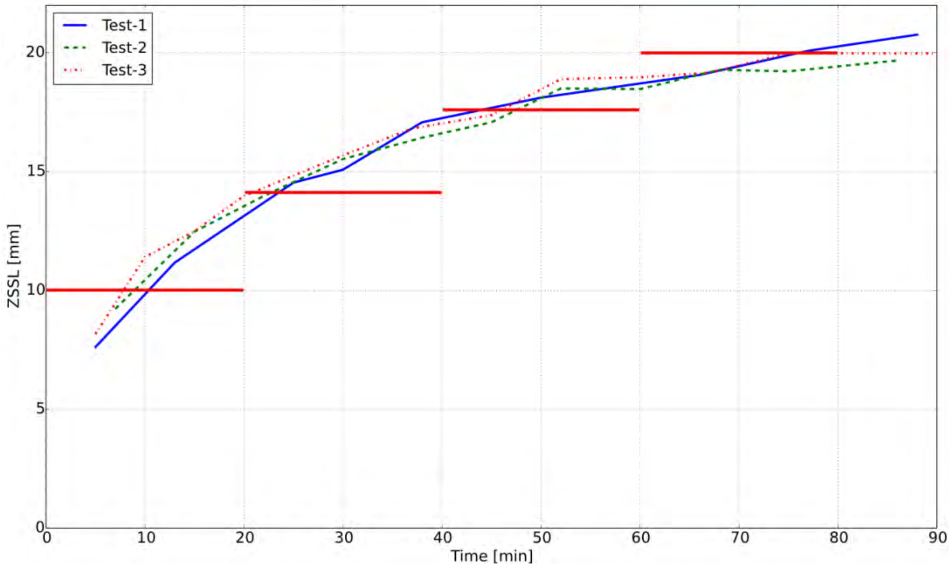

Figure 3.4 Variation of the ZSSL during time exposure for the three tests

On the basis of Figure 3.4, values of ZSSL as a function of time are therefore suggested, in order to take into account the increasing heat flux received by the CLT panel during fire exposure. Finally, a simplified design approach can be obtained setting four values of zero stiffness layer for four ranges of time as in Table 3.2. The slight differences between the estimated values of ZSSL presented in Figure 3.4, for the three tests, show that the four values suggested in Table 3.2 can be used for the new suggested RCSM.

Table 3.2 Suggested values of ZSSL as a function of time exposure

Time t (min)	0<t<20	20<t<40	40<t<60	> 60
ZSSL (mm)	10	14	17	20

4 Comparison of predicted deflection

The comparison between the experimental and predicted mid-span deflection by advanced and RCSM modeling are showed from Figure 4.1 to Figure 4.3. As already introduced, the RCSM-1 method is according to (Schmid et al, 2012), the RCSM-2 is according to (Frangi et al, 2009) and RCSM-3 considers the ZSSL as a function of time (Table 3.2). For the three approaches based on reduced cross section, the k_0 used for the calculation of ZSTL and ZSSL are computed as in EN 1995 1-2 (Figure 1.1).

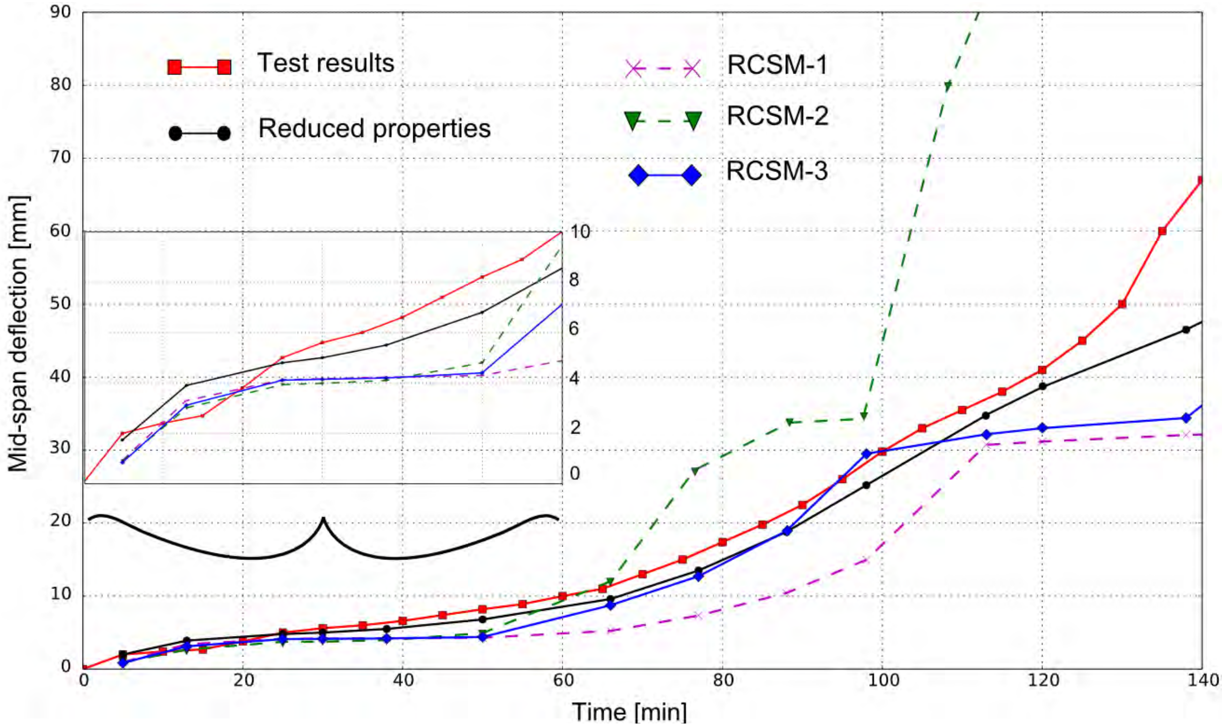

Figure 4.1 Comparison between predicted and experimental deflection of Test-1

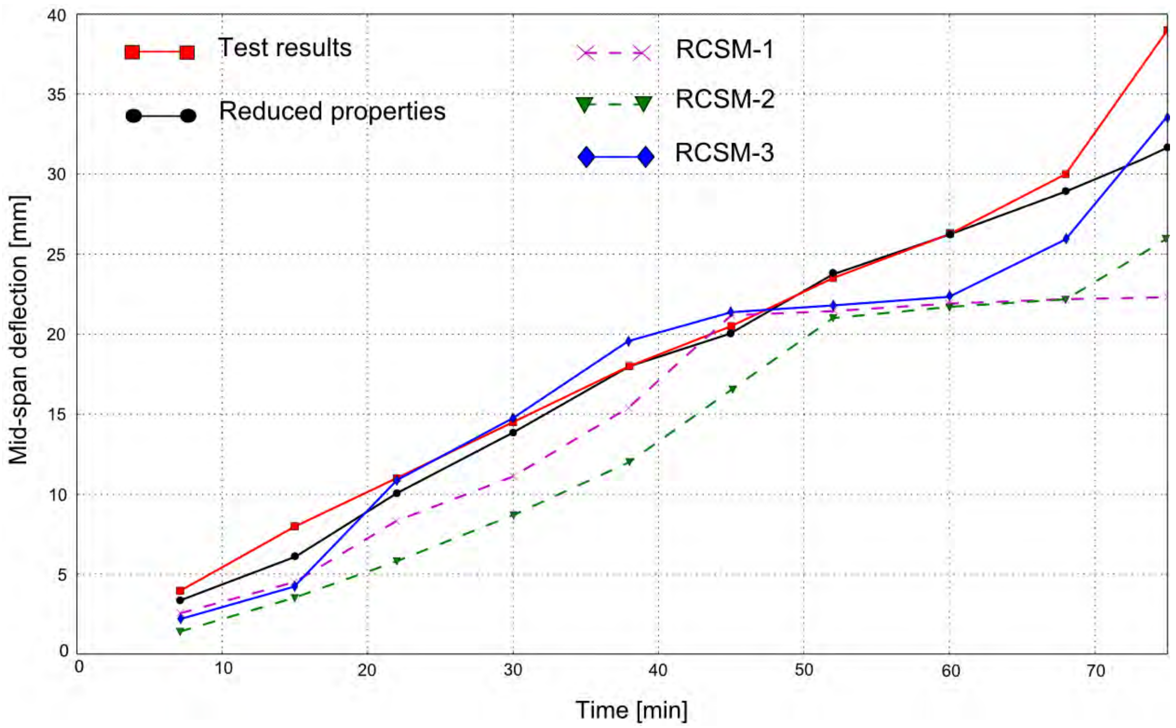

Figure 4.2 Comparison between predicted and experimental deflection of Test-2

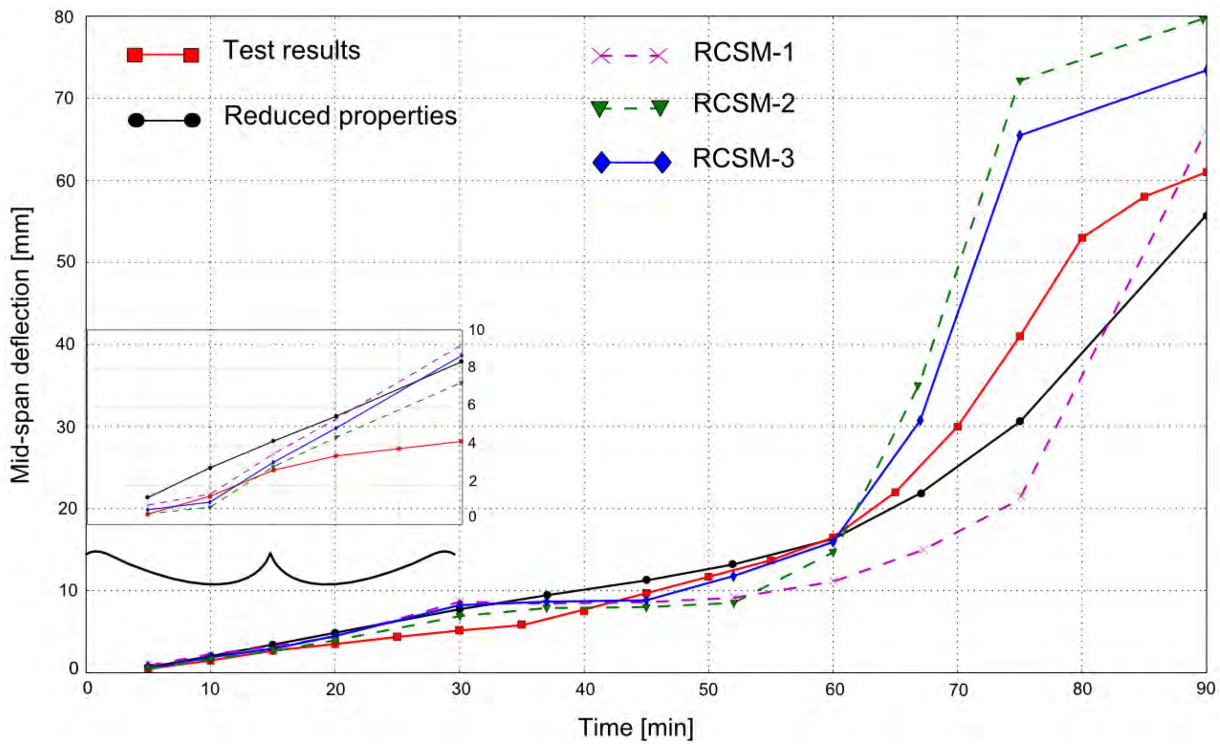

Figure 4.3 Comparison between predicted and experimental deflection of Test-3

The advanced modeling based on reduced properties returns the mid-span deflection that less deviates from experimental results for the three tests. The evolution of the deflection predicted by all RCSM methods shows plateau corresponding to the non-contribution of cross layers to global stiffness but not highlighted by test results. By contrast, the advanced modeling based on reduced stiffness is able to follow the experimental evolution of deflection, showing that the actual phenomenon is a progressive reduction of properties and not a reduction of geometry. The RCSM-3 based on the time-dependency of the ZSSL gives a better description of the measured deflection compared to other RCSM approaches. The RCSM-1 approach underestimates the deflection of the three fire tests. Despite of the delamination of the first layer in Test-1 previously highlighted, the RCSM-2 (derived to take into account such phenomenon) overestimates the Test-1 deflection. The deflection of Test-2 is underestimated by both existing RCSM approaches. Dealing with Test-3, all the RCSM methods show similar slope of the deflection evolution trend, but with an offset due to the different ways of estimating the residual cross section. Indeed, the double charring rate considered by RCSM-2 compensates somehow the higher values of the additional layer to remove of RCSM-3, while RCSM-1 predicts lower deflection since it considers lower values of d_0.

In the final parts of Figures 4.1 and 4.2, most of the methods underestimate the deflection. This is because both of specimens were close to failure at those high exposure times and hence the increasing non-linear contributions to deflection cannot be taken into account by the plate theory.

5 Discussion

The stiffness-based approach presented in this paper shows that, in most of the cases, the calculated deflections are in agreement with the measured deflections while the existing RCSM approaches globally deviate from test results. However, as is known, the existing RCSM approaches were originally derived for predicting the load-carrying capacity of timber elements, hence, the differences observed between measured and calculated deflections are understandable.

Consequently, in order to correctly model the fire behavior of CLT floors, it could be interesting to enhance the research in order to define the best method for the designs of these structural elements. Perhaps the method based on ZSSL suggested in this study could be interesting for CLT floors, but has to be further investigated for different configurations and different load levels.

Dealing with the sensitivity of predicted results, the predicted results can be affected by the variation of input material parameters. Unfortunately, the raw material of CLT has not been tested in ambient conditions and the input mechanical properties for the modeling are based on mean stiffnesses given by C24 strength class in EN 338. However, the model to predict the panel's mechanical behavior in ambient conditions implemented in this work (the plate theory) is based on linear elasticity, like common engineering methods. Hence, a given variation of wood stiffnesses yields the same variation of mechanical response. On the contrary, physical properties of the modeled material such as conductivity, relative humidity or volume specific heat can lead to significant variation of predicted temperatures and therefore even greater variation of the predicted mechanical behavior with the advanced modeling. More accuracy in determining the physical and mechanical properties of the raw material is therefore encouraged for future researches.

The delamination phenomenon is a complex mechanism influenced by a multitude of parameters and therefore very difficult to predict. It can occur locally, with delamination of small pieces of wood, or with a complete falling-off of layer. The charring rate estimation with thermocouples registration pointed out partial delamination phenomena for the three considered tests. In particular, the calculated charring rates of Test-3 pointed out delamination of more than the first layer. The same Test-3 showed an acceleration of mid-span deflection that may be due to such delamination phenomenon. On the contrary, the less pronounced delamination of Test-1 and Test-2 had no visible influence on the global evolution of deflection. This discrepancy confirms the complexity of this phenomenon and suggests enhancing the studies about the effective influence of delamination on structural fire safety of laminated timber structures. It seems that the existing RCSM-2 model can lead to quite conservative results in the cases without delamination and to better results in cases of delamination.

6 Conclusion

In the present paper, the experimental deflection of fire exposed CLT floors has been predicted with advanced modeling based on reduced properties and the simplified approach of the RCSM. The best way to correctly simulate the fire behavior of CLT floors is by means of an advanced modeling. However, the methods based on the RCSM approach are more convenient for practical applications by engineers. This is the reason why it would be interesting to find the best RCSM method for the calculation of deflection and perhaps the design of CLT in fire conditions.

The results presented in this paper show that RCSM-3 based on the time-dependency of the additional layer to remove could be a relevant method for simulating the fire behavior of CLT floors. The approach of the present paper is a research path which seems interesting to investigate, in order to define the relevant method for the fire design of CLT floors to be taken into account by the on-going revision process of EN 1995 1-2 (CEN, 2004). However, this method has to be further investigated for different configuration of floors and under different load conditions.

References

Craft, S., Desjardins, R., Mehaffey, J. (2011): Investigation of the behaviour of CLT panels exposed to fire. Fire and Materials

CEN (2004) EN 1995 1-2 Eurocode 5: Design of timber structures - Part 1-2: Structural fire design. CEN, Brussels

CEN (2009) EN 338 Structural timber: strength classes. CEN, Brussels

Frangi, A., Fontana, M., Hugi, E., Jobstl, R. (2009) Experimental analysis of cross laminated timber panels in fire. Fire safety Journal

Franzoni, L., Lebée, A., Lyon, F., Foret, G. (2016a) Influence of orientation and number of layers on the elastic response and failure modes on CLT floors: modeling and parameter studies. European Journal of Wood and Wood Products

Franzoni, L., Lebée, A., Lyon, F., Foret, G. (2016b) Bending behavior of regularly spaced CLT panels. World Conference on Timber Engineering, Vienna (AUT)

Franzoni, L., Lebée, A., Lyon, F., Foret, G. (2016c) Thick-plate modeling of regularly spaced Cross Laminated Timber panels (submitted)

Klippel, M., Leyder, C., Frangi, A., Fontana, M., Lam, F., Ceccotti, A. (2014) Fire tests on loaded Cross Laminated Timber wall and floor elements. 11th international symposium on Fire Safety Science

Lebée, A., Sab, K. (2011) a Bending-Gradient model for thick plates, Part I: theory. International Journal of Solids and Structures 48, 2878--2888

Lineham, S., Thomson, D., Bartlett, A., Bisby, L., Hadden, R. (2016). Structural response of fire exposed corss-laminated timber beams under sustained loads. Fire Safety Journal , 23-34.

Osborne, L., Dagenais, C., Bénichou, N. (2012): Preliminary CLT Fire Resistance Testing Report. Tech. rep., Advanced Building Systems – Serviceability and Fire Group, Point-Claire, Canada

Perret, O., Lebée, A., Douthe, C., Sab, K. (2016) The Bending-Gradient theory for the linear buckling of thick plates: applicaton to CLT panels. International Journal of Solids and Structures

Piacenza, J., Tumer, I., Seyedmahmoudi, S., Haapala, K., & Hoyle, C. (2013). Comparison of Sustainability Performance for Cross Laminated Timber and Concrete. 8th Design for Manufacturing and the Life Cycle Conference (p. 11). Portland, (USA): ASME

SAFIR (software), version 2011.b.3, ArGEnCo, University of Liege, 2011

Schmid, J., Konig, J., Just, A. (2012) The Reduced Cross Section Method for the design of timber structures exposed to fire – Background, Limitations and new Developments. Structural Engineering International

Schmid, J., Klippel, M., Just, A., Frangi, A. (2014) Review and analysis of fire resistance tests of timber members in bending, tension and compression with respect to the Reduced Cross Section Method. Fire Safety Journal

Schmid, J., Just, A., Klippel, M., Fragiacomo, M. (2015) The Reduced Cross Section Method for evaluation of the fire resistance of timber members: discussion and determination of the Zero-Strength layer. Fire Technology

Schaffer, EL (1984) Structural fire design: wood. US Dept of Agriculture, Madison WI

Discussion

The paper was presented by L Franzoni

A Frangi commented that he did not agree with the conclusion. He questioned why deflection should be calculated in a fire situation. L Franzoni replied that the paper presented a way to compare experimental data to model and it was not intended as an engineering approach. A Frangi commented that stiffness information would not be needed but only load carrying capacity information. He stated that König's work might not be considered accurately in this paper and Frangi's model was also not intended for calculation of deformations. Frangi suggested if the goal was to look at cases without delamination then one should test with melamine otherwise there would be too many parameters.

G Schickhofer also commented that the paper only considered PU and a general model should consider different adhesives.

Fire design of timber connections – assessment of current design rules and improvement proposals

Pedro Palma
Research Assistant,
ETH Zurich, Institute of Structural Engineering (IBK), Switzerland.
palma@ibk.baug.ethz.ch

Andrea Frangi
Professor,
ETH Zurich, Institute of Structural Engineering (IBK), Switzerland.
frangi@ibk.baug.ethz.ch

Keywords: *timber connections*, *fire resistance*, *design, EN1995-1-2*

1 Introduction and scope

The fire resistance of timber connections is one of the key aspects regarding the structural fire design of timber structures. This paper reviews the current design rules of EN 1995-1-2:2004 for timber connections in fire, taking into account the experimental research conducted before and after its publication in 2004. Some design rules are shown to give unsafe estimates of the fire resistance, while others give very conservative results. Shortcomings of current rules discussed and improvements are proposed.

2 Experimental background

According to König and Fontana (2001), some simplified rules on EN 1995-1-2:2004 are based on the test results of Norén (1996) and the reduced load method is based on the test results of Norén (1996), Dhima (1999), and (Ayme 2003). Since then, more fire resistance tests on timber connections have been conducted, namely by Fleischer et al. (2002), Scheer et al. (2004), Laplanche (2006), Lau (2006), Chuo (2007), Peng et al. (2012), and Palma et al. (2013). The number of tests and the connection typologies are presented in Table 2.1; only three-member timber-to-timber and steel-to-timber (with an internal steel plate) connections with laterally-loaded dowel-type fasteners were considered.

During the fire resistance tests, the connections were loaded in tension with a constant load and in mostly similar test conditions. A few remarks, however, should be made about some test series. In the tests by Fleischer et al. (2002), after the target fire resistance was reached (either 30 or 60 min), the load in the connections was increased until failure, unlike in the other tests, where the load wass kept constant until failure. In the tests by Peng et al. (2012), the connections were exposed to the ASTM E119 fire curve (prescribed by CAN/ULC-S101), which is different from the ISO 834 fire curve. Finally, the tests by Lau (2006) and Chuo (2007) were performed in an electrical furnace that was not able to follow the ISO 834 time-temper-

Table 2.1: Fire resistance tests on three-member symmetrical timber connections loaded in tension – number of tests for each connection typology.

Reference	Timber-to-timber			Steel-to-timber	
	Nails	Dowels	Bolts	Dowels	Bolts
Norén (1996)	32 [A]	-	-	-	-
Dhima (1999)	2	10	6	-	10
Ayme (2003)	-	-	-	9	-
Fleischer et al. (2002)	-	-	-	12	-
Scheer et al. (2004)	-	12	-	-	-
Laplanche (2006)	-	5	-	-	-
Lau (2006)	2	-	2	2	2
Chuo (2007)	-	-	2		2
Peng et al. (2012)	-	-	-	-	13
Palma et al. (2013)	-	-	-	2	-

[A] Despite what the great number of tests might suggest, only three different typologies were tested.

ature curve and the connections were assembled with laminated veneer lumber (LVL), as opposed to solid timber or glued laminated timber in all other tests.

3 Assessment of current design methods

3.1 Overview of design methods

The design rules in EN 1995-1-2:2004 apply mostly to symmetrical three-member connections with timber side members and laterally loaded fasteners, under standard fire exposure, and for fire resistances below 30 min (up to 60 min for protected connections). Two approaches are laid out for the designer: the *simplified rules*, in which the required fire resistance is attained by either increasing the dimensions of the side members or by protecting the connection with the addition of wood-based panels or gypsum plasterboards; and the r*educed load method*, in which the load-carrying capacity of the connections after a given fire exposure is estimated, based on the design effect of actions in the fire situation and the load-carrying capacity of the connection at normal temperature. According to König and Fontana (2001), many of the current design rules are based on the experimental research conducted by Norén (1996), Dhima (1999) and Ayme (2003).

3.2 Simplified rules

3.2.1 Unprotected timber-to-timber connections

The simplified rules for unprotected timber-to-timber connections assume that connections designed according to EN 1995-1-1:2004 satisfy a fire resistance of 15 min (nails, screws, bolts, and connectors) or 20 min (dowels), given that a minimum side member thickness is used. For connections with fasteners with non-projecting heads (nails, screws, and dowels), fire resistances greater than those assumed for connections with the minimum end and edge distances prescribed by the design at normal temperature (according to EN 1995-1-1:2004) can be achieved if the thickness of the side members t_1 and the end and edge distances of the fasteners, a_3 and a_4, respectively, are increased by a_{fi} (Equation 3.1 and Figure 3.1).

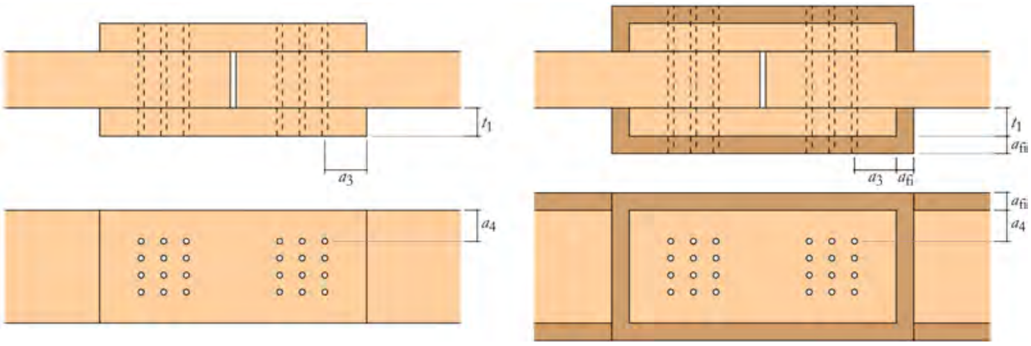

Figure 3.1: Simplified rules for unprotected timber-to-timber connections – extra thickness and extra end and edge distances.

(Equation 6.1 of EN 1995-1-2:2004)
$$a_{fi} = \beta_n \cdot k_{flux} \cdot (t_{req} - t_{fi}) \tag{3.1}$$

where β_n is the notional charring rate, k_{flux} = 1.5 is a coefficient to take into account the increased heat flux through the fasteners, t_{req} is the required fire resistance, and t_{fi} is the fire resistance of the unprotected connection ($t_{fi} = 15$ or 20 min, as mentioned above). According to König and Fontana (2001), this rule is based on Norén's (1996) tests with nailed timber-to-timber connections, which is why it is limited to fire resistances not exceeding 30 min. Further limitations of this rule are a minimum fastener diameter (for connections with nails and screws), and a minimum thickness (for connections with dowels). EN 1995-1-2:2004, however, does not establish a maximum load level in fire (ratio between the effect of actions for fire design and the resistance at normal temperature $\eta = E_{fi}/R_{20°C}$) up to which this rule is still applicable.

For timber-to-timber connections with nails, Figures 3.2a1-2 show that if the simplified method of Equation 3.1 is to always provide conservative results, a minimum side member thickness $t_{1,min} = 35$ mm and maximum load level $\eta \leq 0.3$ must be considered. For connections with dowels (Figures 3.2b1-2), if the same maximum load level is assumed ($\eta \leq 0.3$) this simplified method also provides conservative estimations of the fire resistance. For connections with dowels, the new experimental data (Scheer et al. 2004; Laplanche 2006) shows that the minimum thicknesses prescribed by the *Holz Brandschutz Handbuch* (Scheer and Peter 2009) (Figure 3.2b1) gives conservative estimates of the fire resistance for fire exposures up to 60 min.

In addition to an increase in the side member thickness, EN 1995-1-2:2004 stipulates that also the end and edge distances must be increased by a_{fi}, so that the required fire resistance is reached. Unlike with the increase in thickness, which clearly corresponds to an increase in fire resistance (Figures 3.2a2 and 3.2b2), the effect of the increase in end and edges distances is not so clear. Assuming the minimum end and edge distances prescribed by EN 1995-1-1:2004 for nailed and dowelled connections, the effect of extra end and edge distances on the fire resistance is presented in Figure 3.3. Regarding the extra end distance $a_{fi,a3}$, the available experimental data for nailed connections show that the required fire resistance is achieved with even with negative end distances (i.e. smaller than the minimum distance prescribed by EN 1995-1-1:2004). For dowelled connections, on the other hand, there seems to be a correspondence between an increase in the end distance and in the fire resistance. Regarding the extra edge distance $a_{fi,a4}$, for both nailed and dowelled connections, there does not seem to be a correspondence between an increase in the end distance and an increase in the fire resist-

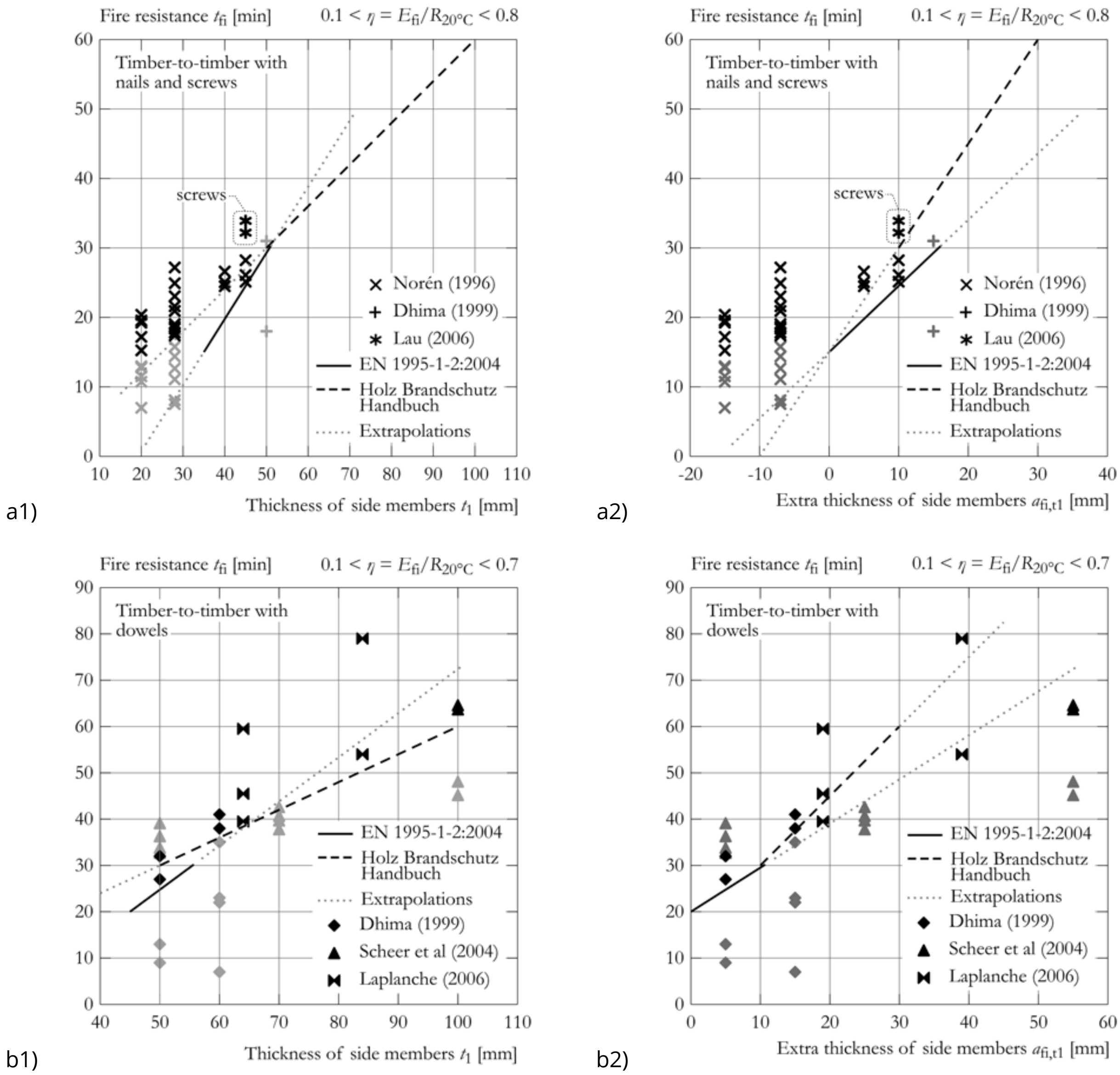

Figure 3.2: Experimental results and current simplified rules for timber-to-timber connections with nails (a) and dowels (b): a1/b1) fire resistance as a function of the side member thickness; a2/b2) fire resistance as a function of the extra thickness of the side member (assuming a minimum side member thickness $t_1 \geq 35$ mm for the nailed connections). Black markers represent tests performed with load levels $\eta \leq 0.3$ and grey markers tests performed with load levels $\eta > 0.3$.

ance (even though connections with more rows of fasteners seem to be less affected by the extra edge distance). It should be noted that the available experimental data does not allow analysing separately the effect of increased thickness, end, and edge distances. Therefore, the current approach of requiring all of these distances to be increased by a_{fi} might be adequate.

3.2.2 Connections with internal steel plates

The simplified rules for steel-to-timber connections with an internal steel plate prescribed by EN 1995-1-2:2004 are based on the width b_{st} and thickness t_s of the steel plate, and the gap depth d_g (Figure 3.4 and Table 3.1). The scope of these rules is not completely clear, as EN 1995-1-2:2004 is omissive about whether the rules are valid for both dowelled and bolted connections. As for timber-to-timber connections, there is no prescribed limit to the load level η.

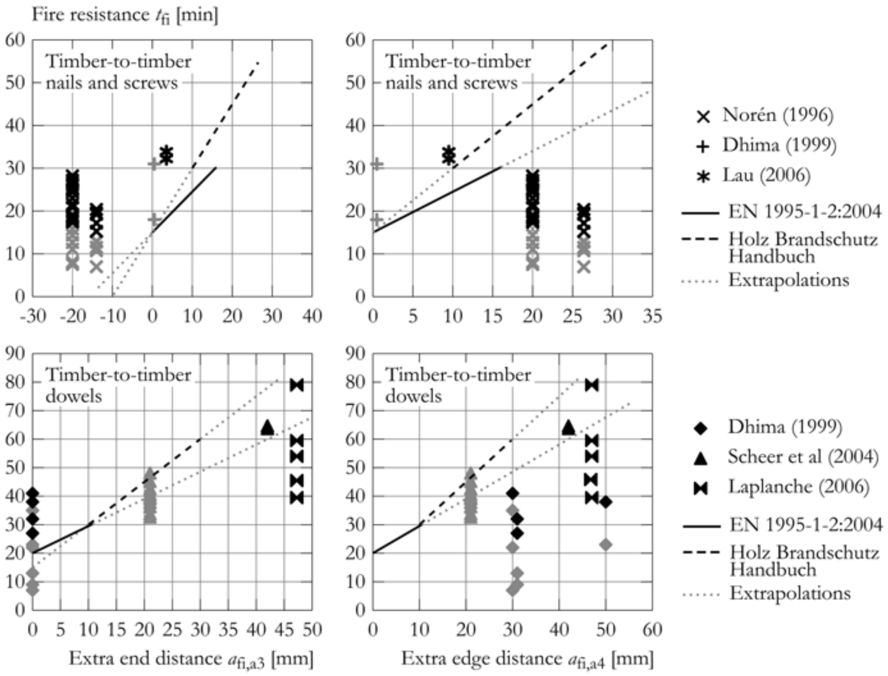

Figure 3.3: Influence of the extra end and edge distances on the fire resistance of nailed and dowelled connections (above and below, respectively). Black markers represent tests performed with load levels $\eta \leq 0.3$ and grey markers tests performed with load levels $\eta > 0.3$.

The prescribed minimum width of the steel plate for a fire resistance class R 60 is the same for plates with unprotected edges in general and for plates with unprotected edges on one or two sides ($b_{st} \geq 280$ mm), which seems to be a mistake. The *Holz Brandschutz Handbuch* (Kordina et al. 1995; Scheer and Peter 2009) prescribes $b_{st} \geq 400$ mm for the former case. Also, the scope of the provisions for steel plates with "protected edges" (without glued-in strips or protective wood-based boards) is limited to plates with rather small thicknesses $t_s \leq 3$ mm.

The comparison between the simplified rules and experimental results (Fleischer et al. 2002; Ayme 2003; Lau 2006; Chuo 2007; Peng et al. 2012; Palma et al. 2013) is presented in Figure 3.5. The collected experimental data only comprises symmetric three-member connections loaded in tension (as in Figure 3.4b), therefore with unprotected edges on one or two sides.

The connections with dowels ($d \geq 6$ mm) exhibited more than 30 min of fire resistance (Figure 3.5a1), regardless of the width of the steel plate and the gap depth. This might indicate that other parameters, such as the load ratio, could be more relevant for the fire resistance.

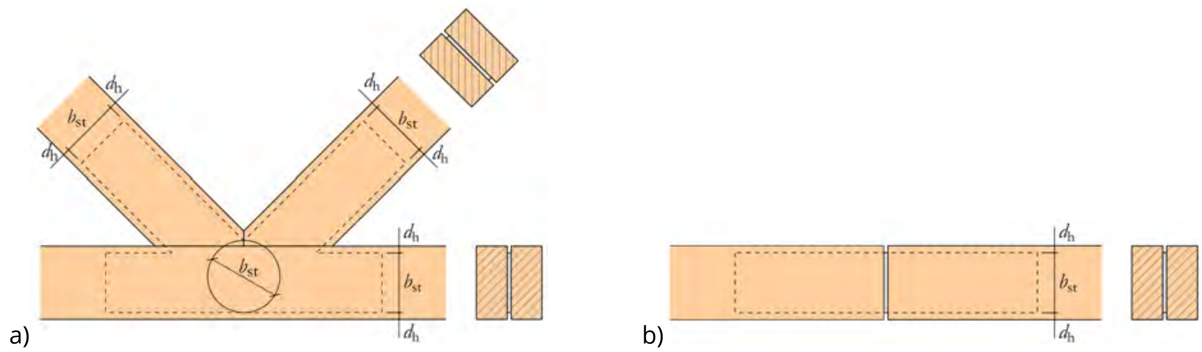

Figure 3.4: Steel-to-timber connections with an internal steel plate: a) plate with unprotected edges in general; b) plate with unprotected edges in one or two sides.

Table 3.1: Fire resistance classes of steel-to-timber connections with an internal steel plate, according to EN 1995-1-2:2004.

Steel plate[a]		Fire resistance class
Edges	Width	
Unprotected edges [A] in general	$b_{st} \geq 200$ mm	R 30
	$b_{st} \geq 280$ mm [C]	R 60
Unprotected edges [B] on one or two sides	$b_{st} \geq 120$ mm	R 30
	$b_{st} \geq 280$ mm	R 60

[A] The plate should be at least 2 mm thick and it should not project beyond the timber surface.
[B] If the steel plate is narrower than the timber member, its edges may be considered as protected if the thickness of the steel plate is $t_s \leq 3$ mm, and the gap depth is $d_g \geq 20$ mm for R 30 and $d_g \geq 60$ mm for R 60.
[C] This value seems to be a mistake: it is the same value as for steel plates with more protected edges; the *Holz Brandschutz Handbuch* (Kordina et al. 1995; Scheer and Peter 2009) prescribes $b_{st} \geq 400$ mm for this same case.

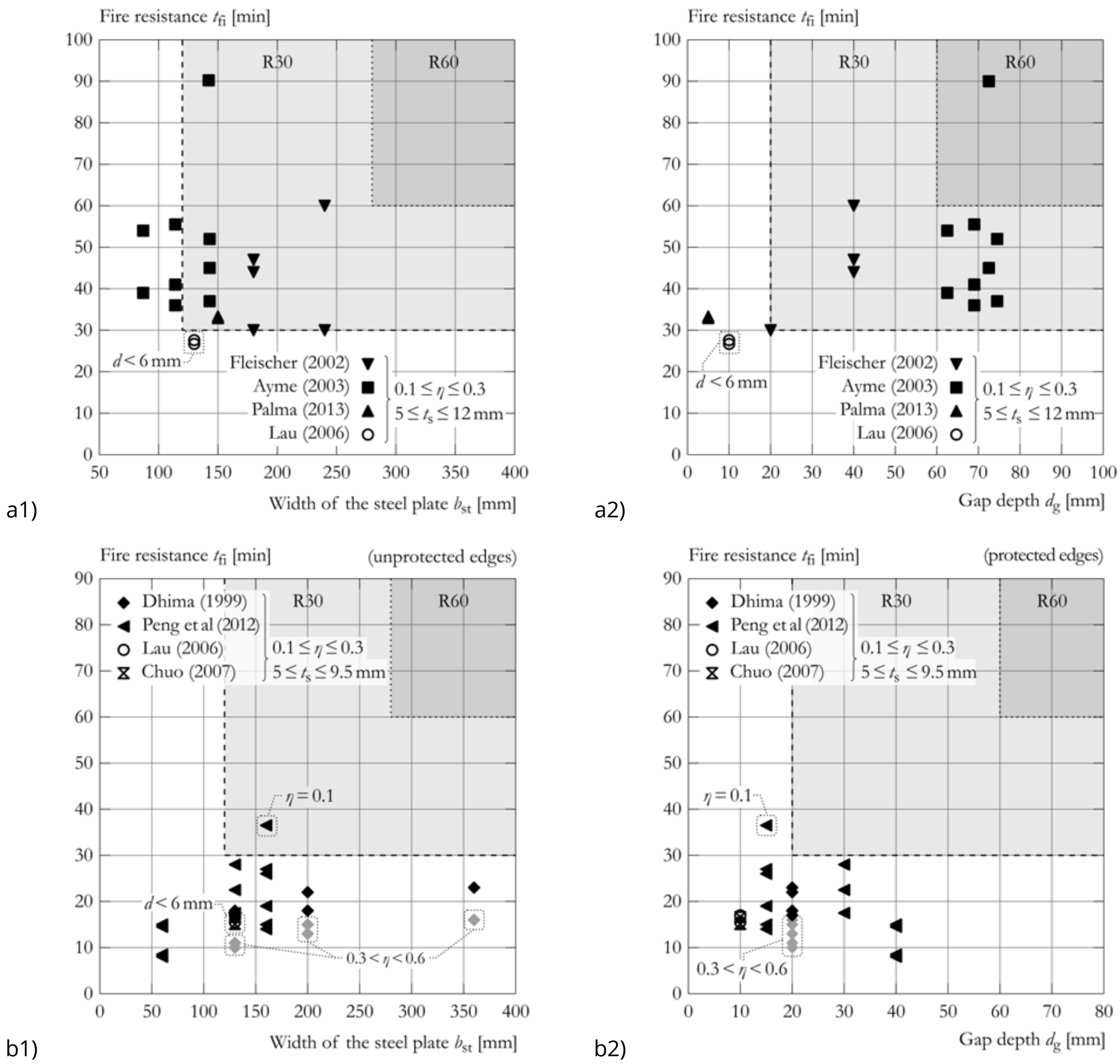

Figure 3.5: Experimental results and current simplified rules for dowelled (a) and bolted (b) steel-to-timber connections with an internal steel plate: a1-b1) fire resistance as a function of the width of the steel plate (minimum width of the steel plate for R 60 is likely to be $b_{st} \geq 400$ mm, instead of $b_{st} \geq 280$ mm); a2-b2) fire resistance as a function of the gap depth (rules for protected edges are only applicable for steel plates with a thickness $t_s \leq 3$ mm).

Regarding the fire resistance class R 60, since the experimental data does not comprise any connections meeting all the corresponding requirements ($b_{st} \geq 280$ mm, or $t_s \leq 3$ mm and $d_g \geq 60$ mm) it is not possible to assess their adequacy.

The connections with bolts did not reach 30 min of fire resistance (Figure 3.5b1-2) (except in one case with a low load level $\eta = 0.1$) and therefore the current rules should not be applicable to bolted connections.

3.3 Reduced load method

The *reduced load method* is based on a negative one-parameter exponential model fitted to the test results of Norén (1996), Dhima (1999) and Ayme (2003). The model gives the load-carrying capacity of the connection after a given fire exposure (verification of the fire resistance in the *strength domain*) or the fire resistance for a given load level (verification in the *time domain*). The method is applicable to nailed, bolted, and dowelled, timber-to-timber and steel-to-timber connections, for fire exposures up to 20-40 min.

3.3.1 Load-carrying capacity after a given period of fire exposure

According to section 6.2.2 of EN 1995-1-2:2004 (including the 2006 and 2009 corrigenda, EN 1995-1-2:2004/AC:2006 and EN 1995-1-2:2004/AC:2009), the characteristic load-carrying capacity of an unprotected connection, with fasteners in shear and side members of wood, after a given period of standard fire exposure should be calculated as

$$F_{v,Rk,fi} = e^{-k \cdot t_{d,fi}} \cdot F_{v,Rk} \tag{3.2}$$

where $F_{v,Rk}$ is the characteristic load-carrying capacity of the connection at normal temperature (calculated according to EN 1995-1-1:2004), k is a parameter describing the reduction of the load-carrying capacity for different connection typologies (Table 3.2 and Figure 3.6), and $t_{d,fi}$ is the design fire resistance of the unprotected connection.

The design load-carrying capacity is calculated based on the 20% fractile of the load-carrying capacity at normal temperature according to

$$F_{v,Rd,fi} = \frac{e^{-k \cdot t_{d,fi}} \cdot \overbrace{F_{v,Rk} \cdot k_{fi}}^{F_{v,20}}}{\gamma_{M,fi}} \tag{3.3}$$

where k_{fi} is a coefficient relating the 5% and the 20% fractiles of the load-carrying capacity at normal temperature ($F_{v,Rk}$ without the effect of load duration and moisture, i.e. $k_{mod} = 1$) (Table 3.3), and $\gamma_{M,fi} = 1.0$ is the recommended partial safety factor for timber in fire.

Table 3.2: Parameter *k*.

Connection with	*k*	Maximum period of validity for parameter *k* in an unprotected connection [min]
Nails and screws	0.08	20
Bolts wood-to-wood[A], with $d \geq 12$ mm	0.065	30
Bolts steel-to-wood[A], with $d \geq 12$ mm	0.085	30
Dowels wood-to-wood[A,B], with $d \geq 12$ mm	0.04	40
Dowels steel-to-wood[A,B], with $d \geq 12$ mm	0.085	30
Connectors in accordance with EN 912	0.065	30

[A] Minimum side member thickness $t_1 \geq \max\{50 \text{ mm}; 50+1.25\cdot(d\text{-}12)\}$, with d in mm)..
[B] The values for dowels are dependent on the presence of one bolt for every four dowels.

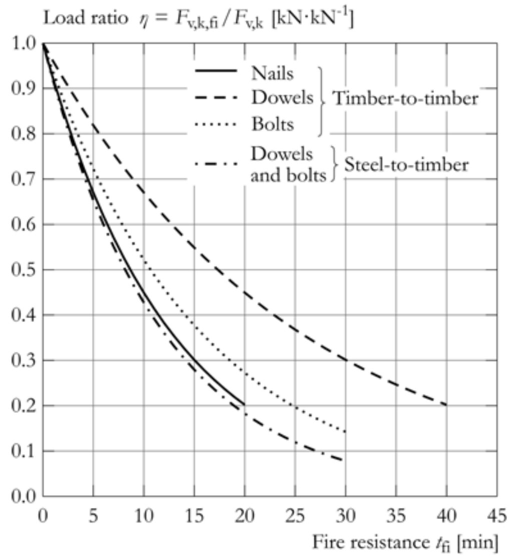

Figure 3.6: Reduction of the load-carrying capacity for different connection typologies, according to the reduced load method of EN 1995-1-2:2004.

Table 3.3: Values of k_{fi} (part of Table 2.1 of EN 1995-1-2:2004).

Connection type	k_{fi}
Connections with fasteners in shear and side members of wood	1.15
Connections with fasteners in shear and side members of steel	1.05
Connections with axially loaded fasteners	1.05

For consistency between EN 1995-1-1 and EN 1995-1-2, the load-carrying capacity of a connection should be denoted as $R_{(\dots)}$ instead of $F_{v,(\dots)}$, which in EN 1995-11:2004 represents the *load-carrying capacity per shear plane per fastener* and not the *load-carrying capacity of the connection*. This inconsistency with the symbols used in EN 1995-1-2 for the load-carrying capacity of a connection has misled several authors and designers.

3.3.2 Fire resistance of a connection loaded by the design effect of actions

According to EN 1995-1-2:2004/AC:2009, the design fire resistance $t_{d,fi}$ of an unprotected connection loaded by the design effect of the actions in the fire situation is

(Equation 6.7 of EN 1995-1-2:2004)
$$t_{d,fi} = -\frac{1}{k} \ln\left(\frac{\eta_{fi} \cdot \eta_0 \cdot \gamma_{M,fi} \cdot k_{mod}}{k_{fi} \cdot \gamma_M}\right) \tag{3.4}$$

where η_0 is the degree of utilisation at normal temperature (ratio between the design effect of the actions E_d and the design load carrying capacity R_d; $\eta_0 = 1.0$ is as a conservative simplification, as it assumes there is no overdesign at normal temperature), η_{fi} is the reduction factor for the load in the fire situation (ratio between the design effect of the actions in fire $E_{d,fi}$ and at normal temperature E_d; as a simplification, EN 1995-1-2:2004 (section 2.4.2) proposes $\eta_{fi} = 0.6$ or 0.7), k_{mod} is the modification factor from EN 1995-1-1:2004 (subclause 3.1.3), and γ_M is the partial factor for the resistance of connections (subclause 2.4.3 of EN 1995-1-1:2004). All the other symbols have already been presented.

Equation 3.4 is not directly obtained by rearranging Equation 3.3. It actually implies a few implicit assumptions that are not clearly stated in EN 1995-1-2:2004, which are shown in the following paragraphs.

According to EN 1995-1-2:2004, it shall be verified, for the required duration of fire exposure t, that

(Equation 2.7 of EN 1995-1-2:2004) $$E_{d,fi} \leq R_{d,t,fi} \tag{3.5}$$

where $E_{d,fi}$ is the design effect of actions for the fire situation and $R_{d,t,fi}$ is the corresponding design resistance in fire.

The design load-carrying capacity after a given period t of fire exposure $R_{d,t,fi}$ can be derived from the design load-carrying capacity at $t = 0$, i.e. at normal temperature, through the conversion factor $\eta = \eta(t)$.

(Equation 2.3 of EN 1995-1-2:2004) $$R_{d,t,fi} = \eta \underbrace{\frac{R_{20}}{\gamma_{M,fi}}}_{R_{d,t=0,fi}} = e^{-k \cdot t_{d,fi}} \frac{R_{20}}{\gamma_{M,fi}} \tag{3.6}$$

where R_{20} is the 20% fractile of the load-carrying capacity at normal temperature, and $\gamma_{M,fi}$ is the partial safety factor for timber in fire. The conversion factor η for unprotected timber connections with side members of wood is the negative one-parameter exponential model (Equation 3.2 and Figure 3.6).

From the previous equations, the fire resistance of a connection loaded by the design effect of actions $E_{d,fi}$ is

$$t_{d,fi} \leq -\frac{1}{k} \ln\left(\frac{E_{d,fi}}{\frac{R_{20}}{\gamma_{M,fi}}}\right) \tag{3.7}$$

and expanding R_{20} according to Equation 2.6 of EN 1995-1-2:2004, the fire resistance $t_{d,fi}$ of a connection loaded by the design effect of actions $E_{d,fi}$ becomes

$$t_{d,fi} \leq -\frac{1}{k} \ln\left(\frac{E_{d,fi}}{\frac{k_{fi} \cdot R_k}{\gamma_{M,fi}}}\right) \tag{3.8}$$

The previous formula is simply a rearrangement of Equation 3.3 (load-carrying capacity after a given period of fire exposure) for the *time domain* ($t_{fi,req} \leq t_{d,fi}$).

Current Equation 6.7 of EN 1995-1-2:2004 is a further simplification of Equation 3.8.

The design effect of actions for the fire situation $E_{d,fi}$ may be obtained, as a simplification, from the analysis for normal temperature as

(Equation 2.8 of EN 1995-1-2:2004) $$E_{d,fi} = \eta_{fi} \cdot E_d \tag{3.9}$$

where E_d is the design effect of actions for normal temperature and η_{fi} is the reduction factor for the design load in the fire situation[1].

1 As a simplification, EN 1995-1-2:2004 recommends $\eta_{fi} = 0.6$ or 0.7.

Consequently, Equation 3.8 becomes

$$t_{\mathrm{d,fi}} \leq -\frac{1}{k} \ln\left(\frac{\eta_{\mathrm{fi}} \cdot E_{\mathrm{d}}}{\frac{k_{\mathrm{fi}} \cdot R_{\mathrm{k}}}{\gamma_{\mathrm{M,fi}}}}\right) \tag{3.10}$$

Since the characteristic load-carrying capacity at normal temperature is

(Equation 2.17 of EN 1995-1-1:2004)
$$R_{\mathrm{d}} = k_{\mathrm{mod}} \frac{R_{\mathrm{k}}}{\gamma_{\mathrm{M}}} \;\Rightarrow\; R_{\mathrm{k}} = \gamma_{\mathrm{M}} \frac{R_{\mathrm{d}}}{k_{\mathrm{mod}}} \tag{3.11}$$

Equation 3.10 becomes

$$t_{\mathrm{d,fi}} \leq -\frac{1}{k} \ln\left(\frac{\eta_{\mathrm{fi}} \cdot \eta_0 \cdot E_{\mathrm{d}}}{\frac{k_{\mathrm{fi}} \cdot \gamma_{\mathrm{M}} \frac{R_{\mathrm{d}}}{k_{\mathrm{mod}}}}{\gamma_{\mathrm{M,fi}}}}\right) \tag{3.12}$$

Finally, given that the ratio between the design effect of the actions E_{d} and the design load-carrying capacity R_{d} is the degree of utilisation[2] η_0 is

$$\eta_0 = \frac{E_{\mathrm{d}}}{R_{\mathrm{d}}} \tag{3.13}$$

Equation 3.12 finally becomes

(Equation 6.7 of EN 1995-1-2:2004)
$$t_{\mathrm{d,fi}} \leq -\frac{1}{k} \ln\left(\frac{\eta_{\mathrm{fi}} \cdot \eta_0 \cdot \gamma_{\mathrm{M,fi}} \cdot k_{\mathrm{mod}}}{k_{\mathrm{fi}} \cdot \gamma_{\mathrm{M}}}\right) \tag{3.14}$$

which is what is currently given in EN 1995-1-2:2004/AC:2009, even though the underlying assumptions are not clearly stated. In a preliminary stage, Equation 3.14 can be useful to get a conservative estimate of the fire resistance, given a design scenario for normal temperature, but it is not equivalent to Equation 3.3.

4 Improvement proposals

4.1 Simplified rules

The scope of the simplified rules for unprotected timber-to-timber connections should be limited to a maximum load level $\eta \leq 0.3$. For nailed connections, if the simplified method is to always provide conservative estimates of the fire resistance, either a minimum side member thickness $t_1 \geq 35$ mm and the current $k_{\mathrm{flux}} = 1.5$ value should be prescribed, or a thinner side member thickness and a higher k_{flux} (e.g. $t_1 \geq 28$ mm and $k_{\mathrm{flux}} = 2.4$). For dowelled connections, it is proposed to maintain the current minimum side member thickness $t_1 \geq 45$ mm, change $k_{\mathrm{flux}} = 1.5$ to $k_{\mathrm{flux}} = 1.9$, and extend the maximum fire resistance from 30 to 60 min. The rules for connections with internal steel plates should be limited to connections with dowels and to a maximum load level $\eta \leq 0.3$. Further tests/simulations should be performed to study the influence of geometric parameters on the fire resistance.

2 The degree of utilisation is $\eta_0 = 1.0$ for optimal design.

4.2 Reduced load method

A simple way to improve the reduced load method would be to make the parameter k dependent not only on the connection typology, as it is now, but also on the thickness of the timber side members t_1. For timber-to-timber connections with nails, Figure 4.1a shows negative one-parameter exponential models fitted to subsets of experimental data with the same side member thickness and the corresponding regression parameters k_{t1}. As it can be observed, there is a clear influence of the side member thickness in the decay rate of the exponential model. The high correlation between the side member thickness t_1 and the regression parameter k is shown in Figure 4.1b, where it can also be seen that a simple linear model can be used to describe the relationship between these two variables.

Therefore, the load-carrying capacity of a connection after a given period of fire exposure R_{fi} would be

$$R_{fi} = e^{-k \cdot t_{fi}} \cdot R_{20°C} \tag{4.1}$$

where $R_{20°C}$ is the load-carrying capacity at normal temperature, and the exponential decay constant k is

$$k = k(t_1) = c_1 + c_2 \cdot t_1 \tag{4.2}$$

where c_1 and c_2 are specific parameters for each connection typology, and t_1 is the thickness of the timber side members.

The parameters c_1 and c_2 for each connection typology (Table 4.1) were obtained by fitting a negative one-parameter exponential model to data subsets comprising experiments with the same side member thickness, therefore obtaining an exponential decay constant k for each side member thickness t_1 (Figure 4.1a). A simple linear model was then fitted to the obtained decay constants and corresponding side members thicknesses (Figure 4.1b), using a weighted least squares method (since the various observations of k are not equally reliable, because there are more results available for some thicknesses than for others).

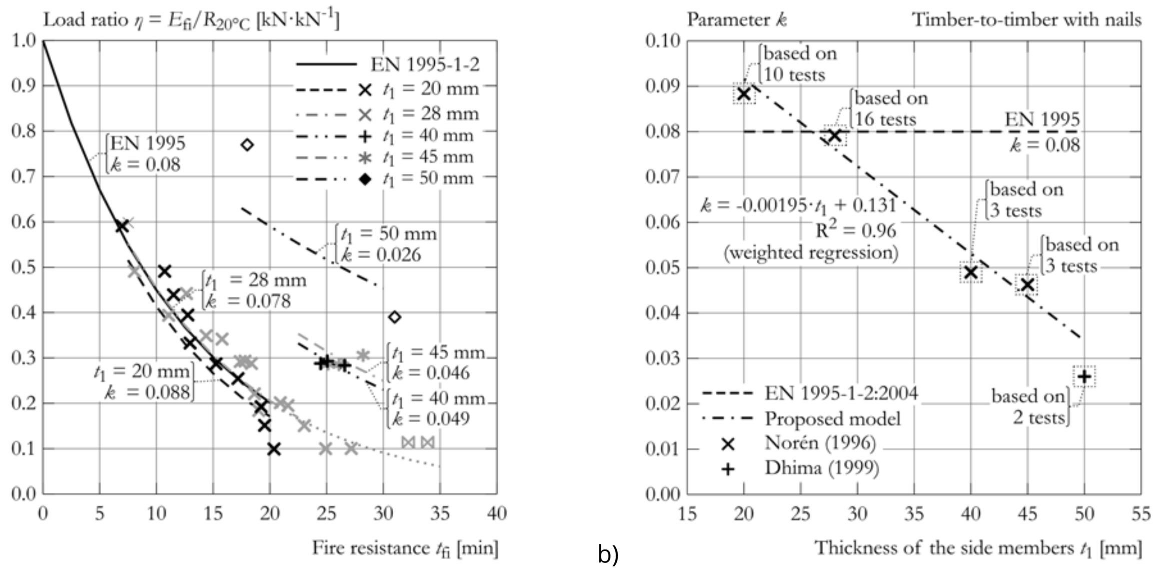

a) b)

Figure 4.1: Timber-to-timber connections with nails: a) negative one-parameter exponential models fitted to subsets of experimental data with the same side member thickness; b) correlation between the parameter k and the side member thickness.

Table 4.1: Proposed parameters k, minimum requirements, and maximum fire resistances for unprotected connections.

Connection		Requirements	Parameter k	Maximum fire resistance [min]
Nails and screws	Timber-to-timber	$t_1 \geq 20$ mm $d \geq 2.8$ mm	$0.1308\text{-}0.00195 \cdot t_1$	$\min\{13.3 + 0.33 \cdot t_1; 30\}$
Bolts	Timber-to-timber	$t_1 \geq 45$ mm $d \geq 12$ mm	$0.0717\text{-}0.00039 \cdot t_1$	$\min\{-10.0 + 0.67 \cdot t_1; 30\}$
	Steel-to-timber	$t_1 \geq 38$ mm $d \geq 12$ mm	$0.2089\text{-}0.00218 \cdot t_1$	$\min\{1.4 + 0.36 \cdot t_1; 30\}$
Dowels	Timber-to-timber	$t_1 \geq 50$ mm $d \geq 12$ mm	$0.0447\text{-}0.00026 \cdot t_1$	$\min\{20.0 + 0.40 \cdot t_1; 60\}$
	Steel-to-timber	$t_1 \geq 75$ mm $d \geq 12$ mm	$0.0711\text{-}0.00039 \cdot t_1$	$\min\{-15.9 + 0.61 \cdot t_1; 60\}$

To restrict the scope of the proposed approach to the underlying experimental data, minimum fastener diameters and side member thicknesses, and maximum fire resistances that can be reached are set for each connection typology (Table 4.1).

The comparison between the proposed method and the current EN 1995-1-2:2004 approach is presented in Figure 6.1, where it can be observed that the proposed method gives better estimates of the load-carrying capacity in fire (lower sum of squared residuals $\Sigma\varepsilon^2$).

5 Conclusions

Current design rules of EN 1995-1-2:2004 for timber connections in fire were compared to available experimental results.

The scope of the *simplified rules* for timber-to-timber connections should be better defined, namely regarding minimum side member thicknesses t_1 and maximum load levels η, and the maximum fire resistance of dowelled connections can be increased from 30 to 60 min. As for steel-to-timber connections, their scope should exclude bolted connections, but even for dowelled connections the influence of the design parameters (width of the steel plate b_{st} and gap depth d_g) on the fire resistance could not be clearly assessed.

The currently called *reduced load method* does not take into account the influence of the side member thickness, which is one of the most relevant parameters regarding the fire resistance of timber connections. The proposed improvements to this method allow to greatly improve the estimated load-carrying capacity of timber connections in fire.

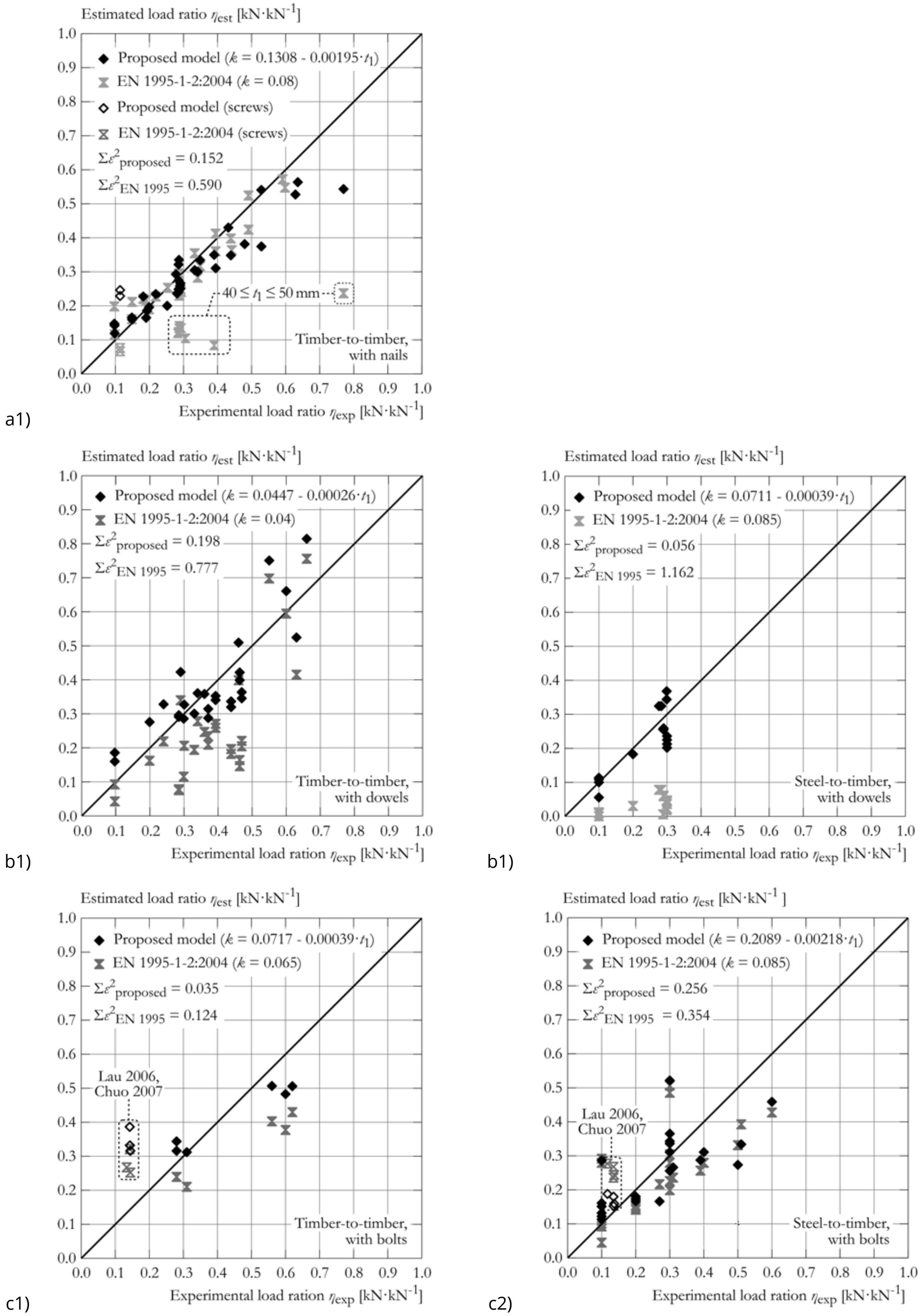

Figure 6.1: Comparison between the proposed method and the current EN 1995-1-2 approach : a1) nailed timber-to-timber connections; b1) dowelled timber-to-timber connections ; b2) dowelled steel-to-timber connections ; c1) bolted timber-to-timber connections ; c2) bolted steel-to-timber connections.

6 References

ASTM E119 - 12a. *Standard Test Methods for Fire Tests of Building Construction and Materials*. (2012). ASTM International, 34.

Ayme, N. (2003). *Rapport du comportement au feu d'assemblages bois – Assemblages bois-métal en double cisaillement*. CTICM, France.

CAN/ULC-S101-07. *Standard methods of fire endurance tests of building construction and materials* . (2007). Standards Council of Canada.

Chuo, T. (2007). "Fire performance of connections in laminated veneer lumber." MSc Thesis, University of Canterbury, New Zealand.

Dhima, D. (1999). *Vérification expérimentale de la résistance au feu des assemblages d'éléments en bois*. Centre Technique Industriel de la Construction Métallique (CTICM), Saint-Rémy-lès-Chevreuse, France.

EN 1995-1-1:2004. *Eurocode 5: Design of timber structures – Part 1-1: General – Common rules and rules for buildings* . (2004). European Committee for Standardization (CEN), Brussels, 123.

EN 1995-1-2:2004/AC:2006. *Eurocode 5: Design of timber structures – Part 1-2: General – Structural fire design* . (2006). European Committee for Standardization (CEN), Brussels, 3.

EN 1995-1-2:2004/AC:2009. *Eurocode 5: Design of timber structures – Part 1-2: General – Structural fire design* . (2009). European Committee for Standardization (CEN), Brussels, 6.

EN 1995-1-2:2004. *Eurocode 5: Design of timber structures – Part 1-1: General – Structural fire design* . (2004). European Committee for Standardization (CEN), Brussels, 69.

Fleischer, H., Fornather, J., Bergmeister, K., and Luggin, W. (2002). Großbrandversuchsreihe 1 - GBV 1 - Versuche an Holz-Stahlblech Verbindungen mit Stabdübeln. Universität für Bodenkultur Wien, Vienna, Austria, 54.

ISO 834-1:1999. *Fire-resistance tests. Elements of building construction. Part 1: General requirements* . (1999). International Organization for Standardization (ISO), 25.

König, J., and Fontana, M. (2001). "The performance of timber connections in fire – Test results and rules of Eurocode 5." *Proceedings of International RILEM Symposium "Joints in Timber Structures,"* RILEM Publications, Stuttgart, Germany, 639–648.

Kordina, K., Meyer-Ottens, C., and Scheer, C. (1995). *Holz Brandschutz Handbuch*. Ernst & Sohn.

Laplanche, K. (2006). "Étude du comportement au feu des assemblages de structures bois: approche expérimentale et modélisation." PhD Thesis, University Blaise Pascal (Clermont-Ferrand), France.

Lau, P. (2006). "Fire resistance of connections in laminated veneer lumber (LVL)." MSc Thesis, University of Canterbury, New Zealand.

Norén, J. (1996). "Load-bearing capacity of nailed joints exposed to fire." *Fire and Materials*, 20(3), 133–143.

Palma, P., Frangi, A., Hugi, E., Cachim, P., and Cruz, H. (2013). "Fire resistance tests on steel-to-timber dowelled connections reinforced with self-drilling screws." *Proceedings of the 2nd Ibero-Latin-American Congress on Fire Safety – 2nd CILASCI*, Coimbra, Portugal.

Peng, L., Hadjisophocleous, G., Mehaffey, J., and Mohammad, M. (2012). "Fire performance of timber connections, Part 1: Fire resistance tests on bolted wood-steel-wood and steel-wood-steel connections." *Journal of Structural Fire Engineering*, 3(2), 107–132.

Scheer, C., Mandy, P., Povel, D., and Maack, S. (2004). Tragfähigkeit von Holzverbindungen mit stiftförmigen Verbindungsmitteln im Brandfall. Teil 2: Brandversuche zur Bestätigung der theoretischen Erkenntnisse. Technische Universität Berlin, Berlin, Germany, 148.

Scheer, C., and Peter, M. (2009). *Holz Brandschutz Handbuch*. Ernst & Sohn.

Discussion

The paper was presented by P Palma

P Zarnani asked why number of fasteners and spacing of fasteners were not important. P Palma clarified that the number of fasteners were important. P Zarnani asked what type of failure mode was encountered. P Palma responded that side member failures were found. P Zarnani and P Palma discussed that the edge distance would be more important if one had fewer rows but the test results are few to make such claims and failure mode was typically embedment.

P Quenneville asked whether Eurocode allows dowelled only connection. It was clarified that at least one bolt is required. P Quenneville asked whether there would be plans to consider cases with at least one bolt. P Palma stated that some results did not have any bolts but some results did have bolts and that the structural engineer can consider the more conservative results.

P Dietsch commented that kflux factor for nailed connection had two values and there was a big jump from 1.5 to 2.5. He asked if the 280 mm values was a mistake in the code and should be corrected to 440 mm, would it mean that the designs in the past were wrong. P Palma stated that it was an obvious typing error in the code and pointed out the source of the 440 mm values as Holz Brandschutz handbook. P Dietsch questioned the conclusion that side thickness was more important than the gap so what about the situation of fire from below. P Palma responded that in such case all 4 sides are exposed to fire and in the case of fire from below they did not have the information.

U Kuhlmann asked why the bolts were worse than dowels. P Palma responded that the influence of exposed bolt head and nut and washer was the reason.

C Rauschen commented about the negative effect of bolt if one protected the steel plate but not the bolt and would it be okay if 20% capacity was still left. P Palma responded that heat would still travel through the bolt to the protected plate.

J Köhler asked whether the characteristic load was used. P Palma responded that the load ratio was taken as 30% of the mean load.

J Köhler, K Ranasinghe and P Palma discussed about using of the 5% percentile load level might be non-conservative because 95% of the connection would have higher strength.

Improved fire design model for timber frame assemblies

Alar Just, Tallinn University of Technology

Mattia Tiso, Tallinn University of Technology

Keywords: fire design, timber frame assemblies, protection by insulations

Abstract

The behaviour of timber frame assemblies in fire is influenced by the protective properties of cladding and insulation materials. The primary protection for a timber member is given by the cladding. After the fall-off of the cladding, secondary protection might be provided by the insulation materials protecting the sides of the timber member.

Annex C of EN 1995-1-2 presents a design model that considers the contribution of stone wool to the fire protection of timber member. The model is extended to assemblies filled with glass wool as long as protected by cladding. The model is valid for cavities completely filled with insulation.

There are many other insulation materials used in buildings, which are not considered by the current EN 1995-1-2. For example wood-based insulations, fire retardant foams etc. Many structures do not have cavities completely filled with insulation. Several studies have been made to investigate the fire resistance of timber frame assemblies with different cavity insulations. The results of these investigations form a basis for an improved design model for timber assemblies proposed in this paper.

1 Introduction

1.1 Design model in EN 1995-1-2

Fire design model for timber frame assemblies is published in Annex C of the current EN 1995-1-2.

According to the model charring of a timber member protected by cladding is considered the protection phase (Phase 2 in Figure 1d). The charring of a timber member after the fall-off of the cladding is considered the post-protection phase (Phase 3 in Figure 1d). Different insulation materials provide different protection depending on their behaviour under elevated temperatures.

The design model is based on stone wool cavity insulations for all protection phases. The model is valid for glass wool cavity insulations for phases 1 and 2.

The charring rates are modified using coefficients to correct the nominal charring rate with the effect of the protection, cross-section width and corner roundings.

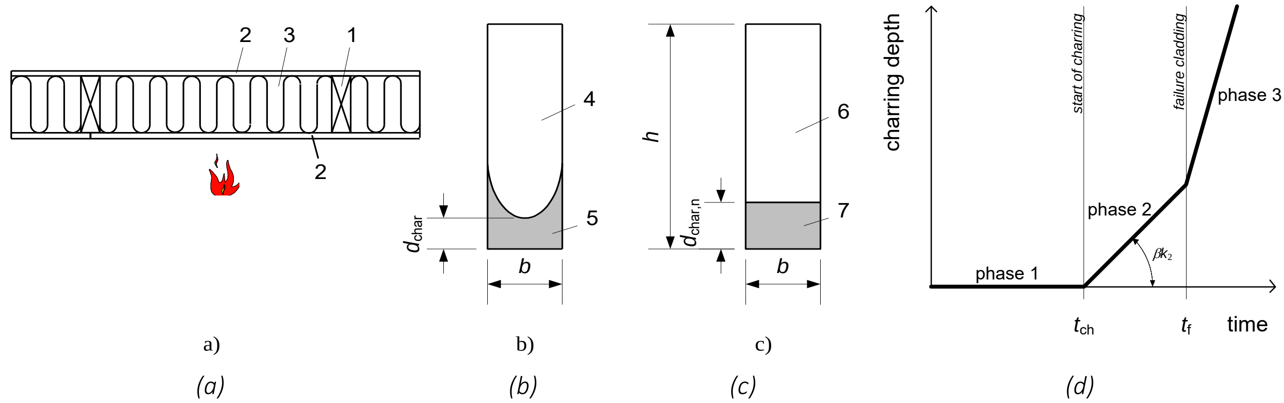

1 Solid timber member (stud or joist)
2 Cladding
3 Insulation
4 Residual cross-section (real shape)
5 Char layer (real shape)
6 Equivalent residual cross-section
7 Char layer with notional charring depth

a) Section through assembly. b) Real residual cross-section and char layer. c) Notional charring depth and equivalent residual cross-section d) charring phases

Figure 1. Charring model for timber frame assemblies at EN 1995-1-2.

Notional charring depth $d_{char,n}$ is calculated as

$$d_{char,n}=\beta_n t \quad (1)$$

The notional charring rate, $\beta_{n,}$ of small-sized timber frame members is given as

$$\beta_n = k_p k_s k_n \beta_0 \quad (2)$$

where β_0 is the one-dimensional charring rate for timber, β_0 = 0,65 mm/min.

1.2 Insulation materials

Insulation materials used in timber frame assemblies have different protection properties.

As a study conducted by Papadopoulus in the early 2000s pointed out the European market of insulation materials shows a predominant presence of stone wool and glass wool (60% of the market) followed by organic foamy materials, expanded and extruded polystyrene and to a lesser extent polyurethane (which account for 27% of the market). In the last decade the demand for bio-based thermal insulation has been increased in the market of timber houses. Most commonly used materials in timber frame assemblies are mineral wool, wood based fibre insulations, PUR, PIR and EPS foams.

The European product standard for mineral wool insulations EN 13162 does not consider the properties used for fire resistance purposes. For example traditional stone wool and traditional glass wool have different behaviour at temperatures over 550°C but the standard does not distinguish them.

1.3 Previous studies

The current concept for the fire design of timber frame assemblies in the Eurocode 5 is based on research by König and Walleij (2000). Model scale tests were made with stone wool and glass wool cavity insulations.

Takeda (2000) researched timber-frame walls with glass wool insulation, developing the WALL2D computer model. Many small-scale experiments were carried out. He concluded that glass wool began to melt at 430-450 °C, and was completely lost at about 650 °C. Rock wool started to shrink at 700 °C, and had decreased in volume by 60 % at about 800 °C. Takeda also noticed a slow melting of glass fibre in the case of a protected structure with no joints between gypsum cladding sheets.

Frangi (2005) performed tests of sandwich elements with stone wool and glass wool insulation. Elements with glass wool lost the insulation ability due to melting. König (2000) studied timber frame assemblies with glass wool insulation and noted the same phenomenon: that glass wool disappeared when exposed directly to fire. This led to the rule in EN 1995-1-2: "where the cavity insulation is made of glass fibre, failure of the member should be assumed to take place at time t_f. (Sub-clause C.2.1 (6))."

Just and Schmid (2012) performed a study with the cavities of timber frame assemblies filled with heat resistant mineral wool. The study concluded that the design method in EN 1995-1-2 does not cover safely all the stone wool products on the market. There are also high temperature extruded mineral wools made of glass that can resist high temperatures in the post-protection phase similarly to stone wool.

Just (2010) made a research on timber frame assemblies with cavities filled with glass wool. The model for post-protection phase was proposed based on recession speed of glass wool – 30 mm/min.

The European guideline *Fire Safety in Timber Buildings* includes a design model that considers the contribution of stone wool and glass wool to the fire resistance during the protection and post-protection phases.

Hakkarainen (2016) made the study with fire safe use of polyurethane insulations in hall buildings. The study showed that the insulations can provide sufficient fire resistance during the protection phase.

2 Fire tests

Model scale and full scale fire tests have been made with timber frame assemblies by Just (2008-2015) consisting of timber frame assemblies with different mineral wool insulations. Tests were made in vertical and horizontal positions.

Tiso (2014-2016) completed the test programme with timber frame assemblies insulated with stone wool (30 to 38 kg/m^3) and glass wool (12 to 14 kg/m^3) as well as cellulose fibre insulation (30 to 40 kg/m^3), EPS, and PUR. Insulation materials involved in this investigation were chosen in order to cover as many different types of products as possible. 30 tests were made in horizontal position in a model scale furnace at SP in Stockholm.

2.1 Methodology

Model scale fire tests with horizontal test specimens measuring 800x1000 mm were performed following the ISO834 fire curve. See Figure 2. The tested timber beam was placed in the middle and insulated with the materials mentioned above. Height of the timber beam cross section was always 145 mm. The width varied between 45 and 120 mm. Both protected and post-protection phase were tested. Fall-off of the cladding was caused at a controlled time, mostly 45 minutes after the start of fire. Temperatures were measured with Type K thermocouples. Measurements were done inside and on the sides of the timber member, and inside the insulation. See Figure 2b. After the test the residual cross-sections were analysed. Duration of each test was 50 to 90 minutes. The fall-off of insulation was not studied. The insulation was glued on the unexposed side and held in place during the entire test.

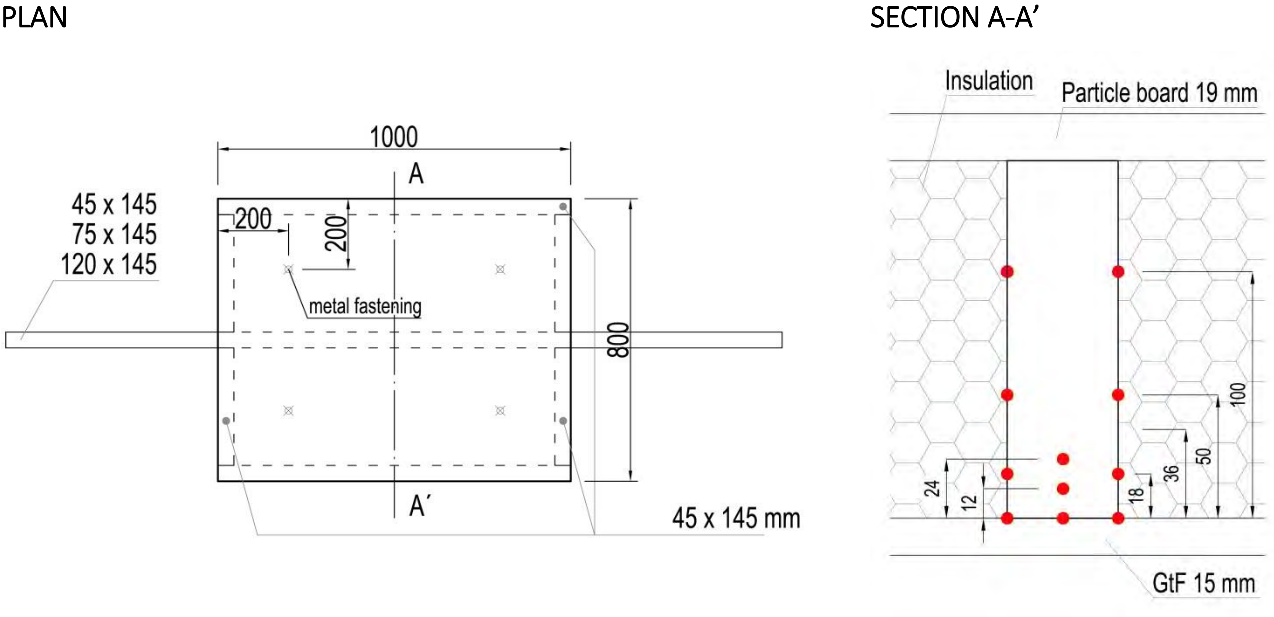

(a) *(b)*

Figure2. Test specimen for the model scale test

2.2 Measurements of the char layer

After the fire tests the char layer was removed from the beams with a metal brush. For each beam the instrumented and the minimum residual cross sections were collected. The residual cross-sections were photographed and analysed with the mass properties function of the AutoCAD software. The outer perimeter of the remaining cross-section (after removing the char layer) was studied further. To verify that the whole cross-section including the darkened zone could be considered timber, a resistograph investigation was made. The specimens were drilled from the unexposed through to the fire exposed side. The resistograph provides the resistance to penetration versus the drilling depth. This method was adopted to obtain in-depth information about the properties of the residual cross-section.

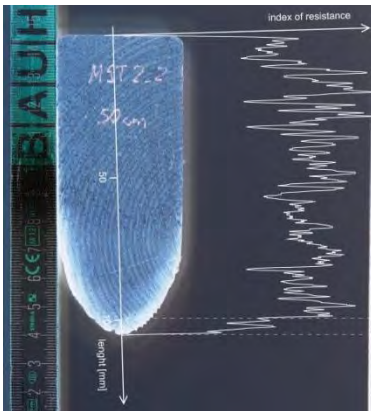

Figure 3. Resistance profile measured by resistograph.

(a) (b) (c)

Figure 4. Residual cross-sections originally protected by different insulation materials. (a)Stone wool (b) glass wool (c) cellulose fibre

Some examples of the residual cross-sections from the fire tests are shown in Figure 4. Cross-section in Figure 4a represents the structure with insulation protecting the lateral sides from charring. Figure 4b and 4c represent the situation with lateral charring. The recession speed of the insulations has been different.

3 Thermal simulations

Effective thermal properties are determined by calibrating the known values according to the fire tests. For numerical heat transfer modelling the change in mass, thermal conductivity and specific heat of a material at a range of temperatures are required. The loss in mass of the insulation materials as a function of the temperature was investigated using thermo-gravimetric analysis (TGA). The thermal conductivity was measured using transient plane source method (TPS) and the steady-state method with a Guarded Hot Plate (GHP) apparatus. An advantage of the latter method is that the obtained results present a full curve of thermal conductivity vs. temperature instead of few points. However, the use of this method is limited to some insulation materials only.

Thermal simulations made with SAFIR are used to study the influence of cross-section dimensions and fall-off of the claddings. Thermomechanical analyses made by FEM programs are used to determine zero-strength layers for the effective cross-section method.

4 Improved design model

4.1 General

The proposed improved design model for timber frame walls and floors is based on a comprehensive series of fire tests and thermal simulations described previously.

The improved design model considers charring from three sides of the timber member. See Figure 5. A wide range of insulation materials is studied and the method is open for new insulation materials and protection systems.

There are two different charring scenarios observed for timber frame assemblies:

- For timber frame assemblies with cavities completely filled with heat resistant insulation materials, the charring occurs mainly on the fire-exposed side of the member, while the lateral sides are protected by the insulation. The lateral charring can be neglected (one-dimensional charring).
- For timber frame assemblies with cavities completely filled with non-heat resistant insulations, the charring is regarded as two-dimensional due to the degradation or recession of the insulation material.

Start time of charring on the lateral side of the cross-section differs from the start time of charring on the fire side. This is caused by recession of the insulation.

The dimensions of the cross-section and the type of insulation have an influence on the charring rates. Charring rates in the protection and post-protection phases are different. Charring rates on the fire side and lateral side are considered differently.

Rounding of corners due to charring from the fire side might partially affect the charring of the lateral sides of the cross section. Corner roundings of the charring on the fire side might effect partially the charring on the lateral side of cross-section. Lateral charring shall be taken into account in the design when if the cross-section will clearly char from three sides. The cross section is considered to char from three sides if more than two thirds of the height of the lateral sides chars. In the proposed procedure 145 mm beam height, the char height criterion is rounded to 100 mm. Time when described point is reached is considered as the start time of lateral charring.

Parameters for the design of assemblies up to 60 minutes and 60 to 90 minutes are obtained separately.

The effective cross-section method is used as the basis for the design model. Determining the zero-strength layers d_0 for different protection levels and fire durations are not covered in the current paper.

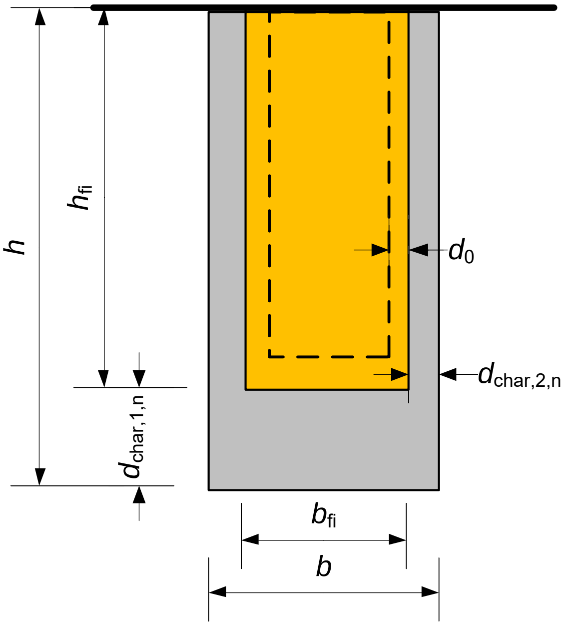

Figure 5. Improved design model for timber frame assemblies.

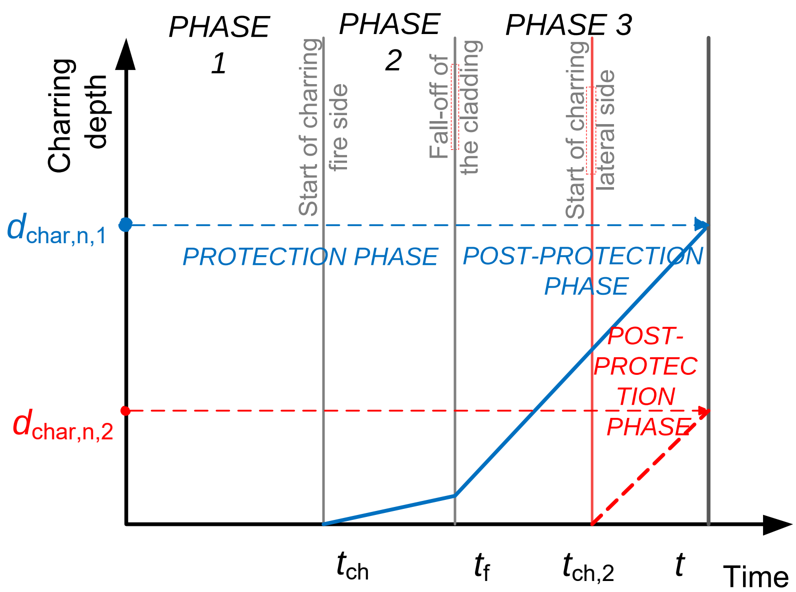

Figure 6. Charring rates and phases for the two-dimensional charring model.

4.2 Protection levels

According to the current research by Tiso and Just (2016) the insulation materials and protection systems could be divided according to the protection provided to timber members. Correlation between the recession of insulation and the residual moment of inertia of the timber beam was shown. The qualification methodology for insulations was proposed where different levels of protection against charring were identified. Figure 7 shows the four different levels of protection up to 90 minutes defined in the qualification methodology.

These protection levels can be summarized as (from stronger to weaker):

- PL1 - insulation materials that can guarantee protection against charring for up to 90 minutes (line A in Figure 7). Such materials are for example stone wool, high temperature extruded mineral wool.
- PL2 - insulation materials which protect at least 1/3 of the height of the beam (45 mm) from charring for up to 60 minutes of the fire test (line B in Figure 7). Such materials are for example stone wool, high temperature extruded mineral wool.
- PL3 - insulation materials which do not guarantee complete protection against charring for up to 60 minutes of fire test (line C in Figure 7). Such materials are for example glass wool, cellulose fibre insulation, fire retardant polyurethane.
- PL4 - insulation materials which do not guarantee complete protection against charring during the protection phase (line D in Figure 7). Such materials are for example extruded polystyrene and other foams.

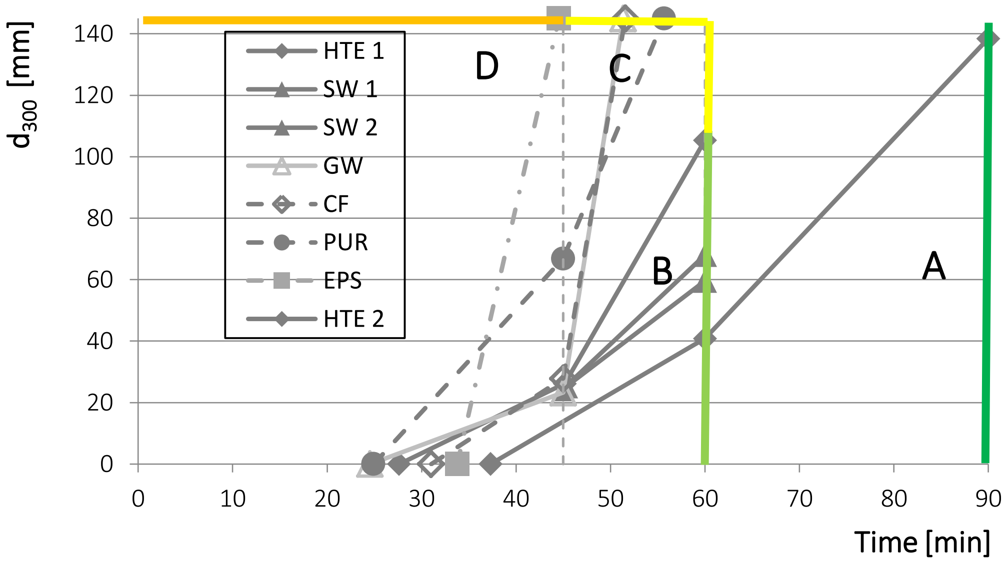

Figure 7. Design model for timber frame assemblies.Examples with different insulations.

The described qualification system should help the designer to distinguish between the wide variety of insulation materials with regard to protection of timber elements against charring. The design method allows the determination of, for example, protection levels of structures with partially filled cavities. Additionally, the protection offered by vertical strips of insulation applied to the sides of the timber element can be calculated.

For the insulation material to qualify as PL1 a successful 90-minute fire test with 20 mm gypsum plasterboard as fire protection is required. The fall-off of the fire protection is imposed at 60 minutes. Charring must be less than 100 mm on the side of timber member. For protection levels PL 2,3 or 4 a 60 minutes fire test with a 15 mm gypsum plasterboard is required. In this case the fall-off of the fire protection is imposed at 45 minutes.

Coefficients for the improved design model can be unified within the protection levels.

4.3 Charring

Charring is considered from three sides. Charring depth from the fire exposed side is $d_{char,1,n}$. Charring depth from the lateral sides of the cross section is $d_{char,2,n}$. See Figure 5 and 6.

Charring depth of timber member is regarded as

$$d_{char,n} = k_{s,n}\, k_{pr}\, \beta_0 \tag{3}$$

where $k_{s,n}$ is the cross-section coefficient and k_{pr} is the protection coefficient. β_o is the basic design charring rate (0,65 mm/min).

The coefficients are characterised in the following subchapters.

4.3.1 Cross-section coefficient

Cross-section coefficient $k_{s,n}$ is used to take into account the notional charring from the narrow side of the cross-section.

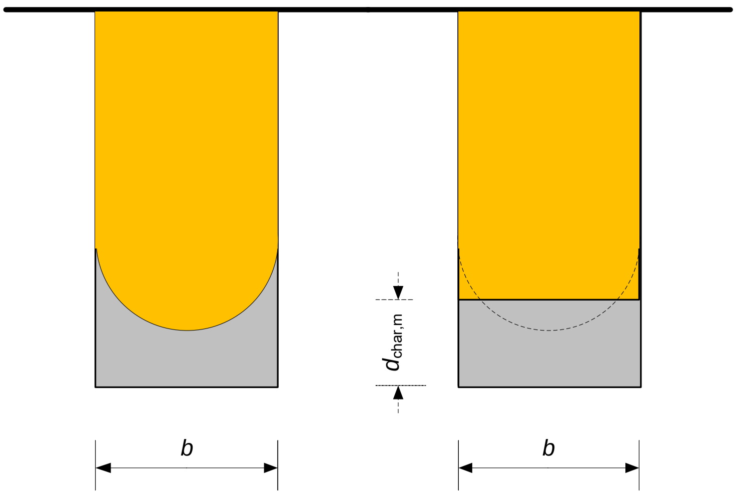

Figure 8. Determining the cross-section coefficient by notional charring depth.

Notional charring depth in the post-protection phase is regarded as

$$d_{char,m}=\beta_m\, t \tag{4}$$

$$k_{s,n}= \beta_m/\beta_0 \tag{5}$$

where β_m is the notional charring rate determined with the unprotected specimen insulated with stone wool (30 kg/m^3).

Coefficient $k_{s,n}$ will be given as function of the beam width b. Different widths may be analysed by means of thermal simulations.

4.3.2 Protection coefficient

Protection coefficient explains the charring rates in the protected and post-protection phases. Subindex indicates the number of the protection phase (see Figure 6).

$k_{pr}=k_2$ (6)

The protection coefficient k_2 takes into account the influence of cladding on the charring rate. The coefficients k_2 for gypsum boards are published in the EN 1995-1-2:2004. For the other cladding materials the coefficients will be determined according to EN 13381-7.

$k_{pr}=k_3$ (7)

Post-protection coefficient k_3 accounts for the influence of faster charring rate after the fall-off of cladding. The coefficient will be determined using the test methodology described in chapter 2. Coefficient k_3 depends on the fall-off time t_f (see Figure 6) of the cladding. Determination of coefficient k_3 for charring on the fire side of the cross-section is shown in Figure 9 and equation (8).

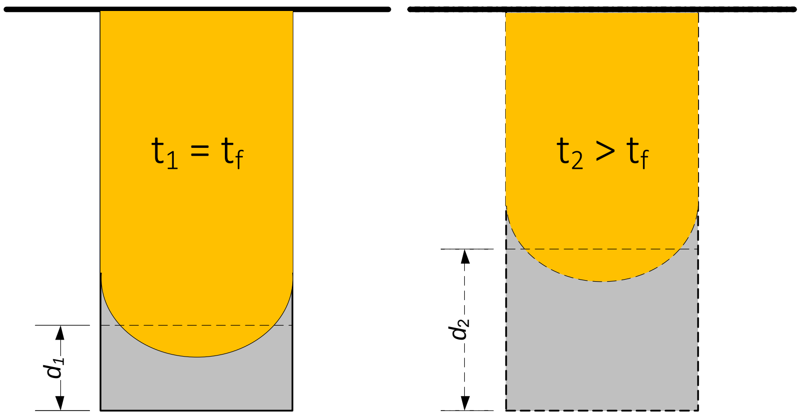

Figure 9. Determination of the coefficient k_3.

$$k_3(t_f) = \frac{d_2 - d_1}{\beta_0 k_{s,n}(t_2 - t_f)} \tag{8}$$

4.3.3 Recession speed of the insulation

Recession speed of the insulation v_{rec} will be defined using model scale tests and measuring the development of the 300°C isotherm between the insulation and timber member in the post-protection phase. See Figure 10.

For the traditional glass wool the recession speed is 30 mm/min. Based on this study the recession speed of cellulose fibre insulation was determined to be 20 mm/min. For stone wool the recession speed can be neglected.

4.3.4 Start time of lateral charring

Start time of lateral charring is defined as the time when charring on the lateral side reaches two thirds of the height of the cross-section. Start time of lateral charring is calculated as

$t_{ch,2}=t_f +0{,}67h/ v_{rec}$ (9)

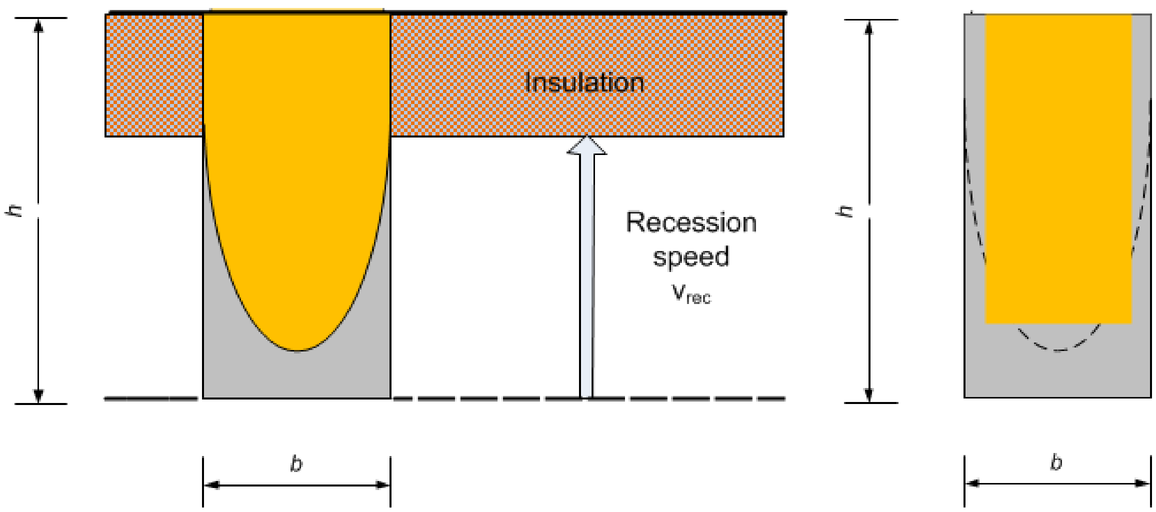

Figure 10. Recession of the insulation and the simplified rectangular residual cross-section.

4.3.5 Lateral charring rate

$$\beta_{3,2} = k_{3,2}\beta_0 \tag{10}$$

The role of lateral charring rate is to provide appropriate residual section modulus. It is derived from test with 145 mm cross-section height according to test methodology described in chapter 2. See equations (11), (12) and (13). The coefficients for fires up to 60 minutes and for fires 60 - 90 minutes have to be determined differently. Following explains the procedure to determine the coefficients for fires up to 60 minutes.

The approach is based on relation:

$$\frac{W_{\mathrm{fi}}}{W_{\mathrm{n}}} = \frac{b_{\mathrm{fi}}}{b} \tag{11}$$

where W_{fi} is the residual section modulus at 60 minutes; W_{n} is the section modulus of the notional rectangular simplified cross-section at 60 minutes considering only charring from the fire exposed side. See Equation (12).

b is the original beam width; b_{fi} is the beam width at 60 minutes considering charring from the lateral sides.

$$W_{\mathrm{n}} = \frac{b(h - d_{\mathrm{char,1,n}})^2}{6} \tag{12}$$

The post-protection coefficient for lateral charring for 60 minutes fire resistance the coefficient $k_{3,2}$ is calculated as:

$$k_{3,2} = \left(b - \frac{6\,W_{\mathrm{fi}}}{[h - d_{\mathrm{char\ 1,n}}(60)]^2}\right)\frac{1}{2\beta_0(60 - t_{\mathrm{ch,2}})} \tag{13}$$

For small cross-sections (height less than 90 mm) lateral charring rate might be multiplied by the cross-section coefficient $k_{\mathrm{s,n}}$.

4.3.6 Charring depth

Charring depth on the fire side of cross-section is

$$d_{char,1,n}=k_{s,n}\, k_2\, \beta_0\, (t_f-t_{ch}) + k_{s,n}\, k_3\, \beta_0\, (t - t_f) \quad (14)$$

Charring depth on the lateral sides of cross-section is

$$d_{char,2,n}=k_{s,n}\, k_{3,2}\, \beta_0\, (t - t_{ch,2}) \quad (15)$$

4.3.7 Examples of calculation for insulations classified as protection level 2 and 3

Firstly, a timber frame assembly with cavity insulation classified as **protection level 3** is considered as an example. For this protection level verification for 60 minutes of standard fire can be made. The cross-section of the timber beam is 45 x 145 mm. Gypsum plasterboard, Type F with thickness of 15 mm is considered as fire protection. Fall-off time is 45 minutes. Coefficients are determined according to the approach described in this paper:

$k_{s,n}$ = 1,3 for beam width of 45 mm

k_3 = 1 + 0,0312 t_f = 2,4 for fall-off time t_f = 45 min

$k_{3,2}$ = 2,05

$t_{ch,2}$ = 50min for t_f = 45 min and recession speed v_{rec}=20 mm/min

Results in terms of charring depth versus time are shown in Figure 11 a.

For insulation classified as **protection level 2** the coefficients are:

k_3 = 1 + 0,0117 t_f = 1,53 for t_f = 45 min

$k_{3,2}$ = 0

Results in terms of charring depth versus time are shown in Figure 11 b.

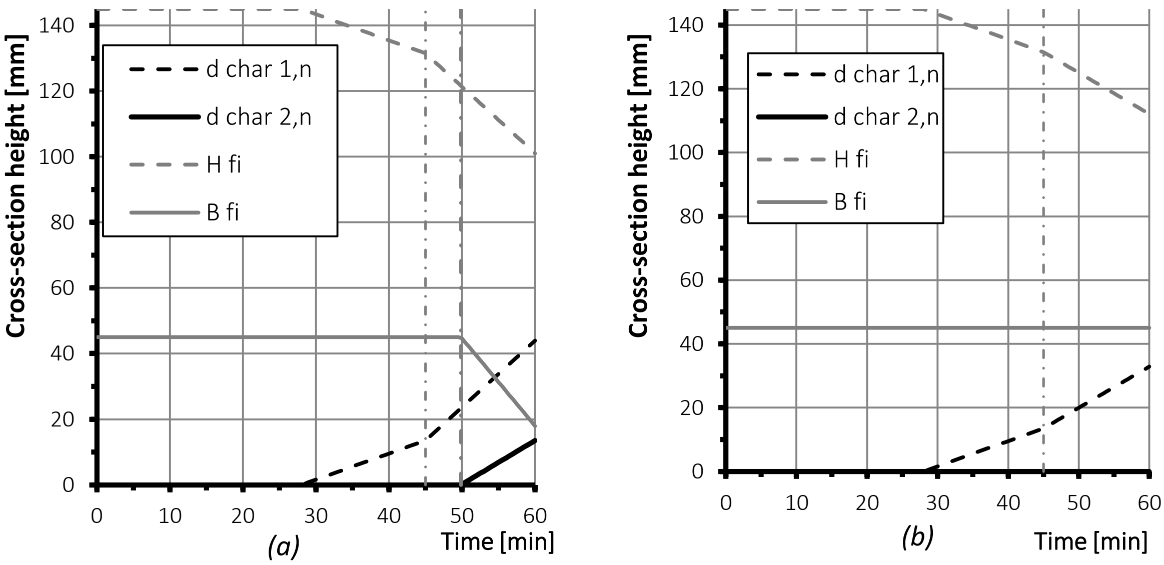

Figure 11: Examples of charring depth according to the improved design model for a timber frame assembly (cross-section 45 mm x 145 mm) with PL3 insulation (a) and PL2 insulation (b) applied.

4.4 Strength properties

Effective cross-section method will be used in the revised Eurocode 5 part 1-2.

Decrease of strength properties at the elevated temperatures is compensated by decreasing the cross-section by the zero-strength layer.

Thermal simulations will be performed in the scope of the ongoing research by Tiso to follow the temperature division within the cross-section and derive the zero-strength layer for various insulation materials. Verification of the results by full-scale fire tests is planned. This paper does not include the values for zero-strength layers.

5 Discussion and conclusions

The improved universal design model for timber frame assemblies is proposed in this paper. The model takes insulation materials with different behaviour in fire into account. The coefficients used in this model are based on timber members with 145 mm cross-section height.

For the improved design method qualification of insulation materials is needed. A recent study by Tiso (2016) introduced a qualification methodology for batt-type insulations based on the fire protection provided to timber elements. The qualification methodology is proposed to be included in the Annex of the revised EN 1995-1-2.

Fall-off of insulations is not dealt with in the proposed design method. To secure the insulation in place proper measures for detailing or fasteners have to be taken if relevant. The method assumes the insulation will not fall off.

Effective cross-section method will be used for taking strength reduction into account. Zero-strength layers for different insulation materials, different fire durations and protection phases will be determined using thermal simulations.

The example given in this paper for cellulose fibre insulation is indicative. An experimental and analytical study should be performed with the most common insulation materials following the procedure proposed in this paper. Compared to the current Annex C of Eurocode 5 Part 1-2 the new design model yields similar fire resistance for assemblies with cavities completely insulated with stone wool for 60 minutes.

6 References

Eurocode 5 Part 1-2 (2004): Design of timber structures – Part 1-2: General – Structural fire design, (EN 1995-1-2:2004).

Papadopoulos, A. M., et al. (2004). Design and development of innovative stone-wool products for the energy upgrading of existing and new buildings Project Interim Report, Thessaloniki.

König, J., & Walleij, L. (2000): Timber frame assemblies exposed to standard and parametric fires: part 2: a design model for standard fire exposure. Rapport-Institutet för Träteknisk Forskning, (0001001).

Just, A., Schmid, J., König, J. (2012): Post-protection effect of heat-resistant insulations on timber-frame members exposed to fire. Fire and Materials, 2012, 36.2: 153-163.

Takeda H, Kahsay F. (2000). The effects of insulation on the Fire Resistance of Wood-stud Walls. World Conference on Timber Engineering 2000, Whistler.

Fontana, M., Frangi, A. (2005). Fire performance-based design of multi-storey timber buildings. Proceedings of the IABSE Symposium on “Structures and Extreme Events”, Lisbon, Portugal, September 14-17, 2005, Conference Report edited by IABSE, ETH Zurich, pp 294 pp.

Just A. (2010). Post protection behaviour of wooden wall and floor structures completely filled with glass wool, Structures in Fire: Proceeding of the 6th international conference. East Lansing, USA. June 2 - 4 2010, pp 584-592; 2010.

Hakkarainen, T., Nissilä, M., Ojanen, T. (2016) Fire Safe Use of Polyurethane Insulation in Hall Buildings. Interflam 2016 proceedings. Volume 2. Pp 1499-1506. Windsor 2016.

EN 13162:2012. Thermal insulation products for building – Factory made mineral wool (MW) products – Specification, European Committee for Standardization; 2012

Östman,B et al (2010): Fire safety in timber buildings. Technical Guideline for Europe. SP Technical Research Institute of Sweden. SP Report 2010:19.

prEN 13381-7:2016. Test methods for determining the contribution to the fire resistance of structural members - Part 7: Applied protection to timber members. Draft standard.

ISO 834-1:1999, Fire-resistance test – Elements of building construction – Part 1: General requirements, International Organization for Standardization; 1999.

Tiso M, Just A. (2016). Parameters influencing the behaviour of timber frame assemblies exposed to fire, development of new design criteria for insulation materials, In: Structures in Fire (Proceedins of Ninth International Conference): Structures in Fire, Princeton University, 8-10 June 2016. Ed. Garlock M. E. M., Venkatesh K. R. K. Princeton (USA): DEStech Publications, Inc, 659−666; 2016

Tiso M, Just A. (2016). Behaviour of insulation materials in timber frame assemblies exposed to fire, World Conference Timber Engineering, Wien 22-25 August; 2016.

Tiso M, Just A, Mäger K N. (2016). Behavior of wooden based insulations at high temperatures, SBE16 Tallinn and Helsinki Conference; Build Green and Renovate Deep, 5-7 October; 2016.

Discussion

The paper was presented by A Just

A Frangi asked with about the possibility to extend the 25 tests by numerical simulations with consideration of the variability. A Just agreed and responded that they could not give numbers for any material and that it was a proposed model approach only. A Frangi commented that companies could do the tests if they were unhappy with the proposed. A Frangi asked whether the authors were sure that the insulation was not falling off. A Just responded that they were not sure and were not dealing with this issue in this approach. He stated that if one did not keep insulation in place then this approach could not be used.

P Zarnani asked about CLT. A Just said that CLT would be a different topic.

K Ranasinghe commented that this proposed approach would require a lot of work to make it usable for designers. He commented that the results in slide 27 suggested that one would need larger cross sections to meet the requirements which would be detrimental to the design. A Just responded that this proposal was neither considered for thin members nor for different material. H Blass added that this meeting is not intended to deliver results to help designers on the spot and the meeting is intended to work on issues related to code.

U Kuhlmann stated that insulation issue is also important for steel structures; in particular, the durability of the insulation has recently been identified as being an issue.

Reliability of large glulam members Part 1: Data for the assessment of partial safety factors for the bending strength

Matthias Frese, Hans Joachim Blaß
Karlsruher Institut für Technologie, Holzbau und Baukonstruktionen

Keywords: size effect, k_h-factor, strength modification

1 Introduction

1.1 Background and concept of the paper

Eurocode 5 allows considering the influence of the member volume on the bending strength. It is explicitly possible to raise the bending strength for beams with a depth smaller than 0.6 m. However, this increase is limited to 10 %. Until now, no Eurocode provisions exist how to modify the bending strength of beams deeper than 0.6 m. Among others, the reason is that at least experimental strength data of very deep beams are not available. Therefore, a comprehensive database was still missing to derive purposeful strength modifications. Consequently, the partial safety factor has to compensate the effects of those member volumes which are larger than the reference size. Up to now, we do not really know whether roof structures as shown in Figure 1 do fulfil the requirements of a consistent reliability.

According to the Eurocode 5 concept based on a k_h-factor, the authors have already suggested approaches for a bending strength modification for beams up to 1.8 m (Frese and Blaß, 2008) and finally up to 3.0 m given by Equation (1) (Frese and Blaß, 2015).

$$k_h = \left(600/h\right)^{1/8.288} \qquad h \text{ in mm} \tag{1}$$

However, this modification of the 5th percentile of a corresponding bending strength distribution does not necessarily provide consistent reliability of small and large glulam members. Hence, a lack of knowledge remains.

This paper intends to give an insight into new bending strength data available for large glulam members. Using efficient scientific computing, these data were obtained from simulations with the Karlsruhe Rechenmodell in its latest amended version (Frese, 2016). With that, the bending strength data were created as accurately as possible. The basis are numerous realisations of simulated bending tests according to the provisions of EN 408. The data contain both the strength of small glulam members, which can be tested experimentally, and the strength of large members, which could not be tested in this way. It is, therefore, the main idea of the work to provide strength data covering a large range of glulam member sizes. This paper is the first part of a two-part contribution. The second part, intended for next year, will report on new tensile strength data of short and long glulam members.

Figure 1. Glulam structure with a span of 40 m and a girder depth of 2.8 m at midspan. Such girders raise the question whether code provisions are realistic enough to provide consistent reliability.

1.2 Benefit of the computational examination of the bending strength

Reliability experts are asked to use the new bending strength data for the reassessment or determination of the level of partial safety factors or modification factors for large glulam members. With that, they may establish a more consistent reliability between small and large glulam members. Furthermore, the authors will provide the original data sets on demand[1] so that interested experts can make their own interpretations or fit their own theoretical probability distributions. Data sets are available as single txt files for beam depths from 0.3 to 3.0 m in 0.3 m steps. Each single 0.3 m step contains 1000 modelled bending strength values. In total, the data sets cover six different characteristic bending strength levels from round 24 to 37 N/mm².

2 Methods

2.1 Computational model

The computational strength examinations were conducted with the Karlsruhe Rechenmodell, a validated finite element based computer model. It is based on the

[1] Experts are asked to express their interest by sending an email to matthias.frese@kit.edu

structural analysis system ANSYS and on its corresponding processors. The integrated design language was employed to control the general programme flow and to build the model with realistic mechanical properties of glulam. To obtain a certain material quality, a corresponding grading process is activated prior to the Monte Carlo analysis. The main features of the computer model are described in the following. For further model characteristics, see Frese 2010. Figure 2 shows the basic model used to simulate a bending test. It applies to arbitrary member sizes. The member size of the modelled body depends on the numbers of elements (150 mm in length and 30 mm in depth) along the total length and depth. After being empirically represented by regression equations, stochastically distributed and auto-correlated mechanical properties are assigned discretely and systematically to the elements of the model. With it, the natural occurrence of knots and glulam specific characteristics as finger joints are taken into account with regard to the local mechanical properties. That enables a computation of realistic resulting tensile and compressive stresses (σ_t and σ_c) for the loaded member.

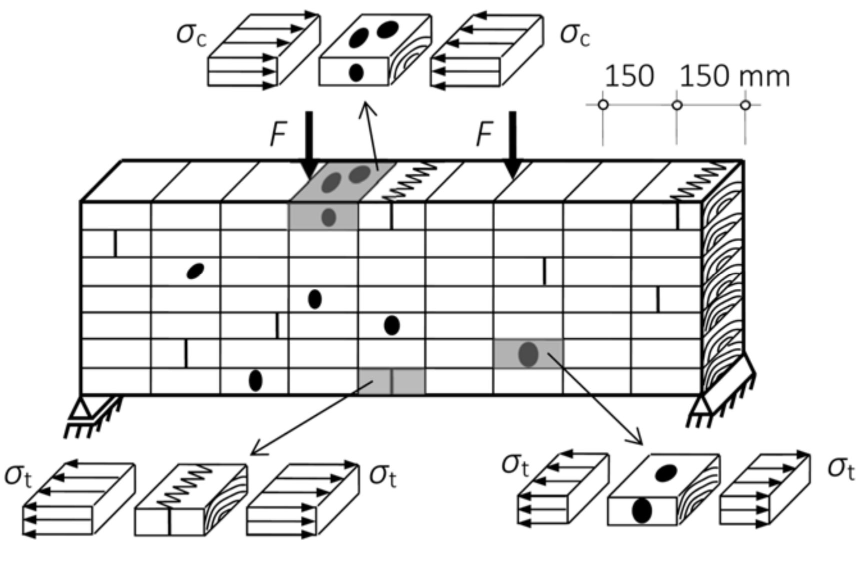

Figure 2. Discretised glulam model with selected elements under tensile and compressive stresses.

2.2 Computationally examined strength classes and member sizes

The computational test programme should meet a certain range of target strength classes and should consider a purposeful size variation. In doing so, the corresponding nominal strength values refer to the member depth of 0.6 m and a member span of 18 times the depth. Table 1 shows in total six different strength levels examined. The paper contains the results of the levels given in bold letters; the results of the other two levels can be obtained on demand. The quoted grading method indicates whether a visual or mechanical procedure is computationally simulated. The tabulated reference strength is the 5th percentile of 1000 modelled strength values. The differences between the nominal strength values (e.g. 24 N/mm²) and modelled values (24.4 N/mm²) are due to the stochastic nature of the process. The last column in Table 1 contains the coefficient of variation of the modelled strength values.

Table 1. Target strength class, grading method and bending strength.

Target strength class	Computationally modelled grading method	reference strength in N/mm²	COV %
GL24	visual	24.4	14.8
GL28	visual	28.1	14.5
GL29	mechanical	29.4	15.4
GL32	mechanical	32.1	14.9
GL34	mechanical	34.0	13.7
GL37	mechanical	37.3	13.4

Figure 3 shows the computationally examined sizes. The smallest beams feature a depth of 0.3 and the largest ones of 3.0 m. Results for sizes, represented with thick contours, are presented in the paper. Those for in-between sizes with contours in broken lines can be obtained on demand.

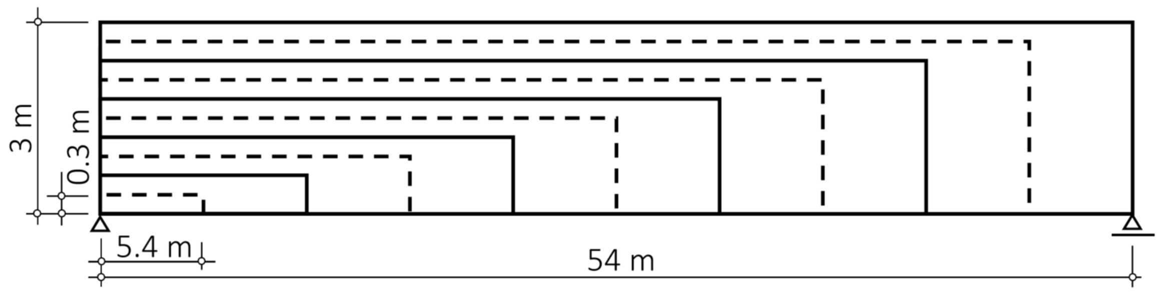

Figure 3. Modelled sizes of bending members with a constant depth to span ratio of 1/18.

3 Results

3.1 Representation of the strength data

The results of each computationally examined strength class are presented in an own section (3.3 -3.6). In order to impart the strength data as clearly and simply as possible, the four following data sections are uniformly arranged. A data section starts with three histograms and appertaining probability plots in the same line. These diagram pairs represent data for the key depths 0.6, 1.8 and 3.0 m. Each histogram contains a fitted Beta density also represented as a cumulative frequency distribution in the appertaining probability plot. The shape parameters alpha and beta are quoted below the probability plots. In these plots, the Beta distributions are compared with the computationally obtained bending strength values (f_m). The tables in each section contain the full set of the parameters for the fitted Beta distributions, also for the in-between depths 1.2 and 2.4 m. As an additional alternative to the Beta distributions, three-parameter Weibull distributions are specified for 2.4 and 3.0 m (C = shape parameter). The two last columns contain the mean values and standard deviations (SD) belonging to the Beta or Weibull fit. The diagram on the second data sheet of each class imparts an overview of selected percentiles and their dependence on the depth. These courses were evaluated from 0.3 to 3.0 m in 0.3 m steps. The vertical broken lines point out the key depths of 0.6, 1.8 and 3.0 m. The horizontal blue line marks the reference strength ($f_{m,k}$) and the red one the calculated design strength using a partial safety factor γ_M = 1.3 and a modification factor k_{mod} = 1.0. The green curve represents the design strength amended with the k_h-factor suggested with Equation (1).

3.2 Data analysis and discussion

With a depth of 0.6 m, the frequency distributions and the Beta densities in the histograms, respectively, are more or less symmetrical; with a depth of 3.0 m, they finally show a negative skewness.
The parameter estimation for the Beta and Weibull distributions follows an automatic procedure available in SAS 9.3. In most cases, this procedure provides a purposeful set containing threshold, scale, alpha, beta and C, respectively. In several cases, one or more parameters could not automatically be estimated so that a threshold was necessary to start the procedure. In these cases, a threshold of zero was defined. Afterwards, the shape parameters alpha, beta and C, respectively, and the scale could be determined automatically. The theoretical distributions were fitted under particular consideration of the lower distribution tails (Foschi et al. 1989; Larsen et al. 1999; Svensson et al. 2000). In this regard, the Weibull distributions, given in the lower lines of the tables, feature a slightly better adaptation to the lower tails compared to the Beta distributions in case of 2.4 and 3.0 m.
The comparisons between the cumulative frequency distributions of the computationally obtained data and the linearised Beta fit prove – even representative for depths of which comparisons are not shown in the paper – that the fitted Beta distributions suitably capture the empirically represented strength values. The tabulated mean values and standard deviations belonging to the theoretical Beta distributions show only marginal differences with the means and standard deviations given in the boxes of the corresponding histograms. Therefore, the fitted Beta distributions at least represent the mean and standard deviation of the original computational data.
The diagrams with the percentile courses show independently of the strength class, that the first percentile falls below the design strength if it is supposed to be constant (red line) and the depth becomes higher than ≈ 2.0 m (the corresponding points of intersection are highlighted by red circles in the Figures 5, 7, 9 and 11). This is particularly evident for GL28: Supposing k_{mod} = 1.0 and γ_M = 1.3, the constant design value of a 0.6 m deep beam comes to 28.1/1.3 ≈ 21.6 N/mm². In case of 0.6 m, a single strength value out of 1000 falls below the constant design strength, in case of 3.0 m finally more than 10 (see Figure 7). This observation may indicate an inconsistent reliability between 0.6 m deep beams and 3.0 m deep ones if both depths are stressed with the same design value. Hence, it is recommended to modify the strength with the given k_h-factor according to Equation (1). In doing so, the so modified depth-depending design strength (green curve) follows a course more or less in-between the minimum bending strength and the first percentile.

3.3 Data for GL24

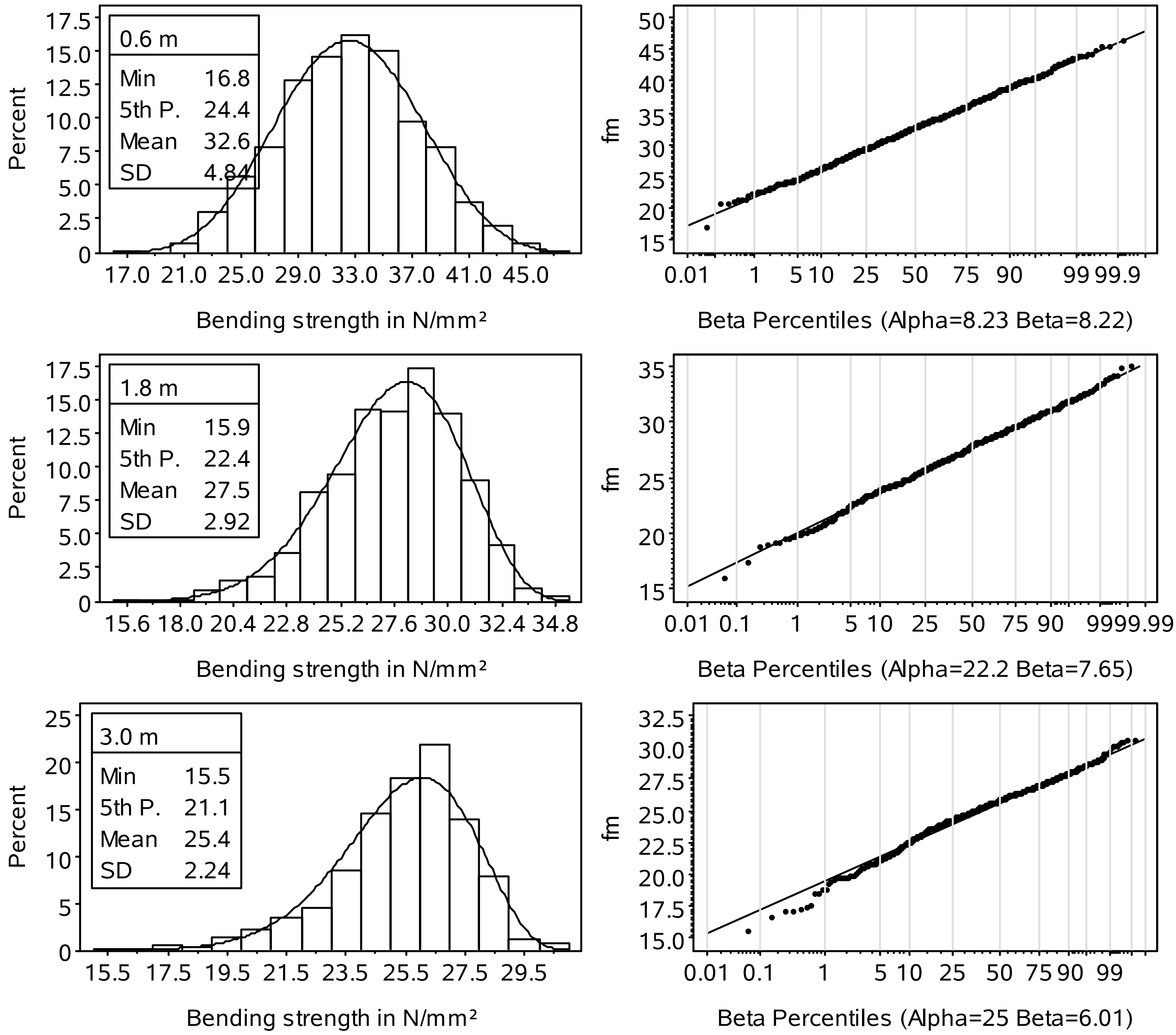

Figure 4. Modelled frequency and fitted Beta probability distributions, 1000 realisations each.

Table 2. Parameters of fitted Beta and Weibull distributions.

Depth m	Distr.	Threshold N/mm²	Scale N/mm²	Alpha -	Beta -	C -	Mean N/mm²	SD N/mm²
0.6	Beta	12.4	40.4	8.227	8.217	-	32.6	4.83
1.2	Beta	4.51	39.3	18.14	10.85	-	29.1	3.48
1.8	Beta	0	37.0	22.20	7.647	-	27.5	2.91
2.4	Beta	0	33.4	21.28	5.950	-	26.1	2.60
3.0	Beta	0	31.5	25.02	6.015	-	25.4	2.20
2.4	Weibull*	-6.96	34.2	-	-	15.42	26.1	2.63
3.0	Weibull*	-0,350	26.7	-	-	14.15	25.4	2.23

*Alternative providing a purposeful adaptation to the lower tail compared to Beta distribution

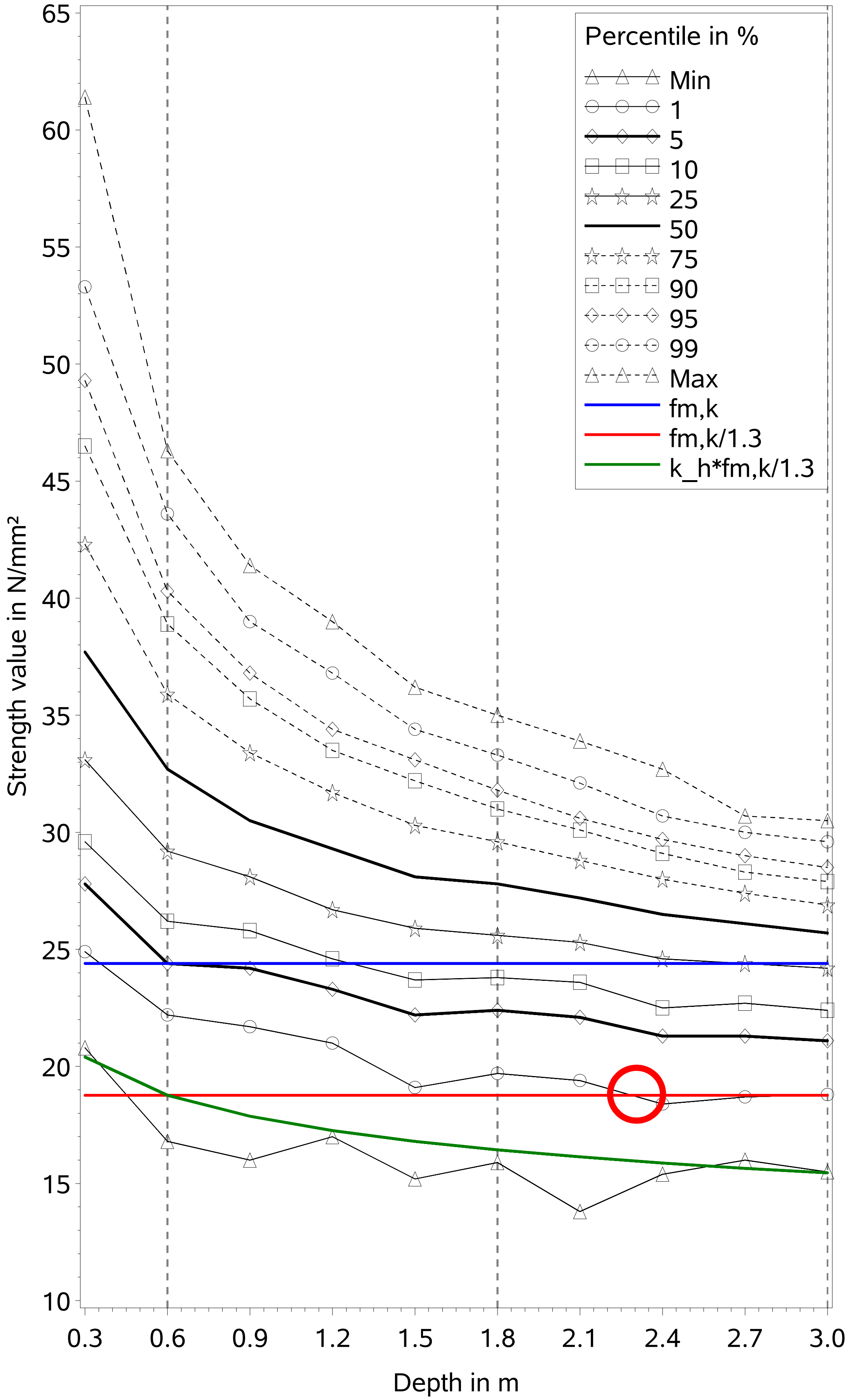

Figure 5. Minimum, maximum and selected percentiles of the bending strength over beam depth.

3.4 Data sheet for GL28

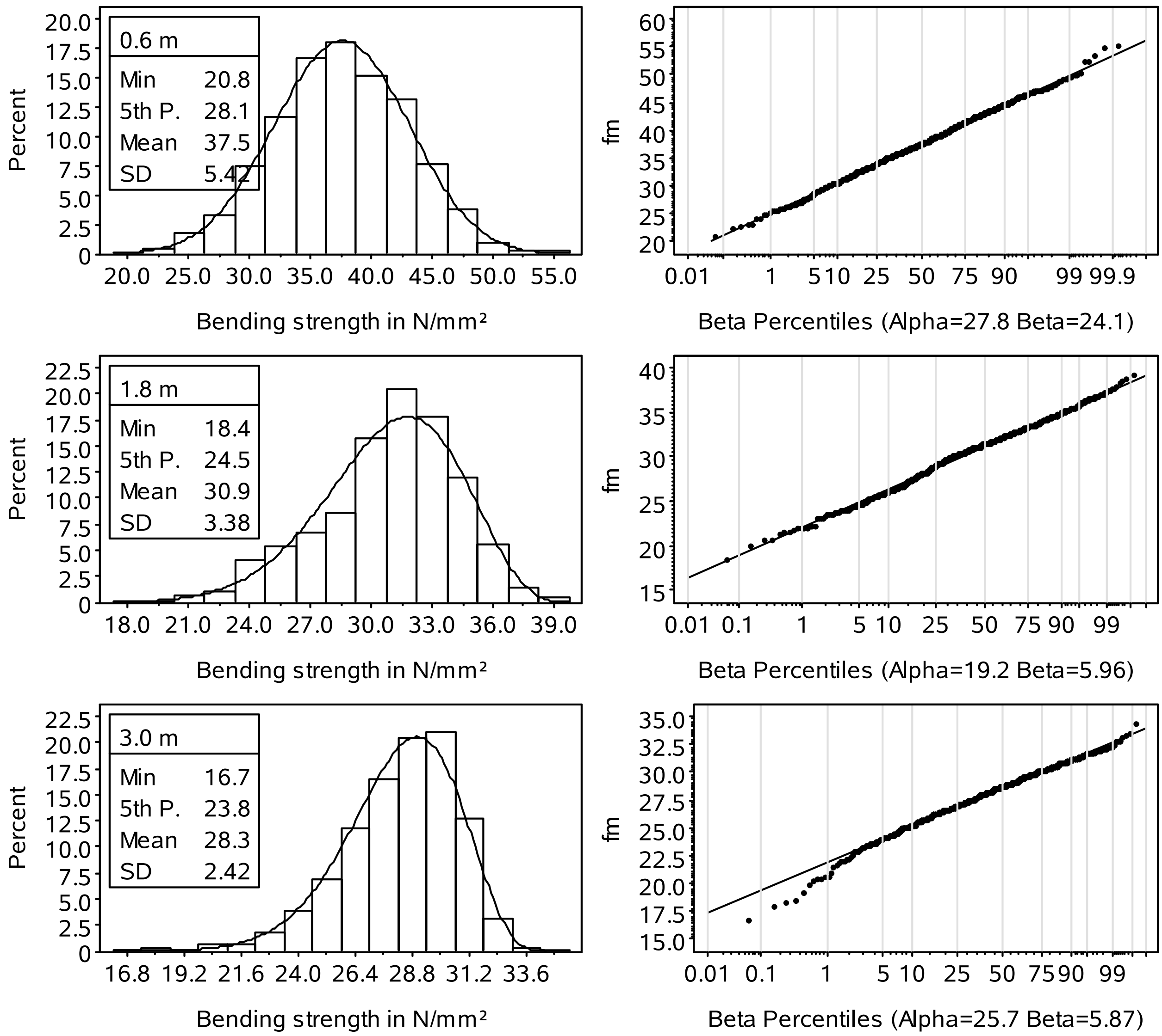

Figure 6. Modelled frequency and fitted Beta probability distributions, 1000 realisations each.

Table 3. Parameters of fitted Beta and Weibull distributions.

Depth m	Distr.	Threshold N/mm²	Scale N/mm²	Alpha -	Beta -	C -	Mean N/mm²	SD N/mm²
0.6	Beta	-4.80	79.0	27.76	24.08	-	37.5	5.42
1.2	Beta	7.62	39.1	12.04	6.542	-	33.0	4.22
1.8	Beta	0	40.4	19.20	5.955	-	30.9	3.36
2.4	Beta	0	36.5	20.73	5.011	-	29.4	2.79
3.0	Beta	0	34.7	25.73	5.867	-	28.3	2.36
3.0	Weibull*	-13.9	43.2	-	-	21.7	28.3	2.41

*Note below table 2

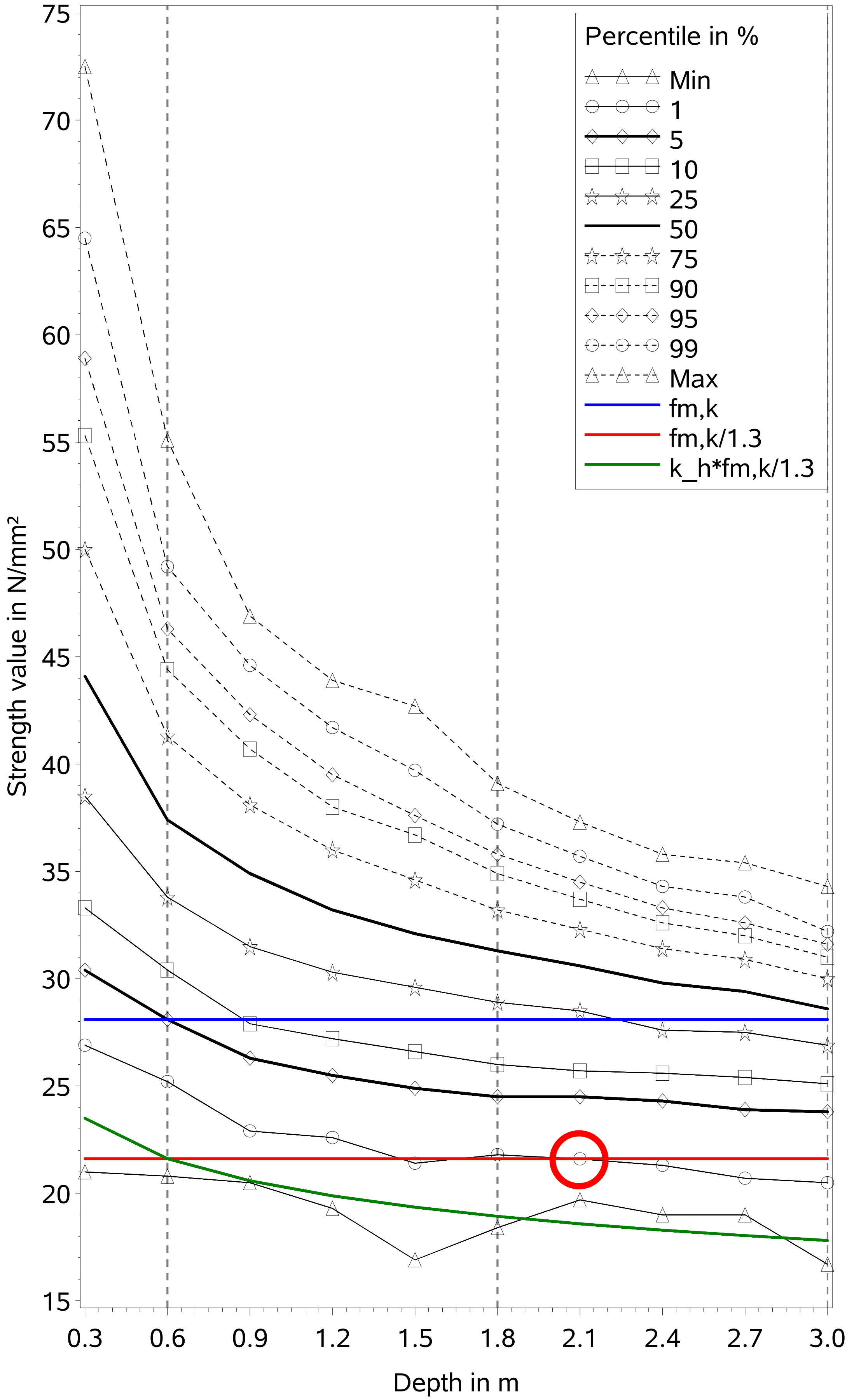

Figure 7. Minimum, maximum and selected percentiles of the bending strength over beam depth.

3.5 Data sheet for GL32

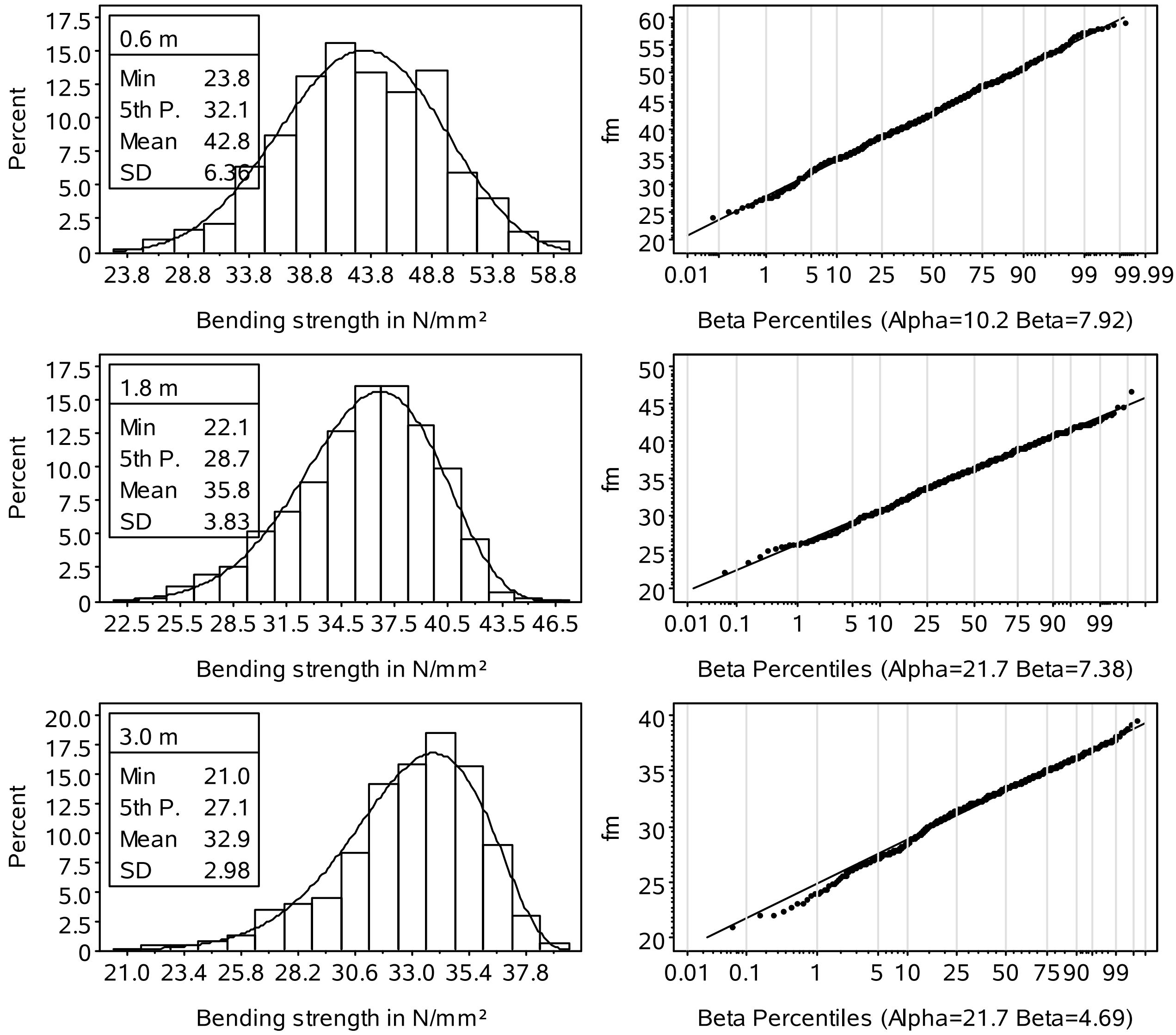

Figure 8. Modelled frequency and fitted Beta probability distributions, 1000 realisations each.

Table 4. Parameters of fitted Beta and Weibull distributions.

Depth m	Distr.	Threshold N/mm²	Scale N/mm²	Alpha -	Beta -	C -	Mean N/mm²	SD N/mm²
0.6	Beta	11.2	56.0	10.19	7.917	-	42.8	6.36
1.2	Beta	8.38	45.0	13.25	6.728	-	38.2	4.64
1.8	Beta	0	48.0	21.74	7.381	-	35.8	3.80
2.4	Beta	0	43.7	19.93	5.787	-	33.8	3.53
3.0	Beta	0	40.0	21.68	4.692	-	32.8	2.92
3.0	Weibull*	-31.9	66.1	-	-	27.28	32.9	2.97

*Note below table 2

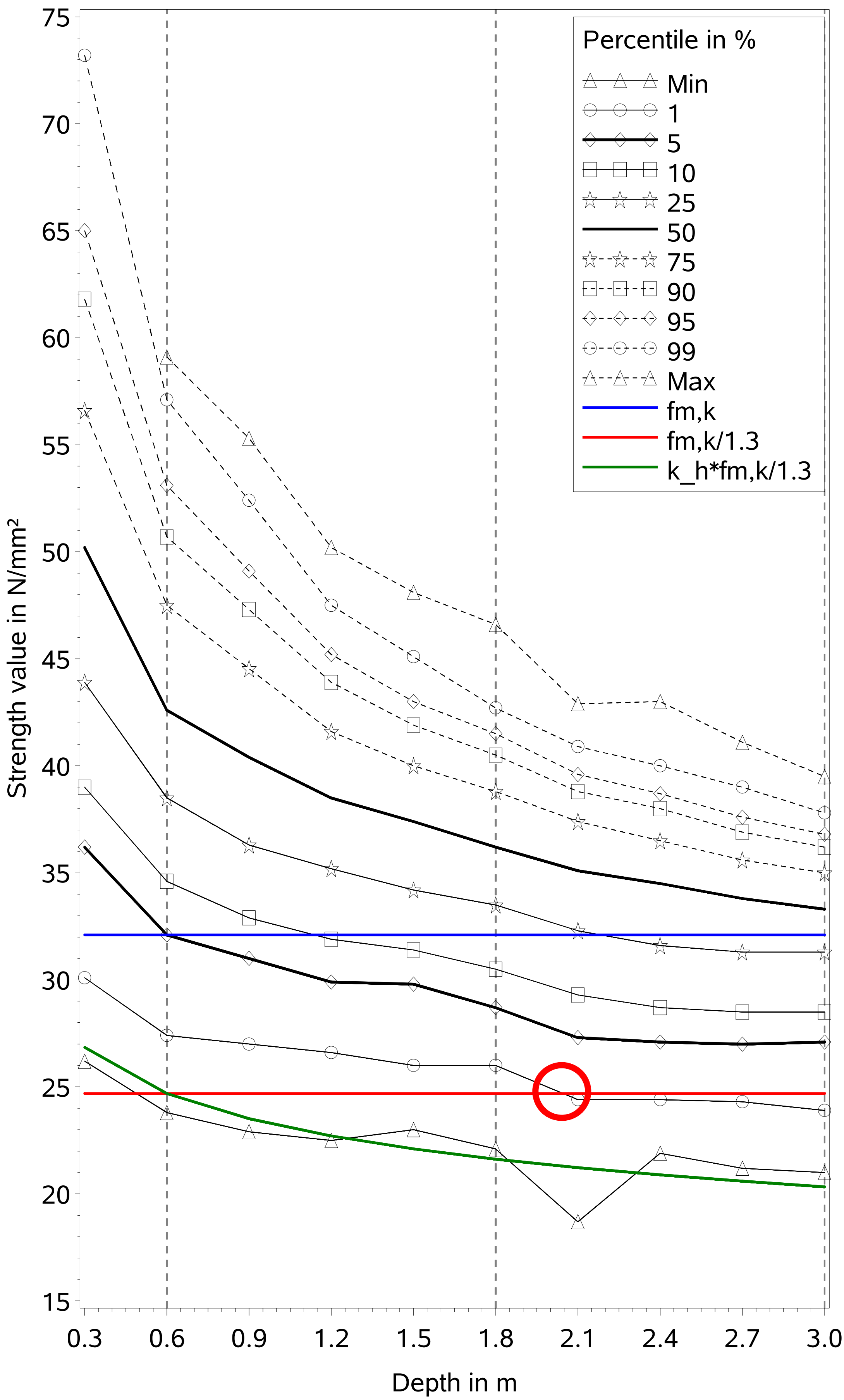

Figure 9. Minimum, maximum and selected percentiles of the bending strength over beam depth.

3.6 Data sheet for GL36

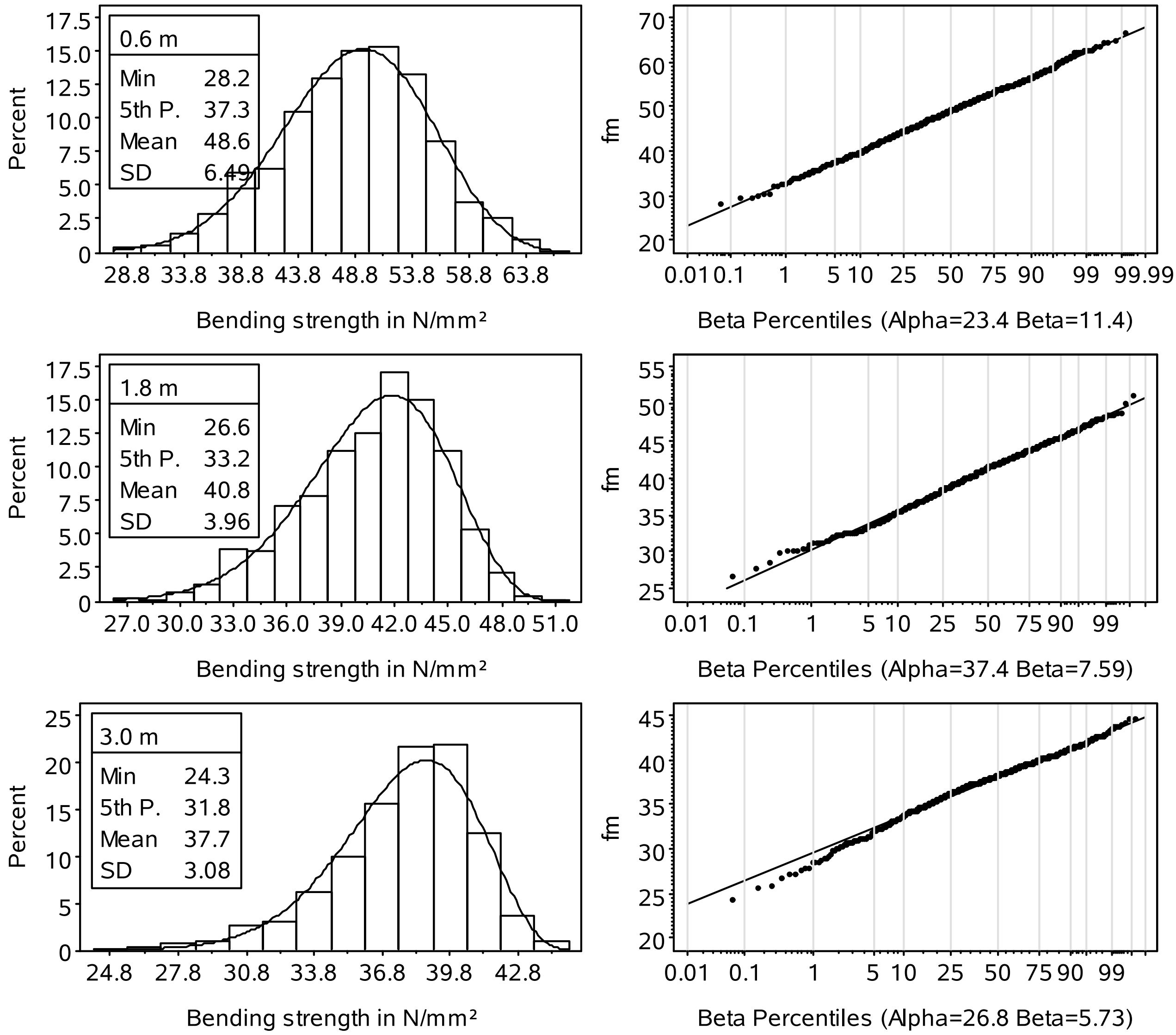

Figure 10. Modelled frequency and fitted Beta probability distributions, 1000 realisations each.

Table 5. Parameters of fitted Beta and Weibull distributions.

Depth m	Distr.	Threshold N/mm²	Scale N/mm²	Alpha -	Beta -	C -	Mean N/mm²	SD N/mm²
0.6	Beta	-6.91	82.6	23.38	11.42	-	48.6	6.48
1.2	Beta	17.3	39.2	8.762	4.489	-	43.2	4.92
1.8	Beta	-18.7	71.5	37.35	7.587	-	40.8	3.95
2.4	Beta	0	47.6	21.82	4.870	-	38.9	3.49
3.0	Beta	0	45.8	26.79	5.727	-	37.7	3.01
3.0	Weibull*	-13.9	52.9	-	-	20.86	37.7	3.07

*Note below table 2

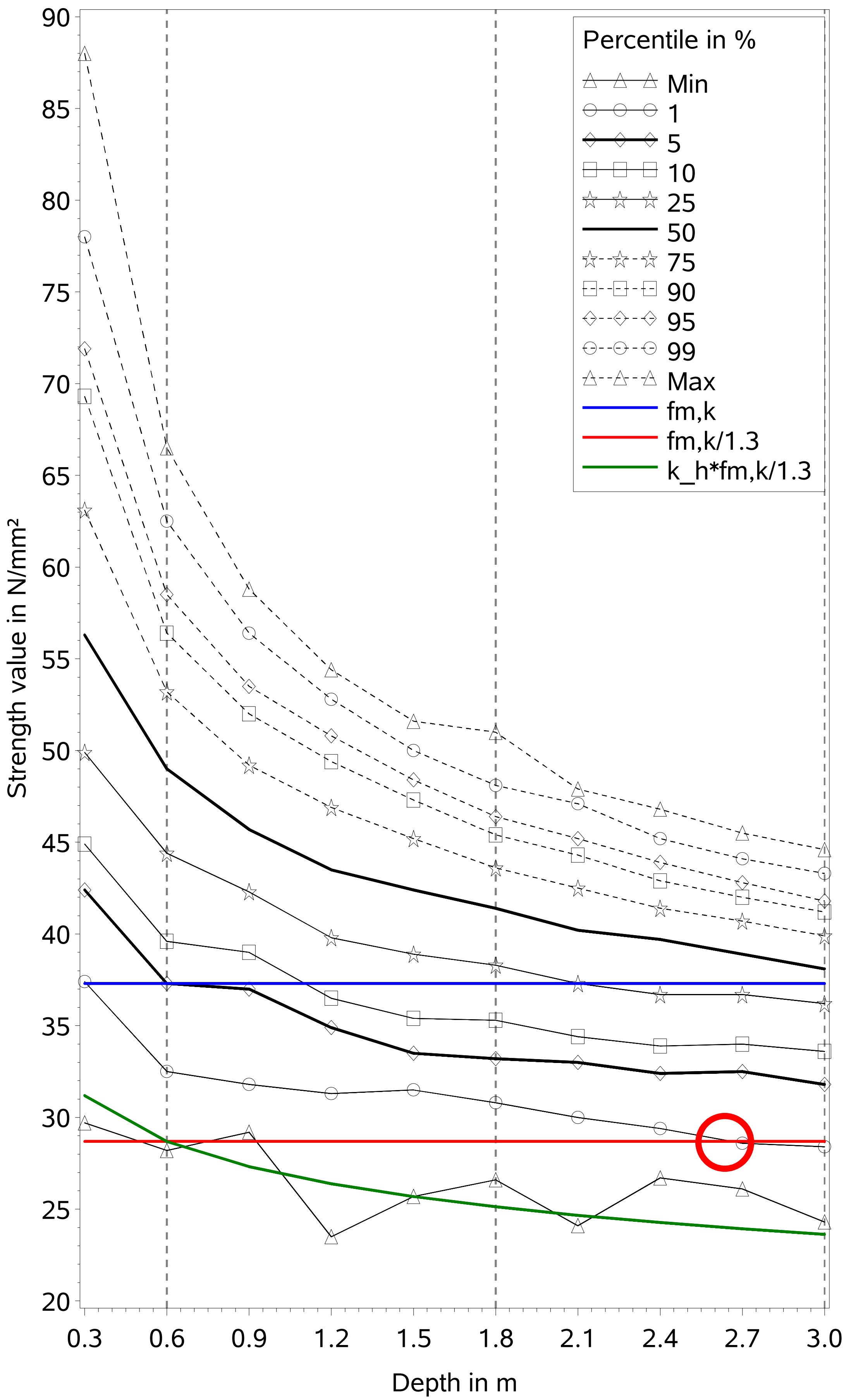

Figure 11. Minimum, maximum and selected percentiles of the bending strength over beam depth.

4 Conclusions

Based on a computationally modelled bending strength for glulam beams with varying volume, it is shown that an inconsistent reliability between small and deep bending members may exist. This assumption refers to computationally examined strength classes complying with GL24 up to ≈ GL36. Using a k_h-factor having an exponent of 1/8.288 according to Eurocode 5 format, one could obviously compensate size effects for beams with a depth of up to 3.0 m. In comparison with current provisions, this compensation would be on the safe side. The computationally determined strength data trigger the reflection whether the extent of consequences in case of bending failure of large members are adequately considered in the current provisions of Eurocodes “0” and 5.
The paper provides purposeful theoretical bending strength distributions so that reliability experts may define precise strength modifications in order to create a more consistent reliability level throughout a depth range from 0.3 up to 3.0 m. All the computationally determined strength data, described in the paper, will be made available on demand in its current txt format. The complete data encompass 60,000 single bending strength values, which are organised in different strength levels and depths.

5 References

EN 1995-1-1:2004 Eurocode 5: Design of timber structures – Part 1-1: General – Common rules and rules for buildings

Frese, M; Blaß, HJ (2008): Bending strength of spruce glulam – New models for the characteristic bending strength. CIB-W18/41-12-2, St. Andrews, New Brunswick, Canada

Frese, M; Blaß, HJ (2015): Numerical description of size and load configuration effects in glulam structures. 12th International Conference on Applications of Statistics and Probability in Civil Engineering, Vancouver, Canada

Frese, M (2016): Computergestützte Verfahren zur pragmatischen Beurteilung der Tragwiderstände von Brettschichtholz. Bd. 31 Karlsruher Berichte zum Ingenieurholzbau, KIT Scientific Publishing

EN 408:2010+A1:2012 Timber structures – Structural timber and glued laminated timber – Determination of some physical and mechanical properties

Frese, M (2010): Computer-aided simulation of glulam strength parallel to grain. 4th European Conference on Computational Mechanics, Paris, France

Foschi, RO; Folz, BR; Yao, FZ (1989): Reliability-Based Design of Wood Structures. Structural Research Series, No. 34, Department of Civil Engineering, University of British Columbia

Larsen, HJ; Svensson, S; Thelandersson, S (1999): Determination of Partial Coefficients and Modification Factors. CIB-W18/32-1-1, Graz, Austria, 1999

Svensson, S; Thelandersson, S (2000): Aspects on reliability calibration of safety factors for timber structures. CIB-W18/33-1-1, Delft, The Netherlands

EN 1990:2002 Eurocode “0”: Basis of structural design

Discussion

The paper was presented by M Frese

J Köhler commented that it was good to propose a size effect for bending strength of glulam. He commented that as this was still artificial data we have to be careful. Because no experiments were conducted it should be mentioned. Choice of distribution function might be better optimized. As comparisons were made with minimum values, this would be sensitive from a probability point of view. M Frese responded that the data were generated for future reliability analysis and the data set would be available for use by reliability experts. J Köhler commented model uncertainties should be considered and more information about the model would be needed to estimate the uncertainties. M Frese responded that a paper will be presented in WCTE 2016 about the model in more detail.

P Dietsch asked about how the model related to experimental evidence and which range could be related. M Frese said that the original data was created in the 1980s on board elements as basic data. There has been a number of series of full scale testing of beams since then to validate the model. This included two series of 20 beams each of two different strength classes and 150 boards and 150 finger joints.

G Fink commented that the characteristic values of the larger beams were not changing as much. The model might not fit the lower tail well. He commented that with a sample size of 1000 beams with low height, one should get some beams with extremely low realizations but this was not seen from the results of the model. He stated that this could be covered by the model uncertainty issue. G Fink and J Köhler and M Frese discussed the importance of variability and the shape of the lower tail of the distribution.

P Quenneville asked about the variability of the loading. M Frese responded this would be a topic for reliability study and not within the scope of this paper.

F Lam commented about the similarity of the k or shape factor between the Canadian study on glulam size effect and this paper. He asked about the effect of width of the laminates. M Frese stated that this was not considered because this was already taken into consideration by grading of the boards. F Lam suggested that study on size effect on shear strength in glulam would also be appropriate.

A Frangi commented that in a study where bending tests were conducted on specimens taken from a failed structure he found a real beam with strength lower than the minimum value. H Blass responded that this could be production error which was not considered in this paper.

Z Li asked about the failure criterion considered in the FEM and what was the size of FEM element considered. M Frese stated that failure of the outmost laminate in tension was considered. The element size in the model was not changed because element size was tied to regression equations used in the basic data set.

G Schickhofer commented that we should consider size effects in our design standards including other properties. M Frese agreed.

P Quenneville commented that large beams are produced with less industrialization. M Frese responded that the quality control for checking of finger joints would be the same for all beam sizes.

P Zarnani asked about the possibility of using the model for LVL. H Blass responded that LVL is a completely different material.

BJ Yeh suggested consideration of width effect because in N America it is a volume consideration.

P Zarnani asked whether the difference was due to grading and not size. M Frese responded no and that in this study only homogeneous beams were considered

V Rajcic commented that it would be a good idea to get data from glulam companies.

Need to consider modal participation in vibration serviceability design of Cross-Laminated-Timber slabs

Ebenezer Ussher, Jan Weckendorf, Kaveh Arjomandi, Ian Smith
University of New Brunswick, Fredericton, NB, Canada

1 Introduction

Vibration serviceability of various types of timber floor systems has received much attention in recent decades, with various design guidelines having been proposed. Proposed design methods range from simple limits of static deflection, to ones intended to limit bounciness, acceleration levels or peak velocity at floor surfaces caused by defined excitations [e.g. 1-3]. However, except for the most sophisticated dynamic analysis based approaches, proposed approaches are based on empirical discriminative pass-or-fail criterion/criteria. Empirical criterion/criteria discriminate between acceptable and unacceptable prospective designs depending on values of a single simply estimated parameter (e.g. d_1 = static deflection under a 1kN concentered load, f_1 = fundamental natural frequency) or a function containing two parameters (e.g. function of f_1 and d_1). Such criterion/criteria are calibrated to achieve a desired balance between errors resulting in under- and over-designed floors [4]. In this context error means in-service performances of particular floors are incorrectly predicted to be acceptable (under-designed) or unacceptable (over-designed) to building occupants. Multiple reasons underpin why errors occur, with common explanations including:

- Criterion/criteria being based on random sampling of perceptions of how floors in occupied buildings perform, with contamination of opinions by factors beyond effects design parameters can mimic (e.g. extraneous visual and audio cues).
- Mismatch between occupancy and design analysis situations, including factors like variations in damping characteristics and effects of non-structural features on static and dynamic responses of floors.
- Application of criterion/criteria beyond the scope of their calibration (e.g. different construction materials, support conditions or plan shape). Even

simple construction detailing and material substitution decisions can invalidate applicability of a criterion/criteria calibration.

Arguments have commonly been advanced that design criterion/criteria must be simple to apply and need only account for effects of easily estimated structural responses (e.g. of f_1 and d_1) [e.g. 1,5]. These arguments have mostly been made by proponents of approaches aimed specifically at design of lightweight joisted floors in domestic residences [e.g. 1], and simple timber slabs [5]. In such specific contexts, and when floors directly match construction details and building occupancy situations employed during calibration of a criterion/criteria, the arguments may be acceptable. However, it is important to remember that resulting surety addresses long-run acceptability of frequencies of under-designed floors (i.e. not performances of individual floors). Setting a bias in criterion/criteria so over-design predominates this is typical [e.g. 1,5], but with long-run material inefficiencies.

Generalized dynamic-response-based approaches have already been recognized as the most reliable approach to vibration serviceability design of lightweight timber floors. Provisions in Eurocode 5 [3] are based on the work of Ohlsson [2] who developed dynamic response criteria applicable to rectangular lightweight joisted floors simply supported along all edges. That approach addresses influences modes other than the fundamental mode have on motions of floor surfaces building occupants will sense and possibly find objectionable [4]. Within the Eurocode 5 approach designers are required to estimate the parameter n_{40}, which is the number of first-order modes with natural frequencies up to 40 Hz. Depending on the type of construction and variables (e.g. floor plan aspect ratio, joist and subflooring flexural rigidities), reliable estimation of modal frequencies and therefore n_{40} can be achievable by explicit formulae or application of numerical analytical approaches (e.g. Finite Element Methods, FEM). In practice n_{40} is the filtering frequency selected by Ohlsson as appropriate to exclude insignificant components of modal participations in aggregated motions occurring at floor surfaces. Important to recognize is appropriate filtering frequencies may not be 40 Hz for other types of floors, or possible not apply to joisted floors that are not rectangular on plan or simply supported along all edges. This reflects that appropriate filtering frequencies can differ (for the same floor construction method) for situations outside the specific conditions studied.

The remainder of this paper addresses questions related to acceptability of vibration serviceability approaches that ignore the contributions of higher order modal frequencies to motions of Cross-Laminated-Timber floor (CLT) slabs. Although for the moment consideration is only given to rectangular slabs with relatively simple support conditions, the findings do address questions such as whether employing a single filtering frequency like n_{40} is viable. The adopted approach is to analyse dynamic time-history responses of CLT slab featuring construction features like plate edges free to vibrate, plan aspect ratio and presence or absence of intra-slab construction joints. The time-history responses are obtained using verified FEM models, with human footfall impacts or unit impulsive force being the loading function. Time-history responses are analyzed to determine how choice of a filtering (modal participation) influences estimation of parameters like peak displacement, acceleration and velocity. This is done because prior experimental investigation revealed modes with higher frequencies up to about 100 Hz participate in CLT floor motions humans perceive [6]. Future papers will address specifics of provisions suitable for inclusion in Eurocode 5 or other design codes.

2 Building occupant sensitivity to floor motion

Humans are sensitive to and disturbed by motion intensities well below those required to damage buildings they occupy. Activities like walking, running, jumping and rhythmic exercises commonly cause objectionable motion levels [2], with human toleration depending on the frequency contents, accelerations and velocities of motions [2,7,8]. The literature implies human sensitivity is mainly to modal frequency or modal frequency separation components that coincide directly or harmonically with natural vibration frequencies of human organs [4,7-10]. Engineering design criteria have often been formulated according to the simple notion that filtering out designs of floors predicted to have fundamental modal frequencies circa < 8 Hz will eliminate most vibration serviceability problems [4]. Unfortunately attractive as the simplicity may be it is inconsistent with scientific studies. Scientifically speaking human toleration of motion relates to acceleration/velocity levels they experience, and is conditional on their activities and physical environment at the time they experience motion [8-10].

Various ways of assessing whether footfall type impacts will cause floor motions objectionable to human observers have been proposed. Floor responses to so-called heel-drop impacts is a popular choice [e.g. 2,4,8]. During a heel-drop impact test a subject raises themselves on their toes and suddenly releases their gravitational weight so that they impact the surface of a floor which will then vibrate to rest. During the free vibration phase subjects are part of the system mass and a supplemental damping source [2]. Preferences for such tests reflect the simplicity and reproducibility (i.e. statistical averaging of acceleration responses or derived velocities) under field investigation conditions [2,8]. Tests have also been performed to characterize footfall loadings during heel-drop, walking, running, exercising and other activities causing impacts on floors. Those tests characterized force levels, durations and frequency contents of individual impacts [e.g. 2,4,7,10,11].

Analytical models have been developed for lightweight joisted floors to predict Weighted Root-Mean-Square Acceleration, A_{RMS}, produced by heel-drop impacts [4], or peak velocity, v, caused by a 1 Ns impulse [2]. The former was developed as part of design criteria developed in the United Kingdom and the latter as part of Swedish criteria [2] subsequently adopted by Eurocode 5 [3]. For the purposes of discussion here responses of floors to unit impulses (1 Ns) or walking and running impacts are considered.

3 Prediction of CLT slab motions

Un-damped free elastic vibration of thin slabs is a function of the geometry (i.e. plan dimension, plan shape), the support conditions, and their inherent properties (thickness, elastic properties and density). Need to consider their through-thickness shear deformations depends on the ratio of plate thickness to the characteristic plan dimension. Un-damped natural frequencies are eigenvalues of equation (1);

$$det([K] - \omega^2[M]) = 0 \qquad (1)$$

where $[K]$ and $[M]$ are stiffness and mass matrices respectively, and ω is the circular modal frequency vector.

Time-history responses for damped forced vibration are obtained by solving equation (2);

$$[M]u''(t) + [D]u'(t) + [K]u(t) = F(t) \qquad (2)$$

where $[D]$ is the damping matrix; $u(t)$, $u'(t)$ and $u''(t)$ are displacement, velocity and acceleration vectors respectively; and $F(t)$ is the loading function. Fourier series expansions can be employed to define $F(t)$, including mimicking human footfall impacts, according to equation (3) [11];

$$F(t) = G[1 + \sum \alpha_i \sin(2\pi i f_p - \phi)] \quad i = 1, n \qquad (3)$$

where G denotes a person's weight, α_i is the Fourier coefficient of the i^{th} harmonic (also called the dynamic load factor), f_p is the activity rate, ϕ is the phase angle, and n is the number of terms in the series expansion for a particular $F(t)$. The common range of walking frequency is between 1.2 and 3 Hz, with frequencies > 3.2 Hz representing jogging or running. The dynamic force of walking has been found to excite frequencies up to the third or fourth harmonic of the walking frequency [10]. Lightweight timber floors typically have relatively low fundamental natural frequencies and other modal frequencies tend to cluster [4]. Therefore, even without quantitative consideration of solutions to equation (2) it is implicit that reliable assessment of vibration serviceability of such floors must address how more than the fundamental mode influence human perceptions of motions caused by footfall impacts. It is equally clear which defines the expected types and frequencies on impacts. Figures 1(a) and 1(b) illustrate force-time histories of foot impacts according to equation (3). To note is the presence of distinct peaks in *F(t)* that correspond to a heel strike and a toe lift-off during walking, but not running.

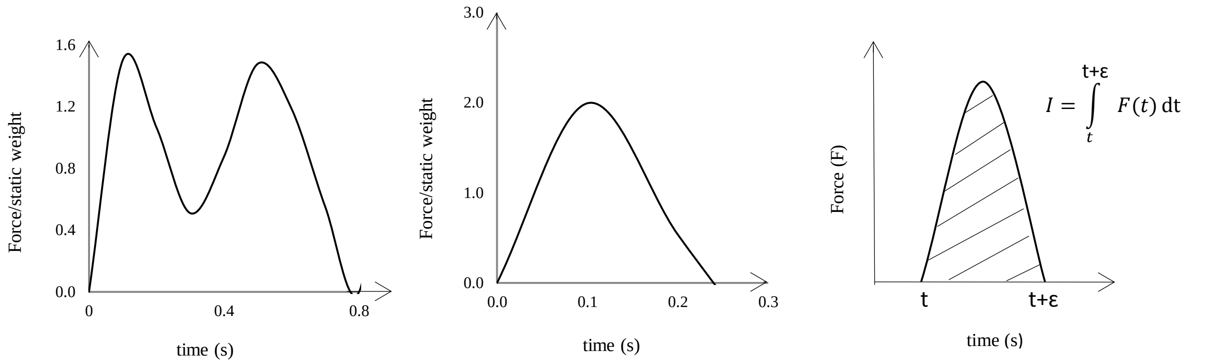

(a) walking *(b) running* *(c) impulsive force model*

Figure 1: Typical human footfall and impulsive loading functions

As an alternative to employing *F(t)* realistically represent footfall impacts it has been defined as an impulsive forces (I) theoretically applied instantaneously [2]. In analyses such impulsive forces have been represented as functions having a very short duration and very large peak value with the area under the function equaling I [12], as illustrated in Figure 1(c).

4 FEM models of CLT floor motions

FEM modelling techniques previously developed and verified by the authors [13] are used as the basis of predicting time-history responses of CLT floors according to equation (2).

Floor systems analyses presented below are for systems matching ones investigated experimentally at the University of New Brunswick. Modal characteristics of those floors have been accurately predicted (Section 5.1), implying time-history responses will also accurately replicate responses of corresponding physical systems. Consequently predictions here about sensitivity of vibration serviceability performances of floors to higher modal order components of *u(t)*, *u'(t)* and *u"(t)* are expected to be reliable for various *F(t)*.

Two floors systems having 175 mm thick 5-ply CLT plate segments [14] were analyzed:

- *Floor 1:* Single rectangular CLT segment with two opposite sides simply supported and other sides free to vibrate; span *L* = 5.5 m, width *W* = 2.28 m.
- *Floor 2:* Two CLT segments with two opposite sides simply supported and other sides free to vibrate; *L* = 5.5 m, *W* = (2 x 2.28 -0.064)m = 4.50m. The CLT segments are edge-to-edge jointed using a full segment-length half-lap joint secured using 6 mm diameter by 160 mm long self-tapping screws placed at 300 mm centres. This enforced vertical motion compatibility but not rotational motion continuity across the half-lap joint.

These two cases were investigated because they exhibit mode shapes that are either symmetrical or unsymmetrical in the slab width direction. *Floor 2* exhibits more pronounced clustering of modal frequencies than *Floor 1* due to its higher plan aspect ratio (*W/L*) and presence of the intra-slab joint. Figure 2(a) shows the physical test version of *Floor 2*, and Table 1 summarizes material properties of the CLT, which is treated as an orthotropic plate [15].

Table 1: Apparent properties of CLT used in dynamic FEM model*

Property	Units	Value
Density, ρ	Kg/m^3	500
Elastic moduli:		
E_1	GPa	11.5
E_2	Gpa	4.0
E_3	Gpa	2.0
Shear moduli:		
G_{12}	GPa	0.900
G_{13}	GPa	0.090
G_{23}	GPa	0.063
Poisson's ratios		
v_{12}	--	0.44
v_{13}	--	0.30
v_{23}	--	0.30
Damping ratio, ζ	%	1.0

* Direction 1 - parallel to span, direction 2 - perpendicular to span, direction 3 - perpendicular to plate

Floor slab models were created using the widely known Abaqus CAE commercial software [16]. Type S4 orthotropic linear shell elements were used to represent CLT segments. Figure 2(b) shows the FEM mesh for *Floor 2* in which elements have side dimensions of about 0.1 m x 0.1 m, selected based on a convergence study that determined suitability of that size. Roller line supports were created along the simply supported end edges, with additional pin constrains to satisfy system equilibrium requirements.

For *Floor 2* the plate segment-to-plate segment half-lap joint was simulated by incorporating orthogonal spring elements interconnecting coincident nodes of the plate meshes. Horizontal springs had stiffnesses matching those of laterally loaded self-tapping screws, and vertical springs were assigned very high stiffnesses to prevent vertical separation of plate meshes.

5 FEM predictions

5.1 Modal characteristics of study floors

Table 2 shows experimentally and FEM derived modal frequencies for the two study floors. The small discrepancies are attributable to FEM models not accounting for minor geometric imperfection and material variability within CLT.

(a) Laboratory specimen

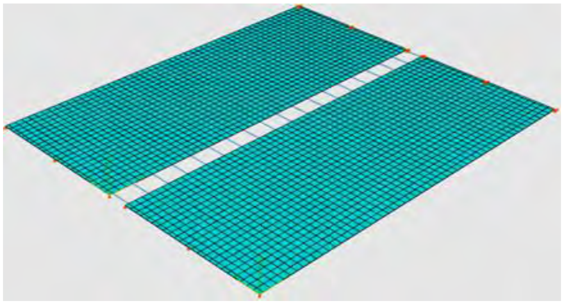

(b) FEM mesh of slab

Figure 2: Two plate segment system simply supported at ends (Floor 2)

Table 2: Comparison of experimental and FEM modal frequencies (Hz)

Mode* (*m*,*n*)	*Floor 1:* single segment slab				*Floor 2:* two segment slab			
	Mode	Test	FE	Error	Mode	Test	FE	Error
1,1	1	12.0	11.9	-0.1	1	11.5	11.9	+0.4
1,2	2	19.7	19.1	-0.6	2	14.3	14.1	-0.2
1,3	6	91.8	87.3	-4.5	3	19.2	19.1	-0.1
2,1	3	41.7	41.1	-0.6	4	39.8	41.1	+1.3
2,2	4	51.4	48.7	-2.7	5	44.7	43.4	-1.3
2,3	-	--	--	--	6	49.1	48.7	-0.4
1,4	-	--	--	--	7	62.2	61.2	-1.0
3,1	5	77.7	77.6	-0.1	8	71.0	77.6	+6.6
2,4	-	--	--	--	9	78.2	78.8	+0.6
3,2	-	--	--	--	10	82.8	79.7	-3.1
3,3	-	--	--	--	11	88.2	84.6	-3.6
1,5	-	--	--	--	12	91.6	87.3	-4.3

**m,n* denotes the degree of curvature in plan and width directions respectively

5.2 Time history responses to a unit impulse

Time history response analyses were performed using a 1 Ns impulsive force as the load function, applied at the floor centre position. That enabled evaluation of the applicability of frequency filtering practices. For example, examination of Eurocode 5 approach which is requiring assessment of the expected peak velocity (*v*) caused by a 1 Ns impulse [3]. The time integral function used to represent a unit impulse force in the FEM models is shown in Figure 3.

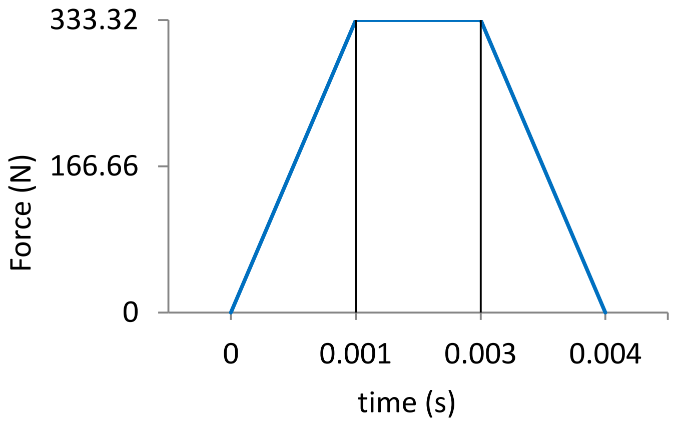

Figure 3: Unit impulse amplitude employed in FE analysis

Table 3 compares peak displacement u_{peak}, velocity u'_{peak} and acceleration u''_{peak} values for a 1 Ns impulse predicted for various frequency filtering thresholds up to 100 Hz. In all cases the shown peak responses occurred at mid-span of floor towards an unsupported side (about 150mm from an unsupported side was considered based on parametric studies). An average of 1% damping ratio was employed with reference to the Canadian CLT Handbook [5,6].

Table 3: Effects of frequency filtering on predictions of peak displacement, velocity and accelerations created by a 1 Ns impulsive force applied to CLT floor slabs

Peak response	Modal participation				
	Fundamental mode only	Modes with frequencies ≤ 40Hz	Modes with frequencies ≤ 60Hz	Modes with frequencies ≤ 80Hz	Modes with frequencies ≤ 100Hz
			Floor 1: single segment slab		
No. of modes	1(1*)	2(2)	4(2)	5(2)	6(3)
Displacement, u_{peak} (10^{-6}m)	25.26	51.76	51.76	54.63	62.85
Velocity, u'_{peak} (10^{-3}m/s)	1.857	5.227	5.227	5.402	8.716
Acceleration, u''_{peak} (m/s^2)	0.634	1.825	1.825	2.295	3.645
			Floor 2: two segments slab		
No. of modes	1(1)	3(3)	6(3)	9(4)	12(5)
Displacement, u_{peak} (10^{-6}m)	12.34	41.90	41.90	43.11	47.40
Velocity, u'_{peak} (10^{-3}m/s)	0.908	3.904	3.904	4.059	5.414
Acceleration, u''_{peak} (m/s^2)	0.310	1.352	1.352	1.627	2.286

*the number in parenthesis indicates the number of first order modes (single curvature in span direction)

Figure 4 shows the FEM predicted acceleration (u'') time-history response for *Floor 2* induced by a unit impulsive force. As shown, taking only the fundamental mode, or modes with natural frequencies up to 40 Hz, into account is very inaccurate. The same applies to derived responses velocity (u') and displacement (u).

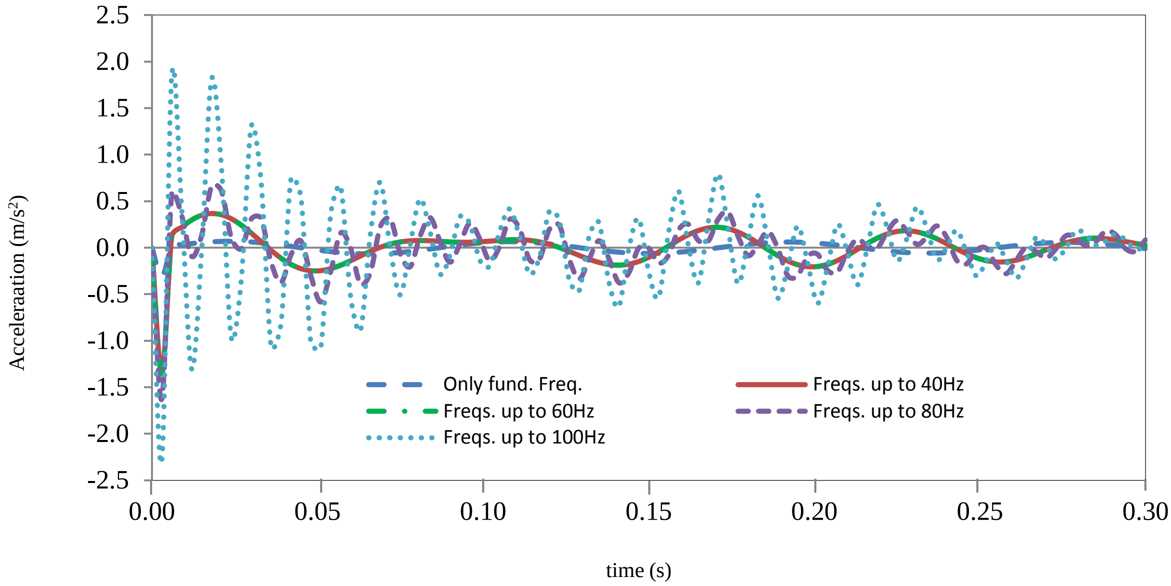

Figure 4: Acceleration (u") time history responses for Floor 2

5.3 Time history responses under walking and running footfall impacts

Responses of the study floors to human footfalls during walking and running were predicted by representing impacts using equation (3), and considering up to the third harmonic. Table 4 summarizes the dynamic load factors (α_i) and corresponding frequencies employed, based on Rainer and Pernica [10] and weight of person causing impacts (G) was assumed to be 700 N.

Table 4: Dynamic load factors, and frequencies for walking and running impact forces

Harmonic	Walking		Running	
	α_i	Frequency [Hz]	α_i	Frequency [Hz]
1	0.52	2.4	1.4	3.6
2	0.24	5.6	0.4	3.2
3	0.06	5.8	0.35	6.6

Although in reality footfall impacts occur as moving loads, the simplification was introduced of applying a single impact at the centre of the floor surface.

Tables 5 and 6 show u_{peak}, u'_{peak} and u''_{peak} values for walking and running impacts respectively, as functions of the filtering frequency. Results in those tables reinforce the findings for a unit impulsive force, by also demonstrating effects of higher order modes on responses of CLT slab floors are significant.

Comparison of magnitudes of u_{peak}, u'_{peak} and u''_{peak} values in Tables 5 and 6 illustrates the importance of matching response evaluation criteria to the type of activities taking place within buildings having different occupancy

Table 5: Effects of frequency filtering on predictions of peak displacement, velocity and accelerations created by a single walking footfall impact

Peak response	Modal participation				
	Fundamental mode only	Modes with frequencies ≤ 40Hz	Modes with frequencies ≤ 60Hz	Modes with frequencies ≤ 80Hz	Modes with frequencies ≤ 100Hz
			Floor 1: single segment slab		
No. of modes	1(1*)	2(2)	4(2)	5(2)	6(3)
Displacement, u_{peak} (10^{-6}m)	391.3	634.2	634.2	643.1	664.5
Velocity, u'_{peak} (10^{-3}m/s)	7.140	10.81	10.81	10.98	11.32
Acceleration, u''_{peak} (m/s^2)	0.331	0.548	0.548	0.585	0.692
			Floor 2: two segment slab		
No. of modes	1(1)	3(3)	6(3)	9(4)	12(5)
Displacement, u_{peak} (10^{-6}m)	191.0	578.5	578.5	584.0	595.5
Velocity, u'_{peak} (10^{-3}m/s)	3.489	9.690	9.690	9.764	9.934
Acceleration, u''_{peak} (m/s^2)	0.162	0.593	0.593	0.598	0.617

Table 6: Effects of frequency filtering on predictions of peak displacement, velocity and accelerations created by a single running footfall impact

Peak response	Modal participation				
	Fundamental mode only	Modes with frequencies ≤ 40Hz	Modes with frequencies ≤ 60Hz	Modes with frequencies ≤ 80Hz	Modes with frequencies ≤ 100Hz
			Floor 1: single segment slab		
No. of modes	1(1*)	2(2)	4(2)	5(2)	6(3)
Displacement, u_{peak} (10^{-6}m)	494.5	826.9	826.9	838.2	865.3
Velocity, u'_{peak} (10^{-3}m/s)	11.00	15.01	15.01	15.08	15.29
Acceleration, u''_{peak} (m/s^2)	0.566	0.885	0.885	0.901	0.956
			Floor 2: two segment slab		
No. of modes	1(1)	3(3)	6(3)	9(4)	12(5)
Displacement, u_{peak} (10^{-6}m)	241.6	748.6	748.6	755.5	770.1
Velocity, u'_{peak} (10^{-3}m/s)	5.374	15.67	15.67	15.69	15.87
Acceleration, u''_{peak} (m/s^2)	0.276	1.035	1.035	1.018	1.097

classifications. Currently such refinement is absent from proposed vibration serviceability assessment methods and criteria. Within Tables 5 and 6, the number of participating modes without parenthesis is the total number of modes for a filtering frequency, and the number in parenthesis is the number of participating first order modes.

6 General Discussions

Findings here highlight difficulties inherent to attempting to generalize conclusions about acceptability of various proposed vibration serviceability design criterion/criteria. For example, applying conclusions about relative lack of sensitivity of lightweight joisted floors components associated with modes having natural frequencies > 40 Hz would lead to wrong predictions of dynamic performance of CLT slab floors. Very strikingly solely accounting for how fundamental modes contribute to motions of CLT slab floors can lead to gross errors in estimation of velocity and acceleration levels caused by unit impulsive force of human footfall impacts. The work of Ohlsson [2] three decades ago on joisted floors with all edges simply supported (implemented in Eurocode 5 [3]) recognized need to consider how various modes influence vibration responses of floors. Unfortunately there was no consideration of whether the n_{40} concept or a variant of it applied in other circumstances.

For slab systems like *Floors 1 and 2* consideration needs to be given to contributions of modes other than first order modes, as results in Tables 3, 5 and 6 demonstrate. Need to only consider first order modes of joisted floors is an artifact of the disparity in such systems between flexural rigidities of floors in their span and width plan directions. The findings here may well point to widespread need to take a different approach to design of floors that have modes that are both symmetrical and non-symmetrical in the floor width direction. If so, an implication is the case most commonly investigated to-date (i.e. rectangular plan floors with all edges simply supported) is a non-conservative case in terms of leading to under-design of floors for vibration serviceability. Careful analysis of this question is a high priority.

It is valid to ask whether for CLT slab or other types of floors the most appropriate filtering frequency actually lies above the 100 Hz value considered here. The choice of 100 Hz as a maximum filtering frequency was guided by experimental findings [6], but was arbitrary in essence. Results in Tables 3, 5 and 6 suggest choice of a higher value might be appropriate for certain types of floor systems. Choosing the suitable value for CLT floors is not a direct objective of the discussion here, but that must be another priority work item enabling creation of fully reliable design code provisions. Reliable choices of an appropriate filtering frequency/frequencies needs to be based on simulation studies that consider effect of relevant variables. These comments also highlight why historical attempts to generalize *ad-hoc* findings are unreliable.

Although not addressed explicitly here there is need to address situations where motions building occupants perceive while standing on floor surfaces are influenced by rigidities and masses of supporting and supported substructures (e.g. multi-storey framework supporting systems). This amounts to defining when consideration of dynamic response characteristics of floors alone is reliable. Possibly this can be dealt with via simple prescriptive provisions.

Making a comment from the general structural engineering perspective is appropriate. Nowadays it has become normal in safety related performance assessments of superstructures to make realistic dynamic response analyses (e.g. seismic or wind design of flexible structures). However, modern tendencies toward use of lightweight materials and elements, including those made of timber, militate toward construction of medium- and high-rise buildings where vibration serviceability often is the design controlling performance consideration [17]. Future design practice can therefore be expected to demand replacement of simplified vibration serviceability design practices applicable to control of lateral motions of complete superstructures or vertical motions of floor substructures. Exploitation of the full potential of timber as an advance construction material will inevitably require application of advanced dynamic analysis tools as part of normal vibration serviceability design practice. Trying to avoid fully dynamic performance criterion/criteria is like trying as King Canute reported did hold back the waves of an incoming tide. In the past proponents of vibration serviceability design methods/criteria dominantly argued need for simple approaches and acceptability of empirical design criterion/criteria. The present work clarifies this is unacceptable.

Standardized criteria for human toleration of dynamic motions, applicable beyond the field of timber engineering [e.g. 7], provide the most reliable basis for direct setting of design criteria. Hence there is no need to resort to design approaches that attempt to correlate building occupant perceptions of floor performance with easily predicted floor response parameters. Combining accurate design predictions of dynamic responses of floor systems (e.g. peak u', A_{RMS}) with toleration of dynamic motion criteria is an infinitely better approach. Widespread availability of modern FEM analysis tools has made it practical to perform the former and the later exists from other fields. Ongoing work by the authors supports development of such an approach.

7 Conclusions

Analyses presented here demonstrate reliable application of vibration serviceability design criteria to CLT floor slabs requires account to be taken of contributions higher order modes make to motions felt by building occupants. There is no one size fits all prescriptive solution to what level of frequency filtering works for all design scenarios. At the moment the best advice is to say a convergence study is required before selecting a filtering frequency for a particular type of design situation. Hopefully ongoing work will mitigate this advice to a less onerous requirements based on the type of construction system and building occupancy involved.

It is important to take proper account during prediction of modal frequencies or time-history responses of features like floor plan shape, support conditions and presence on intra-slab construction joints. Although not the primary focus of the studies reported here it is clear that at least most previously suggested vibration serviceability assessment methods that do not do this are unreliable beyond the scope of their original calibration bases.

Although the present work is incomplete it does set the foundation for a new generation vibration serviceability performance assessment tools that are generally reliable. As demonstrated with proper attention to modal participation it is possible to accurately predict floor motions that building occupants base their evaluation of acceptability of floor designs. Such predictions of floor motions need to be made in a manner consistent with standardized threshold values of acceleration or velocity levels humans will tolerate in specific circumstances.

Provisions in the existing Eurocode 5 are predicated on a correct philosophy but it remains to be demonstrated that those provisions apply beyond the context rectangular plan lightweight joisted floors simply supported along all edges.

Acknowledgements

Financial support was provided by the New Brunswick Innovation Foundation and the Canadian Natural Sciences and Engineering Research Council.

References

[1] Onysko, D. M. (1985): Serviceability criteria for residential floors based on a filed study of consumer response, Proj. Rep. 02-50-10-888, Ottawa, Canada.

[2] Ohlsson, S.V. (1988): Springiness and human induced floor vibration: A design guide: Document No. D-12, Swedish Council for Building Research, Sweden.

[3] Eurocode 5(2004): Design of timber structures – Part 1-1: General and rules for buildings. CEN. (EN 1995-1-1).
[4] Weckendorf, J., Toratti, T., Smith, I. and Tannert T. (2015): Vibration serviceability performance of timber floors, European Journal of Wood and Wood Products, doi: 10.1007/s00107-015-0976-z.
[5] Hu L-J. and Gagnon S (2011): Vibration performance of cross-laminated timber floors, In: Gagnon S. and Pirvu C. (Eds), CLT Handbook: Cross-laminated Timber, FPInnovations, Québec, Canada.
[6] Weckendorf, J. and Smith, I. (2012): Dynamic characteristics of shallow floors with Cross-Laminated-Timber spines, Proceedings of 12th World Conference on Timber Engineering, Auckland, New Zealand.
[7] International Organization for Standardization (ISO, 2003): Evaluation of human exposure to whole-body vibration – Part 2: Continuous and shock-induced vibration in buildings (1 to 80Hz), Standard 2631-2, ISO, Geneva, Switzerland.
[8] Smith, I. and Chui, Y.H. (1988): Design of lightweight floors to avoid human discomfort, Canadian Journal of Civil Engineering 15(2), pp. 254-262.
[9] Polensek, A. (1970): Human response to vibration of wood joisted floors, Wood Science, (3), pp. 111-119.
[10] Rainer, J. H. and Pernica, G. (1986): Vertical dynamic forces from footsteps, Canadian Acoustics, 14(2), pp. 12-21.
[11] Živanović, S. et al (2005): Vibration serviceability of footbridges under human-induced excitation: a literature review, Journal of Sound and Vibration, Vol. 279, No. 1-2, pp. 1-74.
[12] Chopra, A. K. (2012): Dynamics of structures: theory and application to earthquake engineering, 4th Edition, University of California at Berkley, USA.
[13] Ussher, E. and Smith, I. (2015): Predicting vibration behaviour of cross laminated timber floors, Proceedings of IABSE Conference on Elegance in Structures, Nara, Japan.
[14] Anonymous (2011): Limited States Design (CAN), Technical Note S21, Nordic Structures Inc., Montreal, Canada.
[15] American National Standards Institute (ANSI, 2012): Standard for performance-rated Cross-Laminated-Timber, Standard PRG 320, New York, USA.
[16] SIMULIA (2012): Abaqus 6.12, Abaqus/CAE User Manual, SIMULIA, Providence, USA.
[17] Smith, I. and Frangi, A. (2015): Technologies enabling advanced urban timber construction, *Proceedings of the Institution of Civil Engineers, Special Issue 'From Research to Practice',* 168(6), pp. 17–22.

Discussion

The paper was presented by E Ussher

F Sarti asked about the model of CLT panels and connectivity between the panels. E Ussher replied that axial and rotational springs were employed. F Sarti commented about the higher modes at 100 Hz and that human perceptions would not be sensitive at such high frequency. Ussher commented that they were looking at the acceleration at the high modes.

M Augustin commented that conclusions might not be applicable for heavier floors. E Ussher agreed and replied that this had to be considered in a case by case manner. M Augustin commented that test results in lab could be very different from real situations as the influence of non-load bearing elements could not be considered. E Ussher said that boundary conditions could be adapted and one could also recommend some kind of minimum for design considerations.

Design Parameters for Lateral Vibration of Multi-Storey Timber Buildings

Thomas Reynolds, Centre for Natural Material Innovation, University of Cambridge

Angela Feldmann, Technical University of Munich

Michael Ramage, Centre for Natural Material Innovation, University of Cambridge

Wen-Shao Chang, BRE Centre for Innovative Construction Materials, University of Bath

Richard Harris, Honorary Professor, University of Bath

Philipp Dietsch, Technical University of Munich

Keywords: multi-storey buildings, lateral vibration, serviceability

1 Introduction

Timber buildings are now reaching heights at which their lateral dynamic response to wind load is an important consideration in design, and such dynamic effects are particularly important in timber buildings because they have low mass, and they may have relatively flexible connections. The 14-storey Treet building in Bergen, Norway recently became the tallest habitable timber building, and has a total permanent load of 135kg/m^3 (Magne Aanstad Bjertnæs (Sweco), personal communication). This compares with a typical value of 300kg/m^3 for a tall building in concrete (Yang et al. 2004), and 160kg/m^3 in steel (Huang et al. 2007).

Wind-induced vibration may cause discomfort to building occupants or otherwise impair the serviceability of the building. In low-mass structures, it is possible to reduce vibration by changing other parameters: primarily by increasing damping or natural frequency. In steel or reinforced concrete buildings, this may be done by increasing member sizes or adding supplemental damping devices, and such interventions may be necessary in timber construction. Timber is a relatively new material in large multi-storey construction, however, and accurate design guidance specifically for multi-storey timber buildings, particularly for damping, would mean that designers would not be forced to use over-conservative assumptions.

The Eurocodes currently give no guidance on damping ratios for lateral vibration of multi-storey timber buildings. Eurocode 1 Part 1-4 (BSI 2005) gives damping ratios for various materials and structural forms, however the only entry relevant to timber construction is a range of values for timber bridges. There has been a shortage of empirical evidence for the natural frequencies and damping of these buildings in their complete form, but in recent years, some such measurements have been presented in the literature.

A six-storey brick-clad light timber frame building, built in the controlled environment of a former aircraft hangar, is tested using ambient and forced vibration methods by Ellis & Bougard (2001). The use of large cross-section engineered timber elements has subsequently allowed taller construction, and research has started to characterise their dynamic behaviour. Omenzetter et al. (2011) measure the heavy timber frame NMIT building in New Zealand, primarily with an interest in predicting its seismic performance. Hu et al. (2014) present dynamic properties from ambient and forced vibration tests on multi-storey buildings in glued-laminated timber (glulam) and cross laminated timber (CLT) in North America. Reynolds et al. (2014; 2015; 2016) present a series of measurements on cross-laminated timber and light timber frame buildings in the UK, Italy and Sweden, which are included in the present study, all measured using ambient vibration methods.

Results from tests on a 3-storey light timber frame building in Switzerland, by Steiger et al. (2015), show the relationship between forced and ambient vibration tests, which is important given that almost all the data on taller buildings is based on ambient vibration measurements. They show that the ambient vibration tests, at much lower vibration amplitudes of vibration than the forced vibration tests, give lower measurements of damping, and slightly higher measurements of natural frequency. It is reasonable to assume that this is due to a genuine variation of damping with amplitude, rather than inaccuracy in either method. Feldmann (2015) investigates the dynamics of timber towers and multi-storey timber buildings ranging from a 20m-tall multi-storey building to a 100m-tall CLT wind turbine tower.

This body of work means that it is now possible to start to use data on the response of completed buildings to make predictions during design.

In the present study we bring together measurements of the dynamics of multi-storey timber buildings taken over the past four years. Starting with the raw data in each case, we process the data using a common methodology to create a compatible set of measurements of natural frequency and damping, which is then used to discuss appropriate design methods.

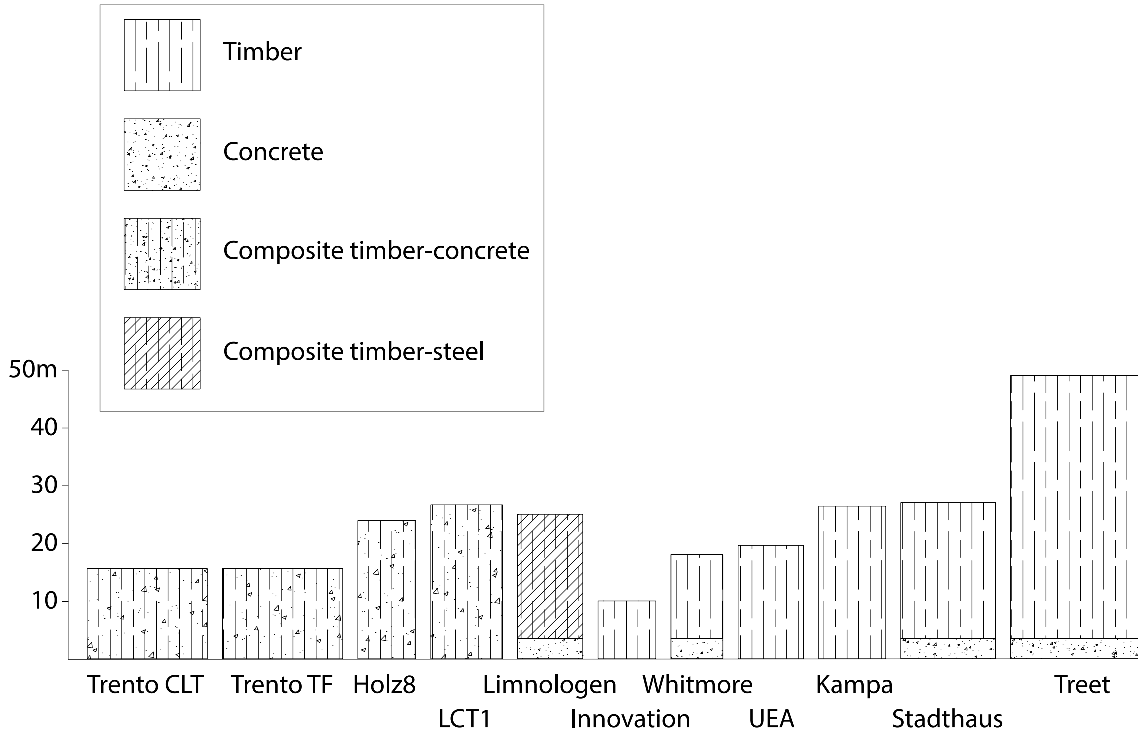

Figure 2.1. Building type, with height and along-wind dimension shown to scale for each of the measured multi-storey timber buildings.

2 Method

In-situ dynamic tests were carried out on 11 multi-storey timber buildings in Central Europe and the UK, relating their natural frequencies and damping ratios in the fundamental mode of vibration in each significant lateral direction.

The buildings are illustrated in Figure 2.1, which shows their construction type and, to scale, their height and their more slender along-wind dimension. They are described as timber, concrete, steel or composite buildings according to the classifications proposed by Foster et al. (2016). We will not reproduce the criteria for classification here, but note that they consider the materials forming the main vertical and lateral load resisting structural elements. Steel used in connections in timber structures and, to some extent, floor materials are not considered to change the classification of a building. The timber in these buildings includes cross-laminated timber, glued-laminated timber and light timber frame structural systems.

Each building was tested using ambient vibration methods. Accelerometers were placed on a part of the structure expected to move in the first few modes of vibration of the building, and a time-series of data, typically approximately 30 minutes in duration, was recorded as the building moved under the ambient wind load. Established modal analysis techniques could then be used to extract modal properties from the data.

We assessed the variation of natural frequency and damping ratio with amplitude. This consideration was important, since modal properties of buildings have been observed to vary substantially with amplitude over the range of excitation imposed by wind. Following the derivation of Jeary (1992), the variation in modal properties with amplitude of vibration can be analysed using the random decrement technique. The amplitude under consideration was expressed as the magnitude of the random decrement threshold used to calculate the modal properties. Since, in the random decrement technique, any contribution from a sinusoid with amplitude greater or less than the threshold level averages to zero, what remains is the decaying sinusoid at a given amplitude (Jeary 1992).

For each building, the variation of modal properties with amplitude was investigated. A slight variation of natural frequency with amplitude was observed, along with a much stronger variation of damping. This observation is common in the lateral vibration of tall buildings, and is attributed to the mobilisation of more and more frictional damping mechanisms as amplitude is increased (Spence & Kareem 2014).

Given this variation of frequency and damping with amplitude, it was necessary to define a reference amplitude to use for comparison of the buildings. Reviewing research and design guidance from around the world on design for human comfort under wind-induced vibration, Burton et al. (2015) state that accelerations below $5mm/s^2$ are considered unlikely to cause “adverse occupant response”. The damping measured at this amplitude would be accurate at this transition point, and also be a conservative estimate for higher amplitudes. $5mm/s^2$ would therefore be a useful reference amplitude for design.

This acceleration was rarely exceeded, however, in the measured data for these buildings, and so it was not possible to assess the modal properties at this amplitude for all buildings. A lower reference value of acceleration was chosen to give comparable data for each building, as shown in Table 2.1. This amplitude was measured at a the point in the structure expected to move most in the fundamental mode, generally at the outer edge of the roof or the top floor of the building.

A reference acceleration of $1mm/s^2$ was chosen. For most of the buildings, this threshold was crossed sufficient times to give repeatable estimates of natural frequency and damping using the random decrement technique at or near $1mm/s^2$. It is noted that, in future work, long-term monitoring of buildings could yield sufficient data at higher amplitude to make an estimate of properties at the higher amplitude.

The geometry of each building considered here is given in Table 2.1, along with the reference amplitude of acceleration used for comparison of measured natural frequency and damping. In Section 3, we look for a correlation between these modal properties and building parameters that could be used in the design process.

Table 2.1 Building data.

Building	Modes	Height (h) (m)	Along-wind dimension (l) (m)	Slenderness (h/l)	Reference amplitude (mm/s^2)
Trento CLT	1	15.6	20.8	0.75	1.0
Trento Frame	1	15.6	20.8	0.75	1.0
UEA Student residence	1	19.6	11.3	1.73	1.0
Treet	1,2	49	24.5	2.00	0.9
Limnologen	1	25	11.3*	2.21	1.0
Murray Grove	1	27	16.4	1.65	0.9
Whitmore Road	1	18	9.0	2.00	1.0
BRE Innovation park	1,2	10	10.0	1.00	0.5**
Holz8	1	23.9	10	2.39	0.9
Kampa	1,2	26.4	11.6	2.28	1.0
LCT1	1,2	26.6	12.4	2.15	1.0,0.9

* This building has two steps in plan dimension, so an average dimension was used.

** The amplitude of vibration for this building was insufficient to estimate the modal properties at $1mm/s^2$, so values for a lower amplitude are stated.

The natural frequency of a building depends only on its geometry and its distribution of stiffness and mass. If the buildings have a similar mean density of mass, and have a lateral stiffness designed to achieve similar displacement criteria, then their natural frequency varies predominantly with their height. A reasonable correlation between height and natural frequency in completed buildings has been shown (Satake et al. 2003), and this correlation is used in the simplified method given in Eurocode 1 Part 1-4 (BSI 2005).

Damping, on the other hand, derives predominantly from friction and very small-scale plastic behaviour, and has proved much more difficult to correlate with any easily measureable parameter. Measurements of over 200 buildings are presented by Smith et al. (2010), and fitted curves for damping against height have coefficient of determination (R^2) below 0.5 for each group of data (steel, reinforced concrete and hybrid steel-reinforced concrete buildings).

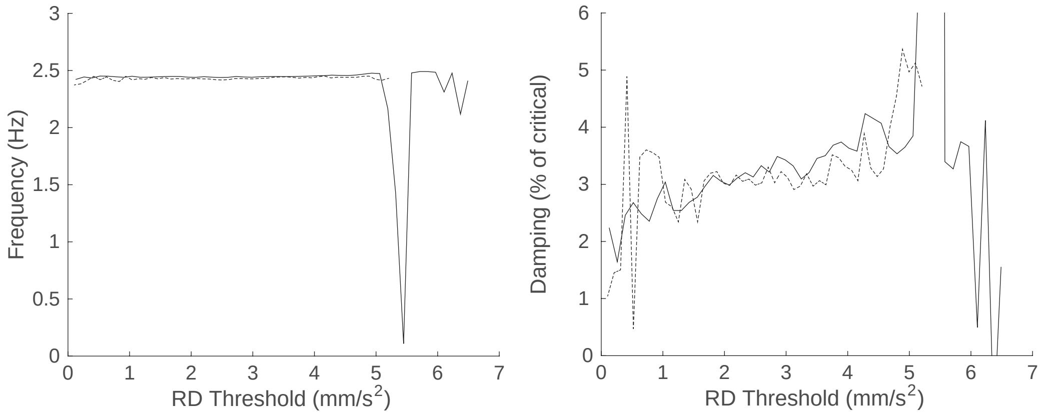

Figure 3.1. Variation of natural frequency and damping with amplitude for the UEA student residence measured in two separate tests to show repeatability.

There is some evidence in the literature that the stockiness of the building may provide an indicator of structural damping. Spence & Kareem (2014) include slenderness as a parameter in their model for damping variation in structures, and Jeary (1986) shows a correlation between the along-wind dimension of the building and the damping.

3 Results and Discussion

For each building, for the measurement point and direction which moved most, the natural frequency and damping ratio of the mode in question could be calculated for a range of random decrement (RD) threshold levels, corresponding to a range of excitation amplitudes. The results of this analysis for the UEA student residence are shown in Figure 3.1. Two lines are drawn, based on data measured on two separate occasions at the same location on the top floor of the building. It can be seen that the results for both natural frequency and damping are repeatable between the two tests over a certain range of amplitudes, in this case between approximately 1mm/s^2 and 5mm/s^2.

The measurements on this building were exceptional in that they were taken during high winds, with a 3-hour peak gust of 17m/s recorded at a nearby weather station. This meant that a substantial variation in damping was evident over the range, whereas buildings measured in lighter winds often showed an approximate plateau in damping measurements.

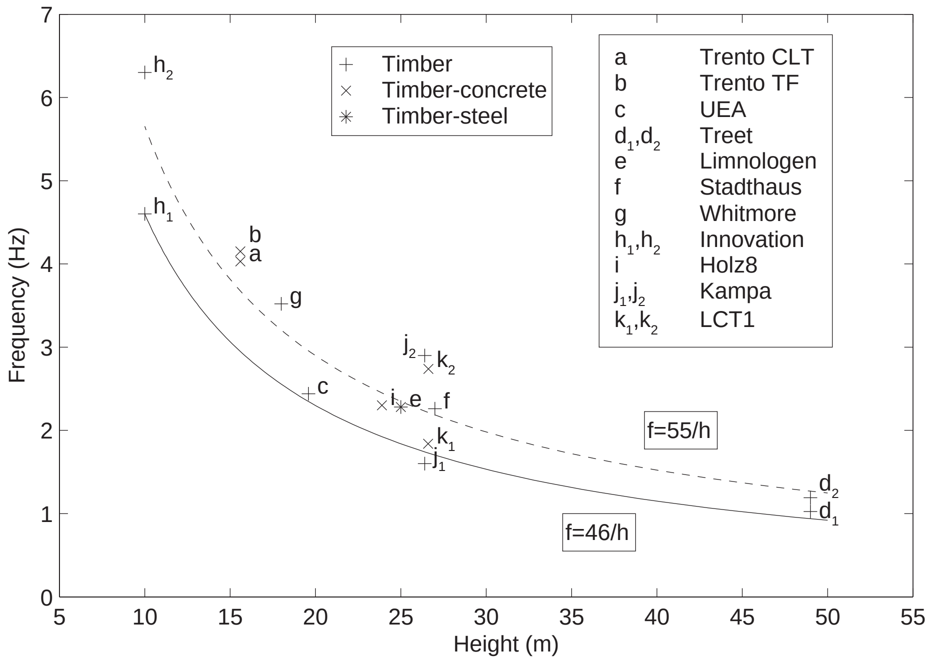

Figure 3.2. Relationship between frequency and height for all buildings.

All the buildings considered in the present study either followed a gradual increase in damping with amplitude, as shown in Figure 3.1, or an apparent plateau with variation less than the random variation of the measurements.

Figure 3.2 shows the relationship between natural frequency and height for the measured multi-storey timber buildings. It shows a clear correlation of fundamental natural frequency with height, which suggests that it may be possible to allow estimation of natural frequency by a simplified rule in the absence of more detailed calculations. Such a rule is given in Eurocode 1 Part 1-4 (BSI 2005), which states that the natural frequency in Hertz of a multi-storey building can be estimated as $46/h$, where h is the height in metres, for buildings over 50m high. None of these buildings exceed 50m in height.

A curve based on this rule is plotted in Figure 3.2, and gives a reasonable conservative estimate of the fundamental natural frequency for these buildings. Applying a least-squares fit equation of this form gives f=55/h. It might be considered that, where this equation is used in design for serviceability, the better estimate given by the least-squares fit would be preferable over a conservative estimate.

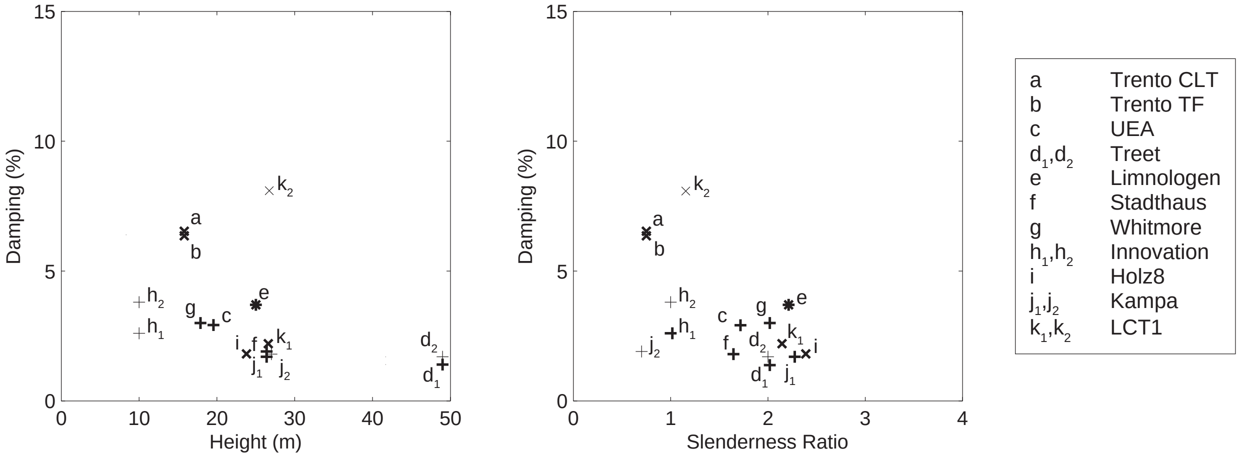

Figure 3.3. Relationship between damping and height or slenderness ratio.

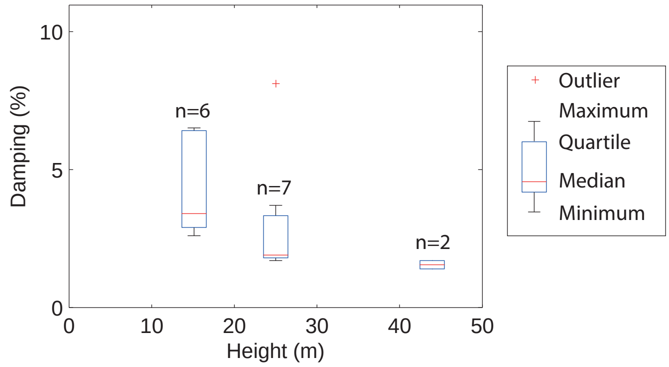

Figure 3.4. Variation of damping in 10m intervals of height.

Calculations based on the estimated natural frequency and damping of the structure can also influence the ultimate limit state design loads according to Eurocode 1 Part 1-4 (BSI 2005), through the dynamic factor. Calculation of this factor would require characteristic values of modal parameters. The low height and light weight of these buildings mean that there would be no increase in load due to dynamic factor, but for taller timber buildings this factor may become important.

Figure 3.3 shows that the relationship between damping and height is not so clear as that for natural frequency, although there is a tendency for damping to reduce with height, and there appears to be a reduction in the scatter of damping ratios with height. Figure 3.3 plots slenderness against damping. Again there is no clear correlation, but the second mode in the LCT1 building is less of an outlier in this case, perhaps suggesting that its high damping ratio may be due to the stockiness of the building in that aspect. What is clear is that the expected value of damping in a taller building is lower than that in a shorter one. This is brought out by classifying each building into a ten-metre range of height, as shown in Figure 3.4, and examining the distribution of damping for the modes in those buildings.

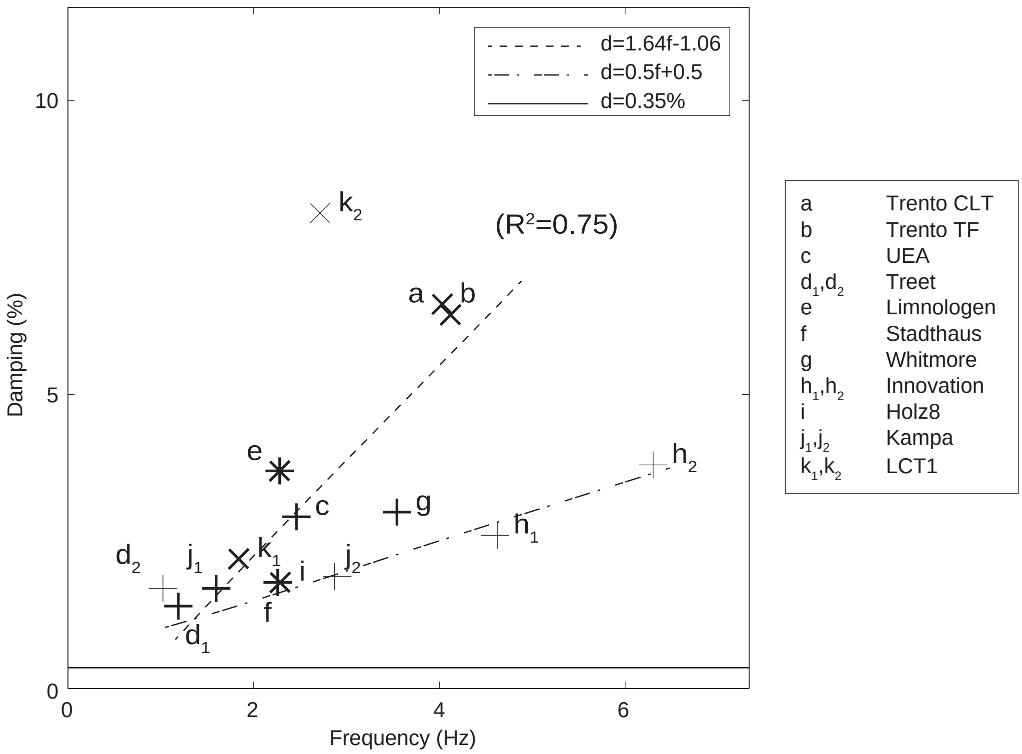

Figure 3.5. Relationship between damping and frequency. The Coefficient of Determination R^2 is given for the fit to the bold markers, which represent damping in the fundamental mode of buildings taller than 15m.

Another approach is to ignore any systematic variation of damping, so that the values can be described by their mean and standard deviation as a single population. This follows the current philosophy of Eurocode 1 Part 1-4 (BSI 2005), which specifies damping for structural forms independent of their geometry. The mean damping in these results is 3.7%, with a standard deviation of 2.5%.

Figure 3.5 shows the variation of damping with frequency in each mode for each building. There is perhaps some correlation evident here, particularly when only the fundamental mode of buildings taller than 15m is considered. These buildings are shown by the bold markers, and have some correlation with the equation shown in the figure. That relationship has two limitations, however: that it predicts damping below zero for frequencies below 0.65Hz, and that it greatly overestimates the damping for the shorter ‘Innovation’ building and underestimates that for the second mode in the ‘Kampa’ building.

For low frequencies, it may be that damping tends towards the value for the material damping of the timber, as the contribution of the structural system becomes dominant over that of non-structural elements. On this basis, a lower-bound for damping of 0.35%, given by the material damping in the timber itself (Yeh et al. 1971), might be appropriate. The lower relationship shown in the figure remains above the material damping of 0.35% at zero frequency, so appears reasonable for all cases.

There is no clear grouping of damping by building type. The composite timber-concrete buildings range from 2.2% to 6.4%, the composite timber-steel building has a damping of 3.7% and the buildings all timber above their first floor range from 1.4% to 5.6%.

4 Conclusion

The proliferation of multi-storey timber construction in the last decade means that a suitable dataset is now available to assess their dynamic performance, and draw conclusions that may be of use to designers. This paper collates dynamic measurements made by the authors, and draws out patterns of natural frequency and damping which may be useful in both preliminary and detailed design.

A high-level assessment is made of the correlation of these properties with relevant measurable parameters of the buildings, including their height and slenderness, as well as the correlation between natural frequency and damping. Design guidance could be based on a simplified relationship between these parameters, or could be founded in the fundamental properties of the system being used. More detailed calculations of natural frequency, for example, rely on knowledge of the stiffness of connections under serviceability limit state dynamic loads, and research is currently ongoing in this area.

The data presented here show that the simplified relationship between height and natural frequency for multi-storey buildings given in Eurocode 1 Part 1-4 (BSI 2005) of f=46/h, where f is frequency in Hertz and h is height in metres, is reasonable and conservative for this group of modern timber buildings. The existing f=46/h relationship is limited to buildings over 50m in height, which is higher than any of these buildings. A relationship of f=55/h is a more accurate fit for this set of buildings, and is therefore the one put forward in this case.

There is evidence of a variation of damping with natural frequency, height and stockiness, although there is a large scatter in each case, as is the case in measurements of damping in tall buildings in steel and reinforced concrete. A relationship of d=0.5f+0.5, where d is damping in per cent of critical and f is frequency in Hertz, is a lower bound for these buildings, and is realistic over a range of frequencies.

5 Acknowledgements

This paper brings together data obtained through various projects funded by different organisations. It was made possible by funding from the BRE Trust, the European Union's COST actions FP1004 and FP1402, and a Leverhulme Trust programme grant. This work has also stemmed from collaborations through the CTBUH Tall Timber Buildings working group. The authors would like to thank: Julie Bregulla and Gordon Breeze of BRE; Jonathan Bawcombe and Gavin White of Ramboll; Andrew Waugh of Waugh Thistleton; Carsten Hein of Arup; Daniele Casagrande and Roberto Tomasi at the University of Trento; and Erik Serrano, Johan Vessby and Åsa Bolmsvik at Linnæus

University for technical advice and access to buildings. Thanks also to Haoyu Huang for support in vibration measurement.

6 References

BSI, (2005). BS EN 1991-1-4:2005 Eurocode 1. *Actions on structures. General actions. Wind actions.*

Burton, MD, Kwok, KCS & Abdelrazaq, A, (2015). Wind-Induced Motion of Tall Buildings: Designing for Occupant Comfort. *International Journal of High-Rise Buildings*, 4(1), pp.1–8.

Ellis, BR & Bougard, AJ, (2001). Dynamic testing and stiffness evaluation of a six-storey timber framed building during construction. *Engineering structures (Online)*, 23(10), pp.1232–1242.

Feldmann, AS, (2015). Dynamic Properties of Tall Timber Structures under Wind-induced Vibration. Technische Universität München.

Foster, RM, Reynolds, TPS & Ramage, MH, (2016). Proposal for defining a tall, timber building. *Journal of Structural Engineering*.

Hu, L et al., (2014). Wind-induced vibration of tall wood buildings - is it an issue? In *World Conference on Timber Engineering*. Quebec City, Canada.

Huang, S, Li, QS & Xu, S, (2007). Numerical evaluation of wind effects on a tall steel building by CFD. *Journal of Constructional Steel Research*, 63(5), pp.612–627.

Jeary, AP, (1986). Damping in tall buildings—a mechanism and a predictor. *Earthquake Engineering & Structural Dynamics*, 14(5), pp.733–750.

Jeary, AP, (1992). Establishing non-linear damping chalacleristics of structures from non-stationary response time-histories. *The Structural Engineer*, 70(4), pp.61–66.

Omenzetter, P et al., (2011). Long-term monitoring and field testing of an innovative multistory timber building. In *Proceedings of SPIE--the international society for optical engineering*. p. 7983.

Reynolds, T et al., (2015). Ambient vibration tests of a cross-laminated timber building. *Proceedings of the ICE - Construction Materials*, 168(3), pp.121–131.

Reynolds, T, Casagrande, D & Tomasi, R, (2016). Comparison of multi-storey cross-laminated timber and timber frame buildings by in-situ modal analysis. *Construction and Building Materials*, 102, pp.1009–1017.

Reynolds, TPS et al., (2014). Ambient Vibration Testing and Modal Analysis of Multi-Storey Cross-Laminated Timber Buildings. In *World Conference on Timber Engineering*.

Satake, N et al., (2003). Damping Evaluation Using Full-Scale Data of Buildings in Japan. *Journal of structural engineering*, 129(4), pp.470–477.

Smith, R, Merello, R & Willford, M, (2010). Intrinsic and supplementary damping in tall buildings. *Proceedings of the Institution of Civil Engineers. Structures and buildings*, 163(2), pp.111–118.

Spence, SMJ & Kareem, A, (2014). Tall Buildings and Damping: A Concept-Based Data-Driven Model. *Journal of Structural Engineering*, 140(5), p.04014005.

Steiger, R et al., (2015). Experimental modal analysis of a multi-storey light-frame timber building. *Bulletin of Earthquake Engineering*.

Yang, J et al., (2004). Benchmark Problem for Response Control of Wind-Excited Tall Buildings. *Journal of Engineering Mechanics*, 130(4), pp.437–446.

Yeh, CT, Hartz, BJ & Brown, CB, (1971). Damping sources in wood structures. *Journal of Sound and Vibration*, 19(4), pp.411–419.

Discussion

The paper was presented by T Reynolds

D Brandon commented about damping versus building height and asked would it be better to separate timber buildings out to see a relationship. T Reynolds replied the reason for not separating the timber from timber concrete system was that the concrete's contribution was considered as part of the system. He agreed that there could be a relationship.

G Doudak asked about the definition of height. T Reynolds clarified it was the height of the building. G Doudak commented that from a dynamic sense the height of the concrete portion in concrete podium cases should not be considered as the building height. T Reynolds agreed that this was a valid point. WS Chang added they could consider only the timber part in such building.

P Quenneville asked whether damping would be related to shear rigidity for shorter buildings. T Reynolds agreed that it would be likely.

A Frangi asked whether the authors would be confident about the proposal based on these unique buildings. T Reynolds replied that it would be important that this work was done so that designers can receive guidance even though the number of cases was limited.

Design of timber floor for vibration: Some design and test questions

Wen-Shao Chang[1], Haoyu Huang[1], Richard Harris[1,2]

[1]Department of Architecture and Civil Engineering, University of Bath, UK

[2] Time For Timber, UK

Abstract

This paper presents experiments on vibration of ten timber floors in various types of construction and discusses how they are compared in different standards, including Eurocode 5, BS 6472 and ISO 10137. These different standards use different parameters to assess the vibration performance of floor in a structure and therefore the compatibility of these standards needs to be reviewed and discussed. The experimental results not only shown the potential for Eurocode 5 to adapt a higher damping ratio for timber floor, but also show necessity of harmonising the parameters in different standards so as to avoid conflict in the future.

1. Background

The human-induced vibration of floors is considered as a serviceability issue that primarily relates to discomfort of occupants. In recent years, there has been an increase in demand for building new floor systems with larger spans; these floors are more susceptible to vibration than conventional residential floor system. Currently, engineers design timber floors based on the approach proposed by Eurocode 5; however, there are some other relevant standards that deal with human exposure to vibration, such as BS 6472 and ISO 10137. The current Eurocode 5 employs a frequency limit criterion, i.e. to limit the floor to have a natural frequency higher than certain threshold, however, approaches adopted by other standards also involve acceleration. Therefore there is a risk that a timber floor designed by Eurocode 5 does not satisfy the requirement set by other relevant standards and causes problems. It is therefore essential to review and compare these standards to inform future design. In this paper, we present the results of measurement of timber floor vibration in different countries. One of the CLT floors was in an office building that was measured for three whole days and we can use the data to compare vibration acceptability levels specified by different standards.

2. Design of timber floor for vibration in Eurocode 5

The current Eurocode 5 [1] provides design guidelines for residential floors, which employs the frequency based criterion, also known as the 8Hz limit criterion. It limits the design of timber floor as only applicable to residential floors with spans up to 6 metres. For floors with a fundamental frequency greater than 8Hz, further checks, including static deflection and unit impulse velocity response checks should be carried out. For those with a fundamental frequency less than 8Hz, a special investigation is required. According to Eurocode 5, natural frequency of the floor can be calculated as:

$$f_1 = \frac{\pi}{2l^2}\sqrt{\frac{(EI)_l}{m}} \quad (Hz) \tag{1}$$

This equation can also be simplified as [2]:

$$f_1 = \frac{18}{\sqrt{w_{inst}}} \quad (Hz) \tag{2}$$

where f_1 is the fundamental frequency of the floor; m is the mass per unit area in kg/m^2; l is the floor span in m; $(EI)_l$ is the equivalent plate bending stiffness of the floor about an axis perpendicular to the beam direction in Nm^2/m; w_{inst} is the instantaneous bending deflection due to permanent action in mm.

Once a timber floor has a fundamental frequency higher than 8Hz, there are two further checks to carry out in the design stage: static deflection under a point load and unit impulse velocity response.

Although design codes for other construction materials, such as concrete [3] and steel [4] do not cover floor vibration, the steel and concrete industries in the UK have provided the design guidelines for design of concrete and steel floors for human-induced vibration [5, 6], and both consider acceleration of the floor vibration.

3. Other relevant standards for vibration

There are other standards that deal with vibration; BS 6472 and ISO 10137 are two examples. BS 6472 categorises the floor having a natural frequency lower than 7-10Hz as a “low frequency floor” whereas those having frequency higher than this range are “high frequency floors”. It also classifies the building vibrations into three different categories: (1) continuous; (2) intermediate; and (3) occasional. It also introduces a frequency weighting, i.e. the vibration data should be filtered according to the frequency weighting as shown in Figure 1 before being processed.

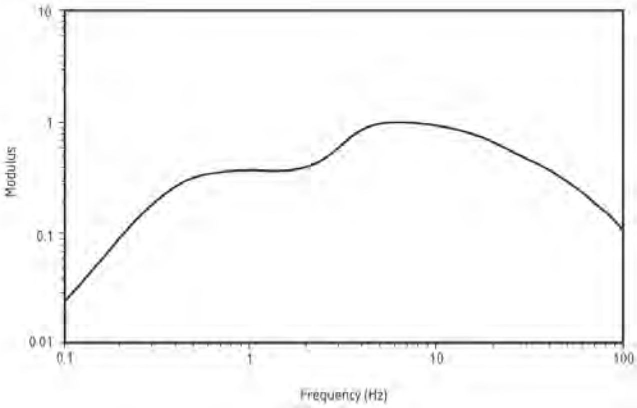

Figure 1 Frequency weighting curve for vertical vibration proposed by BS 6472

BS 6472 then [7] introduces a new parameter called vibration dose value, VDV, to consider intermittent vibrations of walking activities. It can be calculated by:

$$VDV_{b/d,day/night} = \left(\int_0^T a^4(t)dt \right)^{0.25} \tag{3}$$

where $VDV_{b/d,day/night}$ is the vibration dose value (in m/s$^{1.75}$); $a(t)$ is the frequency-weighted acceleration (in m/s^2); and T is the total period of the day or night (in seconds) during which vibration can occur.
Calculation of the VDV implies that the total vibration amount is considered during the period where vibration could occur and, therefore, it is considered that this approach offers improved understanding of the likely acceptability of floors for vibration. Table 1 summarises the VDV ranges for different probabilities to receive adverse comments on vibration in both residential and office buildings.

Table 1 Vibration dose value ranges which might result in different probabilities of adverse comment within residential and office buildings

Place and time	Low probability of adverse comment	Adverse comment possible	Adverse comment probable
Residential buildings 16 h day	0.2-0.4	0.4-0.8	0.8-1.6
Residential buildings 8 h night	0.1-0.2	0.2-0.4	0.4-0.8
Office buildings 16 h day	0.4-0.8	0.8-1.6	1.6-3.2
Office buildings 8 h night	0.2-0.4	0.4-0.8	0.8-1.6

ISO 10137 [8] combines acceleration and acceptability of vibration and this has been acknowledged as a more reliable approach. ISO 10137 proposes to consider, when assessing the serviceability of the floor, the following three parameters: (1) the vibration sources; (2) transmission paths; and (3) the receivers. The receivers of the vibration can be either occupants or specific structure/equipment in the structure. Figure 2 shows the acceptance curve for frequency against acceleration, in which a represent the Root of Mean Square (r.m.s.) value of the acceleration of vibration in m/s^2. ISO 10137 recommends calculating the r.m.s. values of acceleration for 10 seconds. The maximum vibration limit for comfort for a passive person (i.e. occupants who do not expect a vibration) for vertical vibrations may be obtained using Figure 2 as the base curve with a multiplying factor of 200.

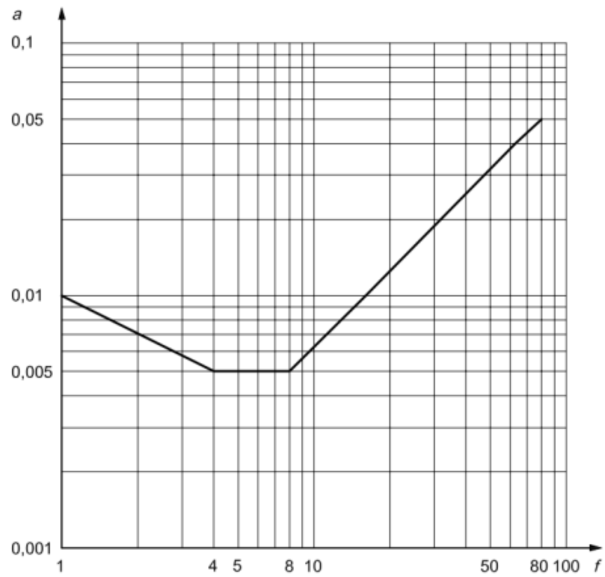

Figure 2 Base curve for perception of vibration from ISO 10137

4. On-site vibration measurement and data analyses

This paper presents the results of vibration measurements on timber floors carried out in various countries, the results are summarised in Table 1.

4.1 Measurement of frequency and damping

To extract dynamic properties of timber floors, accelerometers were placed in the middle of the timber floors, where maximum displacement was expected to occur, to measure the vertical movement. Figure 3 shows the vibration system used for Floor H. There are several ways to excite the floor, such as (1) ball dropping; (2) human jumping; (3) impact hammer; and (4) controlled shaker. In the tests in this paper, the authors jumped on the floor, which generated the floor vibration for analyses. The data was then recorded by the data acquisition system for 1 minute for analyses. The interesting range of the frequency is below 50Hz therefore the sampling rate of the data acquisition was set to be 500Hz. There are several ways to analyse the vibration data, Fast Fourier Transfer is the most common method in frequency domain approach, whereas curve fitting can also be used in time domain approach.

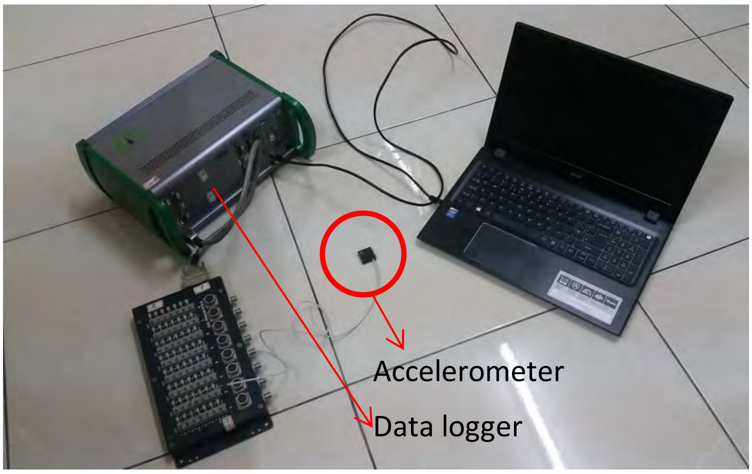

Figure 3 Typical timber floor vibration measurement system

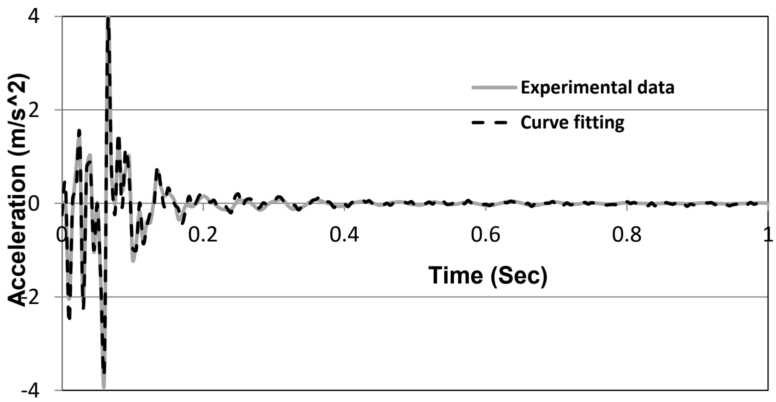

Figure 4 Typical vibration time-history record of floor vibration after a jumping

4.2 Measurement of floor vibration due to daily activities

In this paper, Floor H was chosen to measure the vibration due to daily activities of occupants. It was chosen because it was the only floor that allowed measurement of daily activities. An accelerometer was installed underneath the timber floor where, above the ceiling of the storey below, the measurement lasted for three days. This ensured that the occupants did not know that the vibrations were recorded, so as not to interfere occupants' activities. The accelerations of the floor were recorded by a data acquisition system with sampling rate of 500Hz.

Table 2 Information and the outcomes of the measured timber floors

Floor	Country	Floor system	Natural frequency	Damping ratio	Use of building
A	UK	Timber joist	25.7 Hz	7.1%	Residential
B	UK	Timber joist	34.0 Hz	3.8%	Residential
C	UK	Timber joist	13.2 Hz	4.5%	Residential
D	UK	CLT	12.6 Hz	3.1%	Office
E	UK	CLT*	14.2 Hz	5.3%	School
F	Germany	CLT	18.2 Hz	3.0%	Residential
G	Germany	CLT	11.1 Hz	3.9%	Office
H	Austria	CLT	9.3 Hz	5.3%	Office
I	Sweden	CLT*	13.9 Hz	7.5%	Residential
H	Taiwan	CLT	14.7 Hz	3.1%	Office

* floating floor

5. Results and discussion

5.1 Natural frequency and damping ratio

The vibration of a total of 10 timber floors, with different types of construction, has been measured and the results are summarised in Table 2. The results show that all the timber floors measured have a natural frequency higher than 8Hz, the threshold set up by Eurocode 5. Eurocode 5 prescribes the damping ratio of the timber floors to be 1% whereas in the UK National Annex 2% is specified; the results of our measurement have shown that the damping ratios of all the floors are higher than 3%. Higher damping of the floor means the energy of the vibration will dissipate more quickly which, in consequence, will allow larger unit impulse velocity and imply that the velocity response will not govern the serviceability requirement and therefore its calculation is not necessary. This reflects the conclusion on unit impulse velocity discussed in reference [2].

5.2 Effect of the internal partition

There were two vibration measurements carried out on the Floors A and B, one before and one after the internal finishes of the internal partition walls were completed. The results of these two tests are further summarised in Table 3. It can be seen that, after the plasterboard on the partition walls was installed, the damping of the floor increased. This can be explained by the internal walls contributing to energy dissipation of the timber floor vibrations, echoing the phenomenon, observed by others [9,10], that the non-structural partition walls can have significant impact on the vibration performance of floors.

Table 3 Comparison of two tests in Floor A and B

Floor	Country	$f_{1,p}$ [1]	ζ_p [2]	$f_{1,c}$ [3]	ζ_c [4]
A	UK	25.7 Hz	7.1%	25.7 Hz	5.2%
B	UK	34.0 Hz	3.8%	33.8 Hz	3.2%

[1] Natural frequency of the timber floor after the plaster board in the internal partition walls are installed
[2] damping ratio of the timber floor after the plaster board in the internal partition walls are installed
[3] Natural frequency of the timber floor before the plaster board in the internal partition walls are installed
[4] Damping ratio of the timber floor before the plaster board in the internal partition walls are installed

5.3 Comparison of different standards

Although it has been shown in Table 2 that all the floor tests have a natural frequency higher than 8Hz with damping ratio higher than 3%, it is essential to compare different standards to review the compatibility of these standards. Floor H is a CLT timber floor within an office building, spanning of 6 metres, which has a natural frequency of 14.7Hz and damping ratio of 3.1%. Vibration measurement was carried out on this floor for three consecutive days. The accelerometers were installed in positions that did not interfere with the occupants' activities, who were not informed the measurement. The day time was set to start from 7.00 am until 11.00 pm. The measurement results assessed by BS 6472 are summarised in Table 4. It is obvious that, Floor H has a VDV ranging from 2.2-3.1, which shows the possibility of receiving adverse comment on vibration of the floor. Although during the measurement no adverse comments on vibration was received, this exercise presents the possibility that a timber floor that satisfies one standard, such as Eurocode 5, but could fail in another standard. This can potential cause issues when it happens in the area where these standards are used for legal assessment.

Table 4 Measurement results for Floor H

Time	VDV_{day}	Adverse comment probable threshold
Day 1 day	2.2	1.6-3.2
Day 2 day	3.1	1.6-3.2
Day 3 day	2.6	1.6-3.2

As have been discussed previously, the Eurocode 5 uses frequency as a parameter to assess the timber floor vibration whereas BS 6472 uses VDV and ISO 10137 uses combined frequency and r.m.s. value of acceleration. This exercise shows the necessity to harmonise the parameters in different standards.

5.4 Measurement and analyses techniques

Selection of proper measurement equipment and experimental techniques are important but rarely noticed in the timber community. Factors that should be considered include accelerometers, sampling rate of recording data, excitation sources and analytical approach. In the tests of Floor F, several sampling rates were used to compare the effect of sampling rate. The results are summarised in Table 5. If the sampling rate is too low and the floor has high frequency, there will be insufficient points to describe the vibration behaviour of the floor, and cause errors in analyses. Table 5 shows that tests with a sampling rate of 100Hz would provide the incorrect results when measuring the vibration of the timber floor. It is therefore recommend that, to obtain a more reliable results, the sampling rate of the tests should be at least 10 times of the natural frequency of timber floors. Sampling rate should be considered when different excitation source are used, for example in the tests that impact hammer is used. The contact time between the structure and the impact hammer can be as short as 10ms, therefore it should be ensured that the sampling rate of the tests is high enough to capture the signal generated from the impact hammer. Another important factor to consider is the time length for analyses. From the observation of the tests, it shows that the vibration will attenuate in just a second or two, as shown in Figure 4, therefore it is important to consider the length of time extracted for analyses. The balance between resolution in frequency and signal to noise ratio is important. If the length of time is too short, for example only 2 seconds of vibration is analysed, the resolution will insufficient to capture the natural frequency of the timber floor. In contrast, if the length of time is too long, for example 40 seconds, the signal would include a substantial amount of data that is not needed.

Table 5 Comparison of different sampling rate for Floor F

Sampling rate (Hz)	$f_{1,f}$ [1]	ζ_f [2]	$f_{1,t}$ [3]	ζ_t [4]
100	14.00 Hz	24.1%	13.18 Hz	26.2%
200	18.01Hz	5.3%	18.01 Hz	4.8%
500	18.17 Hz	3.0%	18.17 Hz	3.1%
1000	18.17 Hz	3.0%	18.17 Hz	3.0%
2000	18.17 Hz	3.1%	18.17 Hz	3.4%

[1] Natural frequency of floor obtained from frequency domain approach (FFT)
[2] Damping ratio obtained from frequency domain approach
[3] Natural frequency of obtained from time domain approach (curve fitting)
[4] Damping ratio obtained from time domain approach

6. Summary and recommendation to standards

A total of 10 timber floors were measured in this paper, the following conclusions can be drawn:

1. Timber floors designed according to one standard could fail to satisfy other standards if the parameters used to assess the performance are different.
2. Timber floors measured in this paper have damping ratio higher than that specified in Eurocode 5 and UK National Annex.
3. Non-structural elements in the structure could have a significant effect on the performance of timber floor.
4. Several important factors, such as sampling rate of the data acquisition should be considered when measuring the vibration of the timber floor to assess the performance.

The following recommendations are made from the results of the tests presented in this paper:

1. The current Eurocode 5 only proposes a method to design residential floors with maximum spans of 6 metres, it is recommended that design

of other types of floor types, such as CLT, should be developed and proposed.

2. The damping ratio of timber floor specified in Eurocode 5 could be increased to 2 or 3%.
3. In the design stage, the effect of non-structural elements should be considered.
4. It is recommended that Vibration Does Value (VDV) should be introduced in the design of timber floors.

7. References

1. British Standard Insitution, *BS EN 1995-1-1: 2004 Eurocode 5: Design of timber Structures - Part 1-1: General rules and rules for buildings*. 2006.
2. Institution of Structural Engineers, Manual for the design of timber building structures to Eurocode 5. 2007.
3. British Standard Insitution, *BS EN 1992-1-1:2004 Eurocode 2: Design of concrete structures - Part 1-1: General rules and rules for buildings.* 2004.
4. British Standard Insitution, *BS EN 1993-1-1:2005 Eurocode 3: Design of steel structures — Part 1-1: General rules and rules for buildings*. 2006.
5. Willford, M.R., P. Young, and M. CEng, *A design guide for footfall induced vibration of structures*. 2006: Concrete Society for The Concrete Centre.
6. Smith, A.L., S.J. Hicks, and P.J. Devine, *Design of floors for vibration: A new approach*. 2007: Steel Construction Institute Ascot, Berkshire, UK.
7. British Standard Insitution, *BS 6472-1: 2008 Guide to evaluation of human exposure to vibration in buildings. Part 1: Vibration sources other than blasting*. 2008.
8. International Standard Organisation, *ISO 10137: Bases for design of structures-Serviceability of buildings and walkways against vibrations*, in *International Standard Organisation (ISO)*. 2007.
9. Devin, A., Fanning PJ & Pavic A., Nonstructural partitions and floor vibration serviceability. Journal of Architectural Engineering -- ASCE, 22(1). 2015.
10. Devin, A. & Fanning, P.J.The Evolving dynamic response of a four storey reinforced concrete structure during construction. Shock and Vibration, 19(5), pp.1051–1059. 2012.

Discussion

The paper was presented by Wen-Shao Chang

F Sarti commented that the damping ratio reported seems high. WS Chang responded that the contribution of nonstructural elements including partitions and plaster board might have contributed to the high damping. F Sarti asked about comparisons for higher mode damping and commented that the sampling rate of 100 Hz should be related to how high a frequency one would want to capture. WS Chang responded that the sampling rate was taken as 10x the natural frequency.

F Lam commented Nyquest frequency should be used to establish the sampling rate. A discussion of VDV took place. He commented that the measurements at the tail end of the record might be unreliable because of the low signal to noise ratio. WS Chang agreed but they needed the information.

P Dietsch commented that the measured high damping ratio's depended on nonstructural elements and one would need to clarify that the code damping ratios were based on structural elements only. Consideration of the contribution from nonstructural elements towards damping would be future additions. WS Chang responded that the damping level of 2% in the code was too low.

A Ceccotti received clarification that the ½ band method was used to establish damping the paper.

G Schickhofer agreed with P Dietsch that damping at different stages of the building process should be considered. He also agreed that the damping in actual buildings with non-structural elements was much higher than that based on structural elements only. G Schickhofer commented that VDV was very subjective and may be it is a parameter that could be decided by the client.

P Quenneville received clarification that not all floors considered received complaints. WS Chang answered that it was difficult to gain access to floors for evaluation where complaints had already been launched. Experience from engineers (dynamic's experts) indicated that floors with fundamental frequency higher than 10 Hz should perform well.

R Steiger asked about the relationship between damping ratio and amplitude as increase in amplitude tended to lead to increase in damping. WS Chang answered that the excitation was provided via a heel drop test. R Steiger commented that the formulation of VDV is simply a numerical high pass filter. He asked why an exponent of 4 was chosen. WS Chang answered it was based on ISO standard. R Steiger stated that the choice of this factor would be important and could affect the findings. R Harris stated that the issue is that ISO and British standards which are not timber specific

4 INTER Notes, Graz, Austria 2016

Yield moment of nails

Carmen Sandhaas, Karlsruhe Institute of Technology

Elke Mergny, Université catholique de Louvain

Keywords: nails, yield moment, tension strength

1 Introduction

In Eurocode 5, nailed joints are designed using the Johansen model extended with the rope effect. Necessary input parameters are hence, apart from geometrical data, embedment strength f_h, yield moment M_y and withdrawal capacity F_{ax}. Generally, empirical equations based on regression analyses have been derived for all three parameters f_h, M_y and F_{ax}. However, especially for ring shank nails, no consistent rules are given in the current version of Eurocode 5. Values for yield moments, for instance, must be taken from technical documents of the single nails. The aim of this note is to present first investigations regarding the parameters wire tension strength f_u, nail tension capacity F_t and yield moment M_y. Based on an extensive database comprising more than 5000 test results carried out for certification purposes, regression analyses have been carried out. Potential benefits are more robust design models covering a large range of nails, reduced testing and simplified design equations.

The global database including withdrawal and head pull-through tests consists of in total 9618 tests taken from 96 reports on mostly ring shank nails (rings 77%, threads 5%) and wires (11%). Nails from 33 different producers were considered. Smooth shank nails constituted only 1% of the database. The number of tests per parameter is given in Table 1.

Table 1. Composition of database. Here, only f_u, M_y and F_t are analysed.

	Wire tension strength f_u	Yield moment M_y	Nail tension capacity F_t	Withdrawal capacity F_{ax}	Head pull-through capacity F_{head}
No. of tests	1076	2845	1173	3504	1020
Of which stainless steel	203	370	195	390	60
Of which hdg*	-	265	188	320	220

* hdg = hot-dip galvanised

In current certification practise, all three parameters, f_u, M_y and F_t, are tested according to EN 14592 where a minimum value for the wire strength of f_u = 600 MPa is required. The evaluated values on the characteristic level are then declared in technical documents. For smooth shank nails however, the characteristic yield moment $M_{y,Rk}$ can also be calculated. For round nails for instance, Eurocode 5 gives the following Eq. (1):

$$M_{y,Rk} = 0.3 \cdot f_u \cdot d^{2.6} \quad (= 0.3 \cdot 600 \cdot d^{2.6} = 180 \cdot d^{2.6}) \tag{1}$$

where f_u is the wire tension strength and d is the nominal nail diameter.

Eq. (1) is based on work done by Werner and Siebert [1] and it is valid only when the minimum tension strength of the wire of 600 MPa is inserted, see expression in parenthesis. The exponent of 2.6 in Eq. (1) reflects an observed decrease of yield strength with increasing nail diameter.

2 Analysis

Similar to Werner and Siebert [1], a decrease of wire and nail strength with increasing diameter can be found back in Figure 1 where the nail strength has been calculated using the tension capacity F_t and the nominal diameter. The significant difference between bright wire tension strength and subsequent tension strength of hot-dip galvanised (hdg) nails is obvious.

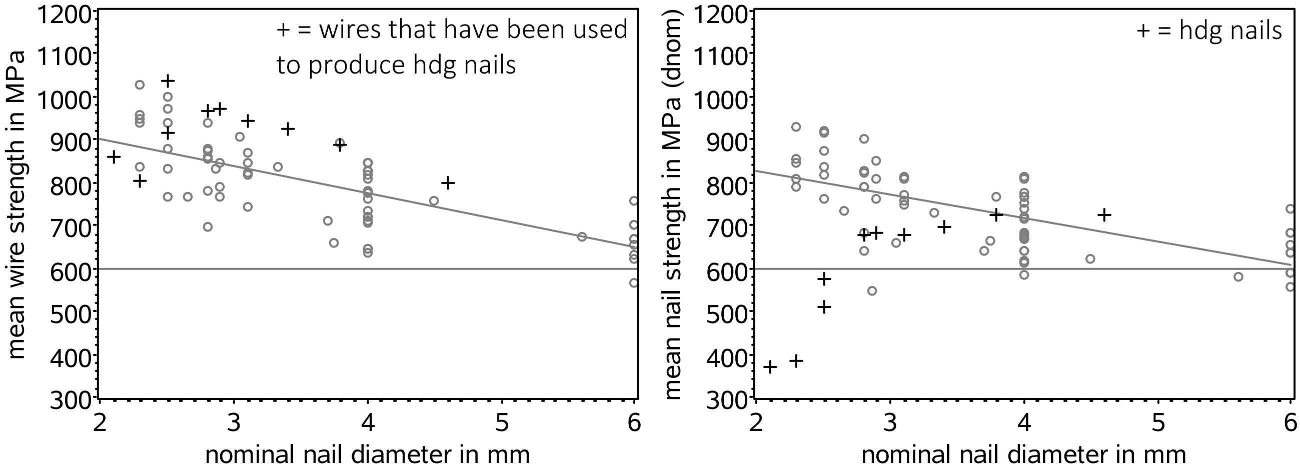

Figure 1. Left: Mean tension strength of wire versus nominal nail diameter. Right: Mean tension strength of nail calculated with F_t and nominal diameter. Data from 78 test series (403 single tests f_u, 918 single tests F_t).

Analogously to Werner and Siebert [1], a regression function with the yield strength f_{My} calculated from the mean yield moment (using a plastic section modulus, see also Eq. (3) in parenthesis) as dependent and the nominal diameter as independent variable has been derived:

$$f_{\mathrm{My}} = 1154 \cdot d^{-0.29} \qquad \left(\text{Werner and Siebert}: f_{\mathrm{My}} = 1320 \cdot d^{-0.41}\right) \tag{2}$$

Outliers having a normalised error larger than 3 (Figure 2 left) have been excluded [2]. The resulting Eq. (2) had a coefficient of determination R^2 of 0.28 and is shown in Figure 2 right.

Furthermore, a nonlinear regression analysis to derive an expression for M_y has been carried out where no differentiations in the database were made, e. g. with respect to different nail types or normal and stainless steel. The dependent variables have been the nominal diameter d and $f_{Ft,dn}$ which is the tension strength calculated from the nail tension capacity F_t and the nominal diameter. One test series leading to outliers had to be eliminated. The resulting regression based on mean values resulted to (with R^2 = 0.99):

$$M_{\mathrm{y}} = 0.18 \cdot f_{\mathrm{Ft,dn}} \cdot d^{2.99} \qquad \left(\text{Theory}: M_{\mathrm{pl}} = \frac{1}{6} \cdot f_{\mathrm{y}} \cdot d^{3}\right) \tag{3}$$

Eq. (3) is basically identical to the theoretical equation shown in parenthesis to calculate the plastic yield moment where however the yield strength f_y is needed to calculate the full plastic yield moment M_{pl} and not the ultimate strength $f_{Ft,dn}$ derived from tension tests on nails that has been used to derive Eq. (3). Figure 3 right shows the experimental mean values versus the predicted values. The very good agreement between tests and model resulting in a bisect line with small scatter can be seen. Figure 3 left shows the model residuals which seem to be not equally distributed, but rather getting larger at larger M_y. This indicates that a logarithmic approach could fit better.

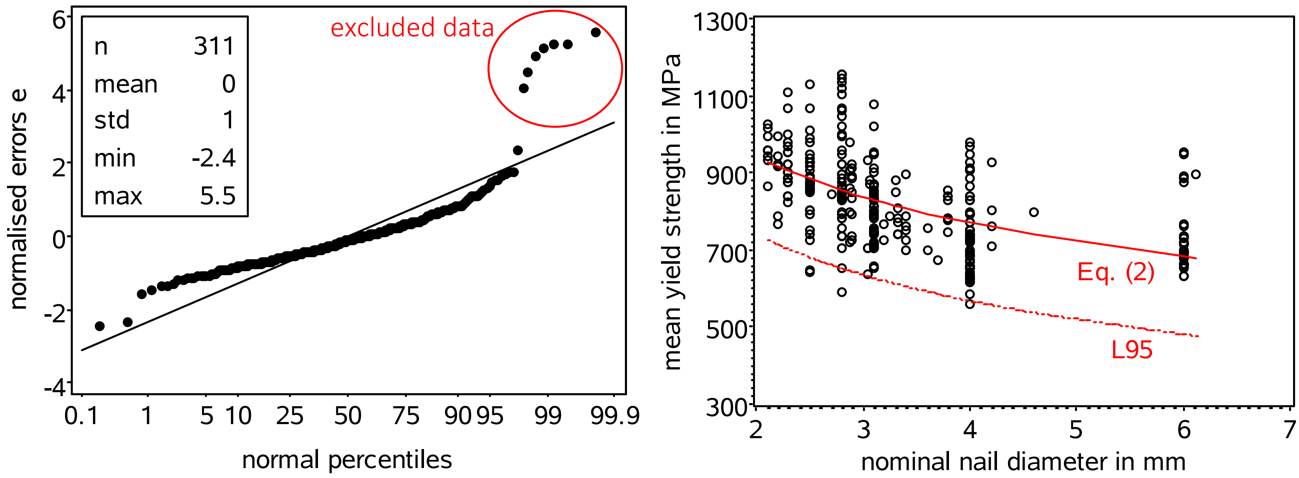

Figure 2. Left: Outliers excluded from analysed database (9 test series excluded). Right: Result of regression analysis (Eq. (2)). Lower 95%-confidence interval is shown, L95. Yield strength calculated from yield moment M_y and nominal diameter. Data from 302 test series (2770 single tests).

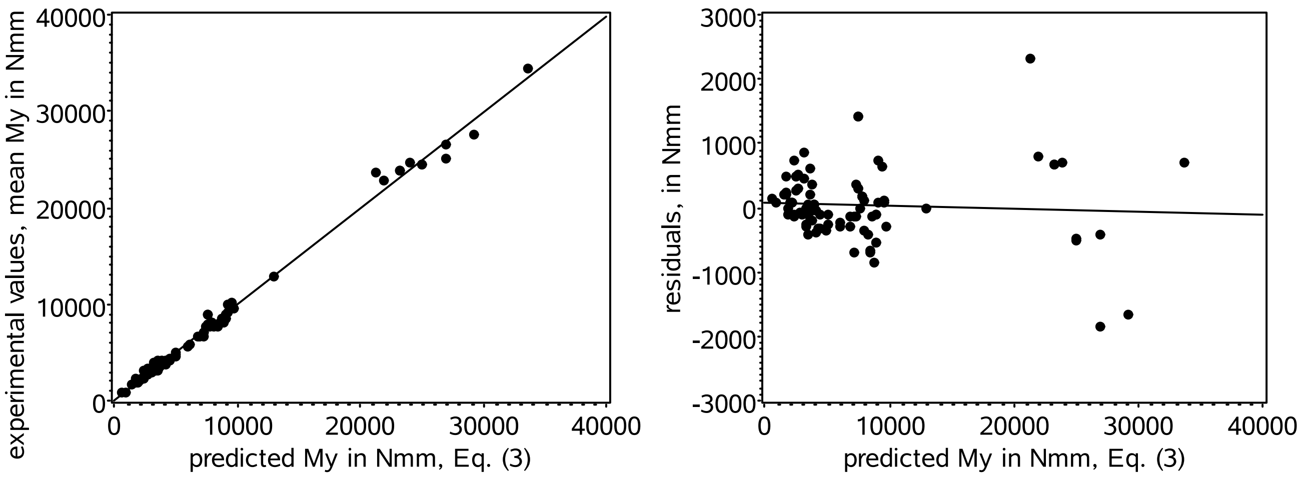

Figure 3. Left: Experimental and predicted values for the yield moment M_y. Right: Residuals. Data from 94 test series (1025 single tests M_y, 1038 single tests F_t).

3 Conclusions

The potentials of the assembled extensive database could be shown with regards to new analyses to evaluate the input parameters M_y, f_u and F_t. As wire and nail strength differ, tension tests on nails could potentially be sufficient to determine the nail properties in terms of tension strength and yield moment. First regression analyses showed that the ultimate strength calculated from the tension capacity of nails and the nominal diameter could possibly be used to calculate the yield moment, independently of nail types. Hardening effects at larger bending angles and strength increase with decreasing diameters seem to be inherently included by substituting the yield with the ultimate strength. Further analyses will be carried out to finalise investigations on direct nail properties (f_u, F_t, M_y) and system properties (f_{ax} and f_{head}), especially with regards to implementation in design standards.

4 References

[1] Werner H und Siebert W (1991) Neue Untersuchungen mit Nägeln für den Holzbau. *Holz als Roh- und Werkstoff*, **49**(5):191-198. [in German].

[2] Frese M, Fellmoser P und Blaß HJ (2010) Modelle für die Berechnung der Ausziehtragfähigkeit von selbstbohrenden Holzschrauben. *European Journal of Wood and Wood Products*, **68**(4):373-384. [in German]. DOI 10.1007/s00107-009-0378-1.

Determination of the effective material properties for thermal simulations

Katrin Nele Mäger, Tallinn University of Technology

Daniel Brandon, SP Technical Research Institute of Sweden

Alar Just, Tallinn University of Technology, SP

Keywords: Effective thermal properties

1 Introduction

Thermal properties of materials are dependent on temperature. Thermal simulations are a recognised alternative to some fire tests of building elements. To conduct the simulations, some material properties are needed. Test methods are available for measuring thermal properties of materials. However, these parameters are dependent on the way of heating. Currently available test equipment allows for either a constant incident heat flux or a constant temperature rise in the specimen. Both of these methods do not correlate well with the standard fire curve and therefore the results cannot be applied directly. Several FEM programs allow the modelling of the behaviour of building structures subjected to fire can be used to perform the thermal analysis. This research note describes how to calibrate the effective thermal properties on the basis of the test results.

2 Methodology

The present study made by Mäger (2016) is performed with FEM software SAFIR and mathematical computing software MATLAB. The MATLAB code is built to suit the specifics of the SAFIR input file.

According to the proposed methodology the software changes the values corresponding to a single temperature repeatedly by a set increment and then calculates the difference between the simulated and test result temperature measurements. This is repeated to find the functions of thermal properties at different temperatures that yield temperature predictions which highly correspond with the used experimental measurements.

The effective thermal properties found can be used in thermal simulations which may be used as an advanced calculation tool for the development of fire resistance properties for structures.

3 Calibration procedure

The main concept for the calculation in SAFIR is that heat is distributed in the structure by conduction since most construction elements are made of solid materials. This means that for some materials (e.g. insulation materials and wood) the calculation is an approximation. The limitations of currently available software and testing equipment create a need for modifying the thermal properties.

On the surfaces heat is exchanged with the environment via convection and radiation. These phenomena are taken into account by specifying the appropriate coefficients. Temperature calculations within solid materials are based on the Fourier equation (Bergman and Incropera, 2011). The Fourier equation describing one-dimensional conduction, such as in the case of the simulations conducted for this work, is presented in (1).

$$k\frac{\partial^2 T}{\partial^2 x} = c\rho\frac{\partial T}{\partial t} \Rightarrow \frac{\partial T}{\partial t} = \frac{k}{c\rho}\cdot\frac{\partial^2 T}{\partial^2 x} \qquad (1)$$

From equation (1) it can be seen that thermal conductivity is divided by the product of specific heat and density. This means that theoretically only one of these values needs to be calibrated to fit test data if there is sufficient certainty in the values of the other components. Generally, it is simpler to determine the mass loss and therefore the decrease in density. In the scope of this work, thermal conductivity and specific heat have been calibrated and density values acquired from separate tests.

In order to calibrate the thermal properties of a new material, the following steps need to be taken:

1) Assumption according to literature to form a starting point for calibrations
2) Appropriate temperature measurements determined by small scale fire tests with some different configurations
3) Mathematical approximation of thermal conductivity and specific heat for a relevant range of temperatures
4) Comparison of simulations and test data

A literature review should be carried out in order to form an initial set of relationships between the material temperature and thermal properties. If data from previous tests is unavailable, some additional tests should be conducted.

The next step is to carry out some small scale fire tests with known configurations. The amount of tests varies depending on the material (if test data is abundant or comparisons can be made with similar products, less testing might be sufficient).

The thermocouple readings from tests are the reference for calibration. For the approach used in this work to be applied, the software used for thermal simulations must have a simple enough system of input and output files. The MATLAB code works through the thermal properties defined in the specified rows of the input file and changes the values by a defined percentage until an acceptable correspondence with experimental results is reached.

In this study, the difference between the simulated and test time-temperature curves was calculated as the residual sum of squares. The software would compare the difference in the curves before and after changing the input and decide if the new value yielded a better fit. As a result the simulated time-temperature curve was iteratively shifted closer to the test curve.

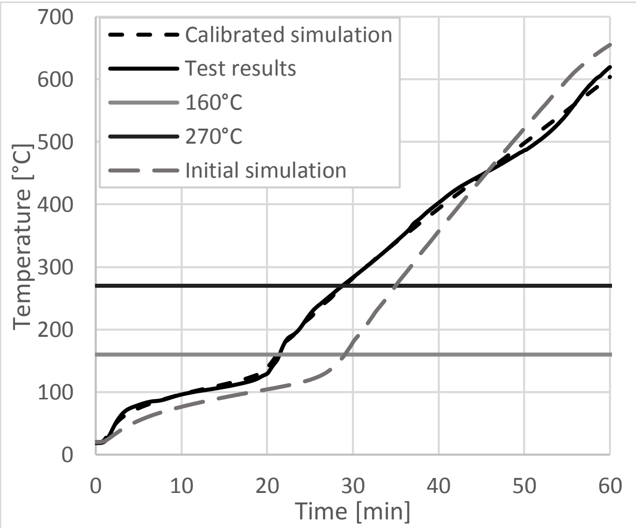

Figure 1. Comparison of tested, initial and calibrated time-temperature relations behind gypsum boards.

Visual evaluation of the fit of the simulated curve was also used. In the context of fire safety engineering of timber structures, there are a couple of characteristic temperatures at which a precise fit was deemed more important. For example 160°C and 270°C behind the gypsum layer shown in Figure 1.

Finally, in order to verify the method, the effective thermal properties were used to simulate the different test setups. Then, a comparison of the results was made with the thermocouple readings.

If all simulations show safe results, the thermal properties developed by calibration are declared to be effective

The effective thermal properties could be used for thermal simulations to evaluate the fire protection behaviour. For example to determine the design equations for improved component additive method to calculate the separating functions of structures (Schleifer 2009).

4 References

Mäger, K. (2016). Implementation of new materials to the component additive method for fire design of timber structures. Master thesis at Tallinn University of Technology. Tallinn, Estonia.

Bergman, T. and Incropera, F. (2011). *Fundamentals of heat and mass transfer*. Hoboken, NJ: Wiley.

Schleifer, V (2009) Zum Verhalten von raumabschliessenden mehrschichtigen Holzbauteilen im Brandfall. Zürich, Switzerland.

Dynamic effects in reinforced timber beams at time of timber fracture

Philipp Dietsch, Heinrich Kreuzinger, Technical University of Munich

Keywords: timber beam, reinforcement, screw, rod, fracture, dynamic effect, spring mass system, energy dissipation, plastic deformation

1 Introduction

In reinforced timber beams, the moment of brittle failure, i.e. the transition from the unfractured to the fractured state, is characterized by dynamic effects. In the unfractured state, the stresses under consideration are transferred proportionally by the timber beam and the reinforcement. Brittle failure in the timber results in associated stress release in the beam. The reinforcement is activated to carry the released stresses by deformations between the beam and the reinforcement. This sudden process leads to dynamic impact, resulting in additional stresses in the system. To receive an idea about the corresponding effects, a simple model is presented.

2 Method

To evaluate this situation, a spring-mass system can be used, see Fig. 2.1. In the unfractured state, the spring stiffness is given by the relevant stiffness of the timber beam k_{timber} (e.g. perpendicular to grain stiffness or shear stiffness) and the additional stiffness of the reinforcement embedded in the timber k_{reinf}. From the moment of brittle failure of the timber, the force has to be solely carried by the spring representing the reinforcement. Due to the reduction of total spring stiffness, the system falls from its original position into its new position of equilibrium. The magnitude of deformations is dependent on the proportion of force and spring stiffness before and after fracture. The system is in vibration, the maximum amplitude is double the static deformation between the original position and the new position of equilibrium. The vibration can be damped by either an activation of friction (k_{μ}) in the fracture plane (e.g. in the case of shear fracture) and/or by the plastic deformation of the reinforcement. See Fig. 2.1.

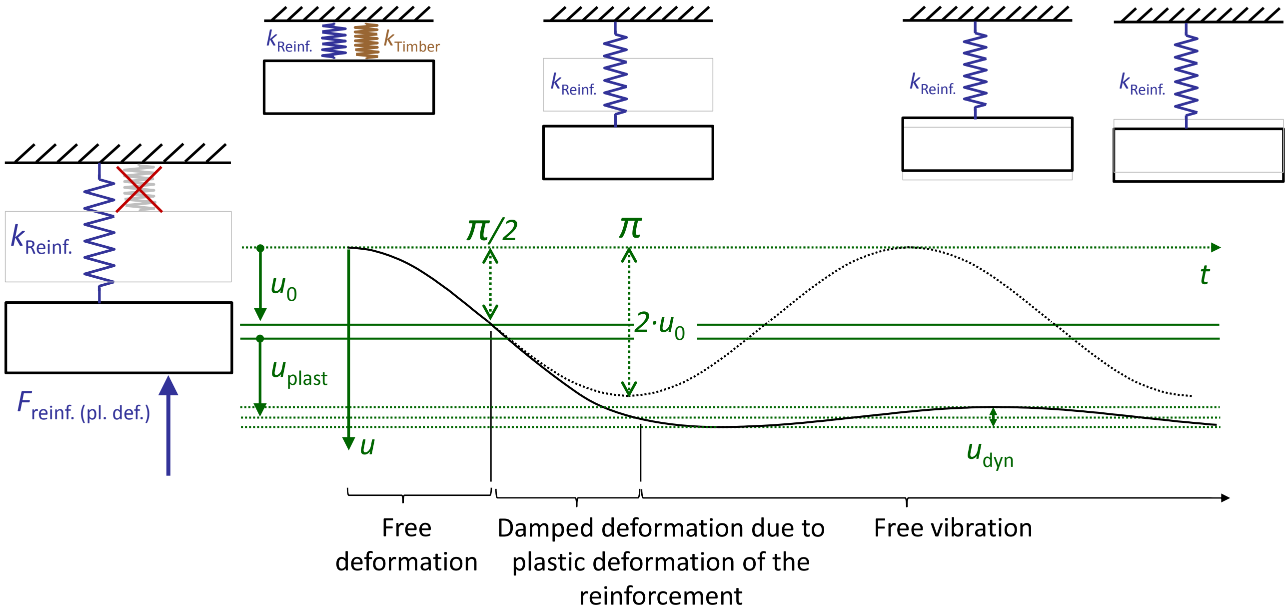

Figure 2.1. Spring-mass-system after timber fracture: free undamped vibration incl. static deformation u_0 between initial position and new position of rest and the dynamic deformation; dissipation of energy through plastic deformation u_{plast} of the reinforcement.

The following explanations concerning the sequence and influencing factors at the time of fracture are given on the basis of a load-deformation diagram that is combined with a time-deformation diagram, as shown in Fig. 2.2. This representation is based on comparable considerations in an unpublished expertise. The following discussion is based on the numbered sequence given in Fig 2.2. The values given are based on the assumption of a pure brittle failure over the full beam length and disregarding potentially higher properties during impact.

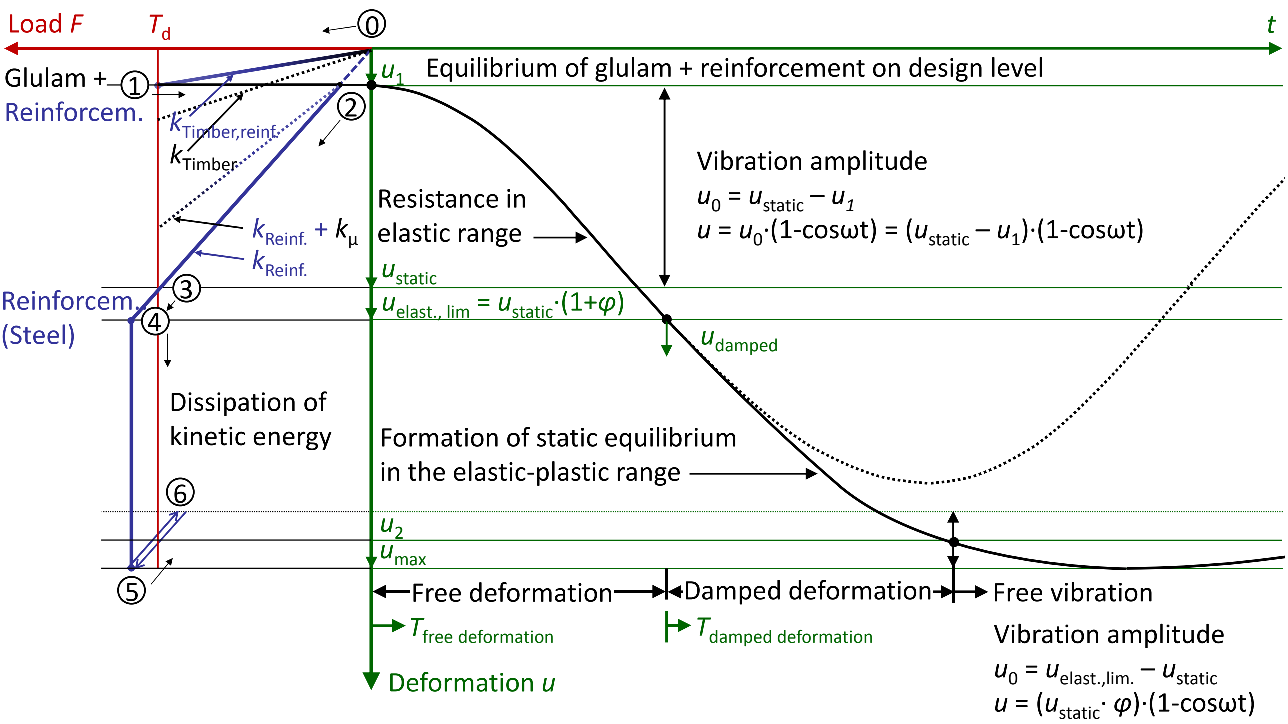

Figure 2.2. Schematic of the processes at the transition from the unfractured state (equilibrium, static position of rest u_1) to the fractured state (equilibrium, static position of rest u_2).

0. The beam is not loaded. Increasing load will lead to increasing deformation. These are smaller in the case of a reinforced beam compared to an unreinforced beam.

1. The load has reached the resistance of the rigid composite beam. The deformation u_1 is dependent on the stiffness of the timber beam and the embedded reinforcement. The exceedance of the design situation results in a sudden, brittle timber failure in the timber cross-section.

2. The elimination of the stiffness of the timber beam in the fracture plane results in a lower stiffness of the interconnection between the now mechanically jointed parts of the composite beam. The stresses that were proportionally transferred by the timber and the reinforcement are now solely transferred by the latter. The activation of the resistance of the reinforcement results in additional deformation. Another potential mechanism to transfer the released stresses is friction, which is activated in the case of shear stresses interacting with compression stresses perpendicular to the grain. Due to the high uncertainty of the friction coefficients, this mechanism is mostly neglected in structural design.

3. The system falls from its original state of equilibrium into the new position of equilibrium whereby it is restrained by the elastic deformation of the reinforcement. In the case of free vibration, i.e. elastic deformation of the reinforcement without energy dissipation, the maximum amplitude would be double the static deformation between the original and the new position of equilibrium (u_{static} - u_1). A corresponding design would result in a considerable increase in necessary capacity of the reinforcement. In [1] it is shown that, in the case of shear reinforcement, the load-carrying capacity of the interconnection would have to be increased by 60 % - 80 %, compared to a pure static design.

4. Another possible approach is to take into account the dissipation of kinetic energy by the plastic deformation of the reinforcement. The limit deformation $u_{elast.,lim.}$, at which a transition from elastic to plastic deformation is acceptable, should have a safe distance from the static position of rest, u_{static}. The relationship between both deformations can be expressed by an increase factor φ ($u_{elast.,lim.} = u_{static} \cdot (1+ \varphi)$). Static equilibrium is established in the elastic-plastic range.

5. The plastic deformation of the reinforcement ends when all kinetic energy is dissipated. The area defined by the resistance of the reinforcement during plastic deformation and the load in the fracture plane equals the dissipated kinetic energy. The larger the difference between resistance and load, the lower the necessary plastic deformation. The maximum deformation u_{max} can be expressed as a function of the static deformation in the unfractured state, u_1, the new position of equilibrium, u_{stat}, and the increase factor φ, as follows (a derivation can be found in [1]).

$$u_{max} = u_{static} \cdot \left\{(1+\varphi) + \frac{((1-u_1/u_{static})^2-\varphi^2)}{2\cdot\varphi}\right\} \tag{1}$$

If the capacity for plastic deformation of the reinforcement is known, the minimum necessary increase factor φ can be determined with Eq. (1).

6. After the damped movement, a free movement around the new static position of equilibrium, u_2, is reached. The vibration amplitude is $u_{static} \cdot \varphi$, equaling the proportion of the elastic deformation, exceeding the static position of rest (u_{stat}).

By increasing the ratio of deformations (u_1/u_{static}) through the stiffness ratio ($k_{Reinf.}/k_{Timber,Reinf.}$) before and after fracture, the magnitude of vibration amplitude u_0 and thus the magnitude of kinetic energy to be dissipated, is reduced. Here, bonded-in reinforcement has some advantage over screwed-in reinforcement, due to its higher withdrawal stiffness. The same effect can be reached by an increase of reinforcing elements.

An important parameter is the ductility of the reinforcement. An increase in plastic deformation capacity is synonymous with a reduction in increase factor φ. Hence the necessary increase in capacity to take into account the additional load from dynamic effects will reduce. Most reinforcing elements used in modern timber structures are optimized for high axial capacity which involves a reduction of ductility of the (high-strength) steel cross-section. Comparative calculations indicate that rather low ductility is necessary to reach a considerable reduction in the increase factor φ. Comparative calculations on shear reinforcement reported in [1] show that, under the assumption of a capacity of plastic deformation equal to three times the elastic deformation capacity, increase factors $0.1 \leq \varphi \leq 0.18$ (mean = 0.15) can be reached.

Self-tapping fully threaded screws that are optimized for high axial capacity feature a rather low relationship between plastic and elastic deformation capacity. Static tensile tests on typical self-tapping screws delivered values in the range of $D_s = v_u/v_y = 2.8 – 3.7$. Self-tapping screws that are less hardened or screwed-in rods feature a larger plastic deformation capacity. For the latter, relationships of $D_s = v_u/v_y = 11.8 – 14.0$ were determined.

3 References

[1] Dietsch, P. (2012): Einsatz und Berechnung von Schubverstärkungen für Brettschichtholzbauteile, Dissertation, Technische Universität München, Germany, 2012. https://mediatum.ub.tum.de/doc/1108735/1108735.pdf

Splitting tendency of nailed roof battens under variation of different parameters

Miriam Kleinhenz, Philipp Dietsch, Technical University of Munich
Chair of Timber Structures and Building Construction, (TUM)

Keywords: timber roof battens, connections, nails, end distance, minimum thickness, splitting, DIN 1052, Eurocode 5

1 Introduction

The splitting tendency of timber connections depends – amongst another factors - on the wood species and the density of the material (Blaß, H.J. & Uibel, T., 2009). (Blaß, H.J. & Schmid, M., 2002) relate requirements for minimum thickness *t* to wood species, inter alia, spruce. Furthermore, the nailing process can be interpreted as an impact process. The resistance of the material influences the energy release rate and, consequently, the splitting development. It can be observed that timber splitting starts at the side facing the nail tip (Ehlbeck, J. & Siebert, W., 1988).

The European timber design standard Eurocode 5 (2004) contains minimum spacing, edge and end distances for fasteners such as nails. The minimum distance to the unloaded end, $a_{3,c,}$ is 10*d*, given a characteristic timber density $\rho_k \leq 420$ kg/m³ and the holes are not predrilled. In the replaced German standard DIN 1052 (2008) minimum distance to the unloaded end, $a_{3,c\,,}$ depended on the nail diameter. For nails featuring diameters ≤ 5 mm, the general limit of 10*d* was reduced to 7*d*. This reduced requirement was applied for nailed roof battens – comparatively small and rarely fully utilized elements – since a reduction of end distances enabled the use of counter battens of smaller cross section.

Requirements for end distances of fasteners are related to the splitting tendency of connections. This behavior is also incorporated in Eurocode 5 in form of requirements for minimum thickness of nailed connections without pre-drilling. In certain cases, the general requirement of a minimum thickness of 14*d* can be reduced to 7*d*. In DIN 1052 (and now in the German NA to Eurocode 5), subordinate elements such as roof battens are amongst these exceptions.

The German timber construction industry proposed to keep the lower required end distances and include them in Eurocode 5 or at least in the German NA to Eurocode 5 (2013). This proposal was justified with good practical experience. Since more specific information was not available, it was decided to start an experimental investigation at TUM to analyze the splitting tendency of roof battens depending on both end distances $a_{3,c}$ (10*d*, 7*d*) under variation of all parameters of practical reference.

2 Materials and methods

Considering former experimental investigations such as Kevarinmäki (2005), the investigation on the influence of end distance $a_{3,c}$ (10*d* / 7*d*) on splitting tendency was realized under variation of different parameters: cross section of the batten, timber moisture content (dry, semi-dry, moist), nail diameter, nail type (smooth shank or threaded shank nail) and nailing process (manually or by nail gun) (see Table 1).

Table 1. Test configurations.

cross section	moisture content [%]	nailing	nail 3,1 mm		nail 3,4 mm		nail 3,8 mm	
			smooth	threaded	smooth	threaded	smooth	threaded
30/50	12 ± 3	manual	3,1x80	3,1x80	3,4x90	3,4x90		
	18 ± 3							
	≥ 24	nail gun	3,1x80	3,1x75	3,4x90	3,4x100		
40/60	12 ± 3	manual			3,4x90	3,4x90	3,8x100	
	18 ± 3							
	≥ 24	nail gun			3,4x90	3,4x100	3,8x110	3,8x120

All variations were tested for two distances to the unloaded end $a_{3,c}$ (10*d*, 7*d*). Seven additional series were realised to investigate an inclination of the nail of 60° to the grain.

In each configuration, ten specimen featuring a length of 60 cm were tested. Two different suppliers from two distinctly different regions of Bavaria supplied the spruce specimens. One charge contained dry battens (supplier A) and another charge contained moist battens (supplier B). The specimens (spruce) featured a mean density (at u = 12 %) of 487 kg/m³ and a characteristic density of 427 kg/m³ according to EN 384 (2010). The main properties of the timber species at delivery are given in Table 2.

Table 2. Properties of timber specimen.

cross section	30/50 (supplier A)	30/50 (supplier B)	30/50 (supplier B)	40/60 (supplier A)	40/60 (supplier B)	40/60 (supplier B)
mean moisture content [%]	13,3	16,9	31,4	12,9	18,1	26,8
coefficient of variation [-]	0,07	0,08	0,20	0,06	0,08	0,07
mean density [kg/m³]	494	519		451	485	
characteristic density [kg/m³]	439	482		388	405	

After each nailing process, a potential crack development was examined. The observations were classified into one of five categories (no splitting, split length ≤ 0,25*t*; split length ≤ 0,5*t*; split length ≤ 0,75*t*; fully splitted). For analysis, all cracks covering more than 50 % of the specimen depth *t* were classified “splitted”.

After this, the specimen were kept in standard climate (20°C, 65 %) for a period of four months. Within this period, the development of moisture content (semi-dry and moist specimen) and potential crack development were examined periodically.

3 Results

During the nailing process, a common observation was, that the crack initiation started at the side facing the nail tip. The majority of observations fell in either one of the categories “no splitting” or “fully splitted”. The drying process from category “moist” (≥ 24 %) to “semi-dry” (18 ± 3 %) took 12 days (30/50) respectively 10 days (40/60), while it took 30 days (30/50) respectively 40 days (40/60) to dry from category “semi-dry” to “dry” (12 ± 3 %). No further crack initiation was observed. The number of cracks with further development during the drying process was small (≤ 1 % in “dry” and “semi-dry”; 5 % in “moist”). It was therefore decided to only show the results for the observations made four months after nailing.

The main results of the observations are summarised in Figure 1, showing the influence of end distance $a_{3,c}$, cross section, nail diameter *d* and slenderness *t/d*.

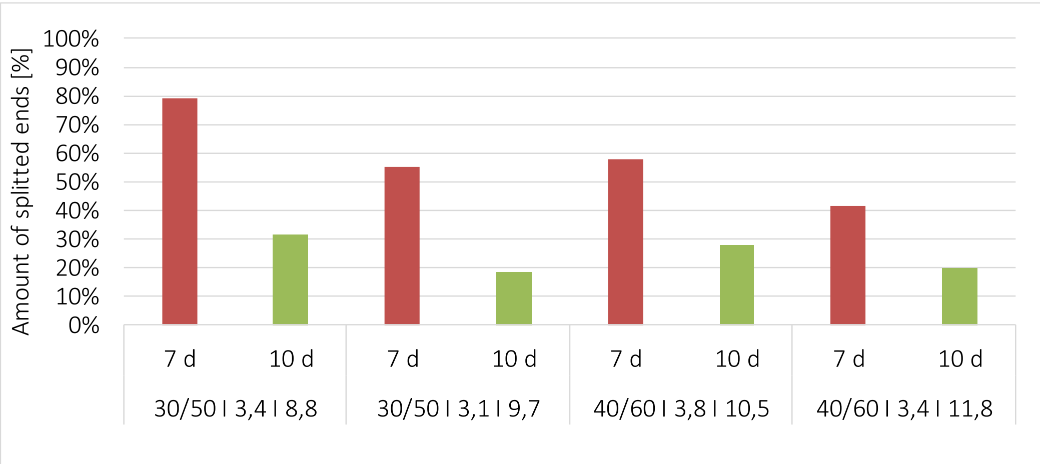

Cross section I ø I slenderness *t/d*	30/50 I 3,4 I 8,8		30/50 I 3,1 I 9,7		40/60 I 3,8 I 10,5		40/60 I 3,4 I 11,8	
End distance	7 *d*	10 *d*	7 *d*	10 *d*	7 *d*	10 *d*	7 *d*	10 *d*
Number of splitted ends *t* = 0	95	38	64	21	52	23	49	23
Number of splitted ends *t* = 4 mon.	95	38	66	22	52	25	50	24
Maximum	120	120	120	120	90	90	120	120
Amount of splitted ends t = 4 mon. [%]	79%	32%	55%	18%	58%	28%	42%	20%

Figure 1. Amount of splitted ends depending on end distance, cross section and nail diameter

Configurations with end distance $a_{3,c} = 10d$ showed much less splitting than configurations with $a_{3,c} = 7d$ (factor 2,4). The amount of splitted ends decreased with increasing cross section thickness *t* or decreasing nail diameter *d*. Even the highest slenderness at $a_{3,c} = 7d$ showed no better results than the series featuring the lowest slenderness at $a_{3,c} = 10d$.

The timber moisture content had no clear influence on the splitting tendency. The same observation was made for the inclination of the nail (60°). Slightly lower splitting tendency could be observed when nailing by hand instead of using a nail gun (11 %) and when using threaded instead of smooth shank nails (13 %). The mean density of all splitted specimen (506 kg/m³) was higher than the mean density of the unsplitted specimen (478 kg/m³) supporting previous examinations, that the splitting tendency is influenced by the timber density (Ehlbeck, J. & Siebert, W., 1988).

4 Conclusion

Based on the results received in the experimental campaign, a reduction of distance to the unloaded end from $a_{3,c}$ = 10*d* to 7*d* based on splitting tendency cannot be supported. If such a reduction shall be enabled, it is recommended to link this to a minimum required thickness of $t > 12\ d$ (compare $t \geq 14d$ in Eurocode 5).

5 Acknowledgement

The authors wish to thank the students David Palotas and Sevan Rashid for supporting the experimental campaign in the frame of their Bachelor Thesis. Gratitude is extended to Andreas Kraft (VBZH), Dieter Kuhlenkamp (Holzbau Deutschland), Jens Hödel (ITW) and Armin Lachmann (MPA BAU TUM) for their input and support.

6 References

Blaß, H.J. & Schmid, M. (2002): Spaltgefahr von Nadelhölzern. Versuchsanstalt für Stahl, Holz und Steine, Abteilung Ingenieurholzbau, Universität Karlsruhe (TH).

Blaß, H.J. & Uibel, T. (2009): Spaltversagen von Holz in Verbindungen, Ein Rechenmodell für die Rissbildung beim Eindrehen von Holzschrauben. Lehrstuhl für Ingenieurholzbau und Baukonstruktion, Universität Karlsruhe (TH).

Ehlbeck, J. & Siebert, W. (1988): Ermittlung von Mindestholzabmessungen und Mindestnagelabständen bei Nagelverbindungen mit europäischem Douglasienholz. Fraunhofer IRB Verlag.

Eurocode 5 (2004): Design of timber structures - Part 1-1: General and rules for buildings. CEN. Brussels. (EN 1995-1-1).

DIN 1052 (2008): Entwurf, Berechnung und Bemessung von Holzbauwerken – Allgemeine Bemessungsregeln und Bemessungsregeln für den Hochbau. DIN. Berlin.

German NA to Eurocode 5 (2013): Nationaler Anhang - National festgelegte Parameter - Eurocode 5: Bemessung und Konstruktion von Holzbauten - Teil 1-1: Allgemeine Regeln und Regeln für den Hochbau. DIN. Berlin. (DIN EN 1995-1-1/NA).

Kevarinmäki, A. (2005): Nails in spruce – splitting sensitivity, end grain joints and withdrawal strength, VTT Technical Research Centre of Finland, Karlsruhe, 2005.

EN 384 (2010): Structural timber - Determination of characteristic values of mechanical properties and density. CEN. Brussels.

5 Peer review of papers for the INTER Proceedings

Experts involved:

Members of the INTER group are a community of experts in the field of timber engineering.

Procedure of peer review

- Submission of manuscripts: all members of the INTER group attending the meeting receive the manuscripts of the papers at least four weeks before the meeting. Everyone is invited to read and review the manuscripts especially in their respective fields of competence and interest.

- Presentation of the paper during the meeting by the author

- Comments and recommendations of the experts, discussion of the paper

- Comments, discussion and recommendations of the experts are documented in the minutes of the meeting and are printed on the front page of each paper.

- Final acceptance of the paper for the proceedings with

    - no changes
    - minor changes
    - major changes
    - or reject

- Revised papers are to be sent to the editor of the proceedings and the chairman of the INTER group

- Editor and chairman check, whether the requested changes have been carried out.

6 Meetings and list of all CIB W18 and INTER Papers

CIB Meetings:

1 Princes Risborough, England; March 1973
2 Copenhagen, Denmark; October 1973
3 Delft, Netherlands; June 1974
4 Paris, France; February 1975
5 Karlsruhe, Federal Republic of Germany; October 1975
6 Aalborg, Denmark; June 1976
7 Stockholm, Sweden; February/March 1977
8 Brussels, Belgium; October 1977
9 Perth, Scotland; June 1978
10 Vancouver, Canada; August 1978
11 Vienna, Austria; March 1979
12 Bordeaux, France; October 1979
13 Otaniemi, Finland; June 1980
14 Warsaw, Poland; May 1981
15 Karlsruhe, Federal Republic of Germany; June 1982
16 Lillehammer, Norway; May/June 1983
17 Rapperswil, Switzerland; May 1984
18 Beit Oren, Israel; June 1985
19 Florence, Italy; September 1986
20 Dublin, Ireland; September 1987
21 Parksville, Canada; September 1988
22 Berlin, German Democratic Republic; September 1989
23 Lisbon, Portugal; September 1990
24 Oxford, United Kingdom; September 1991
25 Åhus, Sweden; August 1992
26 Athens, USA; August 1993
27 Sydney, Australia; July 1994
28 Copenhagen, Denmark; April 1995
29 Bordeaux, France; August 1996
30 Vancouver, Canada; August 1997
31 Savonlinna, Finland; August 1998
32 Graz, Austria; August 1999

33 Delft, The Netherlands; August 2000
34 Venice, Italy; August 2001
35 Kyoto, Japan; September 2002
36 Colorado, USA; August 2003
37 Edinburgh, Scotland; August 2004
38 Karlsruhe, Germany; August 2005
39 Florence, Italy; August 2006
40 Bled, Slovenia; August 2007
41 St. Andrews, Canada; August 2008
42 Dübendorf, Switzerland; August 2009
43 Nelson, New Zealand; August 2010
44 Alghero, Italy; August 2011
45 Växjö, Sweden; August 2012
46 Vancouver, Canada; August 2013

INTER Meetings:

47 Bath, United Kingdom; August 2014
48 Šibenik, Croatia; August 2015
49 Graz, Austria: August 2016

The titles of the CIB W 18 and INTER papers (starting from 2014) are included in the complete list of CIB/INTER papers: http://holz.vaka.kit.edu/392.php